PORT & COASTAL
SOLUTIONS

File Name:
EPBC Referral Report No. 5 - Boskalis Cambridge Gulf - INITIAL MODELLING

Cambridge Gulf Marine Sand Proposal

Metocean & Sediment Dynamics - System Understanding, Conceptual Model and Initial Modelling

P076_R01v03

PCS Output 1- Final

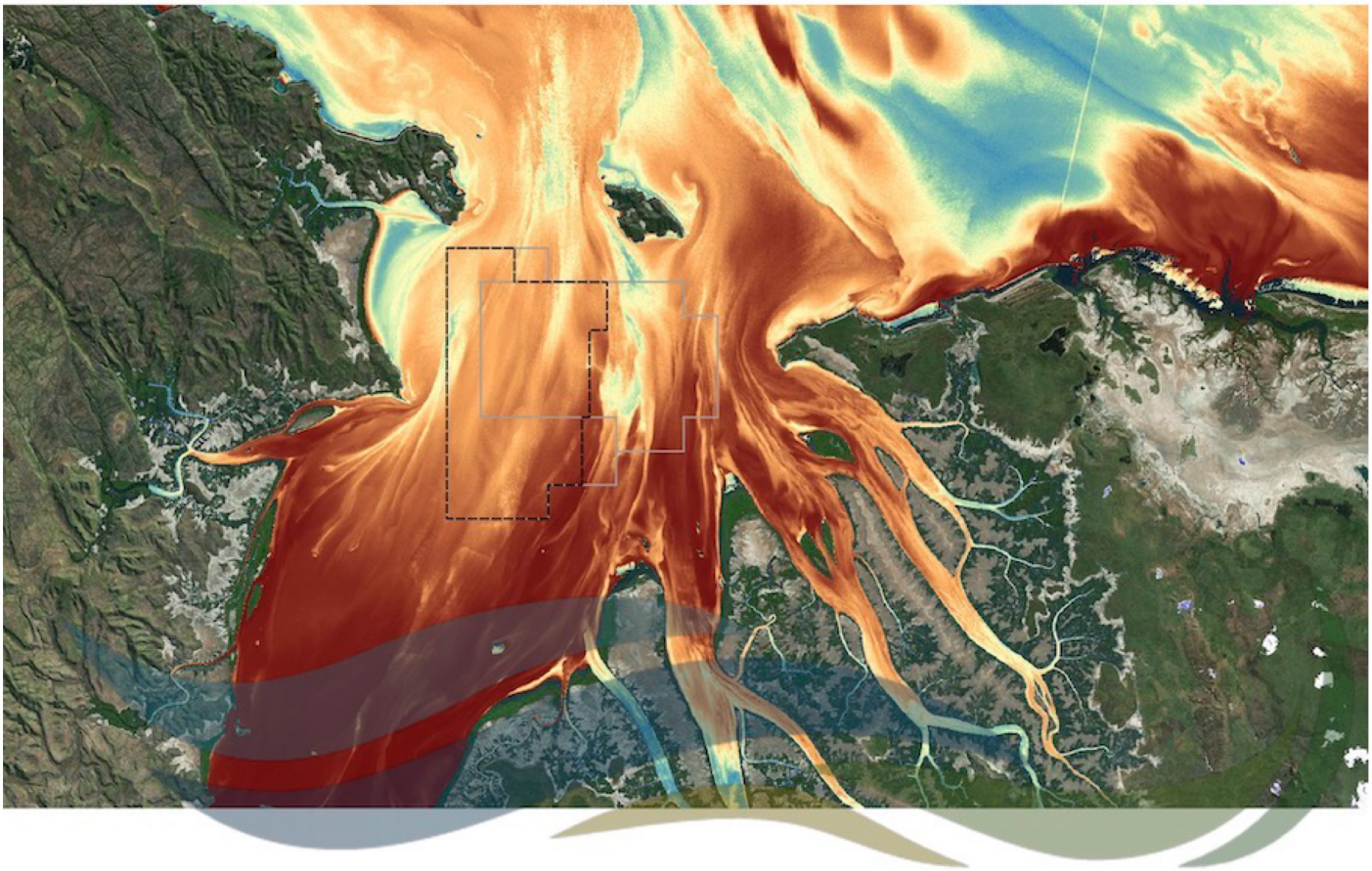

Boskalis
Technical Report
July 2024

PORT & COASTAL
SOLUTIONS

Cambridge Gulf Marine Sand Proposal

Metocean & Sediment Dynamics - System Understanding, Conceptual Model and Initial Modelling

Report No. P076_R01v03

PCS Output 1 - Final

July 2024

For Boskalis Australia Pty Ltd

Version	Details	Authorised By	Date
0.1	Draft	Andy Symonds	27/11/2023
0.2	Reviewed by BKA	Andy Symonds	01/02/2024
0.3	Final	Andy Symonds	26/07/2024

Document Authorisation		Signature	Date
Project Manager	Andy Symonds		26/07/2024
Author(s)	Andy Symonds		26/07/2024
Reviewer	Rachel White		26/07/2024

PORT & COASTAL
SOLUTIONS

CONTENTS

APPENDICES

FIGURES

PORT & COASTAL
SOLUTIONS

TABLES

PORT & COASTAL
SOLUTIONS

ACRONYMS

ADCP	Acoustic Doppler Current Profiler
AHD	Australian Height Datum
AHO	Australian Hydrographic Office
AIMS	Australian Institute of Marine Science
AWAC	Acoustic Wave and Current Profiler
BK	Boskalis
CADDIS	causal/diagnosis decision information system
CAWCR	Centre for Australian Weather and Climate Research
CG	Cambridge Gulf
CSIRO	Commonwealth Scientific and Industrial Research Organisation
D50	Median particle size
DHI	Danish Hydraulic Institute
DSN	Dredging Science Node
EDS	Energy Dispersive X-ray Spectroscopy
EIA	Environmental Impact Assessment
EP	East Profile
EPA	Environmental Protection Authority
EQP	Environmental Quality Plan
FM	Flexible Mesh
GBRMPA	Great Barrier Reef Marine Park Authority
GL	Gigalitre
HAT	Highest Astronomical Tide
HD	Hydrodynamic
H_s	Significant wave height
IMOS	Integrated Marine Observing System
JBG	Joseph Bonaparte Gulf
LAT	Lowest Astronomical Tide
LiDAR	Light Detection And Ranging
MARS	Marine Sediments database
MHWN	Mean High Water Neaps
MHWS	Mean High Water Springs
ML	Megalitre
MLWN	Mean Low Water Neaps
MLWS	Mean Low Water Springs
MP	Middle Profile
MSL	Mean Sea Level
MT	Mud Transport
NISB	National Intertidal Subtidal Benthic
NTU	Nephelometric Turbidity Unit
OBS	Optical Backscatter Sensors
PAR	photosynthetically active radiation
PCS	Port and Coastal Solutions
PSD	Particle size distribution
SEM	Scanning Electron Microscopy
SPV	Sand Production Vessel
SSC	Suspended sediment concentration
SW	Spectral Wave
TSM	Total suspended matter
TC	Tropical cyclone
US	United States
USEPA	United States Environmental Protection Agency
WA	Western Australia
WAMSI	Western Australian Marine Science Institution
WL	Water level
WP	West Profile
WWIII	WAVEWATCH III

Executive Summary

Boskalis Australia Pty Ltd (BKA) commissioned Port and Coastal Solutions (PCS) to undertake metocean and sediment data analysis and numerical modelling for the Cambridge Gulf (CG) Marine Sand Proposal (the proposal). The primary aim of this study is to analyse and interpret metocean and sediment data and then undertake detailed numerical modelling to support the regulatory approval applications for the project, with four objectives as detailed in Section 1, relating to 1) hydrodynamics, 2) sediment dynamics and coastal processes and 3) suspended sediment and turbidity.

The study is designed to support BKA's Environmental Impact Assessment (EIA) and regulatory approval applications for the proposal under the Western Australian (WA) Environmental Protection Act (EP Act). All work has been and is being undertaken in accordance with all relevant guidelines of the WA Environmental Protection Authority (EPA) as listed in Section 1.

This report is aimed at providing a review of the existing metocean and sediment data, a gap analysis, presenting initial numerical model setups and results and developing a system understanding and conceptual model based on the available information. After the preparation of this technical report, data from the 2024 wet season data collection campaign were available. Analysis of these data has been undertaken to provide additional understanding for the project, the analysis is detailed in a supplementary technical note which is included as Appendix A.

The data review showed that the combination of existing data and the data being collected by BKA will be sufficient to provide a good understanding of the hydrodynamics, sediment transport and coastal processes in CG. However, a number of data gaps were identified and based on these it was recommended that the following additional data were collected to fill these gaps:

- high resolution bathymetric data of Blocks 4 and 4A. This was undertaken for the proposed operational area during the 2024 wet season data collection campaign, the data are presented in Appendix A;
- data to show erosion/accretion rates within the proposed operational area (i.e. repeat bathymetric survey). This was undertaken for two target areas within the proposed operational area during the 2024 wet season data collection campaign, the data are presented in Appendix A; and
- topographic data of the intertidal and supratidal areas of the turtle nesting beaches to provide high resolution beach elevation data. This was undertaken during the 2024 wet season data collection campaign, the data are presented in Appendix A.

The available data have shown that CG is a macrotidal environment that regularly experiences strong tidal current speeds of up to 1.5 m/s. It is relatively sheltered from offshore waves due to the shallow bathymetry of King Shoals and Medusa Bank just off the entrance to CG, as well as the sheltering provided by Lacrosse Island. The astronomical tide is the dominant coastal process in CG, resulting in regular transport of the clay, silt and sand that is present within CG. The regular sediment transport results in naturally high suspended sediment concentration (SSC) within CG, with an average value of 50 mg/L and a peak value of more than 200 mg/L recorded to date, which in turn results in low benthic light availability and low chlorophyll-a. Benthic biota surveys identified limited benthic habitats and communities, with no seagrass, coral communities, filter feeder communities or oyster reefs present in the region (BKA, 2024d). The key habitats are the narrow fringes of mangroves around the coast of CG, backed by tidal salt flats and mudflats, including the Ord River Floodplain Ramsar site on the eastern side of CG, and four beaches that are used by marine turtles (mainly *Natator depressus* or Flatback Turtles) for nesting (BKA, 2024d). The seaward beach at Cape Domett is a globally significant Flatback Turtle nesting beach (Whiting et al., 2008).

Satellite imagery was sourced and analysed to assess how the turtle nesting beaches have changed over time. The analysis showed that the seaward beaches outside of CG (Cape Domett and Turtle Beach West, west of Cape Dussejour) have been advancing since 1994, while Turtle Bay on Lacrosse Island has remained stable and the stranded beach ridge at East Bank Point (also known locally as Barnett Point) inside CG has been retreating at either end but remained stable in the centre. The shoreline positions at the two seaward beaches and the beach on Lacrosse Island showed a difference in shoreline position between the wet and dry seasons, indicating a potential change in the beach profile shape due to the different wave conditions which occur during the different seasons.

Satellite imagery was also sourced and processed to assess how the SSC in the region has varied spatially and temporally depending on the metocean conditions. The analysis showed that the SSC in the region is typically high, with low SSC only occurring for short periods during very small neap tides. The SSC was also shown to vary over a tidal cycle, with lower SSC around high water due to offshore waters with low SSC being imported into CG and higher SSC around low water due to upstream waters from the West and East Arms with very high SSC flowing into CG. The imagery showed that the SSC can be increased due to large waves and high river discharge, but the surface water SSC during these events was not significantly higher than during large spring tides.

The initial setup of a hydrodynamic, spectral wave, sediment transport and beach processes models has been presented. The MIKE software suite developed by the Danish Hydraulic Institute (DHI) was applied for all the modelling, with a flexible mesh approach adopted for the hydrodynamic, wave and sediment transport models. The model mesh extends approximately 200 km north to south and 280 km east to west, with the triangular elements side lengths varying from 4 km in the offshore areas to 200 m in CG. An initial model calibration of the hydrodynamic model, and high-level validations of the spectral wave and sediment transport models are presented. Preliminary results from all four of the models are presented to help understand the existing conditions in CG and how these conditions vary spatially and temporally.

There was sufficient confidence in the HD and SW models to allow preliminary impact assessment to be undertaken for the sourcing of 70 million m^3 of sand from the proposed operational area. The HD modelling predicted that the sand sourcing would result in small changes to both water levels and currents in CG. The phasing of the tidal propagation upstream of the proposed operational area was predicted to be changed by 27 s (earlier) and this results in apparent changes in water level and current speed during the flood and ebb stages of the tide. The sand sourcing is not predicted to measurably impact the tidal range within CG (changes of up to 0.06%). The deepening due to the sand sourcing is predicted to result in a localised reduction in current speed within the proposed operational area of up to 1.5% of the peak current speeds.

The SW model predicted that the sand sourcing would not impact the wave conditions for the majority of the time. The deepening of the proposed operational area was only predicted to result in changes to the wave conditions within CG during large wave events such as those which occur during the wet season due to TCs and tropical lows, while the model did not predict any changes to waves offshore of CG. The largest changes were predicted to occur during the largest wave event modelled (due to a TC) when the H_s in CG ranged from 1 to 2 m, with increases in H_s in CG predicted to remain below 0.01 m (0.5 to 1%).

The MT model was not considered to be sufficiently developed to reliably predict changes to sediment transport or erosion and accretion rates. However, the predicted impacts to hydrodynamics and waves were used to qualitatively assess potential impacts to sediment transport and coastal processes. The small and localised predicted changes to the hydrodynamics resulting from the sand sourcing was not considered unlikely to noticeably change the sediment dynamics and sediment transport rates in CG, with the changes potentially resulting in a small increase in sedimentation in the proposed operational area (due to a reduction in current speeds in this area). As predicted changes to wave conditions were limited to within CG and only during large wet season wave events the changes in waves are not expected to directly impact sediment transport rates (of sand and fine-grained silt and clay) or coastal processes (i.e. no changes to beaches or mangroves) either within or offshore of CG.

The proposed approaches for the future modelling to be undertaken as part of the study are outlined along with details as to how the modelling and data analysis approach has and will meet both the study objectives as well as the WA EPA guidelines.

Information from relevant literature, available data and the preliminary model results were used to develop a system understanding of the CG region in terms of coastal processes and sediment transport. In addition, a high-level overview of potential coastal processes and ecological implications resulting from the proposed CG Marine Sand Proposal has been provided along with a conceptual model of the potential different causes and effects. The conceptual model includes changes to the system as a result of the historic Ord River catchment clearing and the construction of the Ord River Dam, to help assess potential cumulative impacts, as required by the WA EPA Guidelines.

The conceptual model identified two potential cause-effect pathways resulting from the CG sand sourcing. The first was the suspension of sediment into the water column by the sand sourcing activity, and the second was a reduction in availability of sand on the seabed. The potential for both pathways to cause negative environmental impacts is considered low, however this will be assessed in detail through the subsequent modelling phase of this study.

1. INTRODUCTION, OBJECTIVES & GUIDELINES

Boskalis Australia Pty Ltd (BKA) commissioned Port and Coastal Solutions (PCS) to undertake metocean and sediment data analysis and numerical modelling for the Cambridge Gulf (CG) Marine Sand Proposal (the proposal). The primary aim of this study is to analyse and interpret metocean and sediment data and then undertake detailed numerical modelling to support the regulatory approval applications for the project, with three objectives as follows:

Objective 1: Hydrodynamics and waves:

a) Define the existing hydrodynamic conditions in the subject areas, under the seasonal range of natural conditions, including any changes since European colonization.

b) Predict potential impacts of the proposed project on the hydrodynamics of the subject areas, including during the operation, at the end of the operation (approximately 15 years) and in 100 years time.

c) Predict likely 'worst-case' and 'best-case' impacts and also potential 'cumulative' impacts of the proposed project on hydrodynamics (with 'worst-case' and 'best-case' being consistent with meanings in relevant WA EPA guidance as listed below, and 'cumulative' meaning in addition to those that may have been caused by previous developments in the area, such as the Ord River dam).

d) Provide hydrodynamics data analysis and modelling to support the other objectives below.

Objective 2: Sediment transport and coastal processes:

a) Define existing sediment transport and coastal processes in the subject areas, including natural sediment sources and pathways, sediment sizes on the seabed and in transport under the seasonal range of natural conditions, and any changes since European colonization.

b) Predict potential impacts of the proposed project on sediment transport and coastal processes of the subject areas, including during the operation, at the end of the operation (15 years) and in 100 years, with particular focus on:

- predicting potential for natural replenishment of sand in dredged areas of the tenements, including likely timeframes for replenishment,
- predicting potential for coastal erosion and accretion,
- predicting potential impacts on turtle nesting beaches both inside and immediately outside Cambridge Gulf, including potential changes in sand grain size and beach geomorphology; and
- predicting potential impacts on mangroves and other coastal and intertidal communities and impacts on the Ord River Floodplain Ramsar site as a result of the sand extraction.

c) This should include prediction of likely 'worst-case' and 'best-case' impacts and also 'cumulative' impacts of the proposed project on sediment transport and coastal processes (with 'worst-case' and 'best-case' being consistent with meanings in relevant WA EPA guidance as listed below, and 'cumulative' meaning in addition to those that may have been caused by previous developments in the area, such as the Ord River dam).

Objective 3: Suspended sediment and turbid plume dispersal & potential impacts on benthic habitats & communities (see note below):

a) Define the existing suspended sediment and turbidity regime in the subject areas, under the seasonal range of natural conditions.

b) Predict potential dispersal of sediment and turbidity plumes from the proposed operation, under the seasonal range of natural conditions, in particular towards King Shoals and the State Marine Park Sanctuary Zone (although noting that benthic

surveys in this area have not identified any sensitive benthic communities (BKA, 2024d)).

This study is designed to support BKA's Environmental Impact Assessment (EIA) and regulatory approval applications for the proposal under the Western Australian (WA) Environmental Protection Act (EP Act). All work has been and is being undertaken in accordance with all relevant guidelines of the WA Environmental Protection Authority (EPA) as follows:

a) Accepted international best practices relating to the hydrodynamics, sediment dynamics and coastal processes and modelling aspects of marine EIAs.

b) Western Australia (WA) Environmental Protection Authority (EPA) 2021 *Technical Guidance for EIA of Marine Dredging Proposals*.

c) WAMSI/CSIRO 2020 *Guideline for Dredge Plume Modelling for EIA* (Sun et al., 2020).

d) WA EPA 2016 *Environmental Factor Guideline - Coastal Processes*.

e) WA EPA 2016 *Environmental Factor Guideline - Marine Environmental Quality*.

f) WA EPA 2016 *Technical Guidance - Protecting the Quality of Western Australia's Marine Environment.*

This report is aimed at providing a review of the existing data, a gap analysis, presenting initial modelling setups and results and developing a system understanding and conceptual model based on the available information. Additional reports will subsequently be developed which cover the detailed modelling associated with each of the three objectives in more detail.

1.1. Overview of the Marine Sand Proposal

BKA currently holds an exploration tenement for marine sands in a designated area of CG, referred to by BKA as Block 4 and corresponding to WA exploration tenement E80/5655 (Figure 1).

BKA undertook initial sand exploration surveys in Block 4 in March 2023 using a sub-bottom profiler, vibro-cores and sediment grabs, to determine the sediment composition and bathymetry and assess the potential sand resource. This survey indicated that there is only limited sand in the eastern part of Block 4 but there is significant sand resource in the western half. Based on indications that the sand resource extends west of Block 4, BKA has applied for a spatial extension of Block 4, referred to by BKA as Block 4A (exploration tenement E80/5910). The proposed operational area would therefore only be the western half of Block 4 and all of Block 4A, with an area of 101 km^2, representing approximately 64% of the combined area of the two blocks (which is 158.4 km^2). (Figure 1).

A total of up to 70 million m^3 of sand is proposed to be sourced from CG by BK over a 15 year period. As the proposed operational area covers 101 km^2 or 101 million m^2, this means that if 70 million m^3 of sand is sourced, on average the layer of sand removed would be less than 1 m.

Further details about the proposed operation including vessel type and the timing of the operational cycle are presented in BKA's EIA submission (EPA Proposal Content Document) (EPA Template, 2024) of which this report is a supporting report. It is relevant for this report to note that the sand sourcing is proposed to be undertaken by a single vessel.

BKA is currently proceeding with the State EIA and other studies to support regulatory approval applications in order to progress towards sand production in CG. As part of these broader EIA studies, BKA developed a data collection plan to provide metocean and sediment data to inform the studies required to support the EIA. The data collection commenced in June 2023 and is planned to continue until January 2025. Extensive metocean and sediment data are being collected over a range of wet and dry season conditions to provide site specific data to inform the project. Further details of the data collected to date and the future data to be collected are provided in Section 2.3. The data collected for the project will be used as follows:

- To provide baseline data for the project.
- As site specific data to inform a conceptual model of CG.
- To inform detailed numerical modelling of the region.

1.2. Cambridge Gulf

Cambridge Gulf (CG) is a large, highly dynamic and highly turbid embayment located on the tropical northeast coast of Western Australia (WA), centered on 14° 52.00' S and 128° 16.00' E, facing northwards and seawards to the larger Joseph Bonaparte Gulf (JBG) (Figure 1). The seaward mouth is bounded to the west by Cape Dussejour and to the east by Cape Domett, with Lacrosse Island located centrally, dividing the mouth into a West Entrance and an East Entrance. Large sand banks at King Shoals and Medusa Banks are located outside CG in JBG beyond Lacrosse Island. The main body of CG extends 40 km from its seaward mouth upstream to Adolphus Island, with the widest point being 20 km (Figure 1). The mean water depth is approximately 12 m LAT (Wolanski et al 2004).

CG is a macrotidal environment with semi-diurnal tides with a spring tidal range of 8 m. The large tidal results in high tidal current speeds resulting in a naturally turbid environment and the tide is likely to have been the dominant process in the formation of CG in its current form (Thom et al., 1975).

The region is semi-arid, with annual rainfall in the region of 500 mm and with the majority of this occurring in the wet season, from December to March. Multiple rivers flow into CG, including the Ord River, Pentecost River, Durack River, King River and the Forrest River (Thom et al., 1975; Wolanski et al., 2001) (Figure 2). High river flows only occur occasionally and only during the wet season. The wet season river discharge has been noted to have considerable inter-annual variability, with order of magnitude variations from year to year. There is also significant daily variability in river flows during flood events, with very high flows following a tropical cyclone only lasting a few days (Wolanksi et al., 2001).

At the upstream end of CG there are two arms, the West and East Arms. The Pentecost and Durack Rivers drain into the West Arm, while the Ord River drains into the East Arm. The total catchment area for CG is approximately 87,000 km^2 and 62% of this area is the Ord River catchment, while the catchments for the Pentecost and Durack Rivers combined represent approximately 27% (the remaining 11% is made up of smaller rivers and creeks and coastal areas) (dataWA, 2023).

The catchments for the Pentecost and Durack Rivers are not dammed and land remains largely uncleared. In contrast, the catchment for the Ord River has been subject to extensive land clearing for cattle and also has two dams, with the Ord River Dam also having created Lake Argyle which is the largest artificial lake in the southern hemisphere. The extensive land clearing commenced around the start of the 20th Century, while the dams were constructed between 1969 and 1972 (Wolanski et al., 2001). The Ord River flows were noted to have experienced significant variability in discharge prior to the construction of the dams, but since the construction the river discharge is now almost constant. The seasonal variability and large floods still occur in the Durack and Pentecost Rivers (Wolanksi et al., 2001).

The rivers that drain into CG all discharge sediment into the Gulf. Over time, this has resulted in the formation of multiple small deltas and tidal flats, with these Quaternary deposits alternating with ancient rock outcrops (Wright et al., 1973). The supply of sediment from the rivers to CG will vary significantly due to the high variability in the river discharge. Peaks in sediment supply from the rivers will occur in the wet season, with limited supply of sediment during the dry season. The rivers supply a combination of sand sized sediment and fine-grained silt and clay. It is likely that the relative contribution of sand and fine-grained sediment supplied by the rivers varies depending on the river discharge, with lower discharge events likely to supply a higher proportion of fine-grained sediment while higher discharge events have the potential to supply a higher proportion of sand.

The sediment deposited in the channels in the CG will be subject to regular reworking by the strong tidal currents that occur in the region, resulting in well-sorted sandy sediment being present in the main channels. Since the damming of the Ord River significant sedimentation of the East Arm of the CG (which is downstream of the dam) has been observed, with average siltation depths of 3 m (Wolanski et al., 2004).

1.3. Report Structure

The report herein is set out as follows:

- an introduction to the study is provided in **Section 1**;
- a review of the data and a gap analysis is presented in **Section 2**;
- the local site conditions are detailed in **Section 3**;

- the modelling approach, setups and preliminary results are included in **Section 4;**
- the conceptual model is developed and detailed in **Section 5**;
- details of how the project adheres to the relevant project objectives and approval guidelines is provided in **Section 6**; and
- a summary of the findings from this report are presented in **Section 7**.

The following conventions have been adopted throughout:

- volumes are in-situ cubic metres;
- depths are provided relative to Australian Height Datum (AHD) unless stated otherwise;
- current directions are quoted as directions to; and
- wave and wind directions are quoted as directions from.

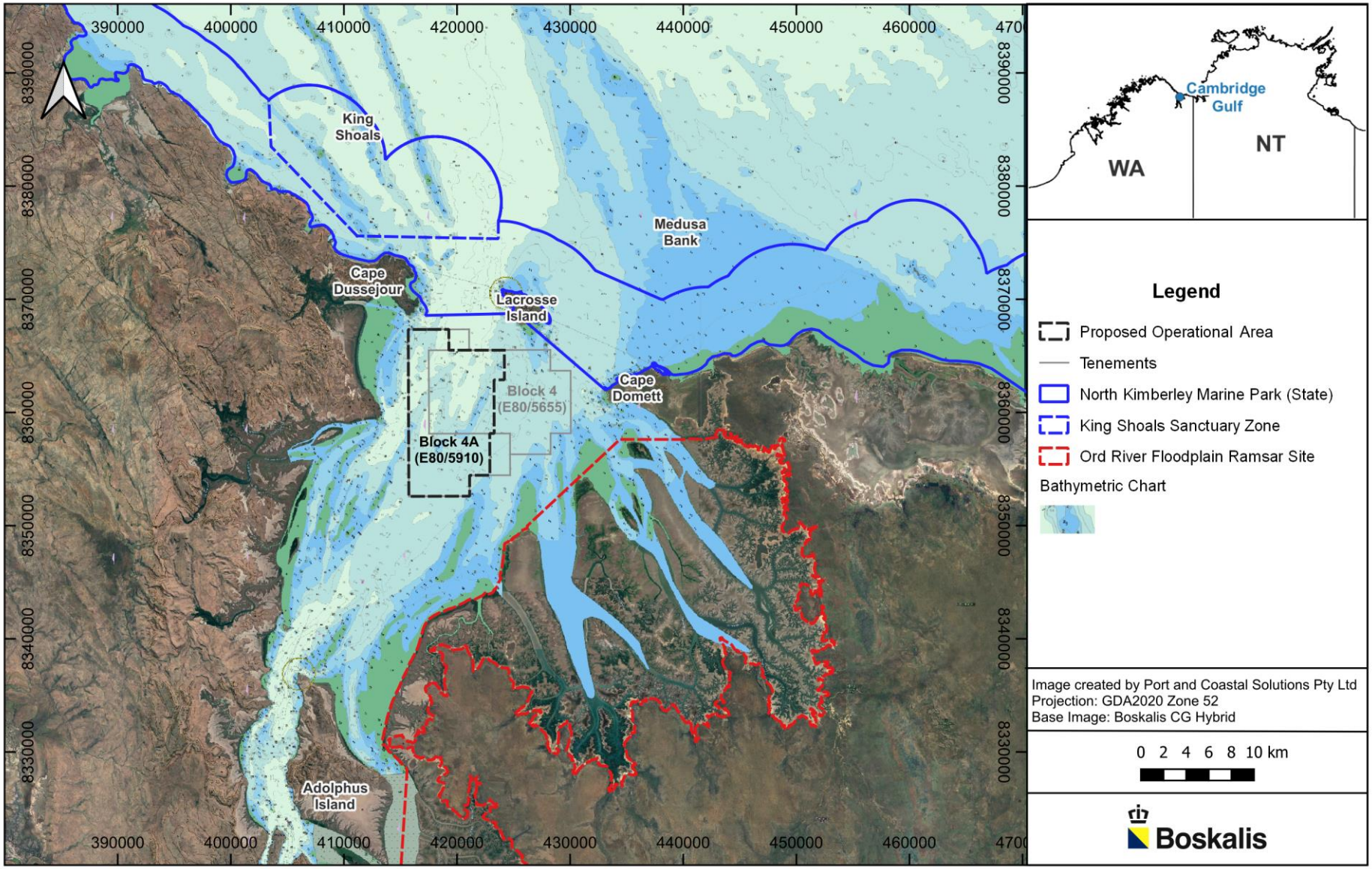

Figure 1. **Map of CG showing areas of interest for this report.**

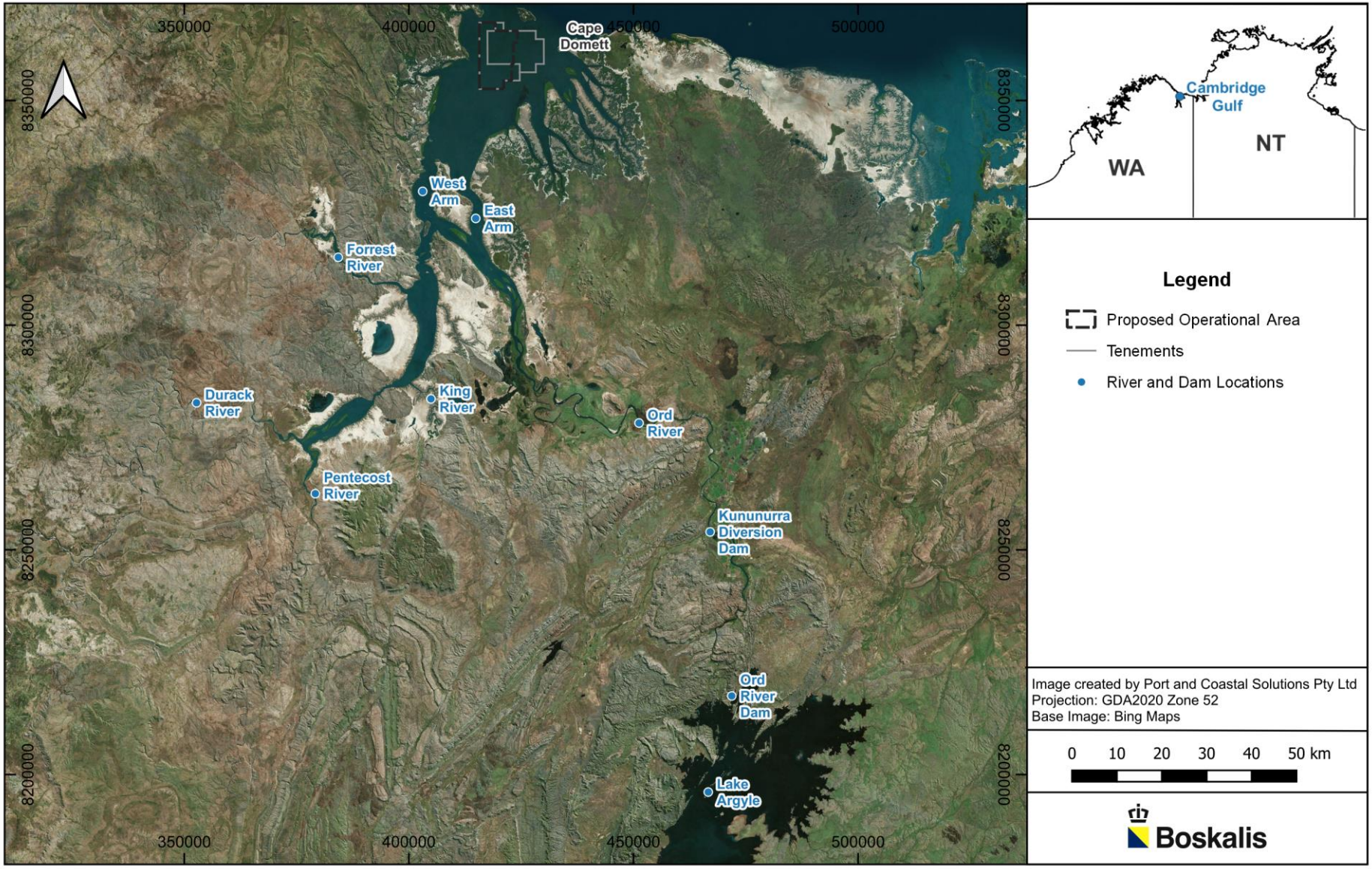

Figure 2. Location of rivers and dams that influence CG along with the West Arm and the East Arm.

2. DATA REVIEW

A significant amount of data and information is already available for CG, which can be used to provide background understanding of the environment and to develop a conceptual model and numerical models. This section discusses the available data and summarises its relevance to the project. In addition, data which have been collected by BKA to date and which is proposed to be collected by BKA in the future are summarised.

A gap analysis of the existing available data and the proposed future data is also presented to determine if sufficient data are available to achieve the EIA objectives and comply with the relevant EPA guidelines as listed in Section 1, and to identify any additional data required.

2.1. Literature

A number of previous studies have been undertaken in the CG region, which provide useful information for this project. All the freely available relevant literature that we have been able to identify was reviewed,, with the following providing the most relevant information for this study:

- Coleman, J.M., and Wright, L.D., 2006. Sedimentation in an arid macrotidal alluvial river system: Ord River, Western Australia;
- DEC (Department of Environment and Conservation) 2012, Ord River and Parry Lagoons nature reserves management plan 77 2012 , Department of Environment and Conservation, Perth;
- Gehrke, P., 2009. Ecological patterns and processes in the Lower Ord River and Estuary;
- Hale, J. 2008. Ecological character description of the Ord River floodplain Ramsar site. A Report to the Department of Environment and Conservation, September 2008;
- Robson, B.J., Burford, M.A., Gehrke, P.C., Revill, A.T., Webster, I.T. and Palmer, D.W., 2008. Response of the Lower Ord River and Estuary to changes in flow and sediment and nutrient loads;
- Robson, B.J., Gehrke, P.C., Burford, M.A., Webster, I.T., Revill, A.T. and Palmer, D.W., 2013. The Ord River Estuary: a regulated wet-dry tropical river system. In Wolanski (ed.) Estuaries of Australia in 2050 and Beyond, Estuaries of the World;
- Thom, B.G., Wright, L.D., and Coleman, J.M., 1975. Mangrove ecology and deltaic-estuarine geomorphology: Cambridge Gulf-Ord River, Western Australia. Journal of Ecology, Vol. 61, No. 1, 203 – 232;
- Wolanski, E., Spagnol, S., and Pattiaratchi, C., 2001. Rapid, human-induced siltation of the macro-tidal Ord River Estuary, Western Australia. Estuarine Coastal and Shelf Science 53, 717-732;
- Wolanski, E., Spagnol, S., and Williams, D., 2004. The impact of damming the Ord River on the fine sediment budget in Cambridge Gulf, Northwestern Australia. Journal of Coastal Research, 20 (3), 801-807; and
- Wright, L.D., Coleman, J.M., and Thom, B.G., 1973. Processes of channel development in a high tide range environment: Cambridge Gulf – Ord River Delta, Western Australia.

These reports and papers provide extensive information on the development of CG over geological timeframes as well as details of changes since European colonisation and specifically changes since the Ord River dams were constructed, including data collected back to the 1950s. They have been used to help inform the description of local conditions, system understanding and the conceptual model. These references are cited throughout the report where relevant.

2.2. Existing External Data Sources

Sections 2.2.1 to 2.2.8 describe relevant data that are available from existing external sources, presented by data type. Locations of the key data sources are shown in Figure 3 to Figure 5.

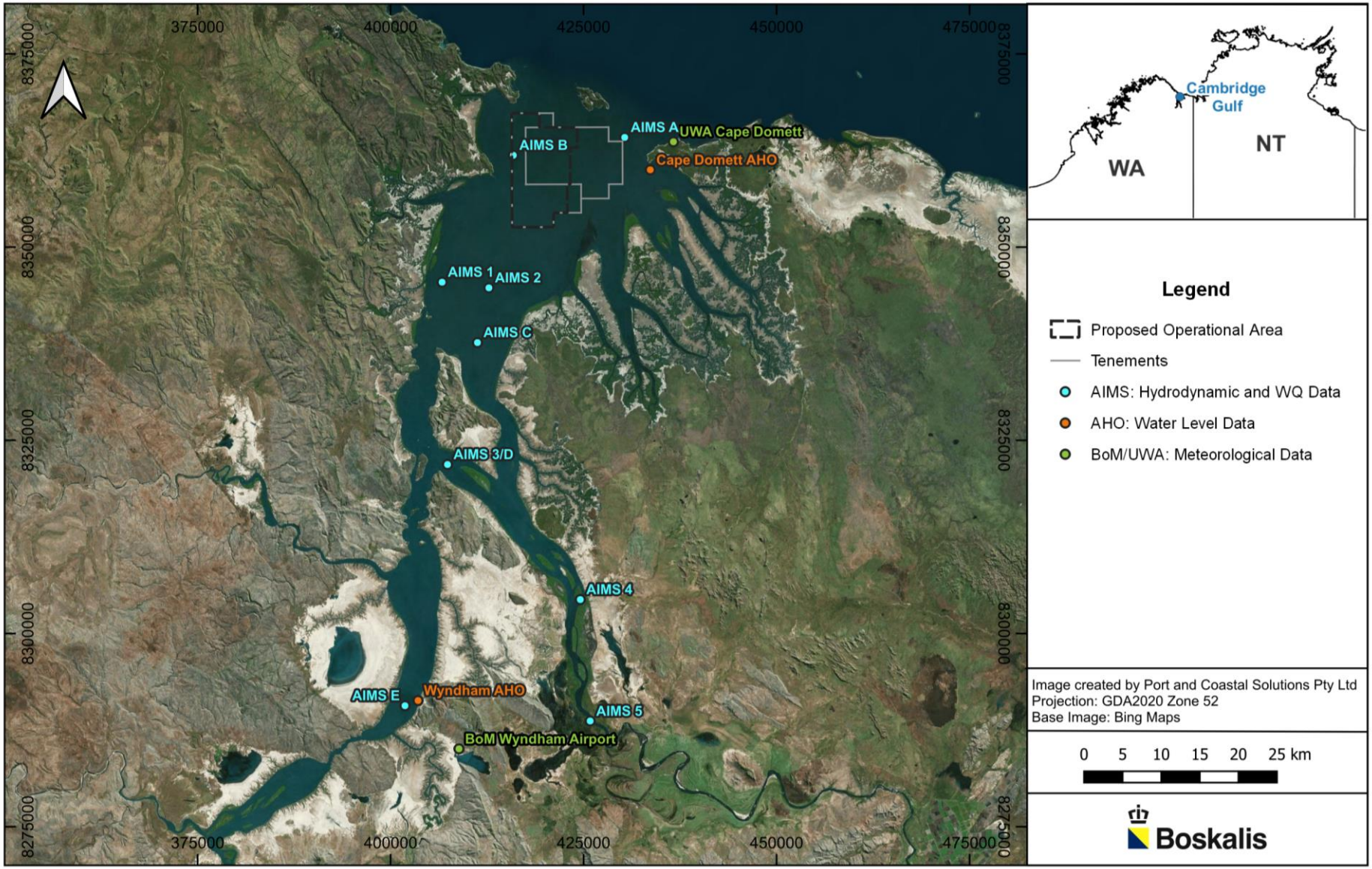

Figure 3. Map showing the locations of existing external sources of hydrodynamic and meteorological data in the CG region.

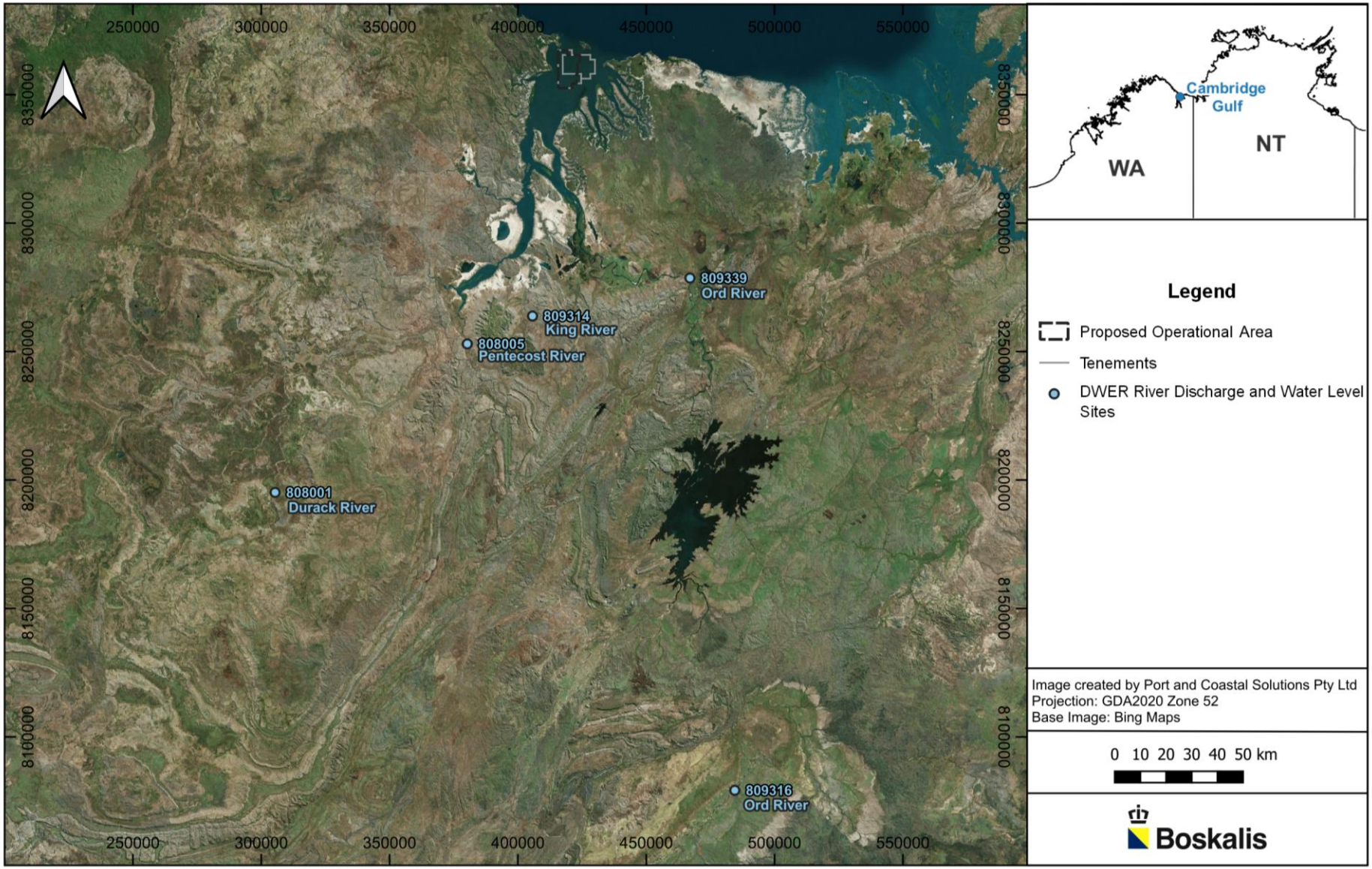

Figure 4. Map showing the locations of river discharge and water level data upstream of CG available from WA-DWER.

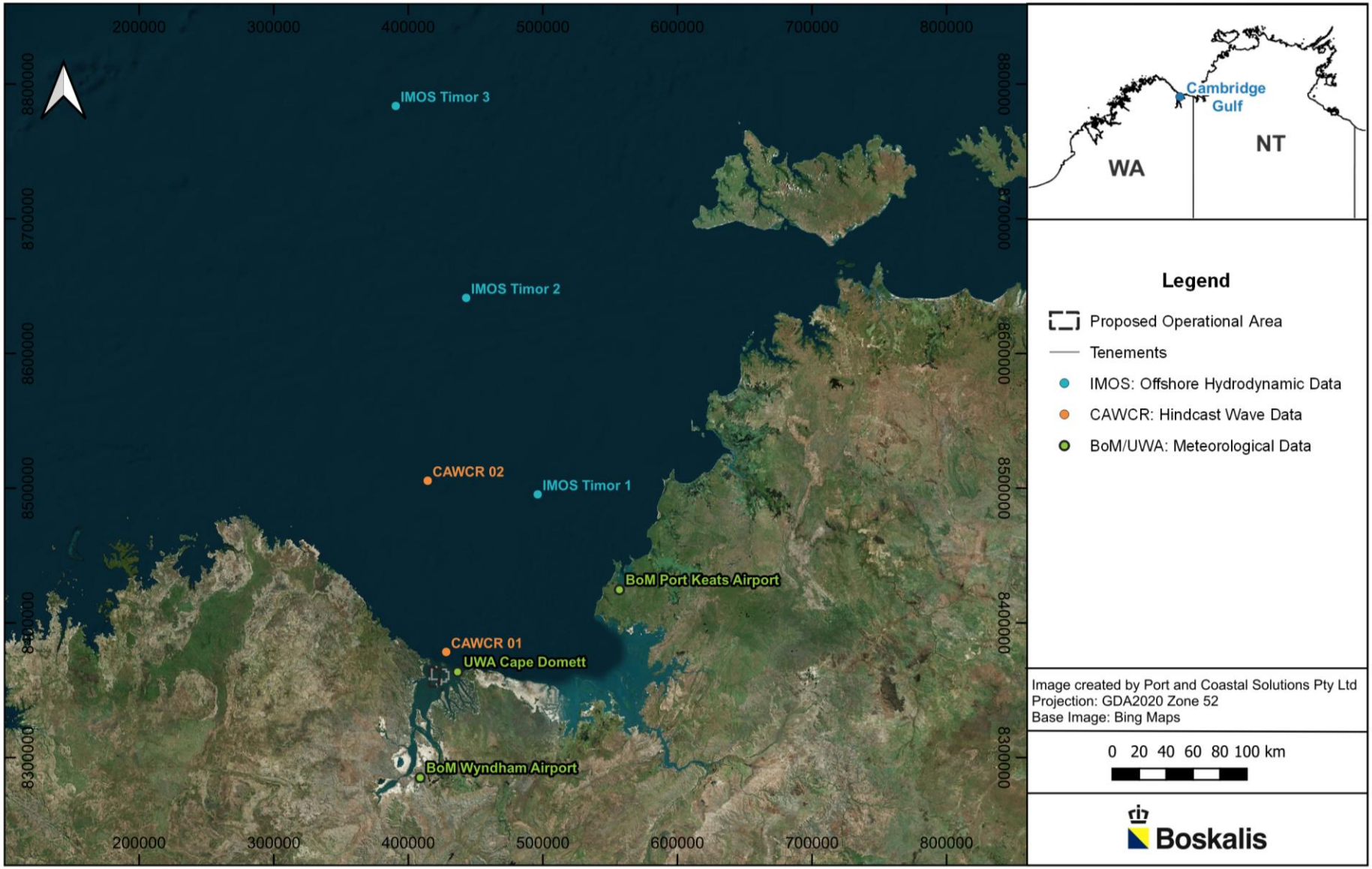

Figure 5. Map showing the locations of existing external sources of regional hydrodynamic, wave and meteorological data.

2.2.1. Hydrodynamic Data

Measured water level (tide) data are available at Wyndham Port from 1985 to the end of 2022 through the Western Australia Department of Transport (WA DoT), with measurements ongoing (WA DoT, 2024). In addition, predicted (modelled) water levels are available through the Australian Hydrographic Office (AHO) software AusTides (AHO, 2023), at the following two standard stations in CG:

- Cape Domett; and
- Wyndham Port.

While AusTides provides predicted water levels for these two sites, the predictions are based on actual measured water level data. The Bureau of Meteorlogy (BoM) provide tide gauge numbers for the two locations (Cape Domett = 63050, Wyndham = 63090 (BoM, 2024a)) but ongoing measured water level data are no longer collected at Cape Domett. Measured water level data are still collected at Wyndham and data have been collected at this location since 1985. The available measured water level data were provided by the BoM from 1985 to the end of 2022 for this project.

There are also three secondary AHO tide prediction stations at Lacrosse Island, Adolphus Island and Pender Point, but the accuracy of the tidal predictions will be reduced at these sites as they are based on less data than at the primary stations (AHO, 2023). As a result, they are not used in this assessment, with the Cape Domett tide predictions considered to be the most reliable for water levels at the proposed operational area.

The Australian Institute of Marine Science (AIMS) provided a range of hydrodynamic and water quality data for the use in this project (AIMS, 2007) They collected various data over seven separate field campaigns between 1999 and 2004, with the primary hydrodynamic dataset of most relevance to this project being mid-water column current speed and direction data collected at three sites over 30 days in 2002 (AIMS A, AIMS B and AIMS E on Figure 3). In addition, water level and water quality data (these are discussed further in Section 2.2.5) are also available at the same three sites as well as two additional sites within the CG (AIMS C and AIMS D on Figure 3).

Current speed and direction data through the water column and water level data are also available from three Integrated Marine Observing System (IMOS) fixed moorings that were deployed offshore from CG from 2010 to 2019 (AIMS, 2023). The moorings extended north from JBG into the Timor Sea (Timor 1 to Timor 3 on Figure 5). Data from these sites can be used to understand how the currents behave offshore from CG and to determine whether ocean circulation processes influence currents in this area.

2.2.2. Wave Data

The only identified external source of wave data for the area is hindcast modelled waves (and winds) from the Centre for Australian Weather and Climate Research (CAWCR) (CSIRO, 2023). The CAWCR model provides 7 km spatial resolution hourly wave conditions from 1979 and the modelling is ongoing with new data available for the previous month at the start of each new month (Smith et al., 2020). The CAWCR wave/wind hindcast uses the WAVEWATCH III (WWIII) model, which is a third generation wave model.

The CAWCR wave model has been validated using all available satellite altimeter data as well as wave buoy data from an Australian network of 37 wave buoys (Durrant et al., 2014; Hemer et al., 2017). Due to the absence of any wave buoys in CG and JBG none of the wave buoy validation sites were located close to CG, but the validation using satellite altimeter will have covered all of Australia (including the JBG). It was noted following the validation that model performance in shallow water, and especially near coastlines can be variable. This has been attributed to variable wind conditions at the transition from land to sea as well as bathymetry and grid resolution limitations (Smith et al., 2020). As a result of this potential limitation, Smith et al. (2020) recommend caution be applied when using wave hindcast results in water shallower than 40 m.

To provide an indication of the waves directly offshore of CG, waves were extracted from the CAWCR wave hindcast from 1979 to 2023 at a location approximately 8 km north of Lacrosse Island (CAWCR01 on Figure 5). The water depth at this location is approximately 25 m and so the data can only be used to provide an indication of the wave conditions at this site. In addition, waves were also extracted from the CAWCR wave hindcast from 1979 to 2023 at the offshore boundary of the wave model located approximately 140 km north of Lacrosse Island (CAWCR02 on Figure 5). The depth at

this location is approximately 70 m which means there is increased confidence in the wave conditions and the data are considered suitable to drive the regional wave model for this project (see Section 4.4.4).

2.2.3. Meteorological Data

Meteorological conditions are measured by the Australian Bureau of Meteorology (BoM) at two weather stations in the CG and JBG region as shown on Figure 3 and Figure 5, as follows:

- Wyndham Airport: This site is located close to Wyndham, approximately 80 km to the south of Lacrosse Island. The site is unlikely to be able to provide a realistic representation of winds in the outer part of CG but the rainfall from this site will provide an indication of when increased river discharge events occur for the rivers that flow into CG.

- Port Keats Airport: This site is located on the east coast of JBG, approximately 140 km to the east north-east of Lacrosse Island. Although the weather station is located close to the coast (approximately 10 km inland), the wind conditions at this site are likely to vary compared to the winds around and in CG and the rainfall at this site cannot be used as an indication for rainfall in CG.

Hindcast modelled wind speed and direction are also available from the CAWCR wave/wind hindcast for the period from 1979 to present day. As with the wave data, the wind data are available at a spatial resolution of 7 km, an hourly temporal resolution and represent the 10 m surface winds. Wind data were extracted from the CAWCR hindcast at the same location as the nearshore wave site (CAWCR01 on Figure 5) to provide an indication of the overwater wind conditions just seaward of, but not within CG.

A weather station was setup at Cape Domett Beach by The University of Western Australia (UWA) as part of a research project from November 2013 to August 2014 (Bentley, 2018). The measured temperature, relative humidity, solar radiation, wind speed and direction and barometric pressure from the station were provided by the UWA for this project. The weather station was setup adjacent to the sand dunes at the upper section of Cape Domett Beach (Figure 3). The wind gauge for the station was located at a height of around 3 m above ground level and due to the station being located adjacent to higher elevation vegetated sand dunes to the south-southeast, it is likely to underpredict winds from southwest through to the east.

2.2.4. River Discharge Data

River discharge and water levels have been measured for the main rivers that drain into CG by the Western Australian Department of Water and Environmental Regulation (DWER) (DWER, 2024). The sites with available data are shown on Figure 4 and a summary of the available data at each site is provided below:

- Ord River: The following long-term datasets are the most relevant for the project:
  - Tarrara Bar, Station 809339: River discharge and water level data are available from 1998 and the data are ongoing. The site is located approximately 70 km downstream of the main Ord River dam.
  - Old Ord Homestead, Station 809316: River discharge and water level data are available from 1970 to 2023. The site is located approximately 110 km upstream of Lake Argyle (i.e. the site is upstream of the Ord River dams).
- Pentecost River, Station 808005: River level data have been measured at this site from February to December 2000.
- Durack River, Station 808001: River discharge and water level data were measured at this location from 1967 to 2000. The site was located approximately 150 km upstream of where both the Durack River and Pentecost River join the West Arm of CG.
- King River, Station 809314: River discharge and water level data are available from 1985 and the data are ongoing. The site is located approximately 35 km upstream of where the King River joins the West Arm of CG.
- Forrest River: No water level or river discharge data are available for the Forrest River.

2.2.5. *In-situ Water Quality Data*

In-situ water quality data were measured by AIMS over seven separate field campaigns between 1999 and 2004 (AIMS, 2007). During the campaigns numerous profiles through the water column throughout CG and in the JBG were collected of the salinity and water temperature using a Conductivity, Temperature and Depth (CTD) logger (Figure 6). Nephelometers were used to collect in-situ measurements during some of the field campaigns, with the nephelometers having been calibrated in-situ to provide suspended sediment concentration (SSC) instead of turbidity (Wolanski et al., 2004).

In-situ water quality data were also collected by the CSIRO within the Ord River, extending up to Adolphus Island (Robson et al., 2008). This included monthly monitoring of nutrients, turbidity, total suspended solids, salinity, temperature, chlorophyll-a, oxygen and water clarity at 11 sites in the Ord River and undertaking wet and dry season field campaigns to monitor water quality at other sites not covered by the monthly monitoring (e.g. tidal creeks). The actual data from the monitoring is not available for this study and the dates and total duration of the data are not detailed by Robson et al. (2008), but results from the monitoring will be used to inform our understanding of the existing water quality in CG.

It is important to note that turbidity measurements are influenced by the properties of the sediment in suspension as the Optical Backscatter Sensors (OBS) used in nephelometers are more sensitive to finer silt and clay particles than to sand particles (Conner and De Visser, 1992). It is noted by Pearson et al. (2021) that the calibration of an OBS using in-situ samples are typically representative of a specific condition (or small range of conditions) and may not be suited to representing the variations in sediment type and mass in suspension over a succession of high and low energy conditions in an environment when the SSC of sand and silt/clay fractions can vary significantly over time.

As the methods used to convert the turbidity data to SSC are not described in the reports by Wolanski et al. (2001, 2004), there is some uncertainty as to the accuracy of the SSC data from AIMS. However, the data can be considered to provide a reasonable representation of the spatial and temporal variability in SSC in CG, although the SSC could be over or underpredicted at specific locations or times resulting in some uncertainty in the absolute SSC values.

Field campaigns by AIMS (2007) collected timeseries of SSC data in the outer estuary of CG and in the East and West Arms over 30 days in October 2000 and in January to February 2002. Timeseries of SSC data are available at three depths through the water column (near-bed, mid-depth and near-surface) at five separate locations. Different measurement locations were selected by AIMS for the two different field campaigns (sites AIMS 1 to AIMS 5 are from the 2000 field campaign, sites AIMS A to AIMS E are for the 2002 field campaign (Figure 3)), with one site replicated between the two campaigns (AIMS D and AIMS 3). Measured depth time series data (which can be converted to water level) were also collected at most of the sites and current speed and direction data were collected at three of the sites during the 2002 field campaign (AIMS A, AIMS B and AIMS E on Figure 3).

It has not been possible to identify any benthic light data for the CG region.

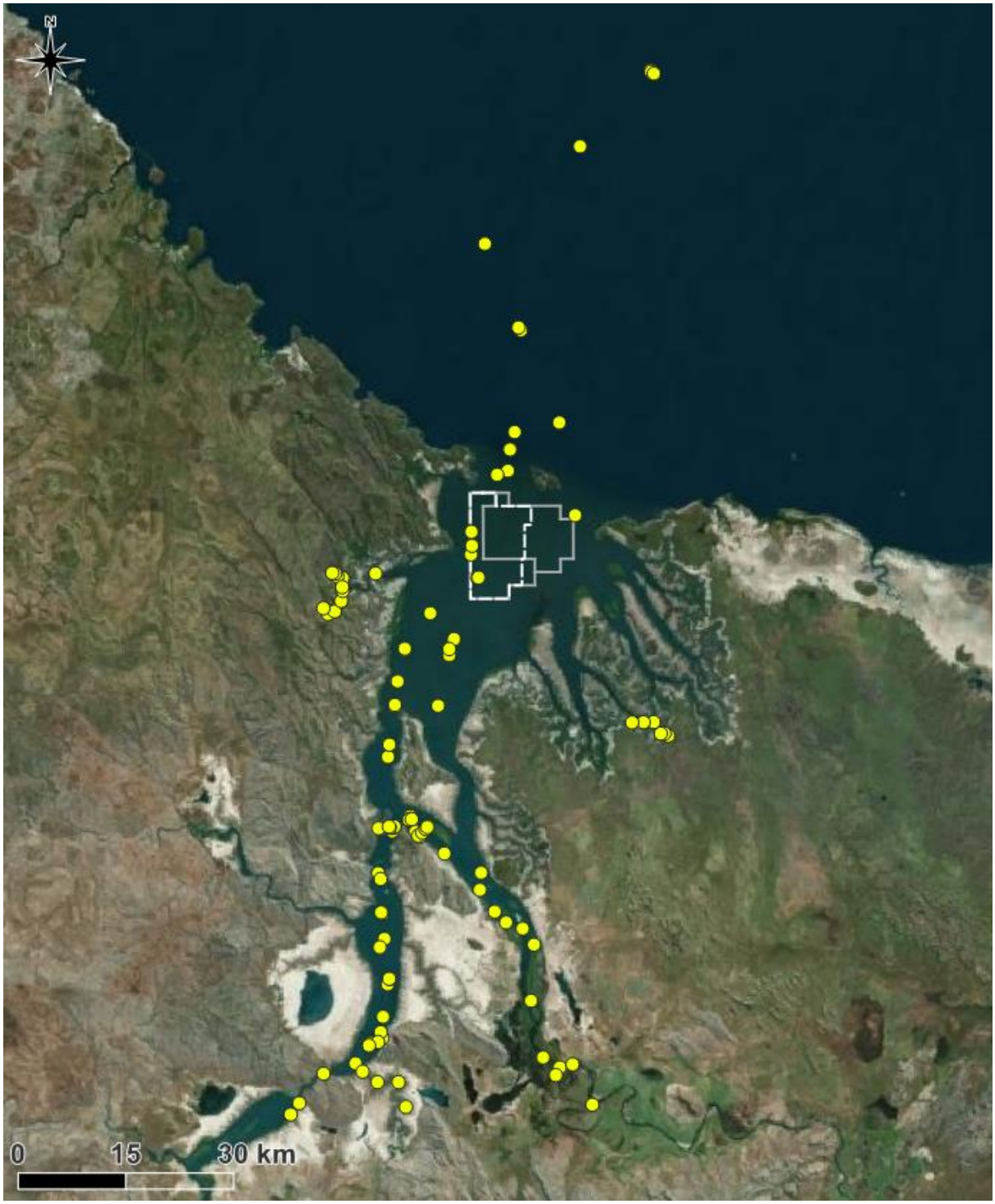

Figure 6. Map showing locations of WQ profile data collected by AIMS between 1999 and 2004.

2.2.6. Sediment Characteristics

Limited data or information on the sediment characteristics in CG is available from external sources, with data available from eight sediment samples in CG from the Geoscience Australia Marine Sediments database (MARS).

Some information is also available from the literature, but this is typically qualitative rather than quantitative. The most relevant information is related to the sizes of flocs in suspension in both the West and East Arms based on measured data collected by Wolanski et al. (2001):

- West Arm: Floc diameters rarely exceeded 100 μm, and the mean diameter was 50 μm and the flocs were slightly larger near the bottom than at the surface.
- East Arm: In the saline water region small flocs of a similar size and shape to those in the West Arm were observed.

Sediment samples collected by CSIRO in the Ord River showed that sediment on the mudflats of the river were generally sandy with a component of silt, while clay dominated the sediment on the channel bed (Robson et al., 2008).

2.2.7. Bathymetry

A number of different bathymetric datasets are available for CG and JBG:

- Australian Hydrographic Office (AHO) Official Navigation Chart (AUS726 & AUS32): The charts provide contours and spot depths throughout the areas of CG (excluding the East Arm of the estuary (the Ord River), the chart does not detail the survey dates that the bathymetry is based on but does note that they are from 'old surveys'. In addition to the published paper charts (although AUS32 is discontinued) these data are available in electronic format from AHO (AHO, 2024).
- Geoscience Australia High-resolution Depth Model: This provides 30 m gridded depth data for Northern Australia based on a compilation of all available sources of bathymetric data. The data covers the majority of CG and the JBG and extends onshore to provide land elevations (based on LiDAR data) (Geoscience Australia, 2023a).
- Digital Earth Australia (DEA) Intertidal Elevation Model: This provides 25 m resolution gridded depth data for the intertidal areas in Australia. The data includes all intertidal areas of CG and JBG (DEA, 2023).

2.2.8. Satellite Data

As a result of the long lifetime of many earth-observing satellites there are significant archives of historical satellite imagery. These can be used to assess natural variations in marine waters and shorelines to help understand baseline conditions and to assist in the development of numerical models (Fearns et al., 2017).

Historical satellite imagery is available for the CG area. For this project the imagery specified below was processed to show the spatial distribution of total suspended matter[1] (TSM) for a range of metocean conditions as well as historical changes to sandy shorelines around CG, as follows:

- Satellite Derived TSM: Selected high resolution (10 m) Sentinel 2 senor imagery available since 2015 was sourced from Copernicus (Copernicus, 2023) and post processed to calculate the satellite-derived TSM based on the approach of Brockmann et al. (2016). This approach has been validated in various studies (Kyryliuk & Kratzer, 2019). An assessment of the accuracy of the satellite derived TSM against the in-situ measured data has also been previously undertaken by PCS (2021) in Albatross Bay in the Gulf of Carpentaria and the results showed that the satellite derived TSM was able to provide a good representation of the in-situ measured SSC data near the seabed (this was possible due to shallow depths combined with relatively low SSC (typically 10 to 20 mg/L) and limited variation in SSC through the water column). Based on this, and for continuity with other datasets, herein the satellite-derived TSM will be referred to as satellite-

[1] This differs to SSC as the satellite image is a remote sensing approach which is not able to differentiate between organic matter and sediment (therefore the TSM includes both), while for in-situ measurements any organic matter can be removed to give a measurement of just the sediment in suspension (SSC).

derived SSC. It is important to note that in high SSC environments such as CG the satellite-derived SSC will typically provide an indication of the SSC in the upper water column and the approach can only determine the SSC up to a certain concentration threshold (as values above that result in the same blocking of the water column). For CG that value is around 50 mg/L. This value was calculated as part of the processing of the satellite imagery. Therefore, although the satellite-derived SSC is not able to differentiate areas of higher SSC within CG, it is able to show the spatial variability in higher and lower values of SSC in the surface layers of the water column.

- Shoreline Changes: The open source Python-based tool CoastSat has been applied to extract the shoreline position from satellite imagery (Vos et al., 2019a, 2019b). The tool was iteratively applied to multiple images from different satellite platforms including the Landsat 5 (30 m resolution, 1988 to 2013), Landsat 7 (30 m resolution, since 1999), Landsat 8 (15 m resolution, since 2013) and Sentinel 2 (10 m resolution, since 2015). The shoreline positions were corrected to 0 m AHD using predicted water levels from Cape Domett.

The usability of the satellite imagery is controlled by cloud cover. Imagery can only be used when there is little to no cloud cover in the area of interest. Sun glare can also limit the usability of some satellite images at certain times of the year. For the CG region both high cloud cover and sun glare can occur over the wet season months, while during the dry season months cloud cover is typically low and there is no sun glare. As a result the satellite imagery provides more information during the dry season compared to the wet season (although usable images are still available during the wet season).

2.3. Data Collected by BKA for the Project

2.3.1. Data Collected up to January 2024

Up to January 2024 BKA has undertaken three data collection campaigns in CG in support of the proposed project and associated EIA studies as follows:

- **February- March 2023:** Sand exploration survey in Block 4 (to define the sand resource):
    - Side-scan sonar and sub-bottom profiler: These instruments were used to identify surface features of the seafloor and stratigraphic structure beneath the seafloor. The vessel sailed in a grid over Block 4, with transects every 500 m north to south and every 1,000 m west to east. Single beam depth measurements were also captured along the transect lines, with a vertical accuracy of 0.5 m (Figure 7).
    - Vibro-core sediment samples: A total of 35 vibro-core samples were collected within Block 4 (Figure 8), with the samples recovering cores of up to 5 m in depth. The cores were sub-sampled with the range of sediment present in each core where the sediment was predominantly sand then analysed in the laboratory for Particle Size Distribution (PSD) using wet sieving.
    - Benthic grab sediment samples: The presence of the sand exploration vessel in CG was utilized to also collect some preliminary environmental data. Duplicate benthic grabs were taken at the 35 vibro-core sites in Block 4 (Figure 8), sieved on-board to 6 mm and assessed for benthic biota. This was an initial environmental reconnaissance to assess if there are any benthic communities in Block 4 such as seagrass, coral, macroalgae, sponge or other communities that might preclude proceeding with the proposed project (none were found). Photographs were taken of all grab samples and the type of sediment recorded, to also inform the sand resource assessment.
    - Secchi-disc & water quality: To provide an initial indication of water clarity/turbidity in CG Secchi-disc readings were taken at the 35 vibro-core sites in Block 4 (Figure 8). Water quality vertical profiles through the water column were also taken using a YSI-DSS multi-sensor, however there were technical issues with the hired instrument, and more reliable and extensive water quality profiles were sampled in the later July-August 2023 environmental survey and are planned for the Feb-March 2024 environmental survey (see below).
    - Drop camera video: A drop camera was deployed to the seabed at all 35 vibro-core sites (Figure 8) in order to provide video assessment of benthic biota – 100% of the videos

showed a completely blacked-out aphotic zone caused by a constantly suspended sediment layer for several metres above the seabed.

- **From June 2023:** In-situ AWAC/ADCP & co-mounted sensor deployments (to provide hydrodynamic and physical parameter data support the EIA including modelling):

  - Acoustic Wave and Current Profilers (AWACs) and Acoustic Doppler Current Profilers (ADCPs) have been deployed on the seabed to measure current speed and direction through the water column, water levels and waves. In addition, LI-COR LI-1500 light sensors and Manta Multiprobes have also been attached to the same frame as the AWAC/ADCPs to measure benthic photosynthetically active radiation (PAR) and temperature, salinity, turbidity, depth, dissolved oxygen and pH, respectively.

    The locations where AWACs/ADCPs and co-mounted sensors have been deployed to date are shown on Figure 9 and are summarized as follows:

    – AWAC-01: An AWAC was deployed on the seabed at this site for 42 days from 9th June to 21st July 2023. Current data at 1 m bins through the water column along with water depth data were successfully recorded. However, there was an issue with the instrument, which meant that the wave data are not usable. There was no light meter or multiprobe co-mounted with this deployment.

    – AWAC-02: An AWAC was deployed on the seabed at this site for 1 day (7th September 2023) along with upward and downward facing light probes and a turbidity probe. Initial processing of the AWAC data has been undertaken and shows reliable water level, current and wave data were recorded.

    – AWAC-04: An AWAC was deployed on the seabed at this site for 1 day (7th September 2023) along with upward and downward facing light probes and a turbidity probe. Initial processing of the AWAC data has been undertaken and shows reliable water level and current data were recorded but no wave data were recorded.

    – AWAC-06: An AWAC was deployed on the seabed at this site for 35 days (from 8th September to 13th October 2023) along with upward and downward facing light probes and a turbidity probe. There was an issue with the light probes and so no measured benthic light data were measured. Initial processing of the AWAC data has been undertaken and shows reliable water level, current and wave data were recorded.

    – AWAC-03: An AWAC was deployed on the seabed at this site for 2 days (from 13th October to 15th October 2023) along with upward and downward facing light probes and a turbidity probe. There was an issue with the light probes and so no measured benthic light data were measured. Initial processing of the AWAC data has been undertaken and shows reliable water level, current and wave data were recorded.

    – AWAC-07: An AWAC is currently deployed on the seabed at this site (since 14th October 2023) along with upward and downward facing light probes and a turbidity probe. It is planned to retrieve the instrument after 90 days of deployment (in January 2024).

  - Additional AWAC and co-mounted sensor deployments are planned from January 2024 as outlined under section 2.3.1 below and shown on Figure 9.

- **July-August 2023:** Dry-season environmental survey (to provide environmental, ecological and biodiversity data to support the EIA):

  - Water quality profiles: Water quality profiles were collected at 53 sites within CG and 20 sites at King Shoals (Figure 11), one site at the Wyndham public jetty and 30 sites ~50 km offshore in JBG (to compare CG with offshore conditions) (Figure 10). A YSI EXO-1 multiparameter probe was slowly lowered through the water column to the seabed and then raised back up to the surface with the instrument measuring salinity, water temperature, turbidity and chlorophyll-a every 3 seconds.

  - SSC-turbidity correlation: At 31 of the sites in CG, three of the sites at King Shoals (Figure 11) and 20 sites ~50 km offshore in JBG (to compare CG with offshore conditions) (Figure 10), turbidity measurements and concurrent water samples using a Niskin bottle were collected at random water depths in order to assess the SSC-turbidity relationship. The

water samples were analysed in the laboratory to measure the SSC and a correlation was then developed between turbidity (in Nephelometric Turbidity Units - NTU) and SSC. The correlation covered a wide range of values and provided a strong linear correlation, which has been used to convert the turbidity measurements to SSC (1 NTU = 1.72 mg/L).

As previously noted in Section 2.2.5, the relationship between turbidity and SSC in an environment where clay, silt and sand can all be in suspension is complex due to the variability in type and mass of sediment in suspension over time. In this case a range of locations and conditions was represented in the relationship, but it is still likely that the relationship will both over- and under-predict SSC at some locations and times. A more detailed investigation will be undertaken during the wet season field campaign with water samples to be collected and analysed to determine the PSD of the suspended sediment (see Section 2.3.2 below).

- Benthic grab biota survey: Benthic grabs (5 litre volume) were sampled at 105 sites throughout CG and 27 sites across King Shoals (Figure 11) in order to assess presence, absence, types, diversity and abundance of sub-tidal benthic biota and provide data to help generate a benthic habitat map for the EIA. Triplicate grabs were collected at most sites, although at a few sites only two or even one could be collected due to extreme tidal currents, rocky seabed or other constrains. Grab samples were sieved to 500 nm and any biota retrieved and preserved in ethanol and sent to Benthic Australia Pty Ltd for identification and analysis. Very little benthic biota was found. A description of the sediment type in all grab samples was collected and the samples were photographed at each stage of processing.

- Drop camera video: A drop camera was deployed to the seabed at all 105 benthic grab sites throughout CG and all 27 benthic grab sites across King Shoals (Figure 11) in order to provide video assessment of benthic biota – 100% of the videos showed a completely blacked-out aphotic zone caused by a constantly suspended sediment layer for several meters above the seabed.

- Benthic grab sediment samples (for chemical analysis): At 21 of the benthic grab sites in Blocks 4 and 4A, representing a range of sediment types (Figure 12), sediment was sub-sampled from the grab sample in accordance with the Australian National Assessment Guidelines for Dredging (NAGD 2009), for analysis for potential chemical contamination. This was to assess whether there is any potential for the proposed sand operation to mobilize contaminants. All samples returned well below the NAGD screening levels for all analytes (not of direct relevance to this report).

- Aerial drone surveys: Aerial drone surveys were undertaken at high-priority shoreline locations to map inter-tidal habitats and communities, with particular attention to identifying possible seagrass areas (none were found), and to provide an understanding of the current extent and state of the mangroves, saltpans and beaches of CG. The drone surveys were also used to determine which beaches have been recently used for turtle nesting, and to record any incidental marine mega-fauna sightings (e.g. crocodiles). The drone footage is of some relevance to this report as it identifies several areas where the coastline and mangroves have been severely impacted by cyclone activity, which is an important driver of coastal processes in CG.

- Marine mega-fauna surveys: Systematic, boat-based marine mega-fauna surveys were undertaken along transects throughout CG and upstream to Wyndham with a focus on recording sightings of snubfin dolphins, humpback dolphins, other cetaceans, marine turtles, sharks and crocodiles (not of direct relevance to this report).

2.3.2. Planned Ongoing Data Collection

As part of BKA's ongoing data collection program to support the EIA and regulatory approval applications, and to build on the data already collected as described above, the following has been undertaken/is planned:

- **From Jan 2024:** In-situ AWAC & co-mounted sensor deployments. A continuation of the AWAC / co-mounted sensor deployments described above is currently underway, this includes:
    - 90-day deployments at AWAC-05, AWAC-06, AWAC-07, AWAC-08, AWAC-09 and AWAC-10 (Figure 9).

    - Longer duration deployments of six months concurrently at AWAC-01 and AWAC-11 (Figure 9).

- **From Jan 2024:** Long-term (initially 12-months) in-situ, data logging seabed light and turbidity is currently underway.

    - In order to provide longer-term seabed light and turbidity data than the shorter period AWAC deployments, seabed frames with a light sensor and turbidity sensor will be deployed for an initial 12-month period at four sites (Pos 12, 13, 14 and 15 on Figure 9) from January 2024 to January 2025). They may be extended should the WA EPA require.

- **As soon as possible** (subject to TO access approval) - Meteorological Data:

    - BKA is planning to install a weather station in the Cape Domett area for an initial 12-months, to measure wind speed and direction, rainfall, air temperature and air pressure, to provide data to support the modelling. A light sensor will be included to measure the available ambient light, for correlation with the seabed light meters (e.g. to account for cloudy days). The exact location of the site is yet to be confirmed in consultation with the Traditional Owners (TOs), but the site is planned to be adjacent to the shoreline with the wind sensor at an elevation of 10 m above ground level and so will provide a good representation of the local wind conditions for CG.

- **Feb-March 2024:** Wet-season environmental survey was undertaken which included the following:

    - This repeated the sampling carried out during the Jul-Aug 2023 dry season survey, so as to allow a comparison between wet and dry season conditions. Based on the very low numbers of benthic biota in the dry season benthic grabs, only 50% of the sites were sampled in the wet season. Drop camera deployments were not repeated based on the total lack of seabed light encountered at all sites during the March 2023 and Jul-Aug 2023 surveys. The following additional sampling was also carried out:

        – Additional sediment samples: To provide data to support the assessment of sediment dynamics, additional grab samples were taken up the mangrove inlets of the Ord River Floodplain Ramsar Site (on the eastern side of CG) and also along East Arm up to the Ord River and along West Arm towards Wyndham. These were analysed by a laboratory for PSD and compositional analysis.

        – Water Column Profiling: Water column profiling was undertaken at three of the AWAC sites to measure currents, turbidity along with concurrent water sampling, from which suspended sediments were filtered and analysed for PSD. The profiling was undertaken throughout a 13-hour tidal cycle at each site to provide data as to how the turbidity, suspended sediment and the PSD of the suspended sediment varied through the water column, over a tidal cycle and spatially between sites. These data help to understand spatial and temporal variation in SSC and modelling sediment dynamics in CG.

        – Drone Lidar surveys: These were undertaken at the turtle nesting beaches around CG to assist in assessing potential impacts on beach morphology, and thus potential impacts on nesting turtles and coastal processes generally.

        – High resolution bathymetric survey of Blocks 4 and 4A (as recommended in Section 2.4 below).

        – Additional biological sampling: Although not directly relevant to this report, this included eDNA sampling for sawfish and river sharks, and plankton net tows to assess the plankton ecology of CG.

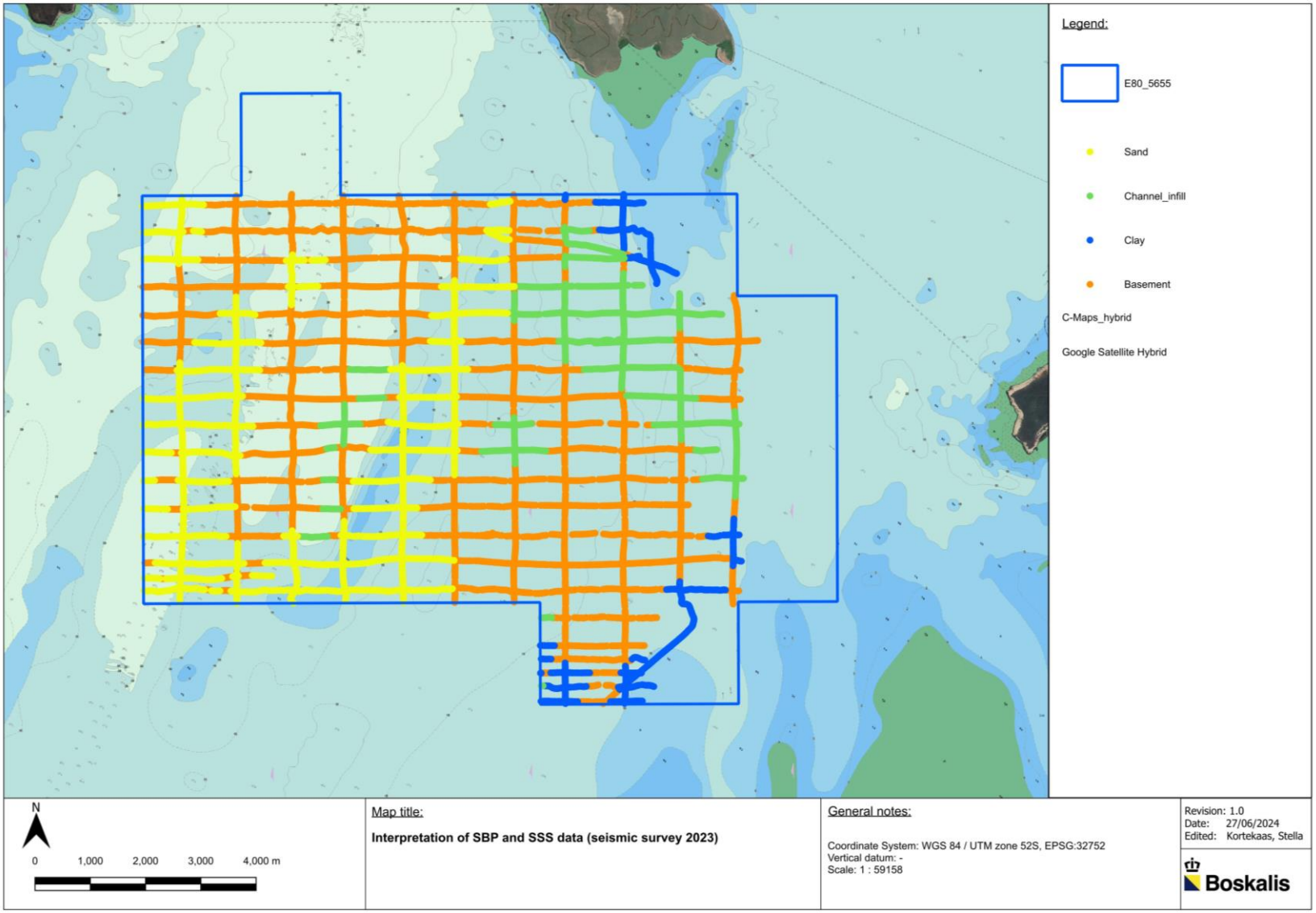

Figure 7. Sub-bottom profiler transects and results from the sand exploration survey in March 2023 (source: BKA, 2024d).

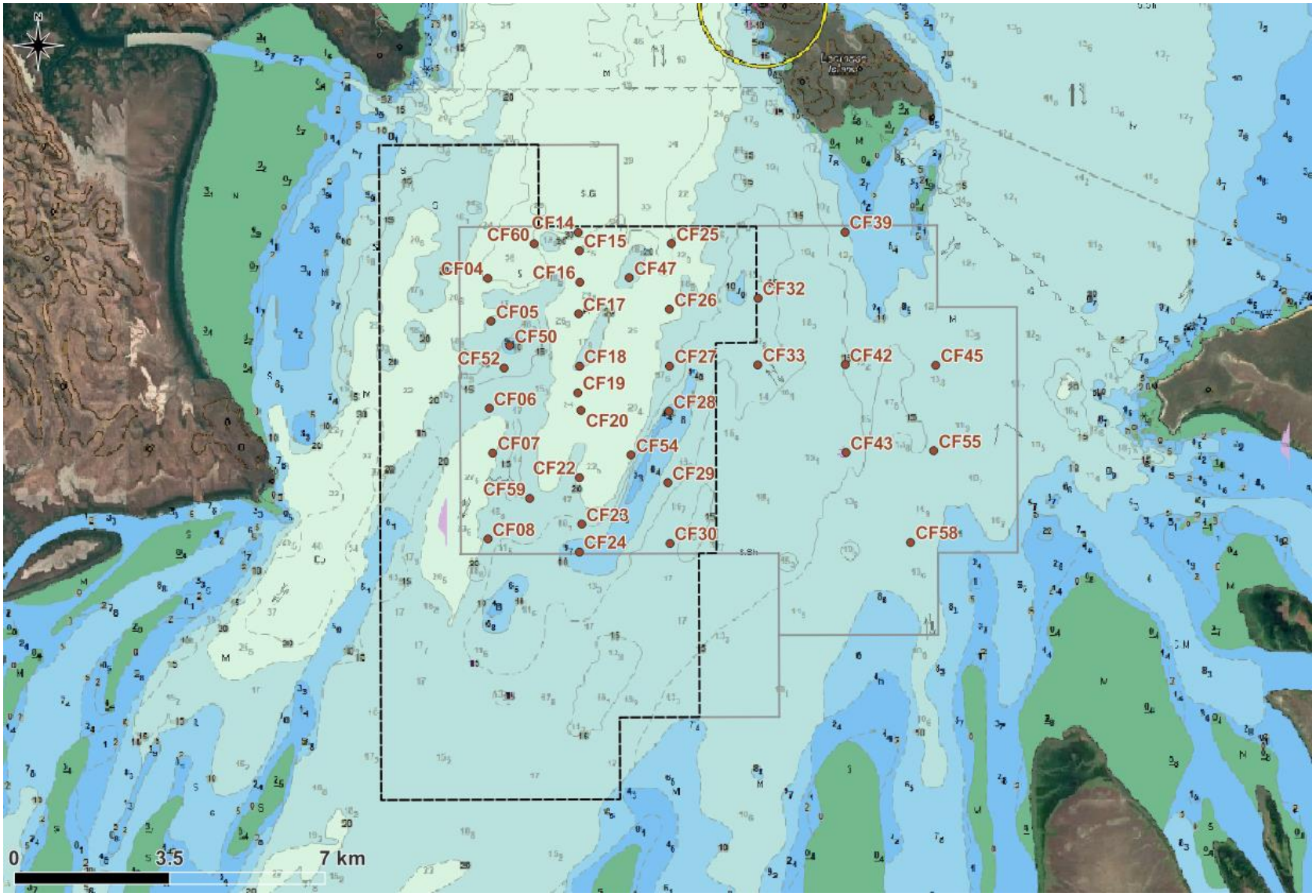

Figure 8. Vibro-core, benthic grab and Secchi disc sample points within Block 4 during the sand exploration survey in March 2023.

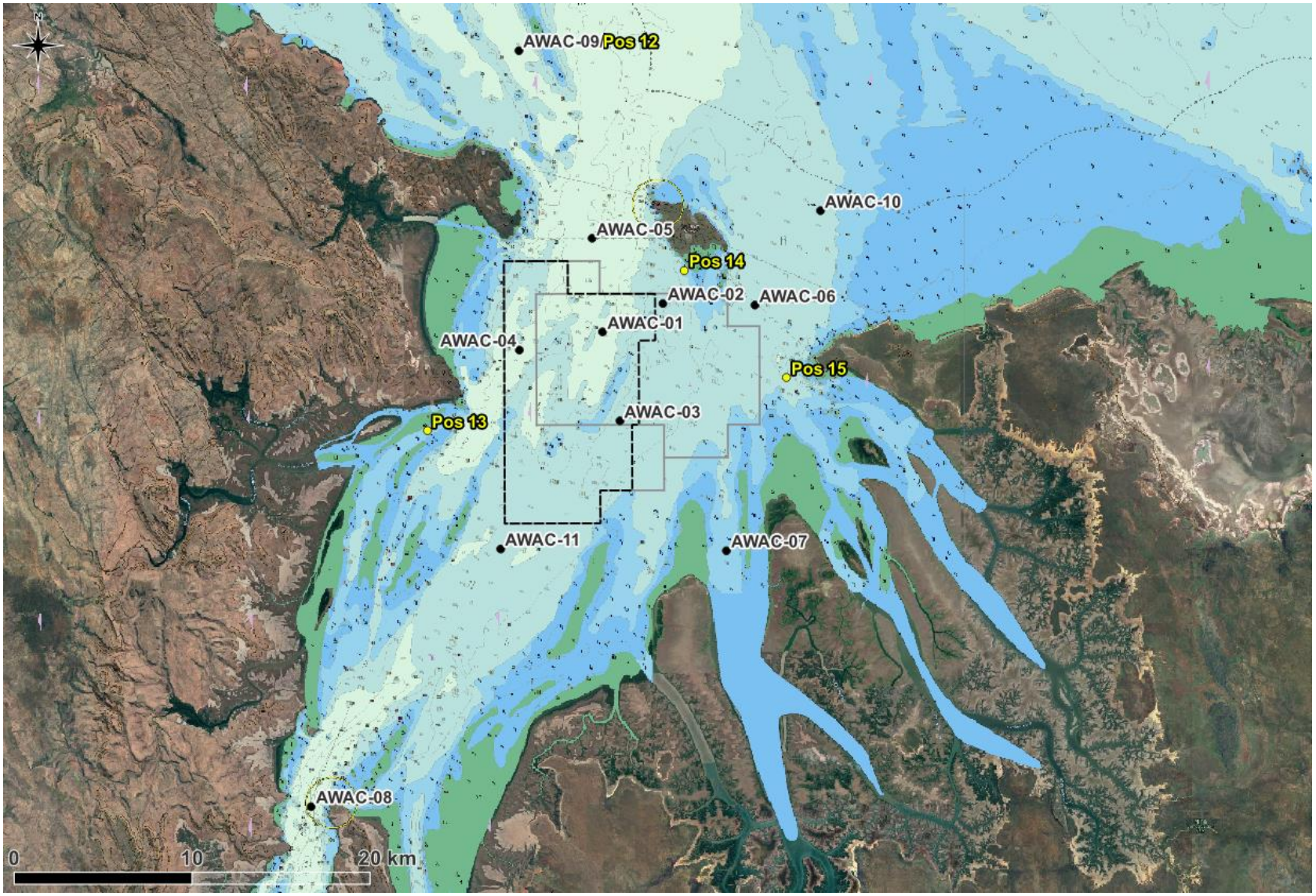

Figure 9. **Sites where AWACs with co-mounted sensors (AWAC 01 to 11) and seabed frames with light & turbidity sensors (Pos 12 to 15) have been or are planned to be deployed for the project.**

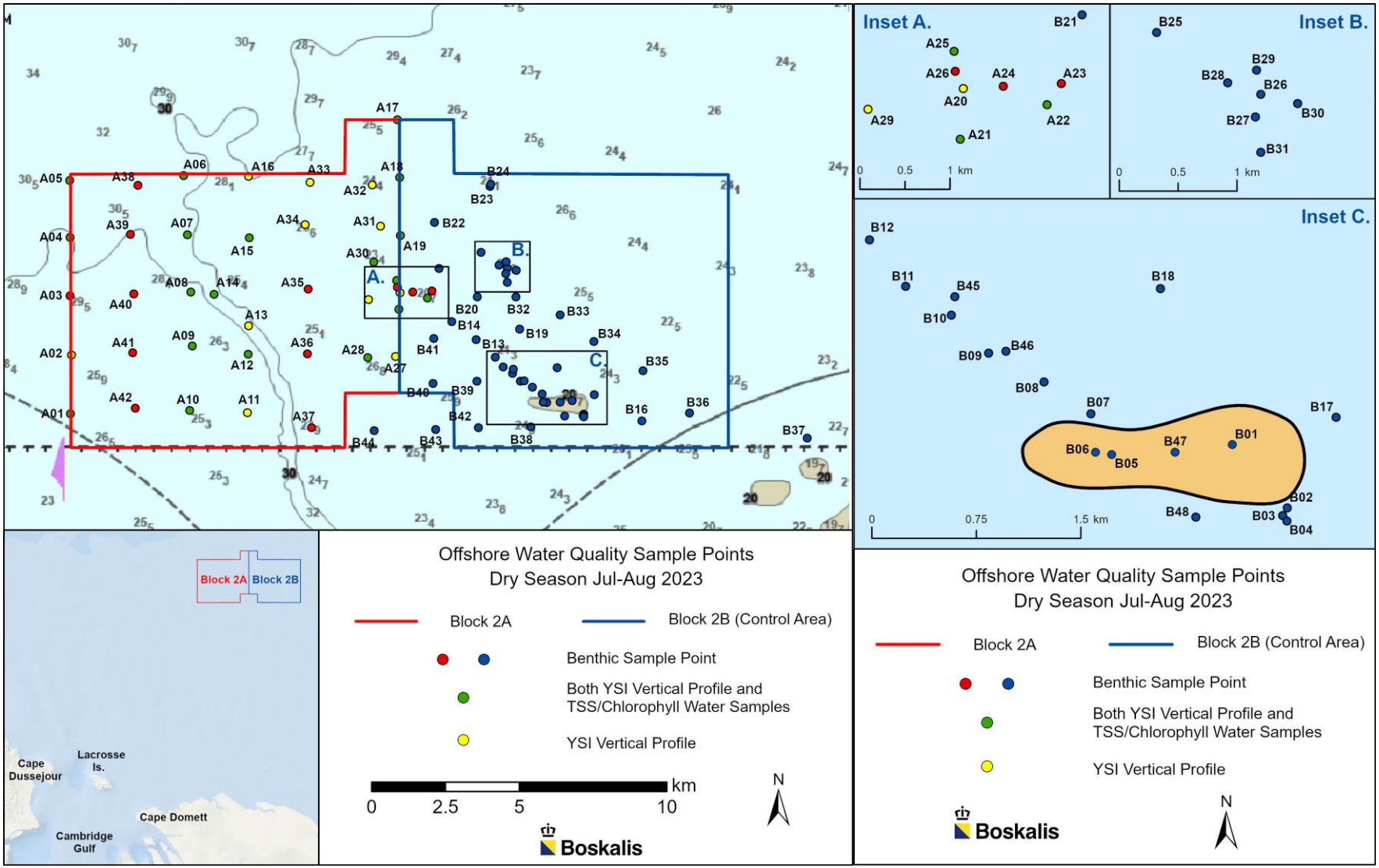

Figure 10. **Sample Points (SPs) ~50 km offshore (OS) for the dry season survey Jul-Aug 2023. Benthic grabs were collected at all SPs (red, green & yellow). For water quality - both YSI vertical profiles and TSS/Chlorophyll samples were collected at the green SPs and only YSI vertical profiles were taken at the yellow SPs (source: BKA, 2024d).**

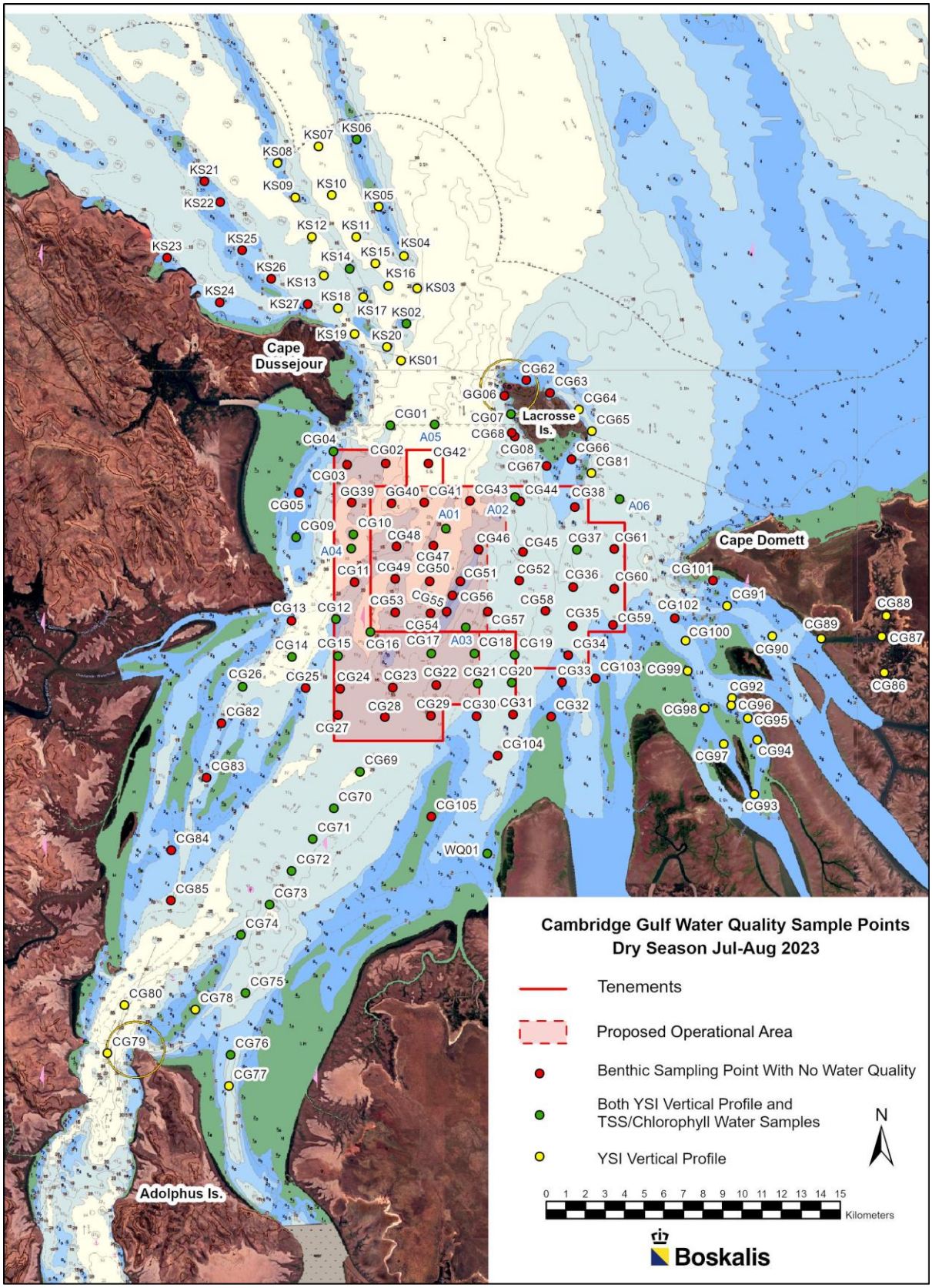

Figure 11. **Water Quality Sample Points (SPs) at Cambridge Gulf (CG) and King Shoals (KS) for the dry season survey Jul-Aug 2023. Benthic grabs were collected and drop camera deployed at all SPs (red, green & yellow). For water quality - both YSI vertical profiles and TSS/Chlorophyll samples were collected at the green SPs and only YSI vertical profiles were taken at the yellow SPs (source: BKA, 2024d).**

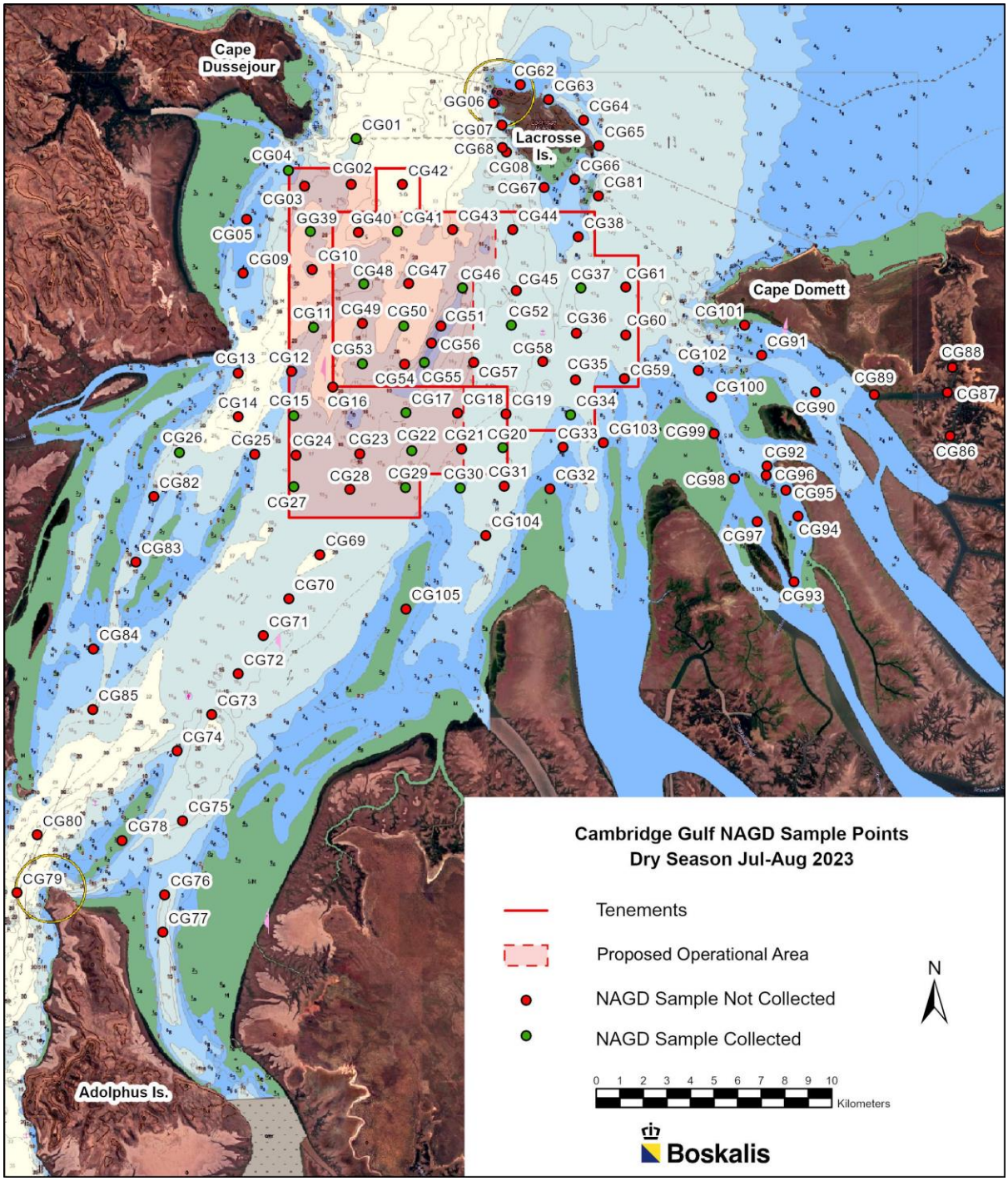

Figure 12. **Benthic & Sediment SPs in CG for the dry season survey Jul-Aug 2023. Benthic grabs were collected and drop camera deployed at all SPs (red & green). Sub-samples of sediment for chemical analysis in accordance with NAGD 2009 were taken at the green SPs (source: BKA, 2024d).**

2.4. Data Gap Analysis

Previous work by Hale (2008) focused on the Ord River Floodplain Ramsar site identified a number of key knowledge gaps. Of these, the hydrological monitoring around the False Mouths of the Ord and long-term water quality remain data gaps which are relevant for this work. The data collection program undertaken to date and planned by BKA for this project will address these data gaps as well as the gaps in the existing available data needed to address the objectives of this study and to meet the WA EPA guidelines listed in Section 1.

It is important to note that when developing the data collection plan for the project, BKA ensured that the data collected would more than satisfy the requirements of the EPA guidelines. This approach will ensure that sufficient data are available for the project even if some data are not able to be collected or data losses occur. Based on the available data and the planned data collection detailed in this section the following key data gaps were identified, prior to the February to March 2024 wet season environmental survey, relative to the said objectives and guidelines (with details provided on their importance for the project):

- High resolution bathymetric data covering Blocks 4 and 4A: Although single-beam bathymetric data were collected over Block 4 it would be beneficial to collect high resolution multibeam data over all of Blocks 4 and 4A (or at least the proposed operational area). These data would ensure that the bathymetry in the numerical models in these key areas will be represented as accurately as possible and any bedforms present can be used to help understand sediment transport processes in the area. In addition, the data will provide a high-resolution baseline bathymetry for the project moving forward. It is proposed that this was collected as part of the February/March 2024 wet season environmental survey (NOTE: BKA subsequently included this in the survey plan and the data were collected during the February to March 2024 wet season environmental survey, the data are presented in Appendix A).

- Erosion/accretion rates in Proposed Operational Area: There were no data available to show the natural erosion and accretion rates in the proposed operational area. For the future numerical modelling it will be important to know the natural erosion and accretion rates in this area to calibrate and validate the model. These data will also help to inform the coastal processes understanding and conceptual model development. It was proposed that the multibeam bathymetric survey was undertaken at the start of the wet season field campaign (as above) and then the survey was repeated for two localised areas (approximately 2.5 km x 2.5 km) within the proposed operational area later in the field campaign. This will mean that there was a spring neap cycle between the two surveys and so the changes will be able to be used to determine the erosion and accretion that occurs over a lunar cycle (NOTE: BKA subsequently included this in the survey plan and the data were collected during the February to March 2024 wet season environmental survey, the data are presented in Appendix A).

- Sediment composition at beaches: Although extensive sediment sampling has been undertaken and is planned by BKA, no sampling has been undertaken at any the turtle nesting beaches. It will be important to understand the composition of the sediment in these areas to help inform the baseline understanding and to input into the beach processes modelling. It is proposed that sediment samples are collected at multiple locations across the beach profile at the beaches where turtle nesting has been observed and the samples are analysed for PSD and sediment composition (sediment composition will only be undertaken for some samples) (NOTE: There are severe crocodile risks on CG beaches and approval to land is also required from TOs as the area is rich with Aboriginal cultural heritage sites, these factors precluded this proposed data collection).

- Detailed beach profile data: The only available data to inform the elevation of the intertidal and supratidal areas of the turtle nesting beaches in the region were 25 m and 30 m resolution gridded datasets based on LiDAR data (DEA, 2023). Higher resolution topographic data are required to ensure that the cross-sectional profiles of the beaches are accurately represented in the beach processes modelling. It was therefore proposed that high resolution LiDAR data were collected at the turtle nesting beaches during the wet season environmental survey (NOTE: BKA subsequently included this in the survey plan and the data were collected during the February to March 2024 wet season environmental survey, the data are presented in Appendix A).

- River discharge data: No river discharge data are available for the Pentecost River (less than 1 year of river level data are available in total), while for the Durack River no recent discharge or river level data are available and for the Forrest River no measured data are available at all. Following the damming of the Ord River in the 1970s, the Durack and Pentecost River catchments have the potential to result in the highest river discharges into CG during an extreme rainfall event. However, there are approximately 30 years of measured data from the Durack River which can provide an understanding of the potential range in wet season river discharge and measured water level data are available at Wyndham which will allow any residual water levels from river discharges to be identified and quantified.

  As the catchments for the Durack, Pentecost and Forrest Rivers are adjacent to each other and of similar sizes (the Pentecost River catchment area is approximately 65% of the Durack River catchment area, while the Forrest River catchment area is approximately 20% of the Durack River catchment area), adopting a scaling factor to represent the Pentecost and Forrest Rivers discharge based on the historic Durack River discharge combined with the measured water levels

at Wyndham should be able to provide a reasonable approximation of the river discharges. Based on this, setting up new river gauges in the Durack and Pentecost Rivers is not considered a priority for this project, given the large seasonal and annual variability in river discharge in the region a relatively short-term data set of 12 months would provide limited benefit.

3. SYSTEM UNDERSTANDING

Analysis and interpretation of available hydrodynamic, wave, meteorological, water quality and sediment data and literature for the CG region is presented in this section to provide an understanding of the local conditions. In addition, this section also provides an overview of the known sensitive receptors present in the region based on the latest available information. Further details of the data analysed, including the locations, to inform the system understanding is provided in Section 2.

3.1. Hydrodynamics

The hydrodynamic conditions are discussed in the following sections on a regional scale for the JBG and then on a local scale for CG.

3.1.1. Joseph Bonaparte Gulf

Plots showing predictions of water levels and depth-averaged tidal currents from a Commonwealth Scientific and Industrial Research Organisation (CSIRO) tidal model as well as tide gauge and current meter observations for JBG were sourced from the IMOS OceanCurrent database (AIMS, 2023). Plots of the predicted water levels and currents over a spring tidal cycle on the 1st to 2nd October 2023 and are shown in Figure 13 and Figure 14. The plots demonstrate a strong tidal influence in currents in JBG, with currents flowing into the Gulf (to the south-east) during the flood stage of the tide and flowing in the opposite direction (to the north-west) during the peak ebb stage of the tide. Current speeds are highest in the south-eastern corner of JBG, although currents speeds in and adjacent to the CG are also typically in excess of 1 m/s. The plots show how both the tidal range and tidal current speeds increase towards the south-eastern corner of JBG, indicating that tidal amplification occurs in this area.

To further investigate the currents in JBG, measured current data from the IMOS database at sites Timor 1 to Timor 3 were sourced. The site locations are shown in Figure 13 and Figure 14. Timor 1 is located within JBG (140 km north of the CG), Timor 2 is located just beyond the northern limit of JBG (likely to be in the Timor Sea) (275 km north of CG) and Timor 3 is located in the Timor Sea, to the north of JBG (415 km north of the CG).

Time series plots of the measured mid depth current speed and direction at the three sites over a five month period, spanning both wet and dry season conditions, are shown in Figure 15. The plots show that there is a very clear and strong tidal signal present at Timor 1 and Timor 2, with similar current speeds (varying from 0.2 m/s during neaps to more than 0.8 m/s during springs) and directions (flood currents of around 140º and ebb currents of around 320º) present at both sites. The currents at Timor 3 also typically show a tidal signal, with higher current speeds during spring tides and lower current speeds during neap tides, but there is more variability in both the current speeds and directions at this site. For example, the red boxes in Figure 15 show a 10 day period where current speeds at Timor 3 become elevated initially during neap tides and when ebb current directions change from being similar to the other two sites (around 320º), to being around 70º.

The currents over just this period are shown in more detail in Figure 16. This change suggests that a separate process is influencing the currents at Timor 3, which does not influence the currents at Timor 1 and Timor 2. Given the location of Timor 3 it is likely that this additional process which intermittently influences the currents at the site is an ocean circulation process. A circulatory eddy centred just south of Timor 3 is visible in some IMOS (2023) imagery and it is likely that this semi-permanent eddy is influencing the currents at Timor 3. This eddy does not influence the currents in the southern area of the JBG near to the entrance to CG. The data therefore show that ocean circulation processes can influence currents in the Timor Sea and in the northern part of the JBG, but that currents within the southern area of the JBG are dominated by the astronomical tide, with little to no influence from large scale ocean circulation processes.

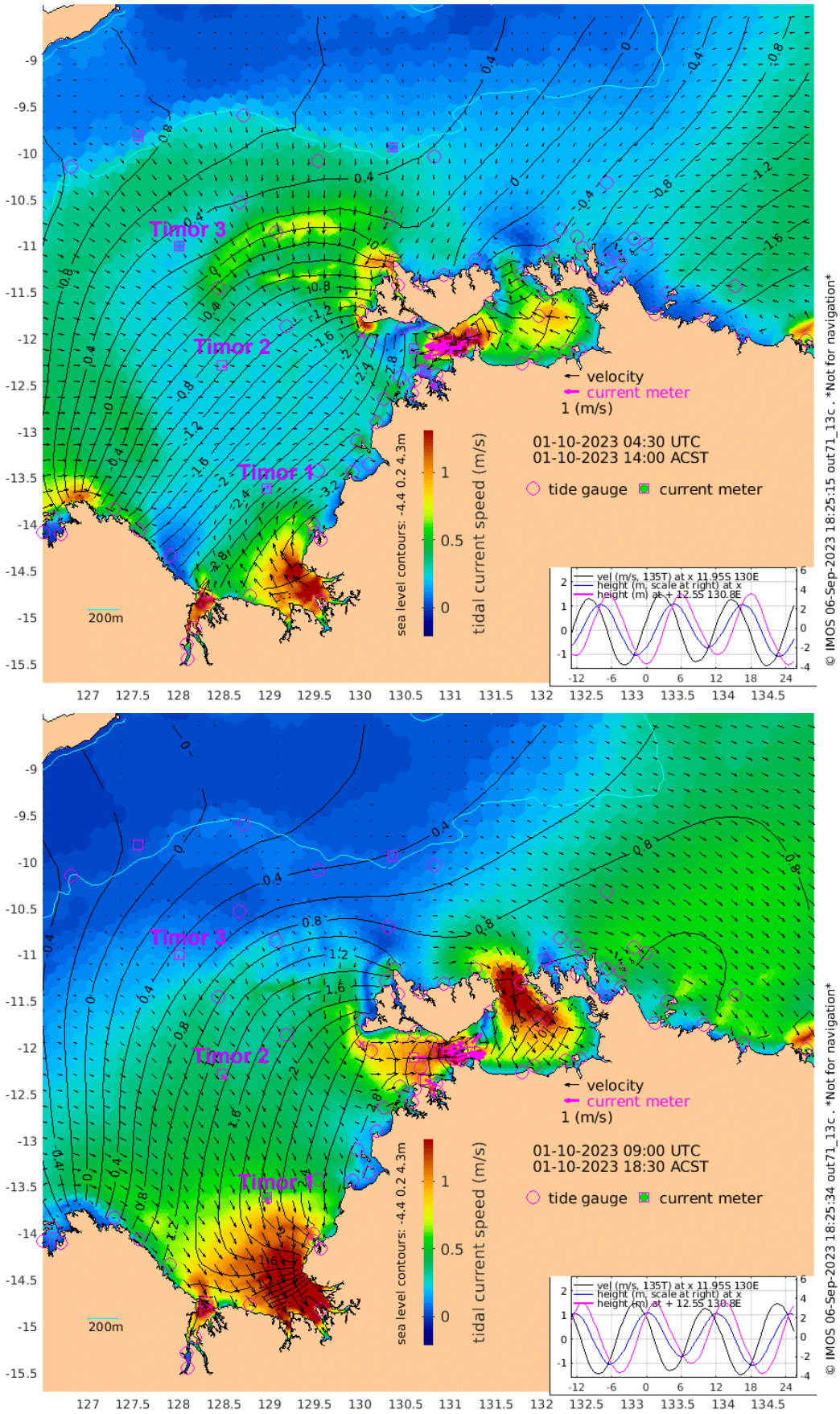

Figure 13. Predicted current and water level (contours) in JBG and the Timor Sea during a spring tide at low water (top) and peak flood (bottom) (source: IMOS, 2023).

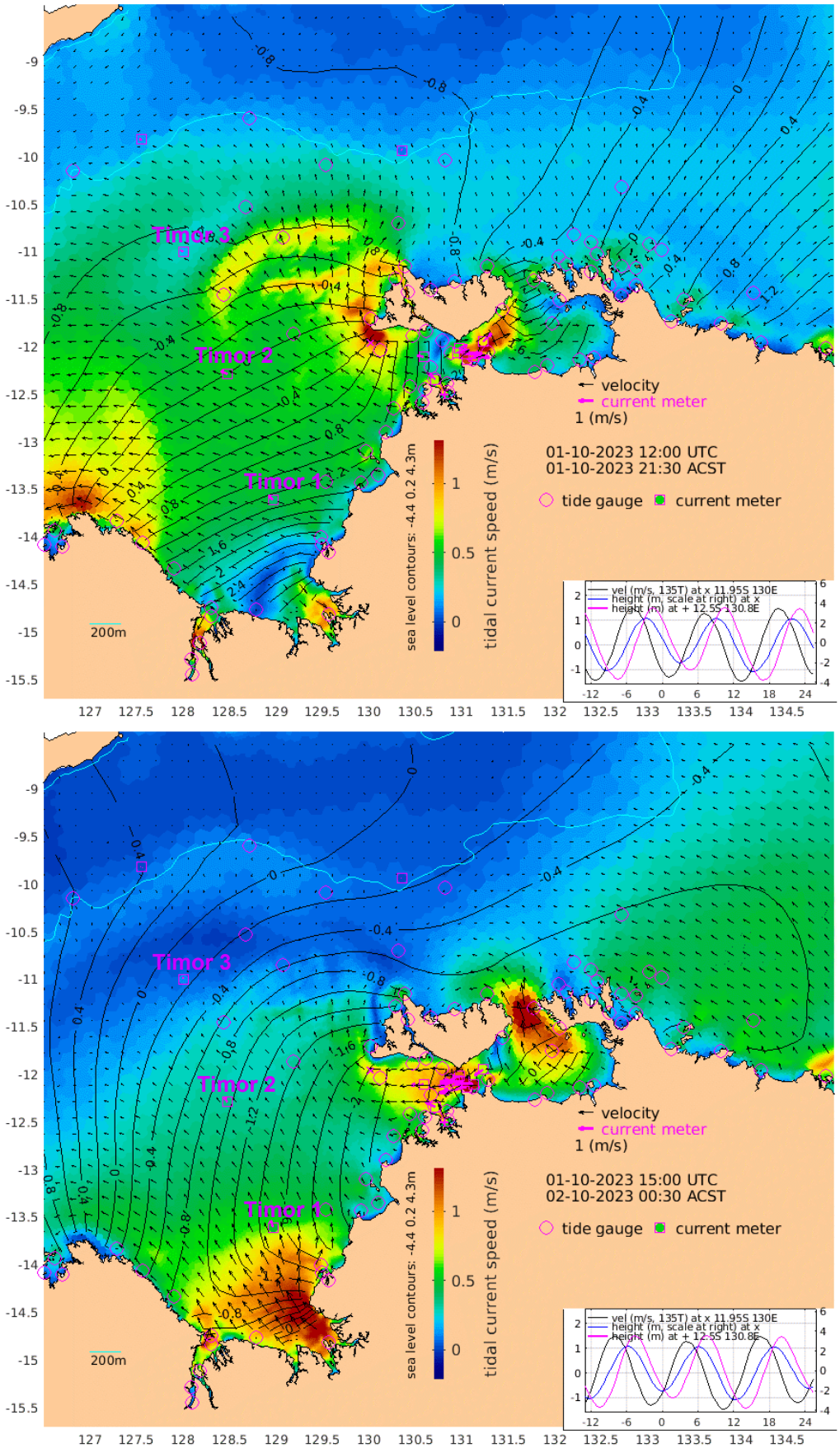

Figure 14. Predicted current and water level (contours) in JBG and the Timor Sea during a spring tide at high water (top) and peak ebb (bottom) (source: IMOS, 2023).

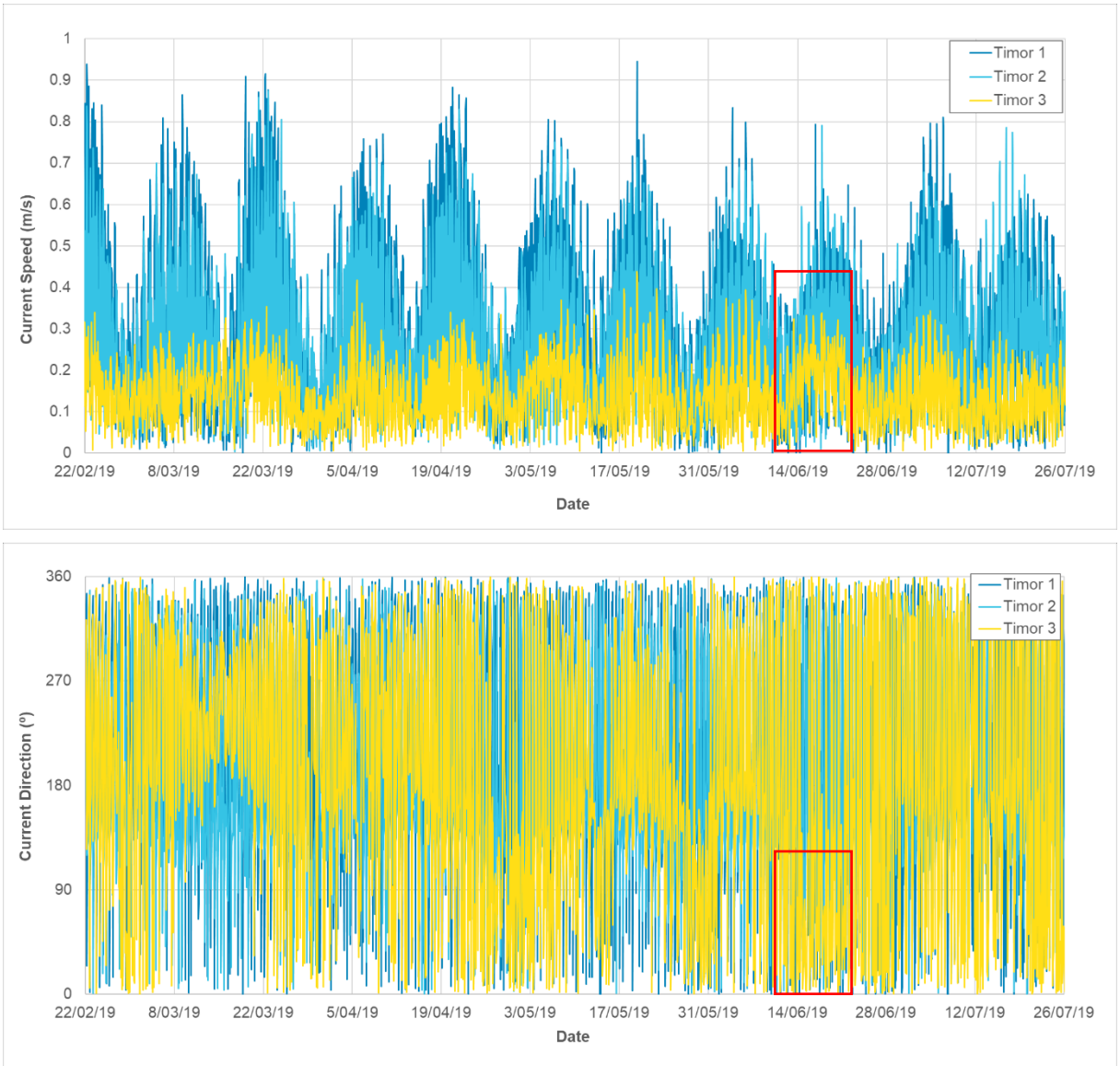

Figure 15. Measured current speed (top) and direction (bottom) at the IMOS Timor 1 to Timor 3 sites over a 5-month period covering both wet and dry season conditions (source: IMOS, 2023).

Figure 16. Measured current speed (top) and direction (bottom) at the IMOS Timor 1 to Timor 3 sites over an 18-day period in the dry season (source: IMOS, 2023).

3.1.2. Cambridge Gulf

As noted in section 3.1.1, CG is located in an area influenced by tidal amplification, resulting in CG being a macrotidal environment with mixed semi-diurnal tides. The tidal planes at the eastern entrance to CG (Cape Domett) and towards the upstream end (Wyndham) are shown in Table 1 and the predicted water levels over an example 14-day spring neap cycle are shown in Figure 17, taken from AHO AusTides predictions (AHO, 2023). The table and the figure both show that the tidal range increases upstream from the entrance to CG. The figure also shows that there is a lag between the time of high and low water at the entrance and upstream, with the time of high and low water at Wyndham being approximately 1 hour 15 minutes later than at Cape Domett.

The measured and predicted water levels at Wyndham were used to calculate the residual water level at the site to show the relative influence of river discharge on the water levels. The measured, predicted and residual water levels are shown over a wet season period when the largest residual water levels occurred in 2021 in Figure 18. The plot shows that over the period the residual water levels ranged from -0.5 m to +1.1 m, with an average residual level of around +0.5 m over the period. The timing of the peaks in residual water level varied over the period shown, with peaks in high water during the first set of spring tides shown and then peaks at low water during the second set of spring tides. The largest residual water levels occurred closer to low water than high water. The data also showed that larger residual water levels occurred during the wet season compared to the dry season, with residual water levels in the dry season varying between ±0.5 m.

There is no information available to determine the relative influence of storm surges in the open bay area of CG. However, given the large tidal range and relatively small influence of upstream freshwater discharges on water levels at Wyndham, it is expected that the highest water levels experienced in CG will be a result of very large astronomical tide combined with a small to medium storm surge (e.g. during Tropical Cyclones).

Measured water level data were also collected up the East Arm in October 2000 (dry season) at AIMS 3 to AIMS 5. AIMS 3 was located where the East Arm joins the West Arm to the south of Adolphus Island, AIMS 4 was located approximately 25 km upstream in the East Arm and AIMS 5 was located a further 13 km upstream. The measured water levels over the period with concurrent measurements are shown in Figure 19. The plot shows how the tidal curve becomes more asymmetrical, the tidal range reduces and the lag in high and low water times increase with distance up the East Arm.

The measured water levels and currents at AWAC-01 over a 15-day spring neap cycle in June 2023 are shown in Figure 20. The plot shows the following:

- Currents increase from the bed to the surface, with peak spring tide current speeds at the bed of 0.8 m/s and almost 1.3 m/s at the surface and peak neap tide current speeds at the bed of down to 0.4 m/s and down to 0.5 m/s at the surface.

- The current direction is to the south south-west (approximately 200º) during the flood stage of the tide and to the north north-east (approximately 20º) during the ebb stage of the tide. There is limited variation in the current direction through the water column, with the main difference being the near-bed current directions are more consistent due to more stronger steering by the bathymetry while the surface current directions are slightly more variable and can be from a more northerly direction during the ebb stage of the tide (approximately 355º).

- Peaks in current speed coincide with the mid-tide levels of the flooding and ebbing stages of the tide. There is typically one peak in current speed each day which is significantly higher than the other peaks over the day (during spring tides the higher peak can be 50% higher than the other peaks). The higher current speed is on the flood stage of the tide (i.e. currents flowing in a southerly direction) due to the diurnal tidal inequality resulting in one flood stage of the tide coinciding with the lower low tide and higher high tide each day. This difference is less noticeable during neap tides as the diurnal inequality also reduces during neap tides.

The water level, current speed and direction over the remaining 25 days of data captured at AWAC-01 show a similar pattern, with the astronomical tide being the dominant process driving the currents. The measured water level and current data at AWAC-01 over a 30 day lunar cycle has also been used to calibrate the hydrodynamic model. This is detailed in Section 4.4.2.

Water levels and currents were also measured at three different fixed sites by AIMS (Wolanski et al, 2004) in 2002. Plots showing the measured water level and current speed and direction at a depth mid-way through the water column in January 2002 (wet season) are shown in Figure 21 (note water levels at AIMS B are not shown as they were the same as at AIMS A). For reference, AWAC-01 is located approximately 10 km to the west of AIMS A and 5 km to the east of AIMS B, while AIMS E is located adjacent to Wyndham. The plot shows the following:

- The measured water levels show similar amplification of the tide in an upstream direction as shown by the AHO predicted water level data. The phase difference between AIMS A and AIMS E is approximately 1 hour 30 minutes.

- At all three sites the peaks in tidal current coincide with the time of mid-tide of the flood and ebb stages of the tide. The currents are lowest at AIMS A, with peak spring speeds of 1.0 m/s and peak neap speeds of 0.5 m/s. The currents are highest at AIMS B, with peak spring speeds of 1.4 m/s and peak neap speeds of 0.8 m/s. The currents at AIMS E have the least variability between spring and neap conditions, with peak spring speeds of 1.3 m/s and peak neap speeds of 1.0 m/s.

- At the three sites the current directions are similar, with average directions of 200º at AIMS A and B and 210º at AIMS E during the flood stage of the tide and average directions of 20º at AIMS A and B and 35º at AIMS E during the ebb stage of the tide.

- The currents at AIMS A and AIMS E have similar peak flood and ebb current speeds, while at AIMS B the ebb current speed is typically slightly higher than the flood current speed. The ebb current speed being comparable to or higher than the flood current speed despite the water level change over the flood stage of the tide often having a larger tidal range (due to the diurnal inequality) differs to the measurements at AWAC-01 (where the highest current speeds were

during the flood stage of the tide) during the dry season. The difference could be a result of the higher river discharge during the wet season resulting in increased ebb flows or differences in the locations of the sites, with AWAC-01 potentially located in a flood dominant area and AIMS B located in an ebb dominant area.

To further investigate spatial variations in the currents around CG and offshore, results from the initial hydrodynamic model are presented and discussed in Section 4.4.3.

Table 1. Tidal Planes at Primary AHO Sites in CG (AHO, 2022).

Tidal Plane	Cape Domett Elevation (m LAT)	Wyndham Elevation (m LAT)
Highest Astronomical Tide (HAT)	8.0	8.7
Mean High Water Springs (MHWS)	6.9	7.9
Mean High Water Neaps (MHWN)	5.2	5.9
Mean Sea Level (MSL)	4.19	4.63
Mean Low Water Neaps (MLWN)	3.2	3.3
Mean Low Water Springs (MLWS)	1.5	1.4

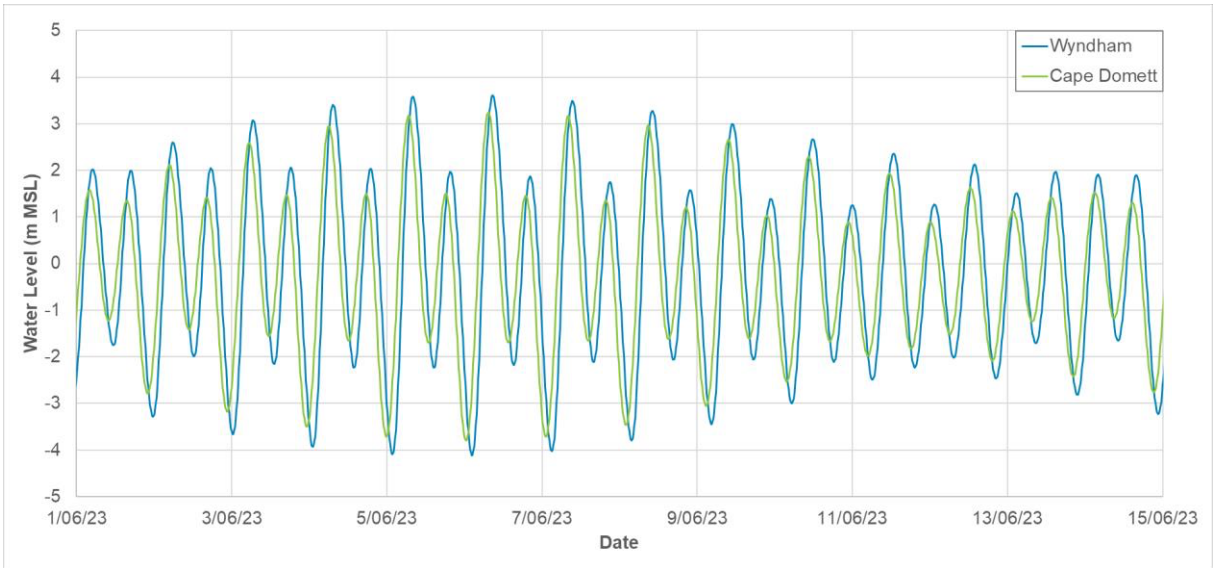

Figure 17. Predicted water levels at the entrance (Cape Domett) and upstream (Wyndham) of the CG (source: AHO, 2022).

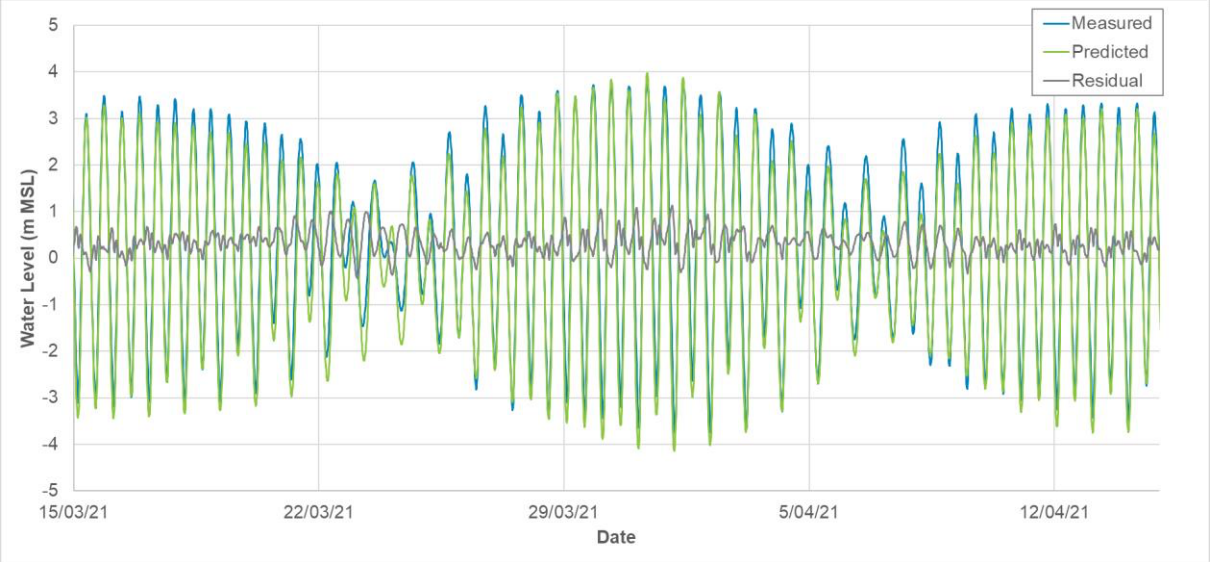

Figure 18. Measured, predicted and residual water levels at Wyndham (sources: BoM, 2024a; AHO, 2023)

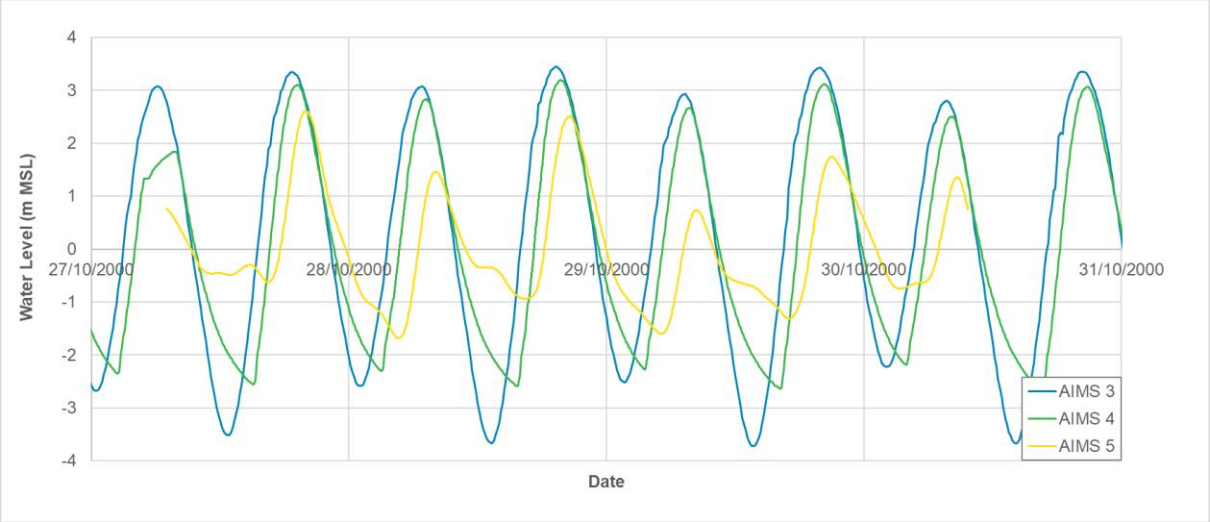

Figure 19. Measured water levels in 2000 along the East Arm (source: AIMS, 2007)

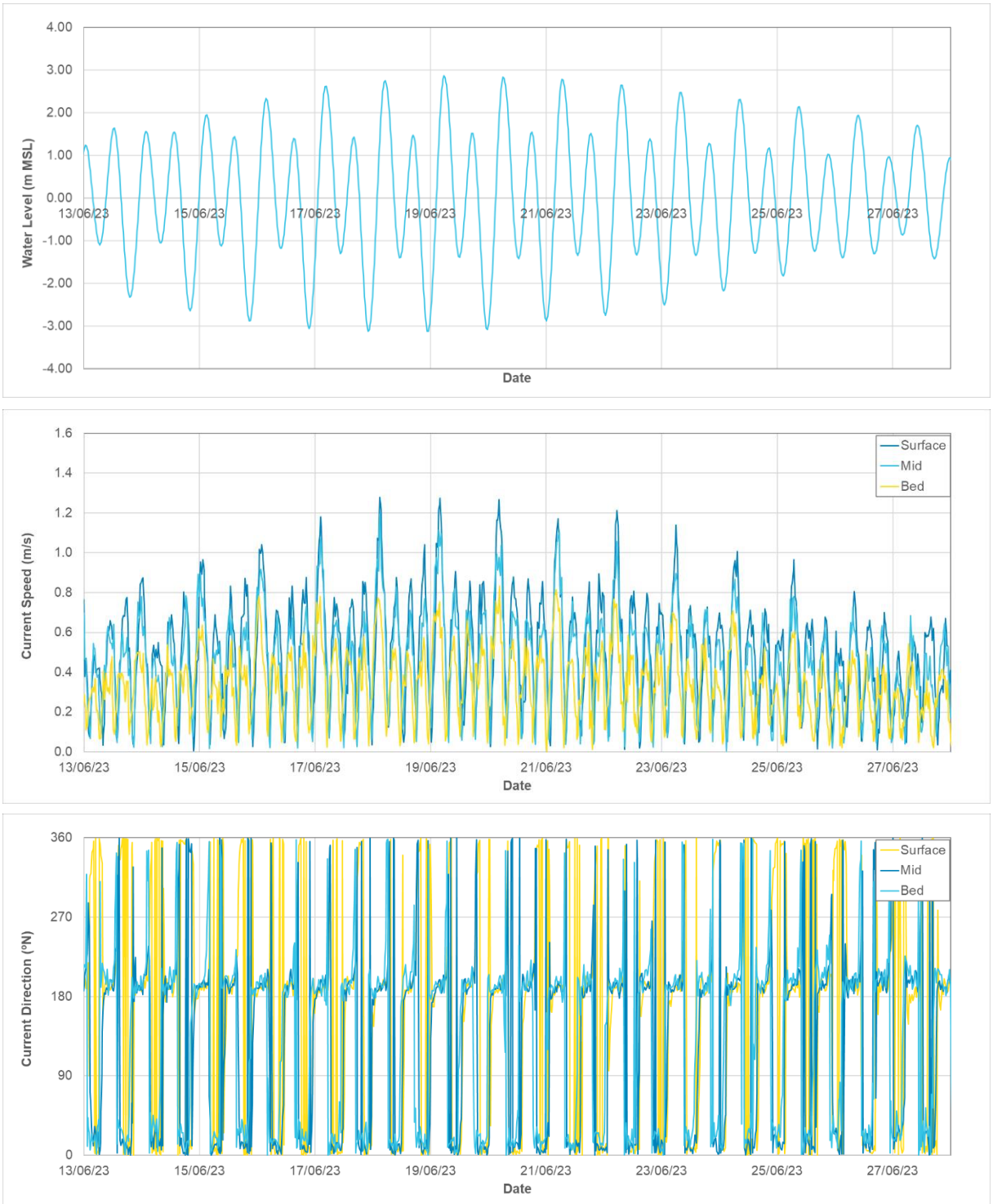

Figure 20. Measured water level and current speed and direction at three depths through the water column at AWAC-01 (source: BKA, 2024d).

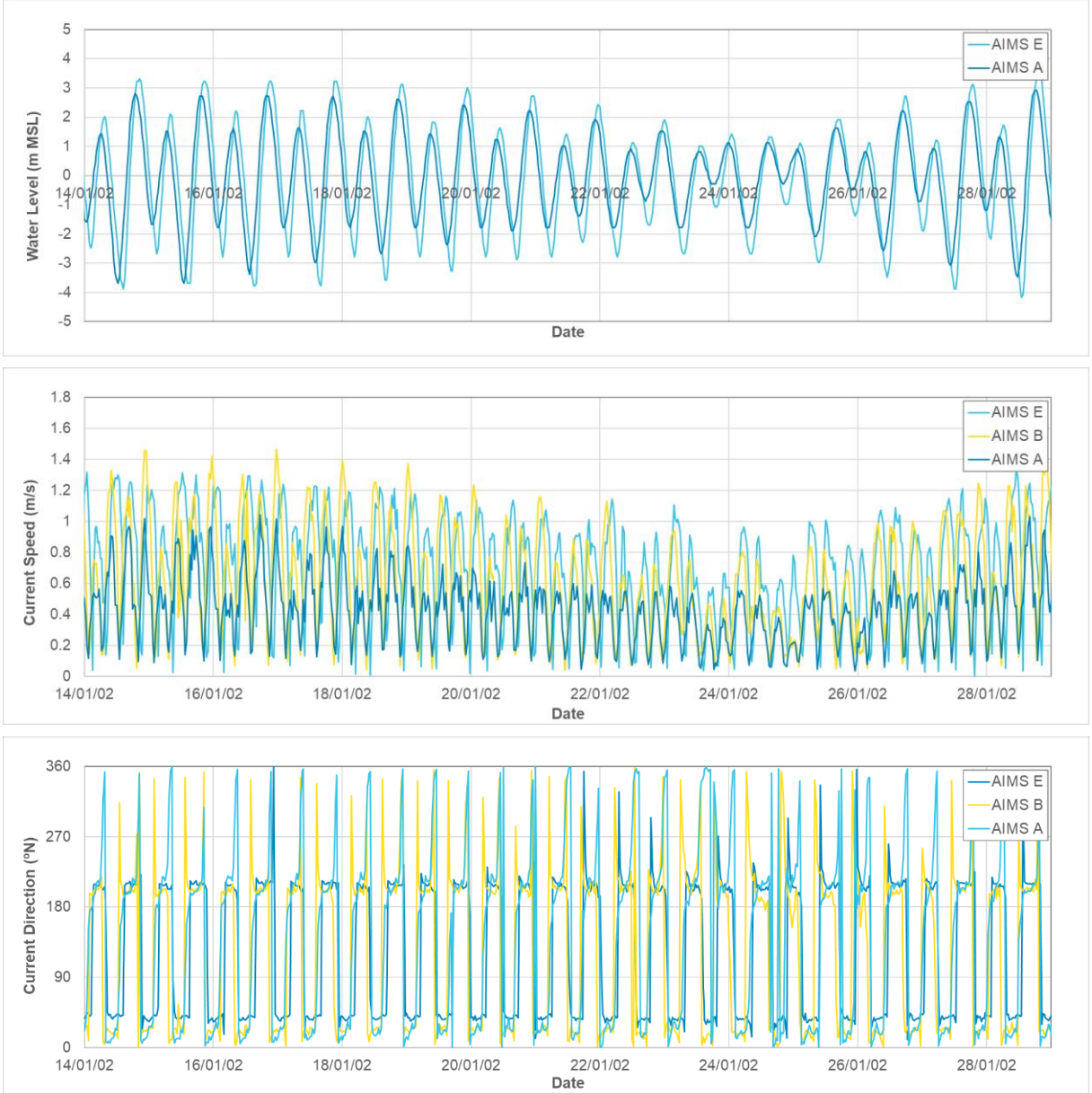

Figure 21. Measured water level and current speed and direction at mid-depth at AIMS A, B and E (source: AIMS, 2007).

3.2. Waves

Time series plots of the hindcast modelled wave and wind conditions directly offshore of CG (at CAWCR01) over a 12 month period (July 2017 to July 2018) are shown in Figure 22 (CSIRO, 2023). The plot shows that over the majority of the year the significant wave height (H_s) remains below 1 m. Larger wave heights can occur during the wet season months (December to March), with four wave events exceeding a H_s of 1 m during this year, with a peak in H_s of just under 3 m. The larger wave conditions typically correspond to a period with wind speeds of more than 10 m/s.

The mean wave period typically remains between 2 and 5 seconds for the majority of the time except during the larger wave events in the wet season when wave periods of 5 to 7 seconds can occur. There is a clear seasonal variability in the wave direction, with waves typically from north to east between April and September (dry season), from northwest to northeast from September to December (transitional period) and from northwest to north from December to April (wet season).

Plots showing wave roses from the two CAWCR hindcast model output points are provided in Figure 23. The wave roses show that offshore of JBG, wave heights are larger and are fairly bidirectional, with waves typically from either west to west northwest or from southeast to east. In contrast, the site directly offshore of CG (nearshore CAWCR01) typically has waves from anywhere between north-

northwest and east, but with waves from north-northwest occurring more regularly and resulting in the largest waves. Wave height is also significantly lower at the site directly offshore of CG compared to the site offshore of JBG, indicating that the shallow bathymetry directly offshore of CG acts to reduce the wave height. Within CG the wave climate will therefore be a combination of offshore waves and locally generated wind-waves which have formed within the fetch limited environment of CG.

Waves roses of the wet and dry season wave conditions at CAWCR01 are shown in Figure 24. The roses further highlight the seasonality in wave conditions directly offshore of CG, with largest waves occurring during the wet season when H_s is predominantly above 0.5 m (H_s above 1 m for around 5% of the time) and with a wave direction predominantly from north northwest. During the dry season the H_s remains predominantly below 0.5 m, while the wave direction varies from north-northeast through to east-southeast. During the transitional periods between the wet and dry seasons the H_s is also predominantly below 0.5 m, but it can occasionally exceed 1 m.

Scatter plots of the hindcast modelled H_s against direction, mean wave period against direction and H_s against mean wave period at CAWCR01 are shown in Figure 25 to Figure 27. The plots show the relative relationships between the different wave parameters, as follows:

- For the H_s to exceed 1 m the wave direction typically must be between 315º to 90º. The largest waves typically occur from northwest to the north.
- For waves from the north-east through to the north-west the mean wave period is predominantly below 5 s, while for waves from northwest through to northeast, the mean wave period is predominantly up to 8 s.
- The waves with a mean wave period of more than 8 s are generally associated with negligible wave heights (e.g. H_s of less than 0.2 m).
- The mean wave period typically increases as the H_s increases, with an average mean wave period of around 5 s for an H_s of 1 m which increases up to around 8 s for an H_s of 3 m.

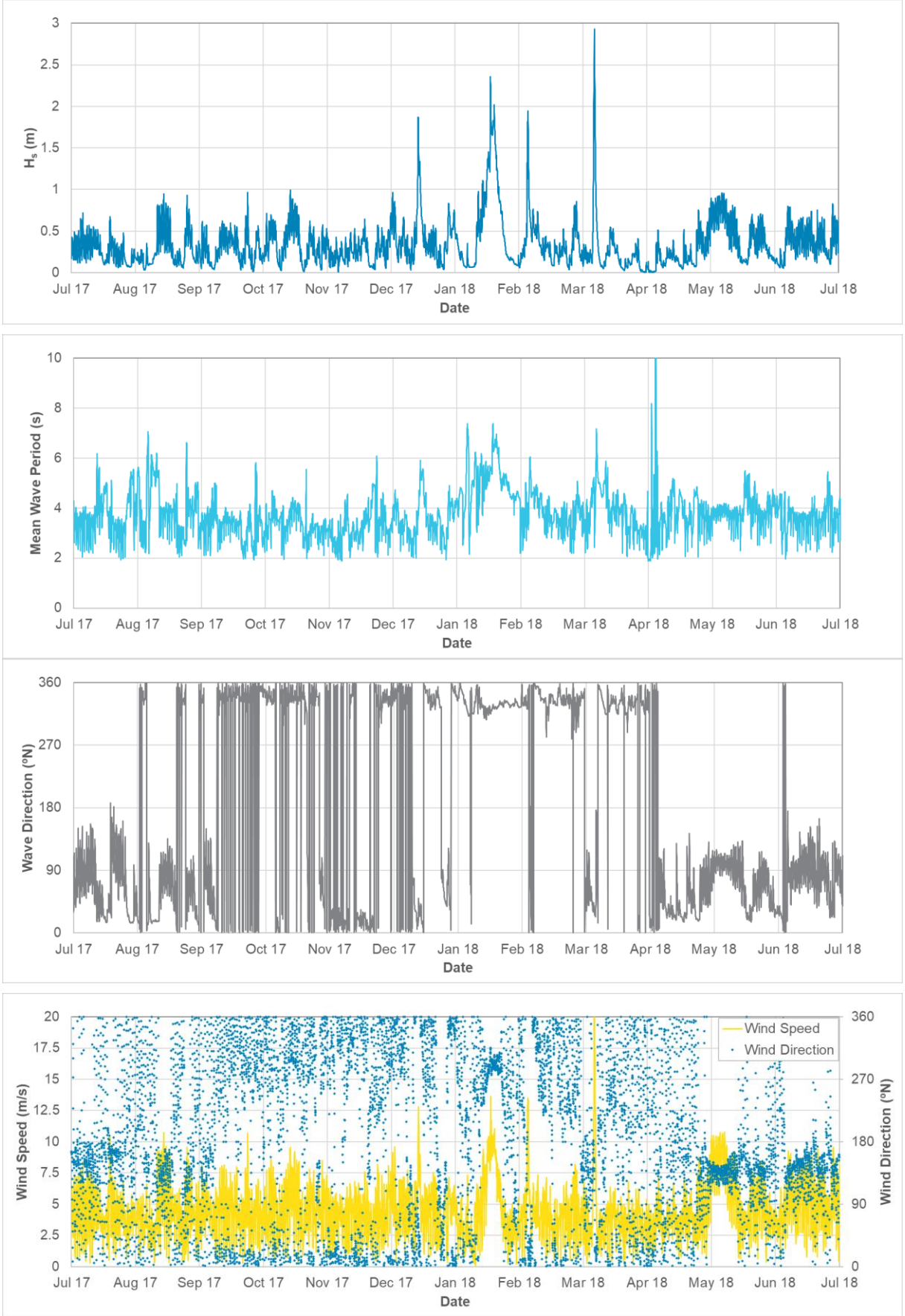

Figure 22. Timeseries of hindcast modelled waves and wind at CAWCR01 over 12 months (source: CSIRO, 2023).

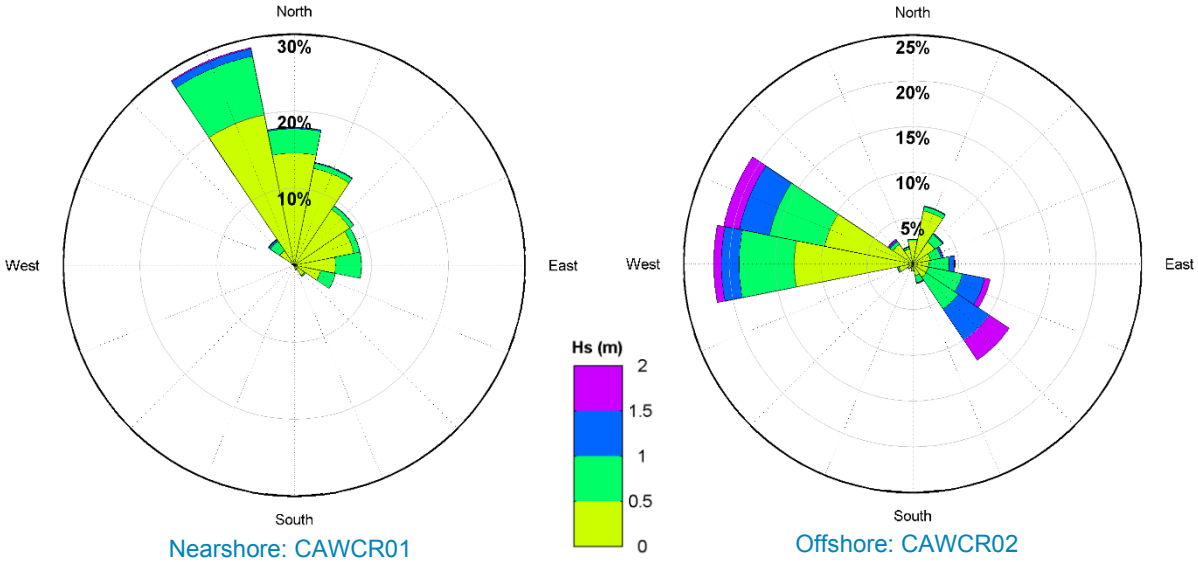

Nearshore: CAWCR01 Offshore: CAWCR02

Figure 23. Wave roses for the nearshore and offshore locations from the CAWCR Hindcast Model (source: CSIRO, 2023).

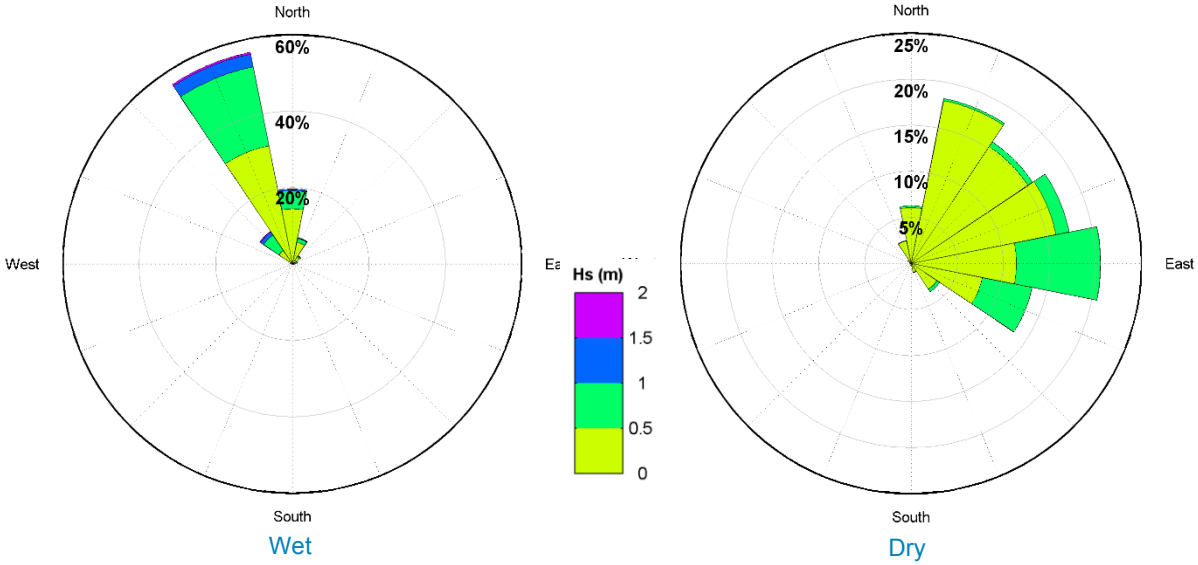

Wet Dry

Figure 24. Wet and dry season wave roses for the nearshore location from the CAWCR Hindcast Model (source: CSIRO, 2023).

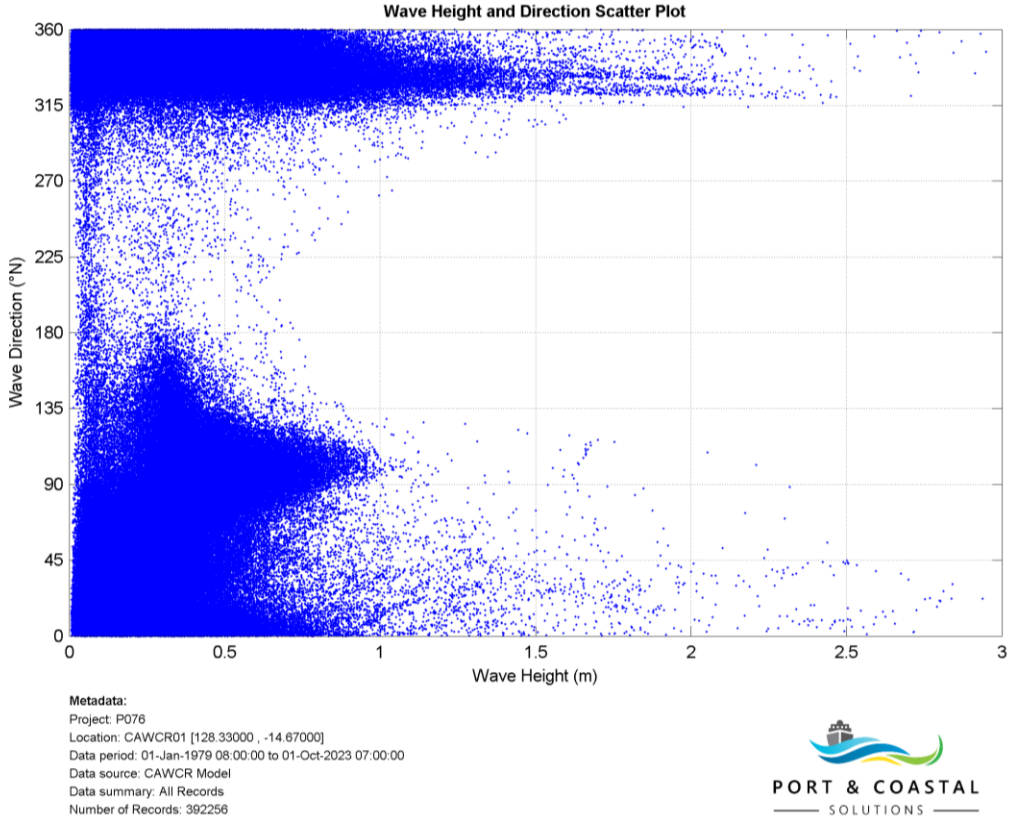

Figure 25. Scatter plot of H_s and wave direction at CAWCR01 (source: CSIRO, 2023).

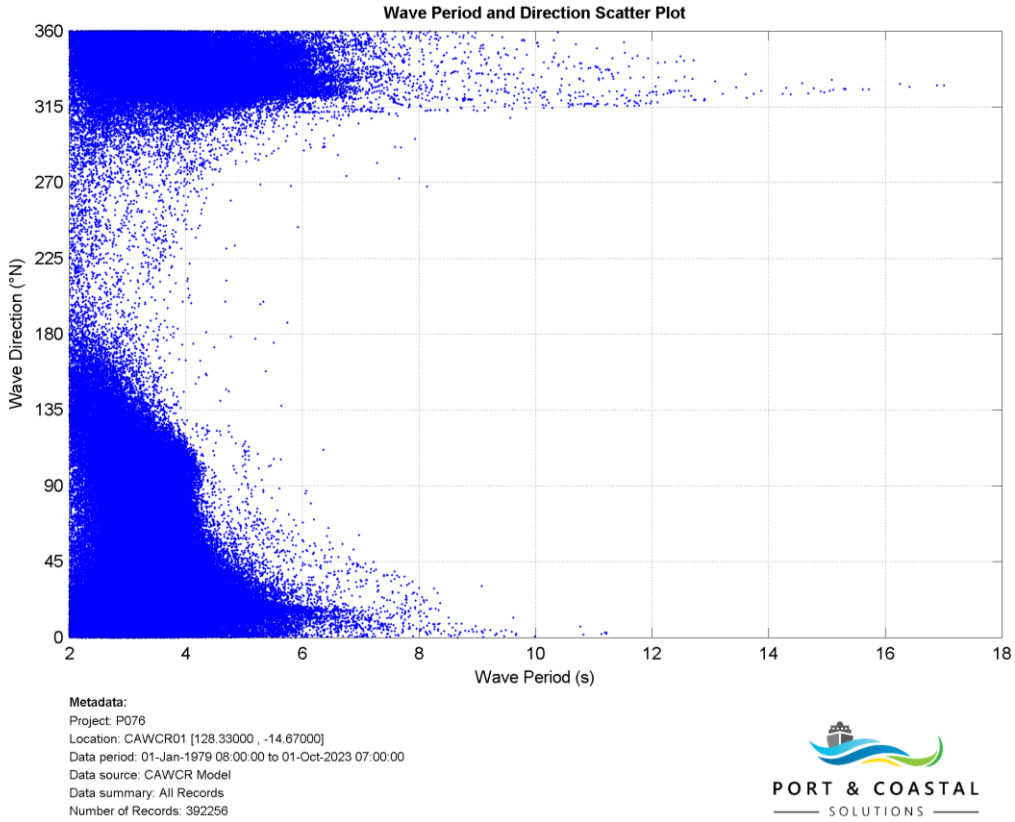

Figure 26. Scatter plot of mean wave period and wave direction at CAWCR01 (source: CSIRO, 2023).

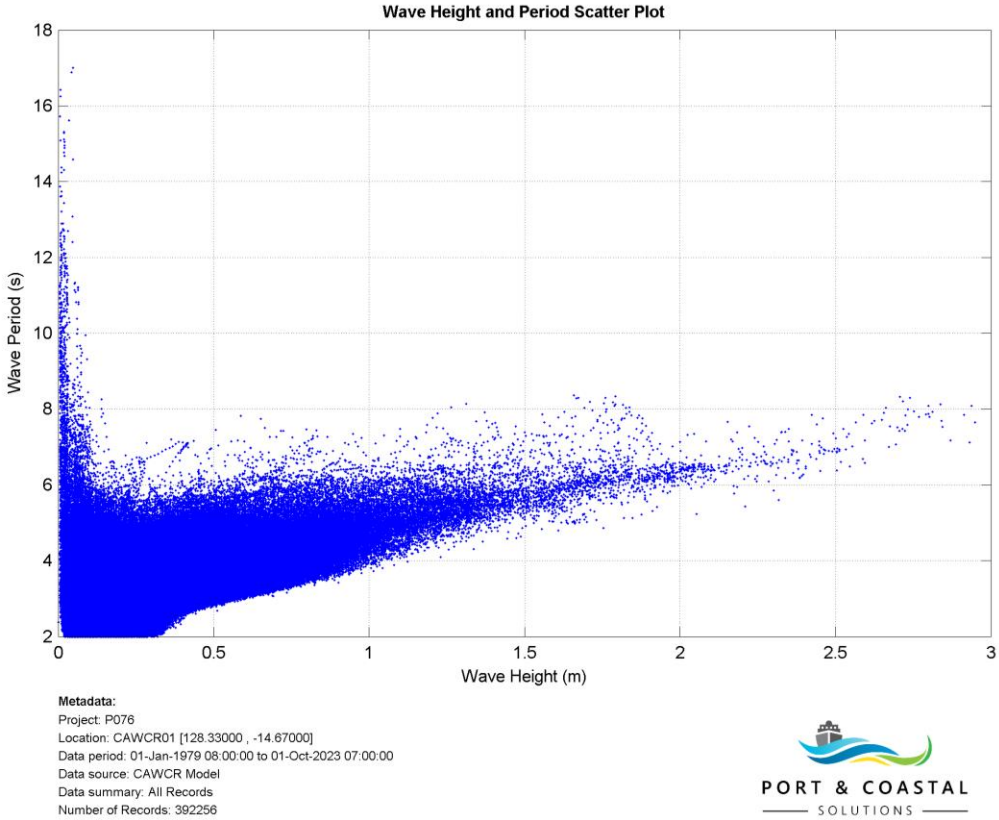

Figure 27. Scatter plot of H_s and wave period at CAWCR01 (source: CSIRO, 2023).

3.3. Wind

The measured wind data at the BoM Wyndham Airport weather station show very dominant winds from east and east-southeast, while the measured wind data at the BoM Port Keats Airport weather station show winds frequently occurring from west through to north, and east through to south directions (Figure 28). The 10 months of measured wind data at Cape Domett by UWA shows dominant winds from northwest through to north-northeast and from east to east-southeast. The hindcast wind data at CAWCR01 shows similar wind direction variability to BoM measured winds at Port Keats Airport, except with higher wind speeds. In addition, the hindcast wind data show a similar dominance in winds from west to north-northeast to the measured winds at Cape Domett, but due to the Cape Domett station being sheltered from the southeast the measured data does not show the same peak in wind from southeast (it shows it from east instead). The dominant winds from an easterly direction measured at the Wyndham Airport is thought to be due to significant sheltering at the site due to hills to the north of the site. Based on the comparison presented, the winds from the CAWCR hindcast model are considered to provide the most representative winds for CG. However, the CAWCR winds are unlikely to be able to accurately represent the mesoscale winds which influence the coastal area or the variability in winds which occur during tropical storms. The adoption of the CAWCR winds will be further investigated when the weather station at Cape Domett is installed as part of the project.

A wind rose for the hindcast wind data at CAWCR01, located directly offshore of CG, from 1979 to 2023 is shown in Figure 28. The rose shows that wind speeds are typically between 4 and 8 m/s, while wind directions are most often from west through to north-northeast and from east-southeast through to south-southeast. Wet and dry season wind roses at CAWCR01 are shown in Figure 29. During the wet season winds typically vary between the west and the north, while during the dry season winds are predominantly from east-southeast to south-southeast.

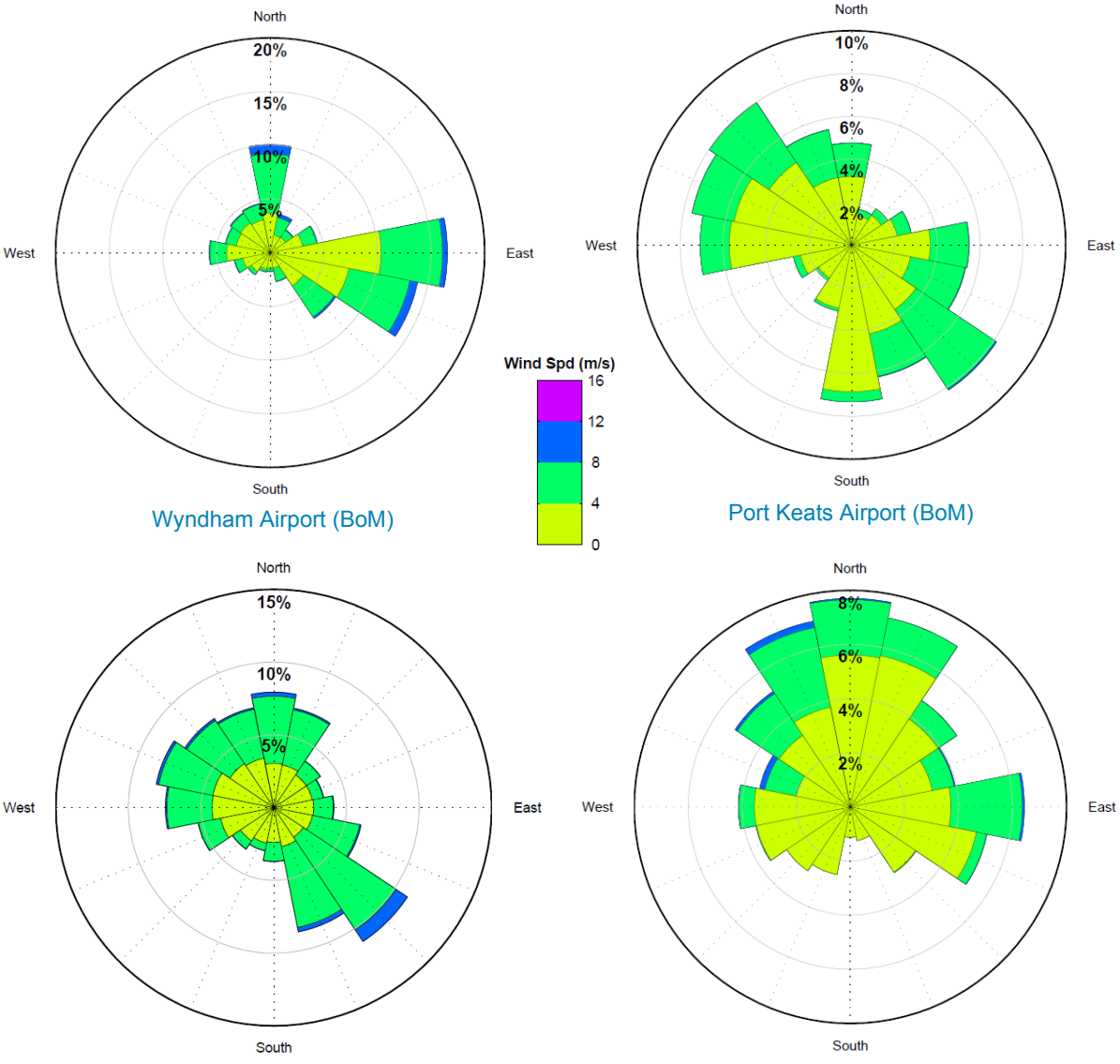

Figure 28. Wind roses for the measured BoM wind data and the hindcast modelled wind at CAWCR01 from the CAWCR Hindcast Model.

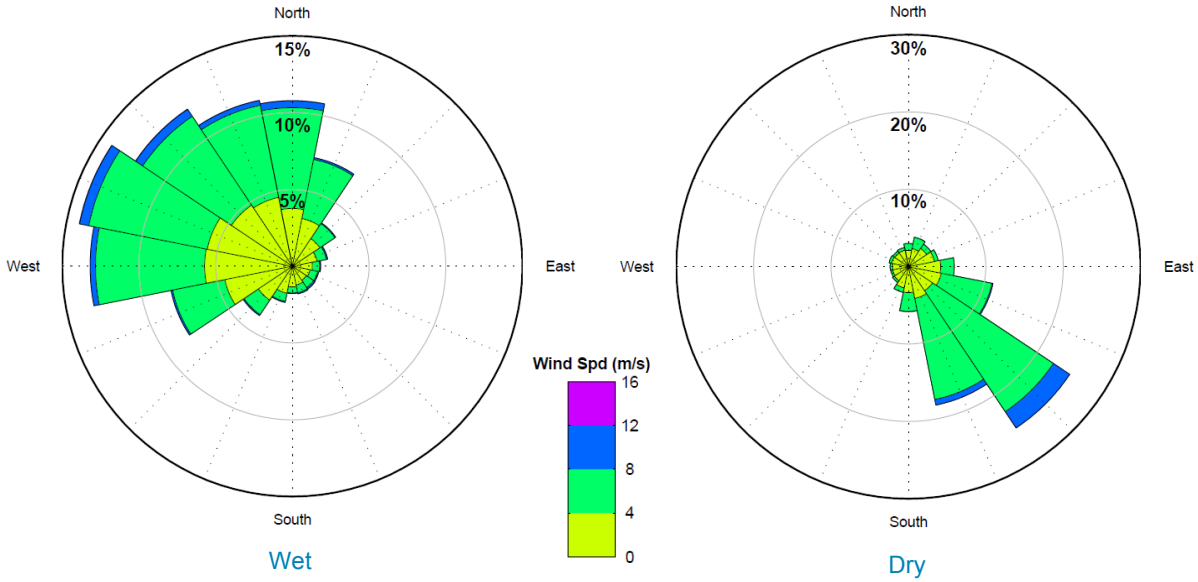

Figure 29. Wet and dry season wind roses for the nearshore location from the CAWCR Hindcast Model (source: CSIRO, 2023).

3.4. Rainfall and River Discharge

As noted in Section 2.2.3, the measured rainfall at the BoM Wyndham Airport weather station can be used to provide an indication of the rainfall in the catchments which drain into CG. The measured daily rainfall at Wyndham Aerodrome over the last 3 years is shown in Figure 30. The plot highlights the interannual and intra-annual variability in the rainfall in the area. It shows how the majority of the rainfall occurs during the wet season period (December to March), with limited rain occurring outside of this period and almost no rainfall occurring from June to October each year. The rainfall which occurs over the wet season is highly variable, typically with days to weeks of no rainfall followed by days to weeks with regular rainfall. The majority of the rainfall occurs during cyclonic events. These can result in very high rainfall over relatively short periods of time (Hale, 2008). The daily rainfall is typically less than 50 mm. This threshold is typically only exceeded a few times each wet season (if at all). Since 2000, the highest daily rainfall measured at the Wyndham Aerodrome station was 230 mm (January 2016).

The measured daily river discharge over the last 3 years at the available monitoring sites on the King River and Ord River is shown relative to the measured rainfall in Figure 30. The daily discharge in the Ord River has been significantly larger than in the King River, which is to be expected given the difference in the catchment sizes (1,500 km^2 for the King River compared to approximately 50,000 km^2 for the Ord River). Comparison of discharge data from the two sites on the Ord River shows the influence that the Ord River Dam has on supressing the flood discharge of the river as well as increasing the dry season discharge, as the Old Ord Homestead site is located upstream of Lake Argyle and the dam, while the Tarrara Bar site is located downstream of them.

During the wet season the majority of the peaks in river discharge which occur upstream of the Ord River Dam are significantly lower at the site downstream of the dam, with most of the peaks downstream capped at around 75,000 ML/day. Over the three-year period shown there is one exception to this with a peak in river discharge in February 2023 downstream of the dam reaching 200,000 ML/day, which is comparable to the peak upstream of the dam. The plots also show that over the dry season there is an almost constant discharge downstream of the dam of around 50,000 ML/day, while upstream of the dam there is typically no discharge in the dry season.

The measured river discharge data at sites in the Ord River, King River and Durack River are shown for all data collected since 1968 in Figure 31. The plots show that peaks in river discharge occur in all three rivers during the wet seasons, with the discharge in the Ord River typically significantly higher than the discharge in the other two rivers. Over the short period when there were concurrent data for the Durack River and the Ord River site downstream of the Ord River Dam (Tarrara Bar), the data show that the daily discharge in the Ord River downstream of the dam was almost double the discharge in the Durack River (350,000 ML/day compared to 180,000 ML/day). The data therefore indicate that even with the Ord River Dam in place the river discharge from the Ord River into East Arm is still likely to be comparable to or higher than the discharge from the Durack and Pentecost Rivers into West Arm.

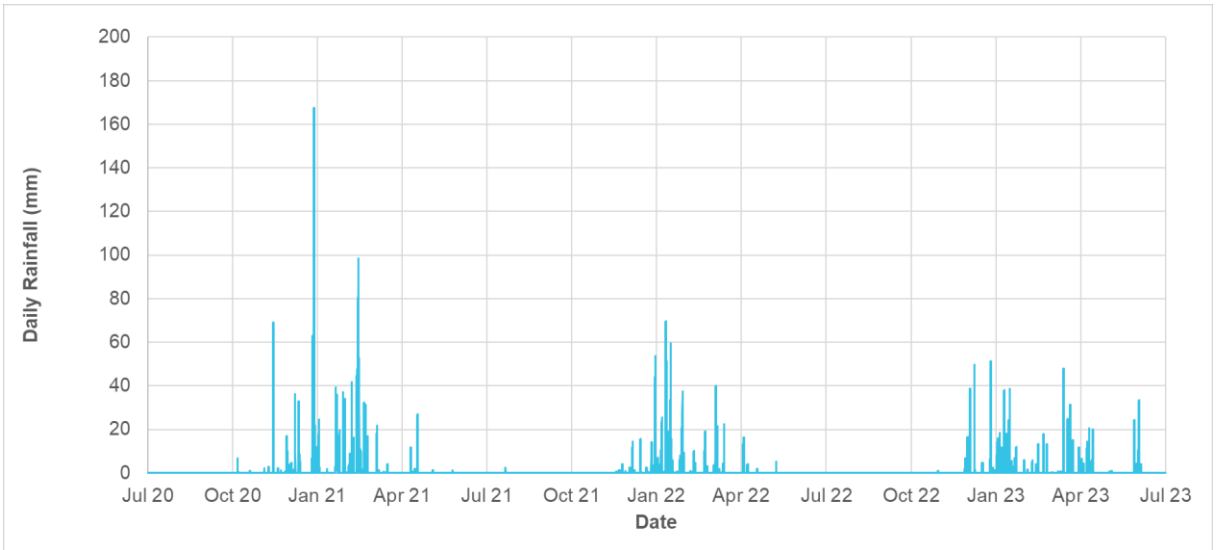

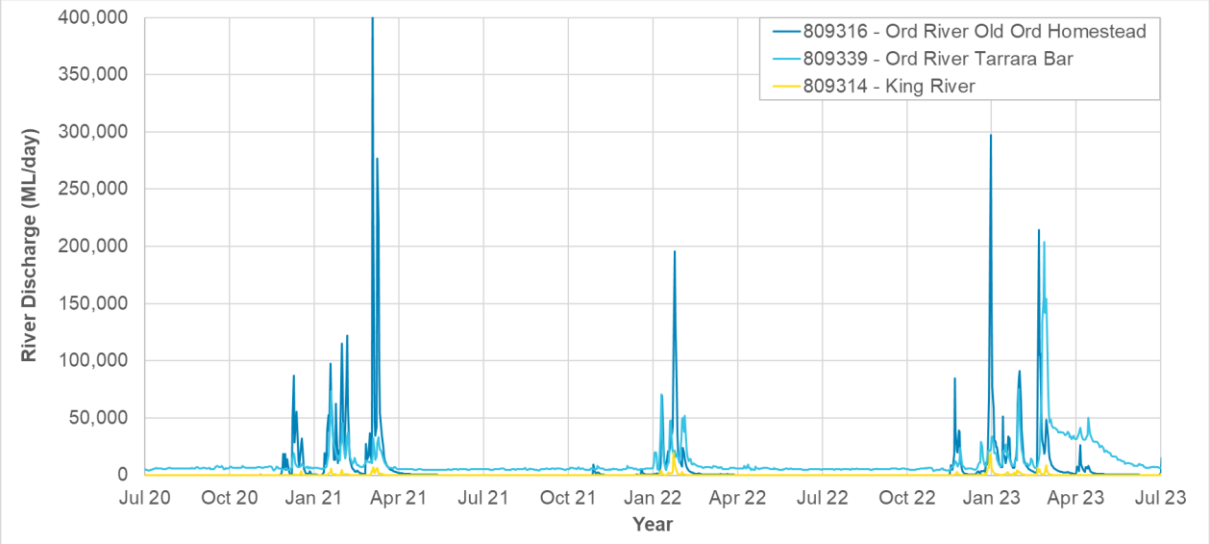

Figure 30. Measured daily rainfall at the BoM Wyndham Airport weather station and measured daily river discharge at the available monitoring sites over the last 3 years (source: BoM)

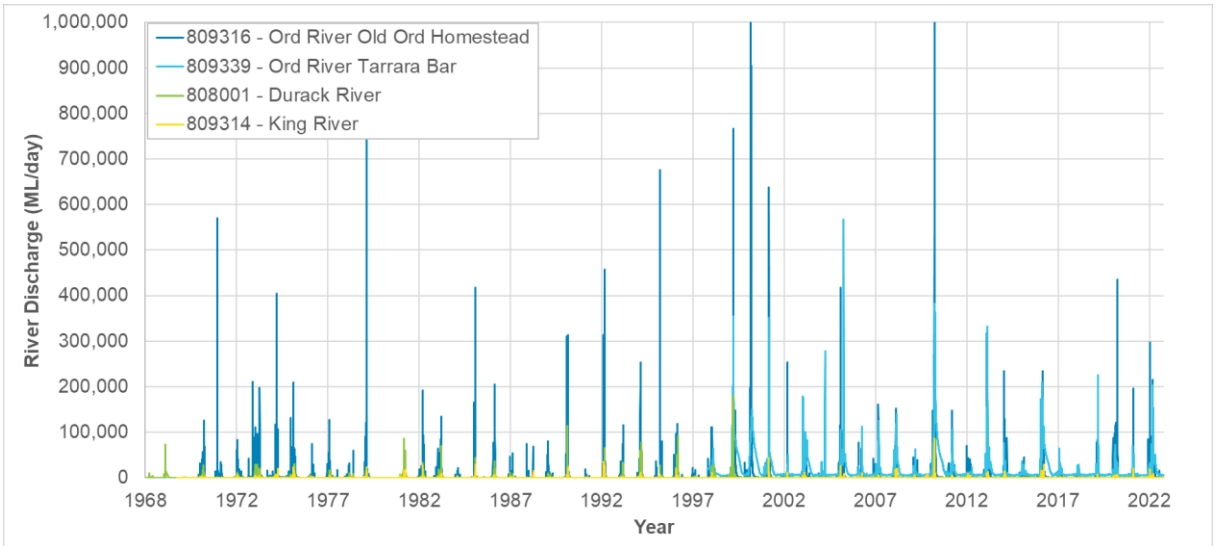

Figure 31. Measured river discharge at the available monitoring sites since 1968 (Source: DWER)

3.5. Tropical Cyclones

CG is located in an area where Tropical Cyclones (TCs) can occur during the wet season. Based on the BoM Southern Hemisphere Cyclone Tracks tool, between 1969 and 2022 a total of 48 TCs have passed within 200 km of the entrance to CG (BoM, 2024b). TCs have the potential to generate large waves, strong currents, storm surge and increased river discharge which can lead to significant resuspension of sediment from the seabed, increased transport of suspended sediment, elevated water levels and changes to shorelines and intertidal/supratidal areas (including mangroves). However, TCs are highly variable with the relative influence of a TC being dependent on multiple factors including its track, intensity and speed and the time of occurrence relative to the astronomical tide. Therefore, some TCs which track within 200 km of CG could result in little to no impact to the metocean conditions in the area, while others could result in significant impacts.

Over the 2017/18 wet season period, the CAWCR hindcast wave results show that four wave events occurred which resulted in an H_s offshore of CG of more than 1 m (Figure 22). Three of these four events were due to TCs:

- TC Hilda: This was a category 2 TC (126-164 km/hr strongest wind gust) which occurred between the 26th and 29th December 2017 (BoM, 2024b). The hindcast wave model predicted that the TC resulted in a peak in H_s of 1.87 m at CAWCR01 (directly offshore of CG) on 26th December 2017.

- TC Kelvin: This was a category 3 TC (165-224 km/hr strongest wind gust) which occurred between the 11th and 21st February 2018 (BoM, 2024b). The hindcast wave model predicted that the TC resulted in a peak in H_s of 1.94 m at CAWCR01 (directly offshore of CG) on 15th February 2018.

- TC Marcus: This was a category 5 TC (more than 280 km/hr strongest wind gust) which occurred between the 14th and 24th March 2018 (BoM, 2024b). The hindcast wave model predicted that the TC resulted in a peak in H_s of 2.93 m at CAWCR01 (directly offshore of CG) on 18th March 2018.

The high energy waves and currents which can occur during TC events, have the potential to mobilise bed sediment in deep water areas which would not normally be subject to bed sediment mobilisation under ambient conditions. Research conducted by Carter et al. (2009) showed that wave-generated bed shear stresses from an intense TC can suspend sediments at water depths of up to 30 to 60 m. Cyclone-induced waves and currents have also been shown to be important in the supply of new sediment to inshore areas through the erosion and advection of seabed sediment from the deeper areas (Gagan et al., 1990; and Orpin and Ridd, 2012).

The rainfall and river discharge data shown in Figure 30 show that the rainfall and river discharge vary significantly over the wet season, with the highest peaks in daily rainfall not always correlating with the highest river discharges. This is because the rainfall in the river catchments can differ from the rainfall at Wyndham and it is sustained rainfall over multiple days that will result in the highest river discharges. The highest annual river discharge peaks in the Ord River between 2020 and 2023 all correspond to TCs:

- TC Marian: This was a category 3 TC with a lowest central pressure of 950 hPa which occurred between the 21st February and 9th March 2021 (BoM, 2024b). The measured rainfall data showed rainfall of up to 100 mm/day over this period, while the Ord River Old Ord Homestead river gauge showed a peak wet season river discharge of 435,000 ML/day as a result of the event.

- TC Tiffany: This was a category 2 TC with a lowest central pressure of 988 hPa which occurred between the 8th January and 12th January 2022 (BoM, 2024b). The measured rainfall data showed rainfall of up to 70 mm/day over this period (the highest of the 2021/22 wet season), while the Ord River Old Ord Homestead river gauge showed a peak wet season river discharge of 195,000 ML/day as a result of the event.

- TC Ellie: This was a category 1 TC with a lowest central pressure of 990 hPa which occurred between the 21st December 2022 and 8th January 2023 (BoM, 2024b). The measured rainfall data showed rainfall of up to 50 mm/day over this period (the highest of the 2022/23 wet season), while the Ord River Old Ord Homestead river gauge showed a peak wet season river discharge of 300,000 ML/day as a result of the event.

The high river discharge events which can occur as a result of TCs will provide a supply of fine-grained sediment to the CG. The fine-grained sediment will have been eroded from the catchments during overland flow and then transported in suspension in the flood waters.

3.6. Water Quality

Plots of the measured temperature, salinity and chlorophyll-a through the water column at selected sites within CG, King Shoals and offshore (see Figure 10 and Figure 11 for site locations) collected by BKA during dry season conditions are shown in Figure 32 to Figure 34 (BKA, 2024d). The sites were selected to show the range of results over the spatial areas sampled. Within CG, sites were selected from the west and east entrances (CG01 and CG37), through to the entrance to West and East Arms (CG79 and CG77). At King Shoals, sites were selected from close to the entrance to CG (KS18 and KS20) up to the furthest sites offshore and to the west (KS06 and KS08). At the offshore area, sites were selected to cover the full extent of the area sampled. The concurrent vertical profiles in SSC at these sites are discussed in the following section. In addition, the water temperature, salinity and chlorophyll-a from all the profiles collected at each of the three areas based on the in-situ probe measurements, are summarised in Table 2 and results from the laboratory analysis from water samples for chlorophyll-a are shown in Table 3. The results are discussed below for each of the three parameters measured.

- Water Temperature: Water temperature in CG in the dry season varied at the profile sites between 23 and 24.5°C, with lower temperatures at the upstream end of CG and higher temperatures close to the entrance. There was less variability in the water temperature at King Shoals, with temperatures varying between 23 and 23.4°C. There was limited variation in temperature with depth at any of the CG and King Shoals sites, with differences in temperature of less than 0.3°C between the surface and seabed (lower temperature at the seabed). At the offshore sites the water temperature was higher than at King Shoals and similar to the water temperatures in CG. The offshore water temperature varied between 23.6 and 24.9°C, with lower temperatures at the western sites and higher temperatures at the eastern sites. At the western sites there was evidence of a temperature gradient through the water column of 1°C, with the variation predominantly in the upper 15 m of the water column. The average mid depth water temperatures from all the profiles shows that water temperatures in CG and offshore were similar, while at King Shoals they were lower by around 0.8°C. This difference between the sites is unlikely to be sustained long term as the strong tidal currents in the region will result in mixing through the area except in the deeper offshore waters with lower tidal current speeds.

- Salinity: Salinity in CG in the dry season varied at the profile sites between 29.5 and 32.5 ppt, with lower salinity at the upstream end of CG and higher salinity close to the entrance. There was limited variation in the salinity at the King Shoals sites, with values ranging from 32.75 and 33.5 ppt. The salinity at the offshore sites was the highest and had the least variability, with the salinity ranging from 35.5 to 35.65 ppt. There was little change in the salinity with depth at any of the sites, with differences in salinity of up to 0.3 ppt between the surface and bed (higher salinity at the bed).

- Chlorophyll-a: Chlorophyll-a levels in the dry season were consistently low at all the profile sites in CG, King Shoals and offshore. The chlorophyll-a remained below 1.5 µg/L at all sites (typically below 0.5 µg/L at King Shoals and below 0.35 µg/L offshore) and for all depths, showing very low phytoplankton (algae) in the region. Wet season data from the literature (Volkman et al., 2007) suggest that chlorophyll levels in CG are lower during the wet season (with measured values reported to range from 0.4 to 1.0 µg/L) than during the dry season, due to higher SSC in the wet season. The chlorophyll-a results calculated based on filtered water samples undertaken in the laboratory indicate that chlorophyll-a was approximately double what the in-situ probe measured. However, the results still show low chlorophyll-a, with mean values of 1.26 in CG, 1.0 at King Shoals and 0.37 offshore. Chlorophyll-a concentrations in the Ord River adjacent to Adolphus Island were shown by Robson et al. (2008) to be low, with the growth of phytoplankton being controlled by nitrogen (of which the monitoring showed a shortage), the low light availability and the vigorous tidal agitation which prevents the growth of algae and other plants on the bed.

The dry season water quality profiles indicate that the water column in CG, at King Shoals and offshore is well mixed in temperature and salinity with no distinct stratification present, but with some minor temperature variations through the water column at the easternmost offshore sites. This agrees with previous findings by Wolanski et al. (2004) who found that the waters in CG were consistently vertically well-mixed in temperature and salinity except for in the West Arm near Wyndham in the wet season (due to the increased freshwater discharge). The large tidal range and resultant strong currents in CG and JBG will limit any stratification of salinity and temperature, whilst also resulting in high SSC in shallower areas with available fine-grained sediment (i.e. CG), which will limit chlorophyll-a levels as the SSC reduces the light available for photosynthesis.

Previous studies indicate that during the wet season the water temperatures are typically 5°C higher than in the dry season (Rothlisberg et al., 2005). Wolanski et al. (2004) found that the longitudinal

gradient in salinity was larger in the wet season, with the potential for very low salinity in West and East Arms due to the increased freshwater discharge. In East Arm, the dry season salinity has been reported as being between 28 and 32 ppt, while during the wet season, the salinity can drop to less than 4 ppt during periods with very high freshwater discharge (Hale, 2008). Despite the lower salinity in West and East Arms, their measurements showed that in the open bay of CG, the salinity remained above 28 ppt.

Table 2. **Results of the dry season (July-August 2023) YSI water quality measurements in Cambridge Gulf, King Shoals and Offshore waters (based on mid-water-depth measurements) (source: BKA, 2024d).**

Statistic	Cambridge Gulf	King Shoals	Offshore Waters
Salinity (ppt)			
Mean	**31.73**	**33.18**	**35.58**
Minimum	29.45	32.78	35.50
Maximum	32.91	33.49	35.65
Mode	31.18	33.10	35.63
Median	32.04	33.18	35.57
Standard Deviation	0.91	0.20	0.05
Standard Error	0.13	0.04	0.01
Number of Sites	52	20	27
Temperature (ºC)			
Mean	**23.87**	**23.05**	**23.91**
Minimum	23.01	22.88	23.46
Maximum	24.42	23.22	24.34
Mode	24.27	22.96	23.62
Median	23.82	23.04	23.90
Standard Deviation	0.40	0.10	0.24
Standard Error	0.06	0.02	0.05
Number of Sites	52	20	28
Chlorophyll-a (µg/L)			
Mean	**0.60**	**0.41**	**0.18**
Minimum	0.29	0.29	0
Maximum	1.17	0.52	0.30
Mode	0.56	0.32	0.21
Median	0.52	0.40	0.18
Standard Deviation	0.17	0.07	0.07
Standard Error	0.02	0.02	0.01
Number of Sites	52	20	28

Table 3. **Results of the dry season (July-August 2023) Chlorophyll-a data from water sampling in Cambridge Gulf, King Shoals and Offshore Waters (based on results from laboratory analysis of filtered water samples) (source: BKA, 2024d).**

Statistic	Cambridge Gulf	King Shoals	Offshore Waters
Chlorophyll-a (µg/L)			
Mean	**1.26**	**1.00**	**0.37**
Minimum	0.90	0.90	0.20
Maximum	2.20	1.10	1.20
Mode	1.1	N/A	0.3
Median	1.1	1	0.3
Standard Deviation	0.33	0.10	0.25
Standard Error	0.06	0.06	0.05
Number of Sites	27	3	21

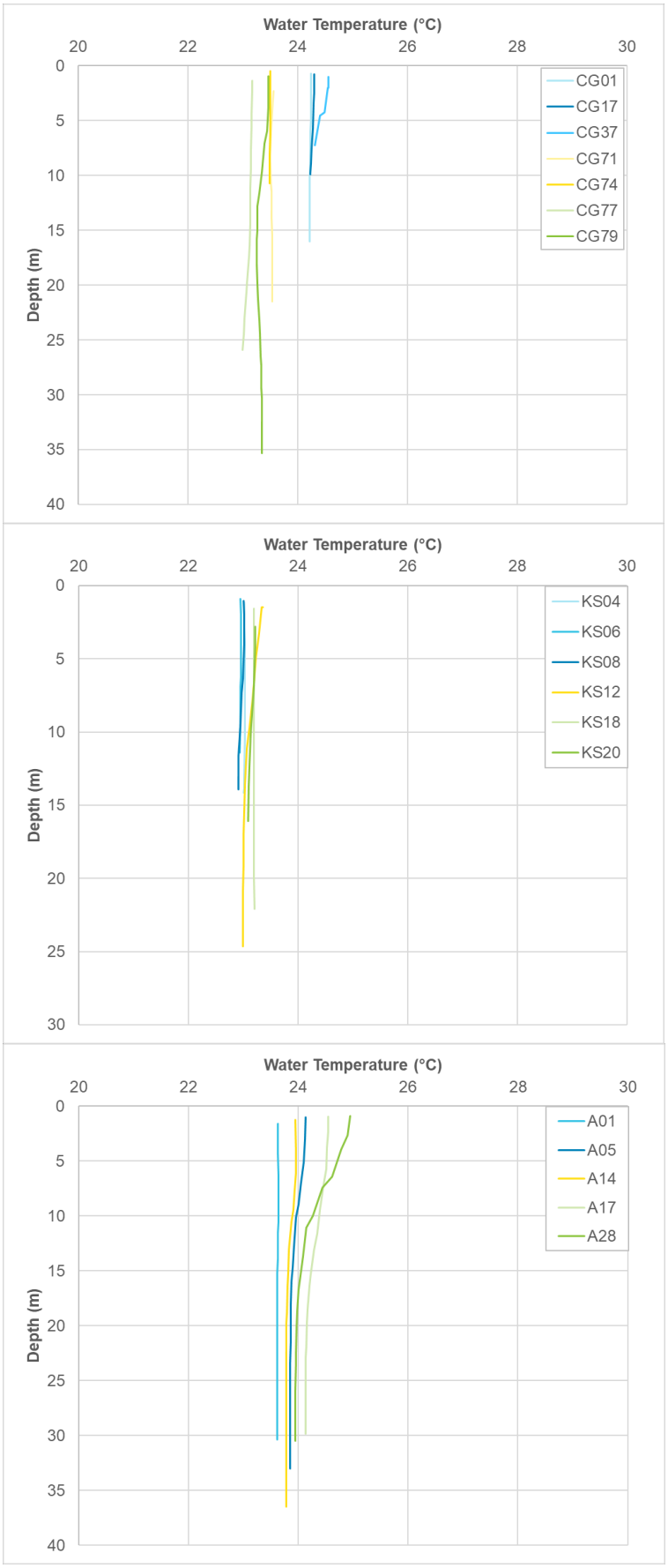

Figure 32. Vertical depth profiles of water temperature at sites in CG (top), King Shoals (middle) and offshore (bottom) measured in July-August 2023 (see Figure 10 and Figure 11 for locations) (source: BKA, 2024d).

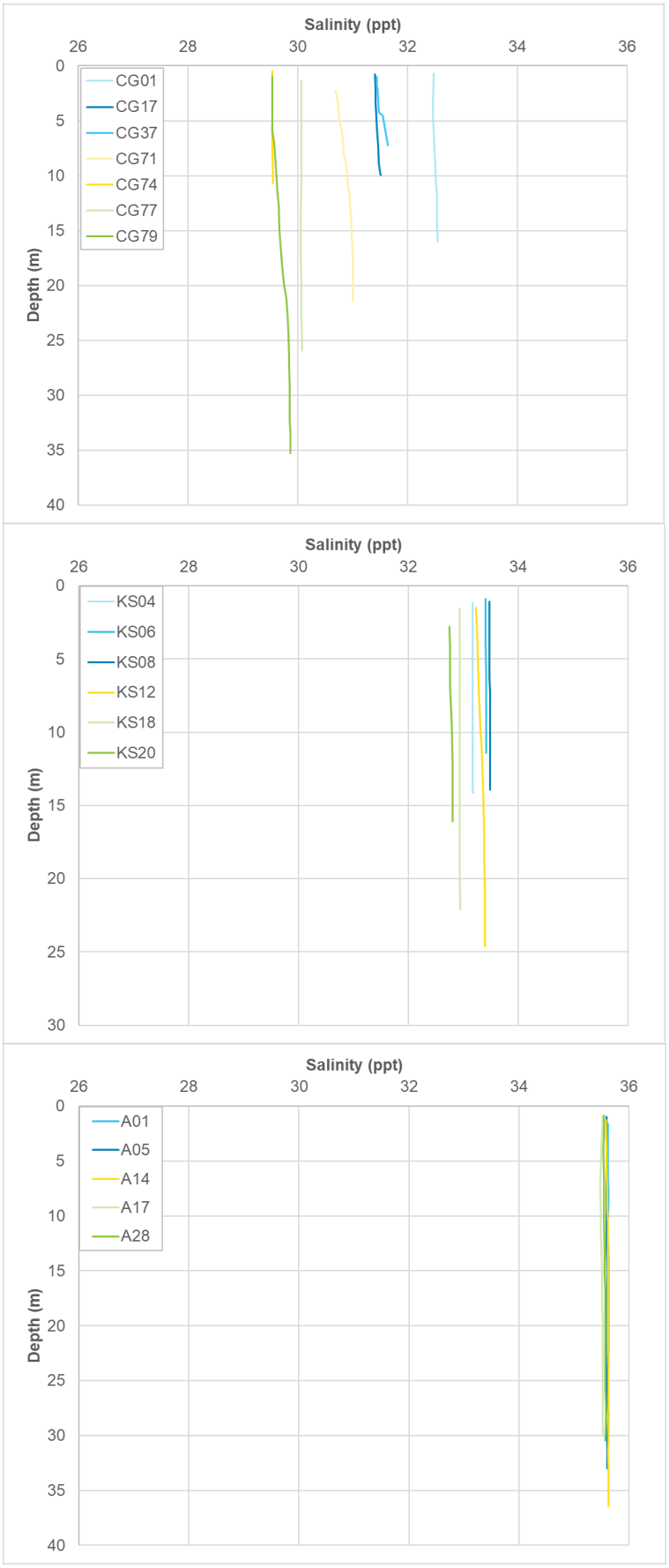

Figure 33. Vertical depth profiles of salinity at sites in CG (top), King Shoals (middle) and offshore (bottom) measured in July-August 2023 (see Figure 10 and Figure 11 for locations) (source: BKA, 2024d).

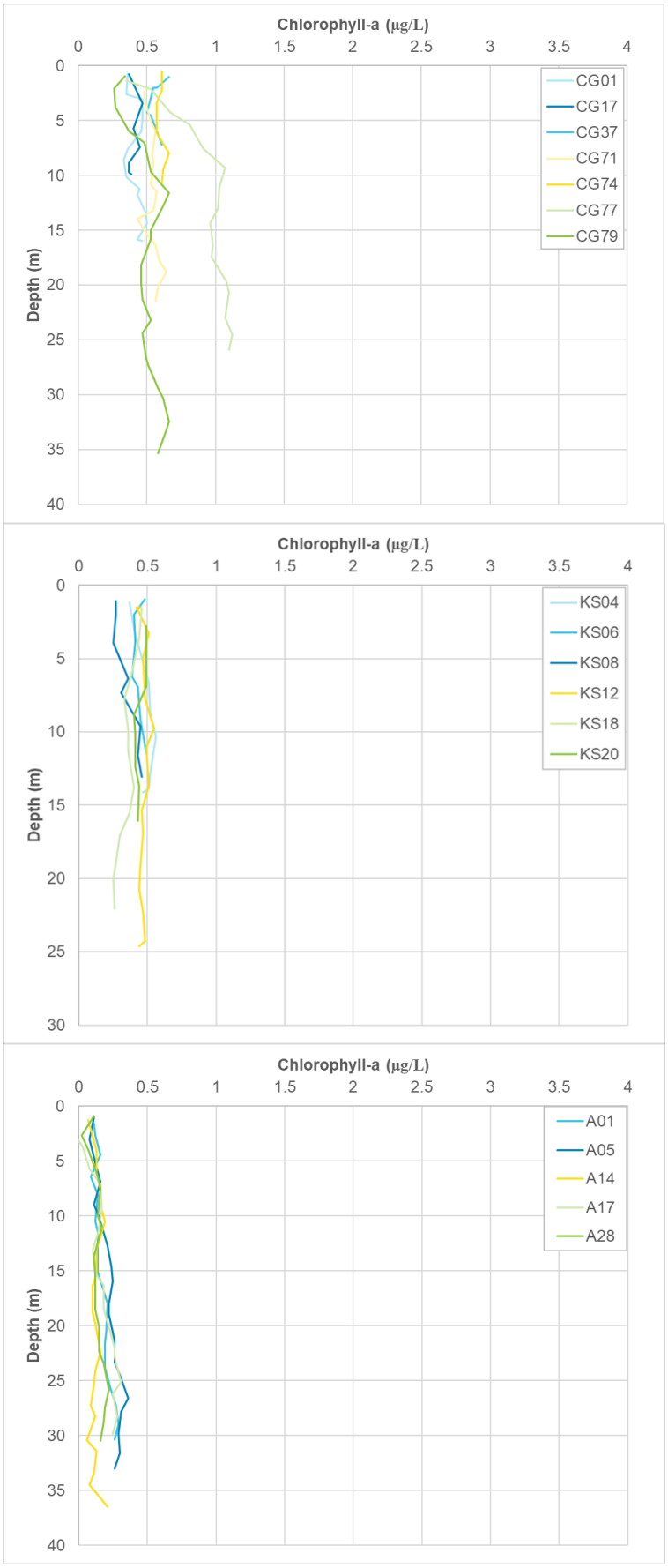

Figure 34. Vertical depth profiles of chlorophyll-a at sites in CG (top), King Shoals (middle) and offshore (bottom) measured in July-August 2023 (see Figure 10 and Figure 11 for locations) (source: BKA, 2024d).

3.7. Sediment Dynamics

The vibro-core samples collected within Block 4 in March 2023 showed that there was some variability in the sediment present on the seabed within Block 4 as well as some variability in the sediment with depth. The sampling showed that the sediment in the western half of Block 4 was predominantly sand sized, although some gravel, silt, clay and rock was also present. The sediment in the eastern half of Block 4 was predominantly clay with some silt also present. In some locations there was some stratification in the upper 5 m of sediment, while in other locations the sediment was all sand. The visual description of the grab sediment samples collected in CG and at King Shoals in July and August 2023 showed the following:

- CG: There were approximately equal samples with predominantly sand and clay present (46% each), with a small number of samples of predominantly rock, gravel or shell grit (8%).
- King Shoals: Samples of predominantly sand were most common (62%), with approximately 14% of the samples being predominantly clay and 25% being predominantly rock, gravel or shell grit.

Based on the sediment samples collected by BKA as outlined above, as well as the benthic grab biota samples and aerial drone imagery collected in July-August 2023 as outlined in section 2.3.1, plus information from the Geoscience Australia Marine Geomorphic Features data layer (Geoscience Australia, 2024), bathymetric chart data and satellite imagery, a map of benthic habitats in CG and at King Shoals was developed (BKA, 2024d) (Figure 35). The figure shows localised areas of predominantly sand present in the region, with the majority of the bed sediment being a mixed substrate (i.e. not predominantly sand).

PSD curves for a selection of the vibro-core sediment samples which cover the range of sediment present within Block 4 are shown in Figure 36. It is important to note that the samples which were selected for PSD analysis from the vibro-cores, were those where the sediment was visually observed as predominantly sand, as the sampling was specifically undertaken to assess the potential sand resource in Block 4. As expected, the curves show that the sediment is predominantly made up of sand sized particles, although some samples also had up to 55% gravel and up to 35% silt and clay present. The D50 (median particle size) of the samples shown ranged from 80 to 800 μm, with an average of 300 to 400 μm. The results do not show any specific pattern in PSD with depth, with some locations having coarser sediment at the surface and finer sediment below and other locations the opposite. Based on the vibro-core sediment sampling an internal Boskalis assessment was undertaken which estimated that there was 150 to 300 million m^3 of sand present in the proposed operational area (BKA, 2024b). This calculation is based on the maximum depth of the vibro-cores which was approximately 5 m.

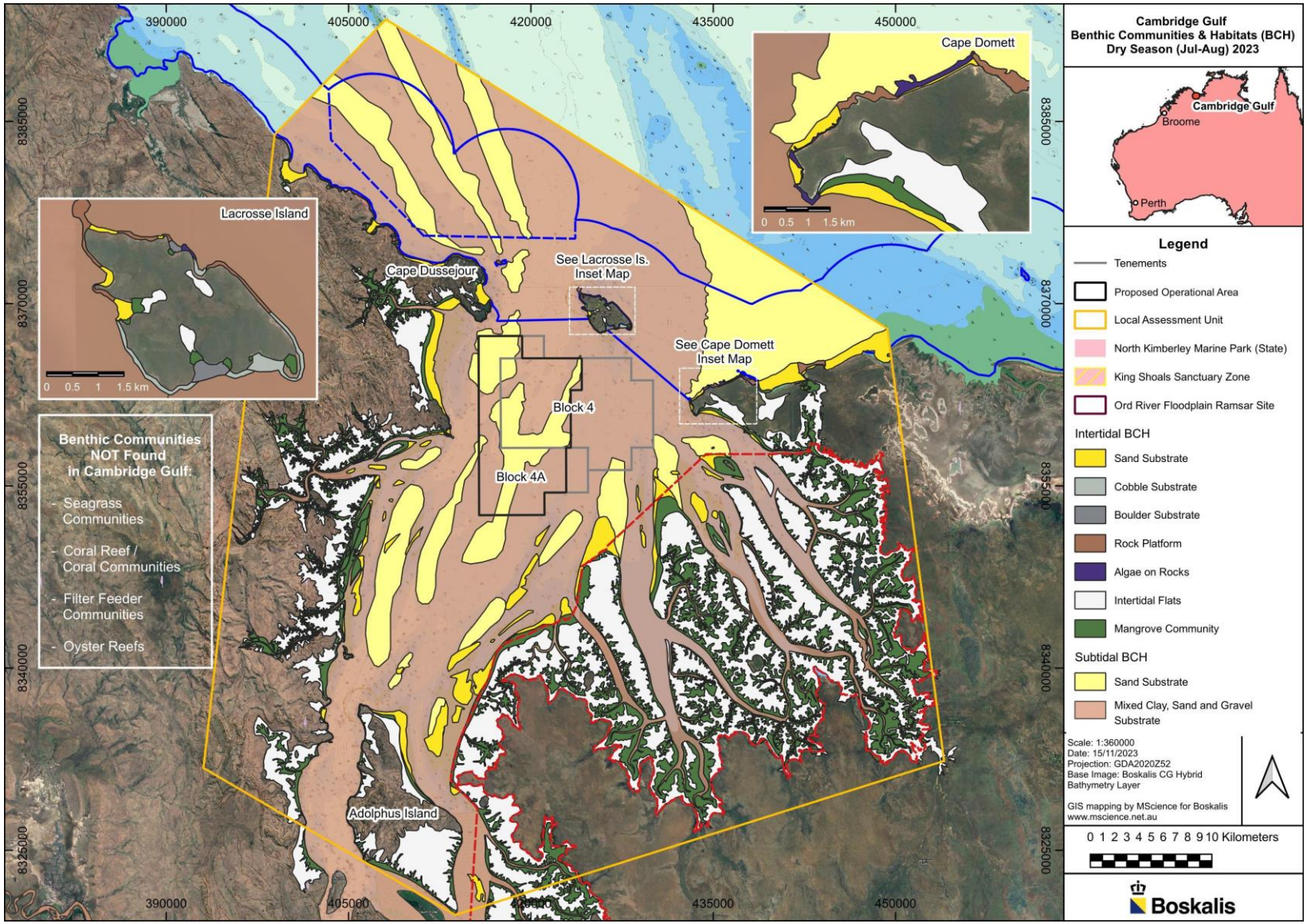

Figure 35. Benthic habitats and communities in the CG region based on the dry season (Jul-Aug 2023) environmental survey (source: BKA, 2024d).

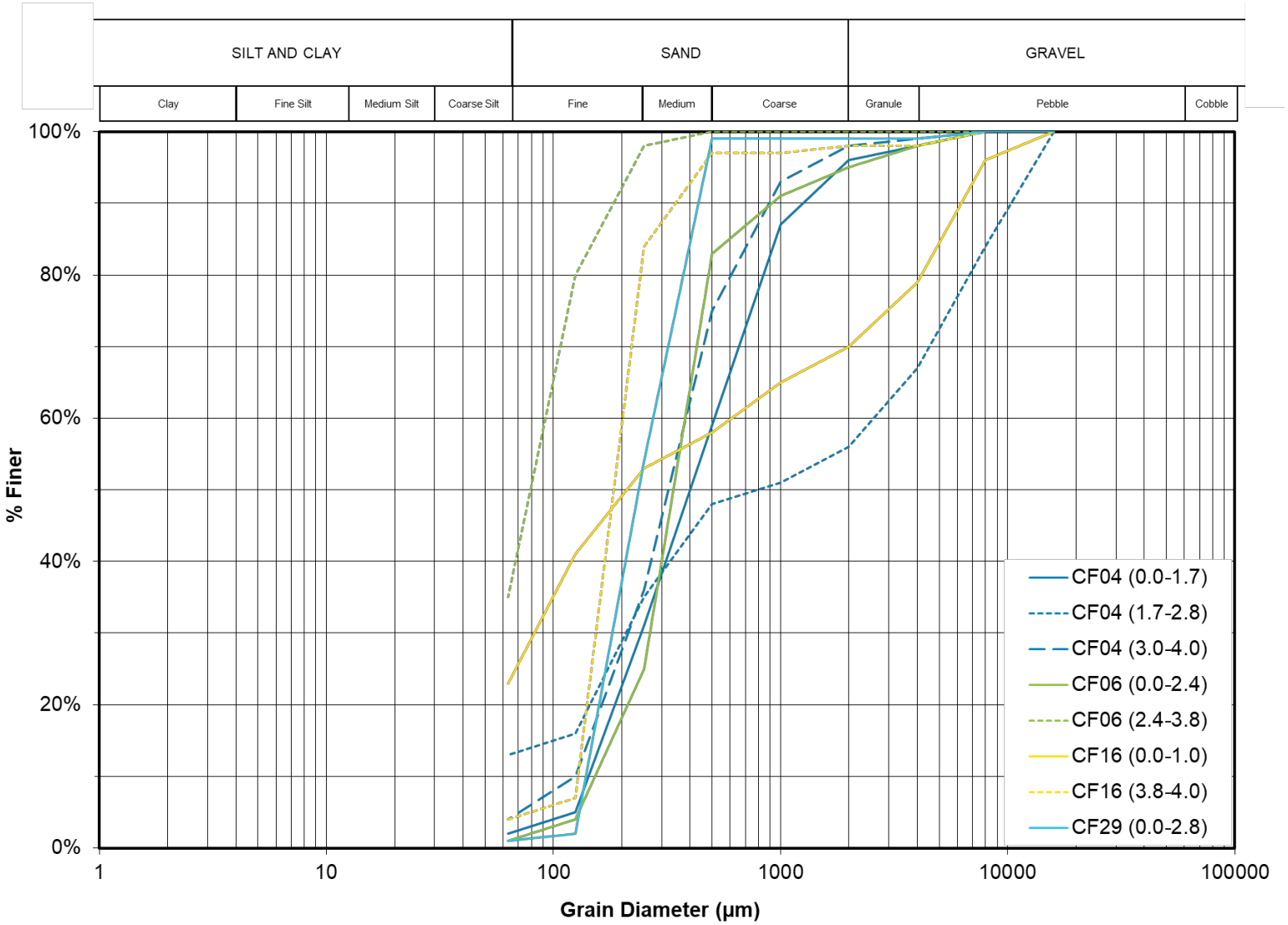

Figure 36. PSDs of predominantly sandy samples collected using vibro-cores from Block 4 in March 2023 (source: BKA, 2024d).

As outlined in section 2.3.1, BKA sampled SSC vertical profiles through the water column at multiple sites within CG, at King Shoals and offshore, in July-August 2023. To show how the SSC varies spatially within these regions, the SSC profiles are shown for selected sites which represent the range of values within the three regions in Figure 37. It is important to note that the time of the profiles relative to the tide varies between the sites and so the exact same metocean conditions are not occurring for each profile. However, despite this limitation, the profiles can still be used to provide an overview of how SSC varies through the water column and spatially within CG, at King Shoals and offshore. A summary of the measured SSC data from all the profiles in each area is provided in Table 4.

Within CG the SSC profiles show significant spatial variability, with the lowest SSC measured at the western (CG01) and eastern (CG37) entrances to CG. The SSC increases in an upstream direction, with the highest SSC measured at the entrance to East Arm (CG77). Close to the downstream entrances to CG, the profiles show a relatively consistent SSC through the water column, with a slight increase in SSC with depth. Further upstream in CG, there is more variation in SSC through the water column, with the SSC close to the bed being almost three times higher than the SSC near the surface at the entrance to West Arm (CG79).

The SSC at the King Shoals sites is broadly similar to the sites in CG close to the entrance, with the SSC remaining below 25 mg/L at all depths. However, two of the sites at King Shoals show that the SSC at the bed is more than double the SSC at the surface, potentially indicating that the distribution of SSC through the water column could be different between the sites. This difference could also be related to different metocean conditions occurring at the time the profiles were collected.

The SSC at the offshore sites is consistently low, with an SSC of less than 1 mg/L at all sites. The data also show very little variation with depth, with consistently low SSC throughout the water column at all the sites.

Based on the measurements undertaken in July-August 2023, the mid-depth average SSC in CG was around 51 mg/L, at King Shoals it was 11 mg/L and at the offshore sites it was 0.3 mg/L. The standard deviation of 47 mg/L shows that there was a significant variation in SSC between the sites in the CG, while at King Shoals the variation was relatively small (standard deviation of 3.8 mg/L) and at the offshore sites there was very little variability between the sites (standard deviation of 0.2 mg/L).

Table 4. Results of the dry season (July-August 2023) YSI turbidity measurements in Cambridge Gulf, King Shoals and Offshore waters (based on mid-water-depth measurements) (source: BKA, 2024d).

Statistic	Cambridge Gulf	King Shoals	Offshore Waters
SSC (mg/L)			
Mean	50.6	11.4	0.3
Minimum	4.9	6.9	0.0
Maximum	197.3	22.2	0.8
Mode	N/A	12.9	0.3
Median	37.1	10.7	0.3
Standard Deviation	46.5	3.8	0.2
Standard Error	6.4	0.9	0.1
Number of Sites	52	20	28

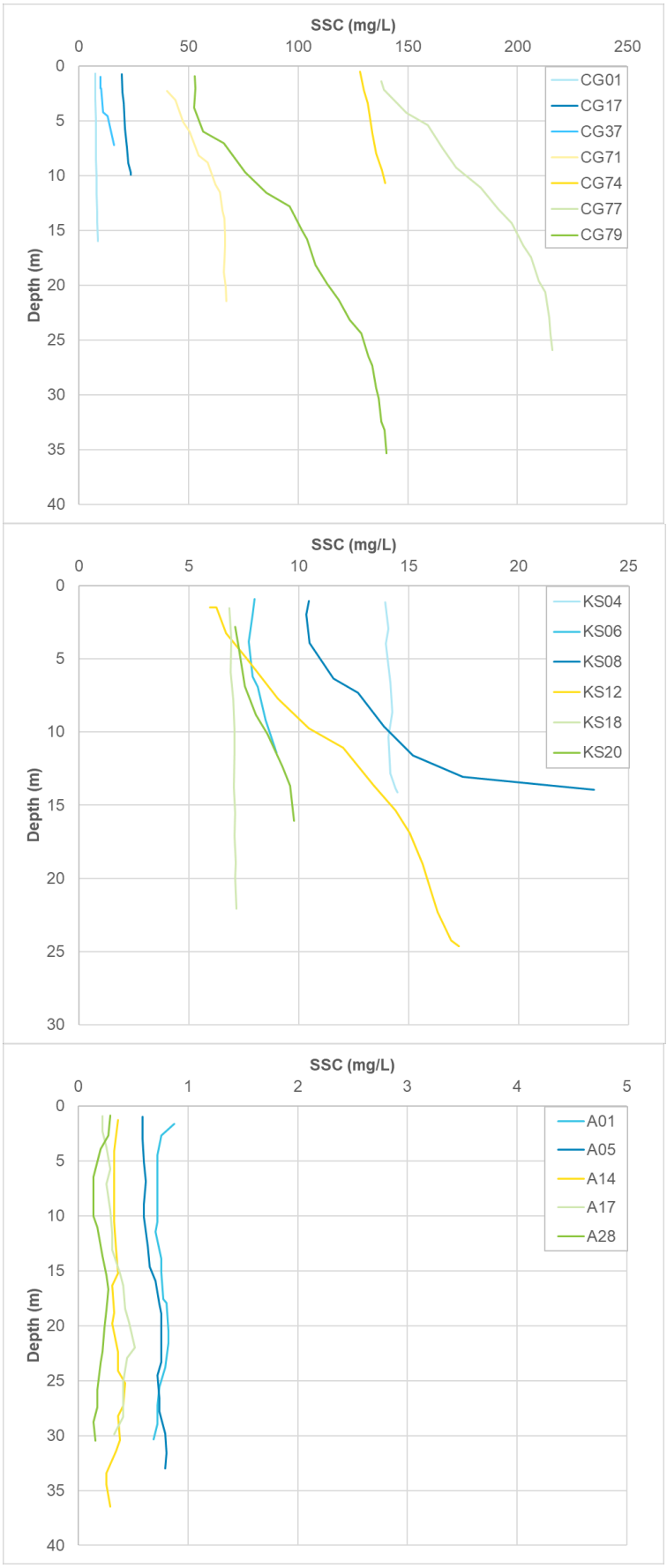

Figure 37. Vertical depth profiles of SSC at sites in the CG (top), King Shoals (middle) and offshore (bottom) measured in July-August 2023 (see Figure 10 and Figure 11 for locations) (source: BKA, 2024d).

In-situ measured SSC data were collected by AIMS (AIMS, 2007) in CG at three depths through the water column during dry season conditions in 2000 and during wet season conditions in 2002. The locations of the sites where they collected data were different between the two campaigns, although AIMS 3 and AIMS D are in approximately the same location, while AIMS 2 is located approximately 6.5 km to the north of AIMS C. Timeseries plots of the SSC through the water column and water level at each site, are shown in Figure 38 and Figure 39 for the dry season conditions in 2000 and in Figure 40 and Figure 41 for the wet season conditions in 2002. The plots show the following:

- There is a general trend of increasing SSC in an upstream direction, with lower SSC in the open bay area of CG and higher SSC in West and East Arms. The peaks in SSC range from around 75 mg/L at AIMS B to approximately 5,000 mg/L in West and East Arms. The data show a significant reduction in SSC between West (AIMS E) and East Arms (AIMS 4 & 5) and where they connect to the south of Adolphus Island (AIMS D & AIMS 3). This reduction was also observed by Robson et al. (2008), with their monitoring showing that the turbidity in the Ord River adjacent to Adolphus Island was typically less than 200 NTU, while the turbidity further upstream in the Ord River estuary was significantly higher. The maximum SSC was observed in the Ord River where the salinity was 5 ppt. In this area, strong tidal currents occurred and the salinity was high enough for flocculation to also occur (Robson et al., 2008).

- Close to the entrance to CG, the SSC at the seabed can be around double the SSC close to the surface, while at the southern end of the open bay area of CG and in East and West Arms, there is limited variation in SSC with depth.

- At all sites except for the two upstream sites in East Arm (AIMS 4 and AIMS 5) the SSC peaks around low water, while the lowest values in SSC occur around high water. This indicates that the peaks in SSC in these areas are due to the transport of sediment suspended upstream of the sites, while the lower SSC around high water is a result of lower SSC from offshore flooding into CG. In East Arm, the peaks in SSC occurred on the flood stage of the tide and then reduced over time until low water, suggesting that the SSC was being imported from downstream.

- There is a clear tidal signal in the sites located within the open bay area of CG, with higher SSC during spring tides and lower SSC during neap tides. This spring neap tidal signal is also present at the upstream site in West Arm and it is assumed that it is also present in East Arm, although the duration of available data (less than three days) is insufficient to show this.

- At all of the sites located in the open bay area of CG (i.e. AIMS A to C and AIMS 1 and 2) there is a delay in the timing of the peak in SSC relative to the tidal range, with the highest SSC occurring a day or two after the largest tide. In addition, the SSC remains elevated relative to the tidal range following spring tides and into the neap tides. The lag in the SSC relative to the tidal curve indicates that much of the sediment in suspension is fine-grained silt and clay which remains in suspension for the majority of the larger tidal ranges (i.e. except for the neaps) and for a day or two once the tidal current speeds have reduced sufficiently to allow deposition to occur.

- Comparison between nearby sites where both wet and dry season data were collected, indicates that at the confluence of West and East Arms (AIMS 3 and AIMS D) the pattern in SSC was similar for the wet and dry season, as were the magnitudes for the majority of the time, but much higher peaks in SSC occurred during the wet season (peaks of around 2,000 mg/L in the wet season compared to peaks of around1,000 mg/L in the dry season). At the southern end of the open bay area of CG (towards Adolphus Island) the data show similar patterns in SSC both over time and through the water column for the wet and dry season, but with the wet season SSC being approximately 50% higher.

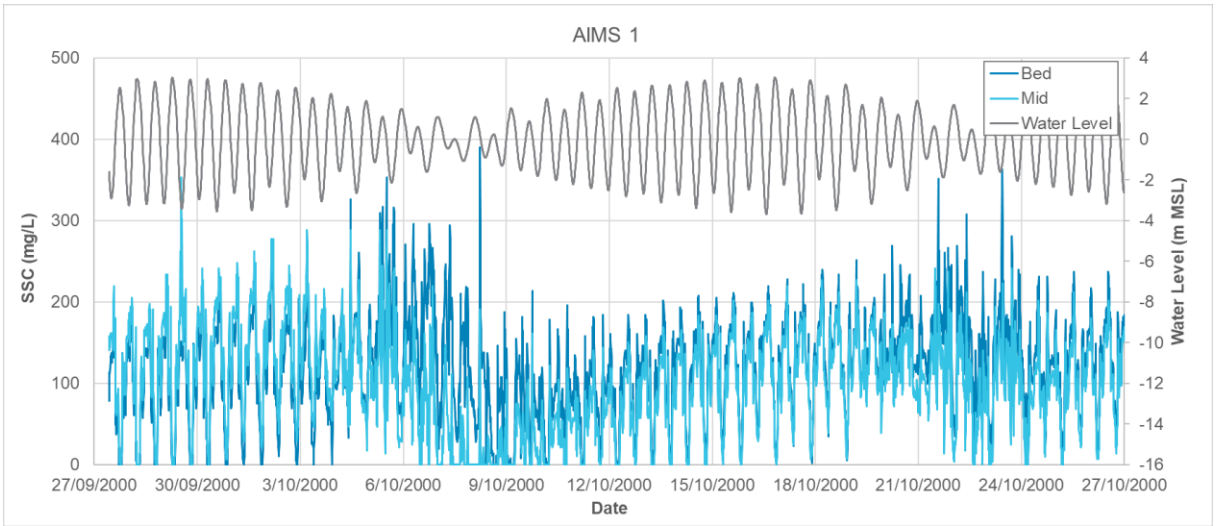

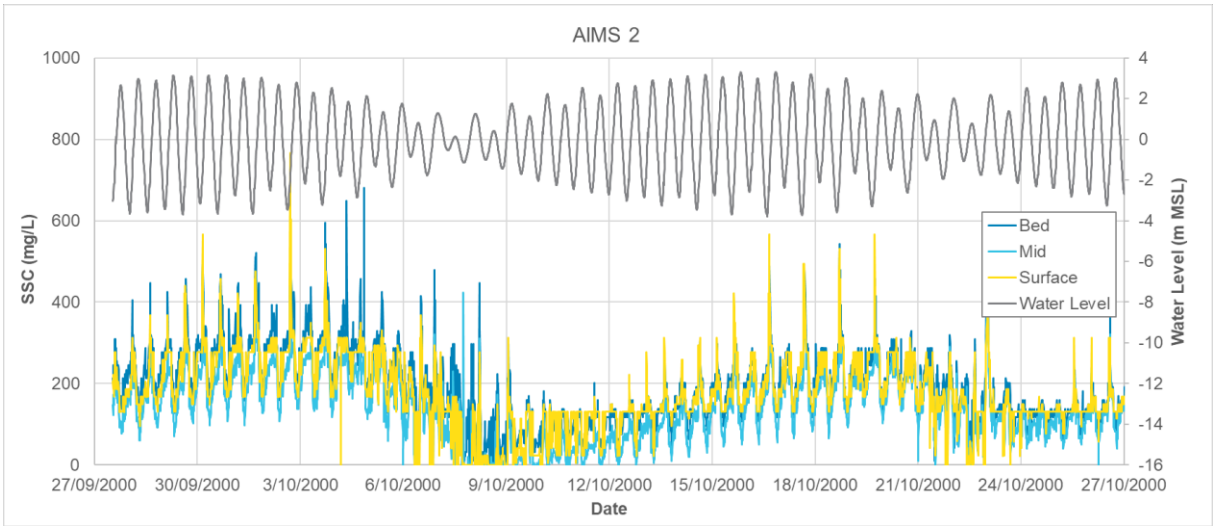

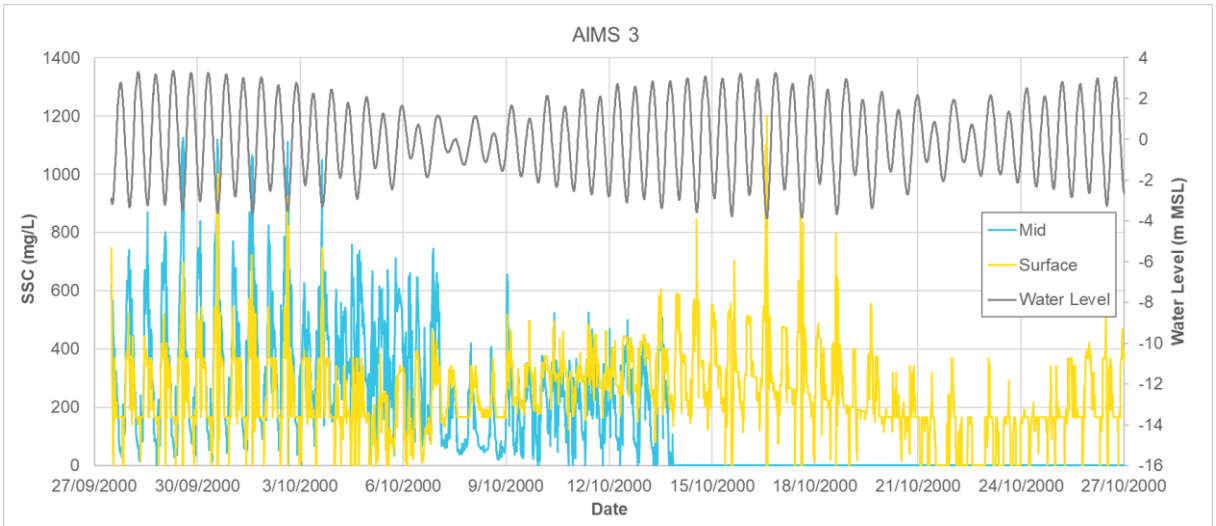

Figure 38. Measured water levels and SSC at sites AIMS 1 to AIMS 3 in the 2000 dry season (source: AIMS, 2007).

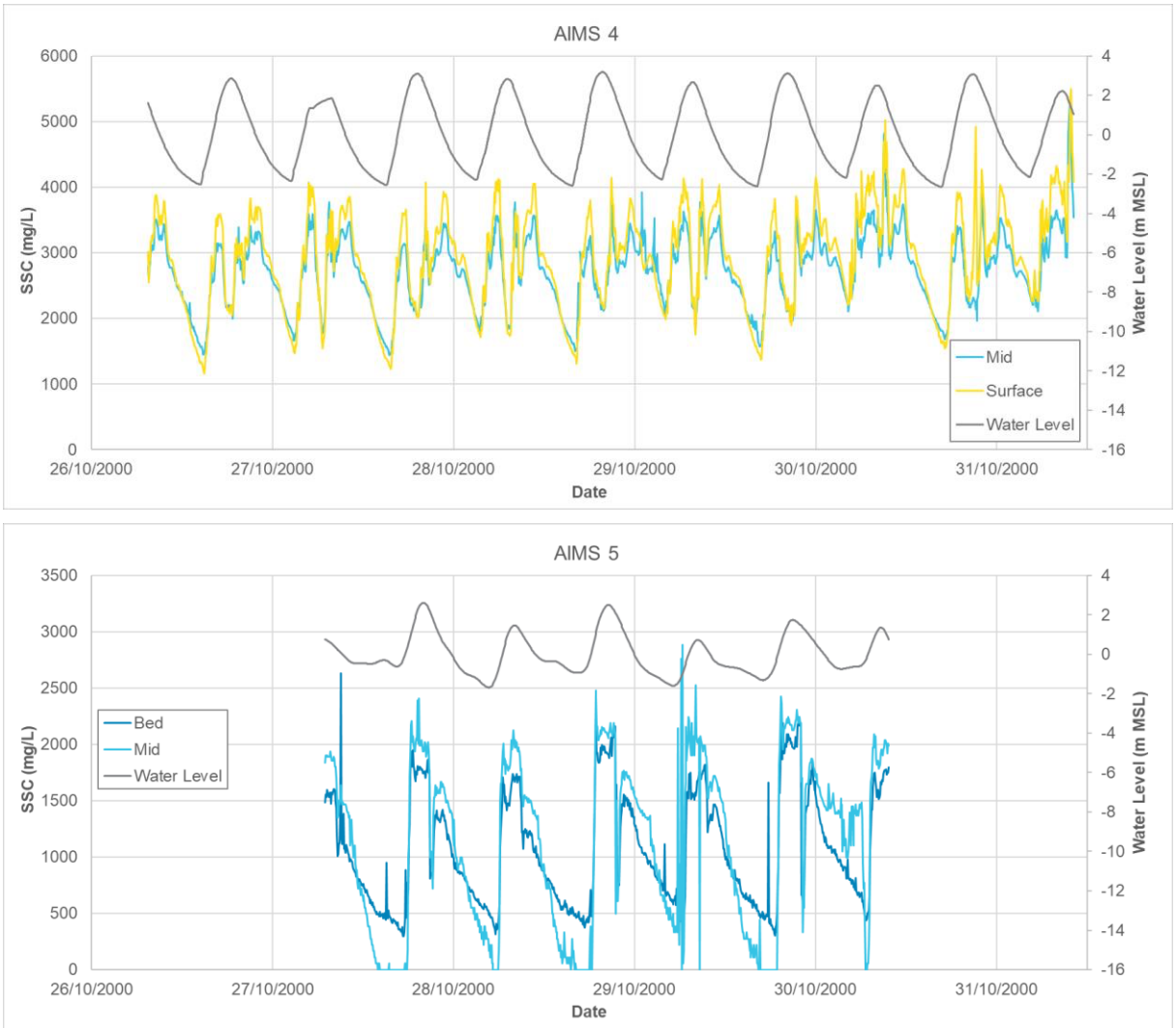

Figure 39. Measured water levels and SSC at sites AIMS 4 and AIMS 5 in the 2000 dry season (source: AIMS, 2007).

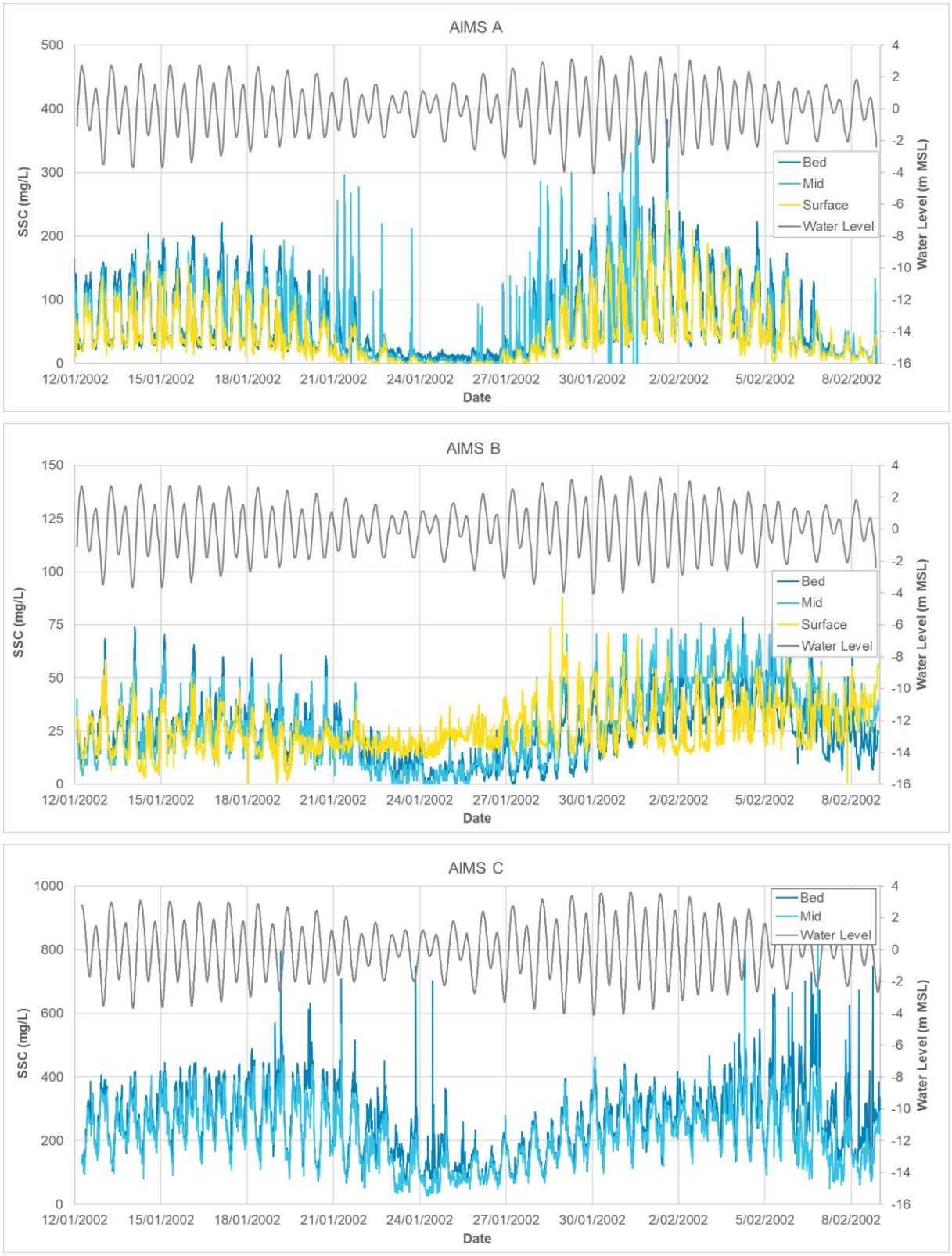

Figure 40. Measured water levels and SSC at sites AIMS A to AIMS C in the 2002 wet season (source: AIMS, 2007).

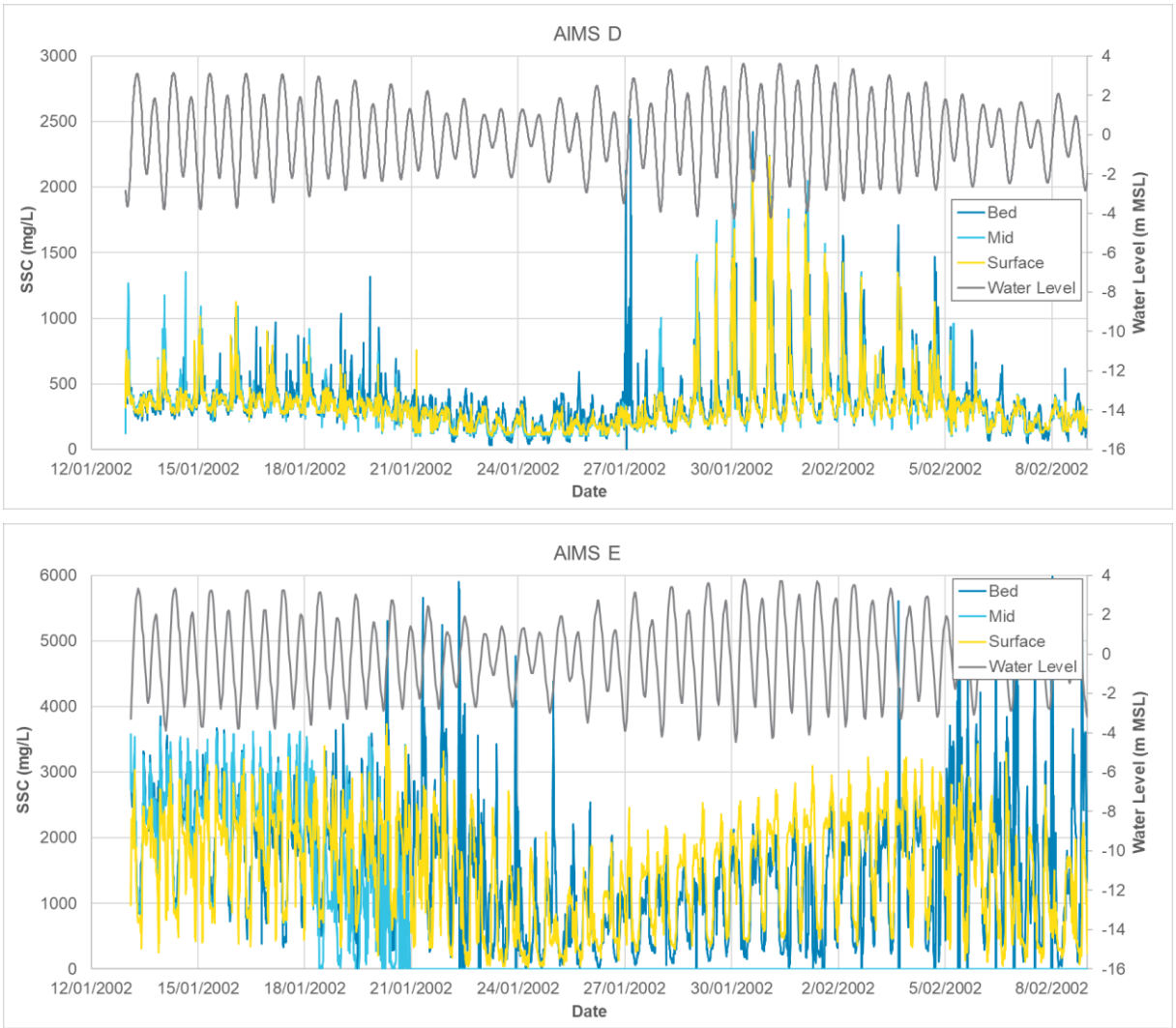

Figure 41. Measured water levels and SSC at sites AIMS D and AIMS E in the 2002 wet season (source: AIMS, 2007).

To better understand the spatial variability in SSC in the CG region and how this is affected by the metocean conditions, satellite imagery was sourced from Copernicus (2023) and processed by PCS to provide satellite-derived SSC spatial maps. In addition, metocean conditions prior to and at the time the images were captured are also presented to provide additional context to the images. Plots are presented for the following range of conditions:

- Dry Season, spring and neap tides (Figure 42 to Figure 44): The plots show a significant difference in SSC between the spring and neap tides. For the spring tide, the SSC offshore of CG is up to 50 mg/L in the shallower areas and typically less than 10 mg/L in the deeper areas, while within CG SSC is 10 to 25 mg/L in the open bay area and 25 to 50 mg/L in East and West Arms and in shallow areas around mangroves and saltpans. For the neap tide, the SSC offshore is less than 10 mg/L for the entire area to the west of Lacrosse Island, while to the east of Lacrosse Island, values of more than 50 mg/L occur along the shoreline and in the shallow nearshore regions. Within CG during the neap tide, the majority of the open bay area, SSC is less than 10 mg/L, around the mangroves is 5 to 15 mg/L and East and West Arms range from 10 to >50 mg/L.

- End of Wet Season, spring and neap tides (Figure 45 to Figure 47): Comparison between these plots and the plots during spring and neap tides in the dry season can be used to infer potential differences in SSC in the region between the two seasons. The wet season spring and neap tide plots show much higher SSC than the dry season plots, with an SSC of 25 to >50 mg/L within CG and offshore to a distance of around 20 km. During the wet season neap tide, there are some localised areas around Blocks 4 and 4A in CG with an SSC of 10 to 15 mg/L, but the majority of the SSC in this area is still more than 25 mg/L.

- Dry Season, flood and ebb stage of tide (Figure 48 to Figure 50): These plots help to show how the SSC in the region varies depending on the stage of the tide. The images shown are for similar small spring tides with relatively calm metocean conditions, but with one image captured close to low water (i.e. at the end of the ebb stage of the tide) and one image captured close to high water (i.e. at the end of the flood stage of the tide). The image captured at low water shows SSC of 25 to 50 mg/L extending offshore from the west entrance to CG along King Shoals, while the image captured at high water shows an SSC of 5 to 15 mg/L for the majority of this area, although high SSC of 25 to >50 mg/L still occurs over the shallow offshore features. Within CG, the majority of the area has an SSC of 25 to >50 mg/L at low water, while at high water the open bay area has an SSC of predominantly less than 15 mg/L, although East and West Arms are still predominantly >50 mg/L and the shallow mangrove areas are also 15 to 50 mg/L. The significant difference between the flood and ebb images is due to low SSC water from offshore of CG flowing in on the flood stage of the tide, while high SSC from upstream drains into CG on the ebb stage of the tide.

- Wet Season, end of a wave event (Figure 51 and Figure 52): Wave events occurred 16 days and 6 days prior to the satellite image being captured. This was the closest high resolution satellite image which could be sourced to a wave event (these events are typically associated with high cloud cover) but it is likely that the SSC shown by the image will be lower than it was at the peak of the wave events. Comparison between this plot and the end of wet season spring tide plot (Figure 46) shows that the wave events resulted in higher SSC extending further offshore into the JBG (although this is likely to be lower than during the peak of the wave event). The image shows that the SSC within CG is not noticeably higher due to the wave events, but this could be a result of the time between the peak in the wave events and when the image was captured (i.e. the SSC in CG has returned to normal conditions over the 6 days following the second wave event).

- Wet Season, period of high rainfall (Figure 53 and Figure 54): Comparison between this plot and the end of wet season spring tide plot (Figure 46) shows that overall the SSC is fairly similar between the two. The high rainfall does appear to result in higher SSC in the mangroves to the south-east of Blocks 4 and 4A, indicating that the increased discharge has resulted in localised resuspension of sediment from the exposed mudflats and saltpan areas which drain into the channels adjacent to the mangroves. The SSC in West and East Arms is high (25 to >50 mg/L), but comparable to other wet season spring conditions. The SSC directly offshore of CG is higher than during wet season spring conditions, with an SSC of more than 25 mg/L extending approximately 40 km offshore of the entrance (around 20 km for wet season spring).

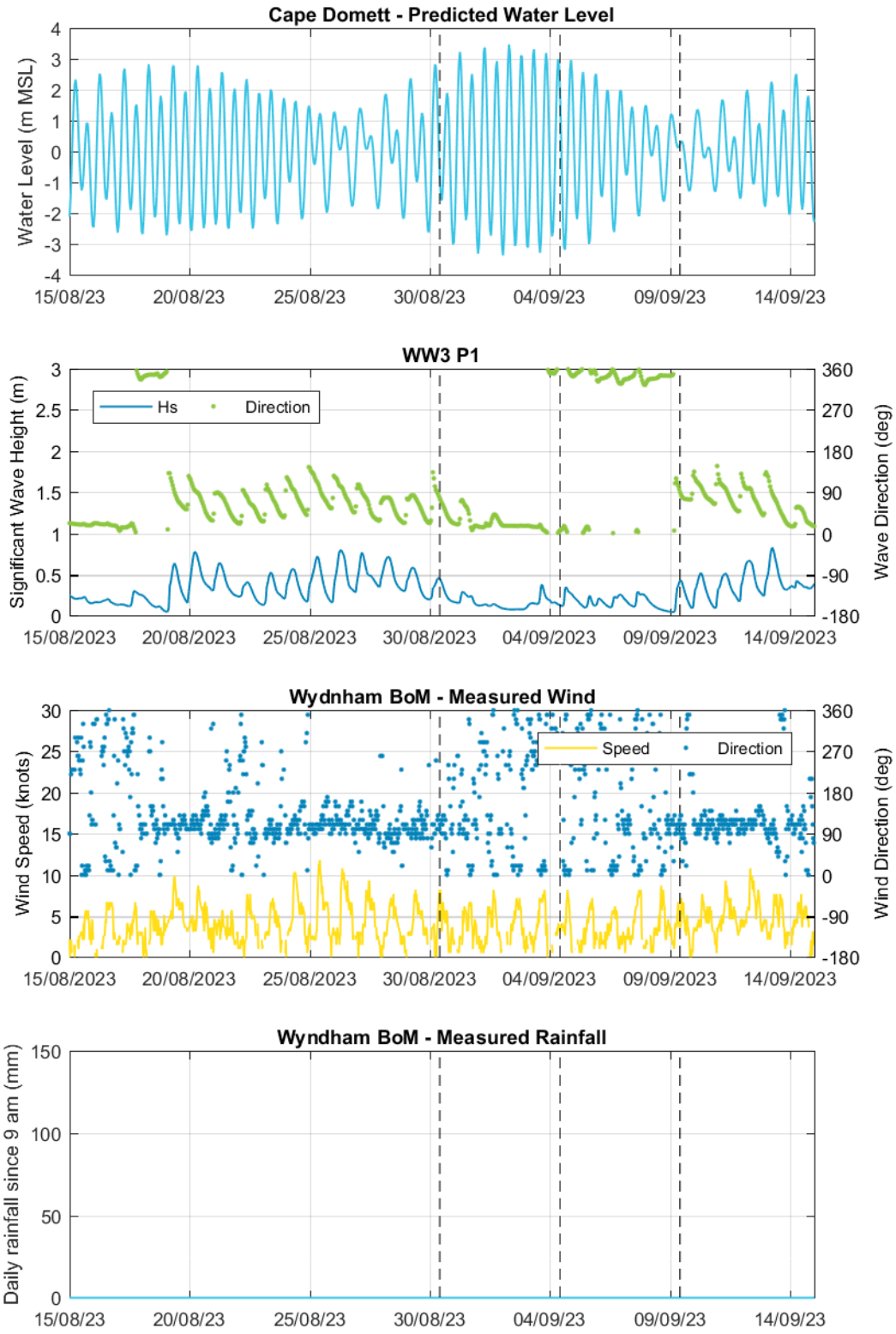

Figure 42. **Metocean conditions in the 2023 dry season for a period when Sentinel 2 images have been processed (times of images shown by dashed lines) (sources: BoM, AHO, CSIRO).**

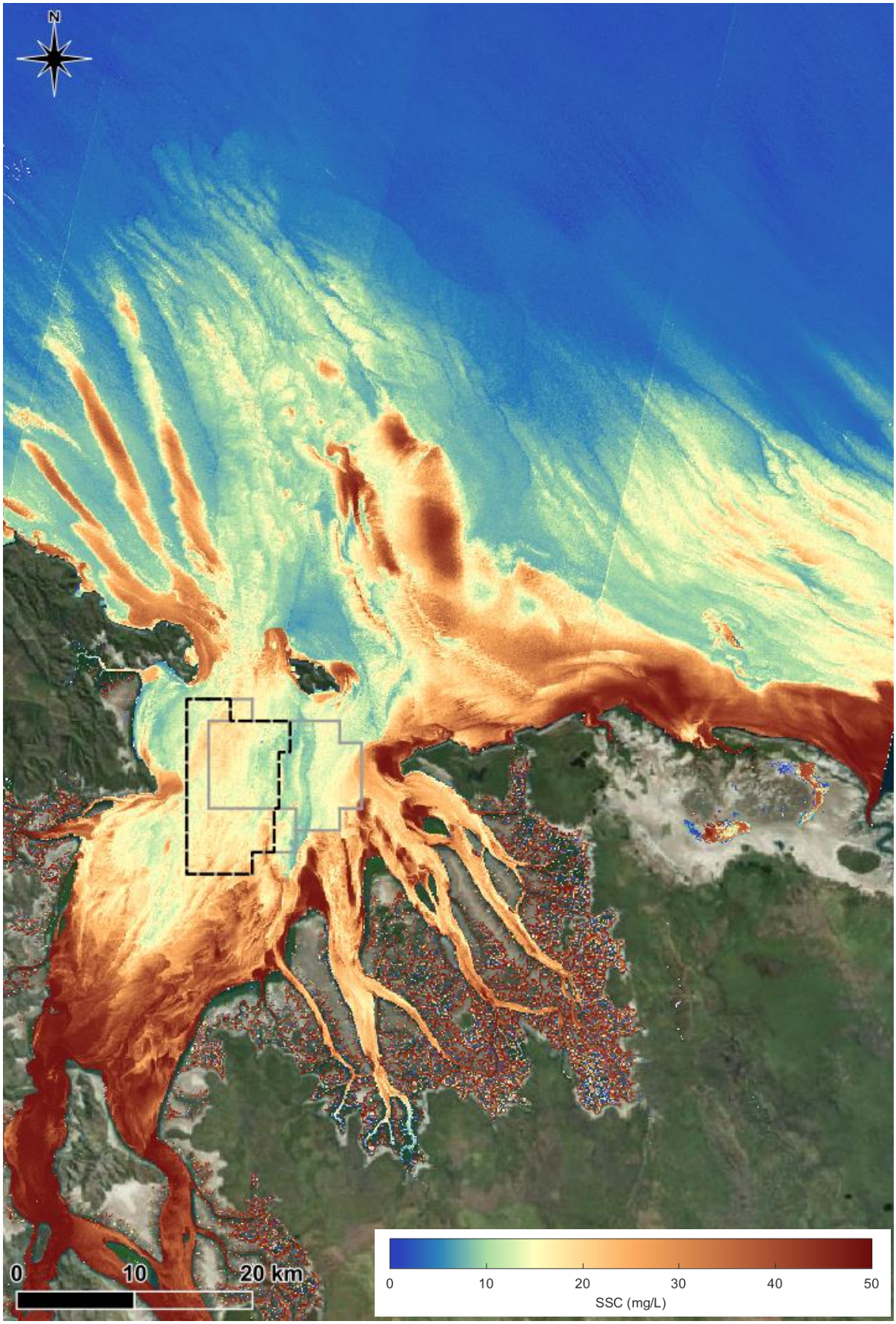

Figure 43. Satellite-derived TSM for Sentinel 2 image captured on 04/09/2023 at spring tidal conditions during the dry season.

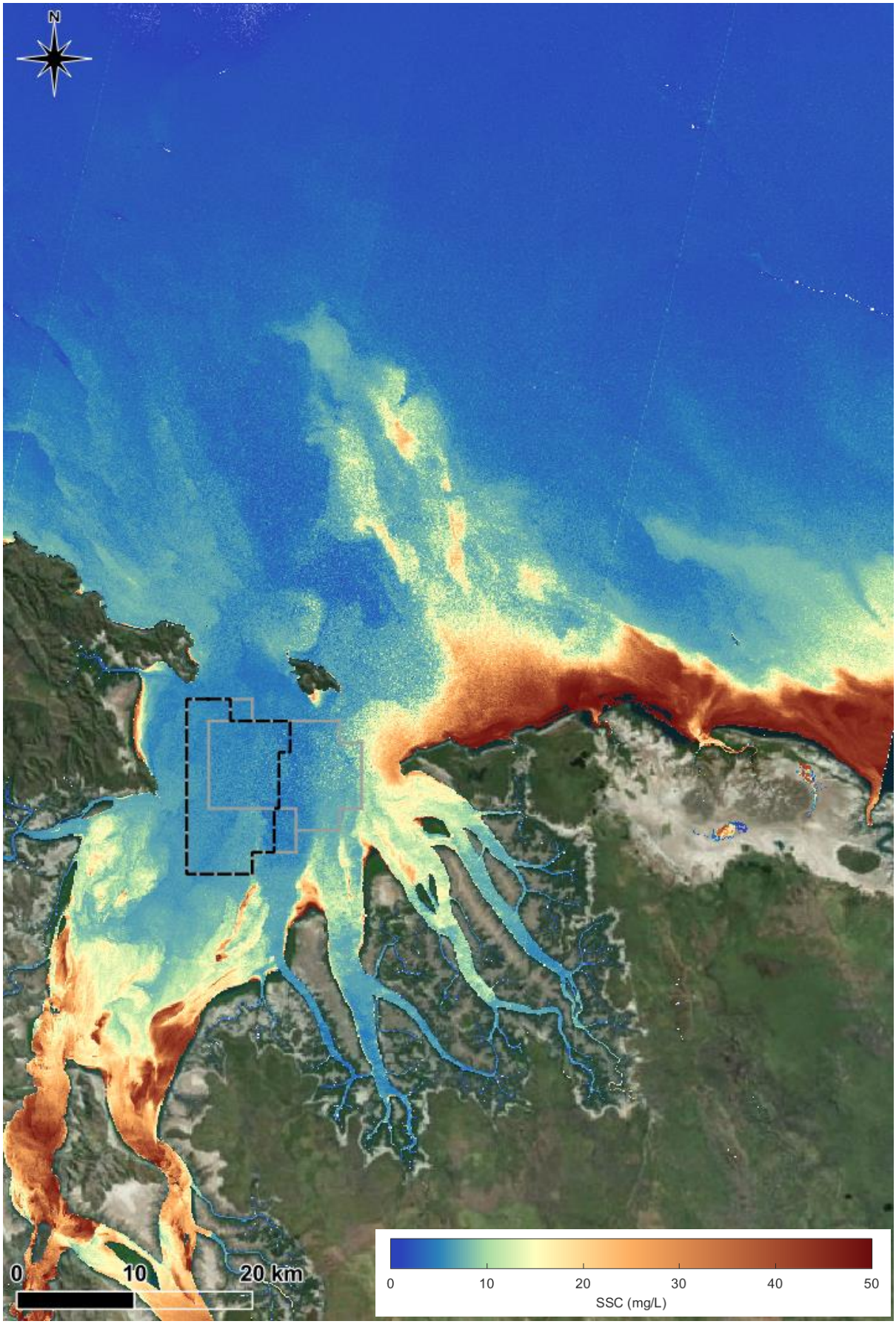

Figure 44. Satellite-derived TSM for Sentinel 2 image captured on 09/09/2023 at neap tidal conditions during the dry season.

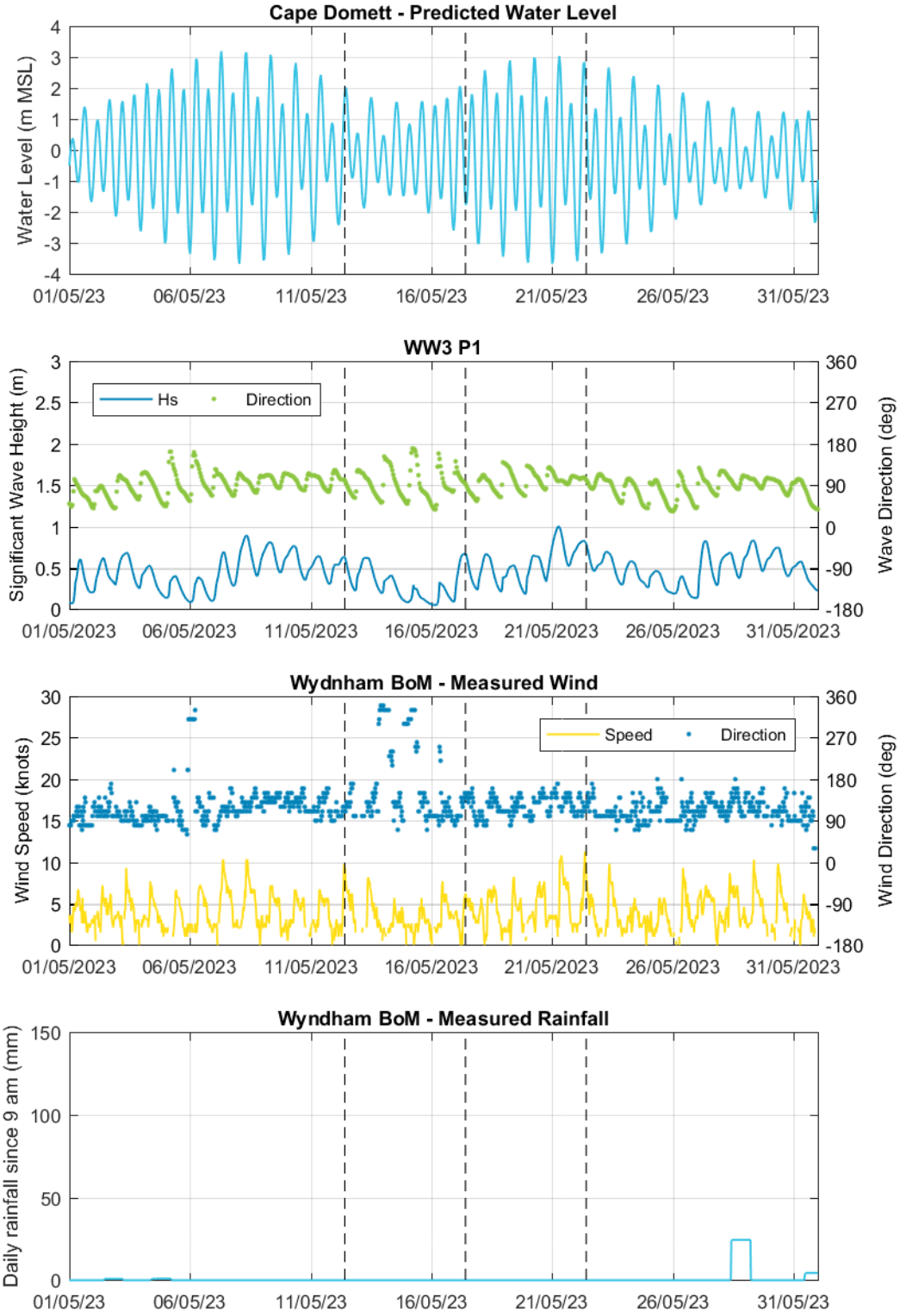

Figure 45. **Metocean conditions at the end of the 2023 wet season for a period when Sentinel 2 images have been processed (times of images shown by dashed lines) (sources: BoM, AHO, CSIRO).**

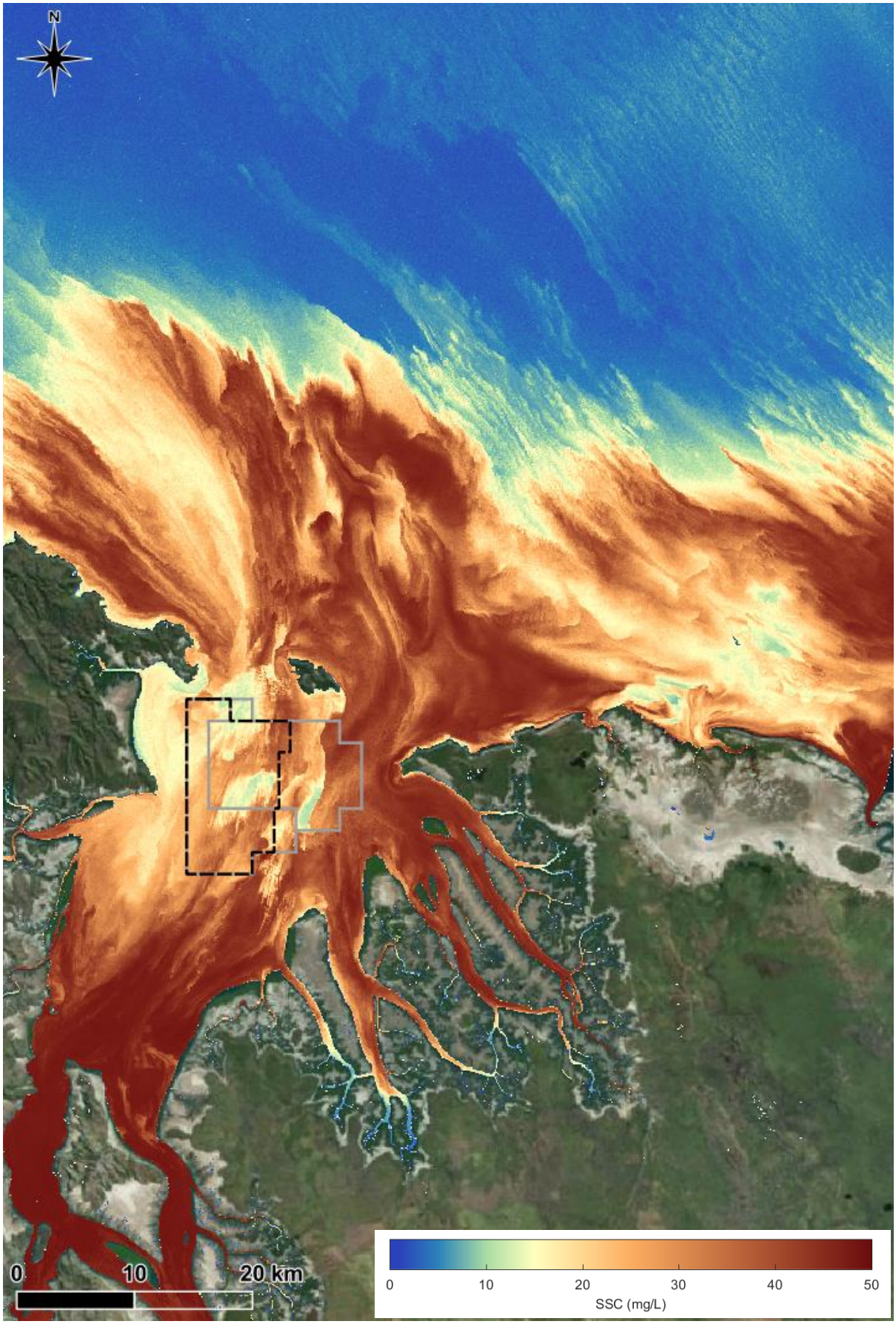

Figure 46. Satellite-derived TSM for Sentinel 2 image captured on 12/05/2023 at neap tidal conditions just after the end of the wet season.

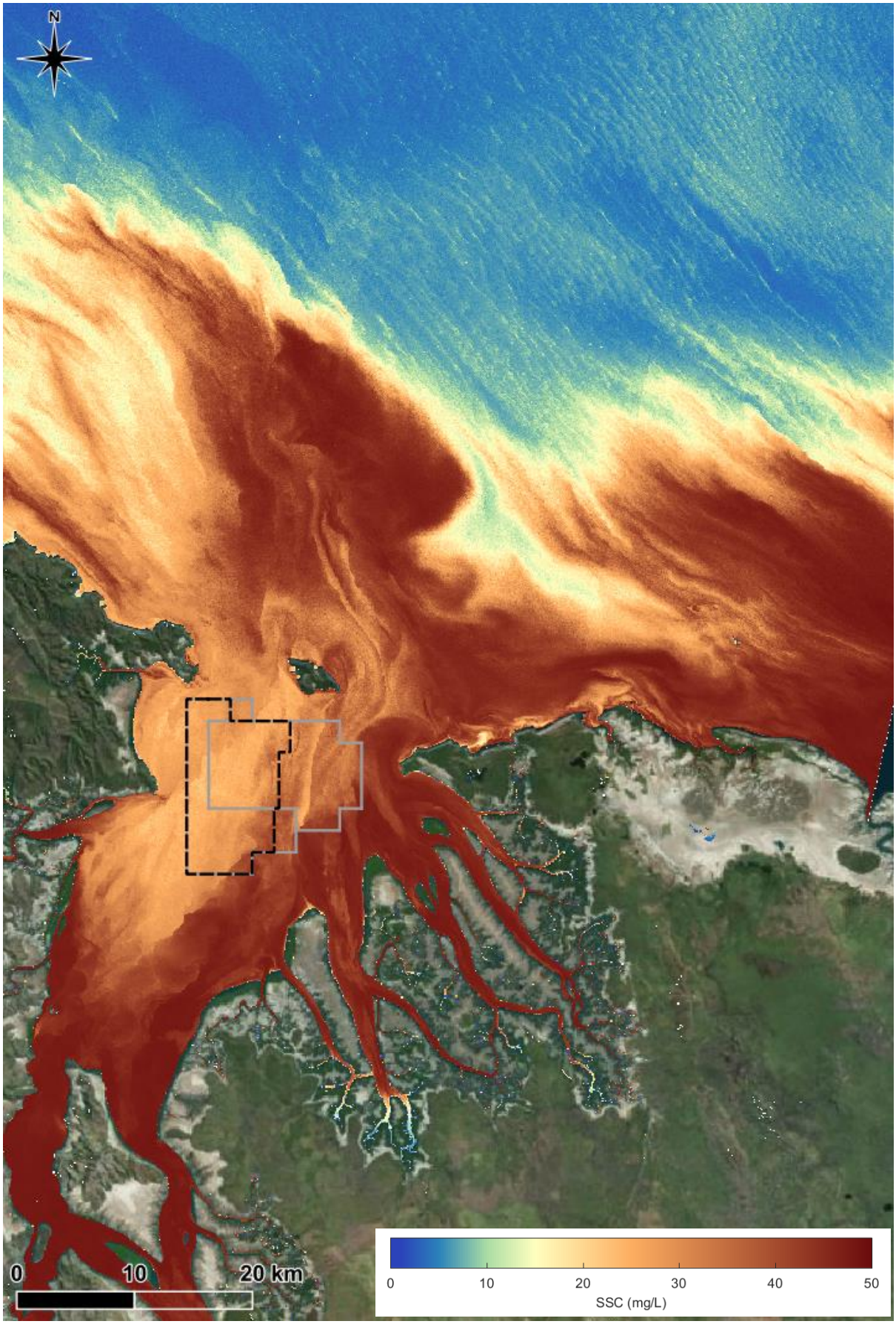

Figure 47. Satellite-derived TSM for Sentinel 2 image captured on 22/05/2023 at spring tidal conditions just after the end of the wet season with an H_s of 0.8 m and a 10 knot easterly wind.

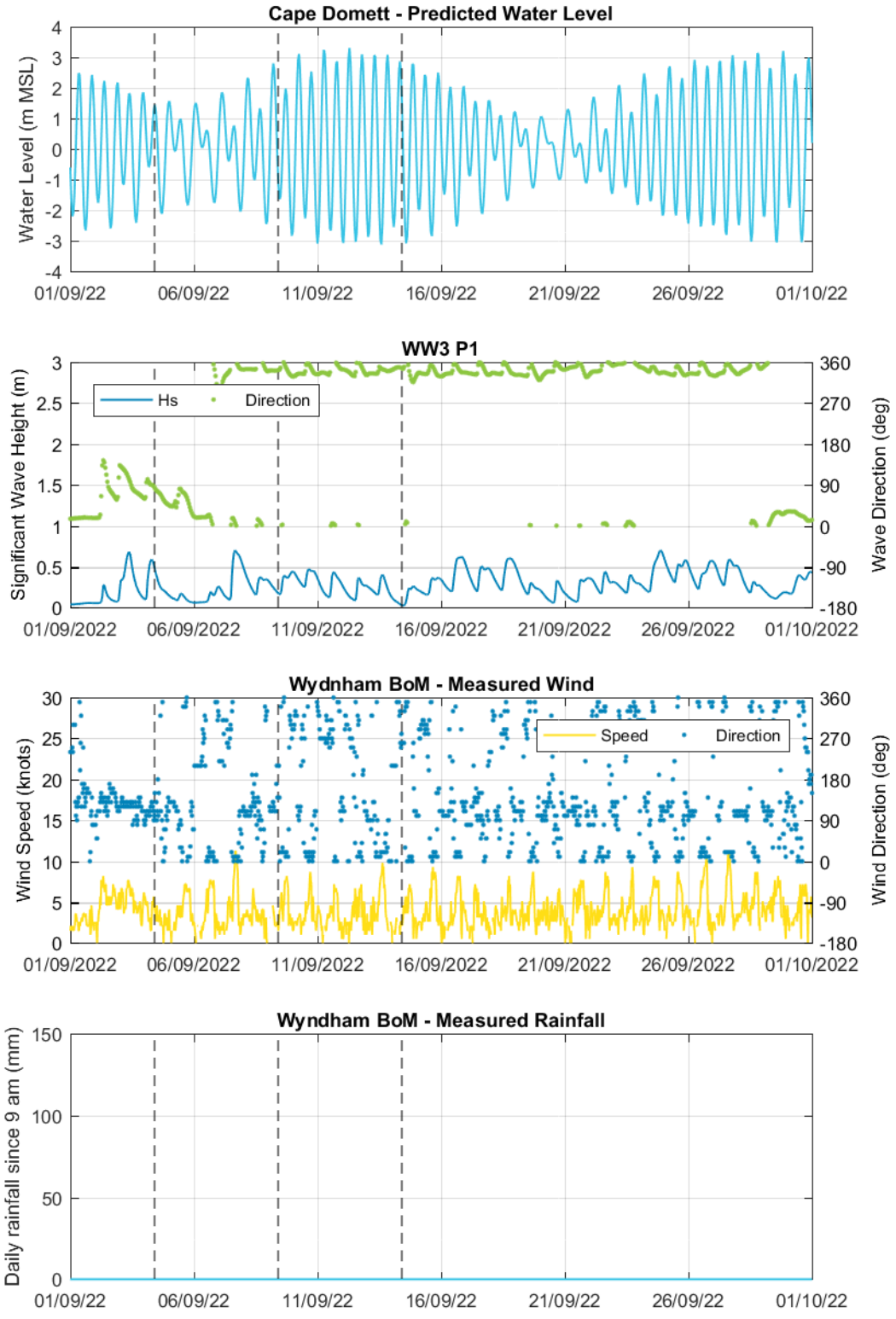

Figure 48. **Metocean conditions in the 2022 dry season for a period when Sentinel 2 images have been processed (times of images shown by dashed lines) (sources: BoM, AHO, CSIRO).**

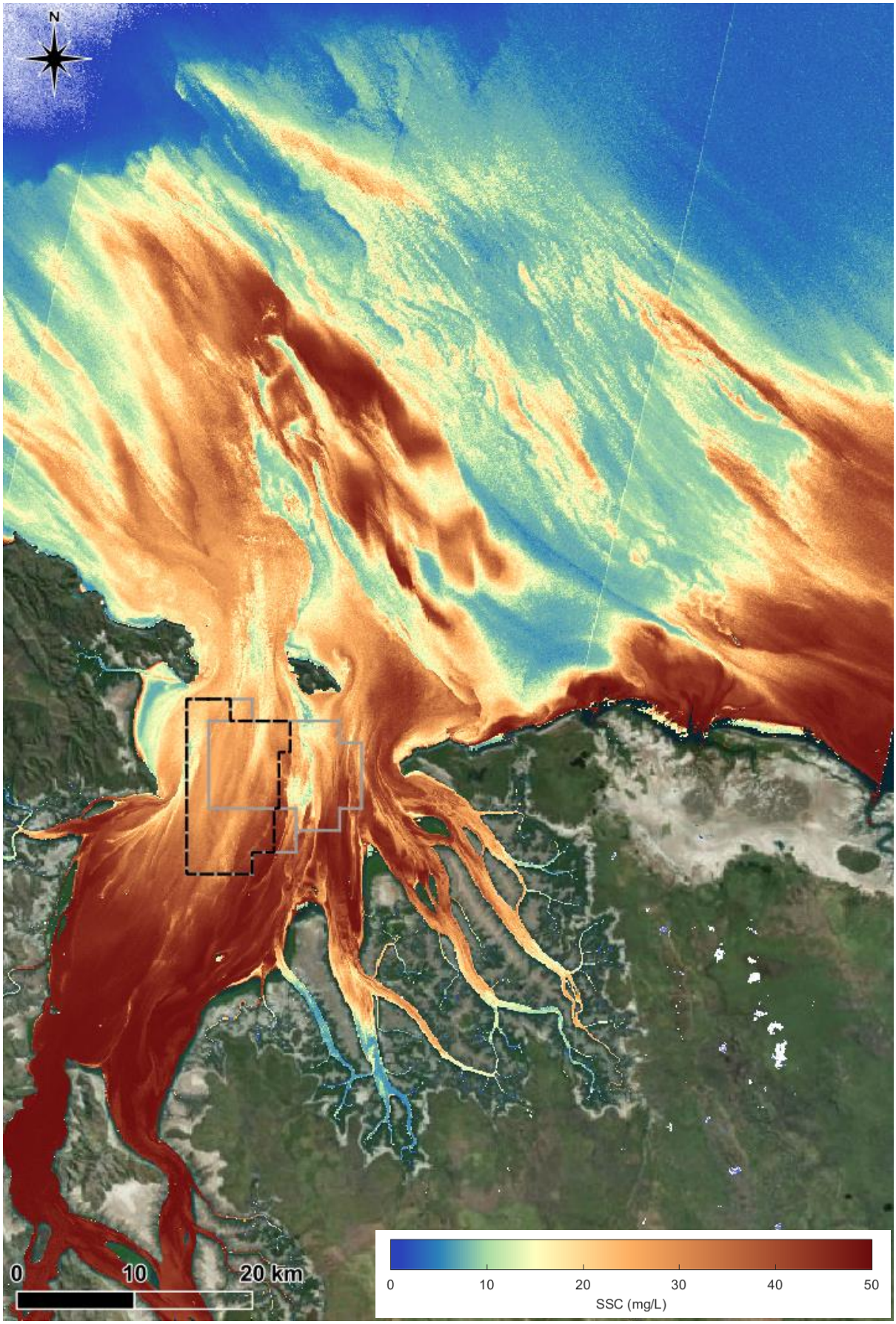

Figure 49. Satellite-derived TSM for Sentinel 2 image captured on 09/09/2022 during a small spring tide in the dry season at the end of the ebb stage of the tide (i.e. at low water).

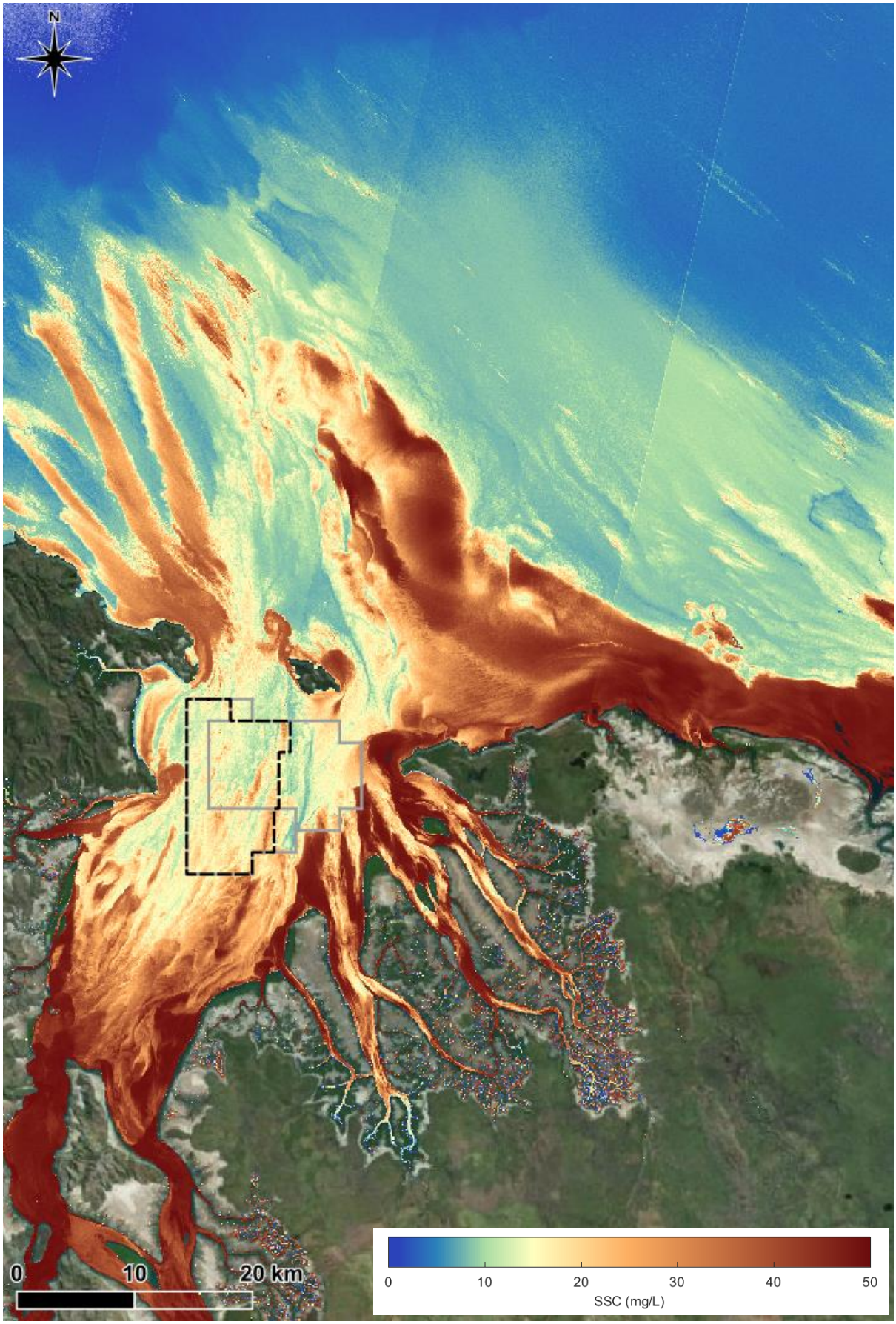

Figure 50. Satellite-derived TSM for Sentinel 2 image captured on 14/09/2022 during a small spring tide in the dry season at the end of the flood stage of the tide (i.e. at high water).

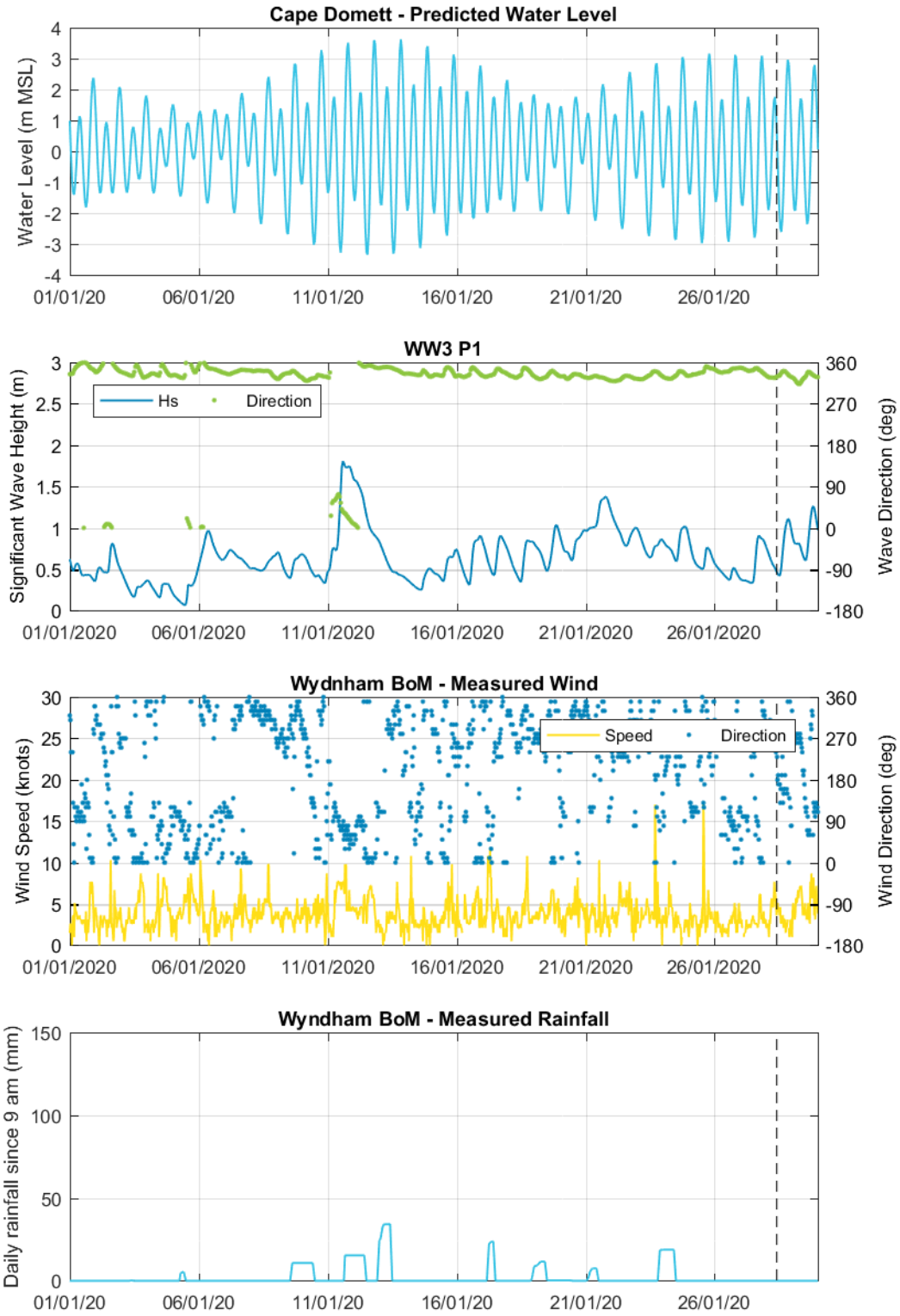

Figure 51. **Metocean conditions in the 2019 wet season for a period when Sentinel 2 images have been processed (times of images shown by dashed lines) (sources: BoM, AHO, CSIRO).**

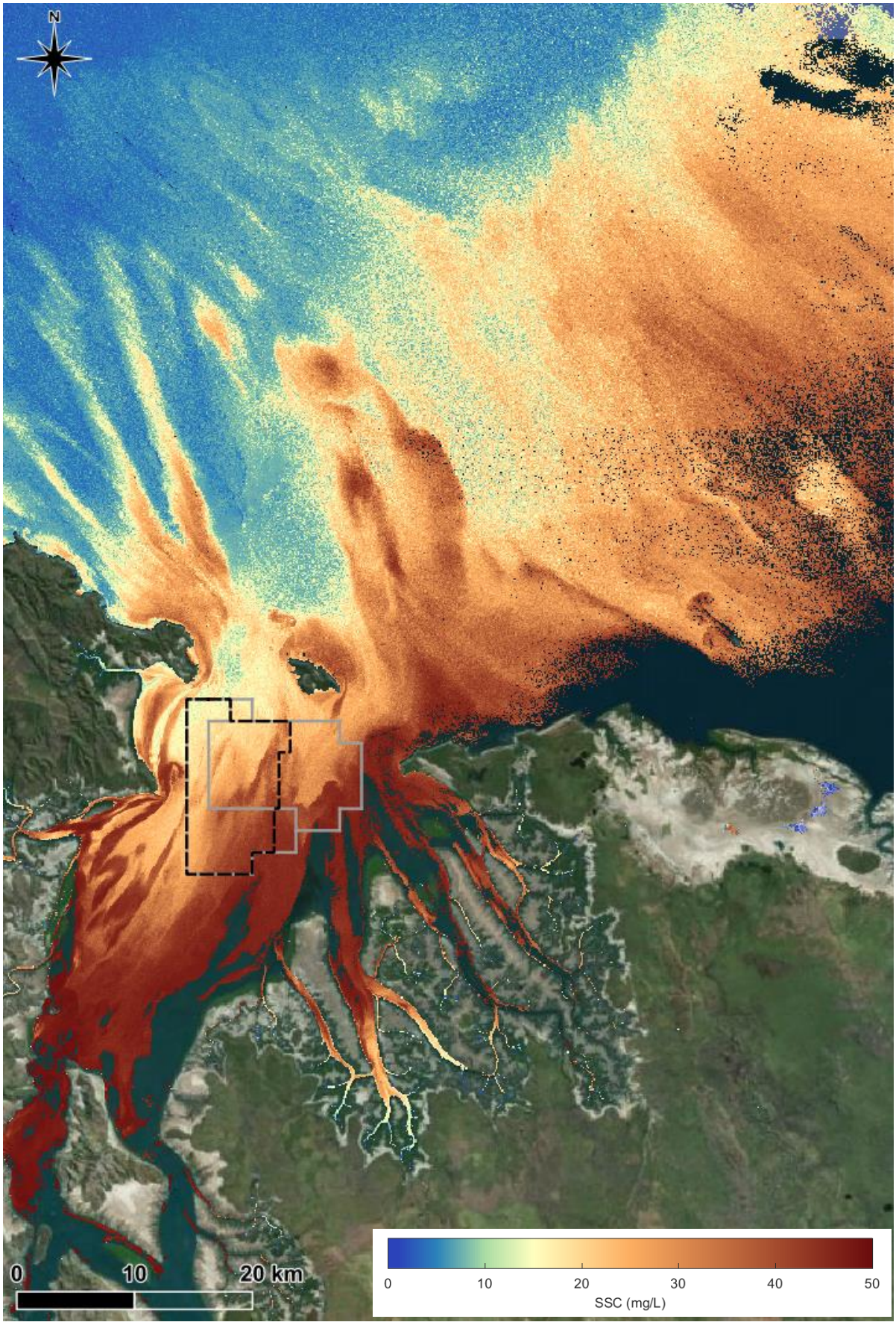

Figure 52. **Satellite-derived TSM for Sentinel 2 image captured on 28/01/2020 during a spring tide during the wet season at the end of a period of above average wave heights (from the north north-west).**

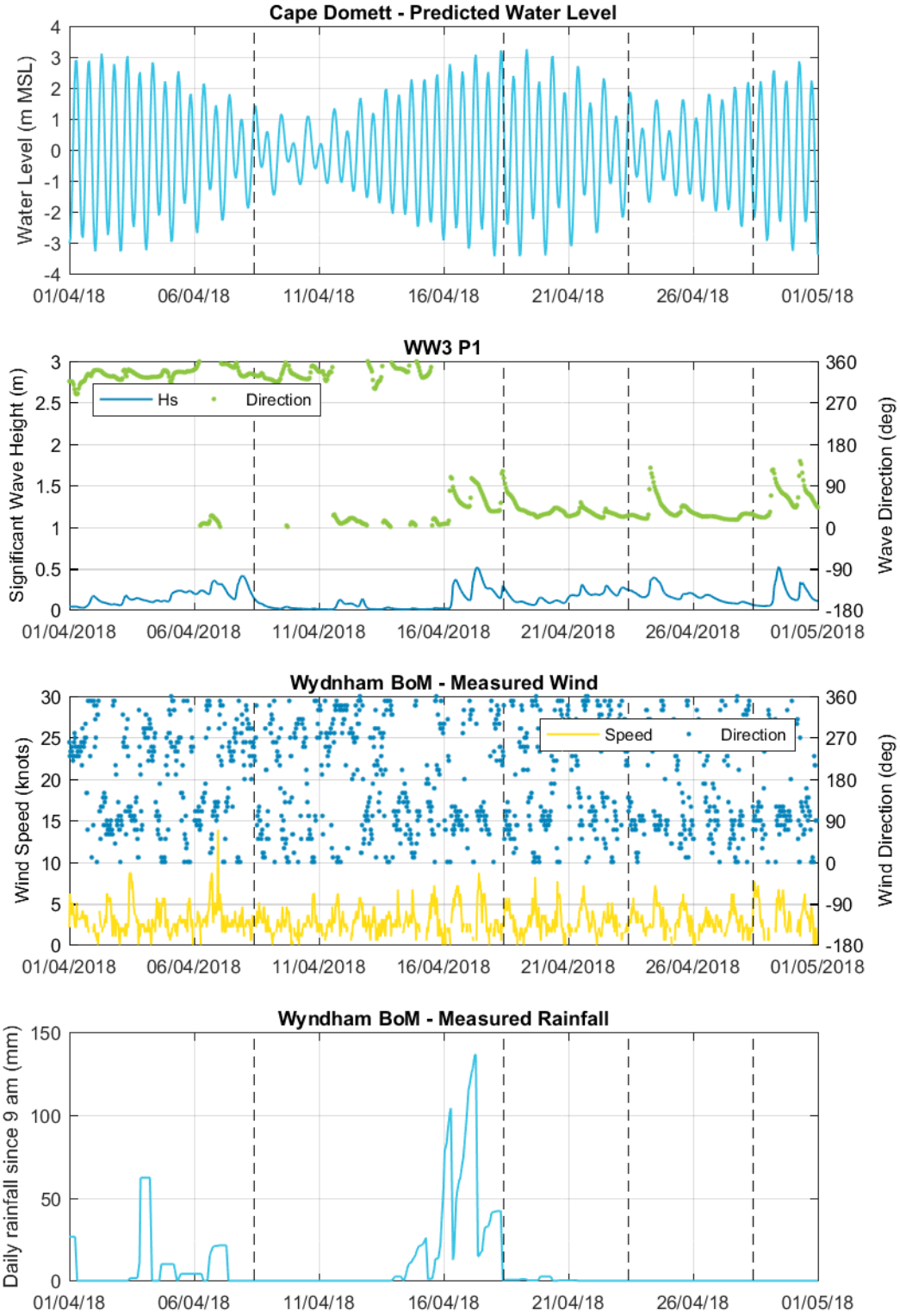

Figure 53. **Metocean conditions at the end of the 2018 wet season for a period when Sentinel 2 images have been processed (times of images shown by dashed lines) (sources: BoM, AHO, CSIRO).**

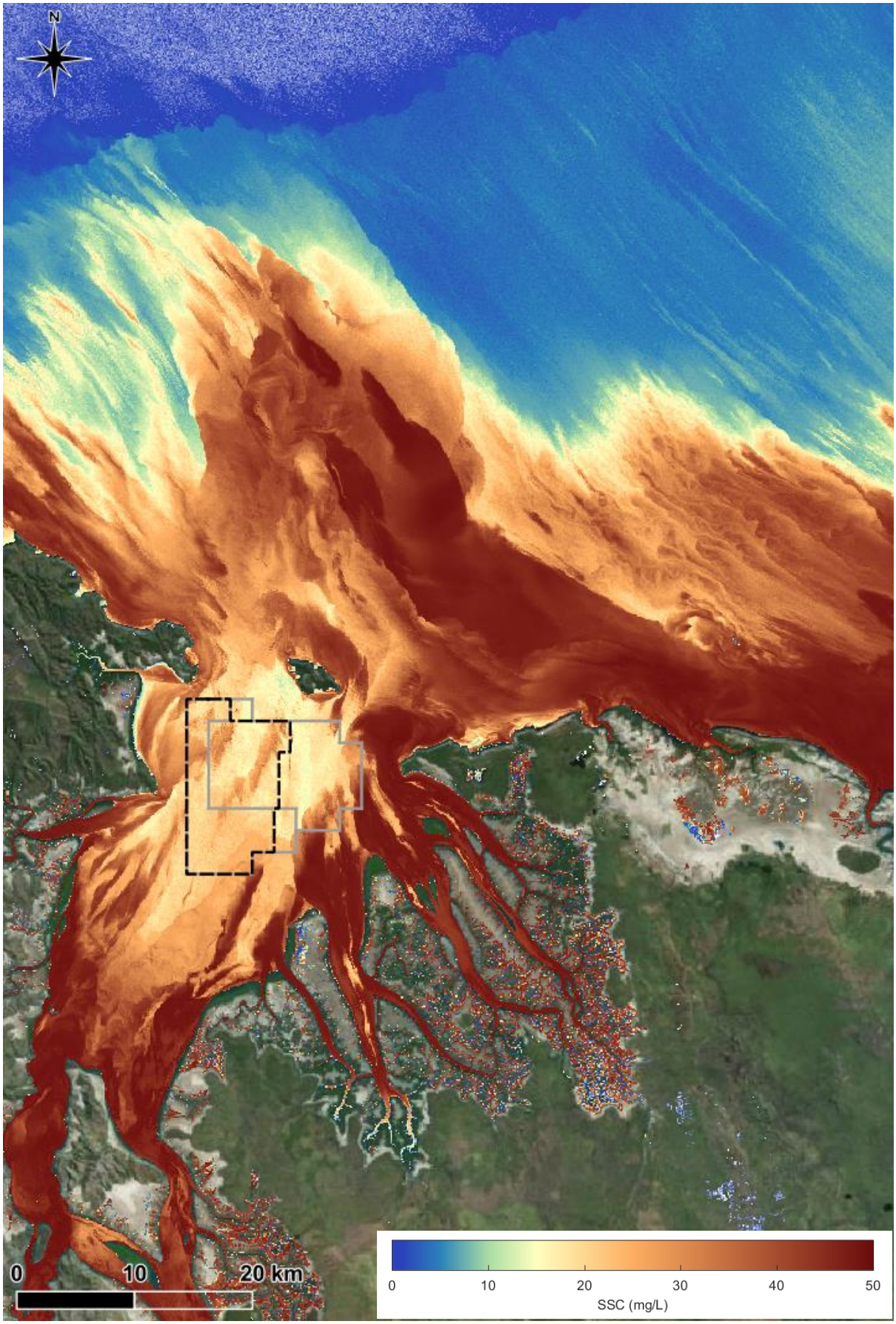

Figure 54. **Satellite-derived TSM for Sentinel 2 image captured on 18/04/2018 during a spring tide at the end of the wet season following multiple days of high rainfall (source: BoM, AHO, CSIRO).**

The hydrodynamic and SSC data collected by Wolanski et al. (2004) in 2000 and 2002, were used to calculate net fluxes of suspended sediment at their measurement sites in CG and West and East Arms (Figure 55). The net fluxes show that East Arm is importing suspended sediment from West Arm, with the calculated flux being more than double during the wet season compared to the dry season. This correlates with a previous investigation by Wolanski et al. (2001), which estimated that based on the sedimentation which had occurred in the East Arm between 1969 and 2000 it had been importing sediment at a rate of around 36,000 ton/day. In addition, monitoring by CSIRO showed that tides in the Ord River estuary were asymmetric, with a flood dominance in the current speed meaning that more sediment is suspended on the flood tide than on the ebb tide, which in turn results in a net upstream transport of fine-grained sediment occurring in the Ord River (Robson et al., 2008).

Based on the available data, Wolanski et al. (2004) calculated that West Arm exports fine sediment at a rate of around 40,000 ton/day, and based on the rate that East Arm has been accreting, this indicates that most of the sediment from West Arm is now imported into East Arm and does not reach the open bay area of CG. However, the satellite-derived SSC data consistently showed high SSC in both West and East Arms and extending into the southern half of the open bay area of the CG. The satellite imagery therefore shows that there is a regular ongoing supply of suspended sediment from West Arm into CG. Based on this, either the import of suspended sediment from West Arm into East Arm has reduced over the last 20 years (since 2002) or the import of suspended sediment from West Arm into the CG was higher than calculated by Wolanski et al. (2004).

In the open bay area of CG, the net flux of suspended sediment shown in Figure 55, during both wet and dry season conditions, was to the north along the west side of the Gulf, and to the south along the east side of the Gulf. The net flux in a northerly direction was consistently higher than the net flux in a southerly direction, suggesting that the west coast of the Gulf is likely to be accreting while the east coast is likely to be receding (Wolanski et al., 2004). The net fluxes indicate that there was a small net export of suspended sediment from CG into JBG.

Sand is reported to constitute at least 50% of the sediment load in catchments such as those which flow into CG (Gehrke et al., 2009). The rates of soil erosion, which transports the catchment sediment into river channels, typically declines during the wet season due to increased ground cover by grass, while land uses such as mining, grazing and cropping greatly increase sediment yields above the low background values (Williams, 1969). It was noted by Gehrke et al. (2009), that of the 23.5 million tonnes per year of sediment entering Lake Argyle due to gully erosion in the upstream catchments, which has been exacerbated by grazing, is predominantly trapped within the lake. As a result, the Ord River is deprived of sediment immediately downstream of Kununurra Diversion Dam, but it does receive sediment from erosion of cropping and grazing lands elsewhere in the catchment and from bank erosion closer to the estuary.

The tidal creeks of the Ord River estuary (located east of Adolphus Island) were noted by Gehrke et al. (2009), as being depositional environments. Observations showed that during the dry season, they act as a sink of sediment which enters from the main estuary.

As noted in Section 3.5, TCs and tropical lows are responsible for the largest waves and highest freshwater discharge in CG. These events can therefore result in acute impacts which can be a major driver of episodic sediment transport in CG, and may contribute to the net recession of the east coast noted previously. During BKA's aerial drone surveys in July 2023, severe natural damage to mangroves and coastal erosion was observed at several locations, mainly on the east coast, which is most likely caused by the last cyclone to hit the area, as shown in Figure 56 and Figure 57. Similar damage to mangroves was noted by Thom et al. (1975) when comparing aerial images from 1948 and 1971. Localised damage to mangroves also results in increased exposure of the mudflats to wave energy, increasing the potential for ongoing erosion to occur in these areas until the mangroves have recolonised.

Another feature of coastal processes at some locations in CG, is stranded sandy beach ridges (also known as chenier plains) directly landward of the mangroves. These stranded beach ridges form through wave-induced onshore sediment transport, with energetic wave conditions washing out the finer-grained silt and clay, while the coarser sand is transported onshore by washover processes (Masselink, 2011). The formation of the beach ridges in CG are thought to have occurred during short erosional episodes, potentially relating to single storm events, with ongoing lateral and vertical accretion of the fronting tidal flats occurring between storms (Thom et al., 1975).

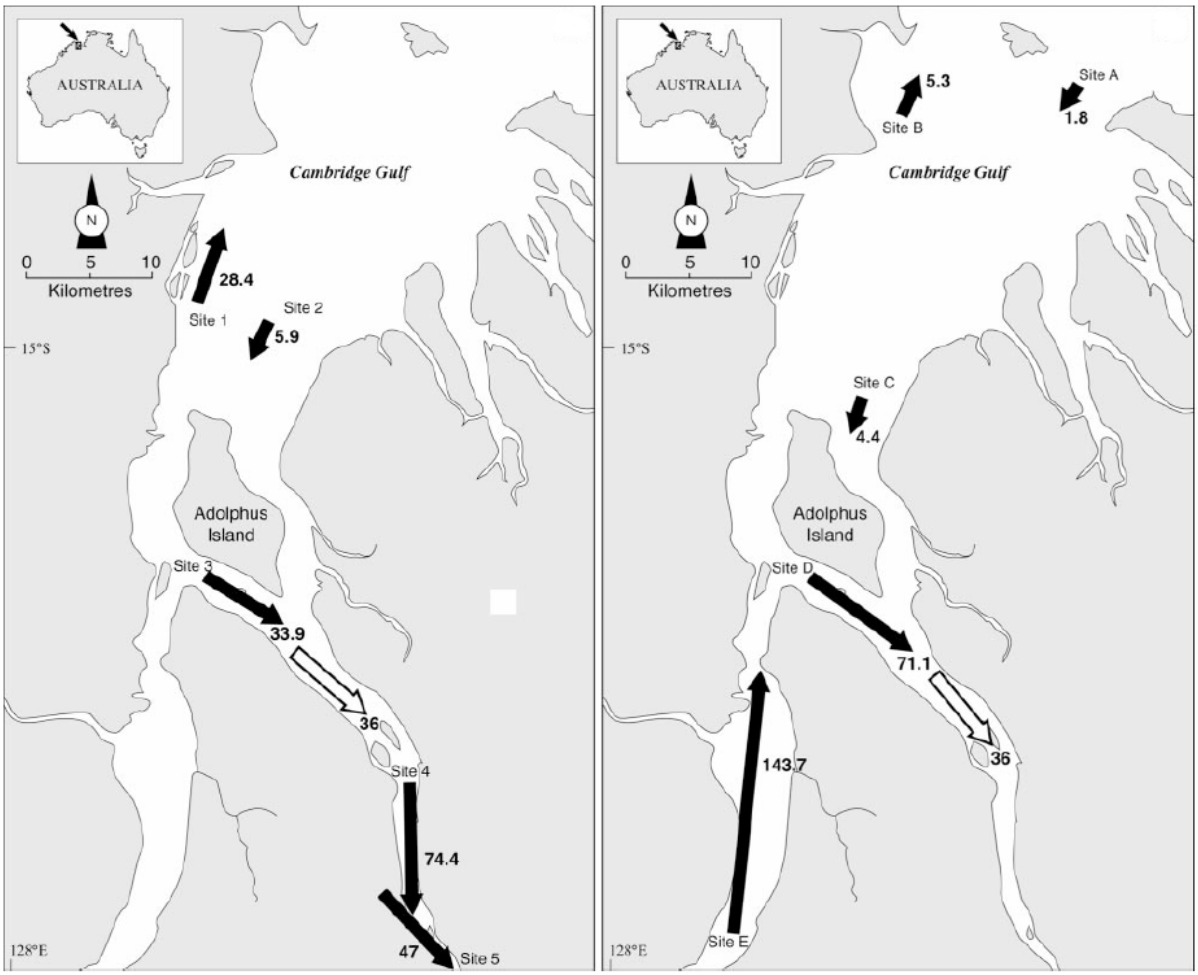

Figure 55. Calculated net suspended sediment fluxes (ton/day/m) at the measurement sites in October 2000 (left) and January to February 2002 (right) (Wolanski et al., 2004). *The open arrow shows the net sediment flux calculated from the siltation rate of East Arm between 1969 and 2000.*

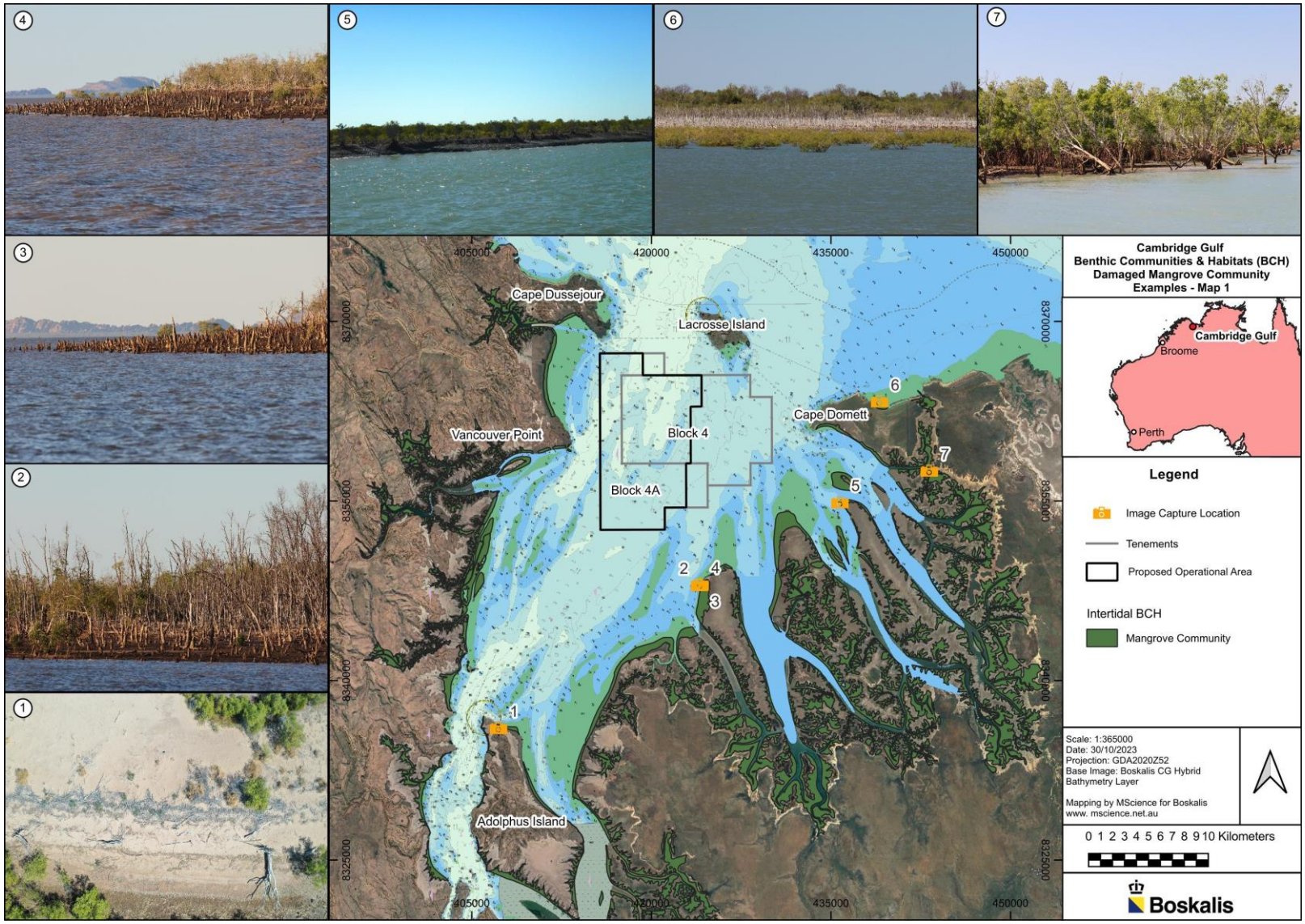

Figure 56. **Areas of CG with natural damage to mangroves observed during the dry season environmental survey, most likely caused by a TC (source: BKA, 2024d).**

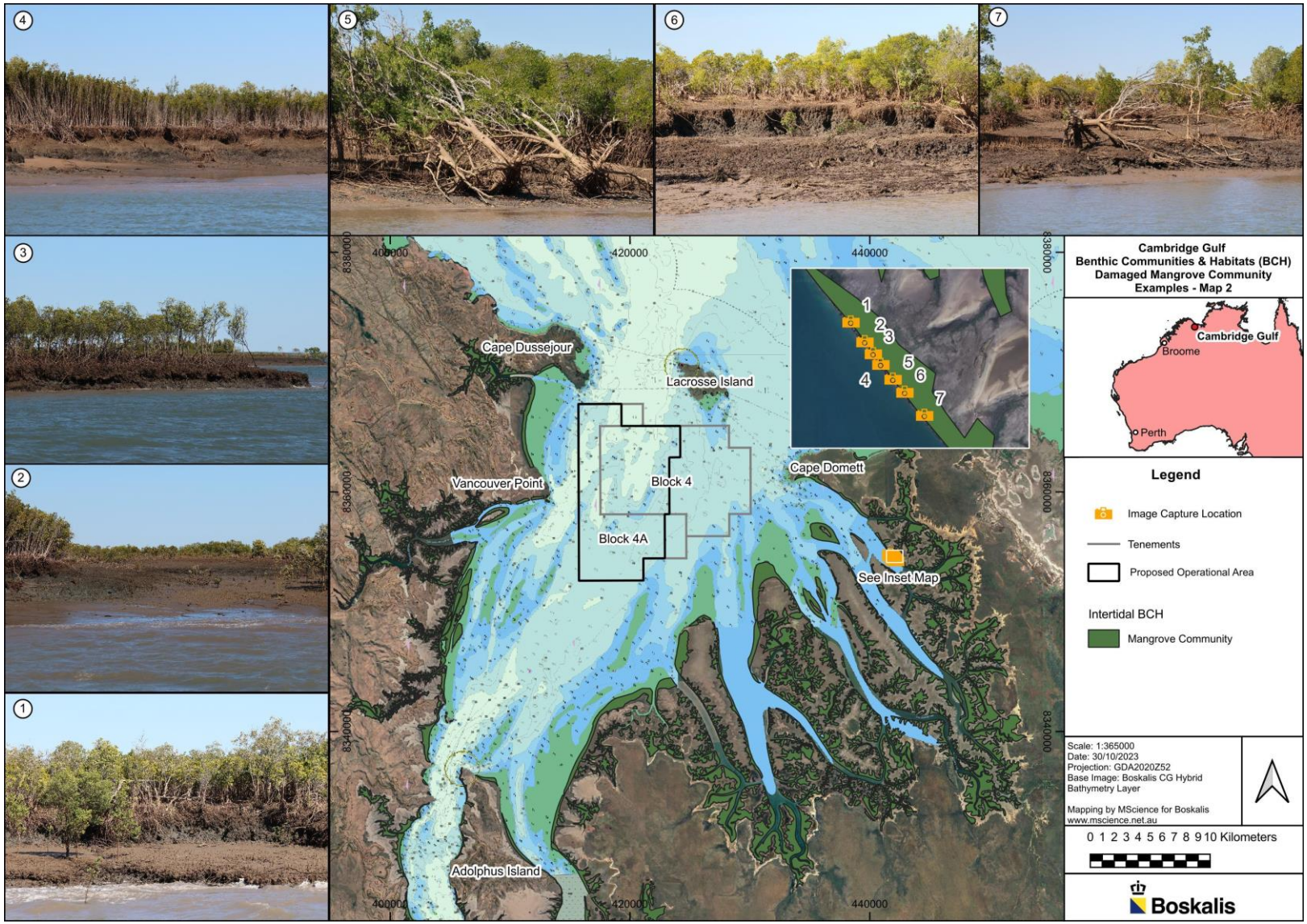

Figure 57. Additional areas of CG with natural damage to mangroves observed during the dry season environmental survey, most likely caused by a TC (source: BKA, 2024d).

3.8. Light Availability

The quantity and quality (wavelength) of available light at the seabed is a major determinant of what benthic biota can survive in an area. Light at the seabed is measured as benthic Photosynthetically Available Radiation (PAR) ($\mu m/s/m^2$) and this is influenced by the available ambient light (sunshine), the water depth and the water clarity.

This study could not identify any pre-existing PAR data for CG. As outlined in sections 2.3.1 and 2.3.2, BKA has started collecting benthic PAR data with light meters co-mounted on the seabed AWAC frames, and plans to deploy four dedicated seabed frames with both light and turbidity meters for an initial 12 months from January 2024 (at Pos 01 to 04 on Figure 9). At the time of writing, benthic PAR data from just one day of measurements in CG were available from the AWAC-02 site, and have been analysed.

The light meters (2 x LICORs, one pointing down and one up on the AWAC frame) were deployed over 24 hours on neap tides with an average water depth over the period of 18 m. The concurrent turbidity measurements ranged from 10 NTU to 70 NTU, indicating that SSC varied from approximately 17 mg/L around high water to 120 mg/L around low water (based on the turbidity-NTU correlation described in Section 2.3.1). The measured benthic PAR values were less than 0.01 $\mu m/s/m^2$ for the upward facing sensor and typically 0 at the downward facing sensor. These are very low values, which indicate that there was essentially no benthic light over this period.

This is consistent with the results from the drop camera that was deployed to the seabed at all 35 vibro-core sites in Block 4 in March 2023 and at all 132 benthic grab sites across CG and King Shoals in July-August 2023, with 100% of the videos showing a completely blacked-out aphotic zone, caused by a constantly suspended sediment layer for several metres above the seabed (Figure 58).

Based on the data collected to date, along with our understanding of the sediment transport in CG, it is expected that the benthic PAR will be extremely low at most, if not all sites. This is a result of the following:

- CG having high natural SSC which is predominantly tidally-driven meaning that the elevated SSC occurs regularly. Satellite-derived SSC data have shown that during small neap tides, the SSC within the open bay area of the CG can be relatively low (5 to 10 mg/L) and so it is possible that short duration periods of elevated benthic PAR could occur at some sites.

- the peaks in SSC within the bay area of CG coincide with the timing of low water, which is when water depths will be shallowest and therefore when there would typically be increased chance of higher benthic PAR. The timing of the lowest SSC is typically around high water, which is when water depths are deepest and so when there is less chance of higher benthic PAR.

As outlined above, additional benthic PAR data are being collected as part of this project (see Section 2.3), with 12 months of continuous data to be collected at four sites (Pos 12 to Pos 15 on Figure 9) and 90 days of continuous data to be collected at six other sites (AWAC-05 to AWAC-10 on Figure 9). These data will provide a good understanding of how the benthic light availability within CG varies both spatially and temporally.

Very low benthic PAR levels will be a significant inhibiter of benthic biota in CG, and along with likely dynamic seabed sediments, explains the very low returns of benthic biota in the benthic grab sampling undertaken by BKA to date. There do not appear to be any significant sub-tidal benthic communities in CG.

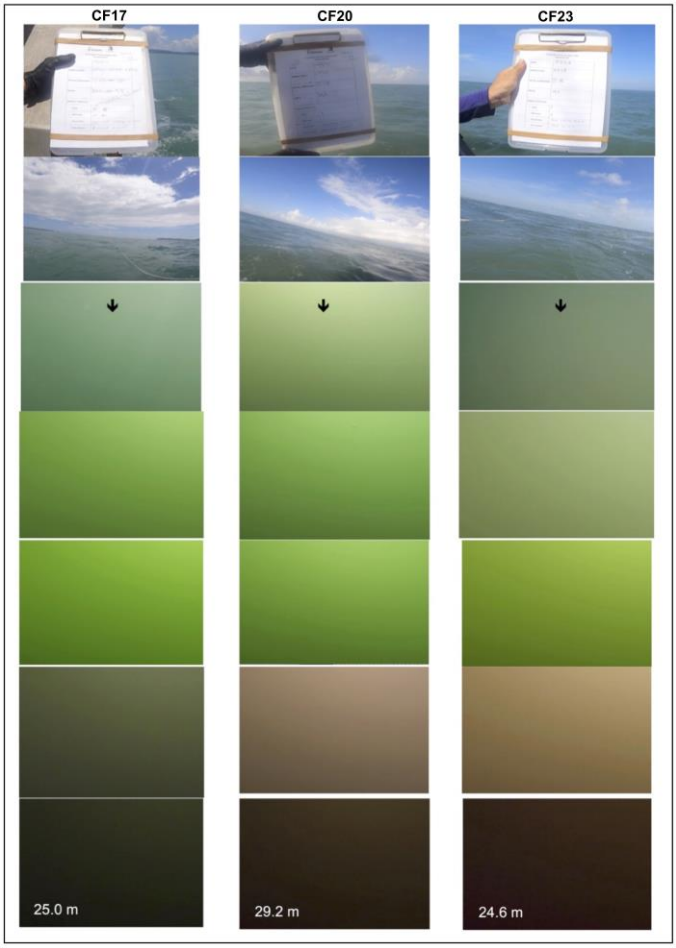

Figure 58 **Screen shots from three examples of the drop camera videos undertaken at 167 sites across CG and King Shoals in March 2023 and July-August 2023, showing a completely blacked-out aphotic zone caused by a constantly suspended sediment layer for several meters above the seabed. 100% of the videos show exactly the same (source: BKA, 2024d).**

3.9. Shoreline Changes

BKA is affording very high priority to assessing the potential for the proposed operation to cause shoreline changes, including at the four beaches in the CG area that are known to host nesting marine turtles. These are Turtle Beach West (west of Cape Dussejour), Turtle Bay on Lacrosse Island, Cape Domett Beach (seaward of Cape Domett) and East Bank Point (inside CG) (equating to sites A, D, E and F on Figure 59 respectively).

Analysis of shoreline position from historic satellite imagery using CoastSat was undertaken at cross-shore profiles across the shoreline at these four beaches (see Section 2.2.8 for further details). The locations of the cross-shore profiles are shown in Figure 60 to Figure 63. The analysis is based on satellite imagery from 1988 to 2023. Over this period a total of 36 TCs have passed within 200 km of the entrance to CG, meaning that multiple extreme wave and river discharge conditions will have occurred. Therefore, the results show how the shoreline at the beaches has changed due to typical conditions and extreme events. The shoreline position has been normalised at each cross-section by subtracting the mean shoreline position throughout the analysis period (1988 to 2023).

At Turtle Beach West, Cape Domett Beach and Turtle Bay, sufficient imagery was available during both the wet and dry season periods to allow the shoreline position to be mapped separately for these periods. At East Bank Point, it was not possible to analyse the shoreline position separately for wet and dry season periods, but the change to the annual shoreline position has been analysed here. The reason for this was that the extensive mudflats fronting the stranded sandy beach ridge limit the ability of the CoastSat tool in identifying the shoreline, which significantly reduced the number of available images.

The results from the CoastSat analysis have been processed to determine the average annual shoreline position at all of the profiles. The results at the profiles at Turtle Beach West, Cape Domett Beach and Turtle Bay have also been processed to determine the average wet and dry season shoreline positions. Results from the analysis are shown in Figure 64 to Figure 69. Results from the analysis are discussed in the points below for each of the four beaches:

- Turtle Beach West: All three profiles at this beach have shown an advance (i.e. beach position moving in an offshore direction) in shoreline position from 1988 to 2023, with the average shoreline position advancing around 10 m in the middle of the beach and 15 m at both the eastern and western ends. At the east and west ends of the beach, there was little difference between the wet and dry season shoreline positions, while at the middle profile, the wet season shoreline was approximately 10 m further seaward than the dry season profile, indicating a potential change in the beach profile shape between the two seasons.

- Cape Domett Beach: Similar to Turtle Beach West, all three profiles have shown an advance in shoreline position between 1988 and 2023, with the average shoreline position advancing between 5 m (east end of beach) and 15 m (west end of beach). At the west end of the beach, there was little difference between the wet and dry season shoreline positions, while at the middle and eastern end, the dry season shoreline was on average 5 to 10 m further seaward than the wet season shoreline.

- Turtle Bay, Lacrosse Island: There was no long-term change to the shoreline position between 1988 and 2023 at this beach. The results do show a 5 to 10 m difference between the wet and dry season shoreline positions, with the dry season shoreline located further seaward than the wet season profile.

- East Bank Point: Out of the four beaches analysed, the largest changes in shoreline position occurred at this stranded sandy beach ridge or 'chenier' beach. The changes varied along the different sections of the beach as follows:

  - eastern side of the beach ridge (profiles East 1 to East 3): relatively constant recession (i.e. beach position moving in an onshore direction) of between 60 and 90 m occurred from 1994 to 2023, with average recession rates of 2 to 3 m/yr since 1994;

  - middle of the beach ridge (profiles East 4, West 1 and West 2): there was no long-term change in the shoreline position from 1988 to 2023; and

  - western side of the beach ridge (profiles West 3 and West 4): as with the eastern side, there was relatively constant recession from 1994 to 2023. The recession was between 55 and 100 m over the period, equivalent to average recession rates of 2 to 3.5 m/yr.

Turtle Beach West and Cape Domett Beach have both experienced similar trends, with a gradual advance of 0.1 to 0.4 m/yr over the last 35 years, while the shoreline position at Turtle Bay on Lacrosse Island has not changed over this period. The shoreline position at all three beaches has shown variability between wet and dry seasons, with the shoreline position at Cape Domett Beach and Turtle Bay being further seaward during the dry season, while the shoreline position in the middle of Turtle Beach West was further seaward during the wet season. This variability is likely to be a result of the cross-shore profile changing its slope and configuration (i.e. sand being moved onshore and offshore in the intertidal and subtidal zones) due to the varying wave conditions over the wet and dry seasons, as opposed to changes in the volume of sand present at the beaches.

The change in the shoreline position at East Bank Point differs from the changes at the other three beaches. This is a result of this beach being a stranded beach ridge (chenier) located on top of a mudflat with little to no ongoing supply of sand (only the small amount of sand present in the mudflat sediment), while the other three beaches are typical sandy beaches which have sand present along the full length of their profiles and have an ongoing supply of sand from offshore. The shoreline recession at the eastern and western ends of the ridge at East Bank Point should be considered as a migration of the beach ridge over the mudflat as opposed to a recession of the ridge. Stranded beach ridges typically continue to migrate landward (and alongshore) instead of building up, due to the lack of additional sandy sediment. As a result, they will continue to migrate landward due to wave washover until their crest is above the spring tide level (Tas et al., 2022).

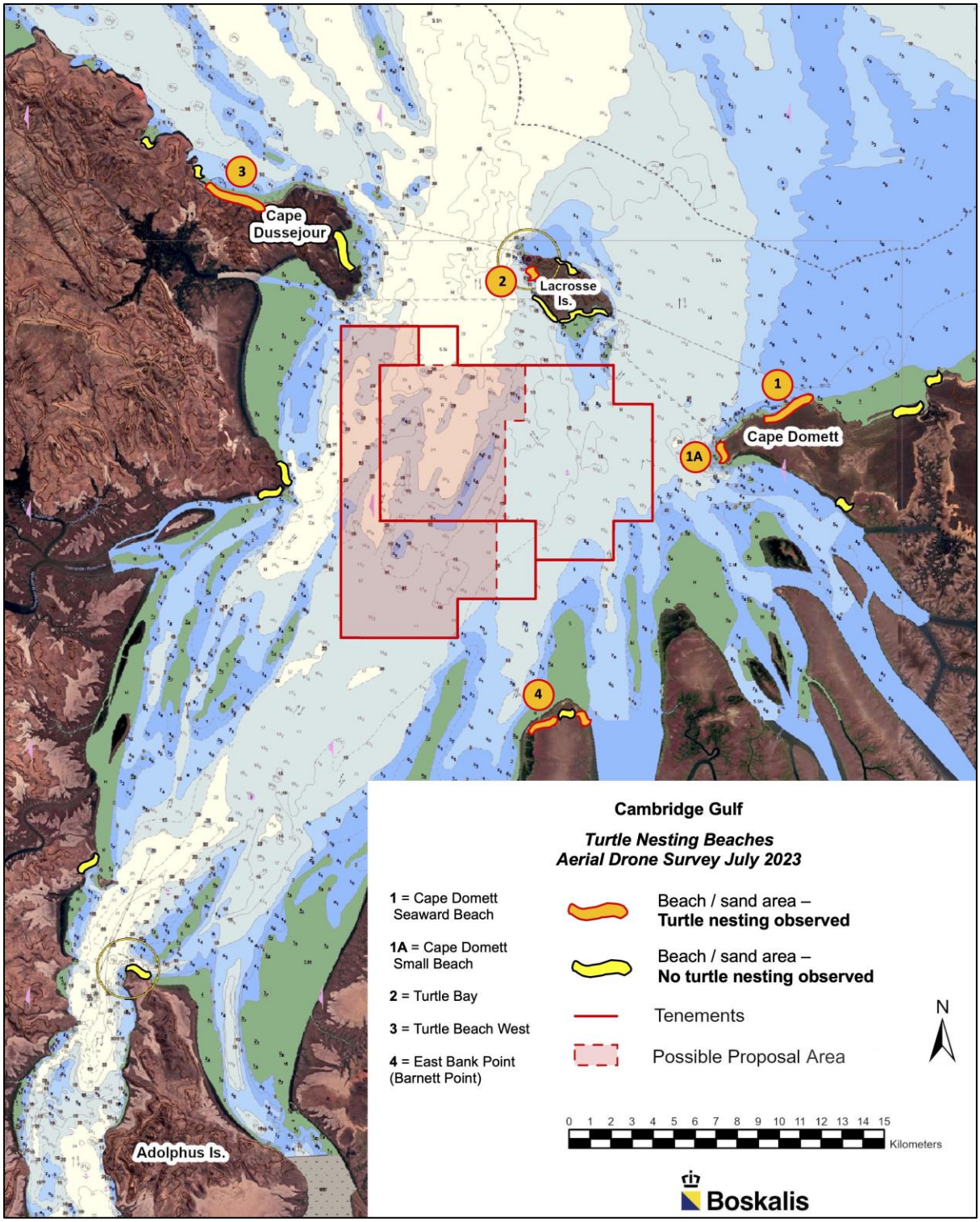

Figure 59. The known turtle nesting beaches in the CG area (source: BKA, 2024d).

Figure 60. Cross-shore profiles adopted to assess historical shoreline change at Turtle Beach West using CoastSat.

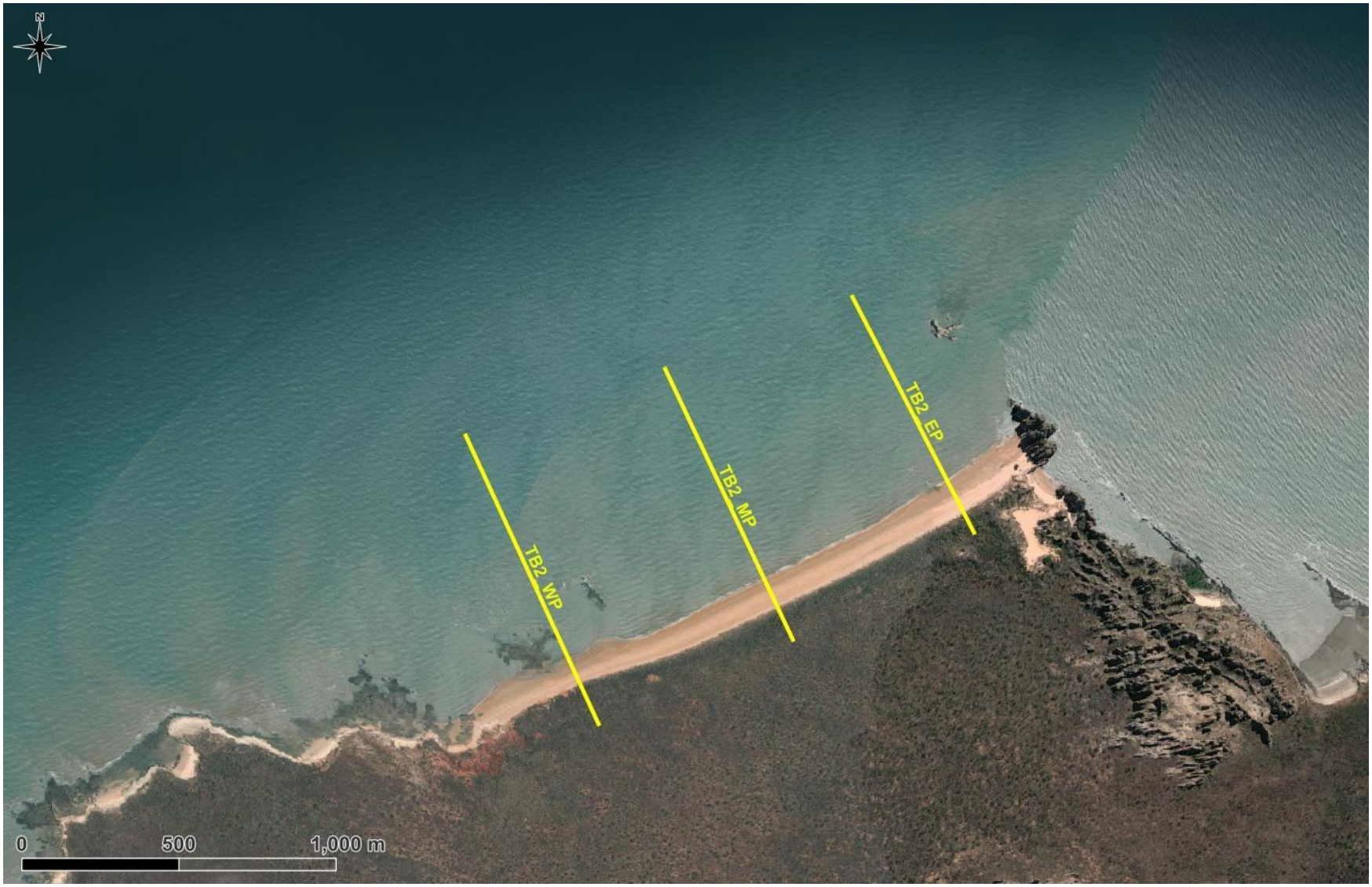

Figure 61. Cross-shore profiles adopted to assess historical shoreline change at Cape Domett Beach using CoastSat.

Figure 62. Cross-shore profiles adopted to assess historical shoreline change at Turtle Bay, Lacrosse Island using CoastSat.

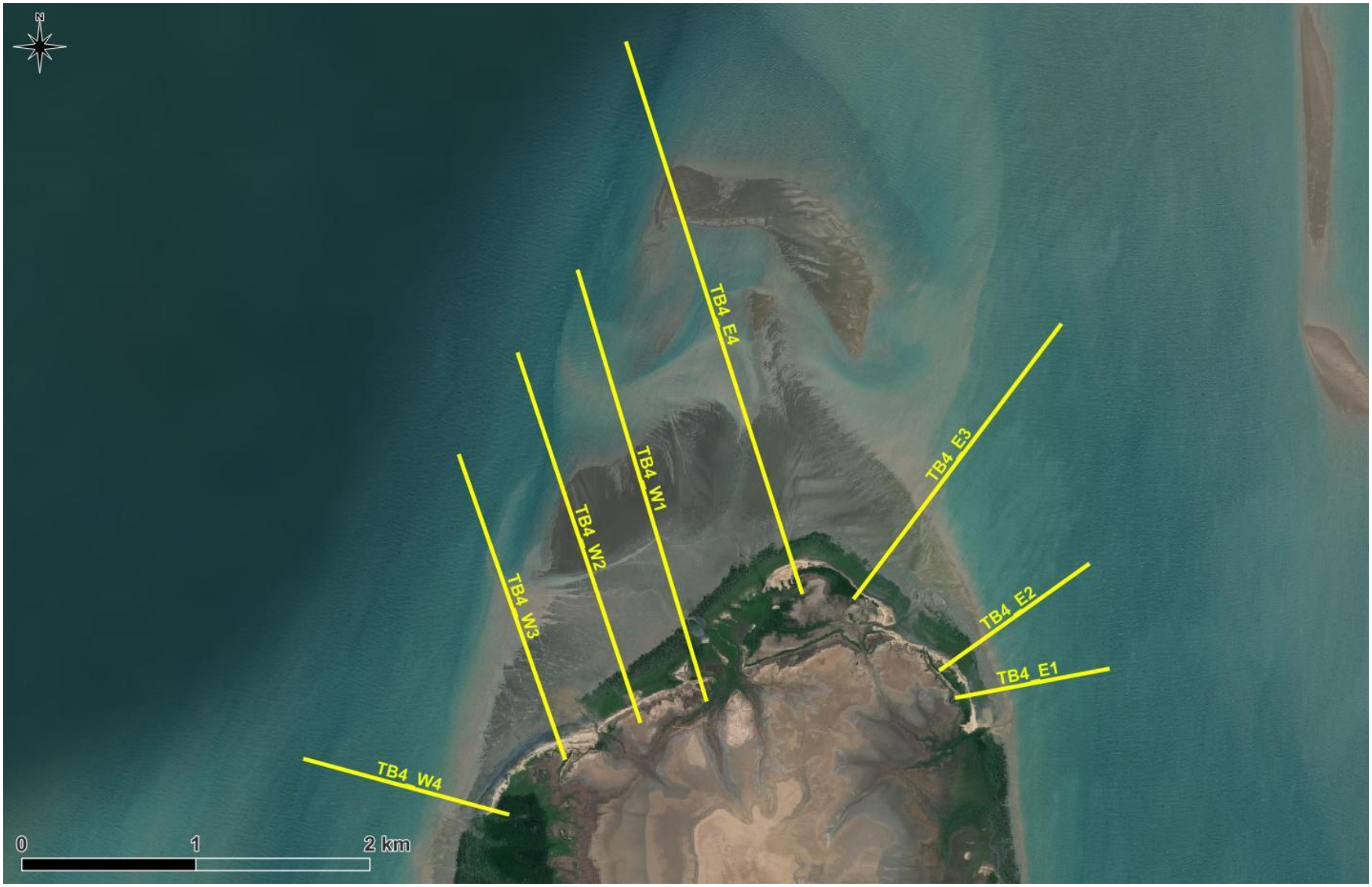

Figure 63. Cross-shore profiles adopted to assess historical shoreline change at East Bank Point using CoastSat.

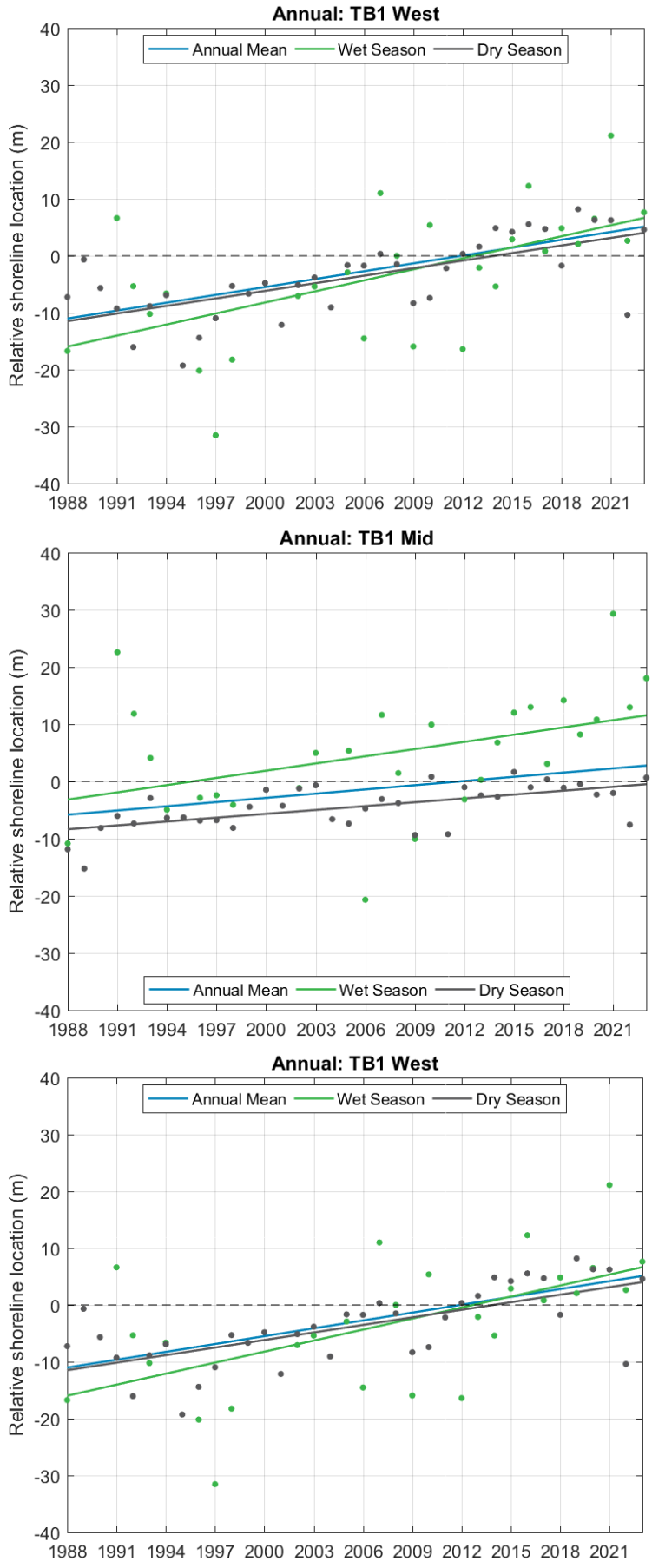

Figure 64. Change in shoreline position from 1988 to 2023 at the Turtle Beach West profiles.

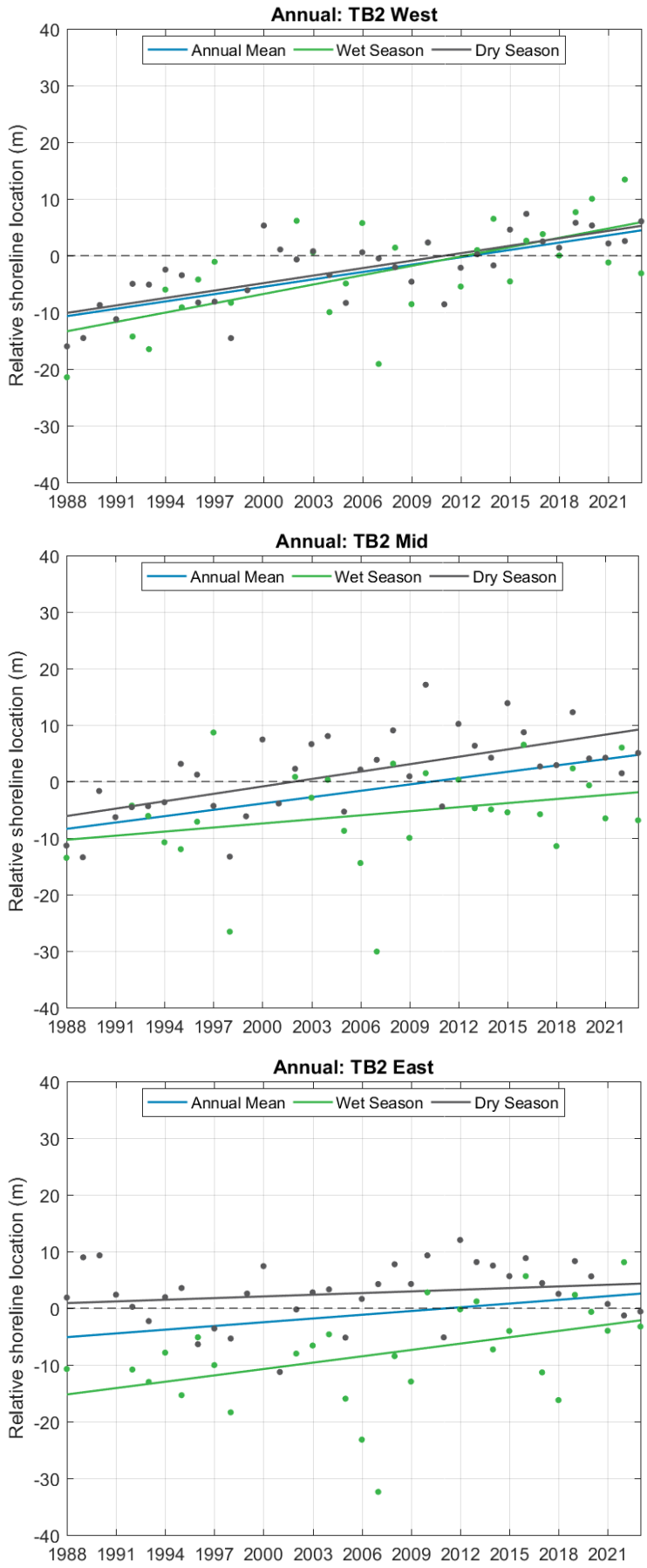

Figure 65. Change in shoreline position from 1988 to 2023 at the Cape Domett Beach profiles.

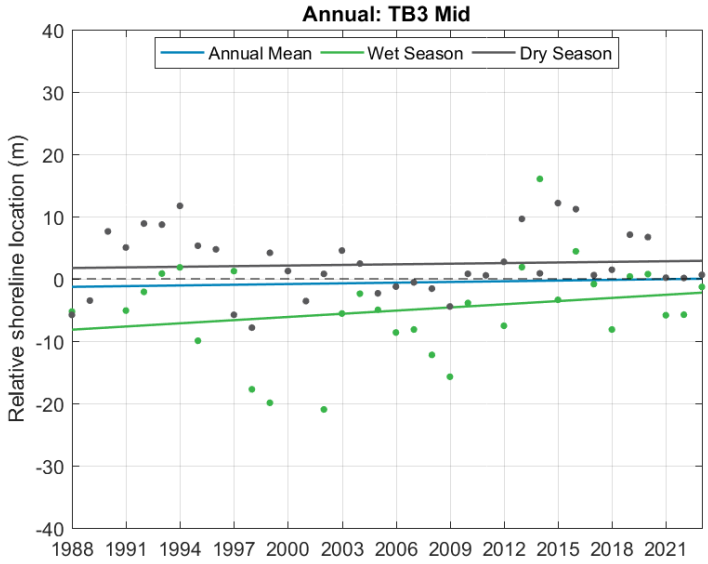

Figure 66. Change in shoreline position from 1988 to 2023 at the Turtle Bay profile.

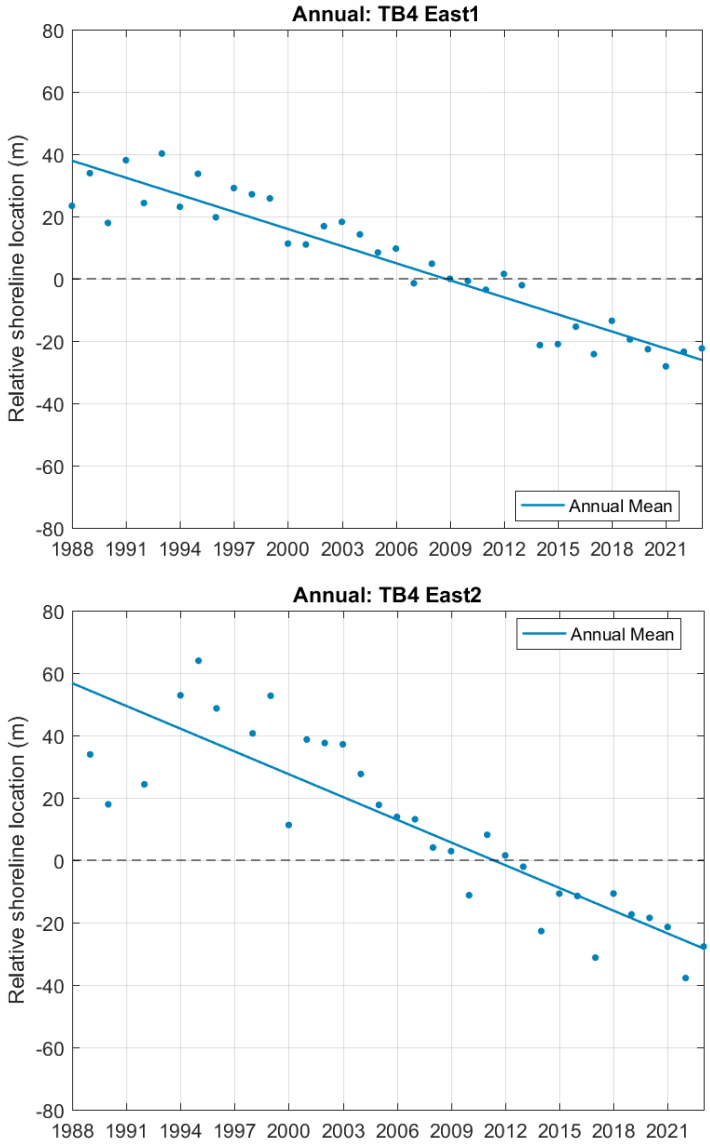

Figure 67. Change in shoreline position from 1988 to 2023 at the East Bank Point profiles TB4 E1 and TB4 E2.

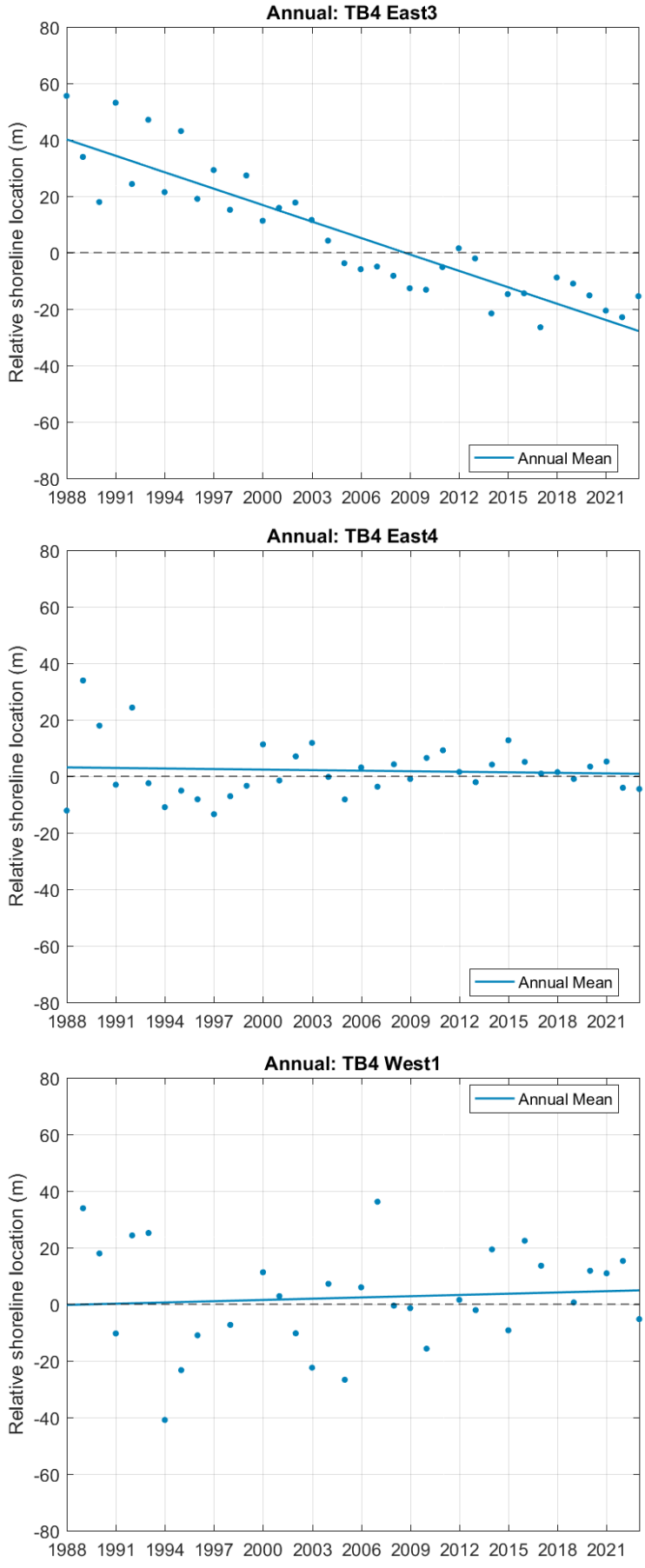

Figure 68. Change in shoreline position from 1988 to 2023 at the East Bank Point profiles TB4 E3, TB4 E4 and TB4 W1.

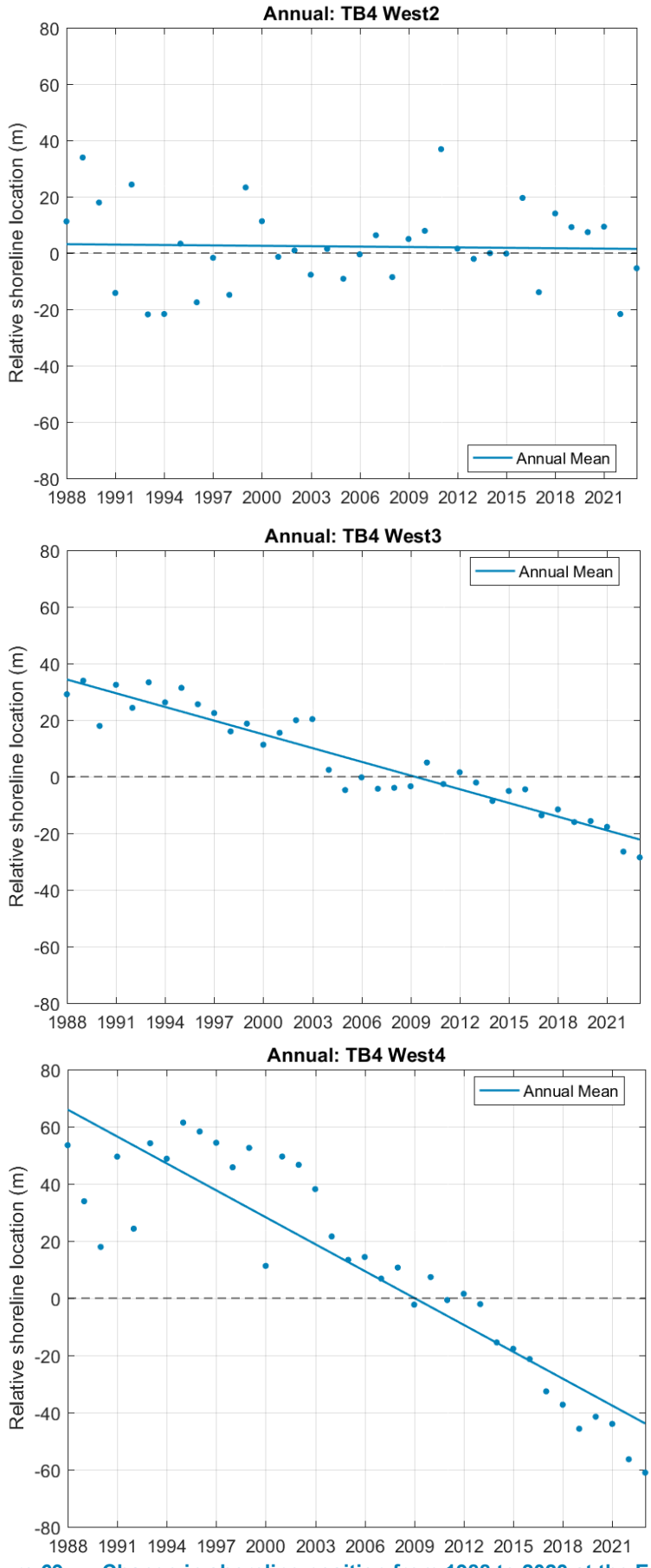

Figure 69. Change in shoreline position from 1988 to 2023 at the East Bank Point profiles TB4 W2, TB4 W3 and TB4 W4.

3.10. Historical Changes in CG Region

The most significant changes that have occurred in the CG region since European colonisation have been in the Ord River catchment area. As noted in Section 1.2, the changes to the Ord River catchment have involved extensive land clearing for cattle since the start of the 20th Century and the construction of two dams in 1969 and 1972 (Wolanski et al., 2001). The land clearing would have resulted in increased surface runoff of both water and sediment from the Ord River catchment, which has the potential to increase the flood discharge of both water and sediment in the Ord River. In contrast, the dams will have acted to suppress the river floods and regulate the discharge of the river. The location of the two dams is shown on Figure 2. Details of the dams are provided in Robson et al. (2013) and summarised below:

- Kununurra Diversion Dam: This dam was completed in 1969, it has a relatively small storage of approximately 100 GL and was created to provide irrigation to approximately 140 km^2 of farmland in the Ord River catchment. The dam was too small to have much impact on the timing or magnitude of annual floods in the Ord River during the wet season.

- Ord River Dam: This was constructed upstream of the Kununurra Diversion Dam in the early 1970s and completed in 1972. The dam created Lake Argyle which is the largest artificial lake in the southern hemisphere. The dam provides water for irrigation of farmland in the Ord River catchment (the Ord River Irrigation Scheme) as well as to supply hydropower and water to the Argyle Diamond Mine (which is now closed) and the town of Kununurra and surrounding region.

A number of studies have investigated the impacts of these changes to the Ord River catchment, noting that the construction of the Ord River Dam will have been the key change resulting in impacts in the CG region (Wolanski et al., 2001; Wolanski et al., 2004; Robson et al., 2008; Robson et al., 2013). Their findings are summarised as follows:

- Prior to construction of the Ord River Dam, the freshwater flows into CG from the Ord River were negligible during the dry season, while flows during the wet season were substantial and were typically characterised by large flood events where peak flows could have exceeded 30,000 m^3/s. Since construction of the Ord River Dam flows during the dry season are maintained at 50 to 90 m^3/s, while peak wet season flows can still exceed 1,000 m^3/s (Robson et al., 2013).

- The reduction in the Ord River discharge during the wet season was estimated to have reduced the total inflow of fine-grained sediment into CG by around 100,000 ton/day, with a negligible inflow of fine-grained sediment now occurring (Wolanski et al., 2004). The reduction is partially a direct result of the dam trapping the sediment discharged during the wet season flood and partially an indirect result of the dam changing the flow patterns in East Arm resulting in the majority of fine-grained sediment discharged into West Arm by the Durack and Pentecost Rivers being transported up East Arm through tidal pumping and subsequently being deposited in East Arm, rather than downstream into CG. East Arm was shown to have silted up significantly between 1972 and 2000, with the cross-sectional area of the channel decreasing by approximately 50% over this time (Wolanski et al., 2001).

- As a result of the construction of the Ord River Dam, East Arm is now considered to be geomorphologically unstable. Numerical modelling undertaken by Wolanski et al. (2001) indicated that East Arm may reach a new equilibrium in as little as 100 years, with the new equilibrium predicted to include a reduction in salinity intrusion length up East Arm/Ord River (by 50%), the channel width and depth in East Arm reducing by 70% and the tidal asymmetry in East Arm becoming stronger.

- Despite the anthropogenic changes to the Ord River catchment, West Arm remains in equilibrium, with the tidal dynamics and river floods responsible for self-scouring of the channel (Wolanski et al., 2001).

- The reduction in supply of fine-grained sediment to the open bay area of CG to a current negligible supply was assumed by Wolanski et al. (2004) to indicate that the fine-grained sediment in suspension within the open bay area of the CG is due to existing sediment being redistributed as opposed to new fine-grained sediment being imported into the area. They also assess that this has possibly resulted in the west coast of CG accreting while the east coast has been receding.

To assess these issues in more detail the planned project numerical modelling described in section 4.8 below will be used to predict how the Ord River Dam has influenced hydrodynamics and sediment transport in CG.

4. NUMERICAL MODELLING APPROACH

This section provides details of the numerical modelling software utilised, the model mesh, initial setup of the hydrodynamic (HD), spectral wave (SW), sediment transport and beach processes models, details of any preliminary calibration undertaken to date and preliminary results from the models. The HD, SW and sediment transport models will be used to simulate the coastal processes in the region for all areas except the beaches, which will be simulated using the beach processes models.

At this stage of the study, only preliminary numerical modelling has been undertaken. This will be further expanded through the course of the project and subsequent reports will be prepared to present the different modelling undertaken and discuss any predicted impacts. This report does not include any initial setup or results from the dredge plume model, as this will be undertaken at a later stage of the project once the HD and SW models have been fully calibrated and validated. A summary of the future modelling that will be undertaken as part of the study is provided at the end of this section.

4.1. Software

For the modelling of a complex estuarine system like CG to be considered best practise, the model should utilise a flexible mesh approach, which allows the resolution of the mesh to vary spatially as required. The Danish Hydraulic Institute (DHI) MIKE Flexible Mesh (FM) software is internationally recognised as state-of-the-art and has been previously adopted by PCS elsewhere in Australia and internationally for similar projects. The MIKE suite includes HD, SW and mud transport (MT) modules (this module includes the transport of silt and clay sized cohesive sediment, and silt and sand sized non-cohesive sediment), which allow all the necessary processes required for this assessment to be represented in the model. The MIKE modules can adopt a FM which allows the spatial resolution of the model mesh to be varied throughout the model domain. This allows suitable model resolutions to be adopted throughout ensuring the model accuracy and efficiency can be balanced. This means that areas of interest can have a higher mesh resolution (e.g. the Blocks and narrow channels) while a lower mesh resolution can be adopted in offshore areas and away from any areas of interest.

For the longshore and cross-shore sediment transport modelling at the beaches used for turtle nesting which are exposed to wave conditions, the MIKE Littoral Processes modelling suite will be adopted. This model can calculate the longshore and cross-shore transport at a series of beach profiles along the shoreline at each beach, with the model being driven by wave conditions extracted from the SW model.

4.2. Model Mesh

The model mesh was developed with consideration to:

- The model needing to be able to accurately represent the hydrodynamics and waves in the CG region.
- Ensuring that the majority of the sediment suspended by sand production activities remain within the model domain, with limited sediment reaching the model boundaries.
- The boundaries are located in a suitable position so that boundary conditions can be adopted to allow the hydrodynamics and waves to be accurately represented in the models.
- The model mesh extends upstream in West and East Arms to locations where model boundary conditions can be adopted for the hydrodynamic model without resulting in unnecessarily high resolution cells to represent the complex bathymetry in these areas.
- Managing the overall model domain so that it isn't overly large which would act to unnecessarily increase the model simulation times.

The final model domain extent and model mesh are shown in Figure 70. The model extends approximately 200 km north to south and 280 km east to west. The mesh extends to Cape Rulhieres to the west, which is approximately 140 km from Lacrosse Island, and Cape Scott to the north-east, which is located approximately 150 km from Lacrosse Island. The same model mesh extent will be used for the HD, SW and MT modelling, and as a result, the mesh has been designed to ensure higher resolution in the areas where dredging will occur (within Blocks 4 and 4A) and where any resultant plumes are likely to be transported (within and close to CG). The arc lengths of the triangular mesh elements range from approximately 4 km in the furthest offshore areas of the domain, to between 200 and 500 m in CG. A close-up of the model mesh in CG is shown in Figure 71.

While the same model mesh extent will be adopted for all the different modelling components of the project, the mesh resolution will be varied. For example, the SW model mesh is coarser than the HD model mesh in some of the smaller tidal creeks within CG as the HD model requires a higher resolution to allow flow connectivity in these creeks while the SW model does not require such a high resolution to propagate the waves.

4.3. Bathymetry

The bathymetry included in the model was selected to provide the most realistic representation of the bathymetry based on data available. Comparison within CG between the Geoscience Australia 30 m gridded data, an interpolation based on the AHO navigation chart (AUS 726 & AUS 32) and an interpolation based on the data within Block 4 measured by BKA in March 2023 showed that the 30 m gridded bathymetry did not accurately represent the shallower areas in the CG. As a result, the following datasets were adopted to represent the bathymetry within CG:

- BKA's measured depths within Block 4.
- AHO navigation chart contours and spot heights.
- Digital Earth Australia 25 m gridded bathymetry for the intertidal areas.

For the JBG region the Geoscience Australia 30 m gridded bathymetric data was adopted. This dataset also incorporates the Digital Earth Australia 25 m intertidal gridded bathymetry in the intertidal areas.

Data from the various sources were converted to MSL and then interpolated onto the model mesh. An overview of the interpolated model bathymetry covering the full extent of the model domain is shown in Figure 72 and a close up of the CG region is shown in Figure 73.

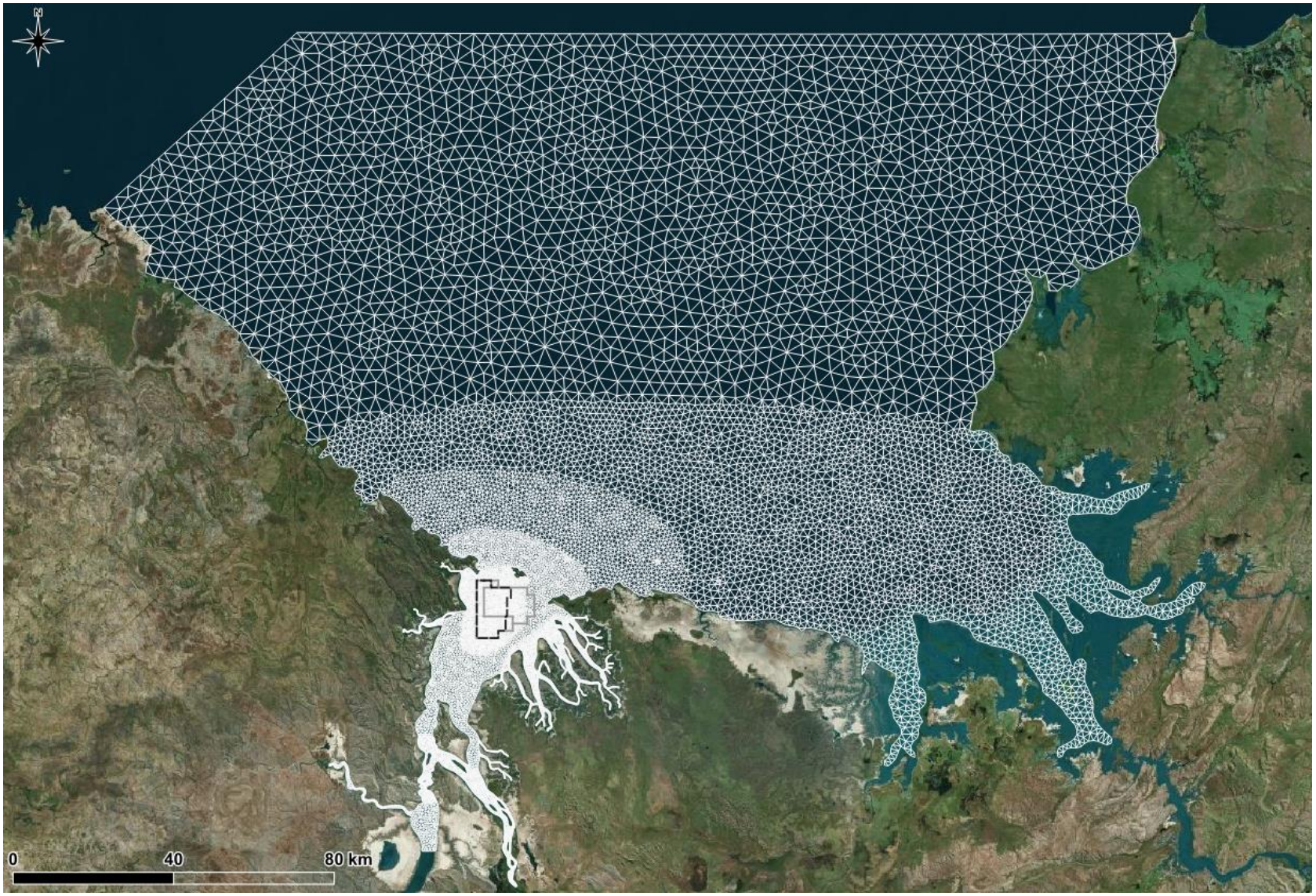

Figure 70. The full extent of the numerical model mesh along with Blocks 4 and 4A (grey polygons) and the proposed operational area (black dashed polygon).

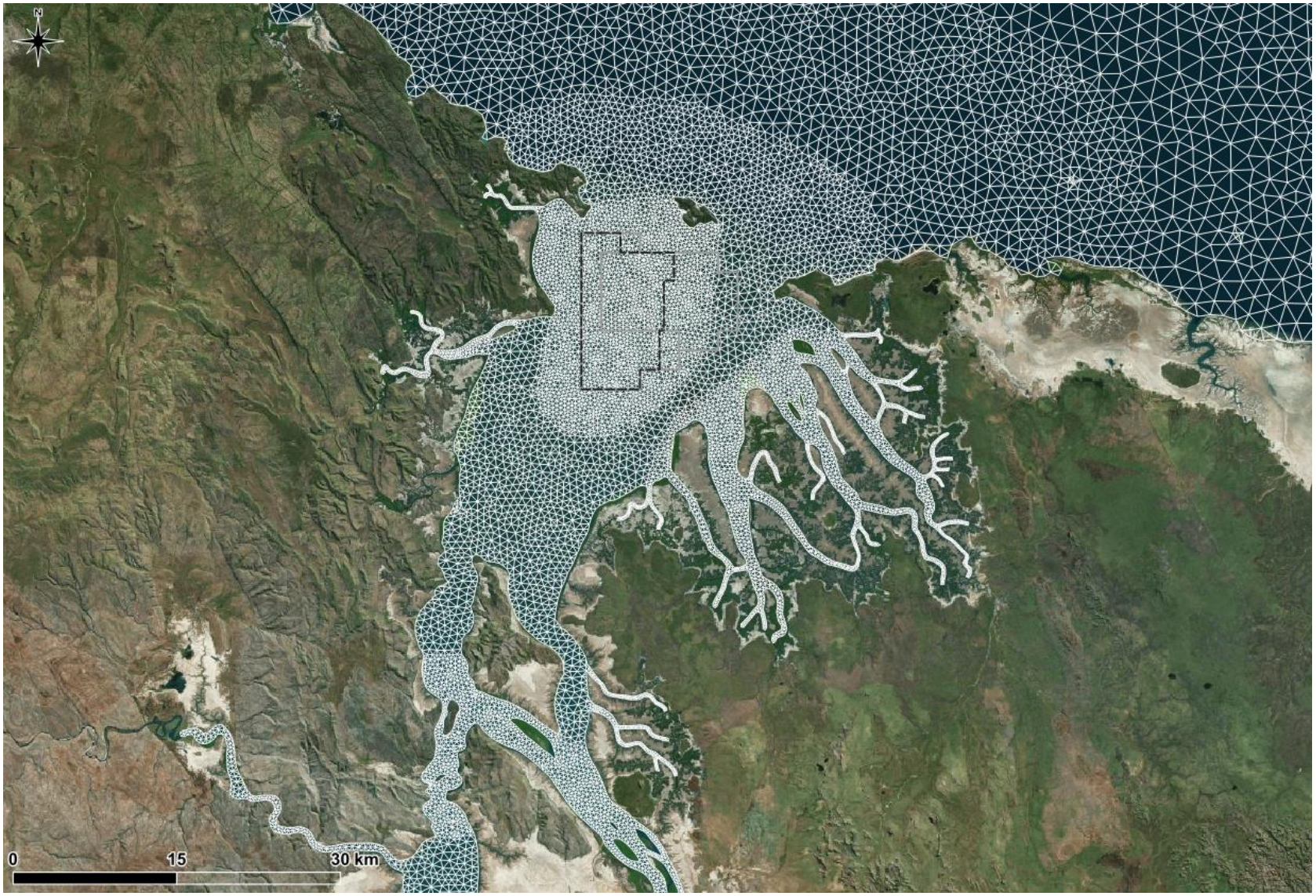

Figure 71. Close up of the numerical model mesh in CG along with Blocks 4 and 4A (grey polygons) and the proposed operational area (black dashed polygon).

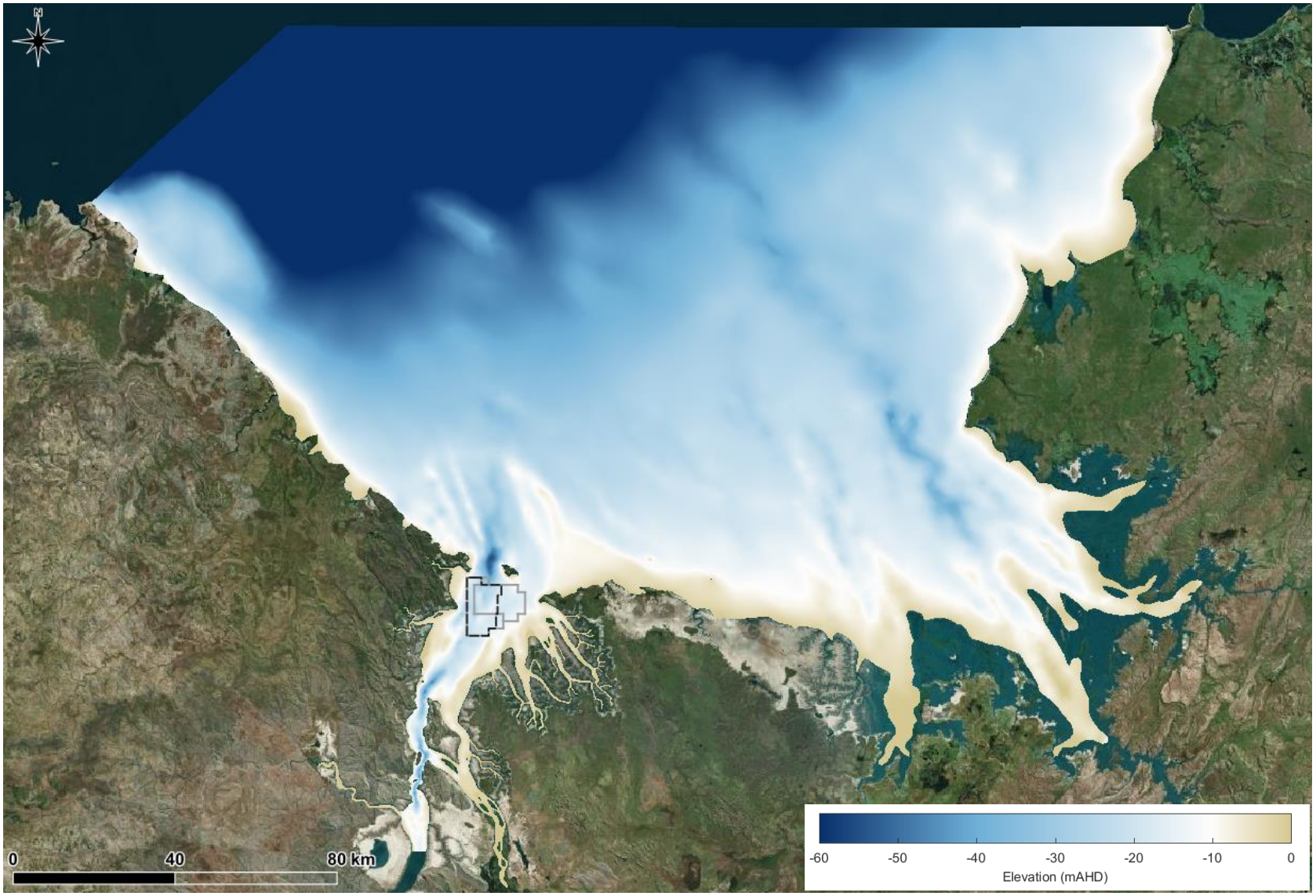

Figure 72. Model bathymetry for the full model domain with Blocks 4 and 4A also shown (grey polygons) and the proposed operational area (black dashed polygon).

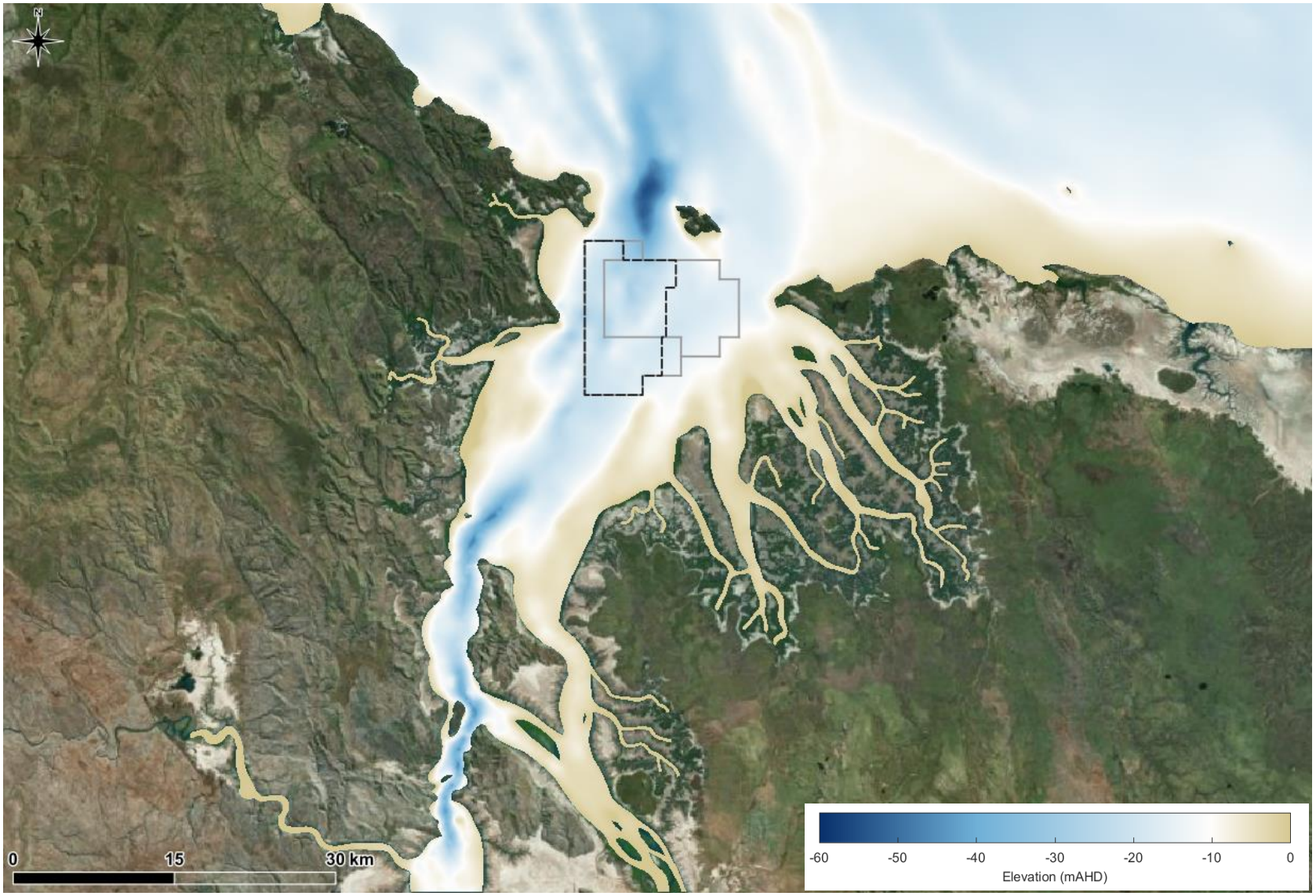

Figure 73. Model bathymetry for CG with Blocks 4 and 4A also shown (grey polygons) and the proposed operational area (black dashed polygon).

4.4. Hydrodynamic Model

The MIKE HD model simulates water level variations and flows in response to a variety of forcing functions in coastal regions and estuaries. Details of the model configuration, initial calibration and preliminary results are provided in the following sections.

4.4.1. Model Configuration

As discussed in Section 3.1.1, currents in JBG are predominantly driven by the astronomical tide, with no larger scale ocean circulation processes influencing the region. Therefore, the hydrodynamic offshore model boundaries were represented using only astronomical tidal water levels which were extracted from the DTU Space Global Tidal Model (DHI, 2007). Tidal constituents were extracted along the two open model boundaries from the 0.125° x 0.125° version of the Global Tide Model, which includes the following 10 major constituents: M2, S2, K2, N2 (semidiurnal), S1, K1, O1, P1, Q1 (diurnal) and M4 (shallow water). The water levels along the boundaries were both spatially and temporally varying.

The upstream boundary in West Arm was represented using predicted water levels from Wyndham (AHO AusTides) and the upstream boundary in East Arm was based on measured water levels collected in 2000 (AIMS, 2007). Further sensitivity testing of the upstream boundary in the East Arm will be undertaken when additional data are available in CG to determine the optimum boundary condition. The model includes the influence of the wind on the currents, with winds from the CAWCR wave/wind hindcast applied in the model.

Initial simulations of the hydrodynamic model were undertaken in depth-averaged 2-dimensional (2D) mode, and the model has also been setup as a 3-dimensional (3D) model, with 5 equally spaced sigma layers for depths of 0 to 40 m, and then an additional 5 z layers with each representing 10 m depth bins (i.e. depths down to 90 m in total). Further sensitivity testing of the configuration of the 3D model layers in the HD model will be undertaken when additional measured data are available and this will be used to inform the final configuration for the HD model adopted in the model setup.

The HD model was setup to simulate a 40-day period from 9th June to 24th July 2023 when measured hydrodynamic data were available at AWAC-01 to allow an initial calibration of the model to be undertaken.

4.4.2. Initial Calibration

Model calibration is the process of specifying model parameters so that the model reproduces measured data to a suitable level of accuracy. Model validation is used to confirm that the calibrated model continues to consistently represent the natural processes to the required level of accuracy, in periods other than the calibration period, without any additional adjustment to the model parameters. The calibration and validation processes provide confidence in the model results and are essential to ensure the accurate representation of variations in water levels and currents.

There are no specific model calibration and validation guidelines adopted by the WA EPA and the available numerical modelling guidelines developed in WA (e.g. Sun et al., 2016; and Sun et al., 2020) and elsewhere in Australia (e.g. GBRMPA, 2012) only provide qualitative guidance. The lack of model performance guidelines for coastal and estuarine areas globally resulted in Williams and Esteves (2017) providing metrics of performance based on practical experience. They suggest the following metrics for HD models of estuaries:

- Water Levels: Modelled water levels (WL) should be ±0.1 m in absolute terms of the observed water levels or within 10% of the spring range and 15% of the neap range in relative terms. Level differences are calculated at the time of high water and low water to ensure that the model captures the tidal range. The calibration guideline standard will be considered to be met if it falls within either the absolute or relative standard Mean tidal phase differences to be within ±15 minutes.

- Currents: Differences should be less than 0.10 m/s in absolute terms (or 10 to 20% in relative terms), these are calculated at the time of peak flood and peak ebb. The calibration guideline standard will be considered to be met if it falls within either the absolute or relative standard. Current directions are within 10 to 15º at the times of peak flood and peak ebb.

Although the guidelines do not provide recommendations for the calibration of tidal residuals it is important to note that these are important for sediment transport and plume dispersion. Based on this the final calibration of the model will include residual currents at key measurement sites.

An initial calibration of the hydrodynamic model has been undertaken using the measured water level and current data collected at AWAC-01 in June to July 2023. Further, more extensive model calibration and validation will be undertaken during subsequent stages of the study. The model will be calibrated and validated at multiple sites using both wet and dry season measured water level and current data.

The measured and modelled water level at AWAC-01 are shown in Figure 74, and the measured and modelled current speed and direction are shown at varying depths through the water column in Figure 75 to Figure 83. A statistical summary of the model calibration is shown for the water levels and currents in Table 5 and Table 6, respectively. The results from this initial calibration adhere to the model performance guidelines recommended by Williams and Esteves (2017) which demonstrates that the HD model is able to provide a realistic representation of the water levels and currents through the water column at AWAC-01.

Table 5. Statistics for comparison of modelled and measured water levels at AWAC-01 during the initial calibration period.

Site	WL difference (m)			WL difference (%)		Phase difference (minutes)		
	HW	LW	RMS	HW	LW	HW	LW	All
AWAC-01	-0.01	-0.05	0.17	0	-1	9	-3	2

Notes: Differences are modelled minus predicted/measured so that positive values indicate that the model value is high/late relative to predicted/measured

Table 6. Statistics for comparison of modelled and measured currents through the water column at AWAC-01 during the initial calibration period.

Period	Speed difference (m/s)			Speed difference (%)		Direction difference (°)		Phase difference (minutes)
	PF	PE	RMS	PF	PE	PF	PE	All
AWAC-01								
Surface	-0.11	0.04	0.14	-7	4	-3	7	-9
Mid	-0.06	0.11	0.11	-5	12	-4	-2	-3
Near-Bed	-0.07	0.09	0.1	-6	11	-6	-10	-4

Notes: Differences are modelled minus predicted/measured so that positive values indicate that the model value is high/late relative to predicted/measured

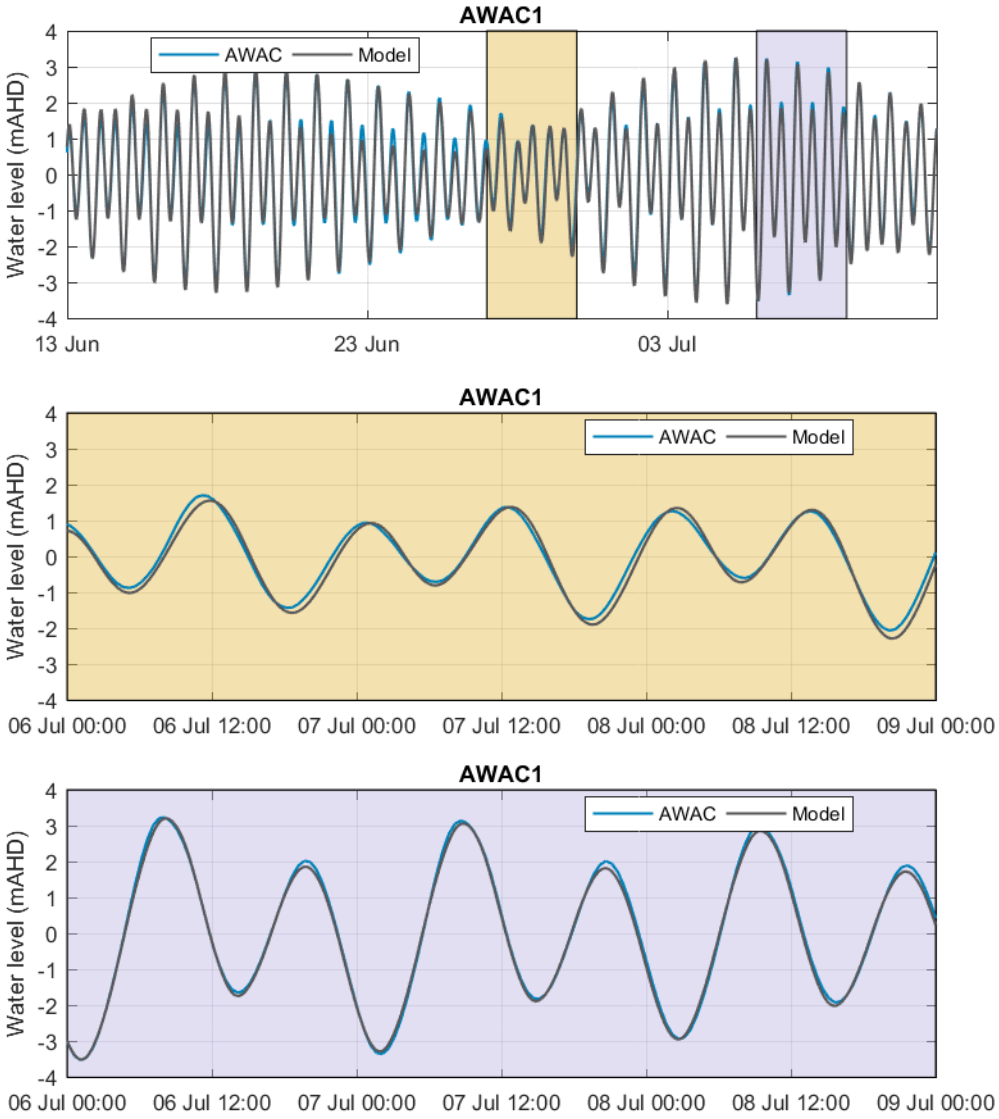

Figure 74. **Modelled and measured water level over the entire 29-day calibration period (top) and during 3 days of neap tides (mid) and 3 days of spring tides (top) at AWAC-01.**

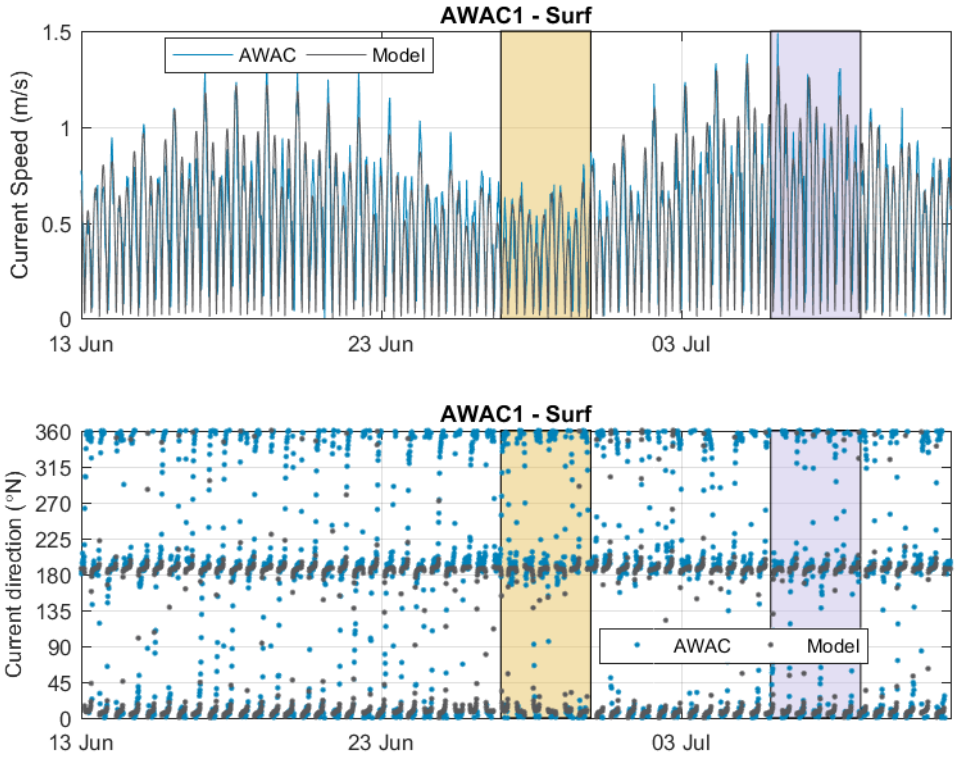

Figure 75. **Modelled and measured current speed in the surface layer over the entire 29-day calibration period at AWAC-01.**

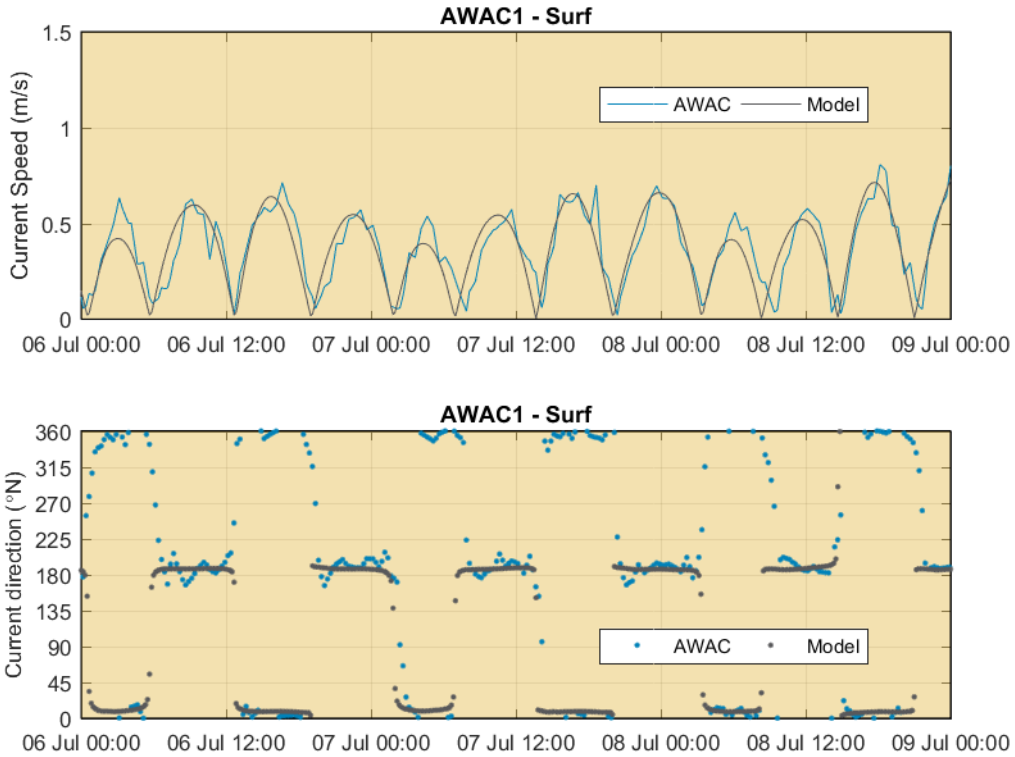

Figure 76. **Modelled and measured current speed in the surface layer over the 3 days of neap tides at AWAC-01.**

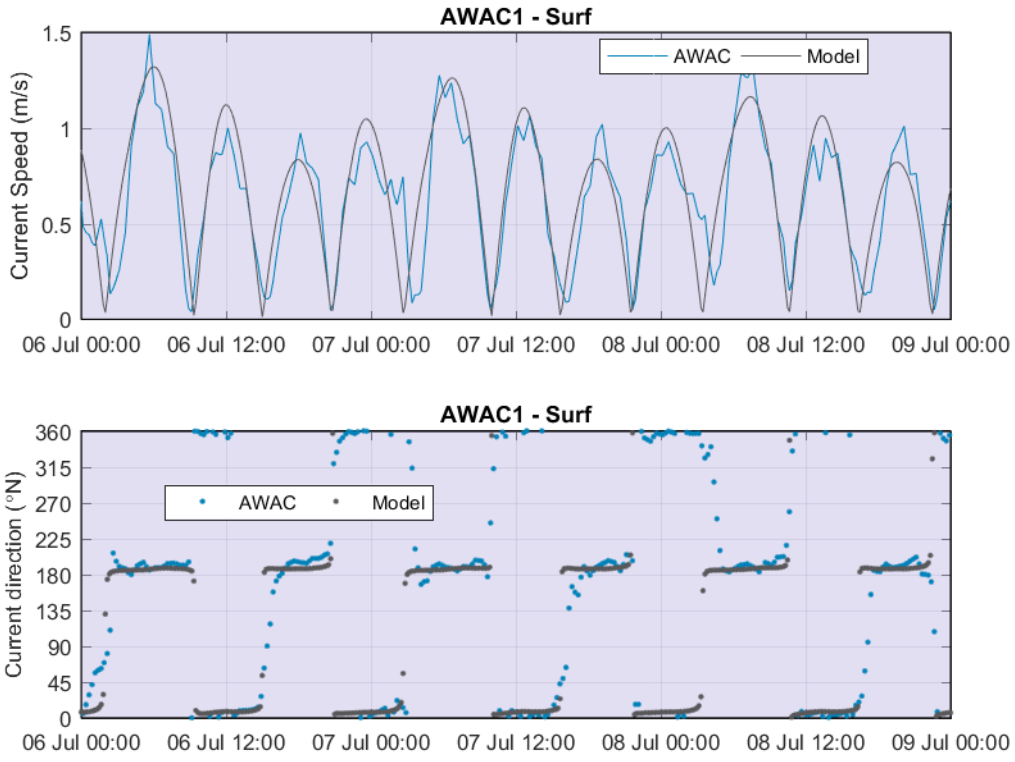

Figure 77. **Modelled and measured current speed in the surface layer over the 3 days of spring tides at AWAC-01.**

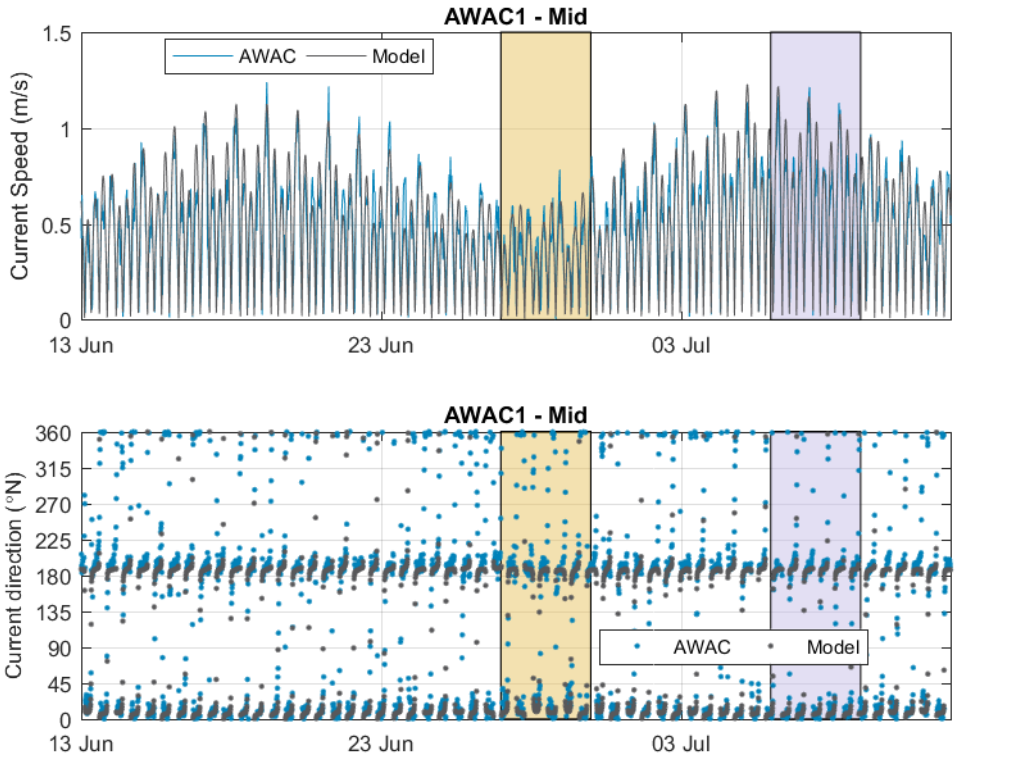

Figure 78. **Modelled and measured current speed in the middle layer over the entire 29-day calibration period at AWAC-01.**

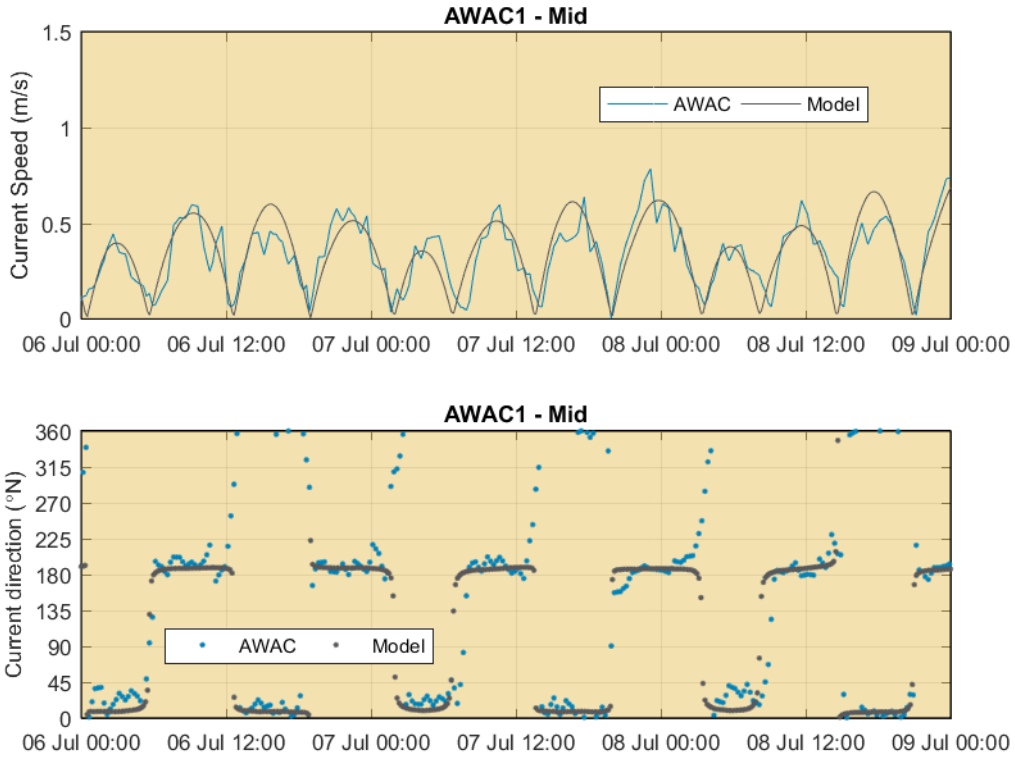

Figure 79. **Modelled and measured current speed in the middle layer over the 3 days of neap tides at AWAC-01.**

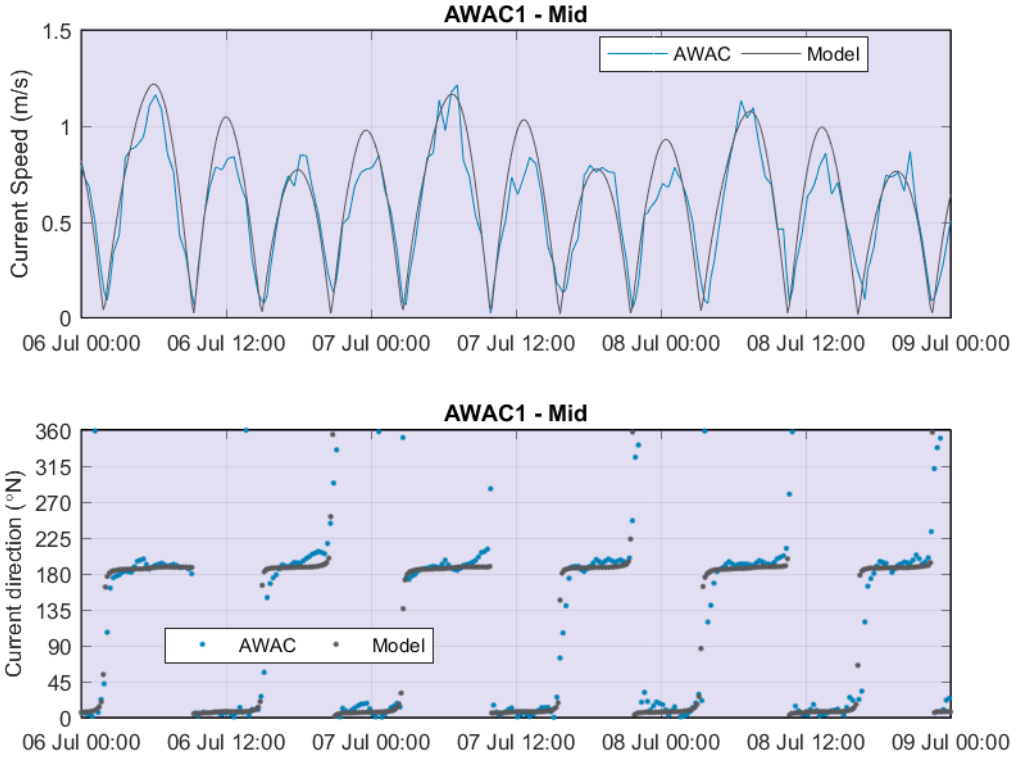

Figure 80. **Modelled and measured current speed in the middle layer over 3 days of spring tides at AWAC-01.**

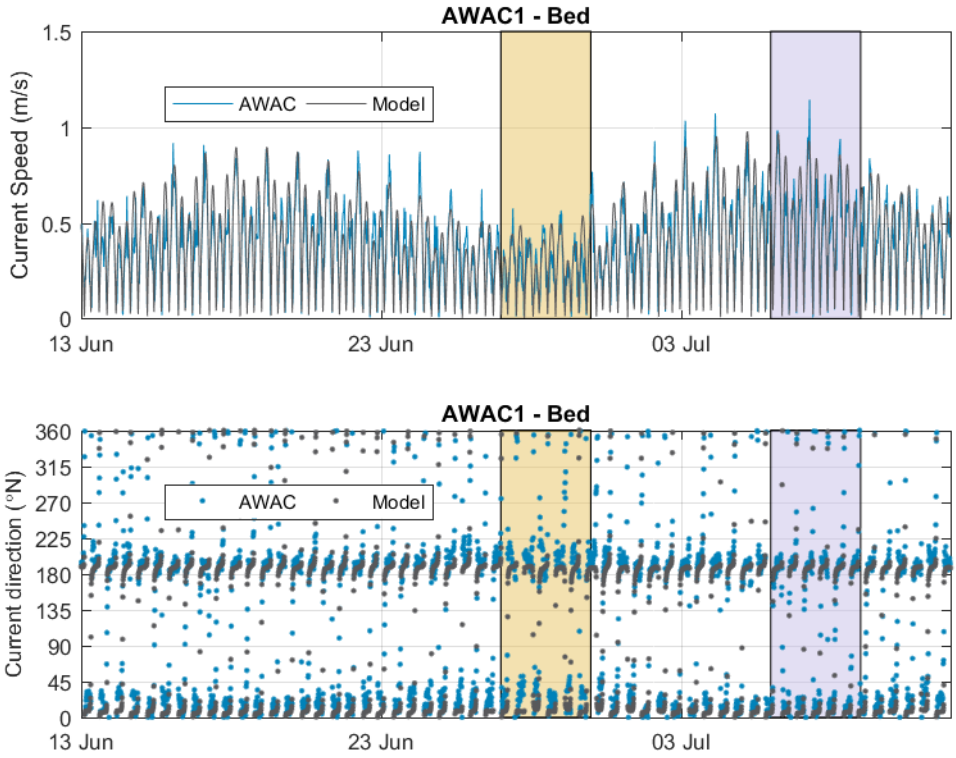

Figure 81. **Modelled and measured current speed in the bed layer over the entire 29-day calibration period at AWAC-01.**

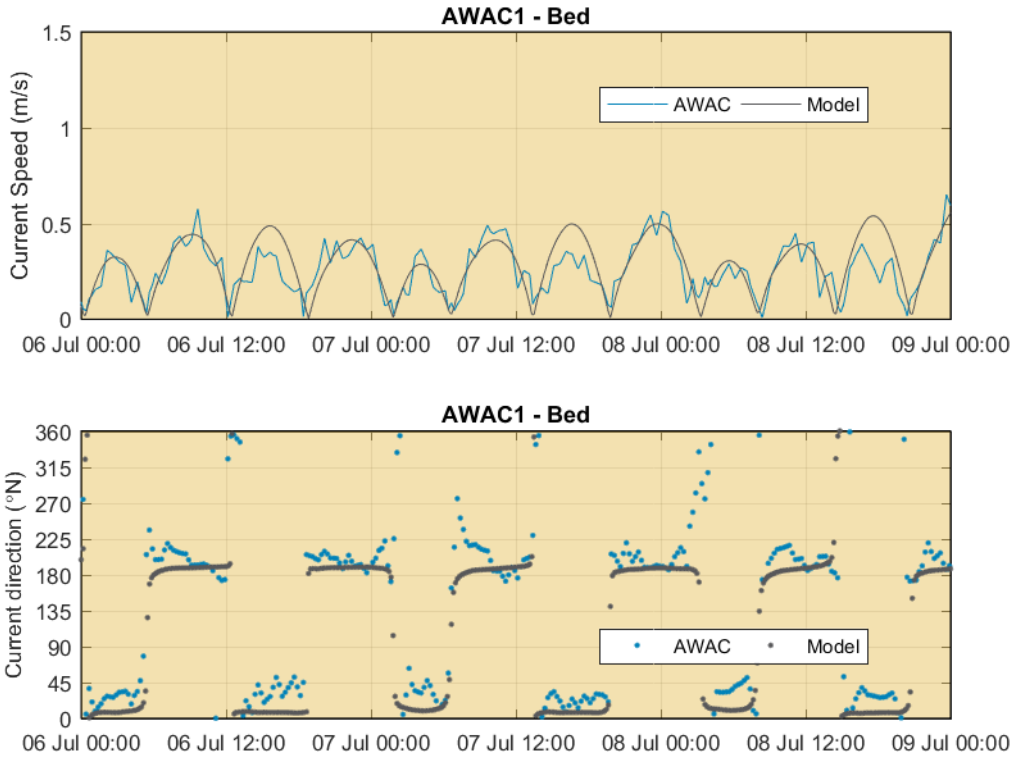

Figure 82. **Modelled and measured current speed in the bed layer over 3 days of neap tides at AWAC-01.**

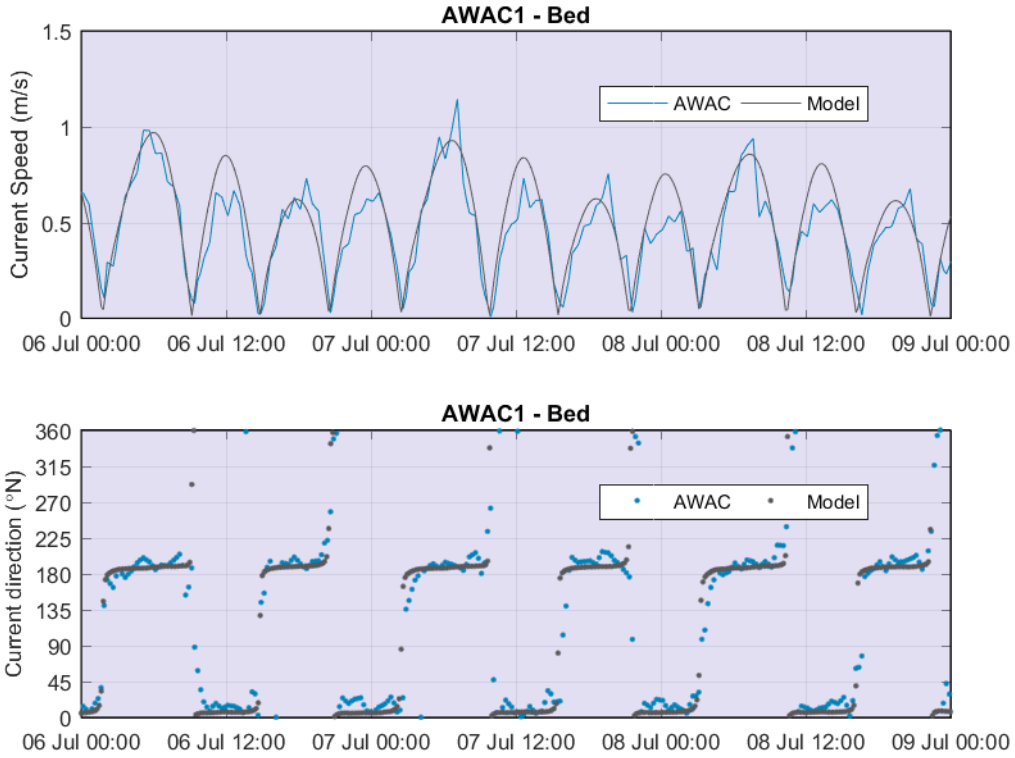

Figure 83. Modelled and measured current speed in the bed layer over 3 days of spring tides at AWAC-01.

4.4.3. *Preliminary Results*

Spatial maps from the HD model of the depth averaged current speed and flow vectors at peak flood and peak ebb during spring and neap tides are shown in Figure 84 to Figure 87. Spatial maps showing the modelled residual current speed over a spring and neap tide are shown in Figure 88 and Figure 89. In addition, a timeseries plot of the flux of water through the western and eastern entrances to CG is shown in Figure 90. The plots show the following:

- Offshore of CG the tide floods and ebbs from/to the north-west, with the highest flows occurring through the deeper channel to the east of King Shoals. Relatively high current speeds also occur around King Shoals and to the west of CG, while the current speeds around Medusa Bank to the north and north-east of CG are consistently low during both the flood and ebb stages of the tide.

- Higher current speeds occur in the western entrance to CG compared to the eastern entrance, with peak speeds in the western entrance of around 1.2 m/s during spring tides compared to 0.8 m/s in the eastern entrance and 0.8 m/s compared to 0.6 m/s during neap tides. The timing of the peak flood and peak ebb currents is the same in the two entrances. The flux of water flowing through the western entrance during both the flood and ebb stages of the tide is in the order of three times larger than the flux of water through the eastern entrance.

- Current speeds within CG are typically higher on the flood stage of the tide than on the ebb stage of the tide, although this dominance does vary spatially through CG and temporally between spring and neap tides (e.g. current speeds in the eastern entrance are flood dominant during spring tides, but ebb dominant during neap tides). The modelled residual current speeds during both spring and neap tides are low, with speeds less than 0.1 m/s over the majority of CG and less than 0.05 m/s for most of the proposed operational area. This shows that despite the current speeds on the flood and ebb stages of the tide differing, the flows in and around CG are relatively balanced over both spring and neap tides.

- The highest current speeds within the open bay area of CG occur to the south of the western entrance, with lower current speeds to the south of the eastern entrance. During spring tides, the peak flows in CG are above 1.0 m/s for much of the area, while during neap tides this reduces to between 0.6 to 0.8 m/s.

- The peak current speeds are typically high (1.0 to 2.5 m/s) in West Arm during both the flood and ebb stages of the tide, while peak current speeds in East Arm are lower (0.4 to 1.5 m/s).

Measured current data collected by BKA to the south of the west entrance to CG (at AWAC-01) and in 2002 at AIMS A (approximately located at AWAC-06) and AIMS B (approximately located at AWAC-04) showed varying flood and ebb current speed dominance and it was unknown if this difference was due to spatial variations or differences in ebb flows between the wet and dry seasons. To help understand this, timeseries plots of water level, current speed and direction from the HD model at multiple locations within CG close to the west and east entrances are shown in Figure 91. The plots show the following:

- At AWAC-01 and AWAC-05, the peak flood tide current speeds are up to 0.2 m/s higher than the peak ebb tide current speeds during spring tides, with the difference reducing to up to 0.1 m/s during neap tides.

- At AWAC-04 (approximately equivalent to AIMS-B) and AWAC-06 (approximately equivalent to AIMS-A), there was very little difference between the peak flood and ebb current speeds, although the flood current speed was typically still slightly higher at both. The data collected in the wet season by AIMS (Wolanski et al, 2004) showed comparable flood and ebb current speeds at AWAC-06, but at AWAC-04 the data showed a consistent ebb current speed dominance which the model does not replicate. The currents at AWAC-04 will be further assessed and compared with the previous measured data and the modelled currents once current data at this site are available.

The results suggests that the difference in flood and ebb current speed dominance between AWAC-01 and AIMS-B is partially due to different currents occurring at the two different sites and potentially also due to increased river flows during the wet season, increasing the ebb current speeds.

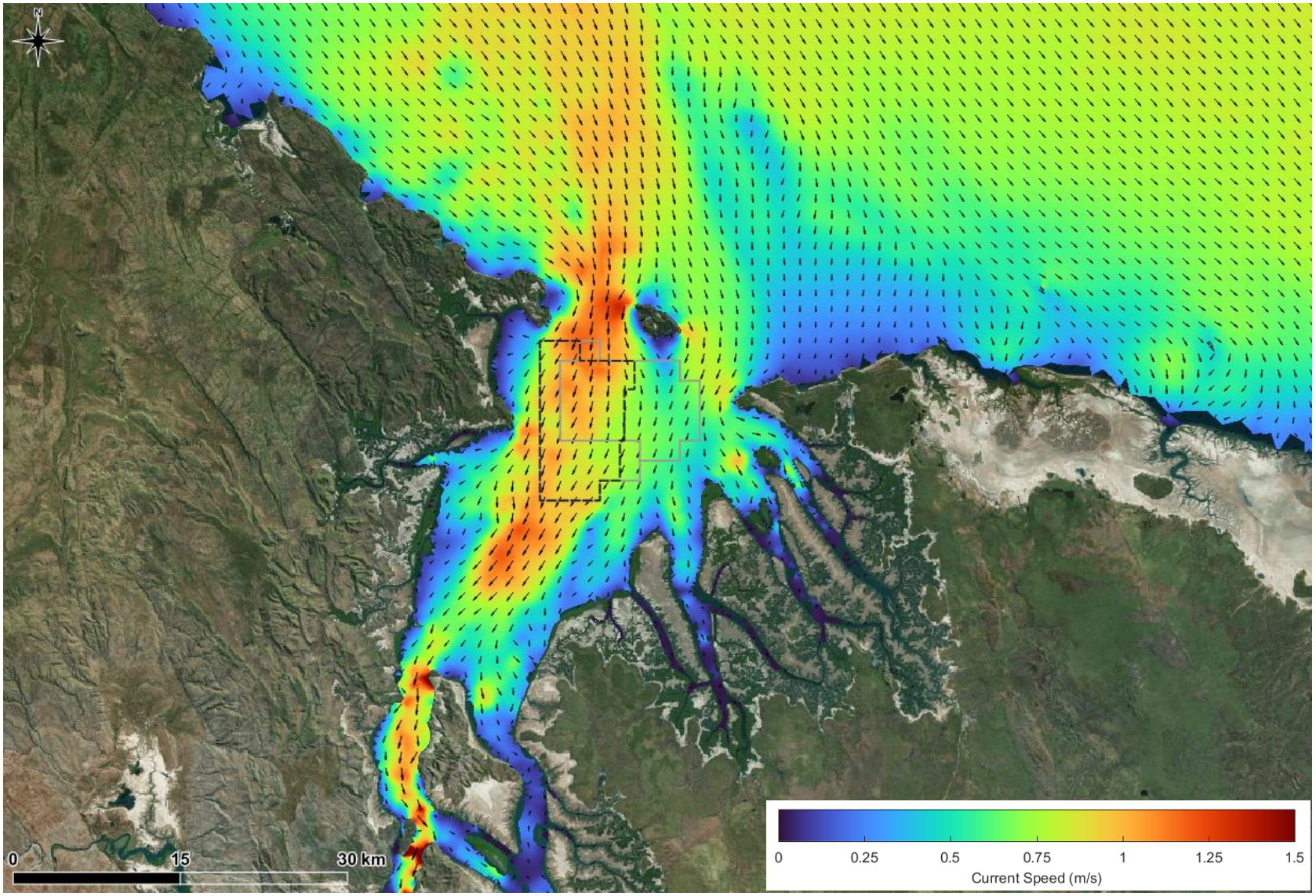

Figure 84. Modelled depth-averaged current speed in CG at peak flood during a spring tide.

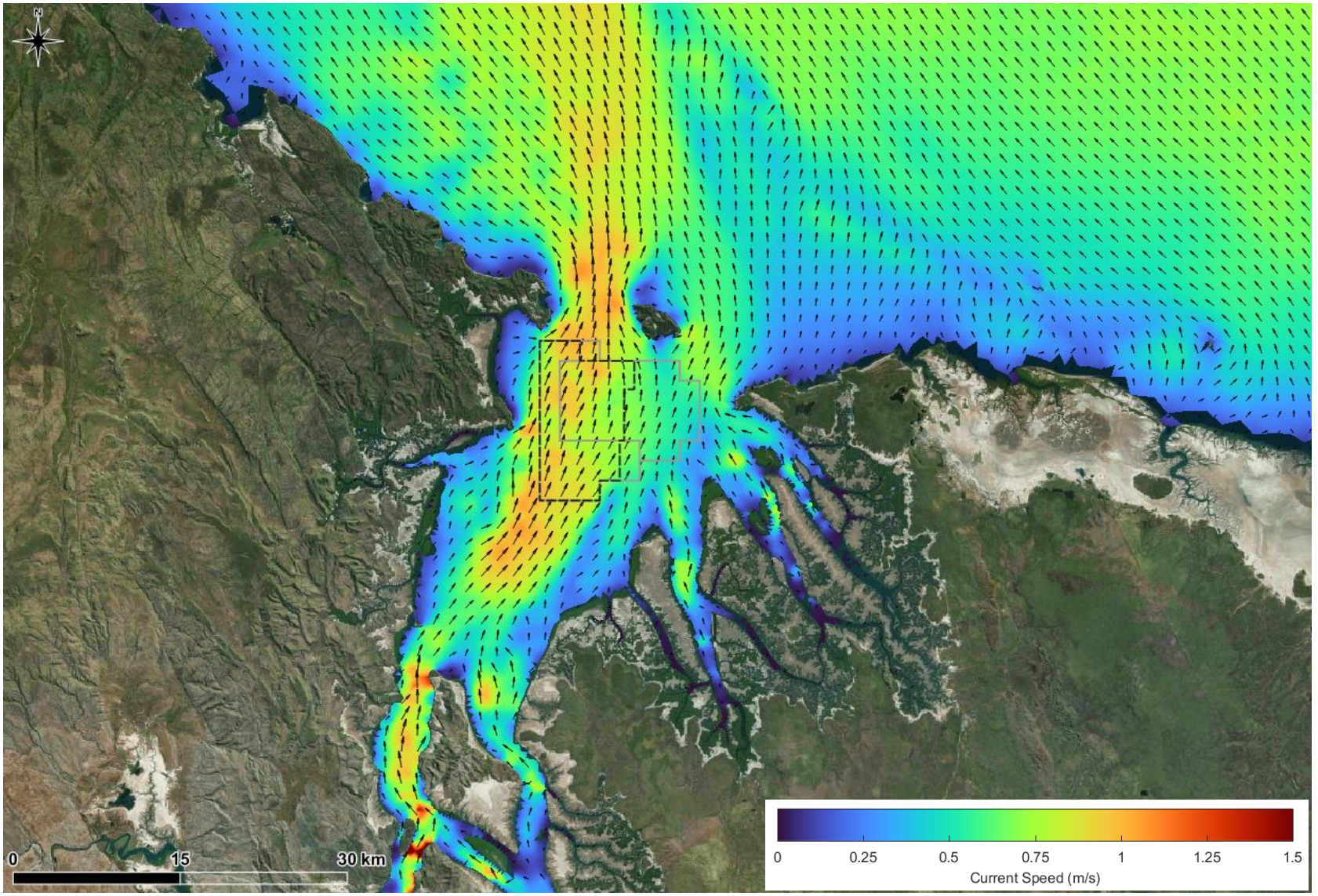

Figure 85. Modelled depth-averaged current speed in CG at peak ebb during a spring tide.

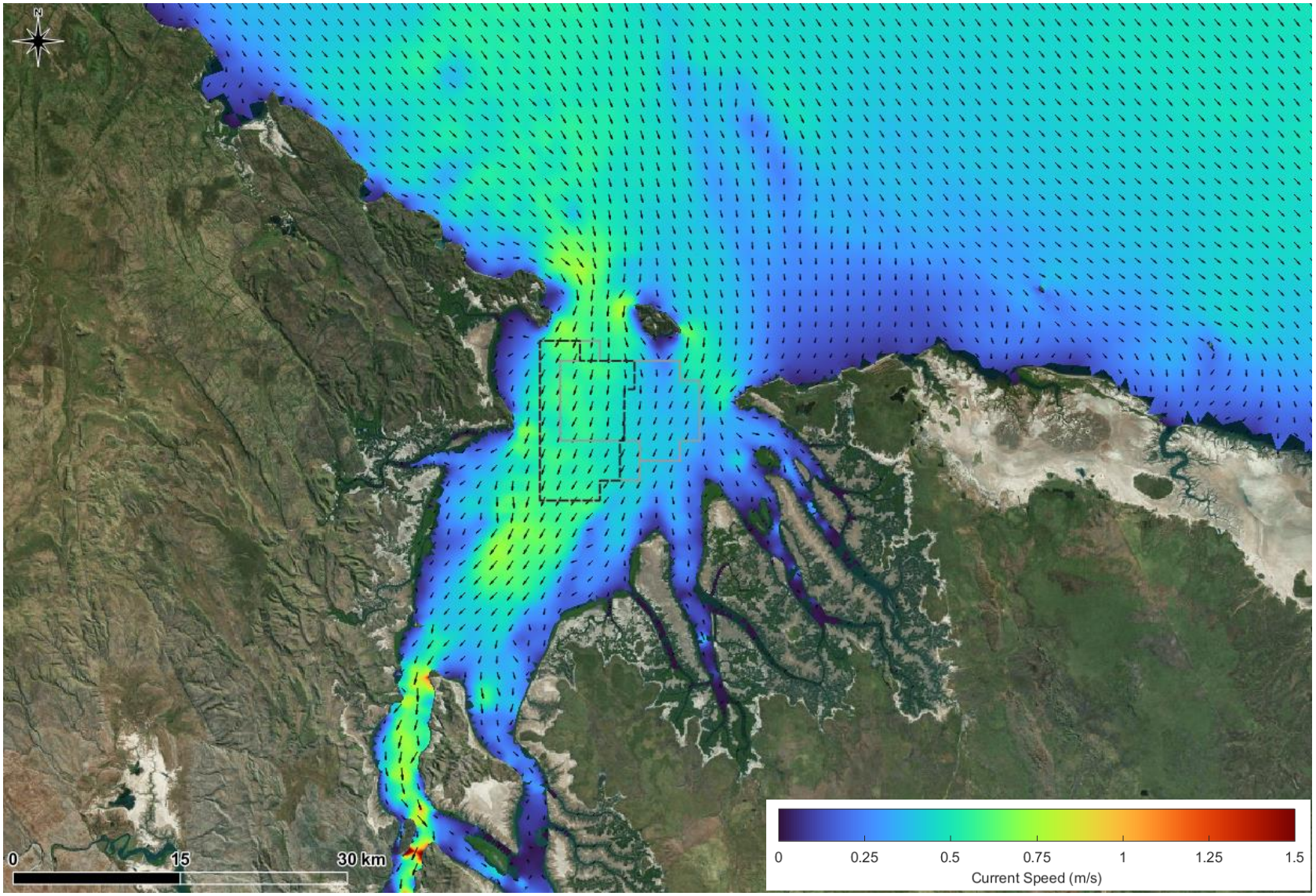

Figure 86. Modelled depth-averaged current speed in CG at peak flood during a neap tide.

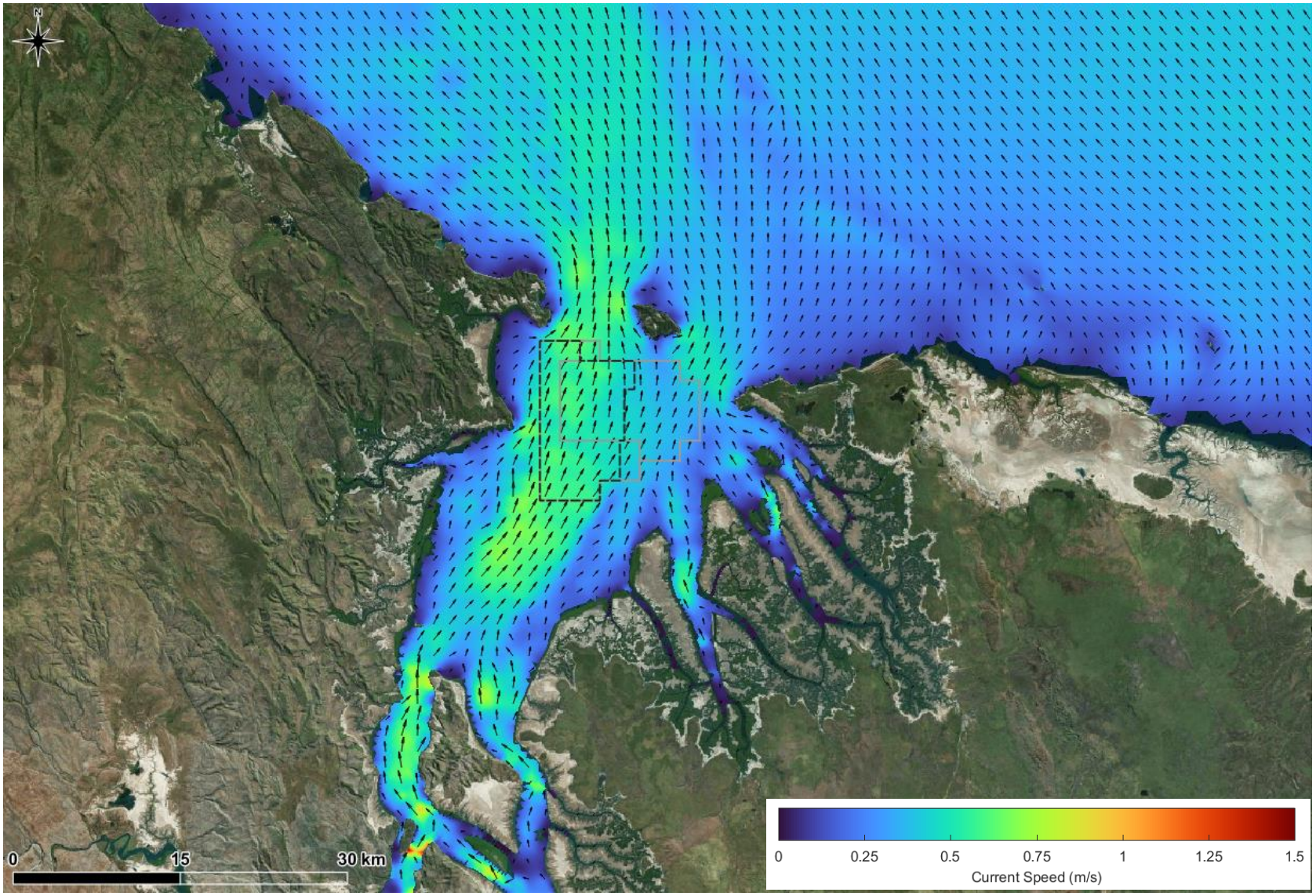

Figure 87. Modelled depth-averaged current speed in CG at peak ebb during a neap tide.

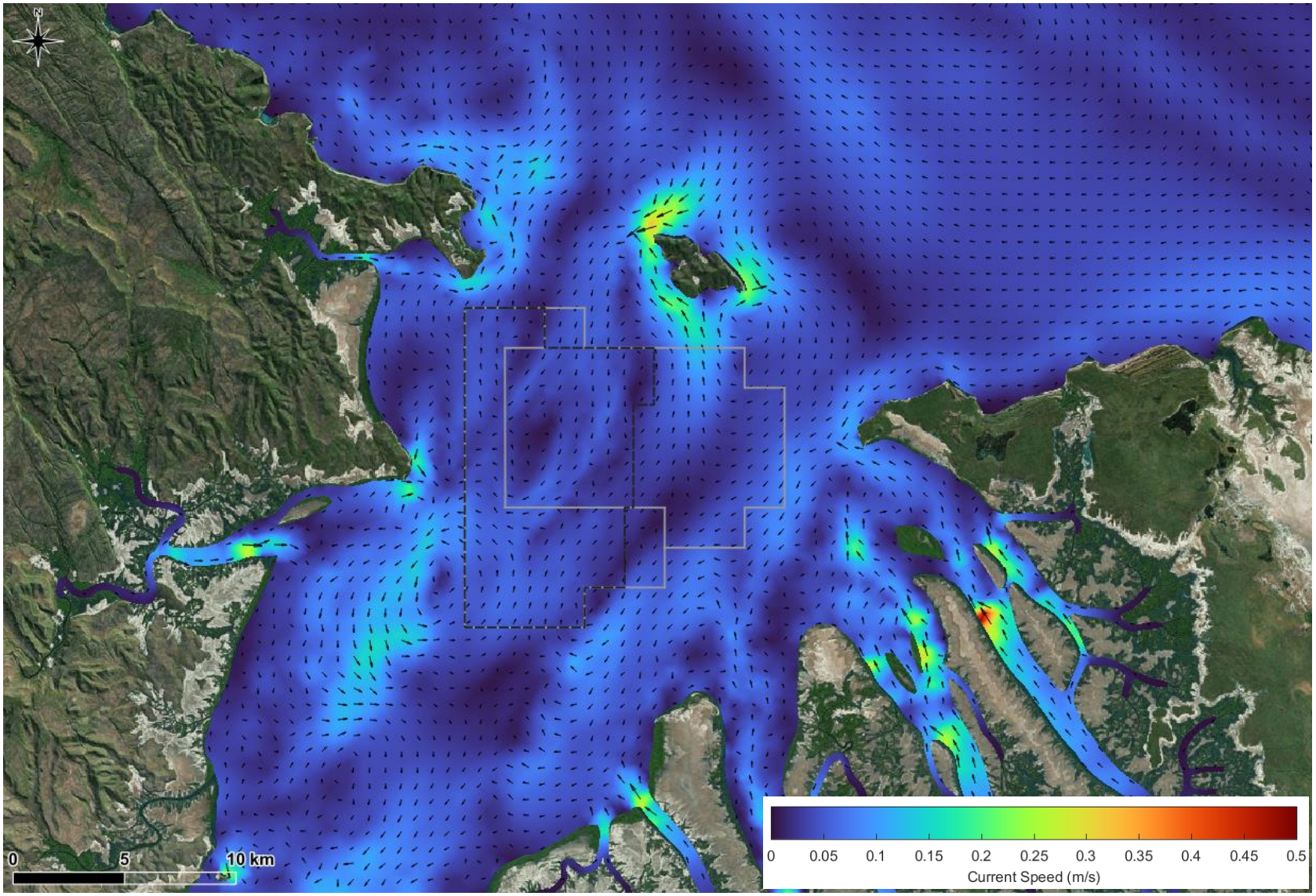

Figure 88. Modelled depth-averaged residual current speed in CG over a spring tide.

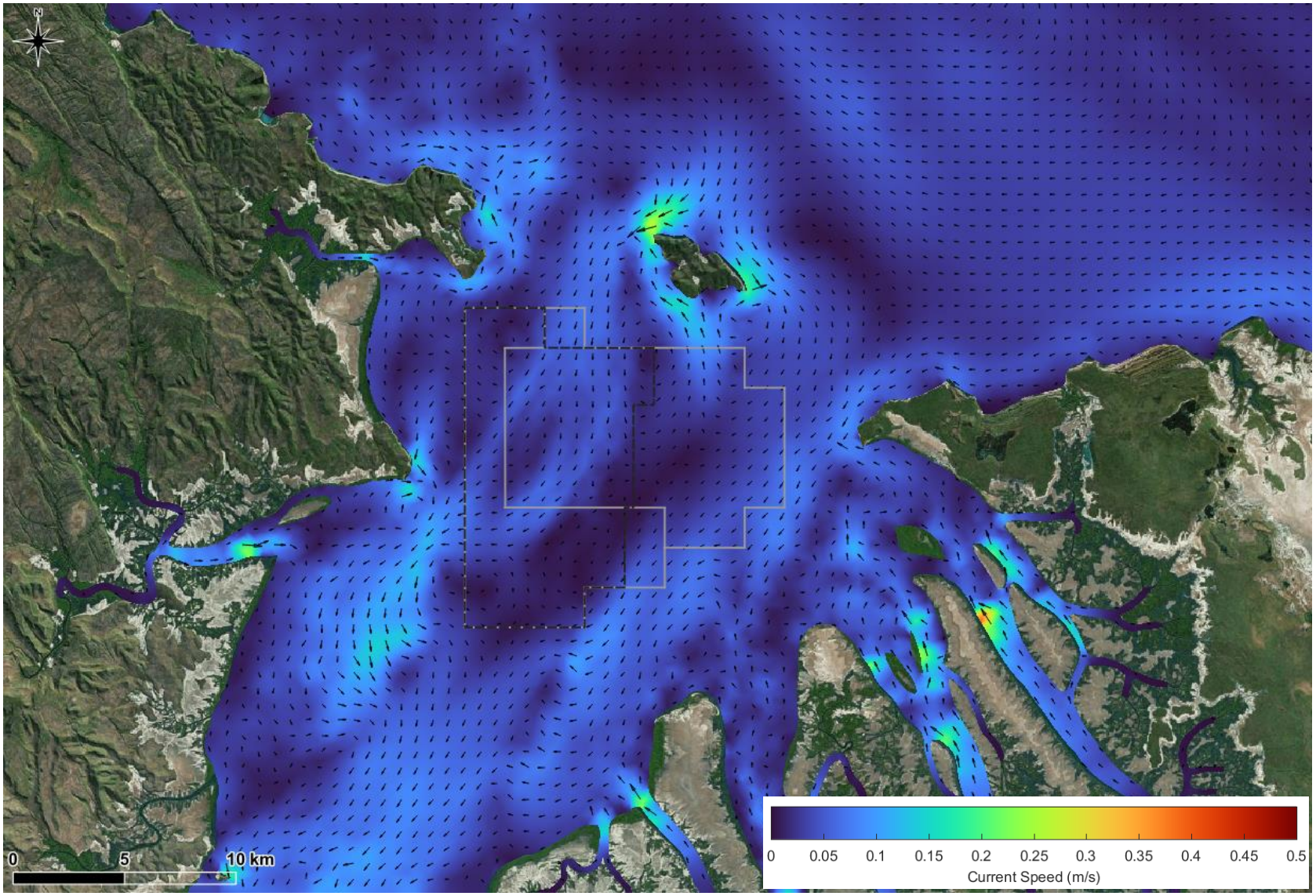

Figure 89. Modelled depth-averaged residual current speed in CG over a neap tide.

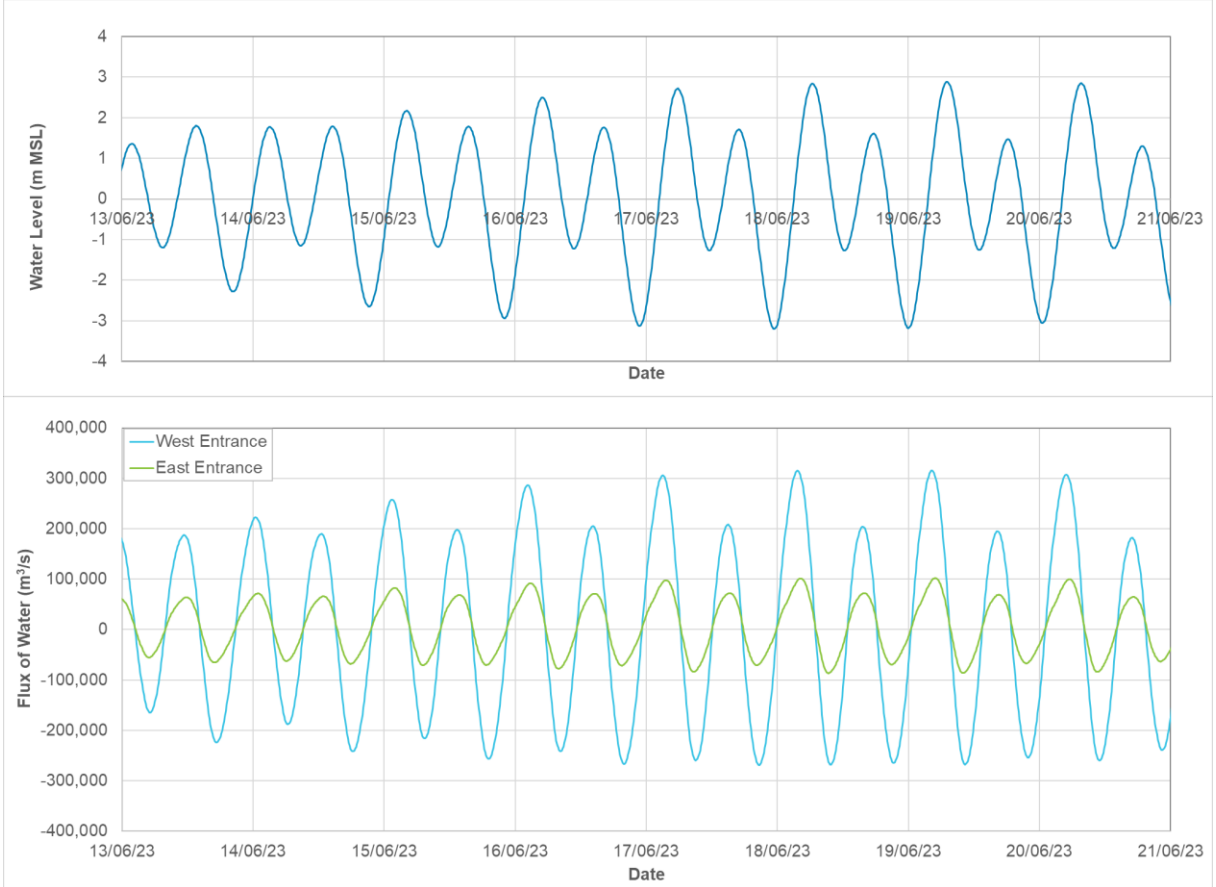

Figure 90. Modelled water level at AWAC-01 and modelled flux of water through the West and East entrances to CG over a 7-day period. *Note: positive flux is flowing into CG, negative flux is flowing out of CG.*

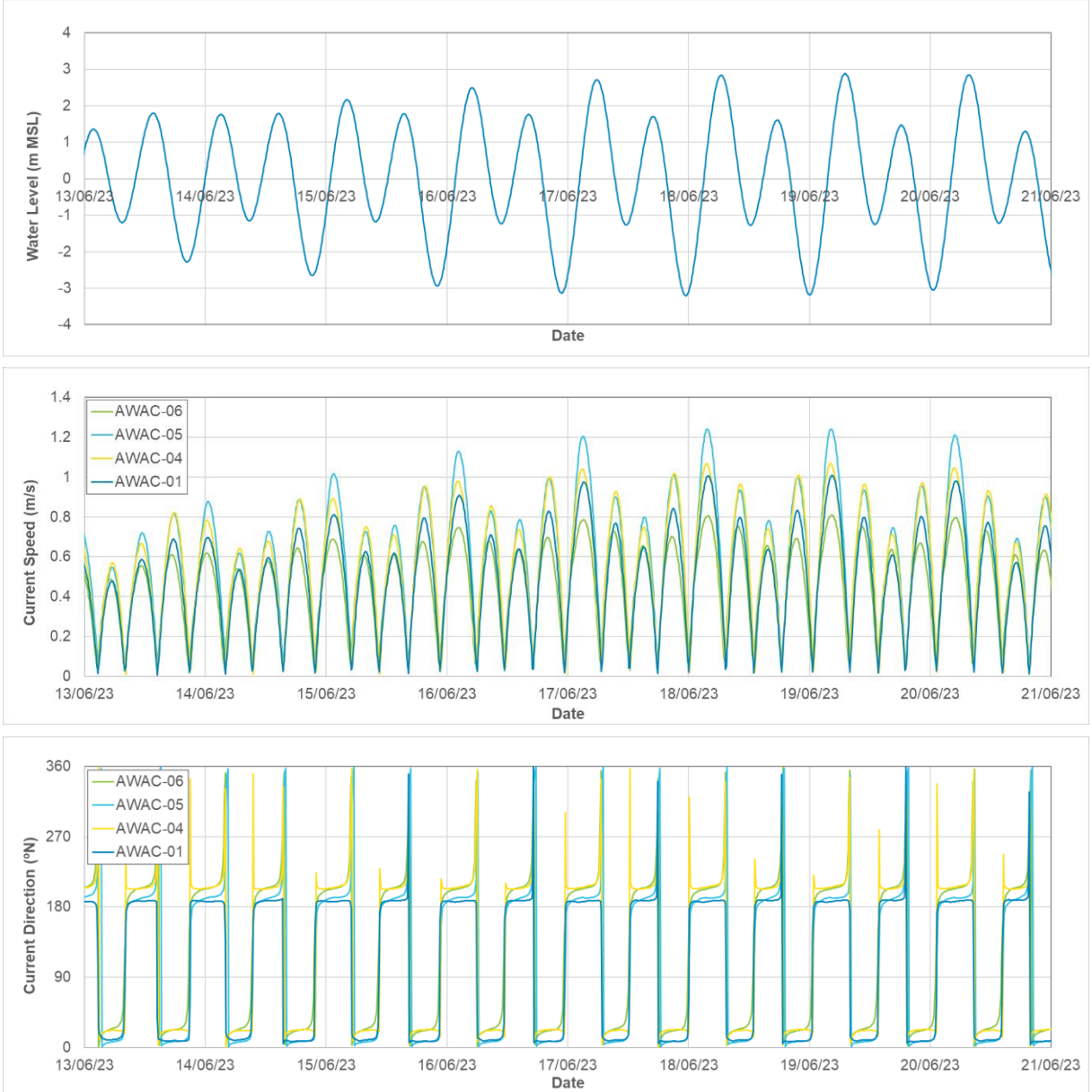

Figure 91. Modelled water level at AWAC-01 and current speed and direction at AWACs 01, 04, 05 and 06 over a 7-day period.

4.4.4. Preliminary Impacts

Based on the initial calibration of the HD model detailed in Section 4.4.2, there is sufficient confidence in the HD model to allow a preliminary impact assessment to be undertaken. The approach adopted and results from this are detailed in this section.

The HD model mesh was setup to represent the existing bathymetry for CG as well as the bathymetry following the sourcing of 70 million m^3 of sand (i.e. the total volume proposed over the 15 years). It has been assumed that the sand is sourced evenly over the entire proposed operational area, resulting in a deepening of 0.68 m in this area. The 3D HD model was setup to simulate the hydrodynamics for the existing base case (no sand sourcing) and the sourcing of 70 million m^3 of sand over a dry season 15 day spring neap tidal cycle.

Spatial maps showing the predicted change in water level and tidal current speed due to the deepening of the bathymetry from the 70 million m^3 sand sourcing are shown in Figure 92 to Figure 95. The results from the existing case simulation were subtracted from the sand sourcing simulation results (i.e. a positive change shows an increase due to the sand sourcing and a negative change shows a reduction due to the sand sourcing). In addition, the change in tidal range during a spring tide relative to the existing tidal range is quantified in Table 7 and the maximum change in current speed

during the flood and ebb stages of a spring tide relative to the peak flood and ebb current speeds is quantified in Table 8. The results show the following:

- Water Level: The spatial changes are predominantly constrained within CG and within ±0.01 m, with the largest changes occurring during the peak flood and peak ebb stages of the tide. As the percent change in tidal range is small (up to 0.06%), the spatial changes shown are actually from a slight change in the phase of the tidal signal as opposed to a change in the tidal range. The change in phase varies spatially within CG, but is in the order of tens of seconds (this is discussed in more detail below).

- Current Speed: The spatial changes in current speed are more localised within and adjacent to the proposed operational area compared to the changes in water level. The changes are predominantly a reduction in current speed within and adjacent to the proposed operational area of up to -0.01 m/s, although localised areas with a predicted increase in current speed of up to 0.01 m/s also occur adjacent to the boundary of the proposed operational area. The percent change in current speed relative to the peak current speeds shows that the largest changes occur within the proposed operational area (around the AWAC-01 site) where current speeds were reduced by 1.3%. The changes outside of the proposed operational area were lower, with both increases and reductions in current speed of up to 0.8% predicted.

To help understand how the proposed deepening due to the sand sourcing could influence water levels and currents in CG, timeseries plots have been extracted from the model at a number of the AWAC locations (Figure 96). Plots of the modelled water level, current speed and current direction for the existing base case and the 70 million m^3 sand sourcing case over an 8 day period (selected to show changes over both spring and neap tides while still showing a short enough duration to allow differentiation between when in the tidal cycle the changes occur) as well as the predicted change due to the sand sourcing are shown in Figure 97 to Figure 102. It is important to note that the plots show results for both the existing base case (no sand sourcing) and the 70 million m^3 sand sourcing case but generally they are almost identical and so it is not possible to differentiate between the two. The plots show the following:

- Water Level: The largest changes are predicted at the sites upstream of the proposed operational area (i.e. AWAC-08 and AWAC-11), with a positive change predicted during the flood stage of the tide and a negative change predicted during the ebb stage of the tide. At high water and low water there is little to no change in water level predicted, showing that the apparent change at these locations is due to a slight change in the phase of the tidal propagation into CG. The change in phase of the tide varies through CG, but based on the spatial maps the largest changes in water level were around the entrance to West Arm, indicating that the phase lag due to the sand sourcing was highest in this area of CG. Therefore, the timeseries data at AWAC-08 have been used to estimate the phase lag. This showed that the 70 million m^3 sand sourcing is predicted to result in the flood and ebb stages of the tide occurring earlier by up to 27s.

- Current Speed: The largest change is predicted within the proposed operational area (AWAC-01) with a reduction in current speed predicted during both the flood and ebb stages of the tide. At the other locations outside of the proposed operational area the changes vary between increases and decreases in current speed, with the changes consistently being small compared to the actual current speed.

- Current Direction: At all sites negligible change in current direction is predicted during the flood and ebb stages of the tide. The results show the potential for short duration changes in current direction due to the sand sourcing when the current switches direction (from flood to ebb or vice versa). This is a result of the slight phase change resulting from the sand sourcing schemes and occurs at a time with very low current speeds and so is considered insignificant.

Overall, the HD modelling results have predicted that the sourcing of 70 million m^3 from the proposed operational area will result in very small changes to both water levels and currents in CG. The phasing of the tidal propagation upstream of the proposed operational area has been predicted to be changed by 27 s (earlier) and this results in apparent changes in water level and current speed during the flood and ebb stages of the tide. The sand sourcing is not predicted to measurably impact the tidal range within CG (changes of up to 0.06%). The deepening due to the sand sourcing is predicted to result in a localised reduction in current speed within the proposed operational area of up to 1.5% of the peak current speeds.

Table 7. Percent change in spring tidal range due to the 70 million m^3 sand sourcing relative to the total tidal range.

Location	Change in Tidal Range
AWAC-01	0.05%
AWAC-05	0.06%
AWAC-06	0.04%
AWAC-07	0.03%
AWAC-08	0.02%
AWAC-11	0.04%

Table 8. Percent change in flood and ebb spring tidal current speed due to the 70 million m^3 sand sourcing relative to the peak flood and ebb spring current speeds.

Location	Flood Current Speed Change	Ebb Current Speed Change
AWAC-01	-1.3%	-1.5%
AWAC-05	0.3%	-0.4%
AWAC-06	-0.4%	-0.7%
AWAC-07	0.3%	0.2%
AWAC-08	0.3%	0.4%
AWAC-11	0.4%	0.8%

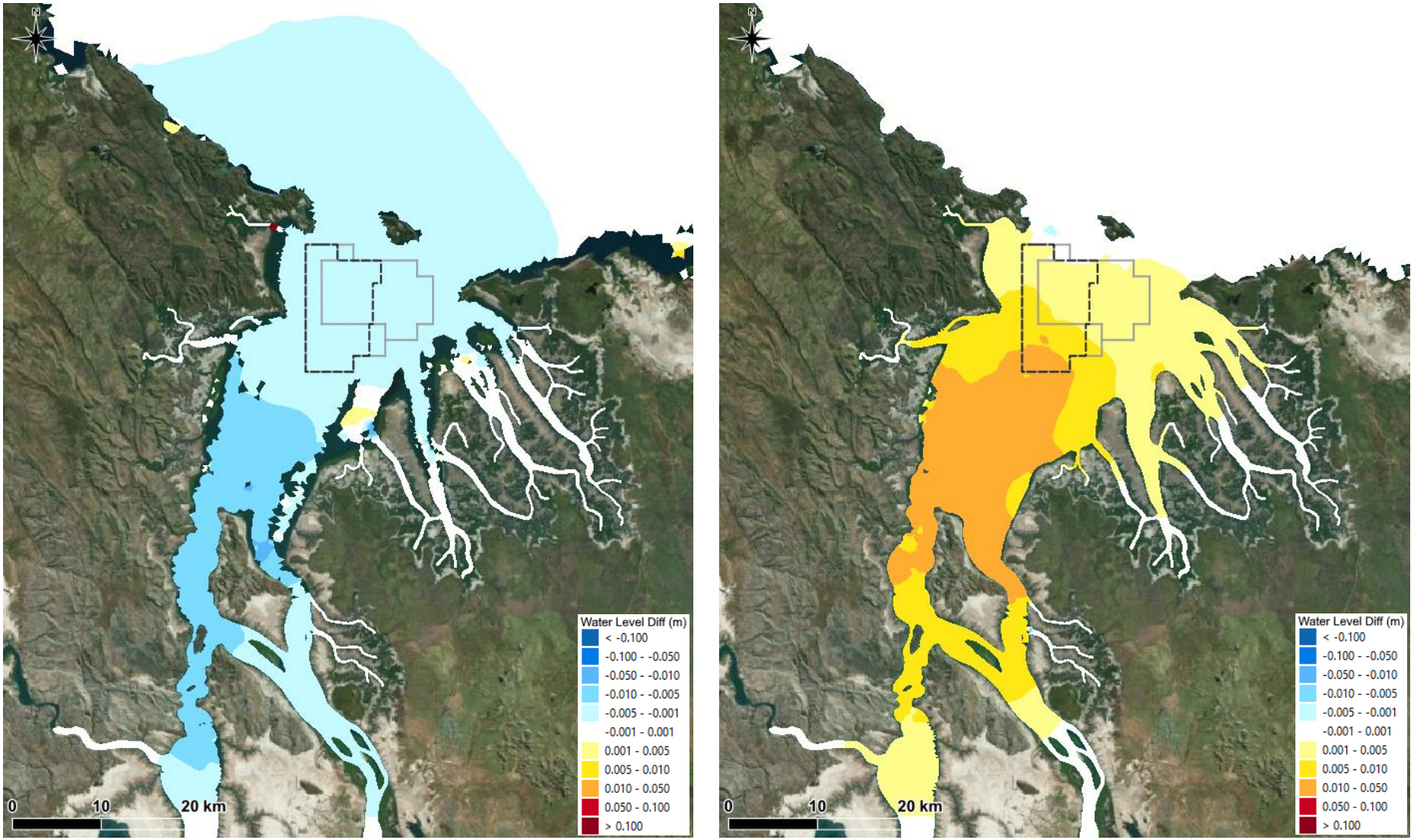

Figure 92. Change in water level at low water (left) and peak flood (right) during a spring tide as a result of 70 million m^3 of sand sourcing.

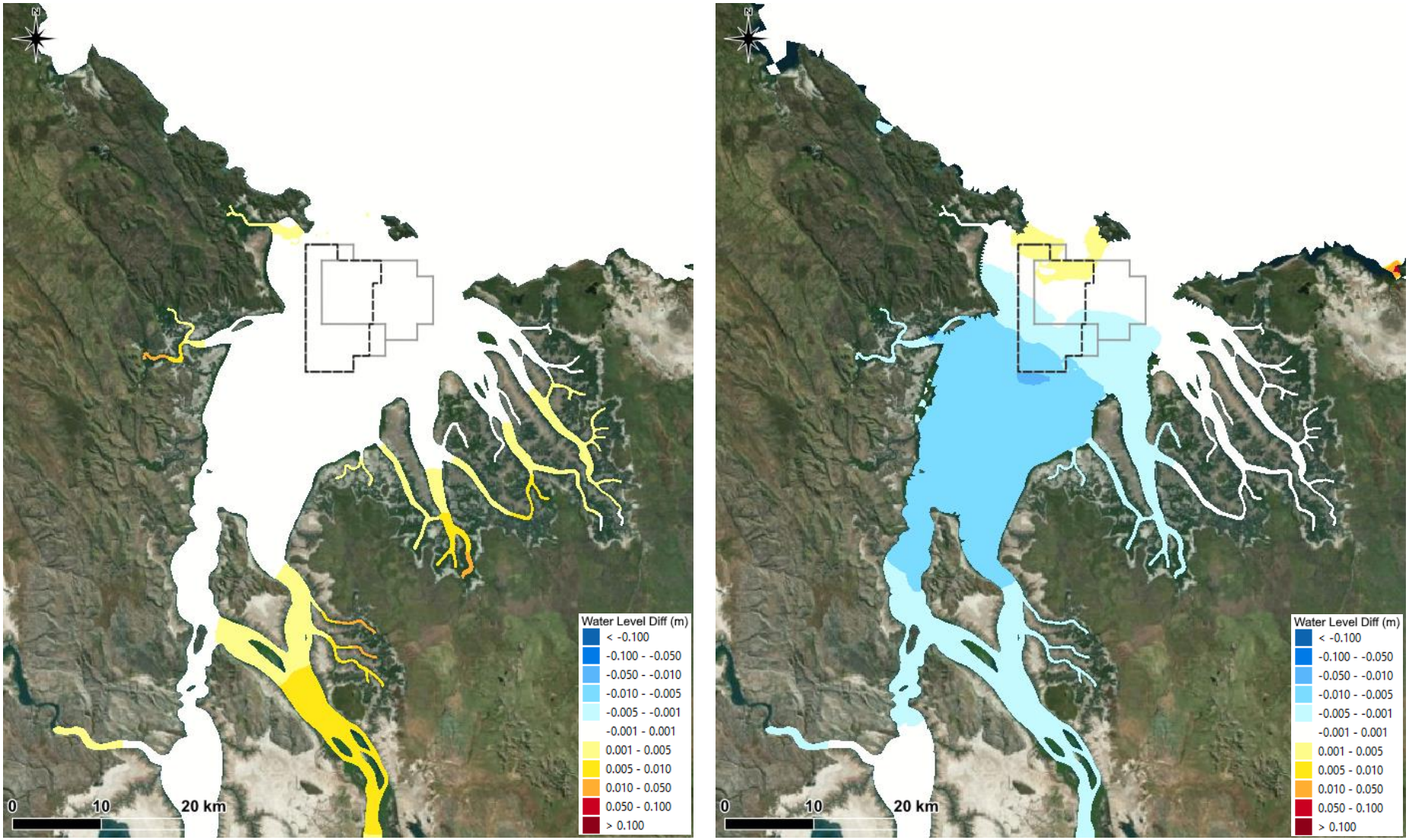

Figure 93. Change in water level at high water (left) and peak ebb (right) during a spring tide as a result of 70 million m^3 of sand sourcing.

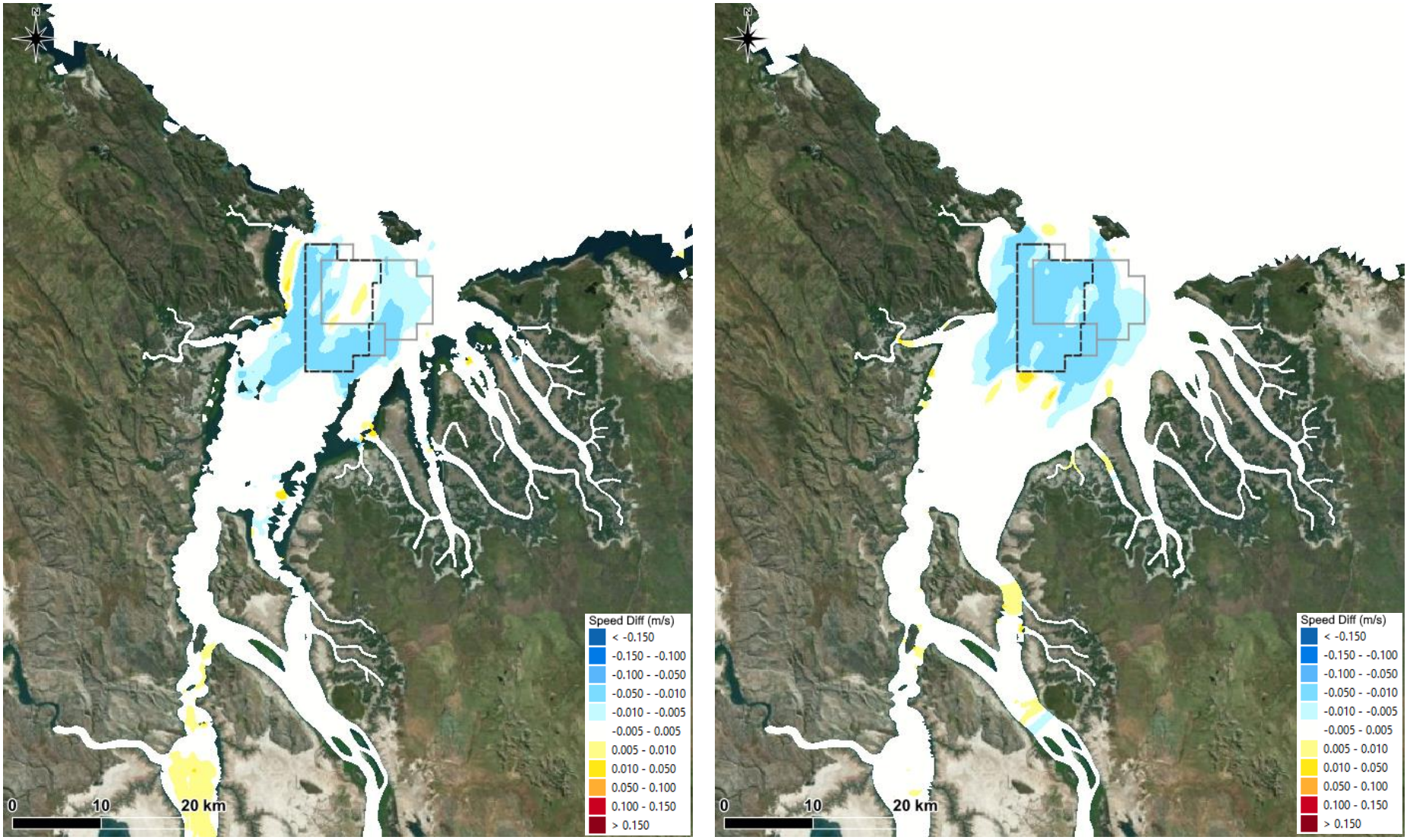

Figure 94. Change in current speed at low water (left) and peak flood (right) during a spring tide as a result of 70 million m^3 of sand sourcing.

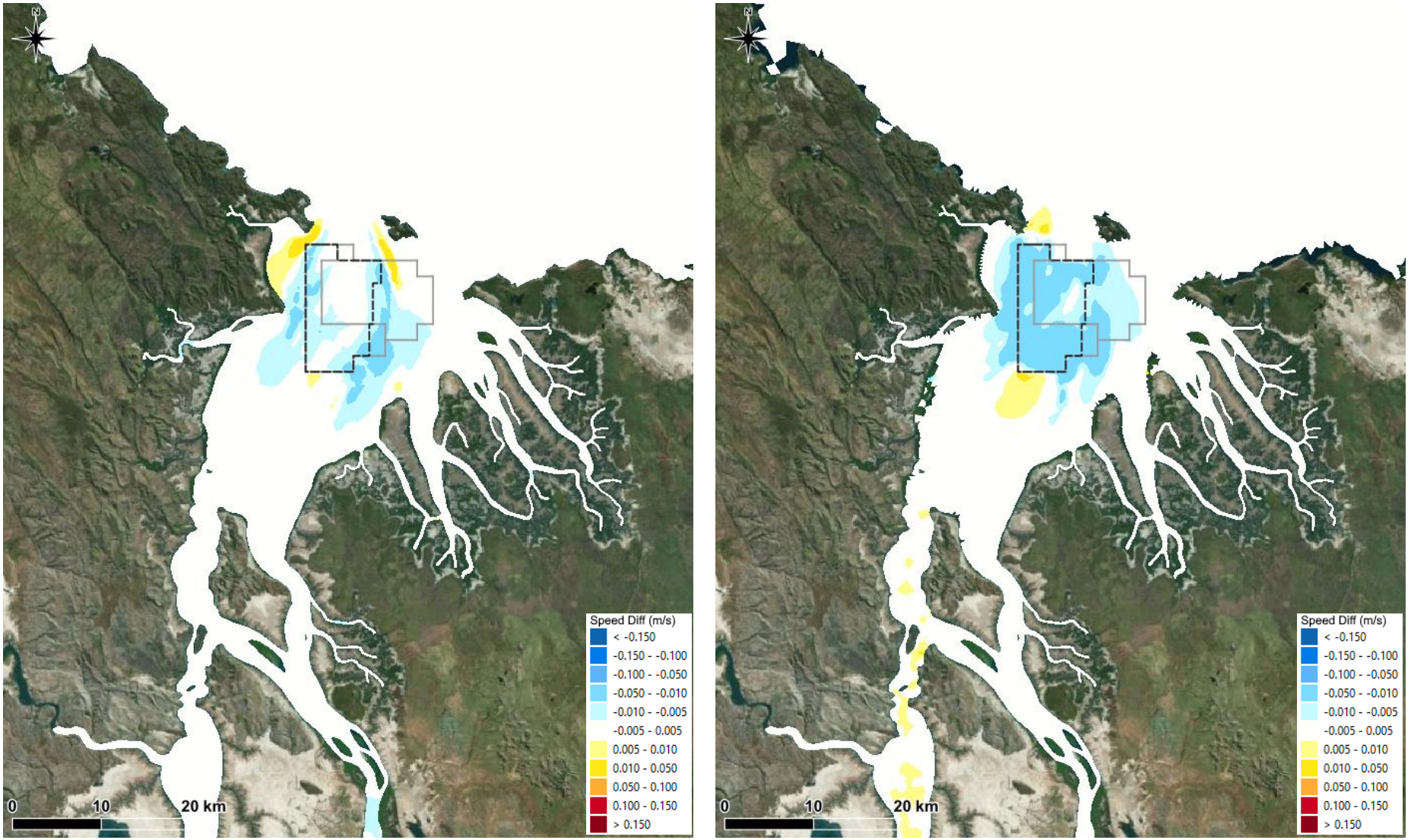

Figure 95. Change in current speed at high water (left) and peak ebb (right) during a spring tide as a result of 70 million m^3 of sand sourcing.

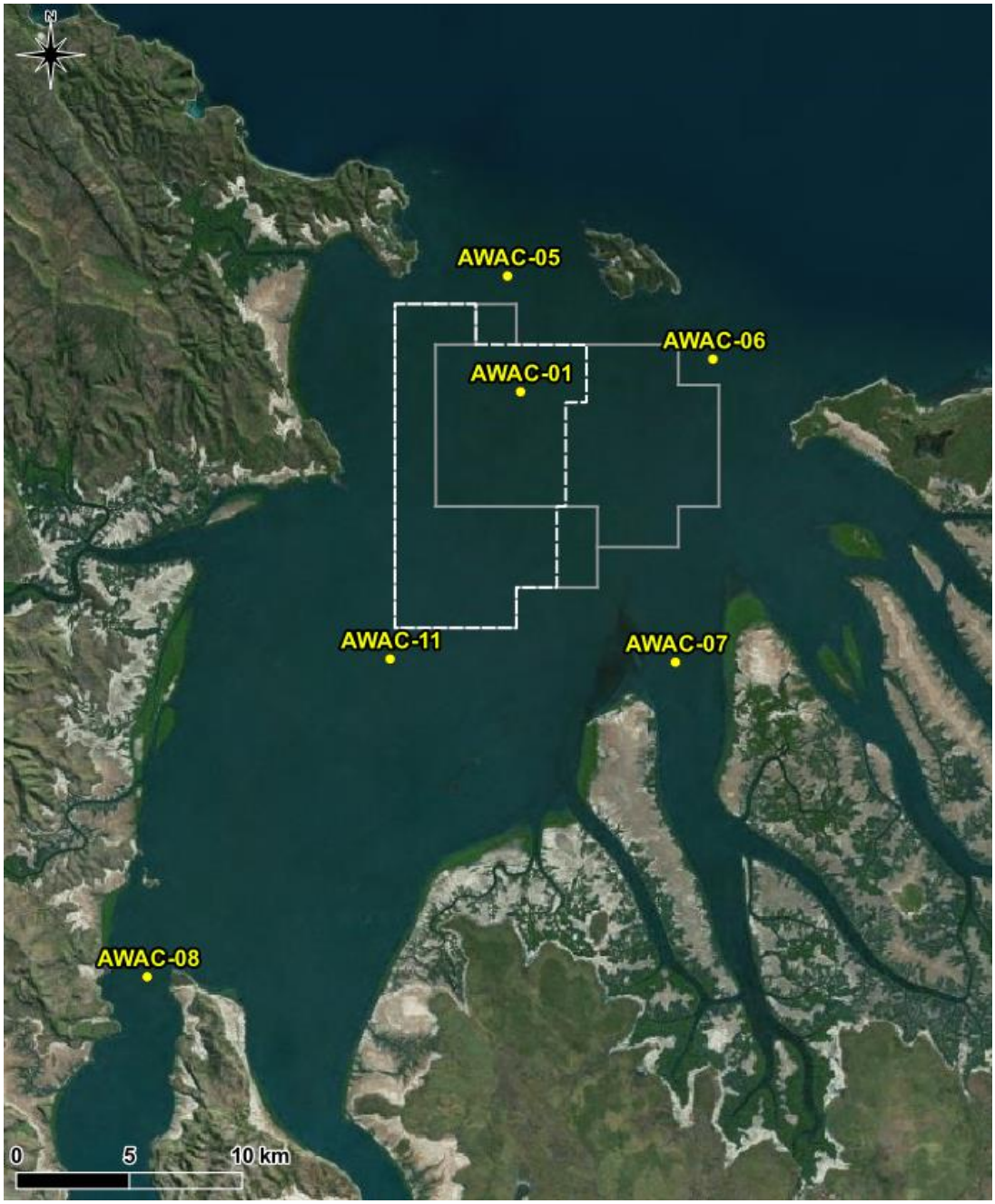

Figure 96. Location of model timeseries points.

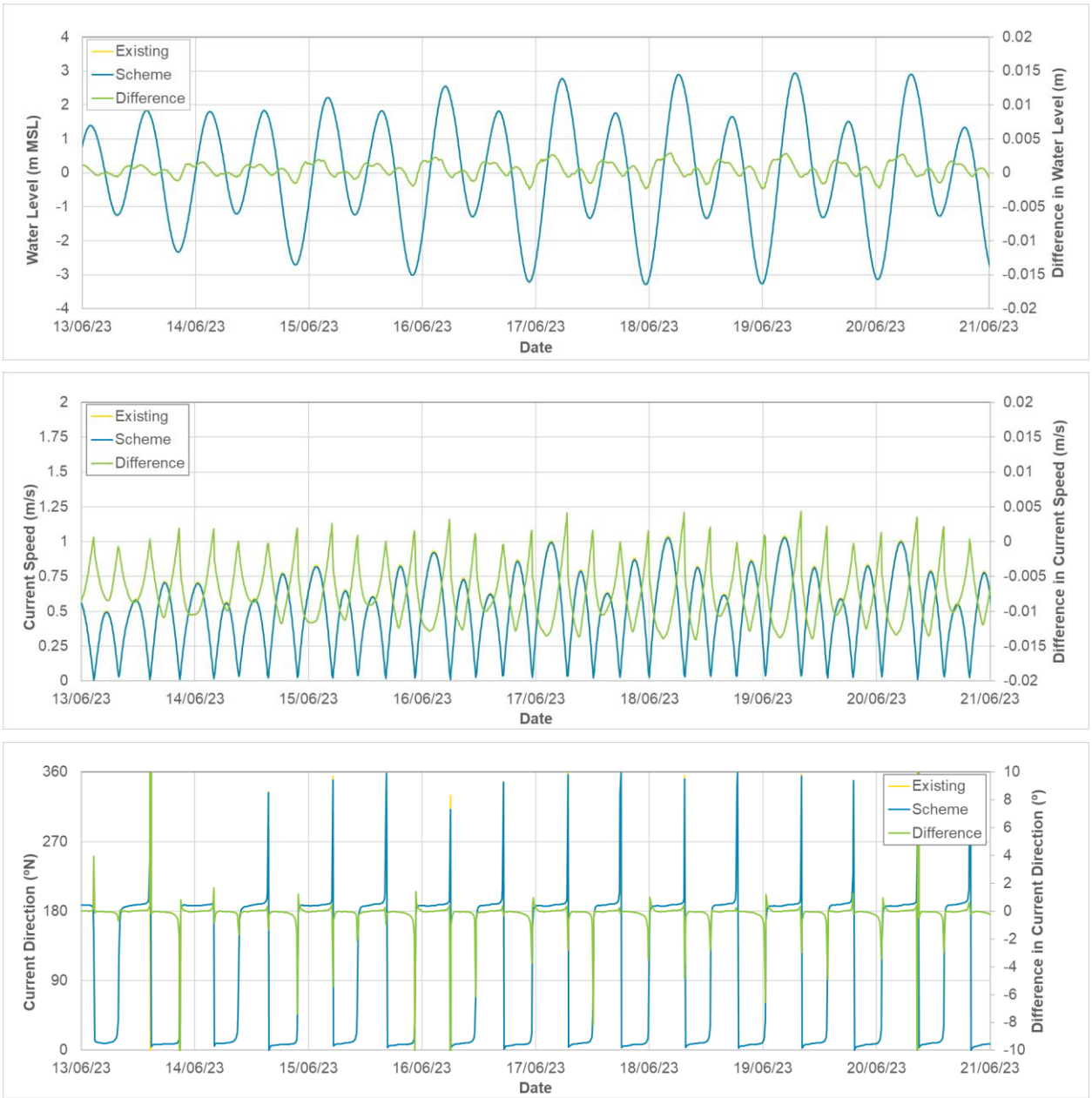

Figure 97. Time series plots showing existing, scheme and difference in water levels, current speed and current direction at AWAC-01 for sourcing 70 million m^3.

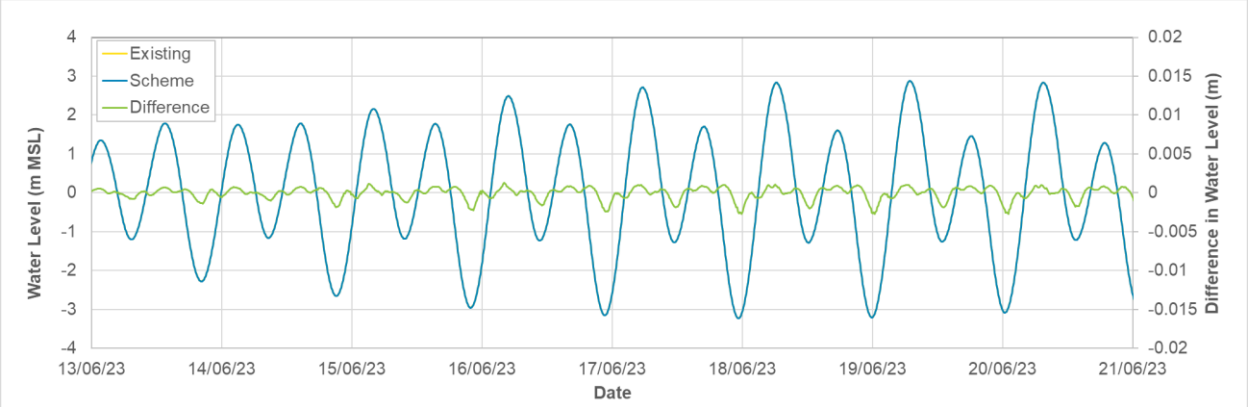

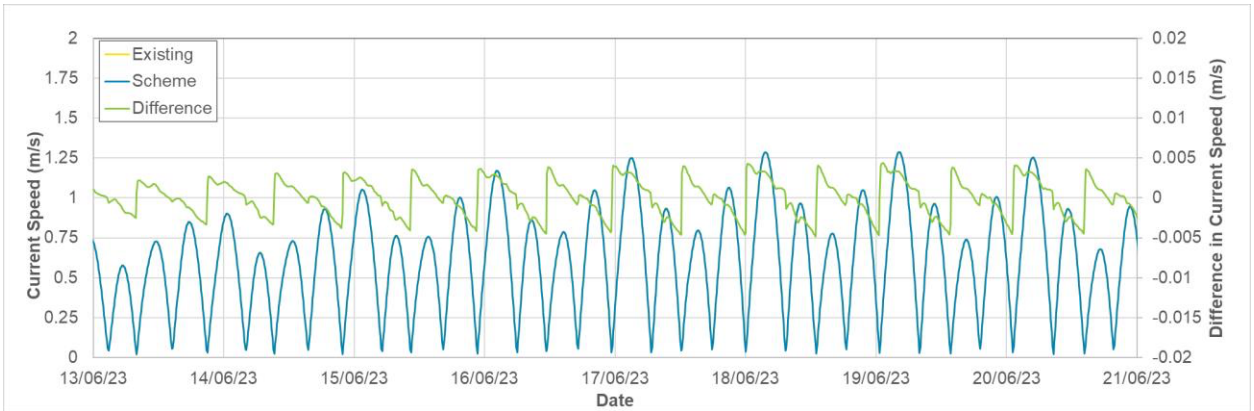

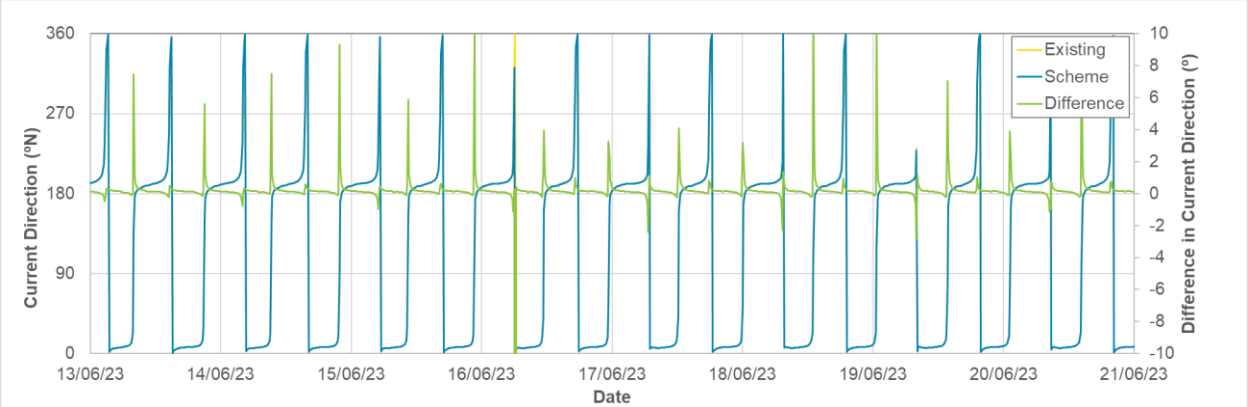

Figure 98. Time series plots showing existing, scheme and difference in water levels, current speed and current direction at AWAC-05 for sourcing 70 million m^3.

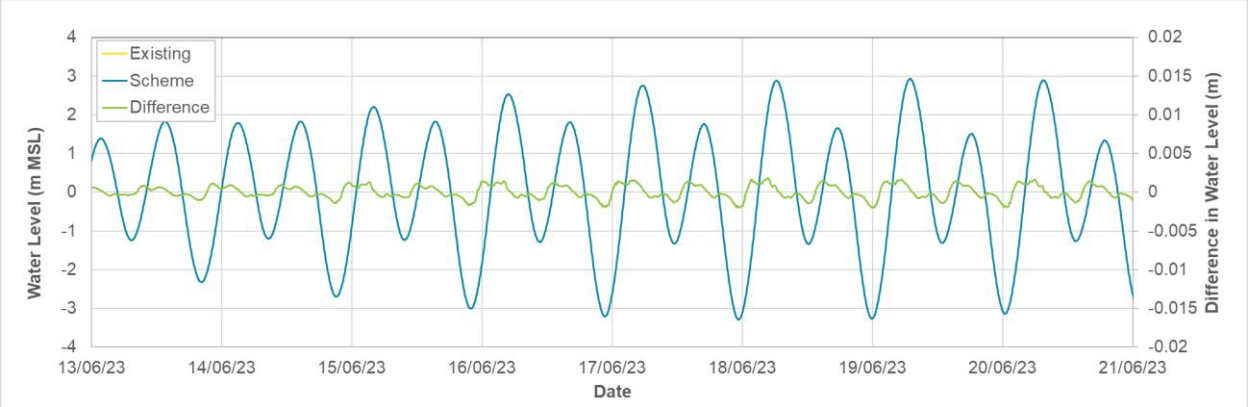

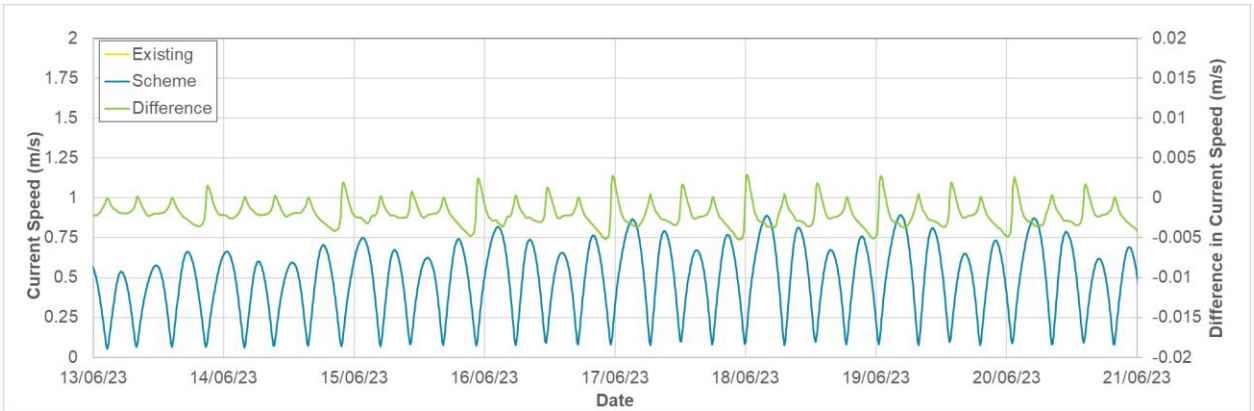

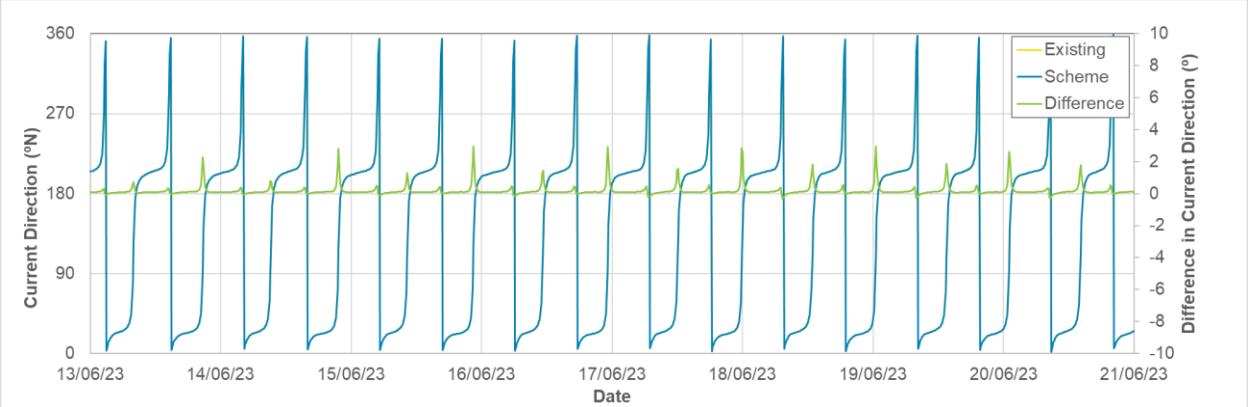

Figure 99. Time series plots showing existing, scheme and difference in water levels, current speed and current direction at AWAC-06 for sourcing 70 million m^3.

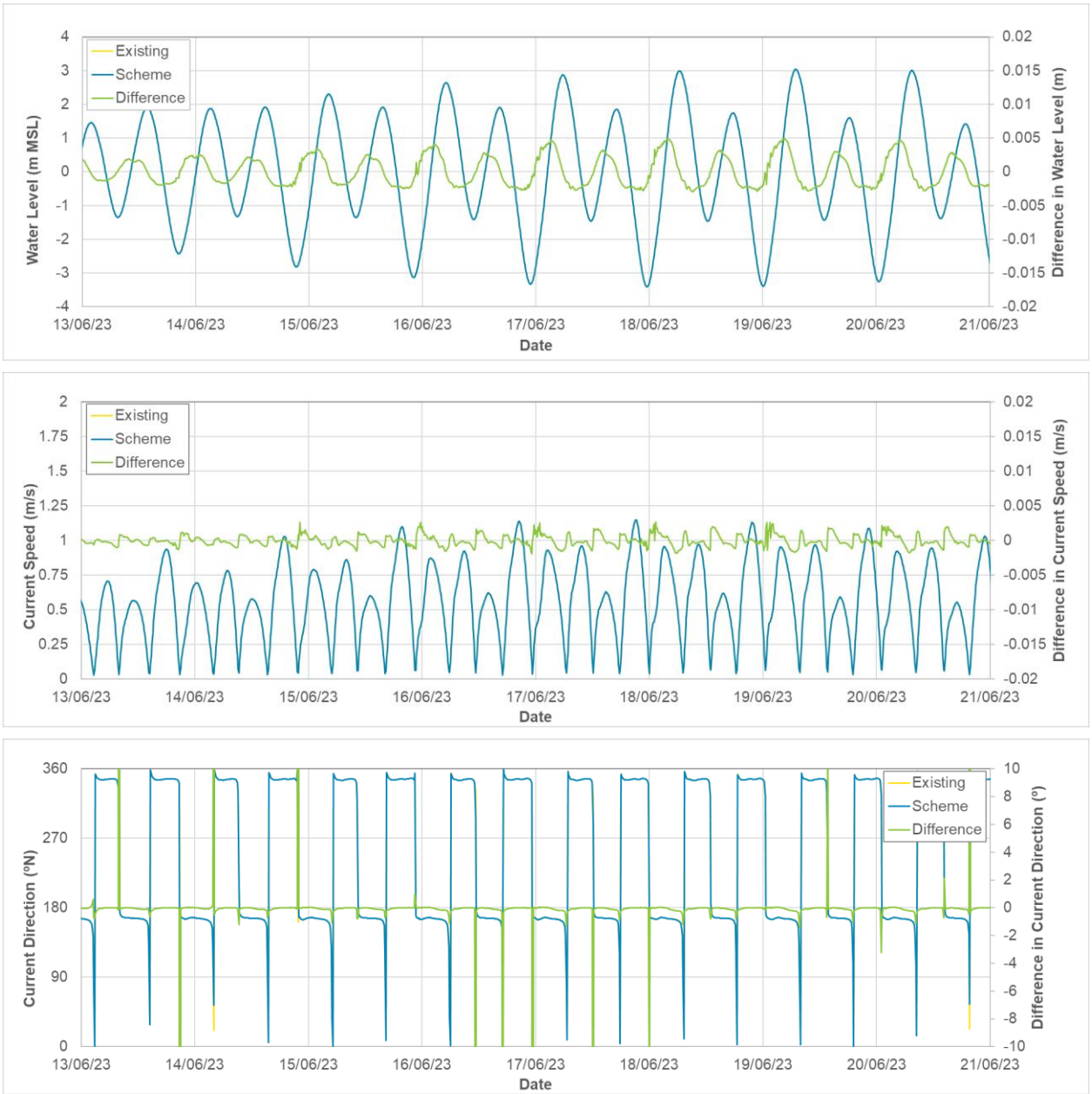

Figure 100. Time series plots showing existing, scheme and difference in water levels, current speed and current direction at AWAC-07 for sourcing 70 million m^3.

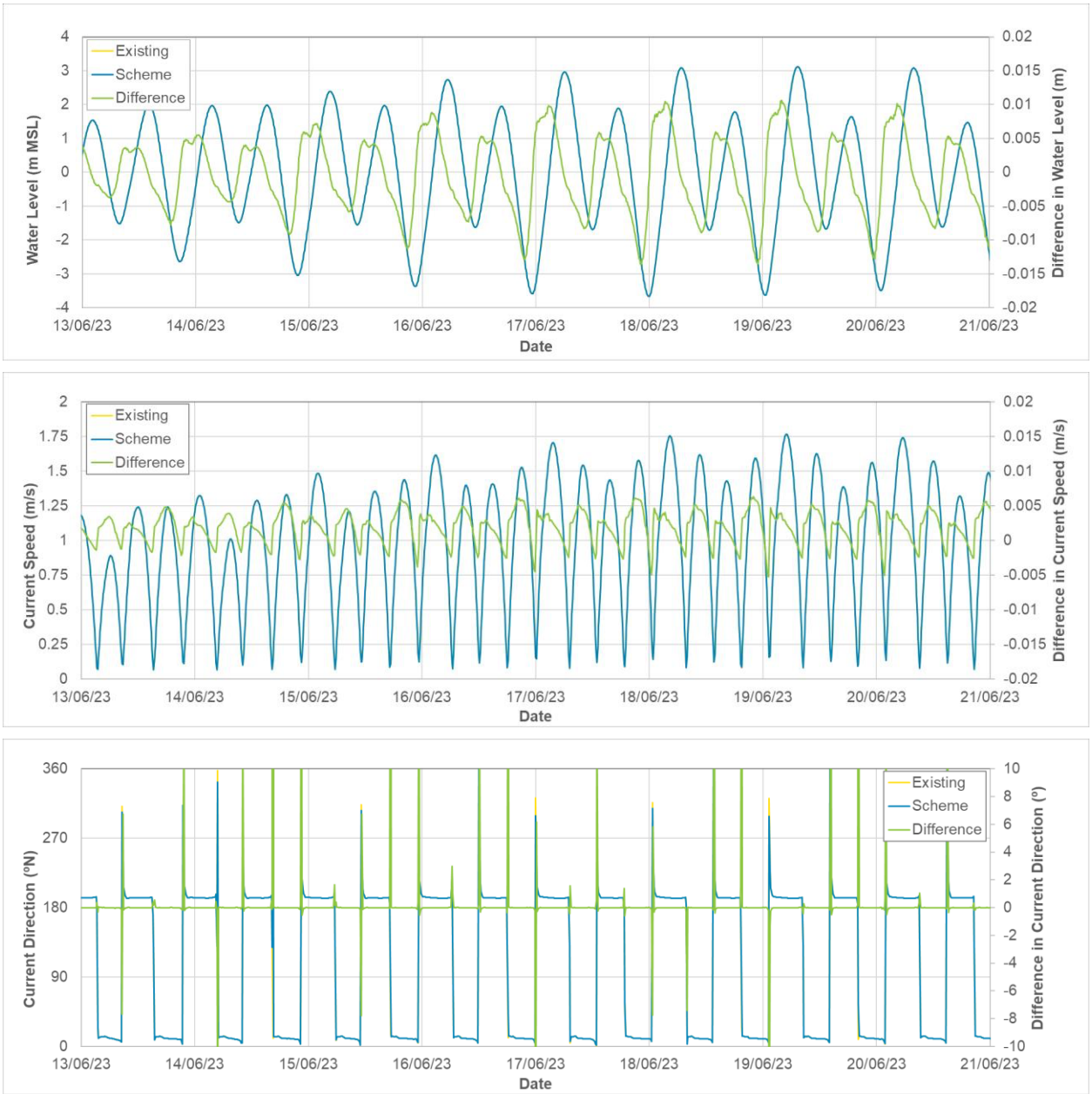

Figure 101. Time series plots showing existing, scheme and difference in water levels, current speed and current direction at AWAC-08 for sourcing 70 million m^3.

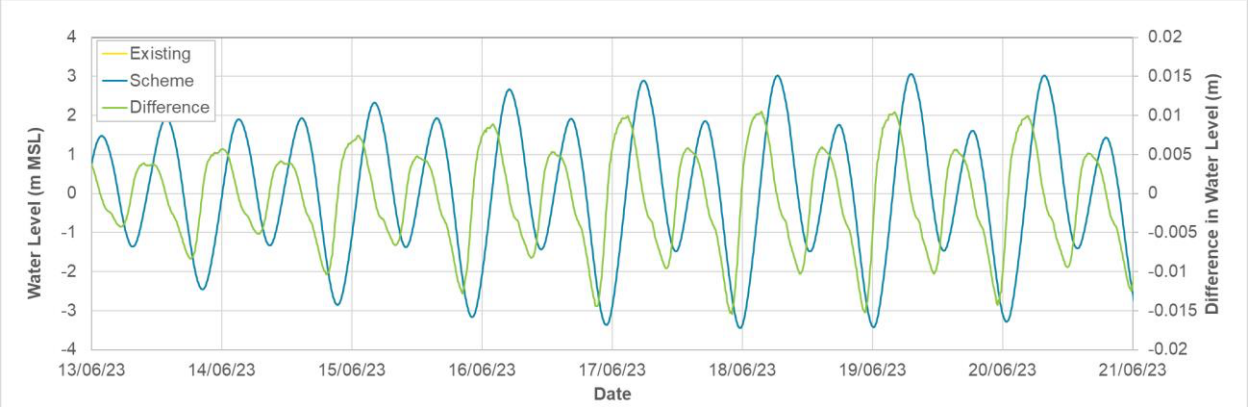

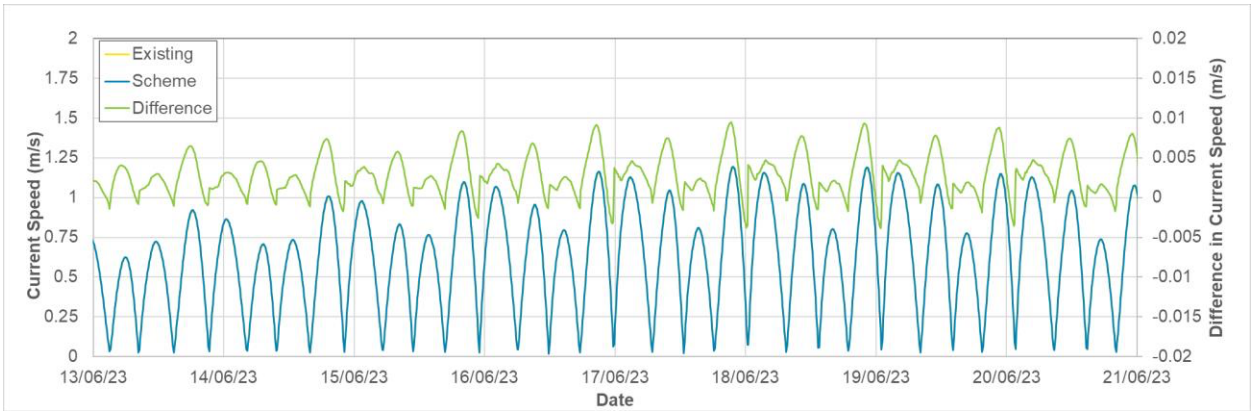

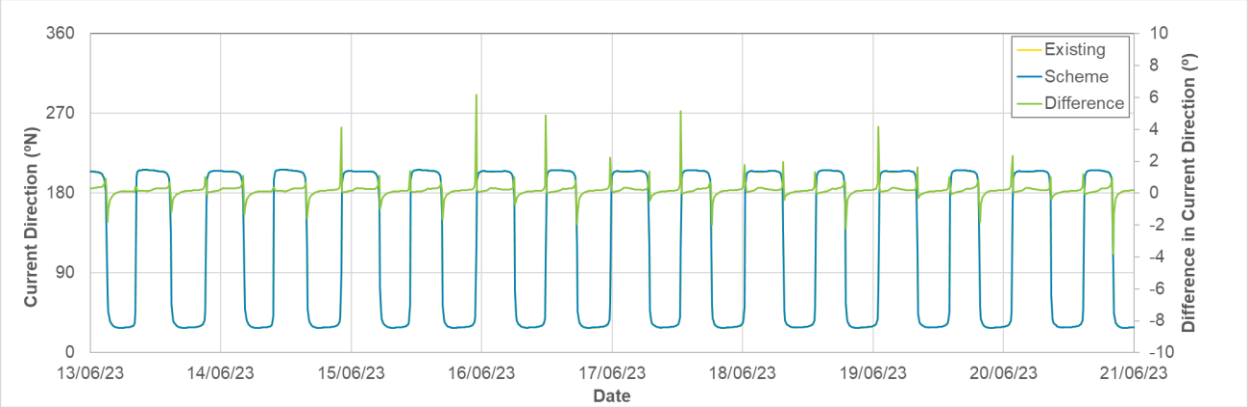

Figure 102. Time series plots showing existing, scheme and difference in water levels, current speed and current direction at AWAC-11 for sourcing 70 million m^3.

4.5. Spectral Wave Model

The MIKE SW model allows for the growth, decay and transformation of wind-generated and swell waves in both offshore and coastal environments. The SW model is able to represent wave processes which are expected to influence wave conditions both in JBG and CG. Details of the model configuration, initial calibration and preliminary results are provided in the following sections.

4.5.1. Model Configuration

Wave parameters were extracted at the offshore model boundary from the CAWCR wave/wind hindcast for Australia (Smith *et al.*, 2020). The CAWCR hindcast was run on a 4 arc minute spatial resolution for the period 1979 to present day and at an hourly temporal resolution. The extracted wave parameters were then applied at the offshore boundary of the model. The model also included winds from the CAWCR wave/wind hindcast in the model so that wave generation and growth by winds could occur within the model domain.

To account for the effect of the large variations in water depth occurring throughout the tide on the wave processes, a time varying water level based on predicted water levels at Cape Domett (AHO, 2023) was applied in the model.

The SW model has been setup to simulate the wave conditions over a five-year period from 2015 to 2020 to provide wave conditions to inform the Beach Processes model. In addition, the wave model was also setup to simulate the wave conditions over the 40-day period when AWAC-01 was deployed from 9th June to 24th July 2023 to provide wave conditions for the sediment transport modelling (MT model). Unfortunately due to an issue with the AWAC deployed at AWAC-01 over this period no measured wave data were available.

4.5.2. *Initial Validation*

The measured wave data collected to date by BKA using the AWACs/ADCPs had not been processed at the time this report was prepared. As a result, the only available wave data in the region were the hindcast modelled waves from the CAWCR hindcast extracted approximately 8 km to the north of Lacrosse Island (at CAWCR01). The fact that these data are from the same hindcast model as the offshore wave boundary and the winds in the model means that the data can only be used to provide an initial qualitative validation that the local wave model is transforming the offshore waves and correctly generating local wind waves in the domain correctly.

The CAWCR and SW modelled wave height, wave period and wave direction at CAWCR01 are shown over a 6 month period, which coincided with the largest waves between 2015 and 2020, in Figure 103.

The plot shows that the SW model provides similar wave conditions to the CAWCR model at the CAWCR01 output location. During the wet season the SW model can result in larger wave heights than predicted by the CAWCR wave hindcast model. This is likely to be due to differences in the nearshore model resolution and bathymetry representation between the two models. More extensive model calibration and validation will be undertaken during subsequent stages of the study using measured wave data. The model will be calibrated and validated using both wet and dry season measured wave data from multiple different sites.

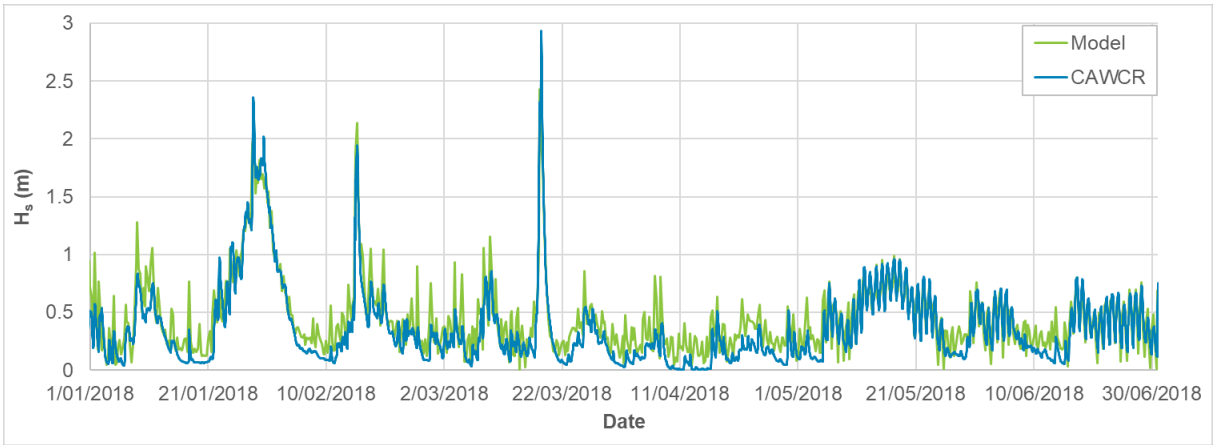

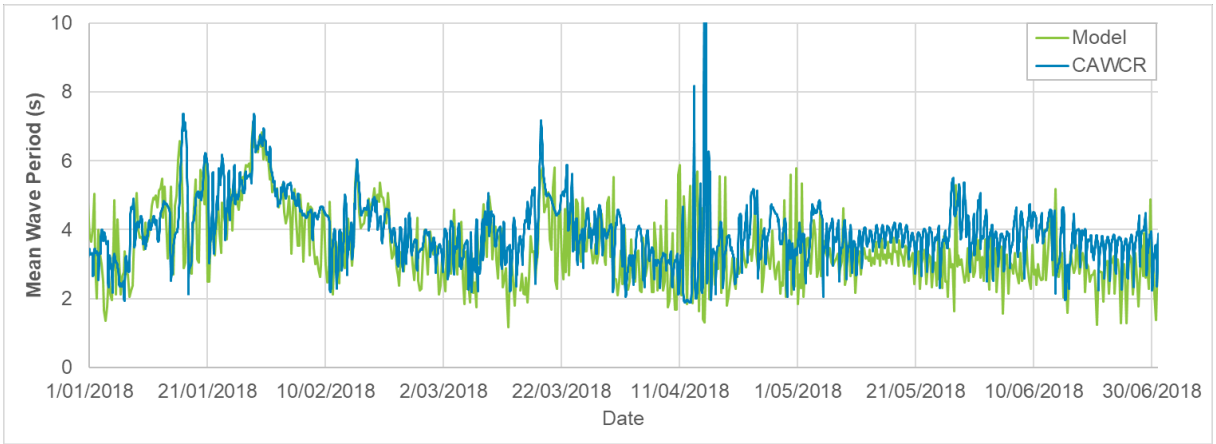

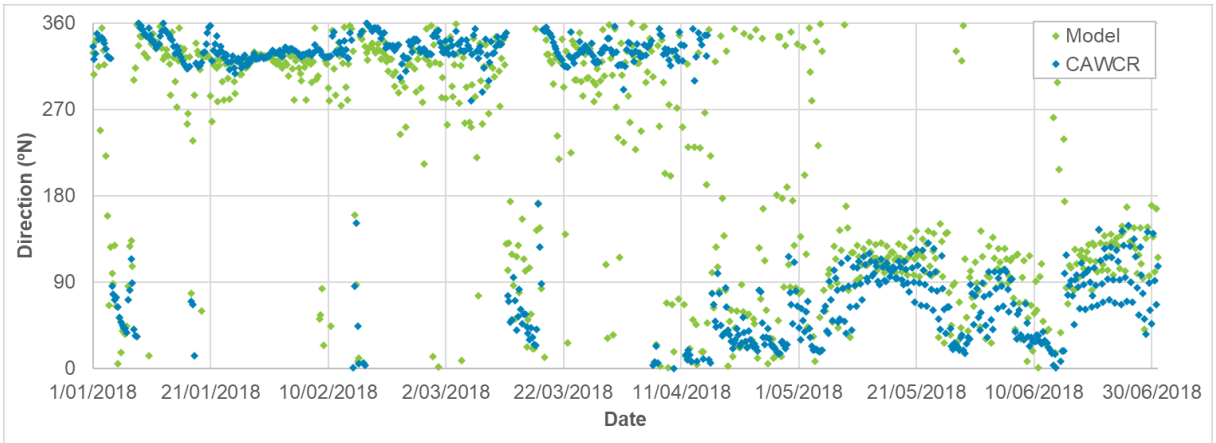

Figure 103. Comparison between hindcast CAWCR and modelled wave conditions offshore of CG over a 6-month period.

4.5.3. *Preliminary Results*

Spatial maps from the SW model of the H_s for a range of different wave events, including a TC (Category 2 when it passed through JBG), are shown for the CG region in Figure 104 to Figure 108. Due to the limitations with the SW model noted in the previous sections the results should only be considered to provide an initial overview of potential wave conditions in the region, further modelling will be undertaken to improve the confidence which can be placed in the model. The plots show how the H_s within CG is significantly lower than the offshore H_s, with Lacrosse Island specifically providing sheltering in its lee. Details of the predicted wave heights which can occur within CG during different wave events are provided below:

- The spatial maps show how the shallow bathymetry at King Shoals and Medusa Bank limit the wave heights which reach the entrance to CG and the beaches to the west and east of the

entrance. The influence of these shallow shoals is greatest during larger wave events, but the reduction in wave height still occurs during the typical wet and dry season wave events.

- The typical wet and typical dry season wave events can result in an H_s of up to around 0.7 m within the CG.
- A large wet season wave event, with waves from the west-northwest, can result in an H_s of up to around 1 m within CG, with these wave heights extending close to the mangroves and stranded beach ridges at East Bank Point (indicating this type of wave event could be responsible for the formation of these features).
- The largest wave event over the 5-year simulation, which occurred during the wet season due to a Category 5 TC (TC Marcus), resulted in varying wave conditions as the TC tracked from east to west in JBG (it was a Category 2 TC at this stage). During this event, waves approaching CG were from the north-northeast and from the east, with the peak in H_s occurring when waves were from the east. During this event an H_s of up to 1.7 m occurred within CG, with the largest waves occurring along the western side of CG. The results show how waves with an H_s of 1 to 1.5 m can occur within CG adjacent to both the eastern and western shorelines.

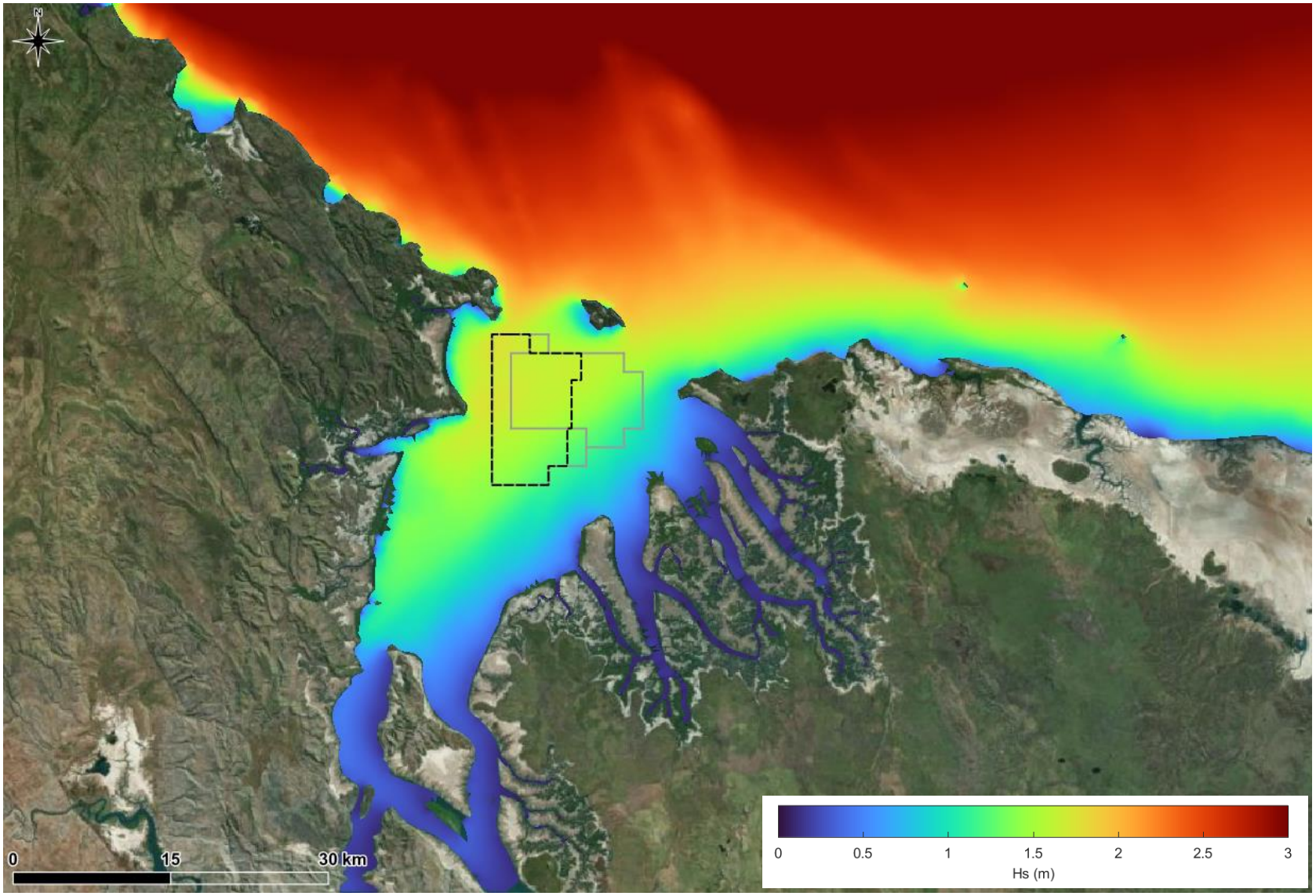

Figure 104. Modelled H_s in the CG region at the peak of TC Marcus on 18/03/2018 12:00 when waves were from the east.

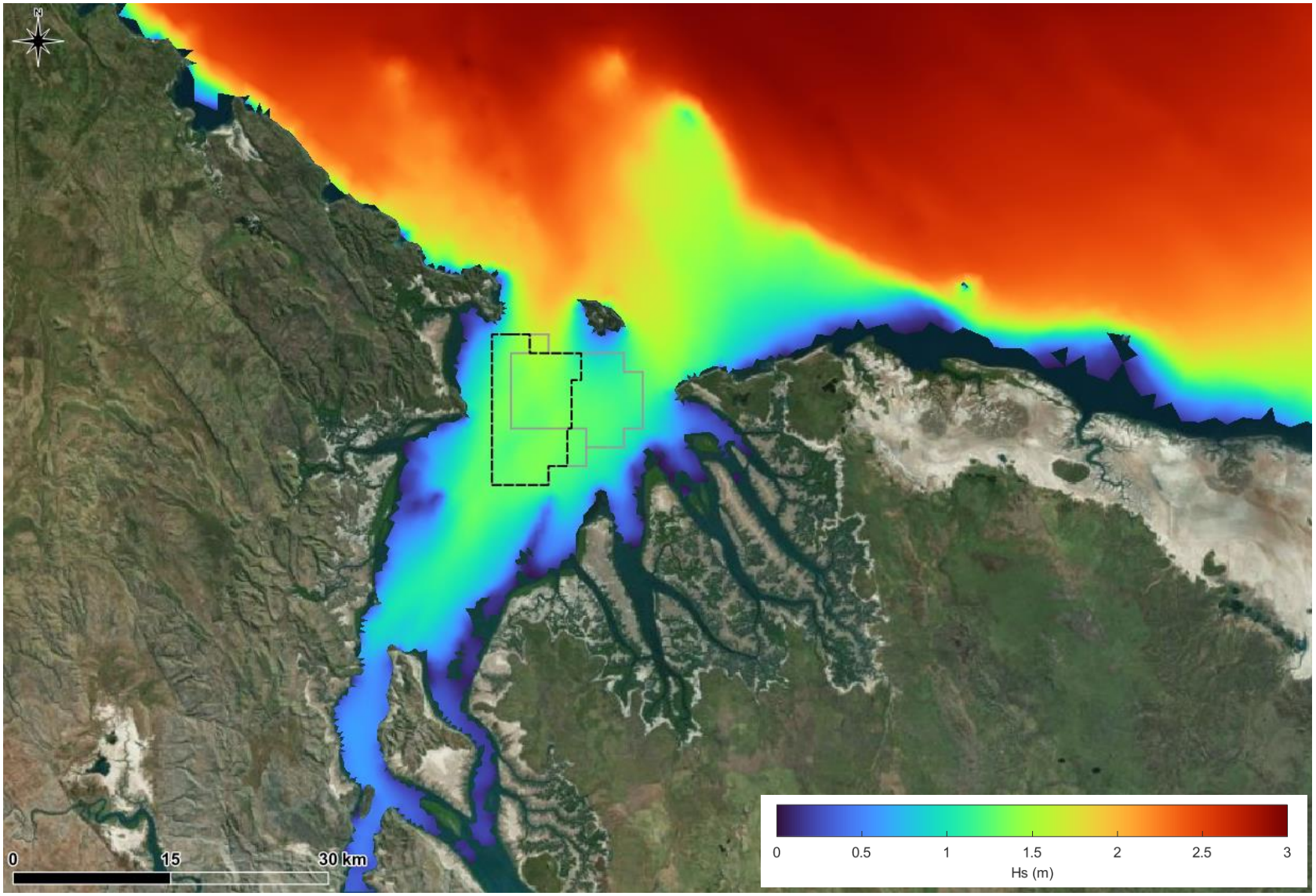

Figure 105. Modelled H_s in the CG region during TC Marcus 18/03/2018 06:00 when waves were from the north north-east.

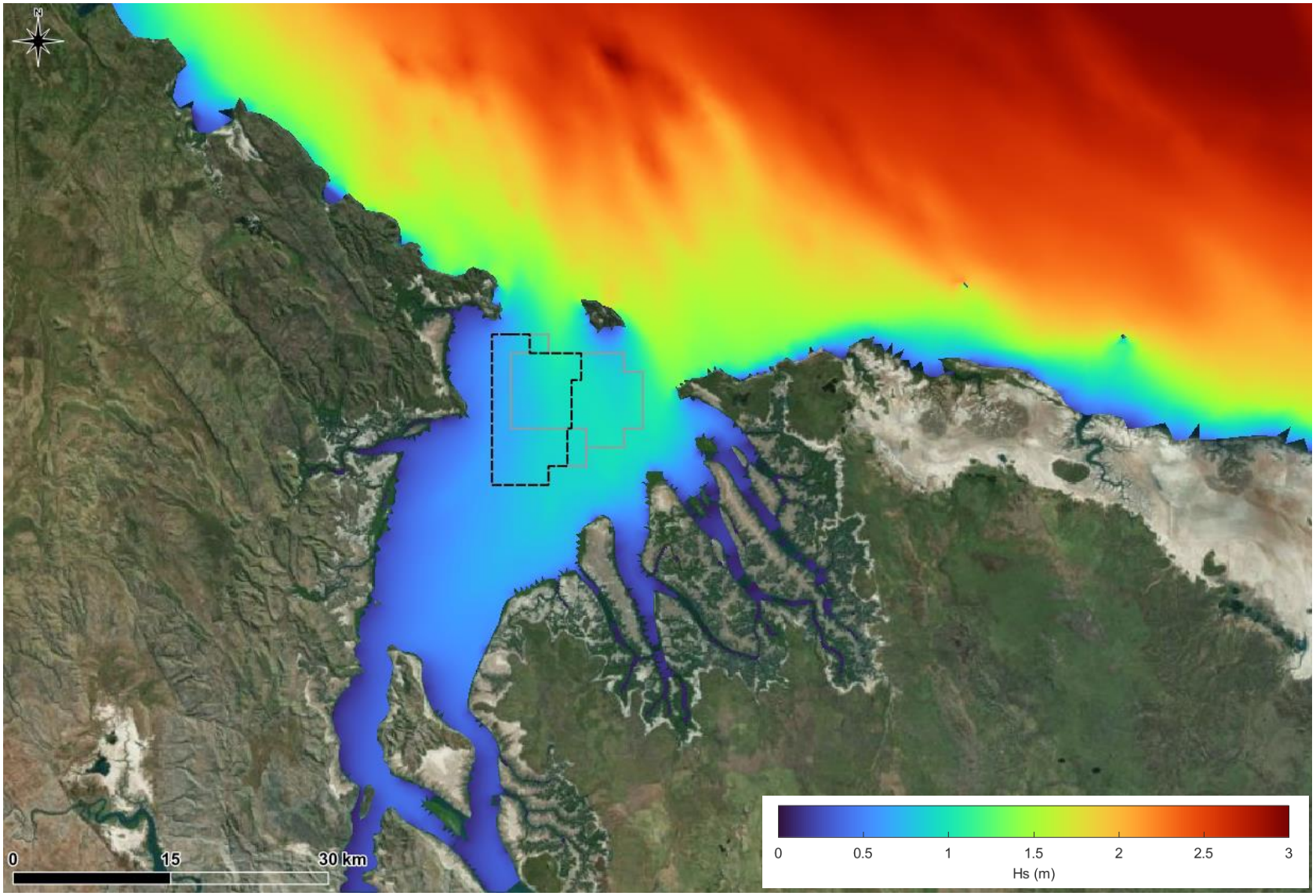

Figure 106. Modelled H_s in the CG region for a large wet season wave event on 28/01/2018, with waves coming from the west north-west.

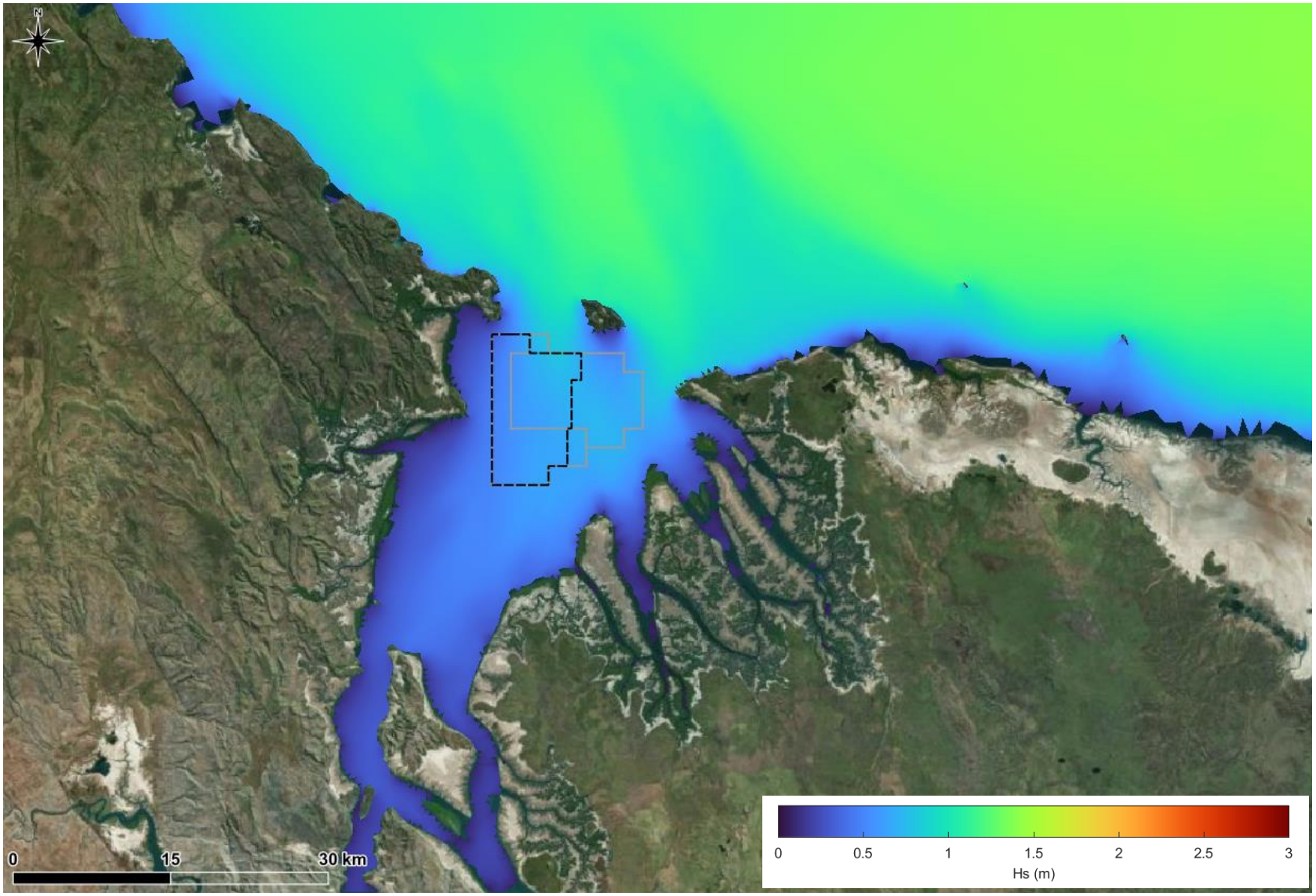

Figure 107. Modelled H_s in the CG region for a typical wet season wave event on 02/12/2018, with waves coming from the north-west.

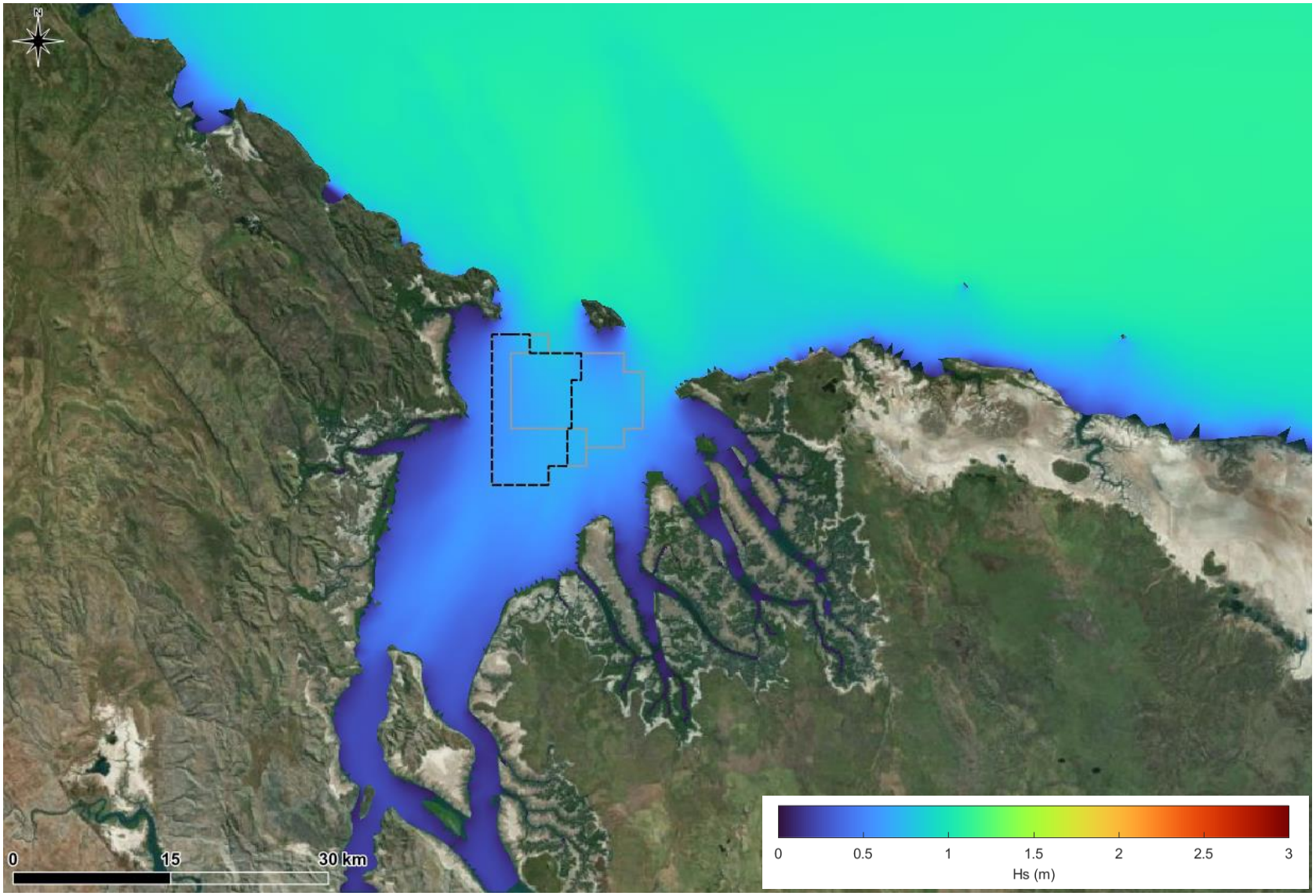

Figure 108. Modelled H_s in the CG region for a typical dry season wave event on 30/08/2018, with waves coming from the north.

4.5.4. *Preliminary Impacts*

Due to the lack of available measured wave data for model calibration and detailed wind data for forcing the model there is limited confidence in the absolute wave conditions predicted by the model. Despite this, the SW model is considered to still be a suitable tool to allow a preliminary impact assessment to be undertaken. The approach adopted and results from this are detailed in this section.

The SW model mesh was setup to represent the existing bathymetry for CG as well as the bathymetry following the sourcing of 70 million m^3 of sand (i.e. the total volume proposed over the 15 years). It has been assumed that the sand is sourced evenly over the entire proposed operational area, resulting in a deepening of 0.68 m in this area. The SW model was setup to simulate the wave conditions for the existing base case (no sand sourcing) and for the sourcing of 70 million m^3 of sand. The model simulated a 5 year period to allow the potential change in waves due to the deepening to be assessed for a range of typical and extreme wave conditions.

Analysis of the results from the SW modelling showed that the sand sourcing is not predicted to impact the wave conditions in CG for the majority of the time. The deepening due to the 70 million m^3 sand sourcing case is only predicted to result in changes to the wave conditions within CG during larger wave events such as those that occur during the wet season due to TCs and tropical lows. Example plots of the predicted spatial change in H_s during the largest wave event of the 5 year simulation (March 2018 during TC Marcus) and during a tropical low (January 2018) are shown in Figure 109. The plots show that the sand sourcing is predicted to result in increases in H_s within the proposed operational area and upstream from the area during these large wave events.

The magnitude of the changes vary depending on the wave conditions, with changes predicted to be significantly larger for the TC wave event compared to the tropical low wave event. During the TC wave event (when the H_s in the area ranged from 1 to 2 m) the increases in H_s are predicted to be predominantly less than 0.01 m (0.5 to 1%). Changes in peak wave period (T_p) and wave direction have also been investigated and the results show that changes in T_p are predicted to be less than 0.1 s while the changes in wave direction are predicted to be less than 0.5º.

The spatial maps show that any changes to wave conditions are predicted to be within the proposed operational area and upstream of it. Therefore, to better understand how the sand sourcing scenarios influence the wave climate in CG, timeseries results from the 5 year simulation were extracted at sites AWAC-01, AWAC-07 and AWAC-11 (see Figure 96 for locations). The H_s timeseries data were then used to calculate percentiles for the existing case and the sand sourcing case over the 5 year period at these three sites (Table 9 to Table 11). The percentile tables show that within the proposed operational area (AWAC-01) the sand sourcing is predicted to result in a 0.001 m increase in the 99th percentile relative to the existing case. Towards the False Mouths of the Ord (AWAC-07) the sand sourcing is also predicted to result in a 0.001 m increase in the 99th percentile H_s. Directly upstream of the proposed operation area (AWAC-11) the sand sourcing case is predicted to result in a small reduction of 0.001 m to the 95th and 0.002 m to the 99th percentile H_s, relative to the existing base case.

Overall, the wave modelling results have predicted that the deepening due to the sourcing of 70 million m^3 of sand within the proposed operation area results in small changes (typically less than 0.01 m) in H_s within CG. The predicted changes are dependent on the wave conditions, with changes only predicted to occur during larger wave events which occur in the wet season due to tropical cyclones and tropical lows.

Table 9. Percentile statistics of H_s over the 5 year model simulation at AWAC-01 for the existing case and 70 million m^3 sand sourcing case. *Note: values in green highlight increases and values in blue reductions in H_s due to the schemes.*

Percentile	Existing	70 Mm^3
5th	0.065	0.065
10th	0.101	0.101
20th	0.155	0.155
50th	0.292	0.292
80th	0.496	0.496
90th	0.631	0.631
95th	0.738	0.739
99th	0.943	0.944

Table 10. Percentile statistics of H_s over the 5 year model simulation at AWAC-07 for the existing base case and 70 million m^3 sand sourcing case. *Note: values in green highlight increases and values in blue reductions in H_s due to the sand sourcing.*

Percentile	Existing	70 Mm^3
5th	0.042	0.042
10th	0.060	0.060
20th	0.086	0.086
50th	0.162	0.162
80th	0.274	0.274
90th	0.359	0.359
95th	0.440	0.440
99th	0.565	0.566

Table 11. Percentile statistics of H_s over the 5 year model simulation at AWAC-11 for the existing base case and 70 million m^3 sand sourcing case. *Note: values in green highlight increases and values in blue reductions in H_s due to the sand sourcing.*

Percentile	Existing	70 Mm^3
5th	0.057	0.057
10th	0.092	0.092
20th	0.138	0.138
50th	0.243	0.243
80th	0.388	0.388
90th	0.487	0.487
95th	0.575	0.574
99th	0.745	0.743

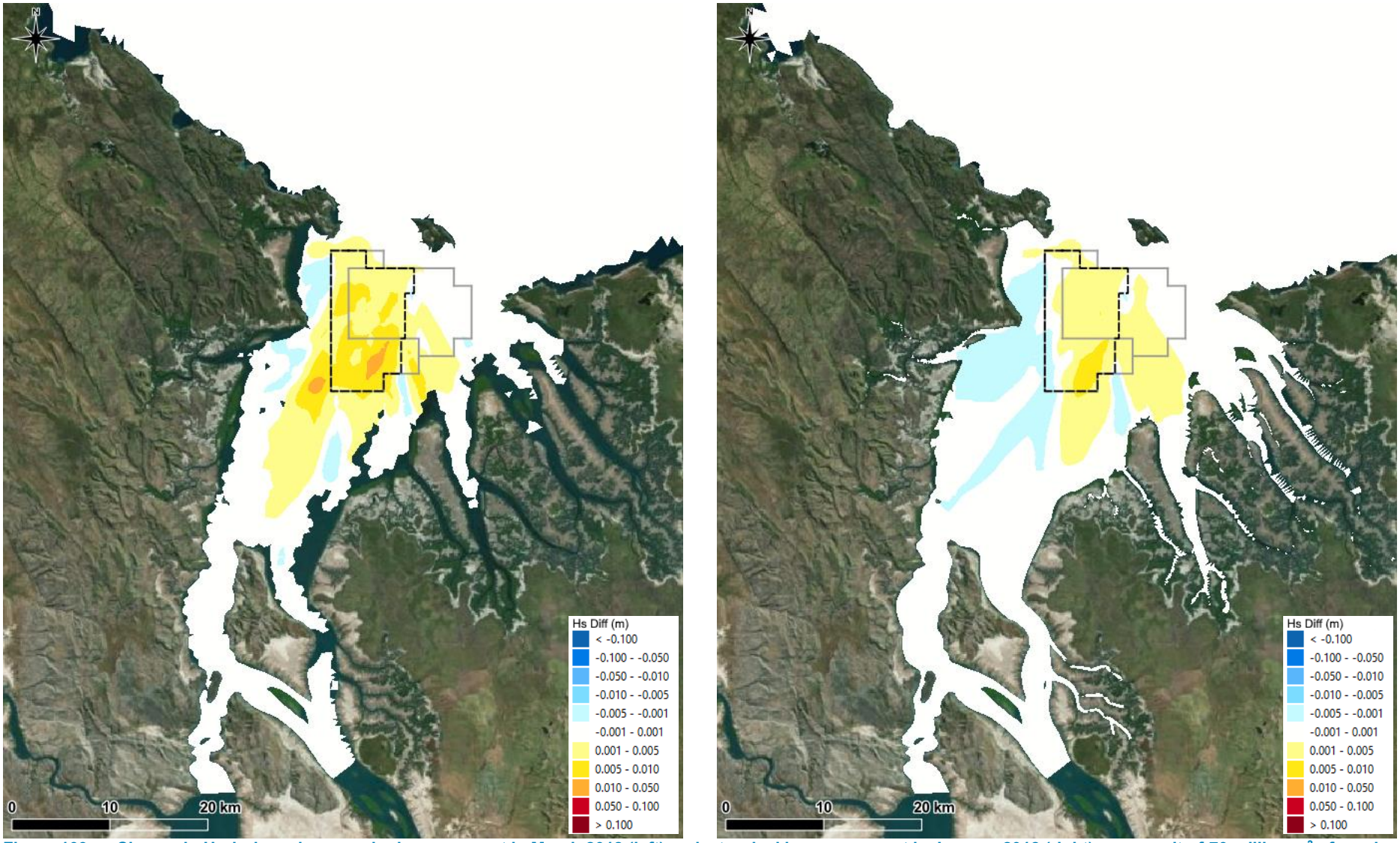

Figure 109. Change in H_s during a large cyclonic wave event in March 2018 (left) and a tropical low wave event in January 2018 (right) as a result of 70 million m^3 of sand sourcing.

4.6. Sediment Transport Model

The MIKE MT module describes the erosion, transport and deposition of mud and sand due to currents and waves. The module is designed specifically for sediment transport studies in coastal and estuarine environments with fine-grained and sand sized sediment, and for dredging studies. Details of the model configuration and preliminary results are provided in the following sections.

4.6.1. Model Configuration

The MIKE MT model is driven by the hydrodynamic and wave conditions from the HD and SW models. A preliminary configuration of the MIKE MT model has been developed at this stage of the study, and will continue to be refined over the duration of the study as additional data and information becomes available. At this stage the MT model has been configured as a depth-averaged model as insufficient data are currently available to justify a 3D model. A 3D model will be developed during the subsequent stages of the study. Details of the preliminary MT model setup are provided below.

The model has been setup with two sediment types, a fine sand (D50 = 100 μm) and a fine silt (D50 = 15 μm). The model has a single bed layer which is made up of 80% sand and 20% fine silt. The percentage sand and fine silt included in the bed layer was a parameter in the model calibration, with the optimum configuration being developed through an iterative testing process. The thickness of the bed layer was developed by running the model for a three month warm up period to allow it to erode and accrete sediment through the domain. This bed layer was then subsequently used as the starting bed thickness for the subsequent simulations. A constant upstream input of fine silt of 700 mg/L was included in the model at the upstream boundary of West Arm.

4.6.2. Initial Calibration

It has not been possible to properly calibrate the MT model using data collected as part of the project at this stage due to insufficient available measured in-situ SSC data (this is being addressed by BKA in the wet season survey Feb-March 2024). However, the data measured at AIMS A and AIMS B in 2002 have been used to undertake an initial calibration to help inform the model configuration. The MT model was setup to simulate the sediment transport over the same 40-day period in June to July 2023 when the HD model was calibrated. Water levels over the model simulation period were matched up with water levels over the 2002 period when data were measured at AIMS A and AIMS B to allow an approximate comparison between the measured and modelled SSC. This approach assumes that the astronomical tide is the dominant driving force for SSC at these two sites, which appears to be the case as outlined in Section 3.7.

A comparison between the modelled and measured SSC at AIMS A and AIMS B is shown in Figure 110 and Figure 111. The plots show that the model is able to provide a good representation of the variability in SSC over a spring-neap tidal cycle, whilst also replicating the peaks in SSC around low water. The model is able to represent the lag between the SSC and the tidal curve which the measured data exhibit (peak in SSC occurs 1 to 2 days after peak in spring tidal range and SSC remains high relative to the tidal range at the start of neap tides), indicating that the relative proportion of fine-grained silt and fine sand in suspension in the model, is a reasonable representation of the actual conditions.

At AIMS A the model tends to underpredict the magnitude of the peak in SSC at the smaller of the two daily low waters. In addition, at AIMS A the model also predicts a peak in SSC around high water while the measured data typically doesn't show a peak in SSC at this time. However, given that the model was not setup to simulate the actual metocean conditions for this period (it was simulating dry season winds and waves when the measured data were from the wet season), it is considered that the model is providing a good representation of the measured SSC, giving confidence that the model can be used to provide an initial overview of the natural sediment processes which influence the CG.

The sediment transport model will be subject to a more rigorous calibration and validation exercise during subsequent stages of the study, including calibration and validation based on the in-situ PSD measurements from the water sampling planned by BKA in Feb – March 2024.

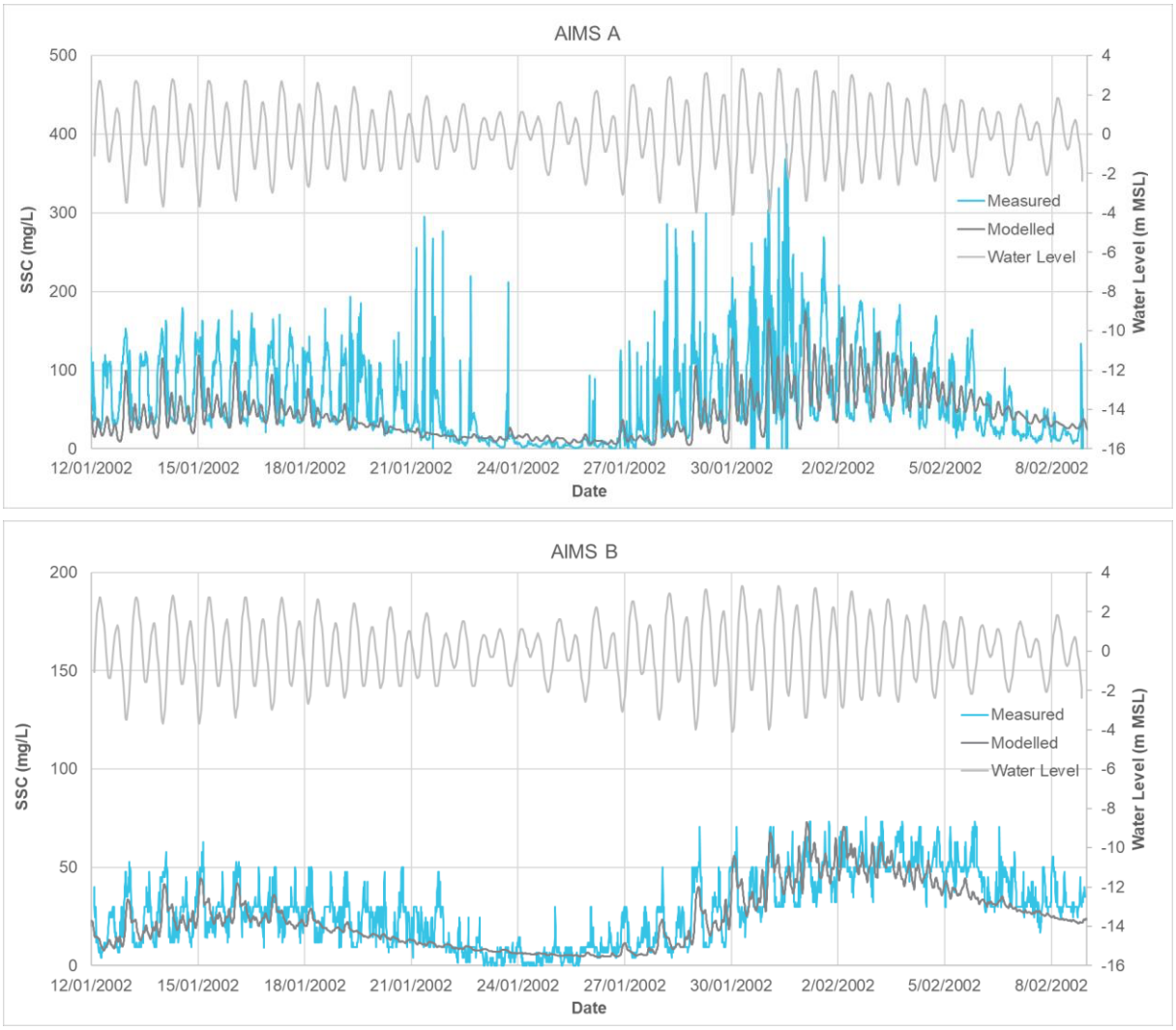

Figure 110. Comparison between modelled (depth-averaged) and measured (mid-depth) SSC at sites AIMS A and AIMS B over a 28 day period.

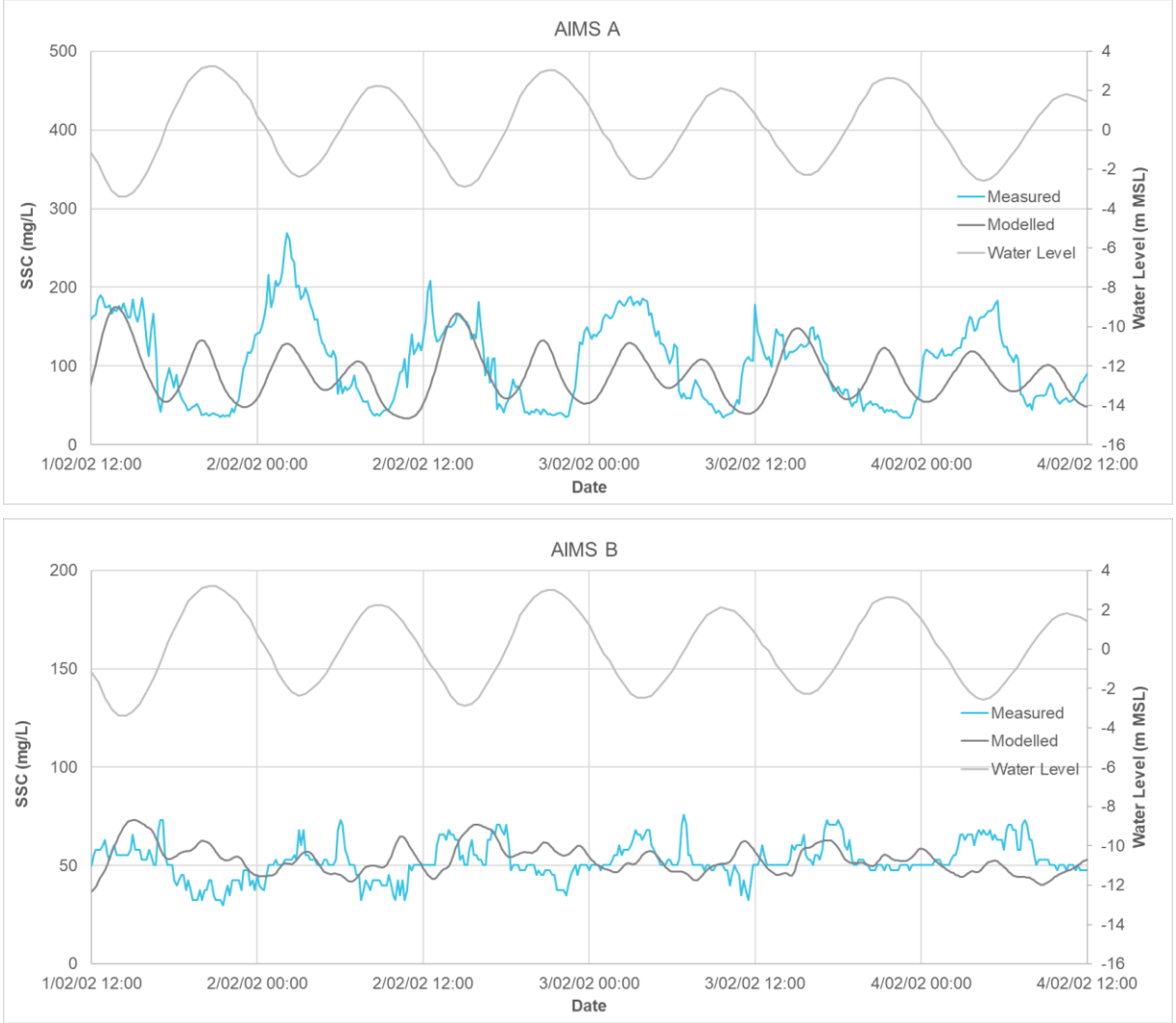

Figure 111. Comparison between modelled (depth-averaged) and measured (mid-depth) SSC at sites AIMS A and AIMS B over 3 days of spring tides.

4.6.3. Preliminary Results

The modelled SSC in the CG region during a neap tide is shown in Figure 112, while the modelled SSC for a spring tide at the end of the ebb and flood stages of the tide are shown in Figure 113 and Figure 114. Comparison between the modelled SSC and the SSC derived from satellite images for comparable tidal states shows similar spatial patterns and magnitudes. It is important to note that the model is not simulating the same timeframes as the satellite images and so differences in SSC offshore of the CG are likely to be a result of different wind and wave conditions. The comparison provides further confidence that the model is able to simulate the sediment transport processes that result in sediment being suspended in CG.

To understand the relative contribution of sand and silt to the SSC in the region, the modelled SSC for just the sand and just the silt sediment during a spring tide are shown in Figure 115 at the end of the ebb stage of the tide and in Figure 116 at the end of the flood stage of the tide. Plots are not shown for the neap tide as the modelling predicts that all of the sediment in suspension in the subtidal areas of CG is fine silt. The results for the spring tide show that the majority of the sediment in suspension is the silt, but there is a continuous path where sand is present in suspension from West Arm in CG to the offshore end of King Shoals, suggesting a potential sediment transport pathway. The location where the sand is present in suspension in Blocks 4 and 4A approximately correlates with the areas where the bed sediment was predominantly sand, based on the sampling undertaken by BKA in March 2023, giving confidence in the modelling results. Further consideration of the modelled SSC of sand sized particles during the flood and ebb stages of the tide, can be used to provide a preliminary indication of the sources and supply of sand from the proposed operational area:

- Ebb Tide: The predicted highest SSC resulting from sand sized sediment during the ebb stage of spring tides was at the southern end of the proposed operational area and directly to the south and southwest of it (i.e. upstream). This indicates that this area of CG is likely to act as a supply of sand to the proposed operational area. The pathway of sand sized SSC from the proposed operational area through the CG western entrance to King Shoals indicates that sand from the area can be transported offshore to King Shoals during the ebb stage of spring tides.

- Flood Tide: The fact that the SSC pattern during the flood stage of a spring tide is similar to during the ebb stage of a spring tide, suggests that sand can be transported backwards and forwards along this sand transport pathway by the flood and ebb currents during spring tides. Comparison between the relative SSC during the flood and ebb can be used to give an indication of where net transport of sand is likely to occur. The SSC of sand around King Shoals, the CG western entrance and the northern half of the proposed operational area, is similar on the flood and ebb, indicating limited net transport of sand. The SSC in the southern half of the proposed operational area and directly to the south and southwest of it is much lower on the flood tide compared to the ebb tide, suggesting a net increase in sand within the proposed operational area due to a supply of sand from upstream in CG. These results therefore suggest that the proposed operational area is a natural sand accumulation area (this would explain why so much sand is present in this area), with a net import of sand from upstream and limited net transport between it and King Shoals.

It is important to note that the results presented in this section are preliminary with only an initial calibration of the sediment transport model undertaken at this stage of the project. PSD measurements of the suspended sediment (which will be undertaken by BKA using water sampling in Feb-Mar 2024) will be used to further understand the particles in suspension and how they vary spatially and temporally. These data, along with additional measured SSC data and measured bathymetric changes in Blocks 4 and 4A will be used to further refine the sediment transport model and improve its robustness.

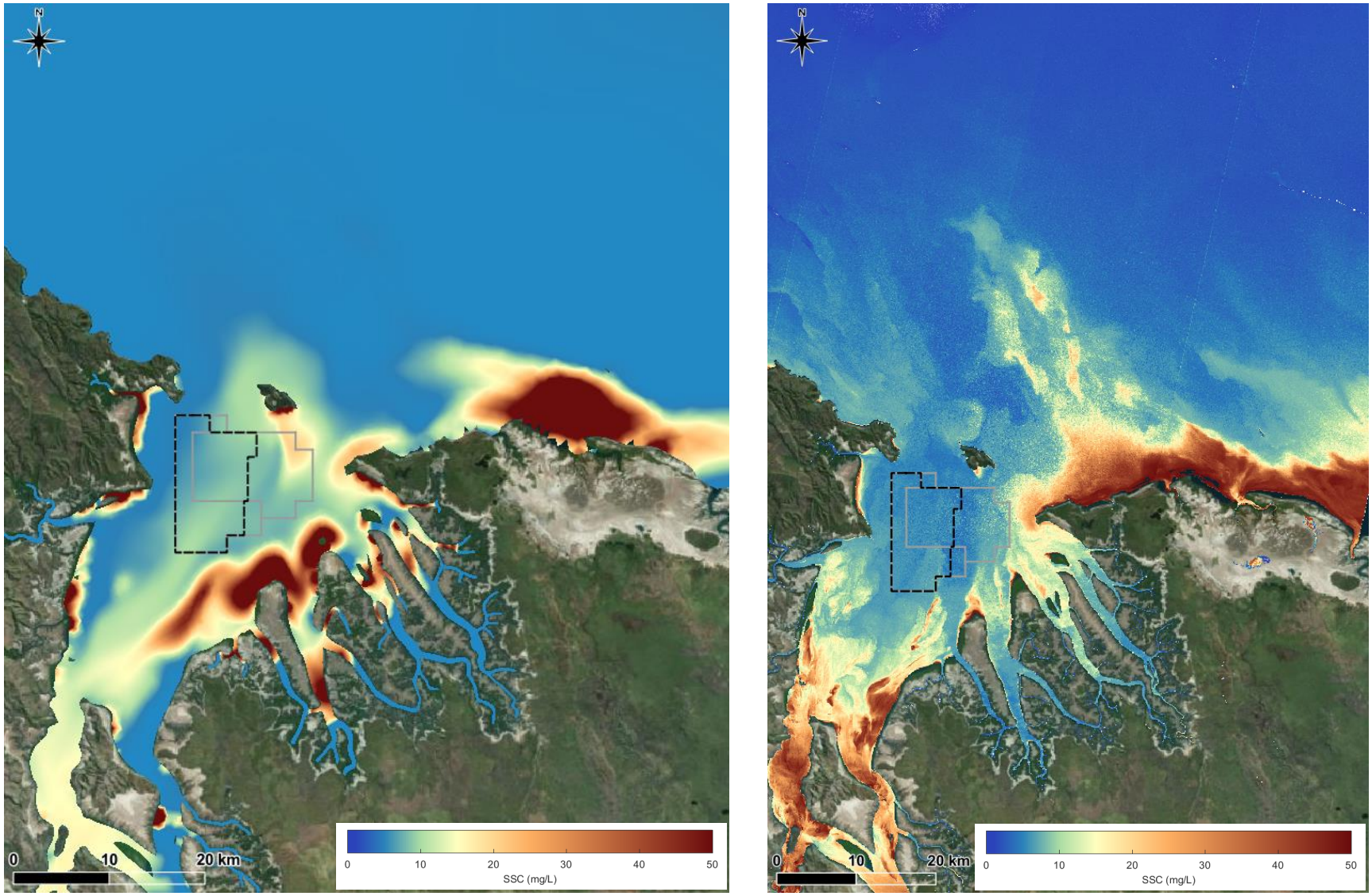

Figure 112. Modelled SSC in the CG region during a neap tide (left) and satellite image showing SSC during comparable neap tide conditions (right).

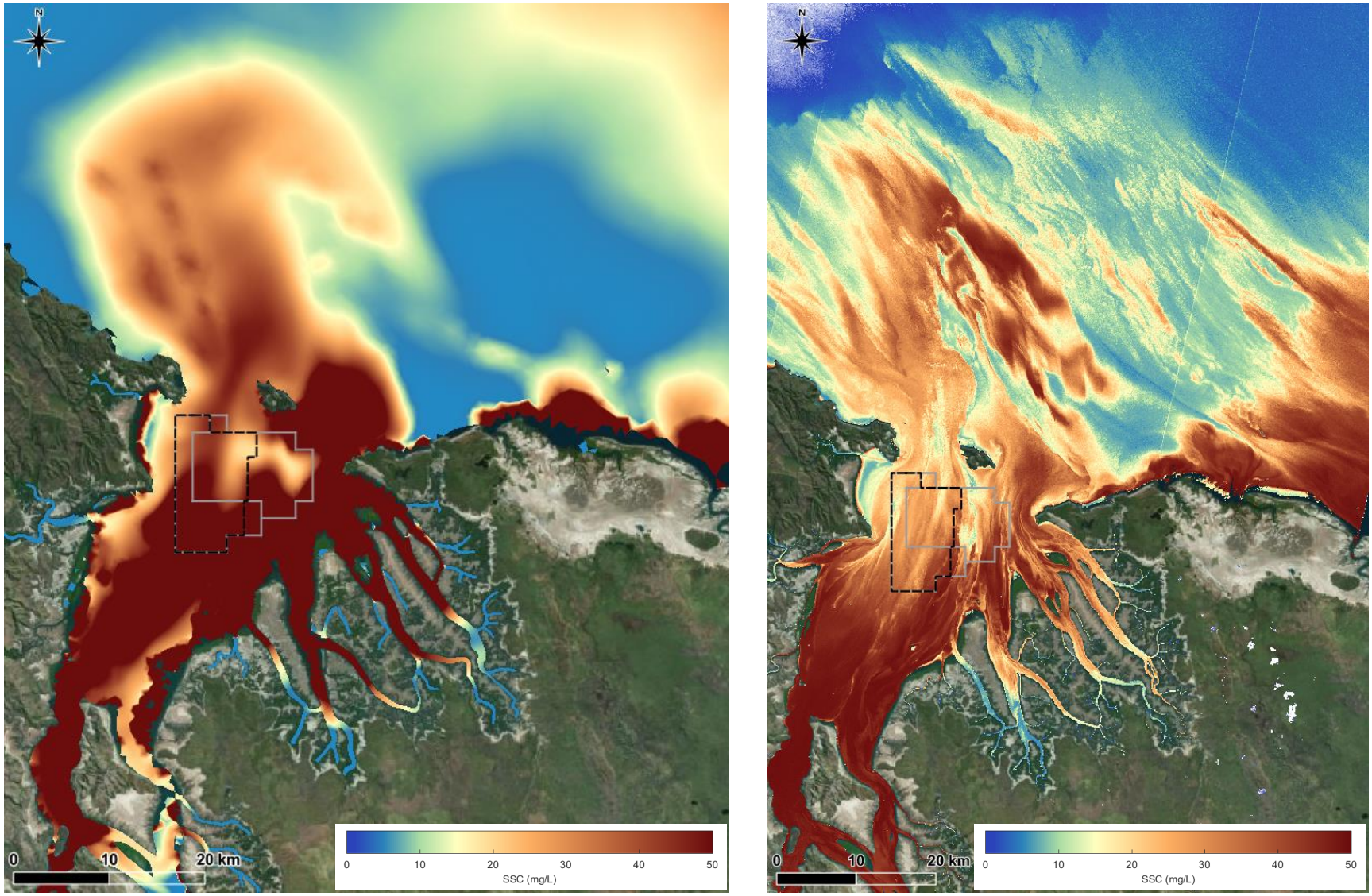

Figure 113. Modelled SSC in the CG region at the end of the ebb stage of the tide during a spring tide (left) and satellite image showing SSC during comparable spring tide conditions (right).

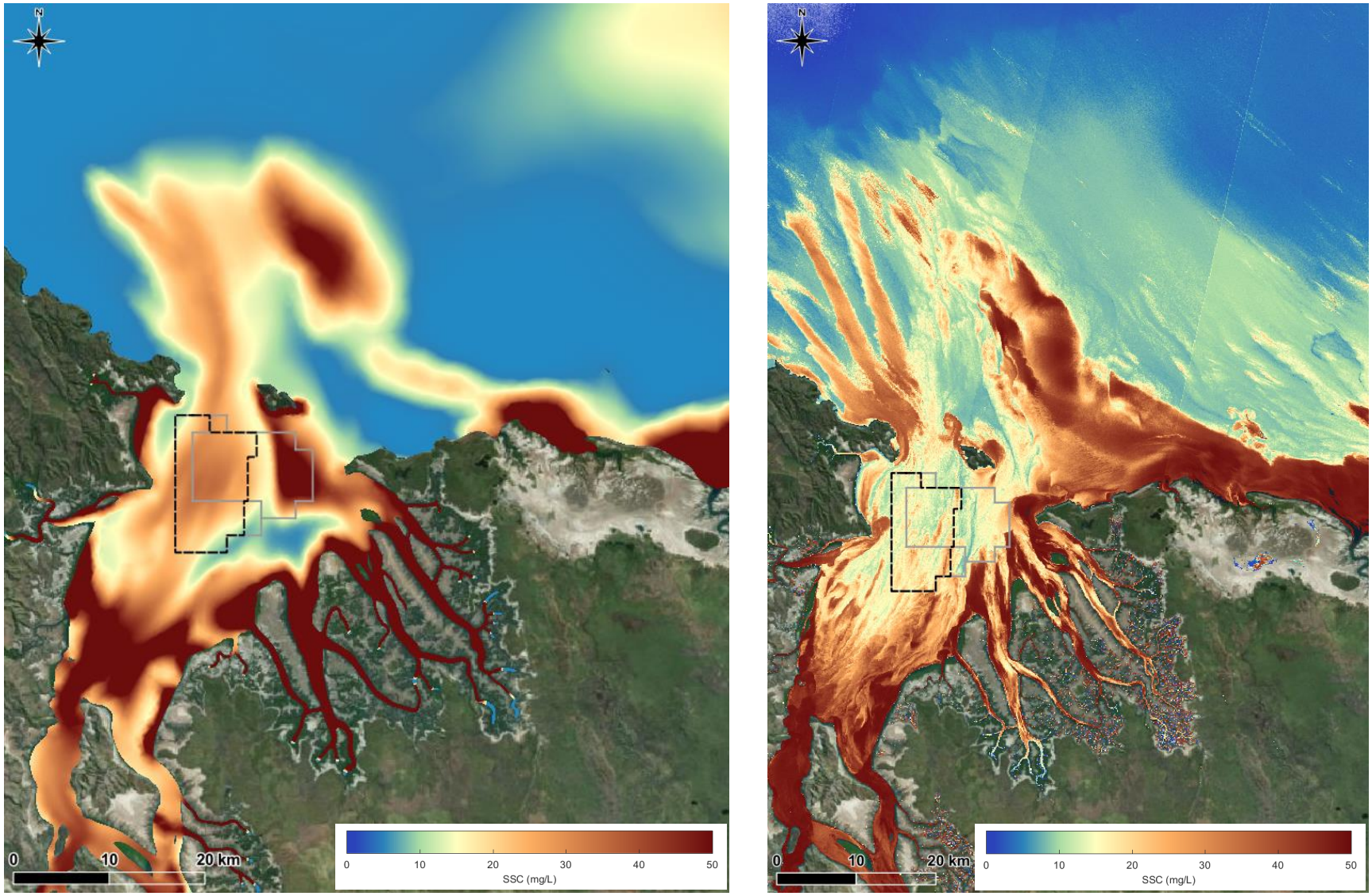

Figure 114. Modelled SSC in the CG region at the end of the flood stage of the tide during a spring tide (left) and satellite image showing SSC during comparable spring tide conditions (right).

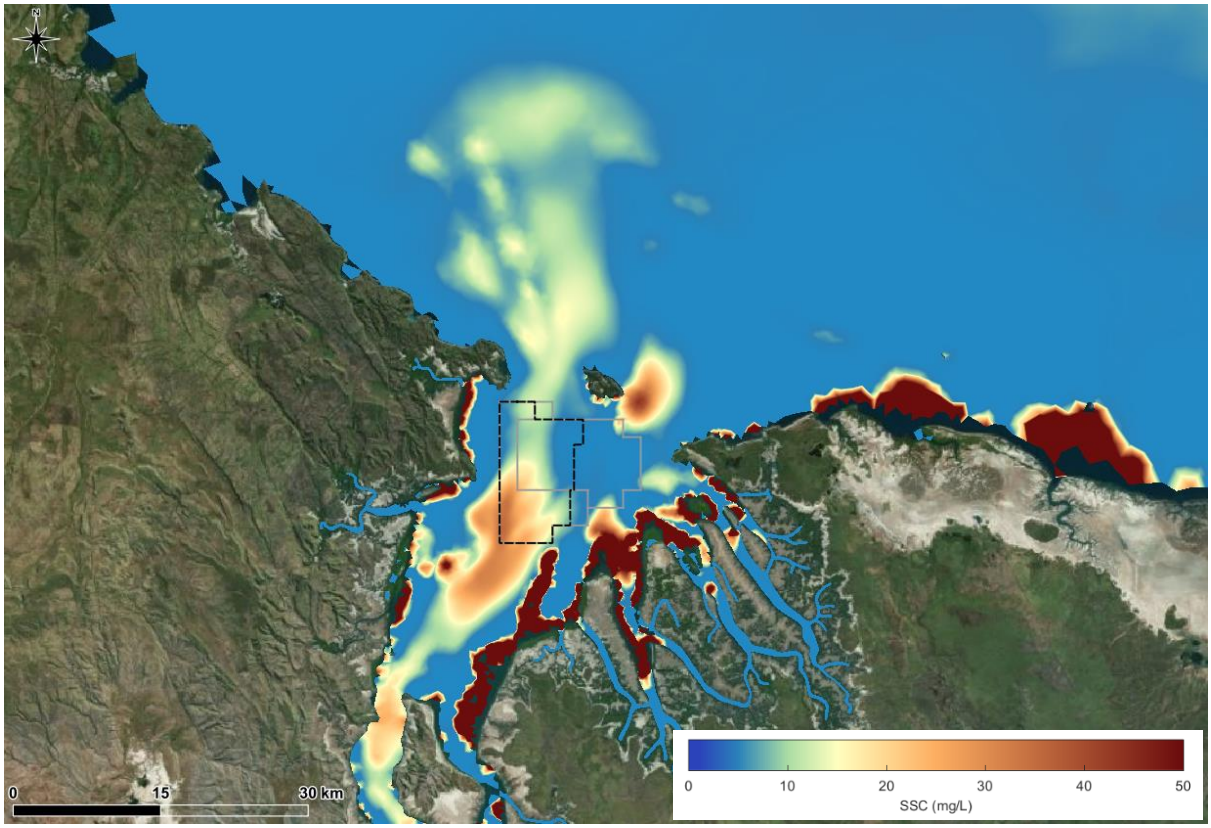

SSC of Sand Sized Sediment

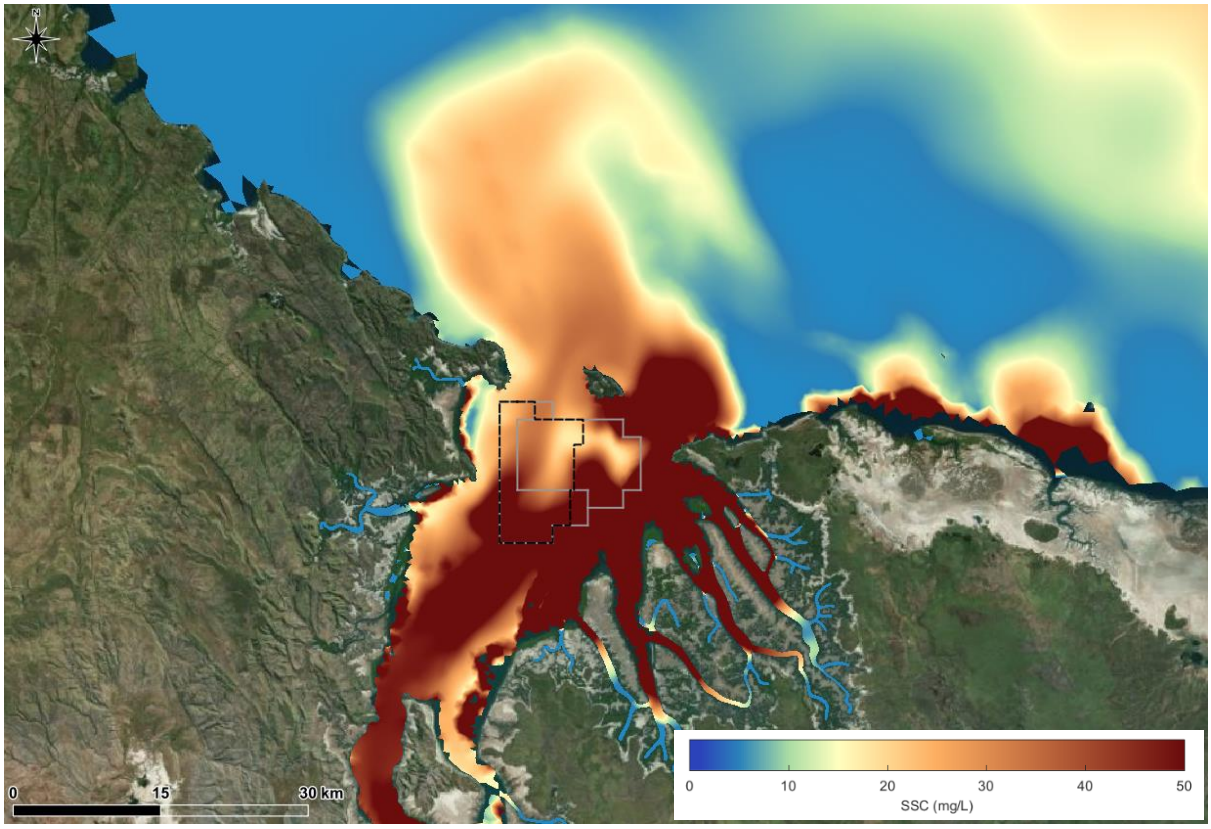

SSC of Fine Silt Sized Sediment

Figure 115. Modelled SSC of the fine sand (top) and fine silt (bottom) fractions at the end of the peak ebb stage of a spring tide.

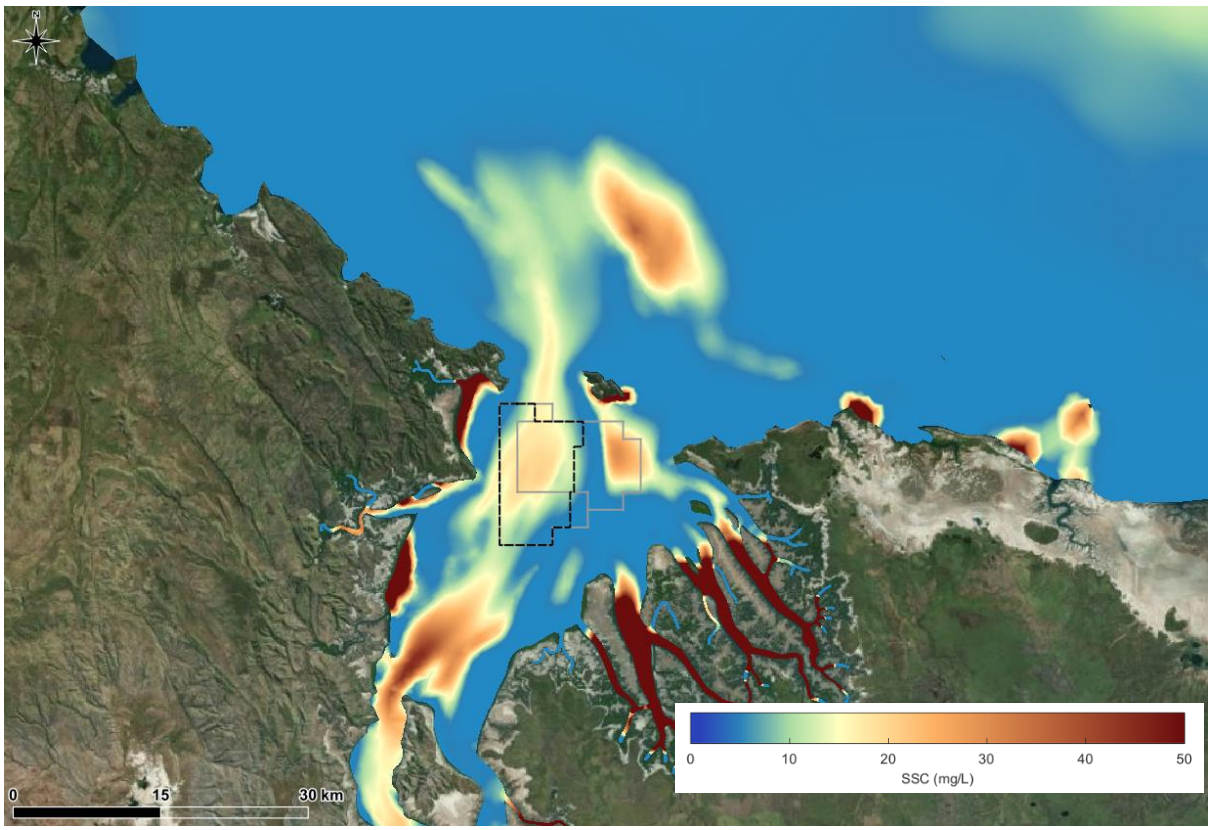

SSC of Sand Sized Sediment

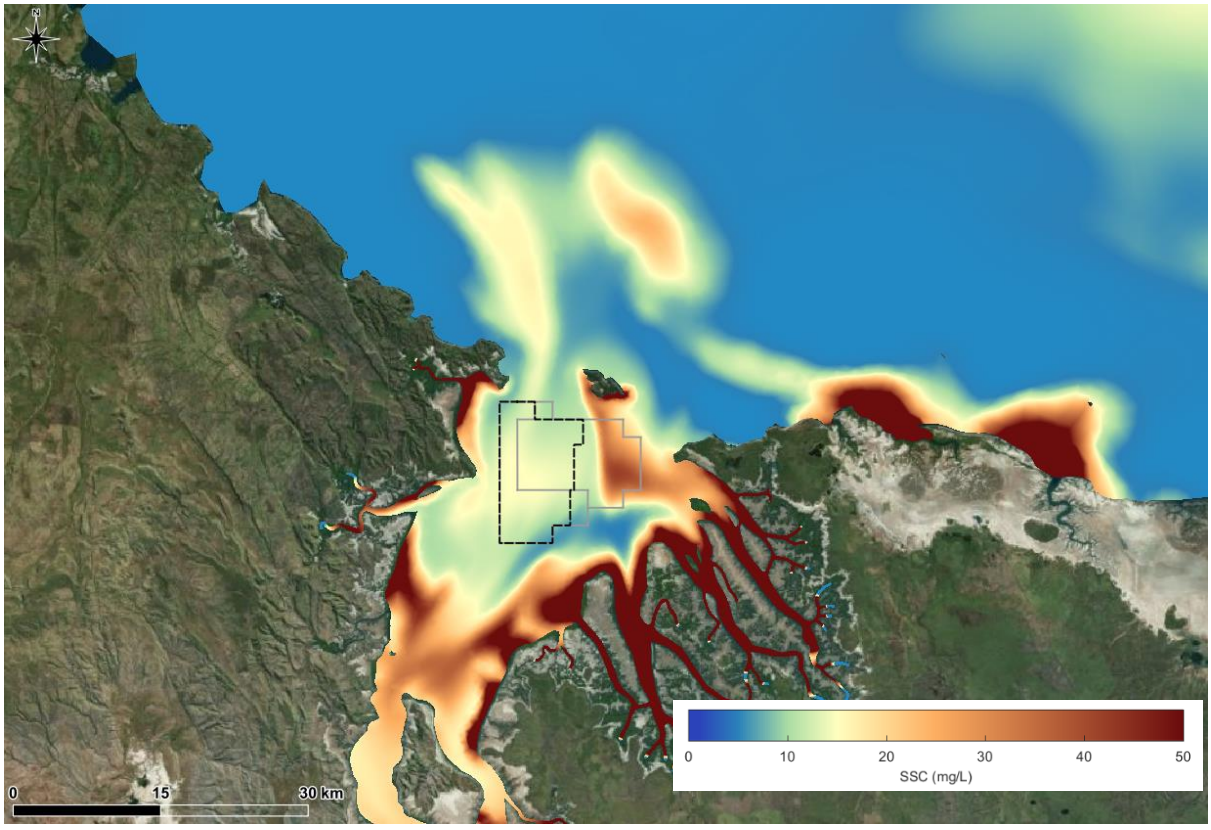

SSC of Fine Silt Sized Sediment

Figure 116. Modelled SSC of the fine sand (top) and fine silt (bottom) fractions at the end of the peak flood stage of a spring tide.

4.7. Beach Processes Model

The MIKE Littoral Processes LITDRIFT and LITPROF modules have been adopted to model the longshore and cross-shore transport of sediment. The LITDRIFT and LITPROF modules calculate the propagation, shoaling and breaking of waves, the momentum balance for cross-shore and longshore currents and the resultant longshore and cross-shore sediment transport.

4.7.1. Model Configuration

For this assessment, the same cross-shore profiles as considered for the shoreline change analysis were adopted at the three turtle nesting beaches offshore of the CG (Figure 117). The modelling has not been undertaken at the East Bank Point stranded beach ridge as the behaviour of this beach ridge is not directly controlled by either cross-shore or longshore transport (see Section 3.9 for further details). Details of the parameters adopted for the profiles are provided below:

- Bathymetry: The beach profile elevation was extracted from the 30 m resolution Geoscience Australia High-resolution Depth Model. For the intertidal areas this depth model is based on the Digital Earth Australia Intertidal Elevation Model and for areas above the intertidal zone it is based on LiDAR data.(DEA, 2023; Geoscience Australia, 2023a).

- Sediment properties: At this stage no sediment data are available for the beaches. In the absence of any data a mean grain size of 200 μm was assumed with no grading. This assumption will be reviewed and a refined grain size adopted should PSD data be collected from the beaches, subject to crocodile safety concerns and TO approval.

- Wave conditions: The wave conditions at the offshore end of each beach profile were extracted from the 5 year SW model simulation. As discussed in Section 4.5.3, this five year period includes multiple TCs which resulted in large wave conditions in the CG region. Therefore, the longshore and cross-shore transport modelling includes for these extreme events.

- Water level: The water level at the offshore end of the beach profiles over the 5 year simulations, was the predicted water level at Cape Domett (AHO, 2023). The model then transforms this water level along the profile to the shoreline to allow processes such as wave setup to be included.

The LITDRIFT and LITPROF modules were then used to simulate the potential longshore and cross-shore transport of sediment at each of the cross-shore profiles over a 5-year period. It is important to note that the modelled transport rates represent the potential transport rate, which assumes an unlimited supply of sand, while the actual transport rates will vary depending on the supply of sand.

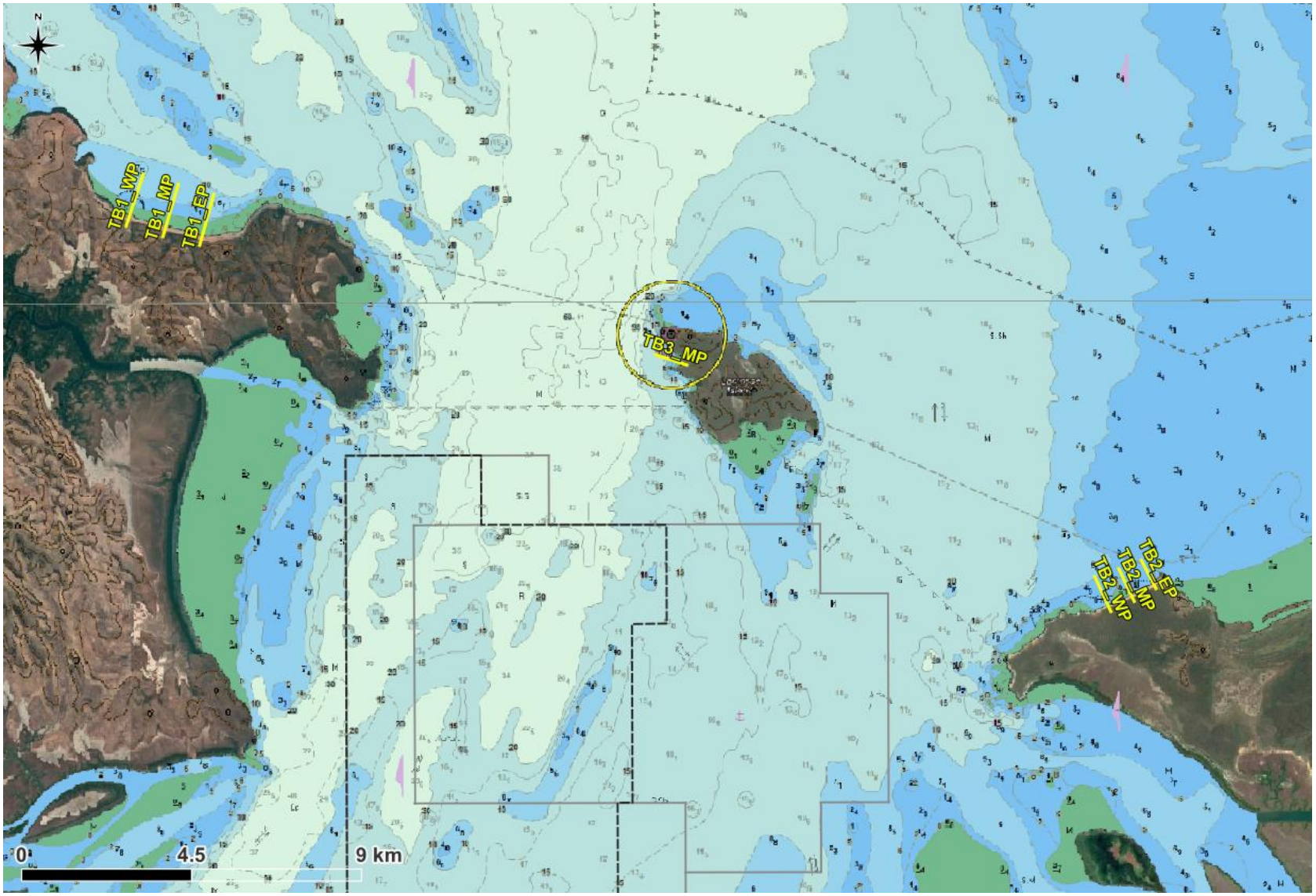

Figure 117. Locations of the cross-shore profiles adopted for the longshore and cross-shore sediment transport modelling.

4.7.2. Preliminary Results

The modelled annual net potential natural longshore and cross-shore transport rates at each of the cross-shore profiles are shown in Figure 118 to Figure 119 (see Figure 60 to Figure 62 for cross-shore profile locations). Positive longshore transport represents transport in an easterly direction, while a negative longshore transport represents transport in a westerly direction (the exact direction varies depending on the alignment of the profile, for example at Turtle Bay positive represents transport to the north, negative represents transport to the south). For the cross-shore transport a positive transport represents net transport in a landward direction, while a negative transport represents net transport in a seaward direction. The results are discussed below for each of the three assessed turtle nesting beaches:

- Turtle Beach West: The natural longshore and cross-shore transport rates are similar, with the longshore transport being higher at the west and east profiles and the rates being approximately the same in at the middle profile. The net longshore transport is predicted to be to the east at all three profiles, with a gradual reduction in the transport rate from the west profile to the east profile. The cross-shore transport is predicted to be in a net landward direction at all three sites, indicating that sand is supplied through the cross-shore transport of sand from offshore. The potential landward transport rates at this beach are predicted to be the highest out of the three beaches modelled, which is in agreement with the finding from the shoreline changes assessment, which showed that this beach was accreting at the highest rate of the four beaches considered. Based on the predicted localised changes to the hydrodynamics and waves resulting from the sand sourcing of 70 million m^3 (detailed in Sections 4.4.4 and 4.5.4) it is considered unlikely that the sand sourcing would directly impact the coastal processes at this beach. The potential longer term impacts of the sand sourcing to the transport of sand in CG and subsequent supply of sand to the beach will be further assessed in more detailed modelling to be undertaken at a later stage of the project.

- Cape Domett Beach: The natural cross-shore transport is predicted to vary along the length of the beach, with net landward transport predicted at the western profile, very little net cross-shore transport at the middle profile and net seaward transport predicted at the eastern profile. The longshore transport at the beach is consistently to the east, with rates gradually reducing from the western profile to the eastern profile. The results indicate that sand from offshore is transported landward at the western end of the beach. The sand is then transported along the beach, with accretion occurring along the length of the beach and then at the eastern end of the beach some of the sand is transported seaward by cross-shore transport. This overall understanding corresponds with the shoreline changes calculated, with the western profile experiencing the highest rates of advance and the eastern profile the lowest. Based on the predicted localised changes to the hydrodynamics and waves resulting from the sand sourcing of 70 million m^3 (detailed in Sections 4.4.4 and 4.5.4), it is considered unlikely that the sand sourcing would directly impact the coastal processes at this beach. The potential longer term impacts of the sand sourcing to the transport of sand in CG and subsequent supply of sand to the beach will be further assessed in more detailed modelling to be undertaken at a later stage of the project.

- Turtle Bay, Lacrosse Island: Both the natural longshore and cross-shore transport rates at this bay are relatively low. The longshore transport rates indicate a small net southerly transport of sand at the bay, while the cross-shore transport rates indicate a small net landward transport of sand from offshore. The relatively low transport rates at this beach correspond to the shoreline changes which showed little change in the shoreline has occurred over time. Predicted localised changes to tidal currents resulting from the sand sourcing of 70 million m^3 occurred close to the western shoreline of Lacrosse Island (see Section 4.4.4). However the changes in current speed were small relative to the absolute current speeds (less than 1%) and there were no predicted changes to waves in this area (see Section 4.5.4). Therefore, it is considered unlikely that the sand sourcing would directly impact the coastal processes at this beach. The potential longer term impacts of the sand sourcing to the transport of sand in CG and subsequent supply of sand to the beach will be further assessed in more detailed modelling to be undertaken at a later stage of the project.

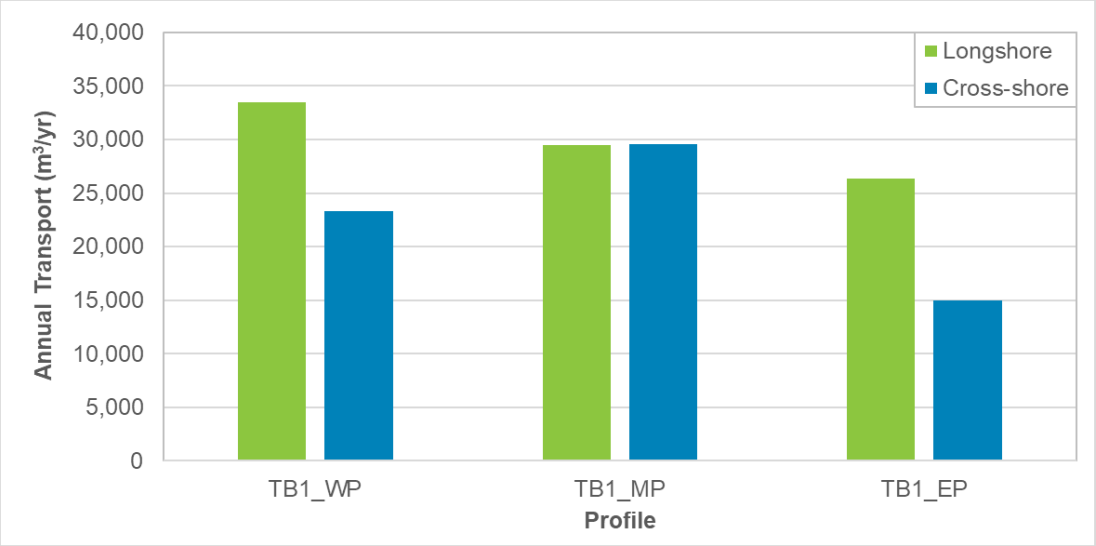

Figure 118. Modelled annual longshore and cross-shore transport at the three profiles at Turtle Beach West.

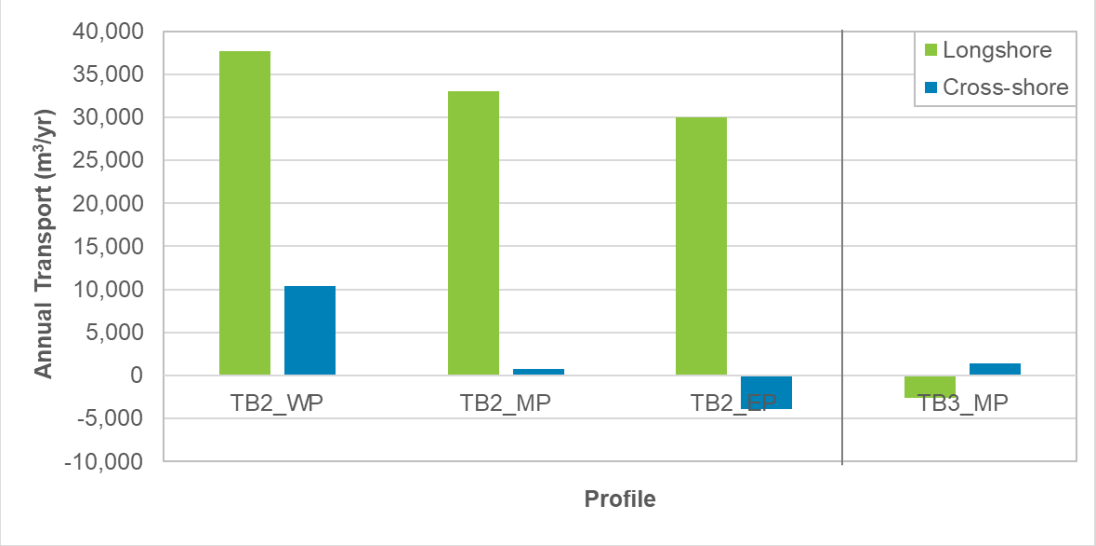

Figure 119. Modelled annual longshore and cross-shore transport at the three profiles at Cape Domett Beach and at the profile at Turtle Bay on Lacrosse Island.

To show how the natural cross-shore and longshore transport varies spatially along the cross-shore profiles and how the transport rates vary over time, plots of the transport across the profile are shown over four months of wet and dry season conditions and the annual transport rates from 2015 to 2019 are shown for the west profile at Turtle Bay West (TB1_WP) in Figure 120 to Figure 123. This profile was selected as both longshore and cross-shore transport rates are relatively high and it provides a typical representation as to how the transport is predicted to vary along the cross-shore profile. The plots show the following:

- Cross-shore transport:
  - There is predicted to be a gradual natural onshore transport of sand from the offshore end of the profile during both the wet and dry season conditions. The onshore transport occurs up to the -2 m AHD level and with a potential offshore transport of sediment then predicted for the intertidal area of the profile above this elevation. The cross-shore natural transport rates are predicted to be significantly higher in the wet season compared to the dry season.
  - There is predicted to be some annual variability in the natural cross-shore sediment transport rates, with the net rates predicted to vary by up to 20% of the maximum annual rate.

- Based on the predicted impacts to hydrodynamics and waves, the sand sourcing of 70 million m^3 in CG is not expected to influence the cross-shore transport at the beach at no changes to waves or currents are predicted in the area.

- Longshore transport:
  - No natural longshore transport is predicted to occur along the profile below an elevation of -2 m AHD. Natural longshore transport is predicted to occur from this elevation up to the 3 m AHD level. The direction of the longshore transport is predicted to vary between the seasons, with transport to the east (positive) during the wet season and transport to the west (negative) during the dry season. As with the cross-shore transport, the longshore transport rates during the wet season are predicted to be significantly higher than the dry season rates.
  - There is significant annual variability in the natural longshore transport rates. The net transport to the east varied from 7,500 to 75,000 m^3, while in 2017 the net transport switched from the east to the west with a net transport of around 50,000 m^3. This indicates that the Turtle Beach West is approximately aligned with the average wave direction and any annual variability in the wave direction can result in significant changes to the longshore transport rates.
  - Based on the predicted impacts to hydrodynamics and waves, the sand sourcing of 70 million m^3 in CG is not expected to influence the longshore transport at the beach and no changes to waves or currents are predicted in the area.

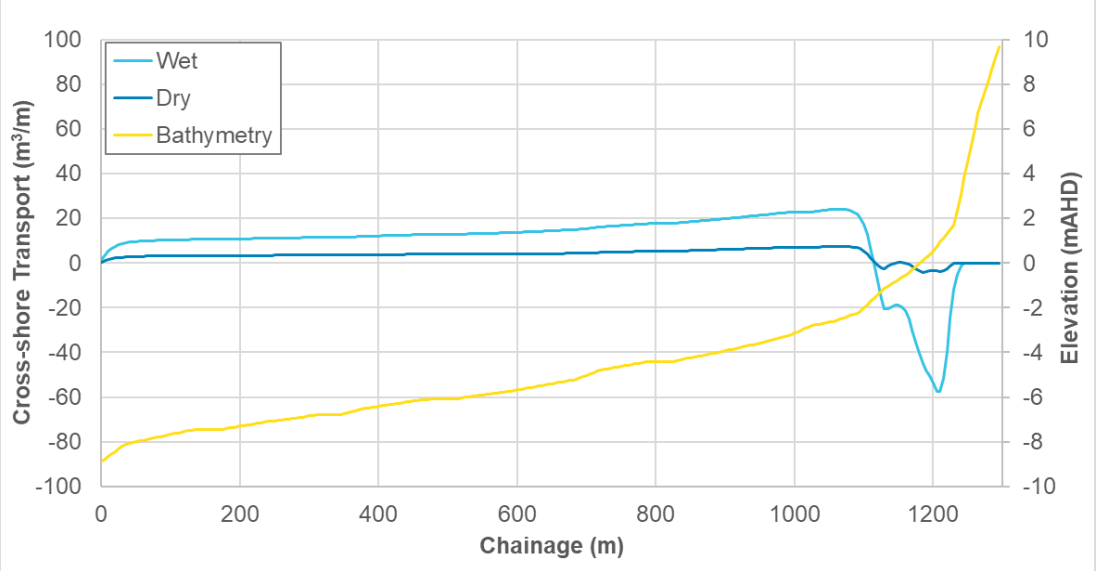

Figure 120. Spatial variation in cross-shore transport along the TB1_WP beach profile over four month wet and dry season periods.

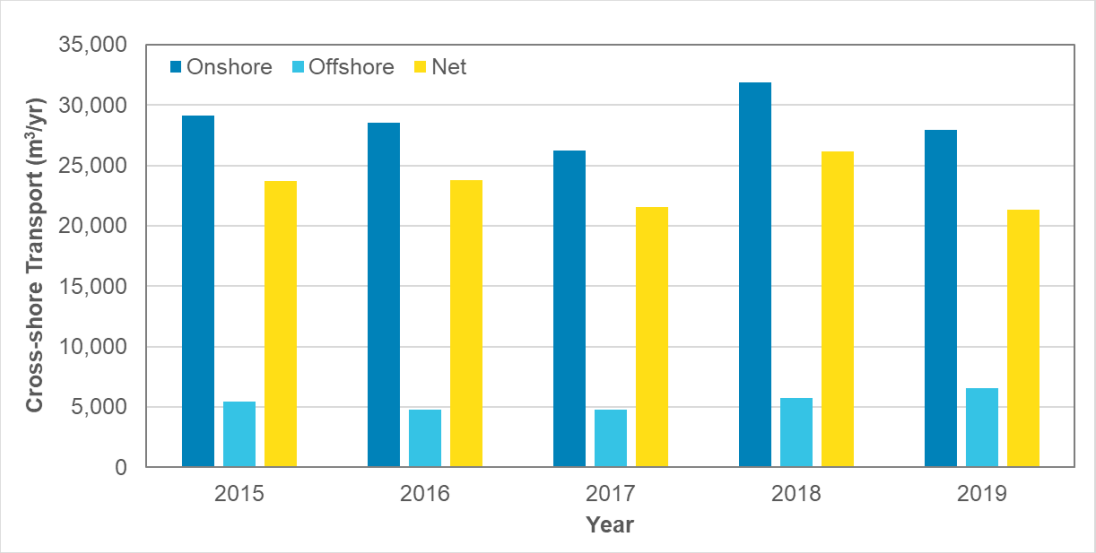

Figure 121. Annual variation in cross-shore transport at the TB1_WP beach profile from 2015 to 2019.

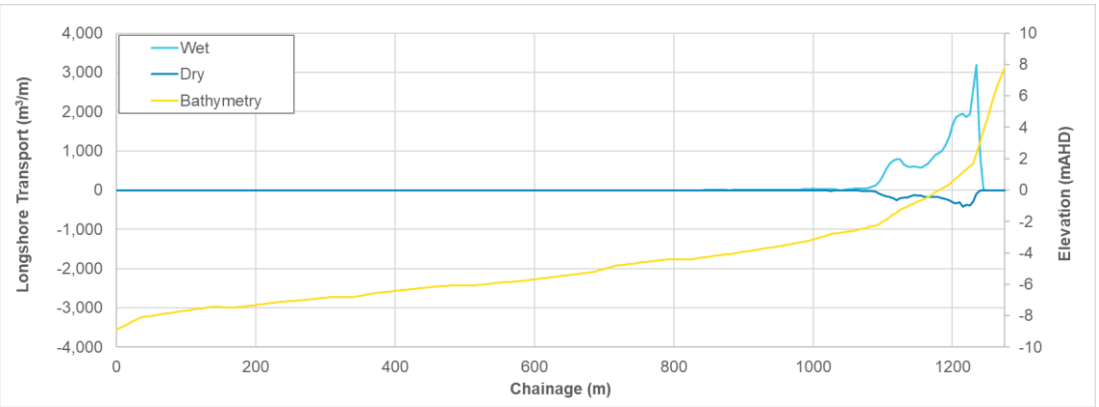

Figure 122. Spatial variation in longshore transport along the TB1_WP beach profile over four month wet and dry season periods.

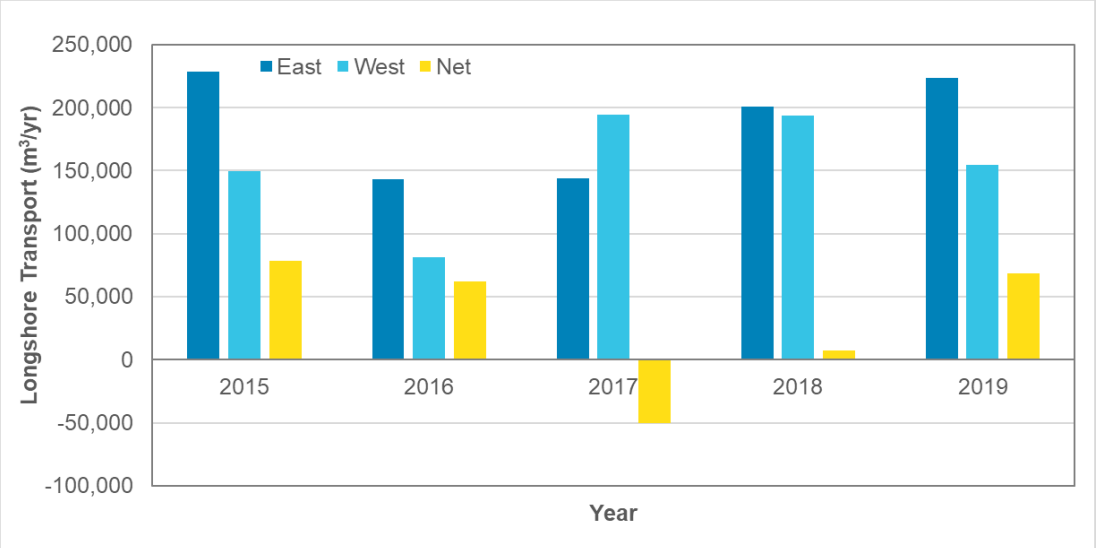

Figure 123. Annual variation in longshore transport at the TB1_WP beach profile from 2015 to 2019.

4.8. Future Modelling

As noted at the start of this section, this report provides details of preliminary numerical modelling which has been undertaken for the study. The numerical modelling will be further expanded through the course of the study and subsequent reports will be prepared to present the different modelling undertaken and to discuss any predicted impacts. The proposed approach for the numerical modelling has been developed in accordance with the study objectives and relevant WA EPA guidelines outlined in Section 1. Further details of how the modelling will meet the objectives and guidelines are provided in Section 6.

This report has provided results from the HD, SW, MT and Beach Processes models for existing base conditions as well as results from HD and SW simulations to assess potential impacts of the sand sourcing. However, these results should be considered as preliminary as the models will continue to be refined throughout the study as more measured data become available. The HD, SW and MT models will be subject to detailed calibration and validation exercises during both dry and wet season conditions to demonstrate whether or not the models are able to represent the range of conditions experienced in CG, in accordance with the required level of accuracy. Following the model refinements and the calibration and validation exercises, the models will be ready to be used to inform the final impact assessment. Details of the proposed modelling approach to meet the four main objectives of the study are provided in the following sections.

4.8.1. Hydrodynamics and Waves

The HD and SW models will be setup to represent the different metocean conditions (including a TC) experienced in CG during the dry season, transitional period and the wet season for the existing conditions (present day, no sand removal) and for pre-European colonisation conditions (this will be based on a number of assumptions which will be defined when undertaking the modelling). Results from these simulations would be used to define the hydrodynamic and wave conditions in the area over the seasonal range of conditions for both existing conditions and pre-European colonisation conditions. The results from the two would be compared to show the change in hydrodynamics and waves due to the European colonisation and how this varies seasonally.

Based on the available information the pre-European colonisation conditions differ from present day primarily due to the creation of the Ord River Dam (with minor changes due to land clearance for cattle grazing and irrigated agriculture in the Ord catchment as well), meaning that during the wet season much higher freshwater discharges occurred in the Ord River along with a higher sediment supply from the river. During the dry season the freshwater discharge pre dam construction would have been lower than it is now, as the dam releases a relatively constant discharge.

The models would then be setup to represent the change in bathymetry due to the sand sourcing activities for the following timeframes:

- During sand sourcing: To represent the change in bathymetry during the sand sourcing, it is proposed that the bathymetry will be updated to represent the sand sourcing over the initial 5 years of operations. The sand sourcing activity will be constant over time, meaning that after 5 years of operations approximately 33% of the total volume will have been removed. It will therefore be assumed for this simulation that 33% of the total volume of sand is removed evenly over the proposed operational area where sand has been shown to be present.

- At the end of the operation: The bathymetry will be updated to represent the total volume of sand sourced over the entire 15 year operational period. It will be assumed for this simulation that the total volume of sand is removed evenly over the proposed operational area where sand has been shown to be present.

- In 100 years time: For this scenario some sedimentation will be assumed to have occurred. The sedimentation to be assumed will be defined based on the available information (e.g. measured bathymetric changes in the area along with results from the sediment transport modelling which is discussed in the following section). The simulation will also include 100 years of sea level rise, an increase in the river discharge and other relevant changes to the metocean conditions based on the latest available guidance.

The HD and SW models will be setup to simulate these three sand sourcing bathymetric scenarios as well as a no sand sourcing existing baseline case for the three metocean periods. The results from the sand sourcing cases will be compared with the results from the no sand sourcing baseline case for each of the three metocean periods. This will result in a range of predicted impacts which will be used

to derive the 'best-case' and 'worst-case' impacts of the proposed project on hydrodynamics and waves during the operation, at the end of the operation and in 100 years time.

The results from the end of operation conditions simulation will also be compared with the results from the pre-European colonisation conditions simulation to show the 'cumulative' impacts of the Ord River Dam and the sand sourcing. Comparison between the predicted changes from these two scenarios and the changes from the existing baseline conditions to the end of operation conditions will put the changes from the sand extraction into context with the changes caused by the Ord River Dam.

4.8.2. Sediment Transport and Coastal Processes

The beach processes model (LITPACK) will be updated to include the detailed beach profile elevation LiDAR data and the PSD results from the sand samples to be collected across the profiles (if they can be safely collected given crocodile risks). The model will then be setup to simulate the longshore and cross-shore transport at the turtle nesting beaches using results from the SW model. The model will be run assuming present day sea levels and sea levels in 100 years time, and for cases where either the sand sourcing or changes since European colonisation are predicted to impact the wave conditions. The model will be run with and without the sand sourcing and for pre-European colonisation for the same three timeframes as the HD and SW models (during, end of operation and 100 years time).

The MT model will be setup to simulate the sediment transport for the same three metocean periods as the HD and SW models (dry, transitional and wet) for the existing conditions and for pre-European colonisation conditions. The results from both the MT and LITPACK model simulations would then be used to define sediment transport and coastal process conditions for the area for existing conditions (including for a TC) and how these have changed from pre-European colonisation conditions. The results, along with results from the analysis of available measured data, will be used to show the natural sediment transport pathways, transport rates, the particle sizes of sediment transported in suspension and on the bed and the longshore and cross-shore transport rates at the turtle nesting beaches. The results from the existing and pre-European colonisation conditions will also be compared to show the change in sediment transport and coastal processes due to the European colonisation and how this varies seasonally.

The MT model will then be setup to simulate the same three bathymetric scenarios as modelled for the hydrodynamics (during operation, end of operation and 100 years time) for the three metocean periods. Results from the end of operation simulations will be used along with measured bathymetric changes to inform the sedimentation rates to adopt for the 100 years time simulations. The results will be compared with the results from the existing conditions in the same way as detailed for the HD and SW modelling to predict 'best-case' and 'worst-case' impacts of the proposed project on sediment transport during the operation, at the end of the operation and in 100 years time. The results from the HD, SW and MT modelling as well as the beach processes modelling will be used to inform the following:

- The potential natural replenishment of sand sourced from Blocks 4 and 4A. This will include estimates of the likely timeframe for all of the sand to be naturally replenished.
- The potential for coastal erosion or accretion as a result of the sand sourcing activity.
- Any potential impacts to the turtle nesting beaches located both inside and immediately outside the CG. This would include any potential for changes in the supply of sediment to the beaches, any changes in sand grain size at the beach or any change to the beach geomorphology.
- Any potential impacts on the mangroves and any other coastal and intertidal communities within the CG and any potential impacts on the Ord River Floodplain Ramsar site.

The results from the end of operation conditions simulation will also be compared with the results from the pre-European colonisation conditions simulation to show the 'cumulative' impacts of the Ord River Dam and the sand sourcing on sediment transport and coastal processes. Comparison between the predicted changes from these two scenarios and the changes from the existing conditions to the end of operation conditions will put the changes from the sand sourcing into context with the changes caused by the Ord River Dam.

4.8.3. Suspended Sediment and Plume Dispersal

It should be noted that the WA EPA *Technical Guidance for EIA of Marine Dredging Proposals* (EPA 2021) require Zones of High Impact (ZoHI), Zones of Moderate Impact (ZoMI) and Zones of Influence (ZoI) to be defined by the model, considering likely impacts of turbidity and sediment plumes on priority benthic communities in the area. This should include biological response modelling and setting of trigger levels, considering the sensitivity of relevant benthic species to turbidity, benthic light reduction and sedimentation, and modelling of likely 'worst-case' and 'best-case' impacts, as defined in the guidance.

However, the benthic surveys by BKA to date as described in section 2.3.1 have found no evidence of potentially sensitive benthic communities in CG or at King Shoals, including the primary producer communities identified as a priority in the EPA Guidance. Due to the strong tidal currents, constant seabed sediment suspension and naturally high turbidity and lack of sunlight near the seabed, there appear to be no seagrass meadows, coral communities, sponge-beds, macro-algae communities or similar inter-tidal and sub-tidal benthic communities in CG or at King Shoals.

The benthic surveys to date (BKA, 2024d) indicates three main types of sub-tidal benthic substrates (physical habitat) in CG and at King Shoals – sand, rock/gravel and silt/clay (with mixtures of these in some areas). The areas of seabed that are dominated by sand, including King Shoals, were found to support very little benthic biota. The areas of seabed that are dominated by rock/gravel were found to support very low numbers of occasional, very small hydroids, bryozoans and similar epi-benthos attached to small rocks and stones. The areas of seabed that are dominated by silt/clay were found to support very low numbers of occasional, very small polychaetes, crustaceans, echinoderms and similar individual organisms.

Additionally, the nature of the proposed operation, using a dredge similar to a Trailer Suction Hopper Dredge (TSHD) is unlikely to cause significant elevation of turbidity above natural background levels. This is because the operation will only target sand and avoid areas of fines, will not involve any dumping (the dredged sand will be retained on the dredge and exported, with the dredge also being the export vessel), the dredge will only be on site for one or two days every two weeks each cycle (it will not be a continuous, turbidity-generating operation), and it will include turbidity control measures (e.g. 'green valve' on the dredge, water overflow discharge at keel etc).

Given the absence of potentially sensitive benthic communities, including the primary producer communities identified as a priority in the EPA Guidance, it is not possible to model ZoHI, ZoMI and ZoI – as there are no benthic communities in the area to model these for. The suspended sediment and turbid plume dispersal modelling will therefore focus on predicting to what degree the sand operation will generate turbidity and sediment plumes, and how far and for how long these will disperse under various conditions, before receding to background levels, generating spatial maps of such dispersal.

The calibrated HD and SW models will be used to drive a plume dispersion model to represent the transport of sediment suspended by the sand sourcing activity using the MT model. As discussed in Section 1.1, a single SPV will be used to source the sand from CG. The SPV will only operate for 1 to 2 days in CG removing the sand every 2 weeks. The source terms adopted to represent the removal of the sand by the SPV will be defined based on the approach detailed in the CSIRO/WAMSI dredge plume modelling guidelines (Sun et al., 2020). The sand sourcing activity will be conceptualised in the model to ensure that the production rate, the time to overflow, depth of overflow and removal methodology (i.e. the tracks that the SPV adopts) are all realistically represented. The source terms will then be defined along with their release location in the water column.

The plume dispersion model will be setup to simulate the dredging for the three metocean periods the HD and SW models were used to simulate. The modelling results will be processed using statistical analysis such as percentiles to show the extent, magnitude and duration of elevated SSC and sedimentation impacts resulting from the sand sourcing. The range of predicted impacts from the simulations will be used to predict likely 'best-case' and likely 'worst-case' impacts of the proposed project on SSC and sedimentation. Results from the modelling will also be compared with the natural SSC and sedimentation predicted by the modelling (and based on measured data) to put the potential impacts into context with the natural environment. The magnitude of any impacts will be assessed through consideration of the natural conditions in the region.

5. CONCEPTUAL UNDERSTANDING

This section presents a system understanding of the CG region in terms of coastal processes and sediment transport. In addition, a high-level overview of the potential coastal processes and ecological implications resulting from the proposed CG Marine Sand Proposal is discussed along with a conceptual model of the potential causes and effects.

5.1. System Understanding

The available data and information have shown that the large tidal range in CG results in high tidal current speeds which in turn result in regular sediment transport and high SSC. Tidal processes are likely to have been the dominant process which resulted in the formation of CG in its current form (Thom et al., 1975). Current speeds in CG are typically higher on the flood stage of the tide than on the ebb stage of the tide, although this dominance does vary spatially and temporally which could be due to the semi-diurnal inequality and bathymetry. Current speeds are higher in the western entrance to CG compared to the eastern entrance.

The wave conditions directly offshore of CG are relatively calm, with the shallow King Shoals and Medusa Bank acting to limit the wave height which can reach the entrance to CG and the adjacent beaches to the west and east. There is a strong seasonal variability in wave conditions in the region, with larger wave events predominantly from the west-northwest occurring during the wet season and calmer wave conditions from the northeastern quadrant occurring during the dry season. The wave conditions result in a combination of cross-shore and longshore transport influencing the beaches adjacent to the entrance to CG. Modelling has shown that at most of the beach profiles, sand is transported onshore to the beaches through cross-shore transport and then transported longshore in the intertidal area.

Waves within CG are further sheltered by the presence of Lacrosse Island in the middle of the entrance to CG, meaning that any influence from wave action in CG is limited to very large wave events during the wet season (e.g. during TCs and tropical lows). These wave events can result in erosion of areas of mudflats and mangroves and also in the formation and landward migration of features such as stranded beach ridges. The influence of waves on sediment transport within the proposed operational area will be small compared to the influence of tidal currents. Waves with an H_s of more than 1 m were predicted to occur for less than 1% of the time in the proposed operational area. Based on an average water depth of 20 m in the area, the peak near bed velocities of a wave with an H_s of 1 m (and corresponding typical peak wave period of 6 s) based on the linear wave theory would be 0.3 m/s (van Rijn, 1993). This is almost three times lower than the measured peak near-bed spring tidal current speeds in the area (around 0.8 m/s).

Sediment sampling results have shown that there is an abundance of sediment available for transport within CG, with a combination of sand, silt and clay all present in the region with an estimated 150 to 300 million m^3 of sand present in the proposed operational area (and likely orders of magnitude more than this within the entire CG and King Shoals). There is significant variability in the sediment transport which occurs in the region, with the tide being the dominant process which influences sediment transport in CG. As a result, the sediment transport varies between the flood and ebb stages of a single tide and between spring and neap tides. Relatively low SSC and transport rates only occur for short durations on small neap tides, while higher SSC and transport rates occur more often due to the larger neap and spring tides which regularly influence CG. The data show consistently very high SSC within West and East Arms throughout the year. The available information suggests that the SSC within CG is typically higher during the wet season compared to the dry season. This will be further assessed using data collected by BKA. Due to the regular high SSC in the region, the benthic light availability is likely to be low throughout most of CG. The peaks in SSC throughout CG occurred (except in East Arm) around low water, indicating that the elevated SSC occurred as a result of sediment which had been suspended upstream of where the measurements were made.

The peaks in SSC in East Arm coincided with the flood stage of the tide, suggesting that the SSC was being imported from downstream. This was previously observed by Wolanski et al. (2004) who estimated that since completion of the Ord River Dam, the majority of the sediment transported downstream along West Arm was subsequently imported into East Arm. Wolanski et al. (2004) suggested that almost no fine-grained sediment was transported into CG from either West or East Arms as a result of the Ord River Dam suppressing the wet season flood flows in the Ord River. However, the satellite-derived SSC data consistently showed high SSC in both West and East Arms, which extended into the southern half of the open bay area of CG, indicating an ongoing supply of suspended sediment from West Arm. The available information therefore indicates that there is a

supply of suspended sediment from West Arm into CG, but there is uncertainty regarding the quantum of the supply.

Very little benthic biota and no significant sub-tidal benthic communities appear to be present in CG, with the low benthic light, strong tidal currents and likely dynamic seabed sediment expected to be the major cause of this. There appear to be no seagrass meadows, coral communities, sponge-beds, macro-algae communities or similar intertidal and subtidal benthic communities in CG or at King Shoals.

The main intertidal community in CG is the relatively narrow fringe of mangroves along most of the coast, especially on the eastern side, which is part of the Ord River Floodplain Ramsar site, backed by intertidal salt flats and mudflats (Figure 1). Evidence of mangrove destruction and coastal erosion was observed within CG during the July-August 2023 environmental survey, assumed to have been caused by a large wave event, storm surge and high winds, probably during a TC (Figure 56 and Figure 57). The last TC to pass over or near CG was TC Ellie in December 2022.

There is a globally important nesting beach for Flat Back Turtles *(Natator depressus)* on the seaward side of Cape Domett, and three other turtle nesting beaches with lesser numbers at Turtle Beach West (just west of Cape Dussejour), in Turtle Bay at Lacrosse Island and at East Bank Point inside CG (Figure 59). The beaches adjacent to the entrance to CG at Turtle Beach West and Cape Domett Beach were shown to have advanced slightly over the last 30 years, while the beach at Turtle Bay on Lacrosse Island was shown to have remained stable. This suggests that any changes to the sediment transport processes in CG that may have been caused by the Ord River Dam have not reduced the supply of sand to these beaches. The western and eastern ends of the beach ridge at East Bank Point was shown to have historically migrated landward over the last thirty years. This is a common response of stranded beach ridges as a result of the limited supply of sand due to their location perched on top of mudflats.

A conceptual sediment transport and coastal processes system understanding for CG is shown in Figure 124.

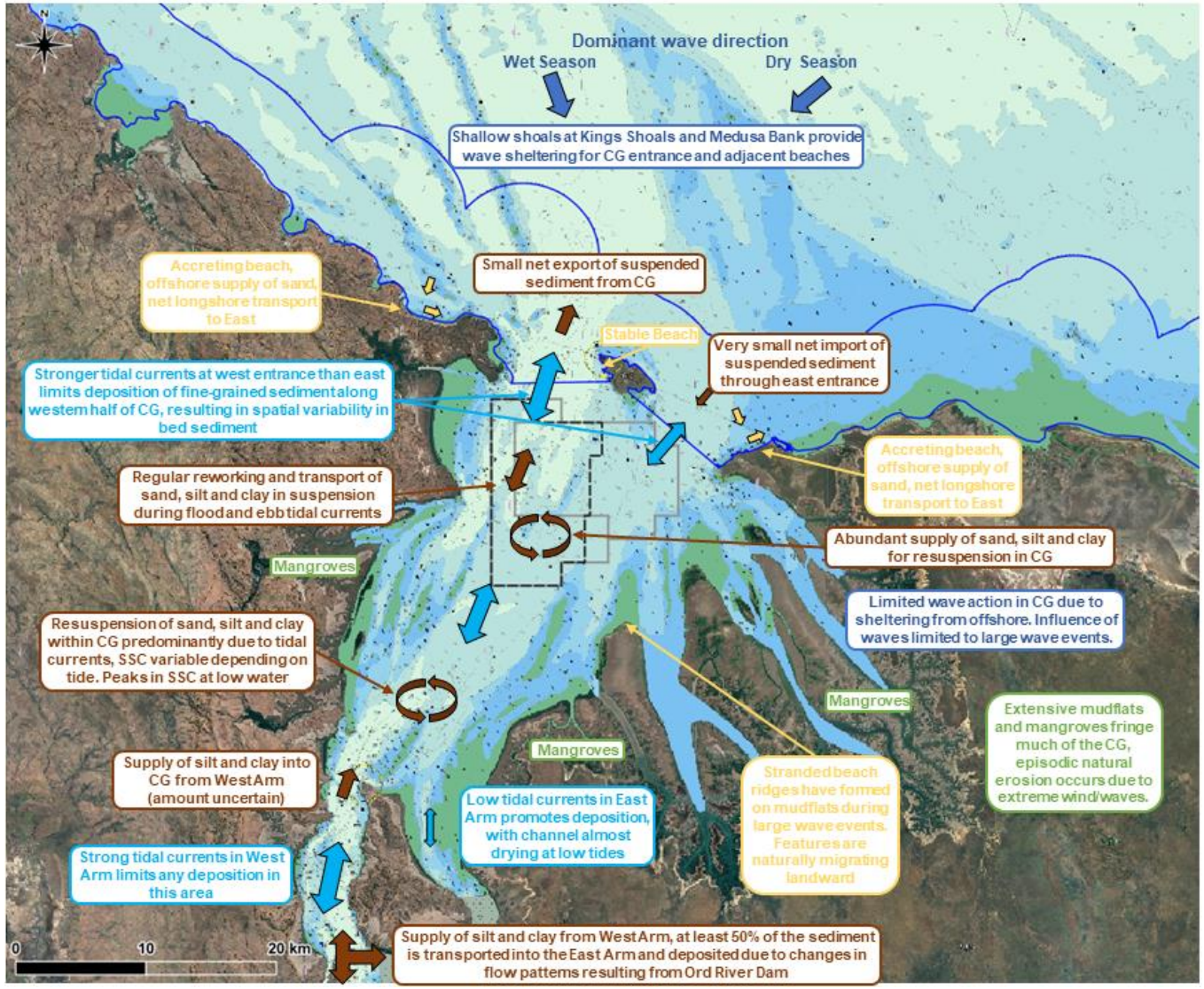

Figure 124. A conceptual sediment transport and coastal processes system understanding for the CG. *Note: text and arrows in dark blue relate to waves, pale blue relates to tidal currents, brown relates to sediment transport, yellow relates to beach changes and local sand supply and green relates to mangroves.*

5.2. Coastal Processes Implications

This section presents a coastal processes assessment that considers the potential impacts of the proposed sand sourcing on the CG region. Initial impact assessment modelling presented in this report has shown that sourcing of 70 million m^3 of sand has the potential to result in minor changes to the hydrodynamics and waves in CG. These changes along with the reduction in sand available in the proposed operational area, will have the potential to influence sediment transport in the region. In turn, these changes could result in impacts to the coastal processes and ultimately to the coastal morphology and ecology. The potential cause-effect pathways for these changes are detailed below:

- Hydrodynamics: The removal of 70 million m^3 of sand has been shown to result in small changes to the flows and water levels in CG. The changes to water levels were predominantly due to a very small change in the phasing of the tide (tide propagating into CG earlier by 27 seconds), with the changes to the spring tidal range predicted to be up to 0.06%. The changes to tidal currents were predicted to remain localised to the proposed operational area and directly adjacent area. Within the proposed operational area, the peak tidal current speeds were predicted to be reduced by up to 1.5%, while outside of the area localised increases and decreases in current speed of up to 0.8% of the peak current speeds were predicted.

- Waves: Changing the seabed morphology can influence how waves propagate across an area, with the potential for changes to refraction, attenuation and reflections. The effects from this are typically more significant in cases where shallow regions are significantly deepened combined with open coastal locations. In this case, the removal of 70 million m^3 of sand from the proposed operational area has been shown to only result in small changes to wave heights in CG (less than 0.01 m). In addition, the predicted changes were shown to be dependent on the wave conditions, with changes only predicted to occur during larger wave events which occur in the wet season due to tropical cyclones and tropical lows. Changes to the modelled wave percentiles due to the sand sourcing were limited to the 95^{th} and 99^{th} percentiles, with maximum changes of 0.001 m.

- Sediment transport and Coastal Processes: The combined changes to hydrodynamics and waves along with changes to the seabed morphology and sediment composition have the potential to result in changes to sediment transport pathways and rates. Changes to the sediment transport pathways have the potential to result in increases in erosion and accretion, changes in the sediment composition and changes to the coastal morphology in some locations. At this stage of the study, the MT model is not considered to be sufficiently developed to reliably predict changes to erosion and accretion rates or sediment transport pathways and rates. However, the predicted impacts to hydrodynamics and waves can be used to qualitatively assess potential impacts to sediment transport and coastal processes. The small and localised predicted changes to the hydrodynamics resulting from the deepening due to the sourcing of 70 million m^3 of sand is not expected to noticeably change the sediment dynamics and sediment transport rates in CG, with the changes potentially resulting in a small increase in sedimentation in the proposed operational area (due to the reduction in current speeds in this area). As predicted changes to wave conditions were limited to within CG and only during large wet season wave events, with H_s increases of less than 0.01 m (0.5 to 1% of the H_s), the changes in waves are not expected to directly impact sediment transport rates (of sand and fine-grained silt and clay) or coastal processes (i.e. no changes to beaches or mangroves) either within or offshore of CG.

  The sand sourcing will reduce the amount of sand present in the proposed operational area, which in turn could limit the supply of sand to other areas. Results from the MT modelling suggest that there is a regular net supply of sand to the proposed operational area from upstream in CG, while there is regular transport due to tidal currents between the area and King Shoals (in both directions) but with limited net transport occurring indicating that the area is a natural sand accumulation area. Based on vibro-coring it has been estimated by BKA that between 150 and 300 million m^3 of sand is present within the top 5 m of the seabed in the proposed operational area, meaning that the sand sourcing represents between 23 and 47% of the sand present in the top 5 m of the seabed. This shows that following the sand sourcing, there will still be a large volume of sand present in this area, with ongoing transport from both upstream and King Shoals expected to occur throughout the 15 years of sand sourcing, meaning that any changes to sand supply are likely to be minor.

  It is also important to note that the Ord River Dam has been shown to have reduced the supply of sediment into CG and so it is important that any potential cumulative impacts to sediment transport due to the sand sourcing are considered in combination with the changes due to the Ord River Dam.

All of these potential coastal processes implications from the sand sourcing will be assessed in more detail as part of the future stages of the study. This will allow a quantitative assessment of the implications to be made and will help to show the extent, magnitude and duration of any changes which in turn will help to understand the relative effects of the changes on the coastal morphology and ecology.

5.3. Ecological Implications

This section briefly summarizes potential ecological implications of proposed sand sourcing in terms of metocean and sediment issues. It does not consider other potential ecological implications such as underwater noise from the SPV, potential interactions between the SPV and marine mega-fauna etc. These are assessed in detail in other reports that have been developed in support of the overall EIA.

The main ecological implications of the proposed operation in terms of metocean and sediment issues are:

- Direct physical impacts on benthic communities in the proposed operational area from the sand-uptake drag head during loading of sand. This is assessed as not being a concern for this project, as surveys indicate that there are no significant benthic communities and species in the proposed operational area. Further benthic surveys will be undertaken in the wet season Feb-March 2024.

- Dispersal of turbidity / sediment plumes from the sand loading operation onto adjacent sensitive benthic communities. This is assessed as not being a concern for this project, for the reasons outlined under Section 4.8.3, including an apparent lack of sensitive benthic communities in the area. However, this will be assessed in detail through further modelling, as outlined in Section 4.8.3.

- Potential changes to hydrodynamics, waves, sediment dynamics and coastal processes from the removal of sand, with potential indirect impacts on coastal morphology and thus on coastal habitats, communities and species, including the fringing mangroves, the Ord River Floodplain Ramsar Site and the four turtle nesting beaches in the CG region. Given that, as outlined above, it is proposed to remove an average of less than 1 m of sand over the area of the proposed operational area (103 km^2) over 15 years and based on the preliminary impact assessment modelling presented in this report, along with the context of broader influencing factors in CG, the potential for such indirect impacts on coastal morphology and ecology is considered low. However, this will be assessed in detail through further modelling, as outlined in Sections 4.8.1 and 4.8.2.

5.4. Conceptual Model

A conceptual model that shows the effects of human activity on sediment transport, morphology and biological activity in the CG is detailed in Figure 125. The conceptual model is based on the causal/diagnosis decision information system framework adopted by Jones et al. (2016) to assess potential impacts to coral from sediment released by dredging in WA (the work was undertaken through the WAMSI Dredging Science Node). The model details the cause-effect linkages for historic human activity as well as proposed future human activity as part of the CG Marine Sand Proposal.

The model shows how the historic Ord River catchment clearing is likely to have resulted in an increase in catchment sediment to the CG, while the Ord River Dam will have resulted in a reduction in supply of catchment sediment to CG. The reduction in catchment sediment supply to the CG due to the Ord River Dam will have been significantly larger than the increase in supply due to the catchment clearing.

The model identifies two potential cause-effect pathways resulting from CG sand sourcing. The first is the suspension of sediment into the water column by the sand sourcing activity and the second is a reduction in availability of sand on the seabed. The suspension of sediment into the column could result in a reduction in the light quality and quantity as well as sediment covering due to the deposition of the suspended sediment. However, due to the naturally high SSC in CG along with the limited benthic flora and fauna present in CG, the suspension of sediment into the water column due to the sand sourcing activity is considered unlikely to result in any effects.

The reduction in the availability of sand on the seabed has the potential to reduce the supply of sand to other areas, with potential effects including changes in morphology and habitat areas and composition, changes in sediment composition and increases in erosion. This cause-effect pathway

therefore has the potential to result in a reduction in the mangrove area within CG along with a reduction in the number of suitable beaches for turtle nesting.

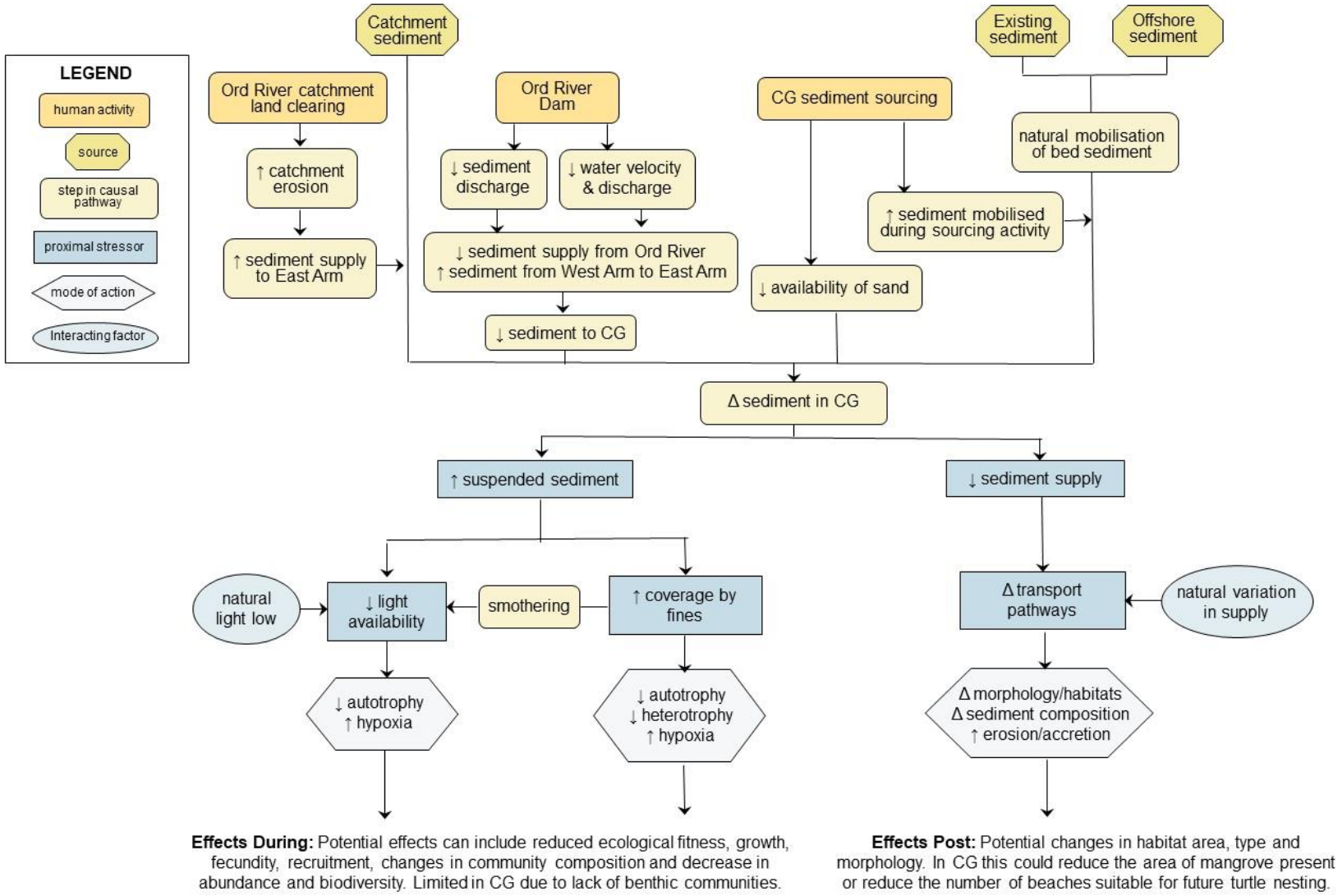

Figure 125. A conceptual model of the effects of possible effects of human changes in the CG based on the causal/diagnosis decision information framework adopted by Jones et al. (2016).

6. ASSESSMENT AGAINST STUDY OBJECTIVES & EPA GUIDELINES

This section provides a summary as to how the metocean and sediment dynamics study undertaken to date as well as the proposed future work for the CG Marine Sand Proposal will meet both the project objectives (detailed in Section 1) as well as the approval requirements.

After the preparation of this technical report data from the 2024 wet season data collection campaign were available. Analysis of these data has been undertaken to provide additional understanding for the project, the analysis is detailed in a supplementary technical note which is included as Appendix A.

Details of how the project objectives have and will be met are detailed in Table 12, while Table 13 provides details of how the WA EPA guidelines have and will be met. These tables are based on the data and information included in this report and in the supplementary technical note (Appendix A).

Table 12. Summary of how the Metocean and Sediment Dynamics work will meet the Consultancy Objectives (from consultancy RFP).

Consultancy Objective	Summary Findings / Conclusions at time of this report (based on best assessment of all existing available data)	Relevant sections of this report	Supporting Data Sources (references)	Assumptions, Qualifications, Limitations & Gaps	Data & Analysis Needs & Recommendations to Address the Objective Fully
Objective 1: Hydrodynamics and Waves:					
a) Define the existing hydrodynamic conditions in the subject areas, under the seasonal range of natural conditions, including any changes since European colonisation.	The existing hydrodynamic and wave conditions during both wet and dry season conditions have been presented in this report and in the supplementary technical note. The results have shown that CG is a tidally dominant environment, with limited influence of waves due to its relatively sheltered nature. The main changes since European colonisation are the Ord River catchment clearing (for cattle grazing and crops) and the construction of the Kununurra Diversion and Ord River Dams in 1969 and 1972, respectively. The catchment clearing may have resulted in an increase in river water discharge and catchment sediment to the CG, while the dams (mainly the Ord River Dam) have resulted in a reduction in river water discharge and catchment sediment to CG. The reduction in discharge and catchment sediment supply to the CG due to the Ord River Dam has been shown by previous investigations to have been the key change in the catchments resulting in impacts in the CG region. The Ord River Dam has reduced the wet season high discharge events in East Arm and increased the river discharge during dry season low discharge conditions. These changes to the river discharge have resulted in changes to the hydrodynamics in East Arm which in turn has changed the sediment dynamics in the area (this is discussed further in under item 2a). The change in hydrodynamics in the CG due to the Ord River Dam is unknown, but changes are likely to have been small due to the strong tidal influence (future modelling will test this hypothesis).	Sections 3.1, 3.2, 3.10, 4.4.3, 4.5.3 and Appendix A	AHO (2023) AIMS (2007) AIMS (2023) BKA (2024d) CSIRO (2023) Wolanski et al. (2001) Wolanski et al. (2004) Robson et al. (2008) Robson et al. (2013)	The wave model has not been validated to measured data in CG and so some uncertainty exists in modelled wave conditions. The hydrodynamic model has only been calibrated during dry season conditions and so there is some uncertainty as to how the modelled conditions vary between the two seasons. The influence of changes since European colonisation on hydrodynamics and waves in CG is unknown. The river discharge from the Ord River during a wet season rainfall event will need to be assumed based on information from the literature to allow modelling of pre European colonisation conditions to be undertaken.	Measured wave data to be collected by BKA in CG during both dry and wet season to better understand waves in CG and to allow the SW model to be calibrated and validated within CG. Measured hydrodynamic data collected by BKA in CG during the wet season will be used to allow the HD model to be calibrated for wet season conditions. The numerical models will be setup to simulate pre European colonisation conditions in CG to better understand the impacts that the dams and land clearing had.

Consultancy Objective	Summary Findings / Conclusions at time of this report (based on best assessment of all existing available data)	Relevant sections of this report	Supporting Data Sources (references)	Assumptions, Qualifications, Limitations & Gaps	Data & Analysis Needs & Recommendations to Address the Objective Fully
b) Predict potential impacts of the proposed project on the hydrodynamics of the subject areas, including during the operation, at the end of the operation (approximately 15 years) and in 100 years time.	Initial modelling of the impacts to hydrodynamics and waves of sourcing 70 million m^3 of sand from the proposed operational area (i.e. at the end of operation) is provided in this report. The modelling predicted small and highly localised changes to both hydrodynamics and waves, with the majority of the changes predicted within and adjacent to the proposed operational area. The magnitude and scale of the predicted impacts are unlikely to cause broader impacts, although further modelling will be undertaken to verify this following additional calibration and validation of the models.	Sections 4.4.4, 4.5.4 and 5.2.	HD and SW models along with the data used to develop and calibrate/validate the models (see Section 4 for further details).	The HD and SW models have only been subject to preliminary calibration and will be further developed using the additional data presented in the supplementary technical note, which could change predicted impacts slightly (changes are expected to still be small). Modelling of impacts during operation and in 100 years time has not been undertaken yet. These scenarios will be undertaken once the models are fully calibrated and validated.	Measured wave and hydrodynamic data presented in the supplementary technical note will be used to allow full calibration of the HD and SW models.
c) This should include prediction of likely 'worst-case' and 'best-case' impacts and also potential 'cumulative' impacts of the proposed project on hydrodynamics (with 'worst-case' and 'best-case' being consistent with meanings in relevant WA EPA guidance as listed in section 4 (of RFP), and 'cumulative' meaning in addition to those that may have been caused by previous developments in the area, such as the Ord River dam).	This report provides predicted HD impacts for a single sand sourcing scenario and single metocean condition (dry season) as well as predicted SW impacts for a single sand sourcing scenario over a 5 year period. As a result, insufficient modelling has been undertaken to date to allow prediction of likely 'best-case' and 'worst-case' impacts and for 'cumulative' impacts. The HD and SW models will be setup to simulate multiple different metocean conditions and based on the range of impacts predicted the 'best-case' and 'worst-case' impacts will be derived. Results from the simulations at the end of the 15 years of sand sourcing will be compared with the results from a pre-European colonisation conditions simulation to show the 'cumulative' impacts of the Ord River Dam, catchment clearing and the sand sourcing.	Section 4.8.1	HD and SW models along with the data used to develop and calibrate/validate the models (see Section 4 for further details).	Insufficient modelling has been undertaken to date to allow likely 'best-case' and 'worst-case' impacts and 'cumulative' impacts to be defined.	Measured wave and hydrodynamic data presented in the supplementary technical note will be used to allow full calibration of the HD and SW models prior to all the simulations being undertaken to derive the range of impacts.
d) Provide hydrodynamics data analysis and modelling to support the other objectives below.	Results from this objective has been used to help inform the conceptual understanding, coastal processes implications and conceptual model. In addition, the HD and SW models have been used as inputs to the sediment transport and beach processes modelling which	Sections 4.6, 4.7, 4.8 and 5	AHO (2023) AIMS (2007) AIMS (2023) BKA (2024d) CSIRO (2023) HD and SW models	The HD and SW models have only been subject to preliminary calibration and will be further developed using the additional data detailed in the	Measured wave and hydrodynamic data presented in the supplementary technical note will be used to allow full calibration of the HD and SW models. Once this has been

Consultancy Objective	Summary Findings / Conclusions at time of this report (based on best assessment of all existing available data)	Relevant sections of this report	Supporting Data Sources (references)	Assumptions, Qualifications, Limitations & Gaps	Data & Analysis Needs & Recommendations to Address the Objective Fully
	is presented in this report. The results from this component of the study will continue to be used to support the other objectives as the hydrodynamics and waves are intrinsic to the other processes. The HD and SW models will also continue to be used drive the other models (sediment transport, beach processes and dredge plume dispersion) required for this study.		along with the data used to develop and calibrate/validate the models (see Section 4 for further details).	supplementary technical note.	undertaken, the models will be suitable for supporting other objectives.
Objective 2: Sediment transport and coastal processes:					
a) Define existing sediment transport and coastal processes in the subject areas, including natural sediment sources and pathways, sediment sizes on the seabed and in transport under the seasonal range of natural conditions, and any changes since European colonization.	The existing sediment transport and coastal processes have been detailed in this report based on literature, existing data and preliminary modelling results. It has been shown that there is significant variability in the sediment transport which occurs in the region, with the tide being the dominant process which influences sediment transport in CG. Extensive sediment sampling has been undertaken as part of the Project, this has shown that there is an abundance of sediment available within CG, with a combination of sand, silt and clay all present in the region. Based on data collected the sediment transport rates are higher during the wet season. Sediment transported in suspension in CG has been shown to be predominantly silt and clay sized sediment meaning that sand transport is likely to occur predominantly through bedload transport. Historic shoreline changes have been determined based on satellite imagery for beaches in the region where turtle nesting has been observed. Beaches offshore of CG were shown to have advanced over the last 30 years, while the turtle nesting beach on Lacrosse Island was shown to have been stable. The beach at East Bank Point inside CG has migrated landward over the last 30 years, this is a common response to stranded beach ridges due to the limited supply of sand from the adjacent mudflats (that they are perched on). Data collected by previous studies in the area	Sections 3.6, 3.7, 3.9, 4.6.3, 4.7.2, 5.1 and supplementary technical note	Wolanski et al. (2004) AIMS (2007) BKA (2024d) Copernicus (2023) MT and Beach Processes models along with the data used to develop and calibrate the models (see Section 4 for further details).	The numerical modelling used to inform the findings at this time are based on models which have not been fully calibrated and validated. Therefore results should be considered to be preliminary. Numerical modelling of the potential changes since European colonisation has not been undertaken at this time and so the results are based on just literature and existing data. Data from the BKA wet season field campaign have not been utilised in the modelling at this stage. Results from the updated modelling will provide additional data to inform the existing sediment transport and coastal processes and how they vary due to seasonal variability.	Measured hydrodynamic, wave, turbidity, sediment PSD and compositional data to be collected by BKA in CG during the wet season (and detailed in the supplementary technical note) will be used to further calibrate and validate the models and to inform the sediment transport and coastal processes understanding. The numerical models will be setup to simulate pre European colonisation conditions in CG to better understand the impacts that the dams and land clearing had.

Consultancy Objective	Summary Findings / Conclusions at time of this report (based on best assessment of all existing available data)	Relevant sections of this report	Supporting Data Sources (references)	Assumptions, Qualifications, Limitations & Gaps	Data & Analysis Needs & Recommendations to Address the Objective Fully
	have shown that the sediment transport patterns have changed since European colonisation, this is predominantly a result of construction of the Ord River Dam in 1971. The Dam was shown to have significantly reduced the sediment supply (both sand and fine-grained silt and clay) to CG from the Ord River. In addition, the Dam also changed the hydrodynamics in the Ord River/East Arm and as a result it is now acting as a net importer of fine-grained sediment, with much of the sediment from West Arm transported into East Arm rather than into the CG. The fact that the beaches offshore of CG have advanced over the last 30 years indicates that any changes to the sediment transport processes in CG that may have been caused by the Ord River Dam have not significantly reduced the supply of sand to these beaches. This finding agrees with results from recent elemental feature analyses detailed in the supplementary technical note which showed that the majority of the sediment at King Shoal was not from the same source as the sediment in CG.				
b) Predict potential impacts of the proposed project on sediment transport and coastal processes of the subject areas, including during the operation, at the end of the operation (15 years) and in 100 years, with particular focus on:	Based on the initial modelling of the impacts to hydrodynamics and waves of sourcing 70 million m^3 of sand from the proposed operational area (i.e. at the end of operation) a qualitative assessment of potential impacts to sediment transport and coastal processes is provided in this report. Based on this it has been noted that the sand sourcing is not expected to noticeably change the sediment dynamics and sediment transport rates in CG.	Section 4.7.2 and 5.2	BKA (2024d) HD and SW models along with the data used to develop and calibrate the models (see Section 4 for further details).	The numerical modelling used to inform the findings at this time are based on models which have not been fully calibrated and validated, therefore results should be considered to be preliminary. No sediment transport or beach processes modelling of potential impacts has been undertaken at this stage as insufficient data were available to inform the model at the time the report was prepared. The impacts predicted to the HD and SW models are based on results for at the end of operation.	Measured hydrodynamic, wave, turbidity, sediment PSD and compositional data and bathymetric data to be collected by BKA in CG during the wet season will be used to further calibrate and validate the models. Further, more detailed modelling will be undertaken to quantify impacts on sediment transport and coastal processes as well as impacts during sand sourcing and in 100 years. .
	A small increase in sedimentation in the	Section 5.2 and	BKA (2024d)	As response to Objective	As response to Objective 2b)

Consultancy Objective	Summary Findings / Conclusions at time of this report (based on best assessment of all existing available data)	Relevant sections of this report	Supporting Data Sources (references)	Assumptions, Qualifications, Limitations & Gaps	Data & Analysis Needs & Recommendations to Address the Objective Fully
• predicting potential for natural replenishment of sand in dredged areas of the tenements, including likely timeframes for replenishment,	proposed operational area is predicted due to the localised small magnitude reduction in current speeds in this area. This indicates that natural replenishment of sand will occur within the area. Measured data have shown that sand is imported into the proposed operational area through sandwave migration from upstream in CG (main supply) and from offshore (minor supply). Insufficient work has been undertaken at this stage to allow a timeframe for replenishment to be estimated.	supplementary technical note	HD and SW models along with the data used to develop and calibrate the models (see Section 4 for further details).	2b)	
• predicting potential for coastal erosion and accretion,	The changes to the waves are not expected to directly impact coastal processes either within or offshore of CG. In addition, following the sand sourcing there will still be a large volume of sand present in the proposed operational area, while ongoing transport of sand into the area from both upstream and offshore will continue to occur over the duration of the sand sourcing activity (15 years). Elemental feature analysis has shown that the sand located in King Shoals is predominantly from a source other than CG. Therefore, any changes to sand supply from the area either to offshore or within CG are likely to be minor and so the sand sourcing is not predicted to result in increased coastal erosion or accretion.	Sections 4.7.2, 5.2 and supplementary technical note	BKA (2024d) SW and Beach Processes models along with the data used to develop and validate the models (see Section 4 for further details).	As response to Objective 2b)	As response to Objective 2b)
• predicting potential impacts on turtle nesting beaches both inside and immediately outside Cambridge Gulf (Figure 3), including potential changes in sand grain size and beach geomorphology; and	Due to the localised changes to waves and hydrodynamics, along with a potential minor change to sediment supply, no potential impacts on turtle nesting beaches inside or immediately outside the CG are predicted.	Sections 4.7.2 and 5.2	BKA (2024d) HD, SW and Beach Processes models along with the data used to develop and calibrate/validate the models (see Section 4 for further details).	As response to Objective 2b)	As response to Objective 2b)
• predicting potential impacts on mangroves and other coastal and intertidal communities and impacts on the Ord River Floodplain Ramsar site as a result of the sand extraction (Figure 3).	Due to the localised changes to waves and hydrodynamics, along with a potential minor change to sand supply, no potential impacts on mangroves and other coastal and intertidal communities or the Ord River Floodplain Ramsar site are expected. The sand sourcing is expected to only result in very small and localised changes to the transport and fate of fine-grained silt and clay (future modelling will test this hypothesis). As a result, the sand sourcing is not expected to	Section 5.2	BKA (2024d) HD, SW and MT models along with the data used to develop and calibrate/validate the models (see Section 4 for further details).	As response to Objective 2b)	As response to Objective 2b).

Consultancy Objective	Summary Findings / Conclusions at time of this report (based on best assessment of all existing available data)	Relevant sections of this report	Supporting Data Sources (references)	Assumptions, Qualifications, Limitations & Gaps	Data & Analysis Needs & Recommendations to Address the Objective Fully
	result in impacts to environments which are dependent on a supply of fine-grained sediment.				
c) This should include prediction of likely 'worst-case' and 'best-case' impacts and also 'cumulative' impacts of the proposed project on sediment transport and coastal processes (with 'worst-case' and 'best-case' being consistent with meanings in relevant WA EPA guidance as listed in section 4, and 'cumulative' meaning in addition to those that may have been caused by previous developments in the area, such as the Ord River dam).	This report provides predicted HD impacts for a single sand sourcing scenario and single metocean condition (dry season) as well as predicted SW impacts for a single sand sourcing scenario over a 5 year period. Based on this a qualitative assessment of impacts to sediment transport and coastal processes has been undertaken. Therefore, insufficient modelling has been undertaken to date to allow either quantitative changes to the sediment transport and coastal processes or to provide likely 'best-case' and 'worst-case' impacts and for 'cumulative' impacts. The models will be setup to simulate multiple different metocean conditions and based on the range of impacts predicted, the 'best-case' and 'worst-case' impacts on sediment transport and coastal processes will be derived. Results from the simulations at the end of the 15 years of sand sourcing will be compared with the results from a pre-European colonisation conditions simulation to show the 'cumulative' impacts of the Ord River Dam, catchment clearing and the sand sourcing.	Section 4.8.2	BKA (2024d) HD and SW models along with the data used to develop and calibrate/validate the models (see Section 4 for further details).	Insufficient modelling has been undertaken to date to allow likely 'best-case' and 'worst-case' impacts and 'cumulative' impacts to be defined.	Measured hydrodynamic, wave, turbidity, sediment PSD and compositional data and bathymetric data collected by BKA and detailed in the supplementary technical note will be used to further develop, calibrate and validate the models. Following the final development and calibration/validation of the HD, SW, MT and Beach Processes models the full suite of proposed simulations will be undertaken and these will be used to derive the range of impacts.
Objective 3: Suspended sediment and turbid plume dispersal & potential impacts on benthic habitats & communities (see note below):					
a) Define the existing suspended sediment and turbidity regime in the subject areas, under the seasonal range of natural conditions.	Measured data and preliminary numerical modelling results have been presented in this report and in the supplementary technical note to understand the existing suspended sediment and turbidity regime. There is significant spatial and temporal variability in the SSC within CG (SSC varying from 5 to 200 mg/L during dry season and from 5 to 800 mg/L around the proposed operation area (double this at the confluence between West Arm and CG) during the wet season), with SSC increasing from the entrances in an upstream direction to West and East Arms where very high SSC can occur (peak of 1,600 mg/L recorded during 2024 wet season but	Sections 3.7, 4.6.3 and supplementary technical note	AIMS (2007) BKA (2024d) Copernicus (2023) MT model along with the data used to develop and calibrate the model (see Section 4 for further details).	The numerical modelling used to inform the findings at this time are based on models which have not been fully calibrated and validated, therefore results should be considered to be preliminary.	Measured hydrodynamic, wave, turbidity, sediment PSD and compositional data and bathymetric data collected by BKA during the wet season and detailed in the supplementary technical note will be used to further calibrate and validate the models.

Consultancy Objective	Summary Findings / Conclusions at time of this report (based on best assessment of all existing available data)	Relevant sections of this report	Supporting Data Sources (references)	Assumptions, Qualifications, Limitations & Gaps	Data & Analysis Needs & Recommendations to Address the Objective Fully
	previous data showed it can be up to 5,000 mg/L). Data indicate that there is seasonal variability in SSC, with higher values in the wet season compared to the dry season. Numerical modelling rand water quality sampling have shown that the majority of the sediment in suspension in CG is fine-grained silt and clay, with limited sand sized sediment present in suspension.				
b) Predict potential dispersal of sediment and turbidity plumes from the proposed operation, under the seasonal range of natural conditions, in particular towards King Shoals, which are within a State Marine Park Sanctuary Zone and therefore considered to be a high priority sensitive receptor environment (Figure 3) (see '**Important Note'** on Objective 3 in the RFP).	This report does not provide any predictions of plumes from the proposed sand sourcing operation. This is because further development of the HD, SW and MT models is required before this modelling can be undertaken. The proposed approach for the modelling is provided in this report.	Section 4.8.3	N/A	The HD, SW and MT models need further development to fully calibrate and validate the models prior to the model being used to predict plume dispersion from the sand sourcing activity.	Measured hydrodynamic, wave, turbidity, sediment PSD and compositional data and bathymetric data collected by BKA during the wet season and detailed in the supplementary technical note will be used to further calibrate and validate the models.

Table 13. Summary of how the Metocean and Sediment Dynamics work will meet the WA EPA Guidelines.

Guideline	Findings / Conclusions at time of this report (based on best assessment of all existing available data)	Relevant section of this report	Supporting Data Sources (references)	Assumptions, Qualifications, Limitations & Gaps	Data & Analysis Needs & Recommendations to Address the Guideline Fully
WA EPA 2021 *Technical Guidance for EIA of Marine Dredging Proposals*: • These mainly relate to impacts of sediment and turbidity plumes on benthic communities, which is not a major issue for this project (due to naturally high turbidities and lack of benthic communities). • However, Objective 3) of the RFP requires this issue to be addressed to a certain extent, and compliance with this Guideline can be addressed when addressing Objective 3).	This report does not provide any predictions of plumes from the proposed sand sourcing operation. This is because further development of the HD, SW and MT models is required before this modelling can be undertaken. Although field investigations have shown that no subtidal benthic communities have been identified within the CG, plume dispersion modelling will be undertaken to show the extent, magnitude and duration of any plumes resulting from the sand sourcing. Our proposed modelling approach will follow the relevant guidance and recommendations provided by Sun et al. (2020) as well as the other Western Australian Marine Science Institution (WAMSI) Dredging Science Node (DSN) guidelines (e.g. Lowe & Ghisalberti, 2016; Mills & Kemps, 2016; Sun et al., 2016; Fearns et al., 2017; Kemps & Masini, 2017; Fearns et al., 2018). For further details on the proposed modelling approach see response to Objective 3 in Table 12.	Section 4.8.3	BKA (2024d)	The HD, SW and MT models need further development to fully calibrate and validate the models prior to the model being used to predict plume dispersion from the sand sourcing activity.	Measured hydrodynamic, wave, turbidity, sediment PSD and compositional data and bathymetric data collected by BKA during the wet season and presented in the supplementary technical note will be used to further develop, calibrate and validate the models.
WA EPA 2016 *Environmental Factor Guideline - Coastal Processes*: • This is the highest priority issue for this project and so all relevant elements of this Guideline need to be addressed thoroughly. • States **objective** is "To maintain the geophysical processes that shape coastal morphology so that the environmental values of the coast are protected".	The literature review, data review and analysis along with components of the numerical modelling detailed in this report and proposed as part of future work is aimed at assessing potential impacts to the geophysical processes which influence coastal morphology. This is further detailed in the following responses.	Sections 3, 4.4.3, 4.5.3, 4.6.3, 4.7.2, 4.8 and supplementary technical note	AHO (2023) AIMS (2007) AIMS (2023) BKA (2024d) Copernicus (2023) CSIRO (2023) HD, SW, MT and Beach Processes models along with the data used to develop and calibrate/validate the models (see Section 4 for further details).	This report only provides preliminary results from the numerical models, with impact modelling only included for the HD and SW models. The beach processes modelling is based on topographic data from the DEA 25 m Intertidal Elevation Model and the sediment properties have had to be assumed due to a lack of data.	Measured hydrodynamic, wave, turbidity, sediment PSD and compositional data and bathymetric data collected by BKA and presented in the supplementary technical note will be used to further calibrate and validate the models. Data from the LiDAR surveys presented in the supplementary technical note will be used to provide high resolution topographic elevation data for the turtle nesting beaches and used in the updated modelling.
• States that **considerations for the EIA** should include (only those directly related to PCS work are listed):	No response required.				

Guideline	Findings / Conclusions at time of this report (based on best assessment of all existing available data)	Relevant section of this report	Supporting Data Sources (references)	Assumptions, Qualifications, Limitations & Gaps	Data & Analysis Needs & Recommendations to Address the Guideline Fully
• the predicted changes to coastal processes based on modelling and analyses to a standard consistent with recognised published guidance,	This report has presented results from preliminary HD and SW modelling of potential impacts of the sand sourcing to hydrodynamics and waves, which are the dominant coastal processes in the region. See response to Objective 1a) in Table 12 for further details of the impacts. Further model development is required based on data presented in the supplementary technical note before the impact modelling for the sediment transport model is undertaken. Therefore, this will be undertaken during the subsequent stage of the study. To ensure that the modelling and analyses are consistent with recognised guidance the model calibration undertaken to date has been in accordance with recognized international standards (e.g. Williams and Esteves, 2017). All future modelling will be undertaken in accordance with relevant published guidelines (e.g. WAMSI DSN guidelines noted above and the GBRMPA modelling guidelines (GBRMPA, 2012)) and future model calibration and validation will be undertaken in accordance to recognised international standards (e.g. Williams and Esteves, 2017; Pye et al., 2017; Los and Blaas, 2010).	Sections 4.4.2, 4.4.4, 4.5.4, 5.2 and supplementary technical note	BKA (2024d) HD, SW, MT and Beach Processes models along with the data used to develop and calibrate/validate the models (see Section 4 for further details).	This report only provides preliminary results from the numerical models, with impact modelling only included for the HD and SW models.	Measured hydrodynamic, wave, turbidity, sediment PSD and compositional data and bathymetric data collected by BKA and presented in the supplementary technical note will be used to further develop, calibrate and validate the models.
• the significance of the likely change to coastal processes as well as the environmental values affected by those changes,	An initial qualitative assessment of the potential implications of changes to hydrodynamics and waves on the supply and transport of sediment in the region is presented in this report. The changes are likely to be small compared to the natural variability of the coastal processes and they are considered unlikely to result in changes to environmental values. Insufficient data were available during this stage of the project to allow detailed numerical modelling of the sediment transport, this will be undertaken as part of future work for the study.	Section 5.2	BKA (2024d) HD, SW, MT and Beach Processes models along with the data used to develop and calibrate/validate the models (see Section 4 for further details).	This finding is only qualitative and is informed based on predicted impacts to hydrodynamics and waves along with the coastal processes understanding developed as part of the study.	Measured hydrodynamic, wave, turbidity, sediment PSD and compositional data and bathymetric data collected by BKA and presented in the supplementary technical note will be used to further develop, calibrate and validate the models.
• impacts to coastal processes in the context of the latest climate change science and projections; and	The potential impacts to coastal processes have not yet been considered in the context of the latest climate change science, but this will be undertaken during subsequent numerical modelling to be undertaken as part of the study.	Section 4.8	N/A	The HD, SW, MT and Beach Processes models need further development to fully develop, calibrate and validate the models prior to them being used to predict quantitative	Measured hydrodynamic, wave, turbidity, sediment PSD and compositional data and bathymetric data collected by BKA during the wet season and presented in the supplementary technical note will be used to

Guideline	Findings / Conclusions at time of this report (based on best assessment of all existing available data)	Relevant section of this report	Supporting Data Sources (references)	Assumptions, Qualifications, Limitations & Gaps	Data & Analysis Needs & Recommendations to Address the Guideline Fully
				impacts.	further develop, calibrate and validate the models. Following this, the models will be setup to include climate change in some simulations.
• the likely change to coastal processes and consequent risks to coastal morphology and associated environmental values.	An initial qualitative assessment of the potential implications of changes to hydrodynamics and waves on the supply and transport of sediment in the region is presented in this report. The changes are likely to be small, with no predicted changes to environmental values. Insufficient data were available during this stage of the project to allow detailed numerical modelling of the sediment transport, this will be undertaken as part of future work for the study. The consequential risks to coastal morphology and environmental values will be assessed using a conceptual model of CG once the quantitative sediment transport changes have been modelled.	Sections 5.2, 5.3 and 5.4	BKA (2024d) HD, SW, MT and Beach Processes models along with the data used to develop and calibrate/validate the models (see Section 4 for further details).	This finding is only qualitative informed based on predicted impacts to hydrodynamics and waves along with the coastal processes understanding developed as part of the study.	Measured hydrodynamic, wave, turbidity, sediment PSD and compositional data and bathymetric data collected by BKA and presented in the supplementary technical note will be used to further calibrate and validate the models.
• States that **Information required for EIA** include (only those directly related to PCS work are listed):	No response required.				
• Characterise the coastal type and current coastal processes, including modelling of the local current and wave climate;	A combination of literature, existing data and numerical modelling results have been used to inform the existing coastal processes. CG has been shown to be tidally dominated, while sediment supply and transport at the beaches offshore of CG is controlled by the wave conditions. Results from the hydrodynamic and wave models have been used to show the existing conditions in the region. For further details see response to Objective 1a) in Table 12.	Sections 3, 4.4.3, 4.5.3, 4.6.3, 4.7.2, 5.1 and supplementary technical note	AHO (2023) AIMS (2007) AIMS (2023) BKA (2024d) CSIRO (2023) HD, SW, MT and Beach Processes models along with the data used to develop and calibrate/validate the models (see Section 4 for further details).	This report only provides preliminary results from the HD and SW numerical models. The HD model has only been calibrated at one location in CG. The SW model has not been calibrated to any measured data in CG.	Measured hydrodynamic and wave data collected by BKA and presented in the supplementary technical note will be used to further develop, calibrate and validate the models. Following this, results from the models will be updated.
• Analysis of long-shore sediment movement and erosion and deposition patterns; beach profiling, and determination of tidal flow and exchange.	The shoreline position at the turtle nesting beaches (i.e. erosion and deposition) over the last 30 years has been shown to vary from accreting at the beaches offshore of CG to migrating landward at the beach within CG. Longshore and cross-shore sediment transport rates have been modelled at the turtle nesting	Sections 3.9, 4.4.3 and 4.7.2	BKA (2024d) CSIRO (2023) HD, SW and Beach Processes models along with the data used to develop and calibrate/validate the models (see Section 4	The SW model which drives the longshore and cross-shore modelling has not been calibrated to any measured data in CG or directly offshore of CG. The beach processes	Data from the LiDAR surveys presented in the supplementary technical note will be used to provide high resolution topographic elevation data for the turtle nesting beaches. Measured hydrodynamic and

Guideline	Findings / Conclusions at time of this report (based on best assessment of all existing available data)	Relevant section of this report	Supporting Data Sources (references)	Assumptions, Qualifications, Limitations & Gaps	Data & Analysis Needs & Recommendations to Address the Guideline Fully
	beaches in the region which are influenced by these processes, with the results showing that sand is moved onshore to the beaches through cross-shore transport. Numerical modelling results have shown that the tidal flow around CG is highly variable both spatially and temporally while the exchange through the western entrance is approximately three times larger than the exchange through the easterly entrance.		for further details).	modelling is based on topographic data from the DEA 25 m Intertidal Elevation Model and the sediment properties have had to be assumed due to a lack of data.	wave data collected by BKA and presented in the supplementary technical note will be used to further develop, calibrate and validate the models. Once the SW model has been calibrated and validated to wave data from the CG region and the Beach Processes model updated based on data collected by BKA during the 2024 wet season field campaign, the longshore and cross-shore sediment transport modelling will be rerun.
• Predict the changes to coastal processes as a result of the proposal, taking into account the appropriate spatial and temporal scales.	A qualitative assessment of the impacts of the sand sourcing to sediment transport and the supply of sand for the region has indicated that the sand sourcing is not expected to noticeably change sediment transport or the supply of sand in CG. Further, more detailed, sediment transport and beach processes modelling will be undertaken to quantify predicted changes to coastal processes.	Sections 4.4.4, 4.5.4 and 5.2	BKA (2024d) HD, SW, MT and Beach Processes models along with the data used to develop and calibrate/validate the models (see Section 4 for further details).	At this stage the MT model is not sufficiently developed for it to be used to assess impacts to sediment transport and sediment supply and therefore inform changes to coastal processes.	Measured hydrodynamic, wave, turbidity, sediment PSD and compositional data and bathymetric data collected by BKA and presented in the supplementary technical note will be used to further develop, calibrate and validate the models. Following this the MT model will be used to quantify changes to sediment transport and any impacts to the supply of sand from the proposed operational area.
• Describe the impacts resulting from the changes to coastal processes.	The predicted impacts of the sand sourcing to hydrodynamics and waves are described in this report, while predicted impacts to sediment transport and sediment supply is discussed qualitatively. Overall, a small phase change of 27 seconds (earlier) is predicted to occur to the tidal propagation, a low magnitude reduction in current speed is predicted within the proposed operational area and small changes to wave heights are only predicted to occur during large wave events. Overall, the results show that the sand sourcing is not expected to influence the broader conditions in CG. Further, more detailed, sediment transport and beach processes modelling will be undertaken to quantify any predicted impacts to coastal processes.	Sections 4.4.4, 4.5.4 and 5.2	BKA (2024d) HD, SW, MT and Beach Processes models along with the data used to develop and calibrate/validate the models (see Section 4 for further details).	At this stage the MT model is not sufficiently developed for it to be used to assess impacts to sediment transport and sediment supply and therefore inform changes to coastal processes.	Measured hydrodynamic, wave, turbidity, sediment PSD and compositional data and bathymetric data collected by BKA and presented in the supplementary technical note will be used to further calibrate and validate the models. Following this the MT model will be used to quantify changes to sediment transport and any impacts to the supply of sand from the proposed operational area.

Guideline	Findings / Conclusions at time of this report (based on best assessment of all existing available data)	Relevant section of this report	Supporting Data Sources (references)	Assumptions, Qualifications, Limitations & Gaps	Data & Analysis Needs & Recommendations to Address the Guideline Fully
• Consider cumulative impacts from and to other existing and approved developments in order to determine whether the proposal, in combination with other developments, will significantly impact coastal processes and any consequential impacts to environmental values in the coastal zone.	The predicted impacts of the sand sourcing to hydrodynamics and waves are described in this report, while predicted impacts to sediment transport and sediment supply is discussed qualitatively. The numerical models are not sufficiently well developed to undertake cumulative impacts at this stage. Future modelling will be undertaken once the models are further developed and have been subject to additional calibration and validation. Results from the simulations at the end of the 15 years of sand sourcing will be compared with the results from the pre-European colonisation conditions simulation to show the 'cumulative' impacts of the Ord River Dam, catchment clearing and the sand sourcing.	Sections 4.8.1 and 4.8.2	HD and SW models along with the data used to develop and calibrate/validate the models (see Section 4 for further details).	Insufficient modelling has been undertaken to date to allow 'cumulative' impacts to be defined.	Measured hydrodynamic, wave, turbidity, sediment PSD and compositional data collected by BKA and presented in the supplementary technical note will be used to further develop, calibrate and validate the models. Once there is sufficient confidence in the models they will be setup to simulate cumulative impacts.
• Determine coastal vulnerability and the potential impacts as a result of climate change.	This report does not include details of coastal vulnerability or potential impacts as a result of climate change. This is because the numerical models are not sufficiently well developed at this stage. Future modelling will be undertaken to account for 100 years of climate change (sea level rise, increase river discharge and relevant changes to other metocean conditions) and potential impacts as a result of sea level rise will be detailed based on this. Coastal vulnerability will be assessed based on results from the sea level rise simulations and the predicted impacts from the sand sourcing.	Sections 4.8.1 and 4.8.2	HD, SW, MT and Beach Processes models along with the data used to develop and calibrate/validate the models (see Section 4 for further details).	Insufficient modelling has been undertaken to date to allow for coastal vulnerability or impacts as a result of climate change to be determined.	Measured hydrodynamic, wave, turbidity, sediment PSD and compositional data collected by BKA and presented in the supplementary technical note will be used to further calibrate and validate the models. Once there is sufficient confidence in the models they will be setup to simulate potential impacts as a result of climate change.
• Identify monitoring strategies, and management and mitigation measures	This report does not provide details of monitoring strategies and management and mitigation measures as insufficient information on the predicted impacts of the sand sourcing is available at this stage to justify developing these. Future modelling will be undertaken once the models are further developed and have been subject to additional calibration and validation and the predicted impacts from the sediment transport and coastal processes modelling will be used to inform monitoring strategies as well as management and mitigation measures.	Sections 4.8.1 and 4.8.2	HD, SW, MT and Beach Processes models along with the data used to develop and calibrate/validate the models (see Section 4 for further details).	Insufficient modelling has been undertaken to be able to fully assess potential impacts of sand sourcing.	Measured hydrodynamic, wave, turbidity, sediment PSD and compositional data collected by BKA and presented in the supplementary technical note will be used to further calibrate and validate the models. Once there is sufficient confidence in the models they will be setup to simulate potential impacts of the sand sourcing and the results used to inform monitoring strategies and management and mitigation measures.
	The only potential impacts of the sand sourcing on the marine environmental quality could be the	Section 4.8.3	HD, SW and MT models along with the	Further development and calibration/validation of	Measured hydrodynamic, wave, turbidity, sediment PSD and

Guideline	Findings / Conclusions at time of this report (based on best assessment of all existing available data)	Relevant section of this report	Supporting Data Sources (references)	Assumptions, Qualifications, Limitations & Gaps	Data & Analysis Needs & Recommendations to Address the Guideline Fully
• WA EPA 2016 *Environmental Factor Guideline - Marine Environmental Quality*: • This Guideline is relevant to the development of the Conceptual Model (but which also needs to address sediment dynamics and coastal processes – perhaps more importantly than MEQ). • Because there will not be any 'operational' discharges of pollutants from the operation, the only potential impacts of the operation on marine environmental quality are turbid plume generation, addressed by Objective 3. • States **objective** is "To maintain the quality of water, sediment and biota so that environmental values are protected", and defines environmental values and beneficial uses.	plume dispersion from the sand sourcing activity. This report does not provide any predictions of plumes from the proposed sand sourcing operation. This is because further data are required to develop the numerical models and allow a robust calibration and validation to be undertaken for the HD, SW and MT models prior to the plume dispersion modelling being undertaken. A conceptual understanding of the coastal processes in the CG as well as a conceptual model of possible effects of human changes in CG are presented in the report. The conceptual model shows that the two main potential stressors caused by human activities are an increase in suspended sediment and a reduction in sediment supply.		data used to develop and calibrate/validate the models (see Section 4 for further details).	the HD, SW and MT models are required prior to plume dispersion modelling being undertaken.	compositional data collected by BKA and presented in the supplementary technical note will be used to further calibrate and validate the models. Once there is sufficient confidence in the HD, SW and MT models the plume dispersion modelling will be undertaken.
• States that **considerations for the EIA** should include (only those directly related to PCS work are listed):	No response required.				
• the marine system that will potentially be affected and the significance of the environmental values that it supports; and	The marine system is described based on a combination of information from the literature, measured data and results from numerical modelling. The significance of the environmental values in the marine system are further detailed by BKA (2024d).	Sections 3, 4.4.3, 4.5.3, 4.6.3, 5.1 and supplementary technical note	AHO (2023) AIMS (2007) AIMS (2023) BKA (2024d) Copernicus (2023) CSIRO (2023) HD, SW, MT and Beach Processes models along with the data used to develop and calibrate/validate the models (see Section 4 for further details).	Data collection by BKA is ongoing in CG and so additional data will be available to inform the later stages of the project.	Future measured hydrodynamic, wave and turbidity data collected by will be used to provide additional understanding of the marine system.
• predictive modelling of the extent, duration and intensity of impacts under normal and most likely worst case scenarios, and in combination with any other changes in marine environmental quality caused by adjacent activities or natural events (cumulative effects)	This report does not provide any predictions of plumes from the proposed sand sourcing operation. This is because further data are required to develop the numerical models and allow a robust calibration and validation to be undertaken for the HD, SW and MT models prior to the plume dispersion modelling being undertaken.	Section 4.8.3	HD, SW and MT and models along with the data used to develop and calibrate/validate the models (see Section 4 for further details).	Further development and calibration/validation of the HD, SW and MT models are required prior to plume dispersion modelling being undertaken.	Measured hydrodynamic, wave, turbidity, sediment PSD and compositional data collected by BKA and presented in the supplementary technical note will be used to further calibrate and validate the models. Once there is sufficient confidence in the HD, SW and MT models the plume

Guideline	Findings / Conclusions at time of this report (based on best assessment of all existing available data)	Relevant section of this report	Supporting Data Sources (references)	Assumptions, Qualifications, Limitations & Gaps	Data & Analysis Needs & Recommendations to Address the Guideline Fully
	Future modelling will be undertaken to predict the extent, duration and intensity of impacts for normal and most likely worst-case scenarios. The plume dispersion modelling will be undertaken for a range of metocean conditions and the results will be processed to define the normal and worst-case impacts. The natural SSC will also be simulated for these periods to determine the cumulative effects in relation to natural variability.				dispersion modelling will be undertaken.
• States that **Information required for EIA** include (only those directly related to PCS work are listed):	No response required.				
• characterisation of the local marine environment including natural background and baseline environmental quality the pre-development EQP for the area including the environmental values to be protected (none exist – we will propose),	The natural background and baseline environmental quality of CG has been detailed in this report and in the supplementary technical note, with measured data during the dry and wet seasons showing variability in water temperature, salinity, chlorophyll-a (data only collected during dry season) and SSC in CG and in King Shoals. During the dry season the data showed that in CG, the water temperature varied from23 and 24.5ºC, the salinity varied between 29.5 and 32.5 ppt, chlorophyll-a was less than 1.5 µg/L at all sites while SSC showed the highest variability, with values in CG varying from 5 to more than 200 mg/L. During the wet season the data showed that in CG, the water temperature varied from 30 and 32.5ºC, the salinity varied between 7 and 34 ppt while SSC showed the highest variability, with values around the proposed operational area varying from 5 to more than 800 mg/L. Based on the field monitoring undertaken, there are no environmental values to be protected in the region and so no pre-development Environmental Quality Plan has been defined.	Sections 3, 4.4.3, 4.5.3, 4.6.3 and supplementary technical note	AIMS (2007) BKA (2024d) Copernicus (2023)	Ongoing water quality data is being collected by BKA, with only the data collected up to June 2024 included in the supplementary technical note.	Ongoing water quality data to be collected by BKA i will be used to provide additional characterisation of the local marine environment.
• a conceptual model of the marine system and the cause effect pathways for each threat or pressure resulting from the proposal (this will be used to assess risk and select relevant indicators),	A preliminary conceptual model has been developed based on the information and data available at this stage of the study. The conceptual model provides details of the cause and effect pathways for threats and pressures to both coastal processes and ecology resulting from the sand sourcing. The conceptual model	Section 5.4	AHO (2023) AIMS (2007) AIMS (2023) BKA (2024d) Copernicus (2023) CSIRO (2023)	The conceptual model will be further developed and refined throughout the study as additional data and information become available.	Additional data collected by BKA and results from future modelling will be used to further develop and refine the conceptual model.

Guideline	Findings / Conclusions at time of this report (based on best assessment of all existing available data)	Relevant section of this report	Supporting Data Sources (references)	Assumptions, Qualifications, Limitations & Gaps	Data & Analysis Needs & Recommendations to Address the Guideline Fully
	shows that the two main potential stressors caused by the sand sourcing are an increase in the sediment mobilised during the sourcing activity and a reduction in the availability of sand.				
• the criteria that will be used to predict the extent, severity and duration of any impacts and how they were derived,	The plume dispersion modelling results will be processed using statistical analysis such as percentiles to show the extent, magnitude and duration of elevated SSC and sedimentation impacts resulting from the sand sourcing.	Section 4.8.3	N/A	Further development and calibration/validation of the HD, SW and MT models are required prior to plume dispersion modelling being undertaken.	Measured hydrodynamic, wave, turbidity, sediment PSD and compositional data collected by BKA and presented in the supplementary technical note will be used to further calibrate and validate the models. Once there is sufficient confidence in the HD, SW and MT models the plume dispersion modelling will be undertaken.
• a description of the extent, severity and duration of effects of the development in the context of the EQP (this is likely to involve predictive modelling); and	This report does not detail the extent, severity and duration of SSC plumes due to the sand sourcing. This is because further data are required to develop the numerical models and allow a robust calibration and validation to be undertaken for the HD, SW and MT models prior to the plume dispersion modelling being undertaken. Future modelling will be undertaken to predict the extent, severity and duration of impacts for normal and most likely worst-case scenarios for plume dispersion.	Section 4.8.3	N/A	Further development and calibration/validation of the HD, SW and MT models are required prior to plume dispersion modelling being undertaken.	Measured hydrodynamic, wave, turbidity, sediment PSD and compositional data collected by BKA and presented in the supplementary technical note will be used to further calibrate and validate the models. Once there is sufficient confidence in the HD, SW and MT models the plume dispersion modelling will be undertaken.
• consideration of the cumulative impacts of the proposal in combination with other existing and approved developments to determine if the EQP can be achieved.	This report does not include any cumulative impacts as further data are required to develop the numerical models and allow a robust calibration and validation to be undertaken for the HD, SW and MT models prior to any cumulative impacts being simulated. However, no relevant in combination existing or approved developments have been identified in the region which could impact on the marine environmental quality in CG and so at this stage no cumulative impacts are being considered.	N/A	N/A	N/A	N/A
WA EPA 2016 *Technical Guidance - Protecting the Quality of Western Australia's Marine Environment*: • Supports the Environmental Factor Guideline (EFG).	This technical guidance will be followed as necessary for the WA EPA 2016 Environmental Factor Guideline - Marine Environmental Quality requirements.	N/A	N/A	N/A	N/A

Guideline	Findings / Conclusions at time of this report (based on best assessment of all existing available data)	Relevant section of this report	Supporting Data Sources (references)	Assumptions, Qualifications, Limitations & Gaps	Data & Analysis Needs & Recommendations to Address the Guideline Fully
• *Please apply when addressing the items under the EFG above.*					
• WAMSI/CSIRO 2020 *Guideline for Dredge Plume Modelling for EIA* (Sun et al 2020): • *In the data analysis and modeling methods sections of your reports please describe how these guidelines have been followed / complied with.*	This report does not provide any predictions of plumes from the proposed sand sourcing operation. This is because further data are required to develop the numerical models and allow a robust calibration and validation to be undertaken for the HD, SW and MT models prior to the plume dispersion modelling being undertaken. When the plume dispersion modelling is undertaken the relevant aspects will be undertaken in accordance with the guidelines provided by Sun et al. (2020).	Section 4.8.3	N/A	Further development and calibration/validation of the HD, SW and MT models are required prior to plume dispersion modelling being undertaken.	Measured hydrodynamic, wave, turbidity, sediment PSD and compositional data collected by BKA and presented in the supplementary technical note will be used to further calibrate and validate the models. Once there is sufficient confidence in the HD, SW and MT models the plume dispersion modelling will be undertaken.

7. SUMMARY FINDINGS & CONCLUSIONS

This report provides an initial assessment for the metocean and sediment data analysis and numerical modelling components of BKA's CG Marine Sand Proposal. The report has reviewed existing data as well as the data available from BKA's collection program for the project, undertaken a gap analysis, detailed the initial numerical modelling setups, provided preliminary results and presented an initial system understanding and conceptual model. After the preparation of this technical report, data from the 2024 wet season data collection campaign were available. Analysis of these data has been undertaken to provide additional understanding for the project, the analysis is detailed in a supplementary technical note which is included as Appendix A.

The data review showed that the combination of existing data and the data being collected by BKA will be sufficient to provide a good understanding of the hydrodynamics, sediment transport and coastal processes in CG. However, a number of data gaps were identified and based on these, it was recommended that the following additional data should be collected to fill the gaps:

- high resolution bathymetric data of Blocks 4 and 4A. This was undertaken for the proposed operational area during the 2024 wet season data collection campaign, the data are presented in Appendix A;
- data to show erosion/accretion rates within the proposed operational area (i.e. repeat bathymetric survey). This was undertaken for two target areas within the proposed operational area during the 2024 wet season data collection campaign, the data are presented in Appendix A; and
- topographic data of the intertidal and supratidal areas of the turtle nesting beaches to provide high resolution beach elevation data. This was undertaken during the 2024 wet season data collection campaign, the data are presented in Appendix A.

The available data have shown that CG is a macrotidal environment that regularly experiences strong tidal current speeds of up to 1.5 m/s. It is relatively sheltered from offshore waves due to the shallow bathymetry of King Shoals and Medusa Bank as well as the sheltering of Lacrosse Island. The astronomical tide is the dominant process in CG, resulting in regular transport of the clay, silt and sand that is present within CG. The regular sediment transport results in naturally high SSC within CG, with an average value of 50 mg/L and a peak value of more than 200 mg/L recorded to date, which in turn results in low benthic light availability and low chlorophyll-a. Benthic biota surveys identified limited benthic habitats and communities, with no seagrass, coral communities, filter feeder communities or oyster reefs present in the region. The key habitats are the narrow fringes of mangroves around the coast of CG, backed by tidal salt and mud flats, including the Ord River Floodplain Ramsar site on the eastern side of CG, and the four known turtle nesting beaches.

Satellite imagery was sourced and processed to show how the turtle nesting beaches have changed over time. The analysis showed that the beaches offshore of CG (Cape Domett and Turtle Beach West) have been advancing since 1994, while Turtle Bay on Lacrosse Island has remained stable and the stranded beach ridge at East Bank Point inside CG has been retreating at either end, and remained stable in the centre. The shoreline positions at the offshore beaches and the beach on Lacrosse Island showed a difference in shoreline position between the wet and dry seasons, indicating a potential change in the beach profile shape due to the different wave conditions, which occur during the different seasons.

Satellite imagery was also sourced and processed to show how the SSC in the region has varied spatially and temporally depending on the metocean conditions. The analysis showed that the SSC in the region is typically high, with low SSC only occurring for short periods during very small neap tides. The SSC was also shown to vary over a tidal cycle, with lower SSC around high water due to offshore waters with low SSC being imported into CG and higher SSC around low water due to upstream waters from West and East Arms with very high SSC flowing into CG. The imagery showed that the SSC in CG can be increased due to large wave events and high river discharges, but the surface water SSC during these events was not significantly higher than during large spring tides (it is possible that the near bed SSC could be significantly higher).

The initial setup of the hydrodynamic, spectral wave, sediment transport and beach processes models has been presented. The MIKE software suite developed by DHI was applied for all the modelling, with a flexible mesh approach adopted for the hydrodynamic, wave and sediment transport models. The model mesh extends approximately 200 km north to south and 280 km east to west, with the triangular elements

side lengths varying from 4 km in the offshore areas to 200 m in CG. An initial model calibration of the hydrodynamic model, and high-level validations of the spectral wave and sediment transport models are presented. Preliminary results from all four of the models were presented to help understand the existing conditions in CG and how these conditions vary spatially and temporally.

There was sufficient confidence in the HD and SW models to allow preliminary impact assessment to be undertaken for the sourcing of 70 million m^3 of sand from the proposed operational area. The HD modelling predicted that the sand sourcing would result in small changes to both water levels and currents in CG. The phasing of the tidal propagation upstream of the proposed operational area was predicted to be changed by 27 s (earlier) and this results in apparent changes in water level and current speed during the flood and ebb stages of the tide. The sand sourcing is not predicted to measurably impact the tidal range within CG (changes of up to 0.06%). The deepening due to the sand sourcing is predicted to result in a localised reduction in current speed within the proposed operational area of up to 1.5% of the peak current speeds.

The SW model predicted that the sand sourcing would not impact the wave conditions for the majority of the time. The deepening of the proposed operational area was only predicted to result in changes to the wave conditions within CG during large wave events such as those which occur during the wet season due to TCs and tropical lows, while the model did not predict any changes to waves offshore of CG. The largest changes were predicted to occur during the largest wave event modelled (due to a TC) when the H_s in CG ranged from 1 to 2 m, with increases in H_s in CG predicted to remain below 0.01 m (0.5 to 1%).

The MT model was not considered to be sufficiently developed to reliably predict changes to sediment transport or erosion and accretion rates. However, the predicted impacts to hydrodynamics and waves were used to qualitatively assess potential impacts to sediment transport and coastal processes. The small and localised predicted changes to the hydrodynamics resulting from the sand sourcing was not considered unlikely to noticeably change the sediment dynamics and sediment transport rates in CG, with the changes potentially resulting in a small increase in sedimentation in the proposed operational area (due to a reduction in current speeds in this area). As predicted changes to wave conditions were limited to within CG and only during large wet season wave events, the changes in waves are not expected to directly impact sediment transport rates (of sand and fine-grained silt and clay) or coastal processes (i.e. no changes to beaches or mangroves) either within or offshore of CG.

The proposed approaches for the future modelling to be undertaken as part of the study is outlined along with details as to how the modelling and data analysis approach has and will meet both the study objectives as well as the WA EPA guidelines.

Information from relevant literature, available data and the preliminary model results were used to develop a system understanding of the CG region in terms of coastal processes and sediment transport. In addition, a high-level overview of the potential coastal processes and ecological implications resulting from the proposed CG Marine Sand Proposal has been provided along with a conceptual model of the potential different causes and effects. The conceptual model includes changes to the system as a result of the historic Ord River catchment clearing and the construction of the Ord River Dam.

The conceptual model identified two potential cause-effect pathways resulting from the CG sand sourcing. The first was the suspension of sediment into the water column by the sand sourcing activity, and the second was a reduction in availability of sand on the seabed. The potential for both pathways to cause negative environmental impacts is considered low, however this will be assessed in detail through the subsequent modelling phase of this study.

8. REFERENCES

Australian Hydrographic Office (AHO), 2022. Australian National Tide Tables 2023. NTM Edition 25, December 2022.

Australian Hydrographic Office (AHO), 2023. AusTides (AHP114). <https://www.hydro.gov.au/prodserv/publications/ausTides/tides.htm>, viewed 7 November 2023.

Australian Hydrographic Office (AHO), 2024. Australian Chart Index: AusGeoTiff. < https://www.hydro.gov.au/prodserv/digital/ausGeoTIFF/geotiff.htm>, viewed 8 January 2024.

Australian Institute of Marine Science (AIMS), 2023. IMOS – AIMS Queensland and Northern Array Moorings. < https://data.aims.gov.au/moorings/>, accessed 18 October 2023.

Australian Institute of Marine Science (AIMS), 2007. Ord River and Cambridge Gulf hydrodynamics and sediment movement study, Western Australia. <https://apps.aims.gov.au/metadata/view/54e833b0-60f5-11dc-9ca3-00008a07204e>, accessed 13 October 2023.

Bentley, B.P., 2018. Predicting the impacts of increasing nest temperatures associated with climate change on Western Australian sea turtles. University of Western Australia, School of Biological Sciences, thesis for the degree of Doctor of Philosophy, April 2018.

BKA, 2024b. Cambridge Gulf Marine Sand Proposal – WA EP Act s38 Referral Report No. 2: *Proposal Setting & Existing Environment Descriptions*.

BKA, 2024d. Cambridge Gulf Marine Sand Proposal – WA EP Act s38 Referral Report No. 4: *Impact Assessments of Relevant Environmental Factors*.

Bureau of Meteorology (BoM), 2024a. Tide gauge metadata and observed monthly sea levels and statistics. < http://www.bom.gov.au/oceanography/projects/ntc/monthly/>, viewed 16 January 2024.

Bureau of Meteorology (BoM), 2024b. Cyclone tracks – Southern Hemisphere. <http://www.bom.gov.au/cyclone/history/tracks/beta/>, viewed 15 January 2024.

Bray, R.N. (Ed.), 2008. Environmental Aspects of Dredging. Taylor & Francis, 396pp.

Brockmann, C., Doerffer, R., Peters, M., Stelzer, K., Embacher, S., and Ruescas, A., 2016. Evolution of the C2RCC neural network for Sentinel 2 and 3 for the retrieval of ocean colour products in normal and extreme optically complex waters. Proceedings of Living Planet Symposium, Prague.

Carter, R.M., Larcombe, P., Dye, J.E., Gagan, M.K. and Johnson, D.P., 2009. Long-shelf sediment transport and storm-bed formation by Cyclone Winifred, central Great Barrier Reef, Australia. Marine Geology, 267 (3), 101-113.

Coleman, J.M., and Wright, L.D., 2006. Sedimentation in an arid macrotidal alluvial river system: Ord River, Western Australia.

Conner, C.S., and De Visser, A.M, 1992. A laboratory investigation of particle size effects on an optical backscatterance sensor. Marine Geology, 108(2), 151–159.

Copernicus, 2023. Copernicus Data Space Ecosystem. <https://dataspace.copernicus.eu>, viewed on 2 November 2023.

CSIRO, 2023. CAWCR Wave Hindcast – Aggregated Collection. < https://data.csiro.au/collection/csiro:39819>, viewed 20 October 2023.

DataWA, 2023. Web Mapping Service, Hydrographic catchments. <https://catalogue.data.wa.gov.au/dataset/hydrographic-catchments-catchments>, viewed 30 October 2023.

Department of Environment and Conservation (DEC), 2012. Ord River and Parry Lagoons nature reserves management plan 77 2012, Department of Environment and Conservation, Perth

Digital Earth Australia (DEA), 2023. Derived data product, DEA Intertidal Elevation. <https://www.dea.ga.gov.au/products/dea-intertidal-elevation>, viewed 11 October 2023.

Durrant, T., Greenslade, D., Hemer, M., and Trenham, C., 2014. A global wave hindcast focussed on the Central and South Pacific, CSIRO Centre for Australian Weather and Climate Research, CAWCR Technical Report No. 070, April 2014.

DWER, 2024. Interactive water science monitoring and data. <https://www.wa.gov.au/service/natural-resources/water-resources/interactive-water-science-maps>, viewed 10 January 2024.

EPA Template, 2024. Project Content Document – Boskalis Cambridge Gulf Marine Sand Proposal.

Erftemeijer, P.L.A., Jury, M.J., Gäbe, B., Dijkstra, J.T., Leggett, D., Foster, T.M. and Shafer, D.J., 2013. Dredging, port- and waterway construction near coastal plant habitats. In: Proceedings of the Coasts & Ports 2013 Conference, Sydney, Australia, 11-13 September 2013.

Fearns, P., Broomhall, M., and Dorji, P., 2017. Optical remote sensing for dredge plume monitoring: a review. Report of Theme 3 - Project 3.1.1, prepared for the Dredging Science Node, Western Australian Marine Science Institution, Perth, Western Australia, 46 pp.

Fearns, P., Dorji, P., Broomhal, M., Branson, P., and Mortimer, N., 2018. Plume Characterisation– Laboratory Studies. Report of Theme 3 – Project 3.2.2, prepared for Dredging Science Node, Western Australian Marine Science Institution, Perth, Western Australia, 57pp.

Gagan, M. K., Chivas, A. R., and Herczeg, A. L., 1990. Shelf-wide erosion, deposition, and suspended sediment transport during Cyclone Winifred, central Great Barrier Reef, Australia. Journal of Sedimentary Research, 60 (3).

GBRMPA, 2012. Guidelines – The use of hydrodynamic numerical modelling for dredging projects in the Great Barrier Reef Marine Park. August 2012.

Geoscience Australia, 2023a. High-resolution depth model for Northern Australia – 30m. <https://ecat.ga.gov.au/geonetwork/srv/api/records/1010ac13-e033-489d-b9ce-ae11fd0e11ef>, viewed 10 October 2023.

Geoscience Australia, 2023b. Digital Earth Australia Map, Coastlines rates of change statistics. <https://maps.dea.ga.gov.au/>, viewed 8 June 2023.

Geoscience Australia, 2024. Geomorphic features of Australia's Marine Jurisdiction MapServer. <https://ecat.ga.gov.au/geonetwork/srv/api/records/dc53a606-8d88-44f6-a1c6-259495a977dc>, viewed 5 January 2024.

Gehrke, P., 2009. Ecological patterns and processes in the Lower Ord River and Estuary.

Hale, J., 2008. Ecological character description of the Ord River floodplain Ramsar site. A Report to the Department of Environment and Conservation, September 2008;

Hemer, M.A., Zieger, S., Durrant, T., O'Grady, J., Hoeke, R.K., and McInnes, K.L., 2017. A revised assessment of Australia's national wave energy resource. Renewable Energy, 114, 85–107.

IMOS, 2023. Integrated Marine Observing System, OceanCurrent – Tidal current and sea level predictions, Arnhem, 2023. <https://oceancurrent.aodn.org.au/tides/Arnhem_spd/2023/>, viewed 16 October 2023.

Jones, R., Bessell-Browne, P., Fisher, R., Klonowski, W., and Slivkoff, M., 2016. Assessing the impacts of sediments from dredging on corals. Marine Pollution Bulletin 102, 9-29.

Kemps, H., and Masini, R., 2017. Estimating dredge source terms – a review of contemporary practice in the context of Environmental Impact Assessment in Western Australia. Report of Theme 2 – Project 2.2, prepared for the Dredging Science Node, Western Australian Marine Science Institution (WAMSI). Perth, Western Australia, 29pp.

Kyryliuk, D. and Kratzer, S., 2019. Evaluation of Sentinel-3A OLCI Products Derived Using the Case-2 Regional CoastColour Processor over the Baltic Sea. Special Issue, Remote Sensing of Ocean Colour: Theory and Applications.

Lowe, R., and Ghisalberti, M., 2016. Sediment transport processes within coral reef and vegetated coastal ecosystems: a review. Report of Theme 3 - Project 3.1.2, prepared for the Dredging Science Node, Western Australian Marine Science Institution, Perth, Western Australia, 27 pp.

Los, F.J. and Blaas, M., 2010. Complexity, accuracy and practical applicability of different biogeochemical model versions. Journal of Marine Systems 81, 44-74.

Masselink, G., Hughes, M., and Knight, J., 2011. Introduction to coastal processes and geomorphology (2nd Edition), Arnold, London.

Mills, D., and Kemps, H., 2016. Generation and release of sediments by hydraulic dredging: a review. Report of Theme 2 - Project 2.1 prepared for the Dredging Science Node, Western Australian Marine Science Institution, Perth, Western Australia. 97 pp.

MScience, 2023. Cambridge Gulf marine sand project, benthic habitat mapping methodology. Unpublished report MSA334.1R01 to Boskalis Australia, Perth Western Australia, pp 16.

Orpin, A.R. and Ridd, P.V., 2012. Exposure of inshore corals to suspended sediments due to wave resuspension and river plumes in the central Great Barrier Reef: A reappraisal. Continental Shelf Research 47 (2012) p.55-67.

PCS, 2021. Port of Weipa, 2021 Maintenance Dredging, Summary of turbidity monitoring. Report No. P042_R2F1, June 2021.

PIANC, 2010. Dredging and Port Construction around Coral Reefs. The World Association for Waterborne Transport Infrastructure (PIANC), Report No. 108, 75pp.

Robson, B.J., Burford, M.A., Gehrke, P.C., Revill, A.T., Webster, I.T. and Palmer, D.W., 2008. Response of the Lower Ord River and Estuary to changes in flow and sediment and nutrient loads.

Robson, B.J., Gehrke, P.C., Burford, M.A., Webster, I.T., Revill, A.T. and Palmer, D.W., 2013. The Ord River Estuary: a regulated wet-dry tropical river system. In Wolanski (ed.) Estuaries of Australia in 2050 and Beyond, Estuaries of the World.

Rothlisberg, P., S. Condie, D. Hayes, B. Griffiths, S. Edgar and J. Dunn, 2005. Collation and Analysis of Oceanographic Datasets for National Marine Bioregionalisation: The Northern Large Marine Domain. A report to the Australian Government, National Oceans Office, CSIRO Marine Research, May 2005, 62 pp.

Pearson, S.G., Verney, R., van Prooijen, B.C., Tran, D., Hendriks, E.C.M., Jacquet, M., and Wang, Z.B., 2021. Characterizing the composition of sand and mud suspensions in coastal and estuarine environments using combined optical and acoustic measurements, Journal of Geophysical Research: Oceans, 126.

Pye. K., S.J. Blott and J. Brown (2017). Advice to inform development and guidance on marine, coastal and estuarine physical processes numerical modelling assessments. NRW Evidence Report 208, July 2017.

Smith, G.A., Hemer, M., Greenslade, D., Trenham, C., Zieger, S., and Durrant, T., 2020. Global wave hindcast with Australian and Pacific Island focus: from past to present. Geoscience Data Journal, Volume 8, Issue 1, 24-33.

Sun, C., Shimizu, K., and Symonds, G., 2016. Numerical modelling of dredge plumes: a review. Report of Theme 3 - Project 3.1.3, prepared for the Dredging Science Node, Western Australian Marine Science Institution, Perth, Western Australia, 55 pp.

Sun, C., Branson, P., and Mills, D., 2020. Guideline on dredge plume modelling for environmental impact assessment. Prepared for the Dredging Science Node, Western Australian Marine Science Institution, Perth, Western Australia. 73pp.

Tas, S.A.J., van Maren, D.S., Helmi, M. and Reniers, A.J.H.M., 2022. Drivers of cross-shore chenier dynamics off a drowning coastal plain, Marine Geology, volume 445,

Thom, B.G., Wright, L.D., and Coleman, J.M., 1975. Mangrove ecology and deltaic-estuarine geomorphology: Cambridge Gulf-Ord River, Western Australia. Journal of Ecology, Vol. 61, No. 1, 203 – 232.

van Rijn, L.C., 1993. Principles of sediment transport in rivers, estuaries and coastal seas. Aqua Publications, Amsterdam.

Volkman, J.K., A.T. Revill, P.I. Bonham and L.A. Clementson, 2007. Sources of organic matter in sediments from the Ord River in tropical northern Australia. Organic Geochemistry 38: 1039-1060.

Vos, K., Harley, M.D., Splinter, K.D., Simmons, J.A., Turner, I.L., 2019a. Sub-annual to multi-decadal shoreline variability from publicly available satellite imagery. Coastal Engineering 150, 160–174.

Vos, K., Splinter, K.D., Harley, M.D., Simmons, J.A., Turner, I.L., 2019b. CoastSat: A Google Earth Engine-enabled Python toolkit to extract shorelines from publicly available satellite imagery. Environmental Modelling & Software 122, 104528.

WA DoT, 2024. Tide data (real time), Wyndham tide, <https://www.transport.wa.gov.au/imarine/wyndham-tide.asp>, viewed 8 January 2024.

Whiting, A.U., Thomson, A., Chaloupka, M., Limpus, C.J., 2008. Seasonality, abundance and breeding biology of one of the largest populations of nesting flatback turtles, *Natator depressus*: Cape Domett, Australia. Australian Journal of Zoology 56(5).

Williams, J.J. and L.S. Esteves (2017). Guidance on setup, calibration and validation of hydrodynamic, wave and sediment models for shelf seas and estuaries. Advances in civil engineering (Volume 2017), 5251902, 25 pages.

Williams, M.A.J., 1969. Prediction of rainsplash erosion in the seasonally wet tropics. Nature 222, 763-765.

Wolanski, E. and Gibbs, R., 1992. Resuspension and clearing of dredge spoils after dredging, Cleveland bay, Australia. Water Environment Research 64, 910–914.

Wolanski, E., Spagnol, S., and Pattiaratchi, C., 2001. Rapid, human-induced siltation of the macro-tidal Ord River Estuary, Western Australia. Estuarine Coastal and Shelf Science 53, 717-732.

Wolanski, E., Spagnol, S., and Williams, D., 2004. The impact of damming the Ord River on the fine sediment budget in Cambridge Gulf, Northwestern Australia. Journal of Coastal Research, 20 (3), 801-807.

Wright, L.D., Coleman, J.M., and Thom, B.G., 1973. Processes of channel development in a high tide range environment: Cambridge Gulf – Ord River Delta, Western Australia.

PORT & COASTAL
SOLUTIONS

Appendices

PORT & COASTAL
SOLUTIONS

Appendix A – Supplementary Technical Note

PORT & COASTAL
SOLUTIONS

Technical Note

Date:	23rd July 2024
To:	Peter Boere, Boskalis Australia Pty Ltd
From:	Andy Symonds
Subject:	Cambridge Gulf Marine Sand Proposal: **Supplementary Technical Note** Metocean & Sediment Dynamics - System Understanding, Conceptual Model and Initial Modelling
Classification:	Project Related
Version:	0.3

1. Introduction

This technical note provides an initial analysis of some of the data obtained by Boskalis Australia Pty Ltd (BKA) during the 2024 wet season data collection campaign in Cambridge Gulf (CG), to support environmental assessment of the Cambridge Gulf Marine Sand Proposal. This note provides supplementary information in addition to the information included in the System Understanding, Conceptual Model and Initial Modelling Report (PCS, 2024a), to support that report, as the wet season data as well as additional data collected by the in-situ self-logging instruments were not available at the time that report was developed. Analysis of the following additional data is detailed in this technical note:

- Bathymetric survey of the proposed operational area: High resolution bathymetric data were collected for the entire proposed operational area and a 1 km buffer zone around the area using a multibeam echosounder in February and March 2024. In addition, the bathymetric survey was repeated at two 2 km^2 'target' areas within the proposed operational area 27 days after the full bathymetric survey was completed, to allow natural changes in bathymetry to be calculated. The repeat surveys were timed to allow two spring tides to occur between the surveys, when currents that drive seabed sediment dynamics are strongest.

- Sediment sampling: Seabed surface sediment samples were collected using a grab at King Shoals, in CG, in West and East Arms and south of Wyndham into the Pentecost River in February 2024. The sediment samples were sent for laboratory analysis to determine particle size distribution (PSD) using a Mastersizer and elemental features using a scanning electron microscope (SEM), to inform assessment of sediment sources and transport pathways.

- Water column profiling: Water column profiling was undertaken at three sites in CG in February 2024, one at West Entrance between Lacrosse Island and Cape Dussejour, one within the proposed operational area and one to the south of that area. The profiling included hourly measurements of a range of water quality parameters through the water column (including turbidity, temperature and salinity) over a 13-hour spring tidal cycle (from low water to low water). In addition to the water quality measurements, concurrent water sampling with two Niskin bottles, one at mid-water and one near the seabed, and current measurements using an Aquadopp Deep were also undertaken. The water samples were subsequently analysed in the laboratory to determine the total suspended solids (TSS) present, the PSD of the suspended sediment and an elemental feature analysis of the sediment using SEM for some of the samples. These data were also collected to inform assessment of sediment sources and transport pathways.

- Acoustic Wave and Current Profiler (AWAC) and Acoustic Doppler Current Profiler (ADCP) data: AWACs/ADCPs have been deployed on the seabed to measure water levels and waves as well as current speed and direction through the water column. Data have been collected at a single site in CG from July to August 2023, with the results discussed by PCS (2024a). This technical note analyses data collected at seven different sites within CG between September 2023 and May 2024.

- In-situ benthic light, turbidity & other data: Benthic light measurements have been collected at multiple sites within CG since September 2023. Upward and downward facing LI-COR LI-1500 light sensors were deployed on the seabed along with Manta multiprobes (turbidity, temperature, salinity etc) and at some sites ADCPs/AWACs, to collect timeseries of the near-seabed light availability, physical water quality and current, wave and water level conditions.

- LiDAR data: Drone-based LiDAR data were captured for the four main turtle nesting beaches in the CG area, the small and large beach at Cape Domett, Turtle Bay on Lacrosse Island and Turtle Beach West, west of

Cape Dussejour. The LiDAR data provides significantly higher resolution topography for these beaches compared to other datasets (e.g. 0.02 m for the LiDAR compared with 25 m Digital Earth Australia (DEA) Intertidal Data), providing an important baseline for the beaches to assist in assessing coastal processes and beach dynamics.

The following sections provide details of the data and the analysis undertaken as part of this technical note.

2. Bathymetric Data

2.1. Data Overview

The extent of the multibeam bathymetric data along with the areas where repeat surveys were undertaken is shown in Figure 1. The plot shows that the bathymetric survey covered the entire proposed operational area and typically extended at least 1 km beyond its boundary (except where proximity of the coast on the northwestern side is closer than 1 km and the southeastern corner where bathymetry was too shallow for the survey vessel). The total area surveyed was 155.3 km^2. The survey was undertaken using a Norbit Multibeam echosounder with a frequency of 400 kHz and an average opening angle of 130°. The average horizontal and vertical errors were calculated as 0.69 and 0.11 m, respectively, which are within the requirements for the International Hydrographic Organisation (IHO) Special Order.

The multibeam survey was undertaken over two periods as follows:

- Period 1, 7th February to 14th February 2024: 60% of the total area was surveyed over this period including Target Areas 1 and 2 which were surveyed on the 8th February 2024.
- Period 2, 3rd March to 6th March 2024: The remaining area was surveyed over this period and Target Areas 1 and 2 were surveyed for a second time on the 6th March 2024.

There were 27 days between the two surveys of Target Areas 1 and 2, with the first survey undertaken midway between neap and spring tides and the second survey undertaken during neap tides. Two spring tides occurred between the surveys around the 11th and 25th February, with maximum tidal ranges of 7.09 and 5.52 m respectively, when seabed currents are strongest. The changes in the bathymetry between the surveys can therefore be considered to be due to changes over a tidal lunar cycle (29 days).

The bathymetric data were post-processed by BKA so that the vertical data were relative to mean sea level (MSL). Point data were provided to Port and Coastal Solutions (PCS) at horizontal resolutions of 1 m for the two Target Areas and 5 m for the whole area. These were used by PCS to generate digital elevation models (DEMs) of the surveyed areas with the same resolution as the point data. These DEMs were then further analysed, including overlaying the repeat DEMs for the two Target Areas to assess changes in bathymetry and sediment movement over the 27-day intervening period.

2.2. Results

The bathymetry for the whole survey area is shown in Figure 1, with close ups of the northern and southern halves shown in Figure 2 and Figure 3. The plots show that sand wave bedforms are present throughout much of the proposed operational area. The sand waves have heights ranging from 1 to 8 m, with wavelengths of between 50 and 200 m. The crests appear to be predominantly aligned approximately perpendicular to the direction of the flood and ebb tidal currents and they are generally asymmetrical with the steeper lee side of the sand wave facing the north-northeast and the more gradual sloping stoss side facing the south-southwest. This suggests that the ebb tidal current is the dominant process influencing the sand transport where the bedforms are located, indicating a net offshore transport of sand by bedload transport through the region. The areas between and adjacent to the sand waves are typically relatively flat with varying depths of between -25 and -55 m MSL.

The bathymetry at the northern end of the proposed operational area, to the south and east of Target Area 1 has an area of approximately 3.5 km by 5 km with irregular bathymetry which includes very steep slopes with depth variations of more than 15 m as well as areas with large areas of flat bed and no obvious bedforms present. Overall, the bathymetry in these areas suggests that the bed is rock or consolidated clay with limited loose surface sediment present. This correlates with the analysis undertaken by BKA to estimate the volume of sand within the proposed operational area, which concluded that there was limited surface sand present in these areas (BKA, 2024b). The sand resource assessment by BKA considered the multibeam survey data along with results from previous vibrocores, grab samples, sub-bottom profiling and sidescan sonar. It was estimated by BKA (2024b) that sand covers approximately 75 km^2 of Blocks 4 (DMIRS E80/5655) and 4A (DMIRS E80/6009) (predominantly within the proposed operational area) and that the average depth of the sand is 4 m, resulting in an estimated minimum volume of sand within this area of 300 million m^3.

The 1 m resolution DEM of Target Areas 1 and 2 developed using the multibeam survey are shown in Figure 4 to Figure 7. The two areas represent different ranges in depth, with Area 1 having depths of between -25 and -45 m MSL, while Area 2 has depths of between -10 and -35 m MSL. Despite the difference in depths between the two areas, they are both predominantly covered by sand waves, with the sand waves in Area 1 extending approximately the width of the area (2 km), while in Area 2 they extend beyond the area, with widths of around 3 km. The zoomed-in plots (Figure 5 and Figure 7) show that in both areas the large sand waves are typically covered by mobile

sediment with undulatory megaripples present. The megaripples have heights of up to 0.4 m and wavelengths of up to 8 m.

The changes in bathymetry between the two surveys of Target Areas 1 and 2 undertaken 27 days apart have been calculated and are shown in Figure 8 and Figure 9. The plots show that erosion and accretion has occurred in a pattern similar to the sand waves. The changes typically show erosion on the southern side of the sand wave and accretion on the northern side, showing that the sand waves have typically migrated in a northerly direction. To better understand how the bedforms have changed over the 27 days, transects have been plotted for each area (Figure 10 to Figure 15). The plots show a consistent shift in the bedforms over the 27 days, with all transects showing a northerly migration of the sand waves except for Transect 2b which showed a southerly migration. The migration distances over the 27-day period were 5 to 10 m for the sand waves migrating in a northerly direction and up to 5 m for the sand waves migrating in a southerly direction. The plots also show that the sand waves are typically asymmetrical, with the steeper lee side facing in a northerly direction, except at Transect 2b where the lee side faces in a southerly direction. At Transects 1a and 2c, the sand waves are more symmetrical, suggesting a smaller difference between the flood and ebb currents at these locations, although the sand waves are migrating in a northerly direction at both transects which indicates that the ebb current is dominant.

It is likely that the migration rates of the sand waves were predominantly due to the astronomical tide, as no extreme conditions (rainfall or wind/waves) occurred over the 27 days, but it is possible that higher migration rates or changes to the migration patterns could occur during extreme conditions. However, during typical conditions it is likely that the migration rates will remain consistent throughout both dry and wet season conditions. It is likely that the sandwaves are in a dynamic equilibrium with the flood and ebb currents. This means that although the individual sandwaves are migrating, their morphology is likely to change with the local currents and so the overall morphology of the sandwave field is likely to remain similar over time.

The migration directions of the sand waves shown by the repeat multibeam survey of Target Areas 1 and 2 have been used along with the asymmetry of the sand waves to predict the net bedload sand transport directions in and immediately around the proposed operational area (Figure 16). This shows that the net bedload sand transport is in a northerly direction, with the edges of some of the sand wave regions experiencing a net southerly bedload transport, which is likely to be a result of strong flood current speeds close to the entrance to CG. The extent of the sand waves indicates that there is a sand transport pathway from within CG, with an upstream supply of sand to the proposed operational area. The sand is then predominantly transported in a northerly direction towards the western entrance to CG, but strong flood currents close to the central and eastern part of the entrance means that the sand waves are forced to the western and eastern sides of the entrance. The strong flood currents also have the potential to result in a supply of sand from offshore of CG to the proposed operational area through the middle of the western entrance.

The sand wave migration rates, along with the dimensions of the sand waves present at the southern boundary of the proposed operational area, can be used to estimate the input of sand into the area due to sand wave migration. The sand waves in this area are approximately 5 m tall, have a wavelength of 100 m and cover a width of approximately 1,500 m. If an average weekly migration rate of 2 m in a northerly direction is assumed to consistently occur due to the astronomical tide, then the annual input of sand into the proposed operational area through sand wave migration would be in the order of 375,000 m^3. It is important to note that higher migration rates may occur during extreme events and that additional transport of sand by bedload and suspended load will also occur as well as the sand wave migration and this transport is also likely to provide an ongoing supply of sand to the area. In addition, there is the potential for an import of sand to the proposed operational area from offshore through the western entrance. Further numerical modelling is being undertaken to provide an estimate of the sand transport into and out of the proposed operational area due to bedload and suspended load.

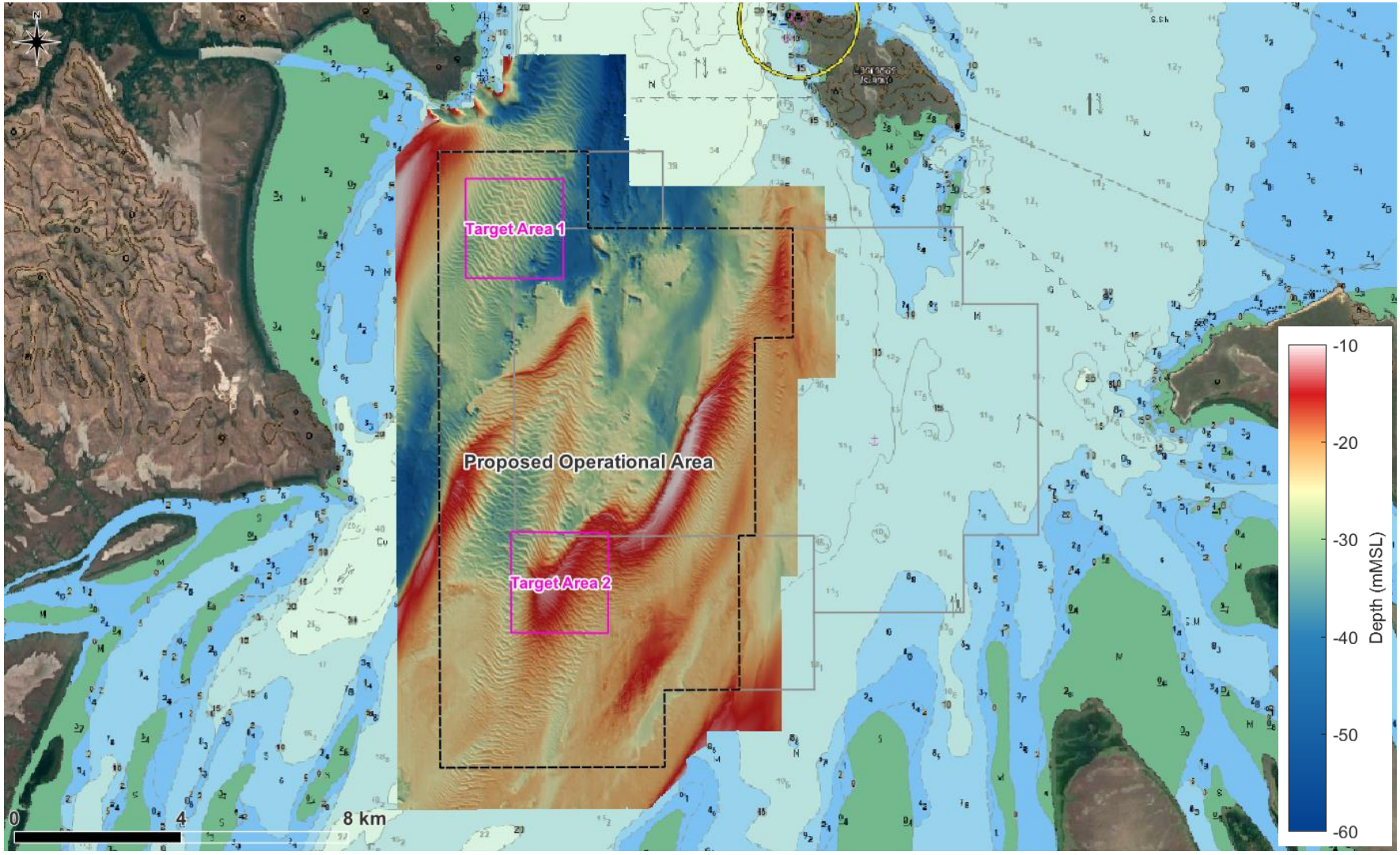

Figure 1. Multibeam bathymetric survey extent along with Target Areas 1 and 2.

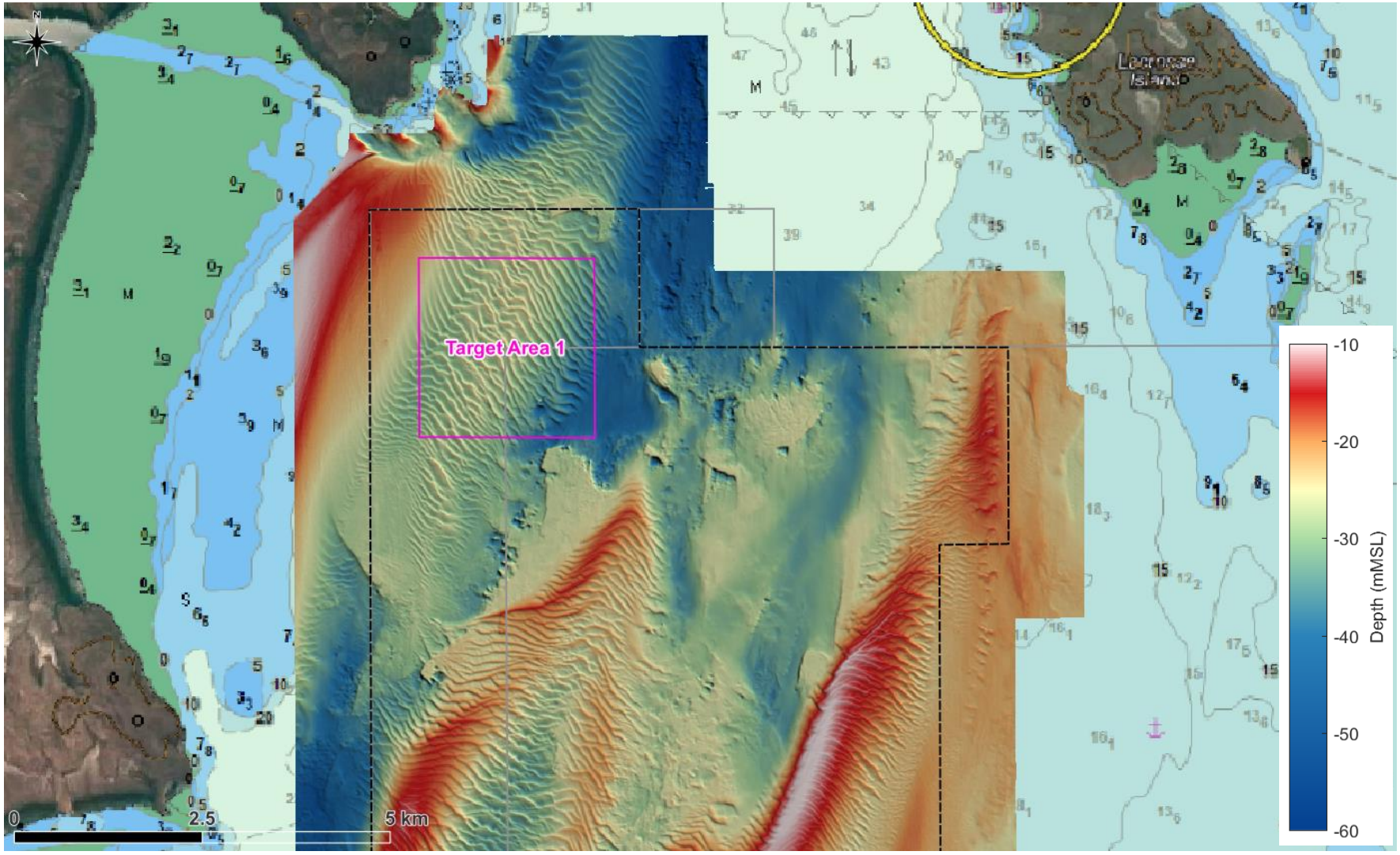

Figure 2. Close up of the northern half of the multibeam bathymetric survey, showing Target Area 1.

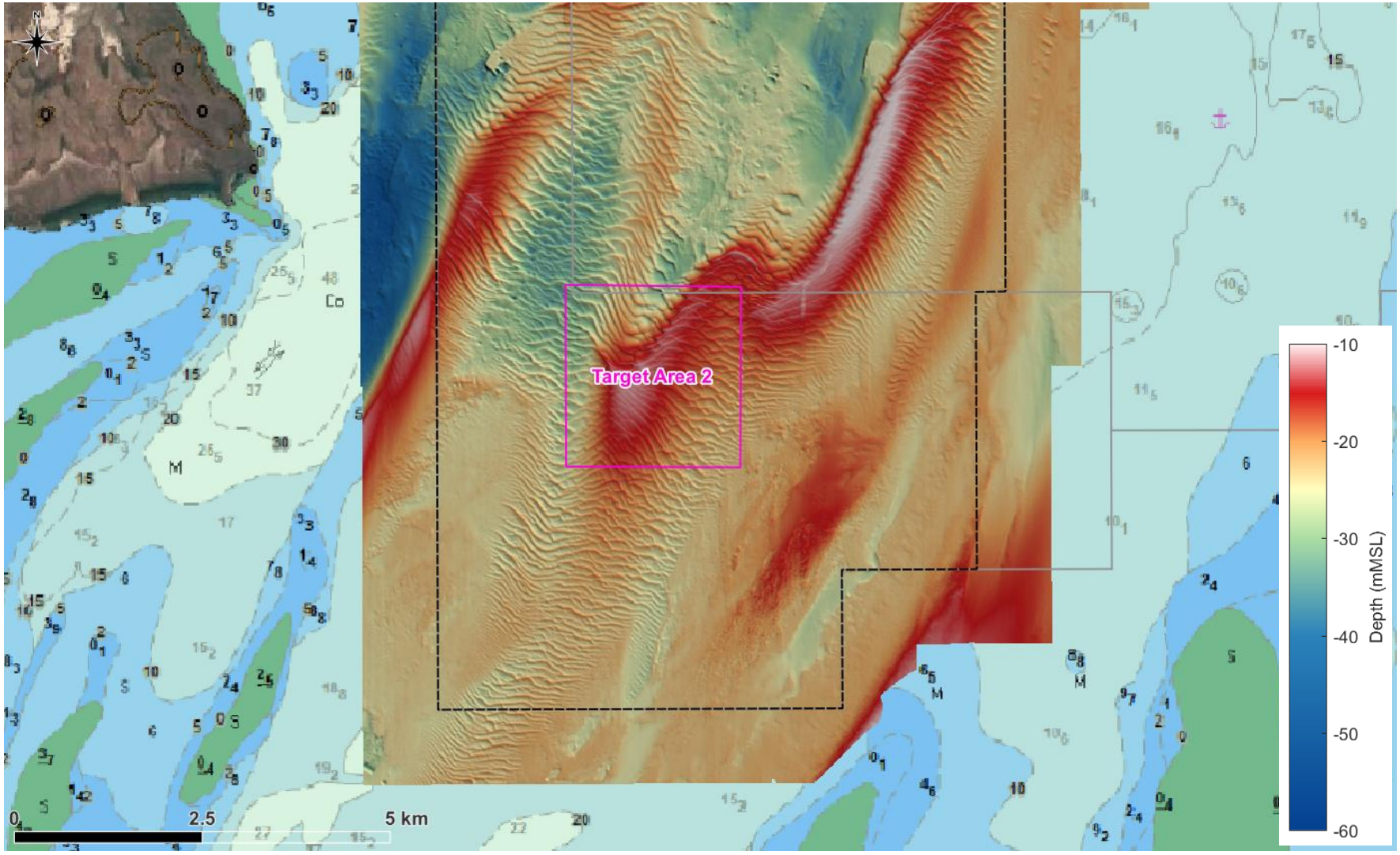

Figure 3. Close up of the southern half of the multibeam bathymetric survey, showing Target Area 2.

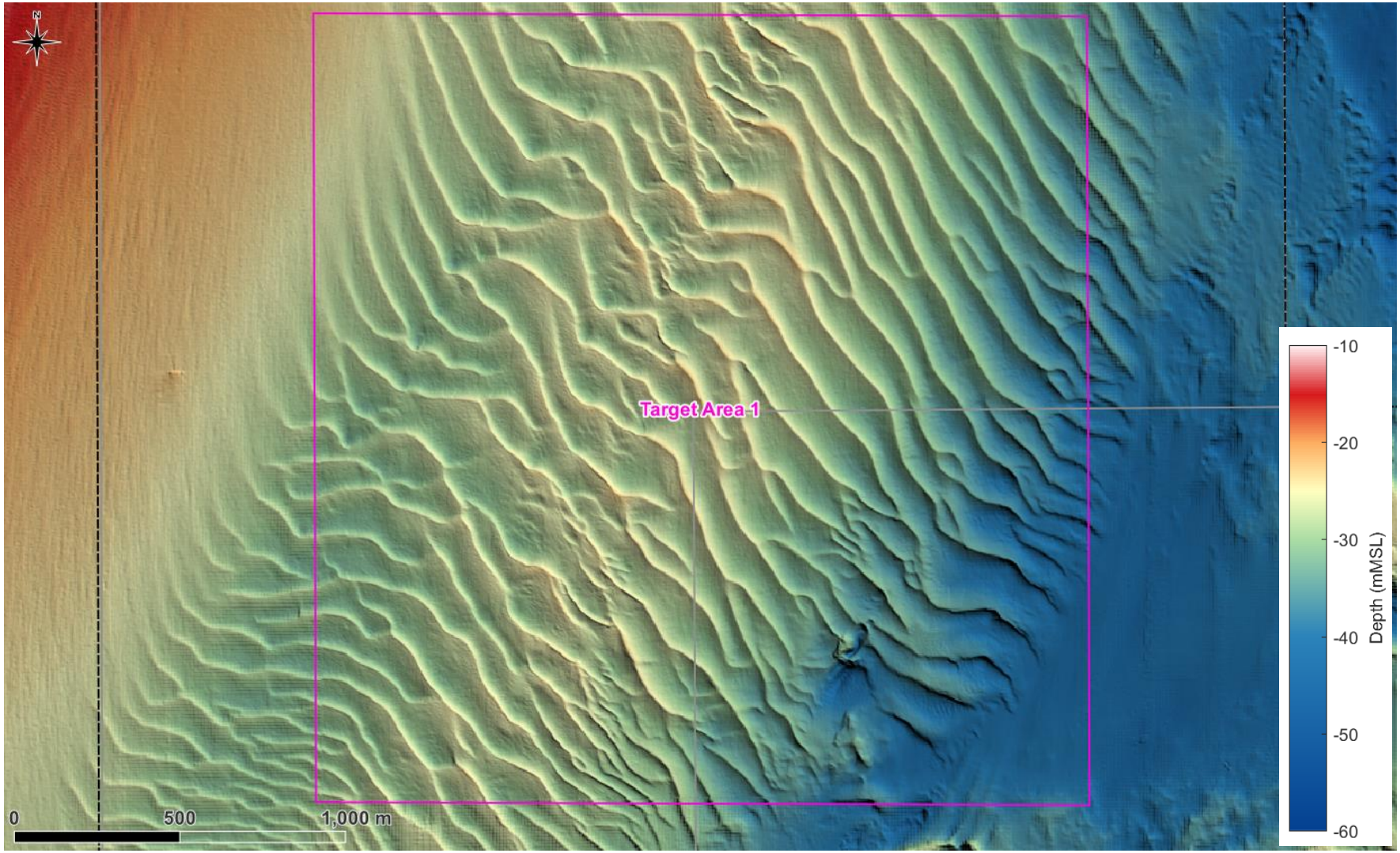

Figure 4. **The 1 m resolution DEM of Target Area 1 based on the multibeam data.**

Figure 5. Close up of part of the 1 m DEM of Target Area 1 showing mega-ripples present on the sand waves.

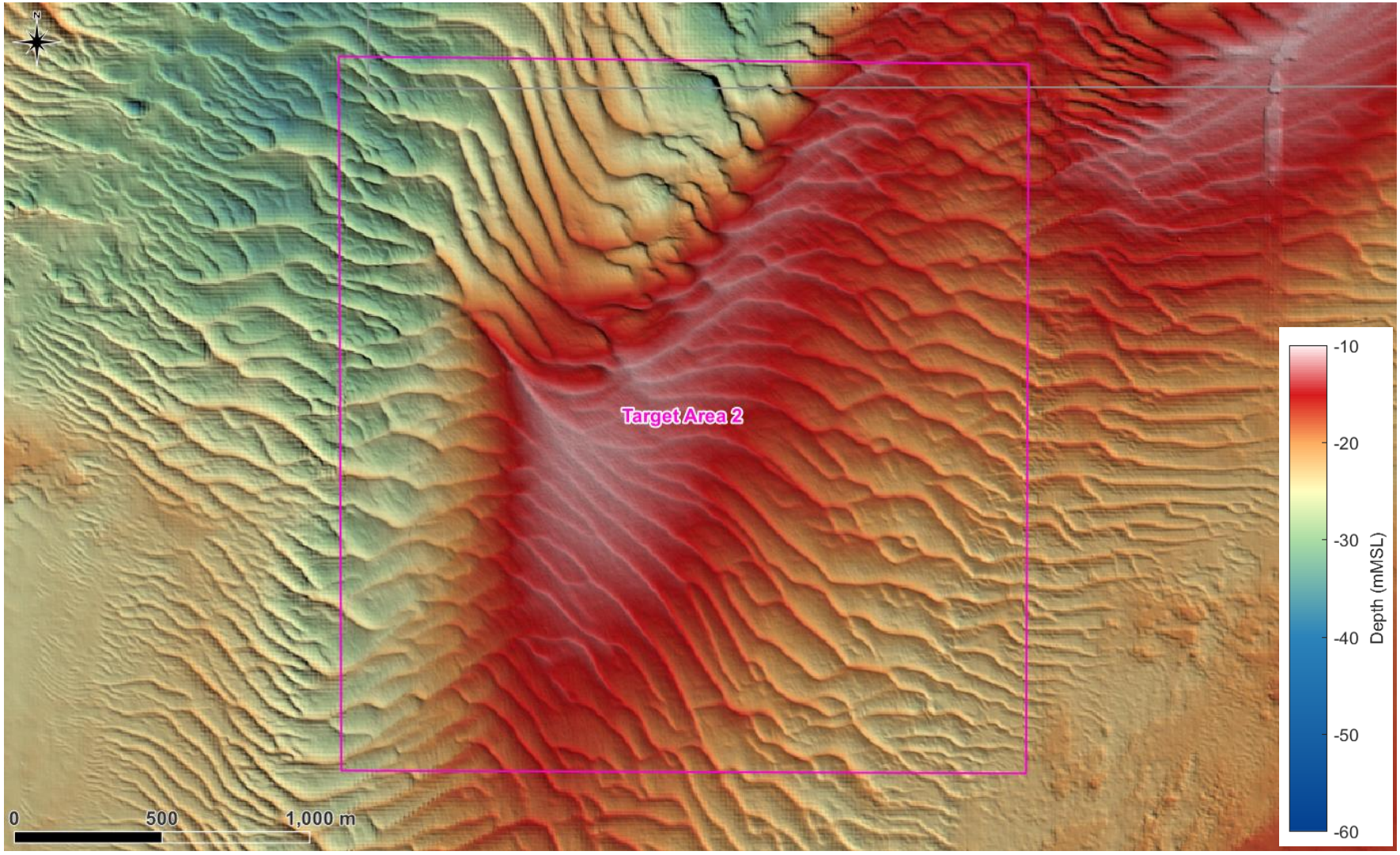

Figure 6. The 1 m resolution DEM of Target Area 2 based on the multibeam data.

Figure 7. Close up of part of the 1 m DEM of Target Area 2 showing mega-ripples present on the sand waves.

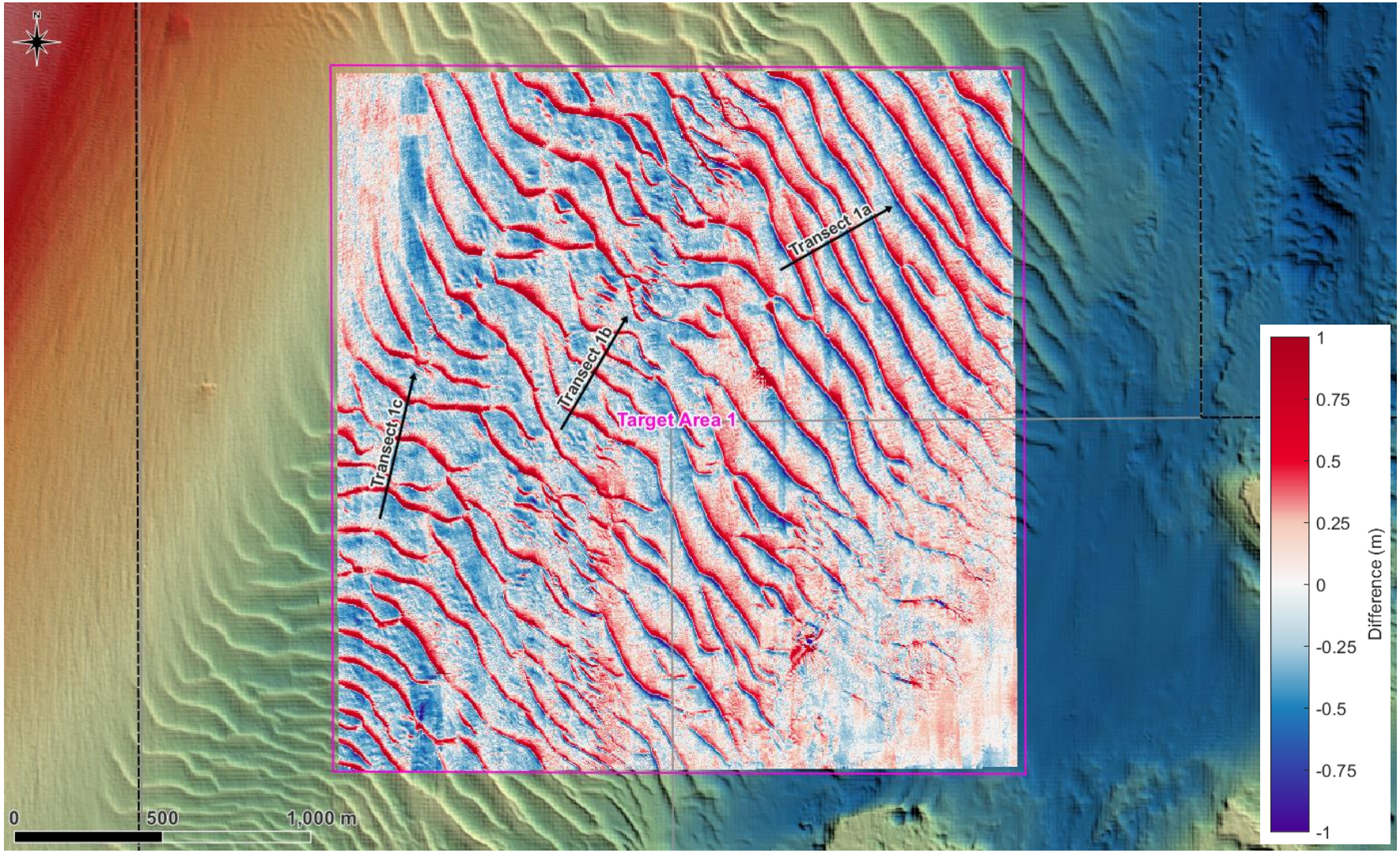

Figure 8. **Change in bathymetry in Target Area 1 over 27 days along with transect locations.**

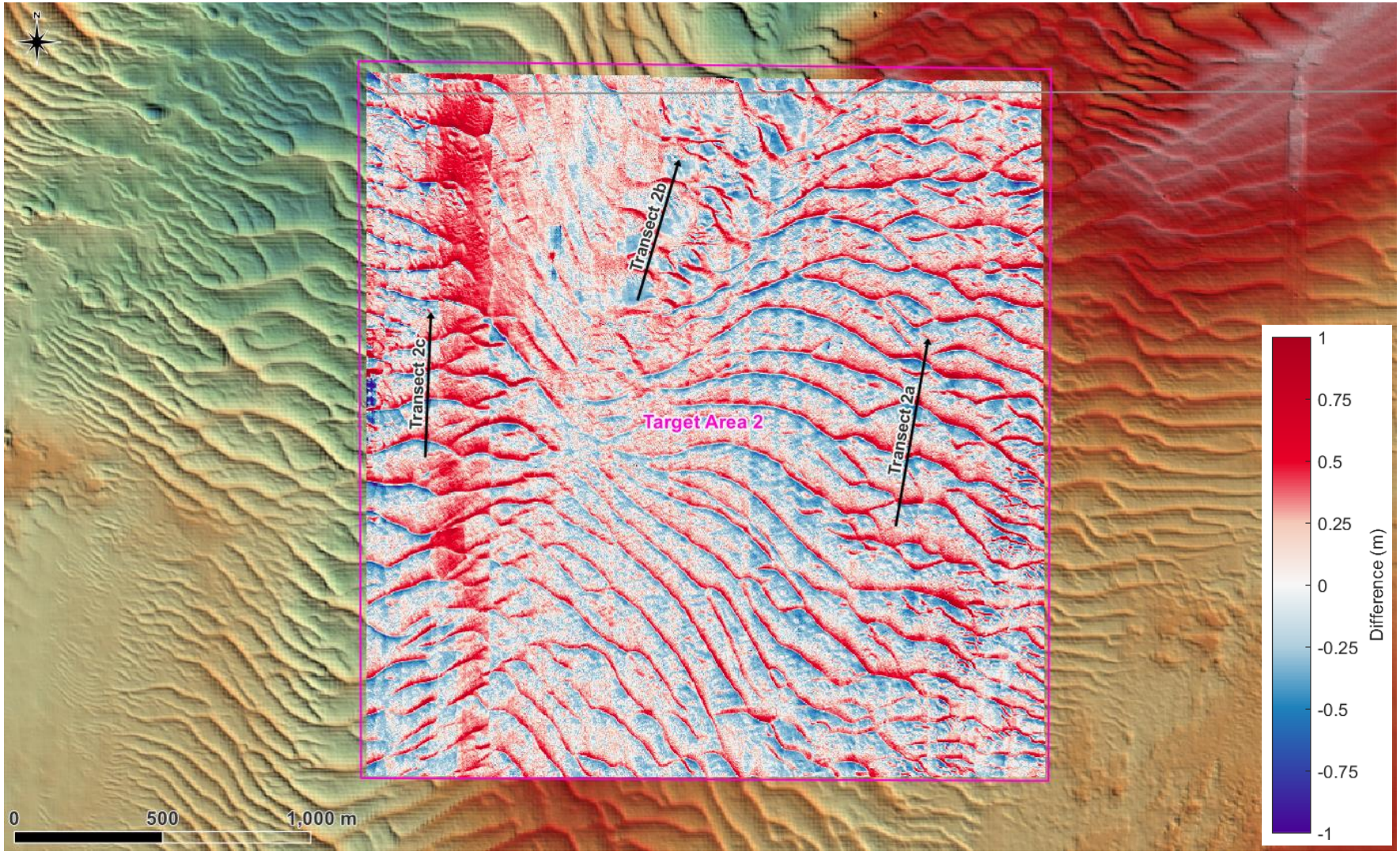

Figure 9. **Change in bathymetry in Target Area 2 over 27 days along with transect locations.**

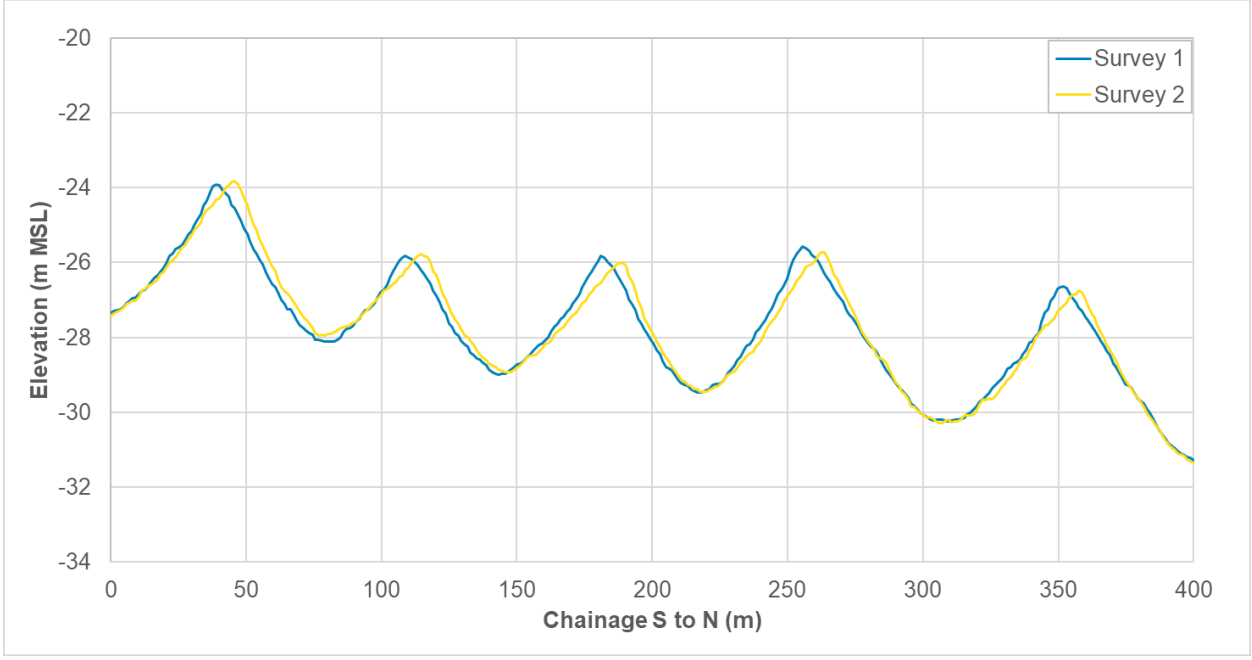

Figure 10. **Bathymetry at Transect 1a on 8th February 2024 (Survey 1) and 6th March 2024 (Survey 2).**

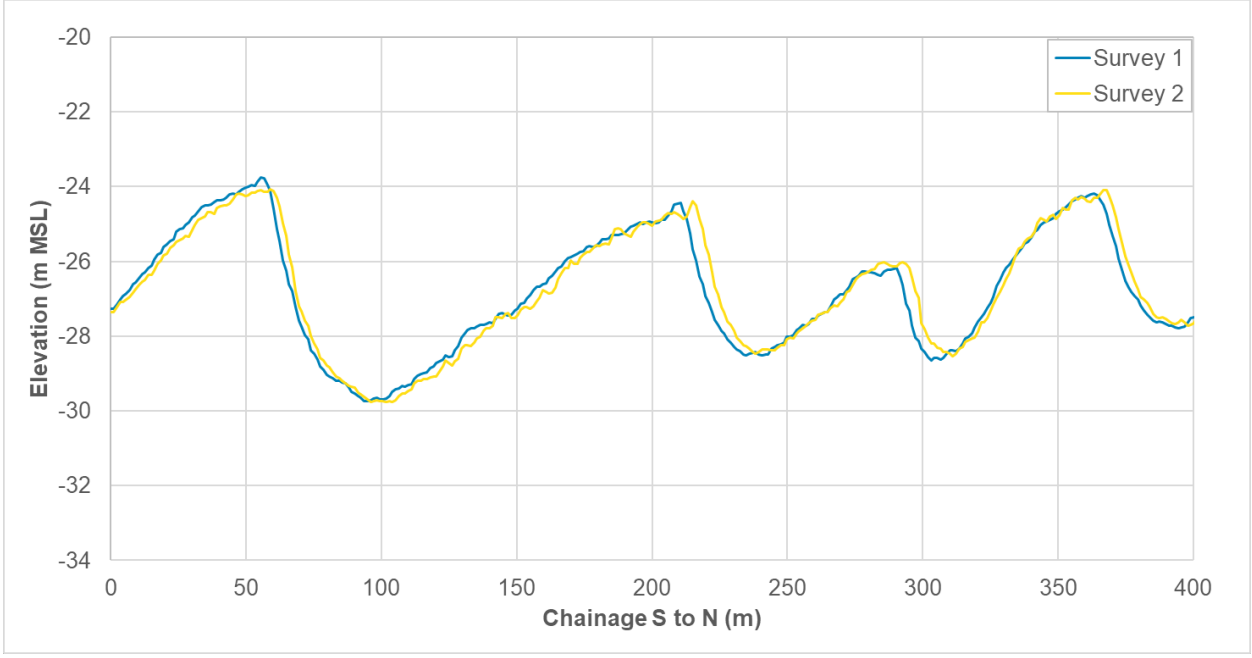

Figure 11. **Bathymetry at Transect 1b on 8th February 2024 (Survey 1) and 6th March 2024 (Survey 2).**

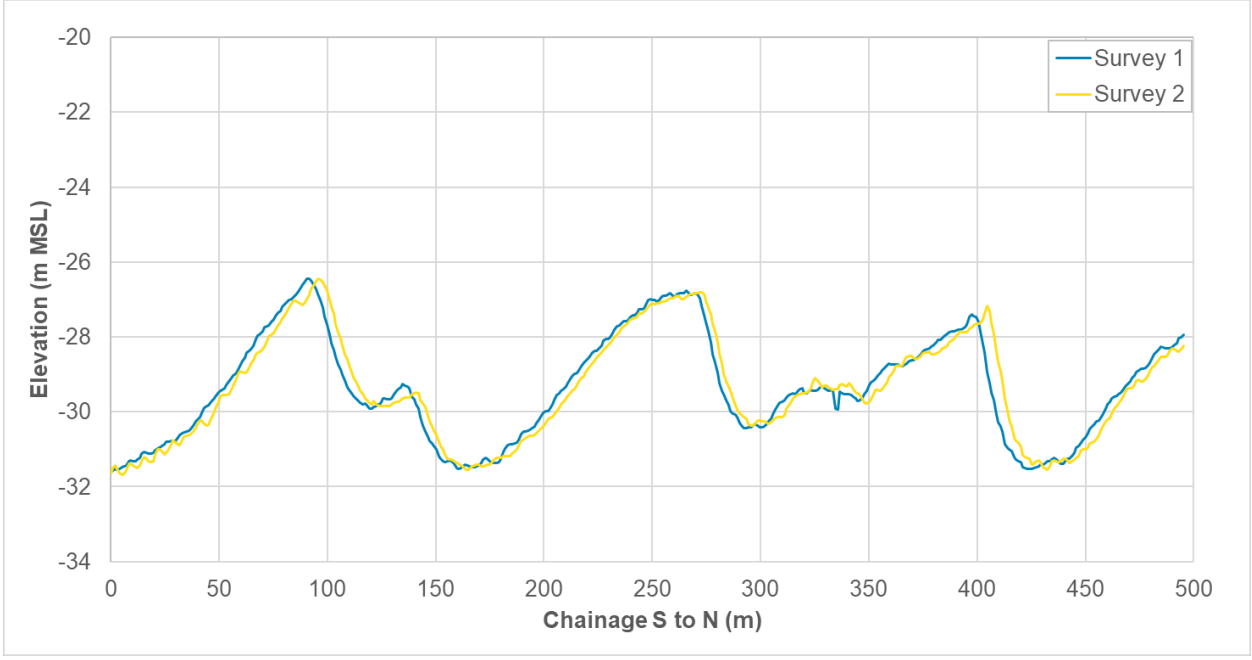

Figure 12. **Bathymetry at Transect 1c on 8th February 2024 (Survey 1) and 6th March 2024 (Survey 2).**

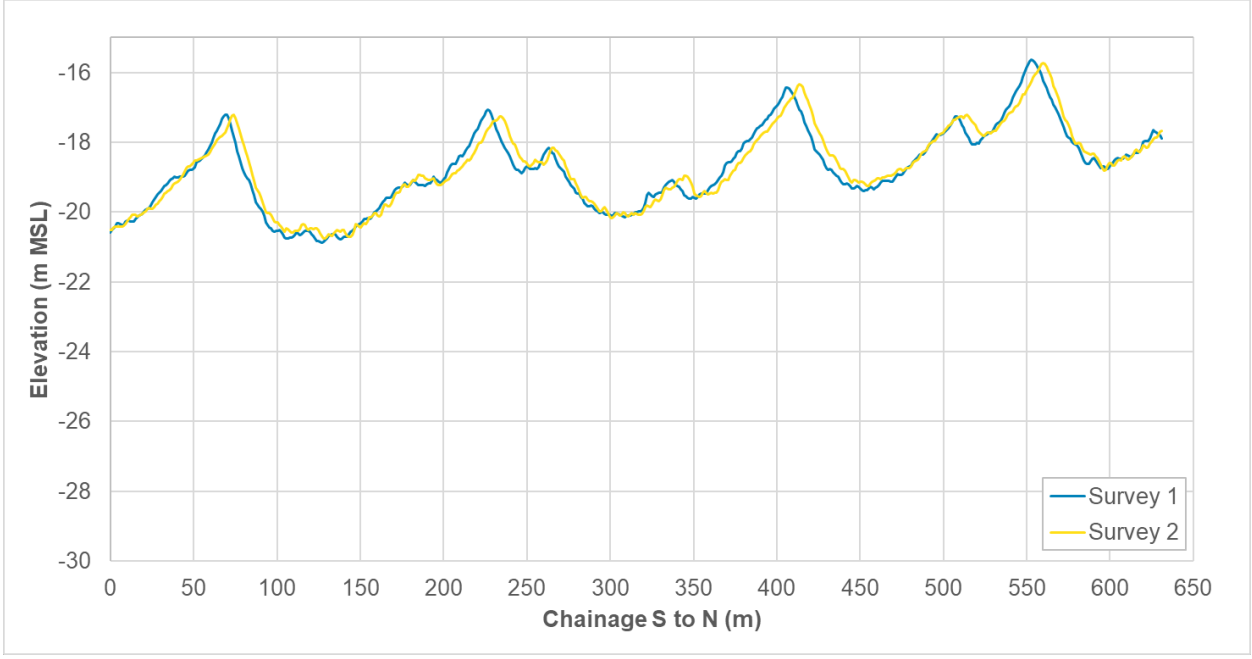

Figure 13. **Bathymetry at Transect 2a on 8th February 2024 (Survey 1) and 6th March 2024 (Survey 2).**

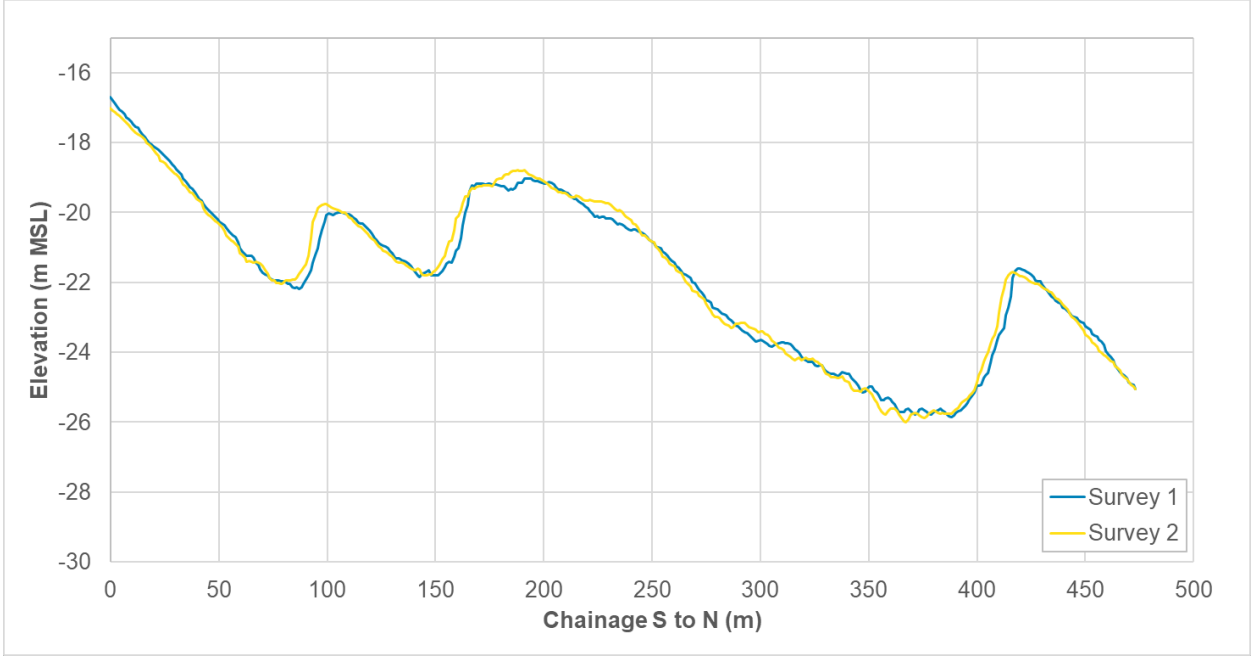

Figure 14. **Bathymetry at Transect 2b on 8th February 2024 (Survey 1) and 6th March 2024 (Survey 2).**

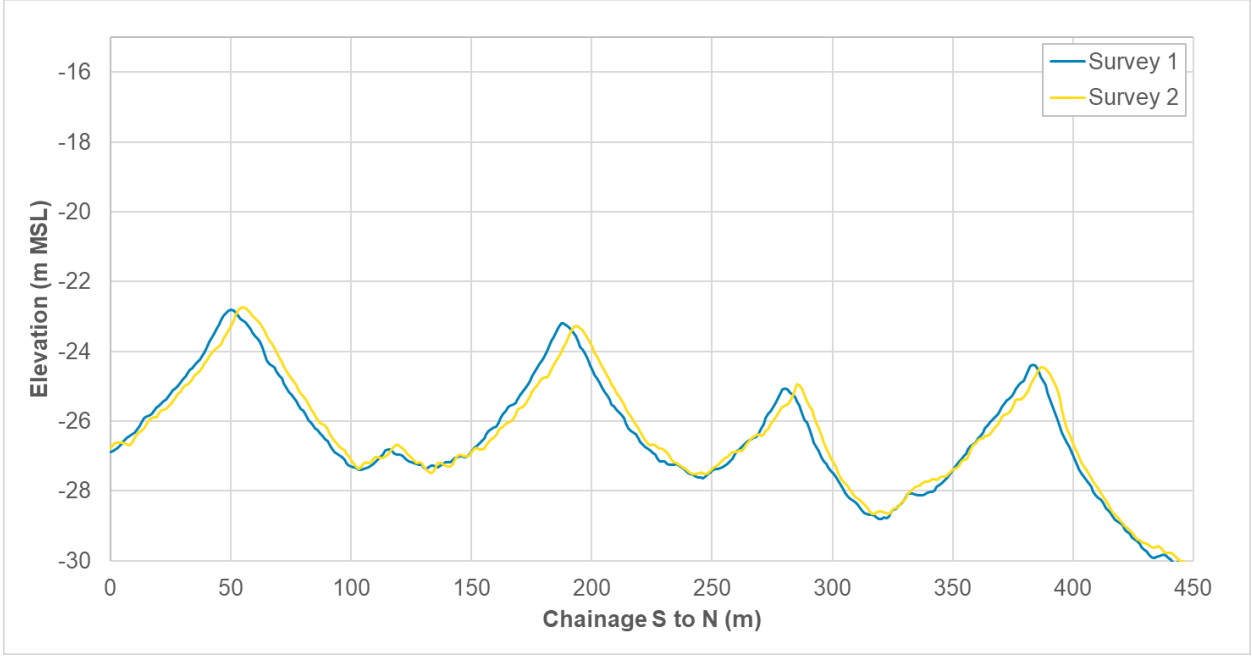

Figure 15. **Bathymetry at Transect 2c on 8th February 2024 (Survey 1) and 6th March 2024 (Survey 2).**

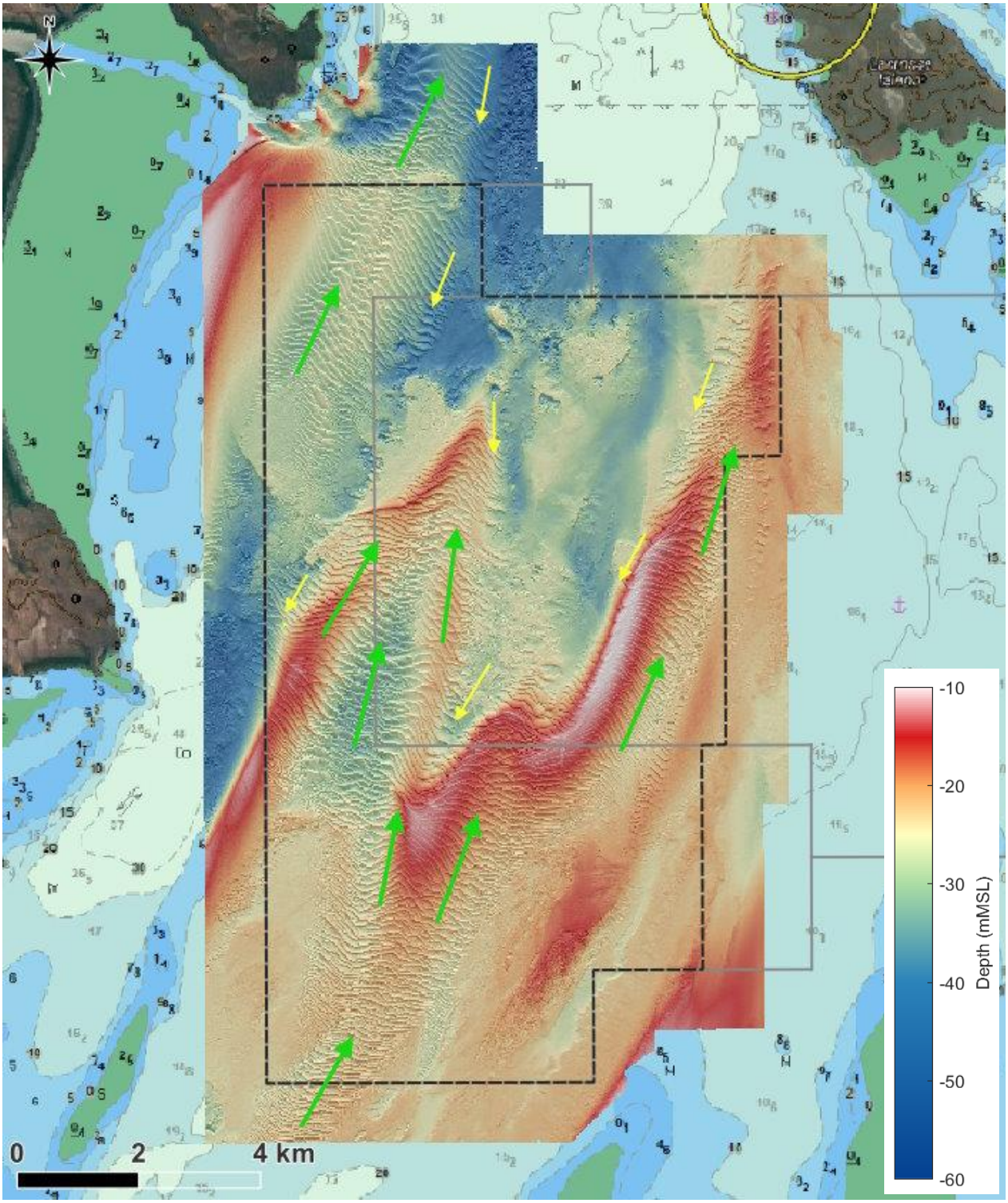

Figure 16. **Multibeam bathymetry in the proposed operational area along with predicted net bedload transport directions (green arrows = northerly transport, yellow arrows = southerly transport).**

PORT & COASTAL SOLUTIONS

3. Sediment Sampling

3.1. Data Overview

The locations of seabed surface sediment grab samples collected in February 2024 are shown in Figure 17. A total of 74 sites were sampled extending offshore from King Shoals, within and around CG including the inlets, creeks and small rivers on both sides of the gulf, and upstream (south) to where the Durack and Pentecost Rivers join the West Arm. The following laboratory analysis was undertaken on the sediment samples by NATA accredited Microanalysis laboratories in Perth (www.microanalysis.com.au):

- PSD analysis: All 74 samples were wet sieved to separate particles larger than 500 µm. Any particles larger than 500 µm were subsequently analysed through wet sieving, while the particles finer than 500 µm were analysed through laser diffraction using a Mastersizer. For the laser diffraction analysis, a dispersing agent (sodium hexametaphosphate) was applied along with sonication to disperse any existing flocs or agglomerates. Following the analysis, the results from the coarser and finer fractions were combined to provide a complete PSD for all particle sizes in each sample.

- Feature analysis: Out of the 74 sample sites, a total of 45 sites were analysed using the SEM, as shown on Figure 17, with the sites with a higher percentage of clay-sized particles present not being analysed as the clay particles can prevent individual particles from being identified. A representative sub-sample was sieved at 500 µm, sonicated, dried and applied evenly to a double-sided carbon tab and then carbon coated. The sample was then analysed using a Carl Zeiss EVO 50 SEM fitted with an Oxford INCA X-Max energy dispersive spectrometer (EDS). Image acquisition, image processing and a compositional analysis was undertaken using the Oxford Instruments Feature software.

PSD results using the same approach as detailed above for surface sediment samples collected within Block 4 (DMIRS E8-/5655) as part of the vibro-coring undertaken in March 2023, have also been used to provide additional data within the proposed operational area. The locations of these samples are shown in Figure 18 along with the locations of samples collected in the February 2024.

3.2. Results

The sediment type, based on the Shepard (1954) classification as modified by Schlee (1973), for all the available surface sediment samples, is shown in Figure 19 and Figure 20. The results show that the sediment in CG is predominantly classified as sand, except for in the inlets, creeks and small rivers around CG where sandy silt, silty sand, sand-silt-clay and gravelly sediment can all be present. Gravelly sediment and gravel were also present in a number of locations throughout the main bay in CG.

- One sample in the West Arm (the majority of samples in this area are sand).
- Multiple samples in the inlets, creeks and small rivers around CG in CG.
- Multiple samples within Block 4 (E80/5655) and at King Shoals.

Overall, the results show that sand is present throughout much of the region, with sand being the dominant sediment in the West and East Arms and in the main body of CG. The sand present in the region was predominantly made up of fine sand (43%) and medium sand (38%), with some coarse sand also present (12%). The sand present within the proposed operational area was predominantly made up of medium sand (50%) and fine sand (37%) with some coarse sand also present (8%). The sediment was more variable in the inlets, creeks and small rivers around CG, where most silt and clay was present as well as areas with gravel.

The SEM elemental feature analysis showed that in total, 31 different elements are present in the analysed samples. However, four of these were classified as agglomerates which contained multiple different elements (silicate, halite, titanium phase, calcite and iron), although the order of the minerals specified by the SEM indicates the dominance of the minerals in the agglomerate. The agglomerates were generally present as a result of clay-sized particles encasing larger particles, meaning that the particles were not sufficiently separated to allow the individual particles of each element to be determined, although they could also be clasts from rocks which have not been broken down to individual minerals. A variety of preparation techniques were adopted by the laboratory to minimise the impact of this, including suspension, redeposition, sonication, dilution and filtration and multiple abstractions, but for some samples the agglomerated particles still represented a larger proportion of the sample.

Eight dominant elements were identified throughout all the samples. These had an average percent composition, based on the particle area, of more than 1% and a maximum percent composition throughout all samples of more than 5%. These elements were quartz, feldspar, magnesium aluminosilicate, titanium phase, calcite, calcium silicate and two agglomerates (silicate with halite (i.e. predominantly silicate) and calcite with halite and silicate (i.e. predominantly

calcite)). It is important to note that the silicate with halite agglomerate is predominantly made up of silicate and so could potentially represent significant amounts of quartz and feldspar particles.

To appreciate the relative importance of these elements, it is important to understand the terrestrial sediment in the catchments which drain into CG and where the elements are present. The catchments are predominantly made up of pre-Cambrian sandstones, with some Pleistocene sediments and felsic volcanic rock also present (Tyler, 1996; Sheppard et al., 2001).

Quartz is the most dominant mineral in sandstone due to its exceptional physical properties (hardness and chemical stability). Feldspar is the second most abundant mineral but it is much more susceptible to abrasion and chemical weathering compared to quartz, which results in the particles typically being reduced down to clay-sized particles. In addition, both the Pleistocene sediments and felsic volcanic rock are likely to be made up of predominantly quartz and feldspar particles.

As well as quartz and feldspar, terrestrial sandstone can also include lithic framework grains (ancient source rock which is yet to weather down to individual particles) which can include clasts from volcanic rock, accessory grains which can be made up of different minerals and cement which can be silicate minerals or non-silicate minerals such as calcite, gypsum or clay.

Clay minerals are mainly known as being complex silicates which include various ions such as aluminium, magnesium and iron. For example, magnesium aluminosilicate is a smectite clay, which is typically formed from the weathering or chemical breakdown of igneous and metamorphic rocks. Titanium can also be present in igneous and metamorphic rocks as an accessory mineral, and so is likely to be formed by the weathering or chemical breakdown of these rock types.

Calcium silicate is from limestone and diatomaceous fossil beds, while calcite is a common constituent of sedimentary rocks and much of it is formed from the protective calcite shells of dead marine organisms.

Halite is a chemical sediment which forms in very arid environments through evaporation. Trace amounts of this mineral could be present from residual seawater present in the samples, although the samples were washed several times to remove the salts.

To better understand how the elemental composition of the sand present in the region varies spatially, a selection of samples from upstream in the West and East Arms to King Shoals made up of predominantly sand-sized sediment (> 90% sand-sized sediment based on the PSD results) have been analysed. The composition of the sediment based on the eight dominant elements is shown in Figure 21. The plot shows the following.

- At the upstream end of the West Arm, the sediment was predominantly made up of quartz with some feldspar also present (88% quartz, 8% feldspar). In the East Arm, the sediment was also predominantly made up of quartz, but with a higher percentage of feldspar (60% quartz, 30% feldspar). Magnesium aluminosilicate was also present in both locations, but with a higher percentage in the East Arm (9% compared to 1%). The West Arm also had small quantities of titanium phase and agglomerates with calcite, halite and silicate (1% for both). The results suggest that the sediment from these two potential upstream sources is not identical, but that both are dominated by quartz particles while feldspar particles have the second highest percentages. As both quartz and feldspar are known to be present in high percentages in the catchments which drain into CG, the sediment in these locations can be assumed to be supplied from the upstream catchments.

- At the confluence of the West and East Arms, the sediment composition is still dominated by quartz and feldspar particles (66% quartz, 19% feldspar). In addition, an agglomerate of silicate with halite is also present (14%) along with traces (<1%) of magnesium aluminosilicate and titanium phase. The sediment in this location can be considered to be representative of a combination of sediment from both the West and East Arms, and if the agglomerate of silicate with halite is considered to be predominantly silicate, then this is also likely to be predominantly quartz or feldspar particles. The halite present in the agglomerate could be a result of the adjacent intertidal and supratidal areas promoting the formations of halite, or due to residual saltwater present in the samples.

- Where the West Arm joins CG, the sediment composition is similar to at the confluence of the West and East Arms, with quartz and feldspar particles still present (63% quartz, 15% feldspar) along with the agglomerate of silicate with halite (18%). This agglomerate is likely to be predominantly made up of quartz or fledspar, meaning that the total percentage of these two minerals present will be higher. This suggests that the sediment from these two locations is from the same upstream source, showing that sediment is being imported into CG from upstream and that limited additional sediment input has occurred between the confluence and the upstream entrance to CG.

- The sediment composition in the central part of CG and at the southern end of the proposed operational area are similar, with the majority of the sediment made up of quartz (approximately 60%), followed by calcite, halite and silicate agglomerates (approximately 30%) and then feldspar (approximately 7%). The remainder of the sediment

is made up of magnesium aluminosilicate and titanium phase, with a trace of calcite (<1%) also present in the central CG. The agglomerate in this region is predominantly made up of calcite minerals. These were not present in the upstream samples which suggests that they are from a different source. The similarity of the sediment at the central CG and at the southern end of the proposed operational area, combined with the generally similar composition to where the West Arm joins CG, indicates that the sediment throughout the southern and central areas of CG is predominantly from an upstream source, although the agglomerate with calcite is likely from a different source.

- The composition of the sediment in CG close to the western and eastern entrances is variable, with a much higher percentage of quartz close to the eastern entrance compared to the western entrance (73% compared to 45%). The western entrance has a higher percentage of feldspar present (11% compared to 1%) and a higher percentage of calcite, halite and silicate agglomerate (28% compared to 8%). Both sites have some magnesium aluminosilicate present (1% and 5%), while only the western entrance has a trace amount of titanium phase (<1%). Both sites have a significantly higher percentage of calcite present than elsewhere in CG (12% and 5%) and the eastern entrance also has calcium silicate present (3%) which is not present elsewhere in CG. The higher percentage of calcite, calcium silicate and agglomerates with calcite, halite and silicate at these locations (combined 33% at the western entrance and 23% at the eastern entrance) than elsewhere in CG, suggests an offshore source for these particles, indicating that a quarter to a third of the sediment present at these locations is transported into CG from offshore. The higher percentage of quartz presence at the eastern entrance, combined with the higher percentage of calcite (and the agglomerate with calcite) at the western entrance, indicates that more offshore particles are imported through the western entrance than the eastern entrance.

- The sediment sample at King Shoals shows a significant reduction in quartz and feldspar particles compared to within CG, with 23% quartz and 1% feldspar. In addition, the percentage of the calcite with halite and silicate agglomerate is significantly higher than at any other sites (46%), with this agglomerate being predominantly made up of calcite. Similar to the sediment in CG close to the western and eastern entrances, the sediment at King Shoals also had calcite (4%) and calcium silicate (9%) present, while none of the samples from the upstream area of CG contained these particles. The combined amount of the calcite agglomerate along with calcite and calcium silicate at the King Shoals sample was 59%, indicating that the majority of the sediment at King Shoals could be from an offshore source rather than from within CG. The sample also has a higher percentage of titanium phase compared to all samples in CG, except one (central CG which also had 4%). Titanium minerals are resistant to weathering and so have the potential to become more concentrated over time in sands in higher energy coastal environments, suggesting that titanium minerals from CG could have built up in King Shoals resulting in a higher percentage present in this area compared to within most of CG. The King Shoals sample suggests that the majority of the sediment in this area could be from an offshore source as opposed to it being from within CG.

The results above show that the dominant minerals supplied from the upstream catchments into CG are quartz and feldspar, while the minerals which are likely to be from an offshore source are calcite and calcium silicate. To show how the elemental composition of the sediment from the upstream catchment and from offshore vary spatially, the combined percentage of quartz and feldspar, along with the combined percentage of calcite and calcium silicate present, are shown in Figure 22 and Figure 23. It is important to note that the agglomerates identified by the SEM feature analysis also contain quartz, feldspar and calcite, and so not all of these minerals present are represented by the maps, but they can however be considered to provide an overview of the spatial trend in these minerals (as the presence of these minerals aligns with the presence of the individual minerals). The plots show the following.

- The sediment in the West and East Arms and in the main body of CG up to the northern half of the proposed operational area, is predominantly made up of quartz and feldspar (>60%), with the highest percentages present in the West and East Arms and in the creek at the eastern side of CG, potentially indicating that these could all be sources of the minerals. The samples show that the sediment close to the western entrance to CG and at King Shoals had lower percentages of quartz and feldspar present, with 40 to 60% present at the northern end of the proposed operational area and 20 to 40% present at the sample at King Shoals to the northwest of the entrance to CG. A reduction in feldspar percentage from the upstream source to King Shoals is expected, as the mineral is prone to ongoing weathering which reduces the particle size and therefore increases the time the particles remain in suspension, as well as limiting the locations where it will accumulate to sheltered areas with low current speeds and small waves.

- The samples throughout CG show a low percentage of calcite and calcium silicate, except near to the western and eastern entrances, where the percentage increases to above 5%. The samples at King Shoal also all show percentages of more than 5%. Even though it is possible that the percentage of calcite present in the samples could be higher than shown, with some calcite potentially present in the agglomerates, the sites with the agglomerate which contains calcite were limited to those from the central CG to the north (with the highest percentages close to the western entrance of CG and in King Shoals). Therefore, the results still show an increasing amount of calcite from the central CG in an offshore direction. Based on the fact that there is no calcite or calcium silicate present in the bed sediment in the West or East Arms, it can be concluded that these minerals present in

the bed sediment are from an offshore source and the calcite and calcium silicate present in CG are from the import of offshore sediment through the western and eastern entrances.

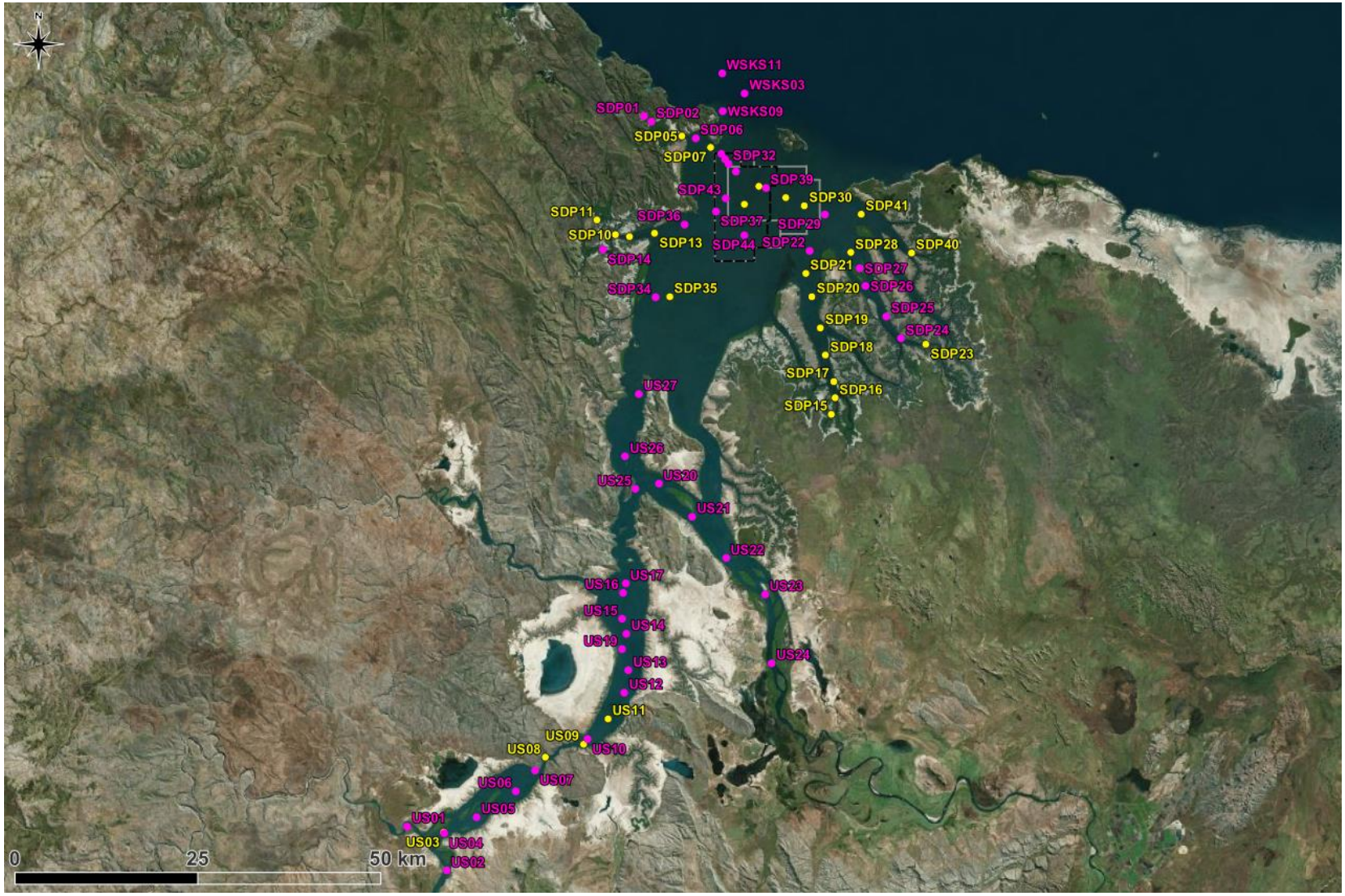

Figure 17. **74 seabed surface sediment samples collected during the 2024 wet season campaign (February 2024) analysed for just PSD (yellow dots) and analysed for PSD and elemental features (pink dots).**

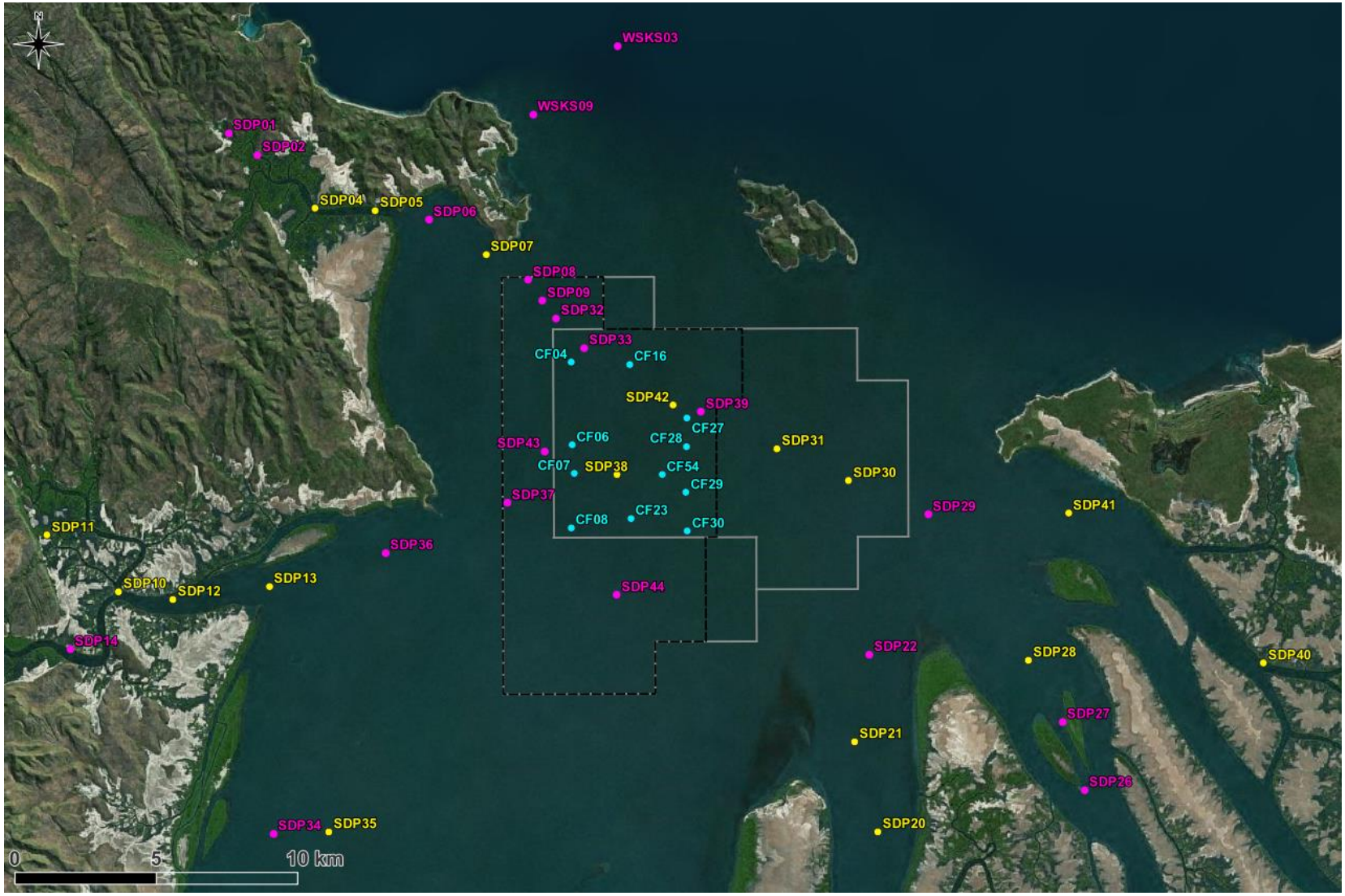

Figure 18. **Close up of the seabed surface sediment samples collected in CG in February 2024 wet season campaign (analysed for just PSD (yellow dots) and analysed for PSD and elemental features (pink dots)) along with seabed surface sediment samples collected in March 2023 (blue dots).**

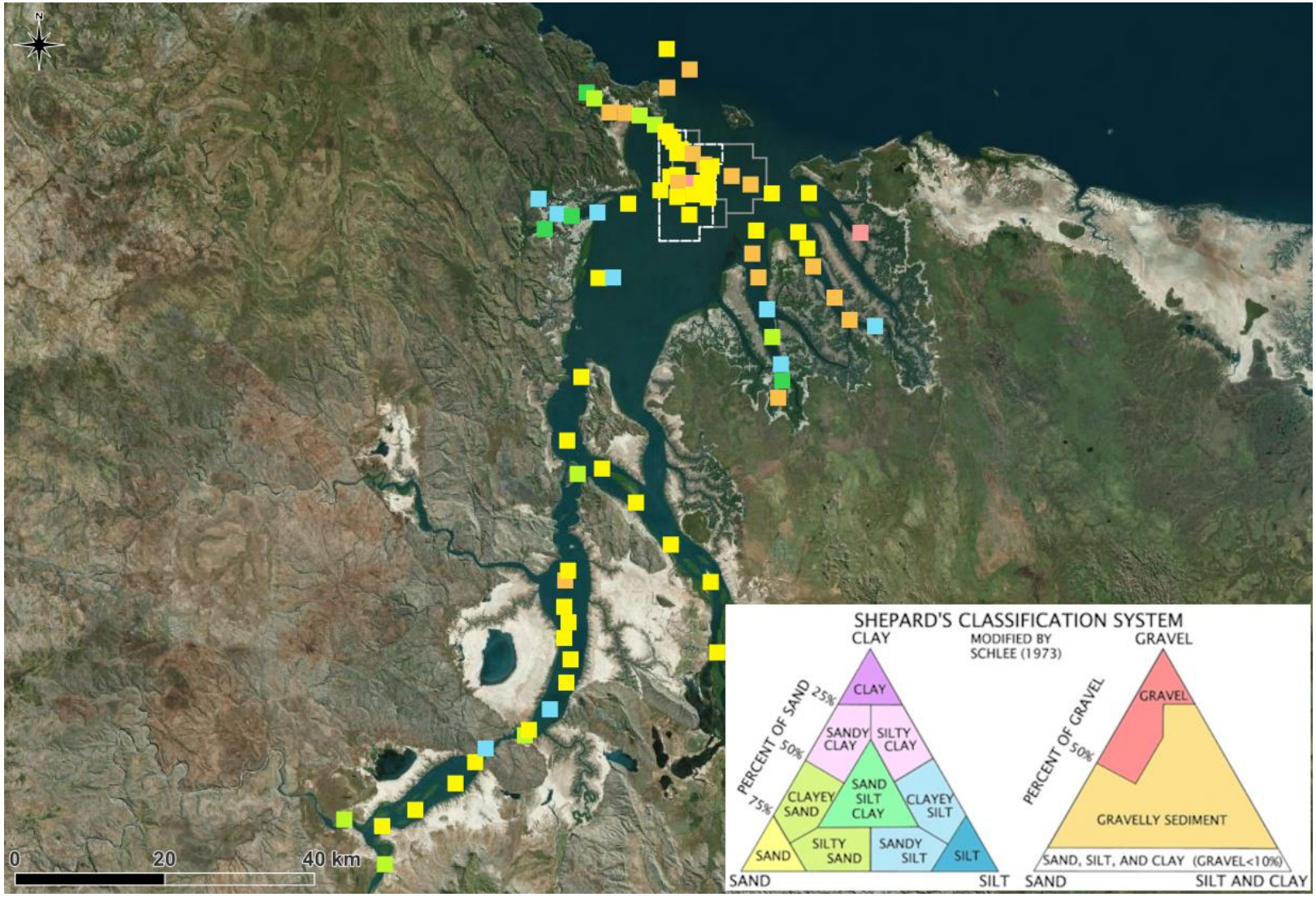

Figure 19. Map showing sediment type for all samples based on Shepard's classification system using the percentage of clay, silt, sand and gravel in the sample.

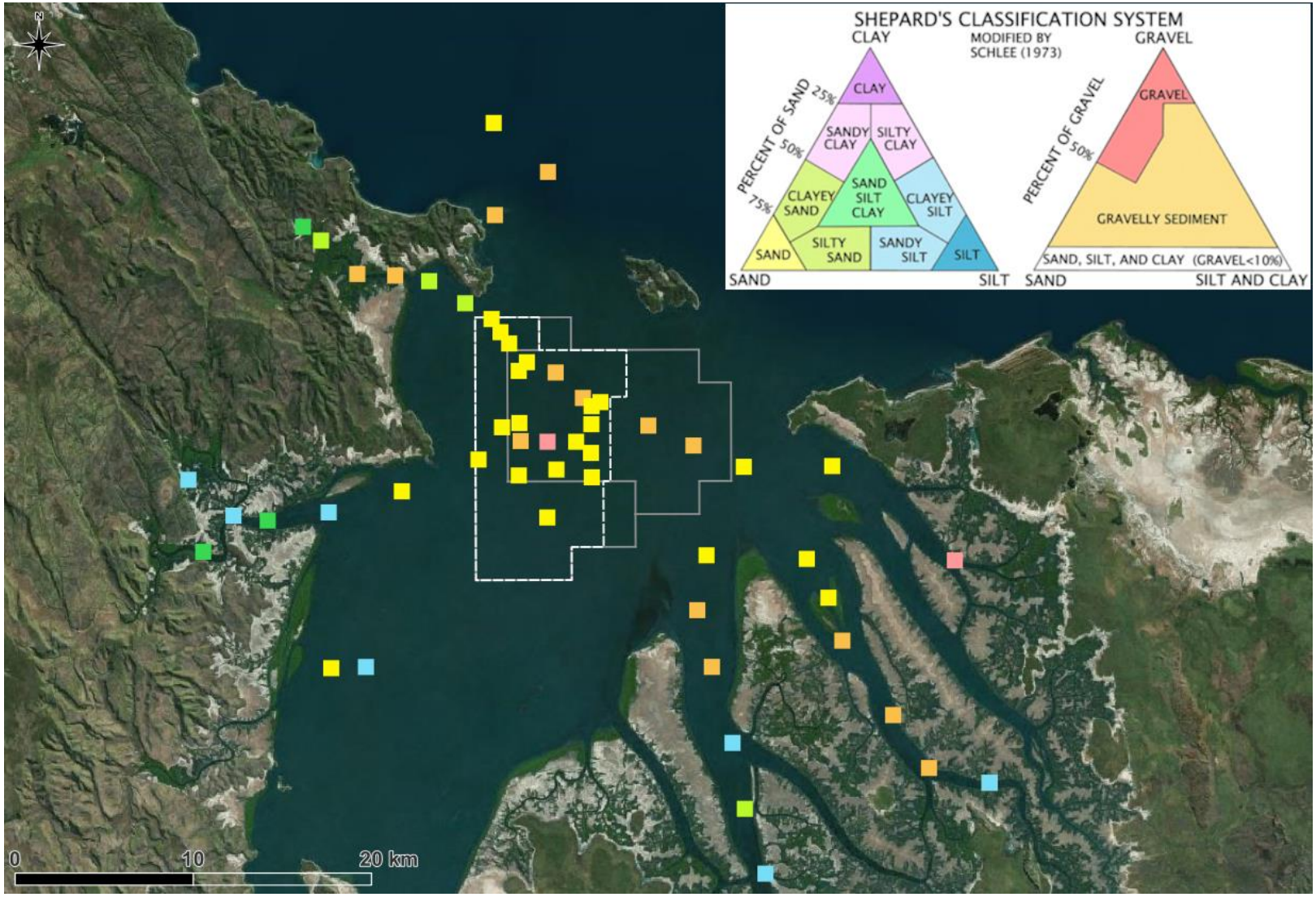

Figure 20. Close up map of CG showing sediment type based on Shepard's classification system using the percentage of clay, silt, sand and gravel in the sample.

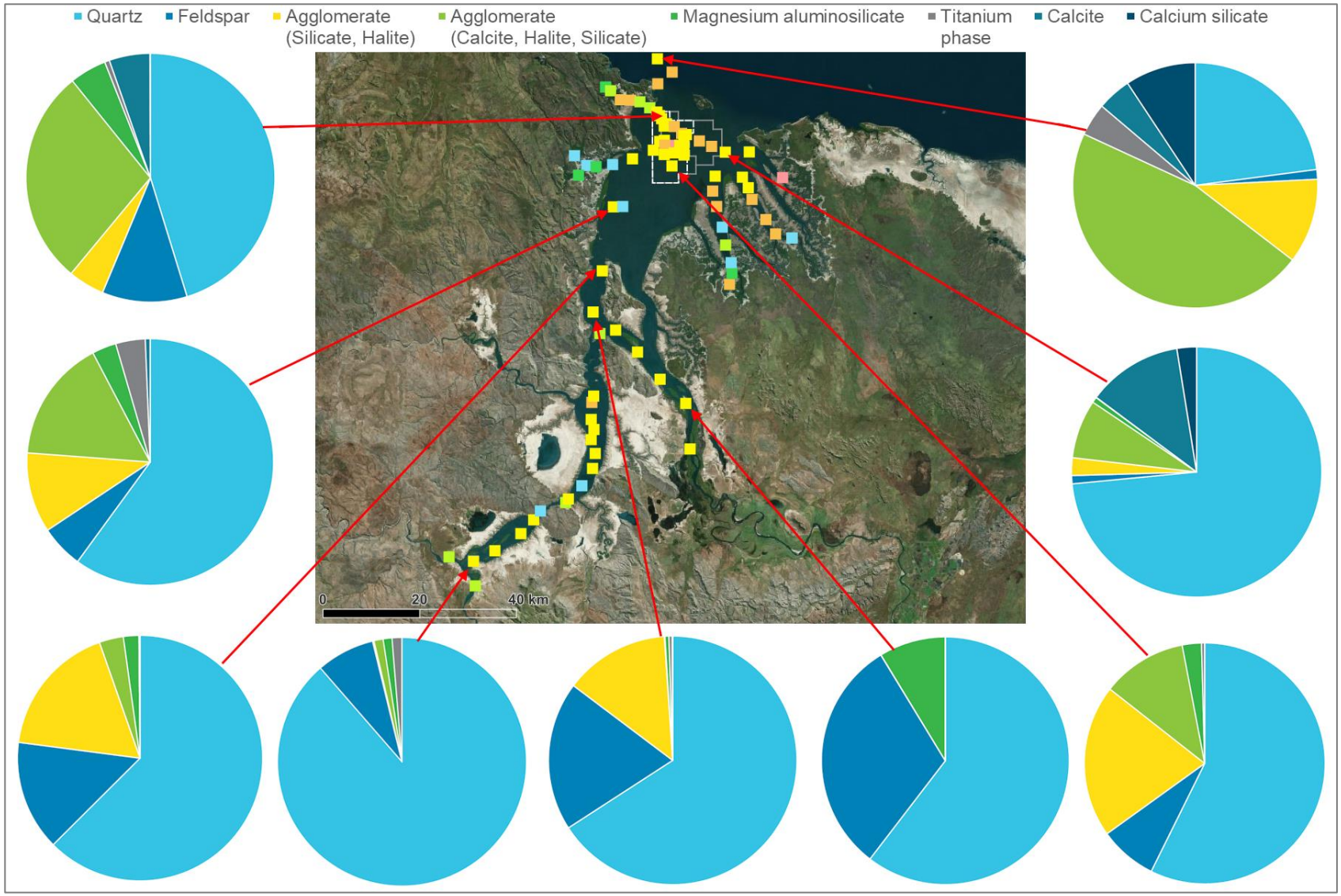

Figure 21. Selected elemental feature results from the SEM shown relative to the sediment classification map.

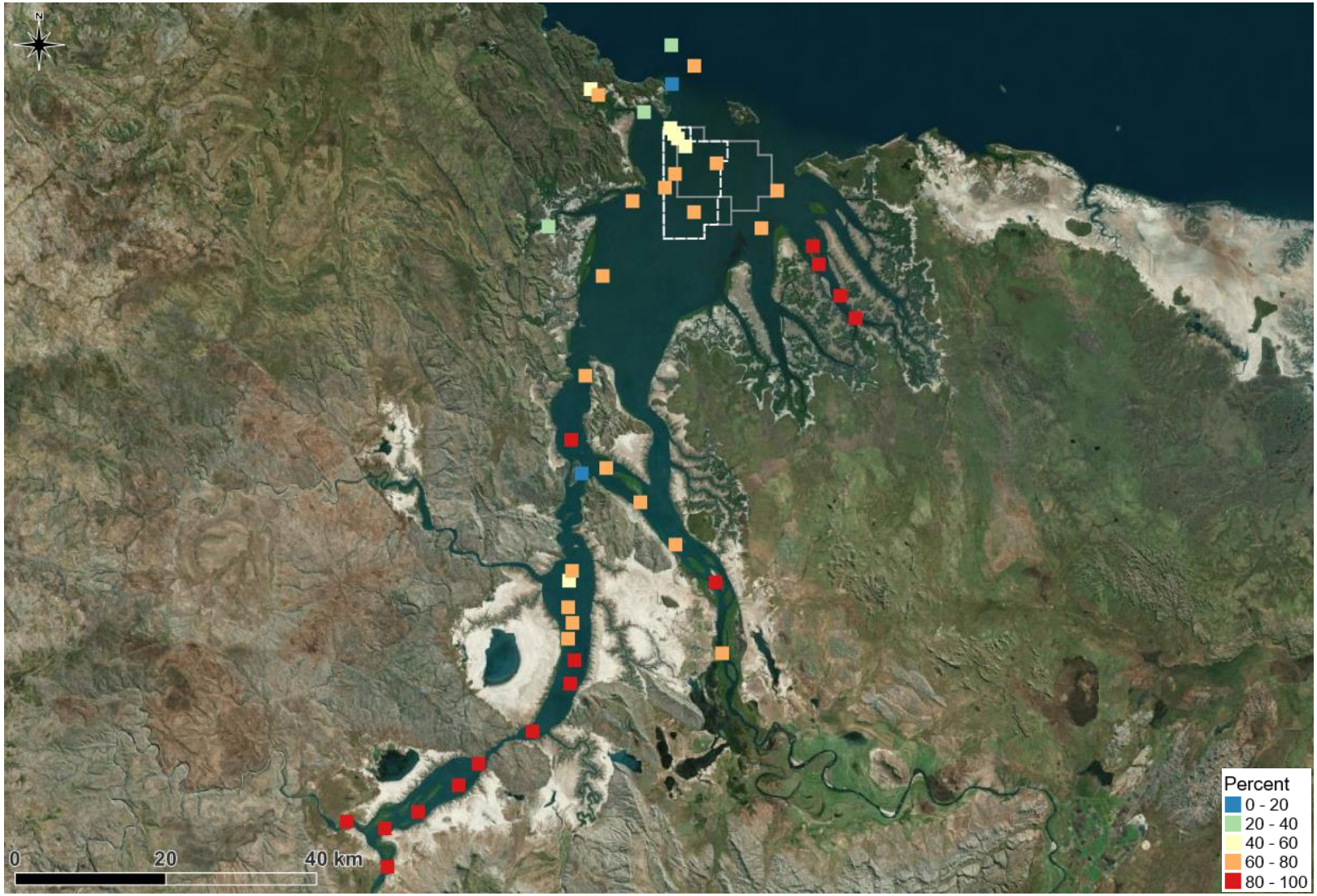

Figure 22. Map showing combined percentage of quartz and feldspar present in the sediment samples.

Figure 23. Map showing combined percentage of calcite and calcium silicate present in the sediment samples.

4. Water Column Profiling

4.1. Data Overview

The three sites where hourly water column profiling over a 13-hour spring tidal cycle was undertaken, are shown in Figure 24. Each of the three sites coincides with where BKA has also deployed AWACs on the seabed as part of a separate data collection campaign, hence the equivalent AWAC site numbers next to each profiling site number. Details of each site are provided below.

- Site 1, AWAC01: This site is located in the northern half of the proposed operational area in a water depth of around -30 m MSL. The site is in an area with a relatively flat seabed which is likely to be predominantly rock or consolidated clay, although sediment sampling has shown that some surface sediment can be present. The profiling was undertaken on the 24th February 2024, with the 1st drop at low tide at 11:53 and the 13th drop at the following low tide at 23:30. The predicted tidal range at Cape Domett for the profiling was 5.24 m. At Cape Domett, the mean spring tidal range is 5.4 m and mean neap tidal range is 2.0 m[1], meaning that the tide when the profiling was undertaken was just below a mean spring tide.

- Site 2, AWAC05: This site is located at the western entrance to CG, just north of the proposed operational area, in a water depth of around -30 m MSL. The site is in an area where sand waves are present, meaning that the bed sediment is predominantly sand. The profiling was undertaken on the 25th February 2024, with the 1st drop at low tide at 12:30 and the 13th drop at the following low tide at 00:00. The predicted tidal range at Cape Domett for the profiling was 5.45 m, meaning that the tide was just above a mean spring tide.

- Site 3, AWAC11: This site is located to the south of the proposed operational area in a water depth of around -21 m MSL. The site is in an area where sand waves are likely to be present, meaning that the bed sediment is expected to be predominantly sand. The profiling was undertaken on the 27th February 2024, with the 1st drop at low tide at 13:37 and the 13th drop at the following low tide at 01:00 (on 28th February). The predicted tidal range at Cape Domett for the profiling was 5.42 m, meaning that the tide was just above a mean spring tide.

The following instruments were attached to a frame and used to collect data during the water quality profiling (Figure 25).

- YSI Multi-Sonde Probe: The multi-sonde collected measurements of depth, temperature, salinity, pH, chlorophyll and turbidity every second.

- Nortek Aquadopp Deepwater: The Aquadopp collected current speed, current direction and pressure data every 5 seconds.

- Niskin Water Sampler: Water samples were collected during each vertical profile using Niskin water samplers at mid depth and near the seabed. The water samples were then chilled and freighted to the laboratory to be analysed for TSS and PSD. An elemental feature analysis of the samples collected at low water and high water was also undertaken using a SEM (see Section 3.1 for details of SEM method).

For each vertical profile, the frame was slowly lowered through the water column until it reached the middle of the water column and the frame was left at this depth for at least 60 seconds while a water sample was collected and while the Aquadopp measured the currents without any vertical change. The frame was then slowly lowered to the seabed and it was left at this depth for a further 60 to 120 seconds while a second water sample was collected and while the Aquadopp measured the near bed currents. The frame was then lifted back through the water column and retrieved on the vessel. The data from the downward drop of the frame has been analysed.

The vertical profile data were processed to show how the measured parameters varied through the water column during each vertical profile. The times when the instruments remained at the same depth were removed from the dataset, so the data represents a continuous vertical profile. In addition, results from the mid water column and near-bed were extracted from each vertical profile, to show how the measured parameters varied over time at each site. The Aquadopp current data were averaged for the periods the instruments remained stationary at the mid water column and near-bed to also provide time series of current speed and direction over the duration of the profiling at each site.

[1] The predicted water levels and tidal planes at Cape Domett are based on limited data (116 days) and the data were collected over 50 years ago (1972). Therefore, the data are not as reliable as at other stations, but they are sufficient to provide an indication of the state in the spring/neap cycle that the water column profiling was undertaken during.

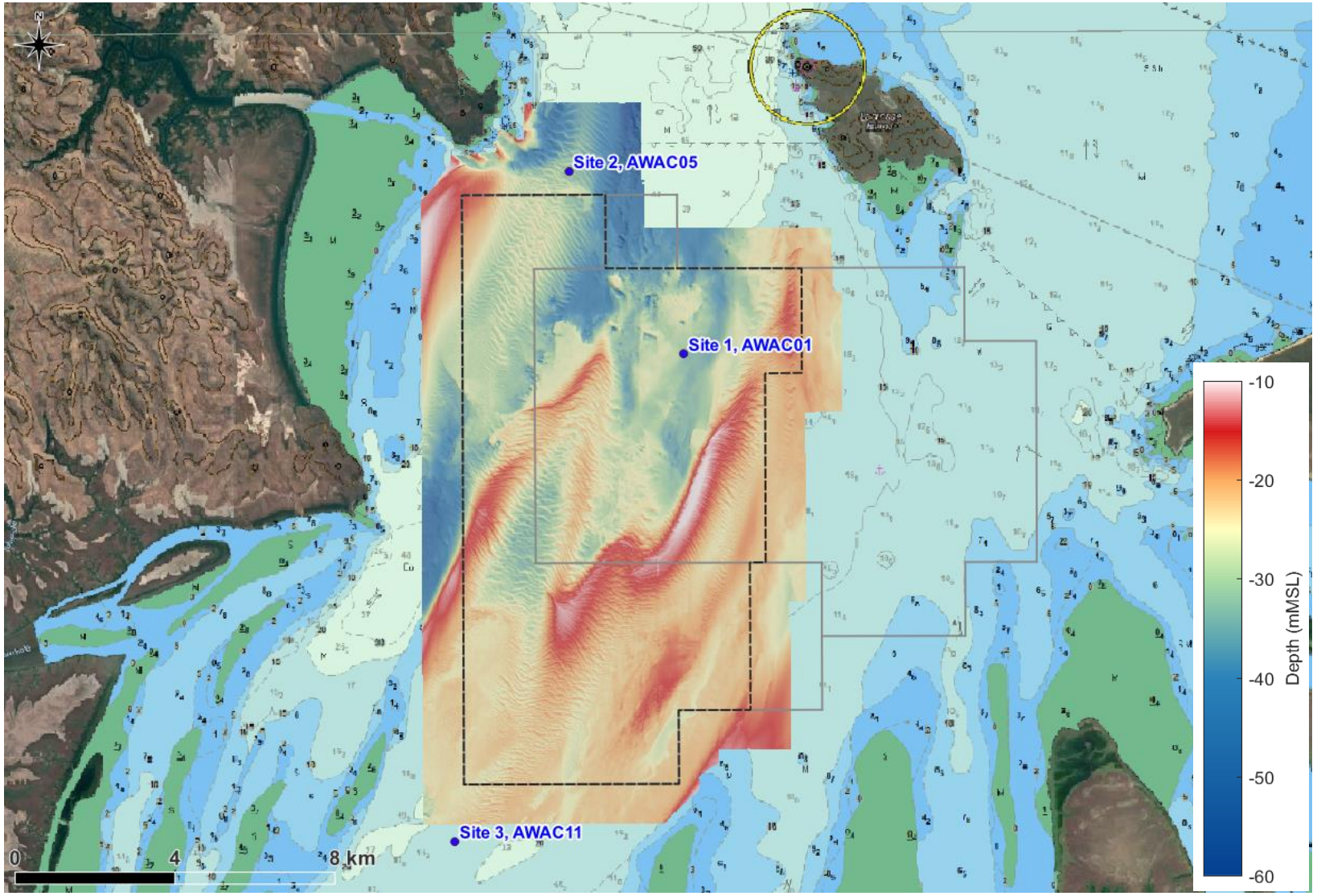

Figure 24. **Locations of the three water column profiling sites.**

Figure 25. **Setup for the water column profiling equipment. Included two Niskins, one near seabed above the Aquadopp and Multi-sonde frame (right image), and one at mid water (the midwater Niskin is shown in left image before deployment).**

4.2. Results

Vertical profiles of the water quality parameters at the three sites during specific stages of the tide are shown in Figure 26 to Figure 31. Plots of the vertical profiles for all stages of the tide at the three sites are included in Appendix A. In addition, time series plots of the water quality parameters over the duration of the profiling at mid and near-bed depths are shown for the three sites in Figure 32 to Figure 34.. The plots show the following.

- Temperature: Mean temperature for all data from all profiles was 31.1 ºC with a range of 30.8 ºC to 31.5 ºC. These are normal values for northern Australian coastal marine waters at this time of year. There was little variability in water temperature through the water column or through the tidal cycle at any of the three sites. The temperature remained at approximately 31ºC throughout.

- Salinity: Mean salinity for all data from all profiles was 30.8 Practical Salinity Units (PSU) with a range of 26.9 PSU to 32.5 PSU. These are normal values for tropical coastal marine waters. There was limited variability in the salinity through the water column, although at Site 3 during the flood stage of the tide, the salinity varied between the surface and the bed by up to 1 PSU (higher near the bed). At all three sites the salinity was shown to vary through the tidal cycle, with a lower salinity around low water and higher salinity around high water. The variation in salinity was smallest at Site 2, where it varied from 30.8 PSU at low water to 32.5 PSU at high water, and highest at Site 3, where it varied from 26.9 PSU at low water to 30.9 PSU at high water. The spatial variability in salinity between the sites is due to variations in the influence of low salinity freshwater inflows from upstream of CG and high salinity seawater from offshore of CG.

- Chlorophyll: Mean chlorophyll for all data from all profiles was 0.07 Relative Fluorescence Units (RFU) with a range of 0.02 RFU to 0.47 RFU. These are relatively low values for tropical coastal marine waters. Chlorophyll was low at all three sites (typically below 0.2 RFU) and uniform through the water column. The only exception to this was the second vertical profile at Site 1 where chlorophyll was up to 0.47 RFU in the upper 6 m of the water column and then less than 0.1 RFU below this.

- Turbidity: Mean turbidity for all data from all profiles was 15.2 Nephelometric Turbidity Units (NTU) with a range of 4.0 NTU to 55.6 NTU (Note: The YSI sonde collected data in FNU, which for YSI instruments gives the same values as NTU. The reported units are NTU as that is what has been historically used for marine assessments in WA). The higher values are high for tropical coastal marine waters. The turbidity at Sites 1 and 2 were similar, with values ranging between 5 and 20 NTU. Both sites typically showed a gradual increase in turbidity down the water column, with the near-bed turbidity being up to twice as high as the surface turbidity. The turbidity at Site 3 was higher than at the other two sites, with values ranging from 7.7 to 55.6 NTU. As with the other two sites, the turbidity typically increased down the water column, with differences in turbidity between the surface and near-bed of up to 25 NTU. The highest turbidity at Site 3 was 55.6 NTU and occurred around low water and the lowest turbidity was 7.7 NTU and occurred around high water. There was a reduction in turbidity during the second half of the flood stage of the tide and an increase in turbidity during the second half of the ebb stage of the tide at Site 3. This shows that the higher turbidity occurred due to the ebbing tide, meaning that the suspended sediment causing the higher turbidity was transported from upstream of Site 3.

- Currents: Mean current velocity for all data from the mid depth and near-bed data (when the instrument was stationary in the water column) for all profiles was 0.55 metres per second (m/s) with a range of 0.05 m/s to 1.22 m/s. The higher values are very high current velocities. Time series plots showing the measured current speed and direction over the duration of the profiling at the mid and near-bed depths are shown at the three sites in Figure 35 to Figure 37. The plots show that peaks in current speed occurred mid-way through the flood and ebb stages of the tide, with lower current speeds occurring around high water and low water (slack water), which is fully consistent with what would be expected. At Sites 1 and 2, the peak flood and ebb current speeds were approximately comparable (mid depth peaks of 1 m/s and near-bed peaks of 0.8 m/s). At Site 3 the ebb current speeds were higher both at mid depth and near-bed (1.2 m/s at mid depth and 1.0 m/s near-bed) while peak flood current speeds were 0.8 m/s at both depths.

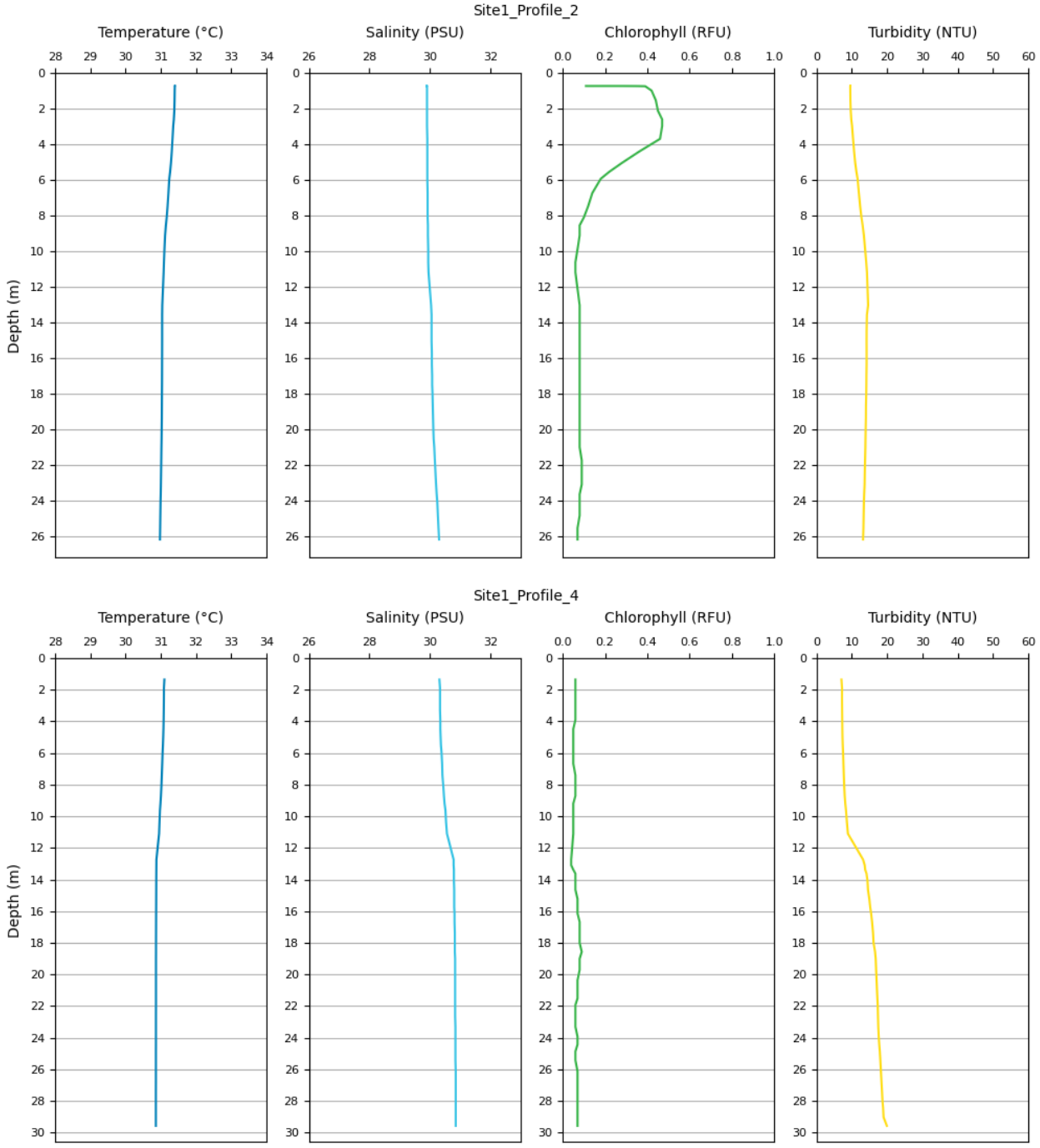

Figure 26. Measured temperature, salinity, chlorophyll and turbidity through the water column at Site 1 close to low water (top) and during the flood stage of the tide (bottom).

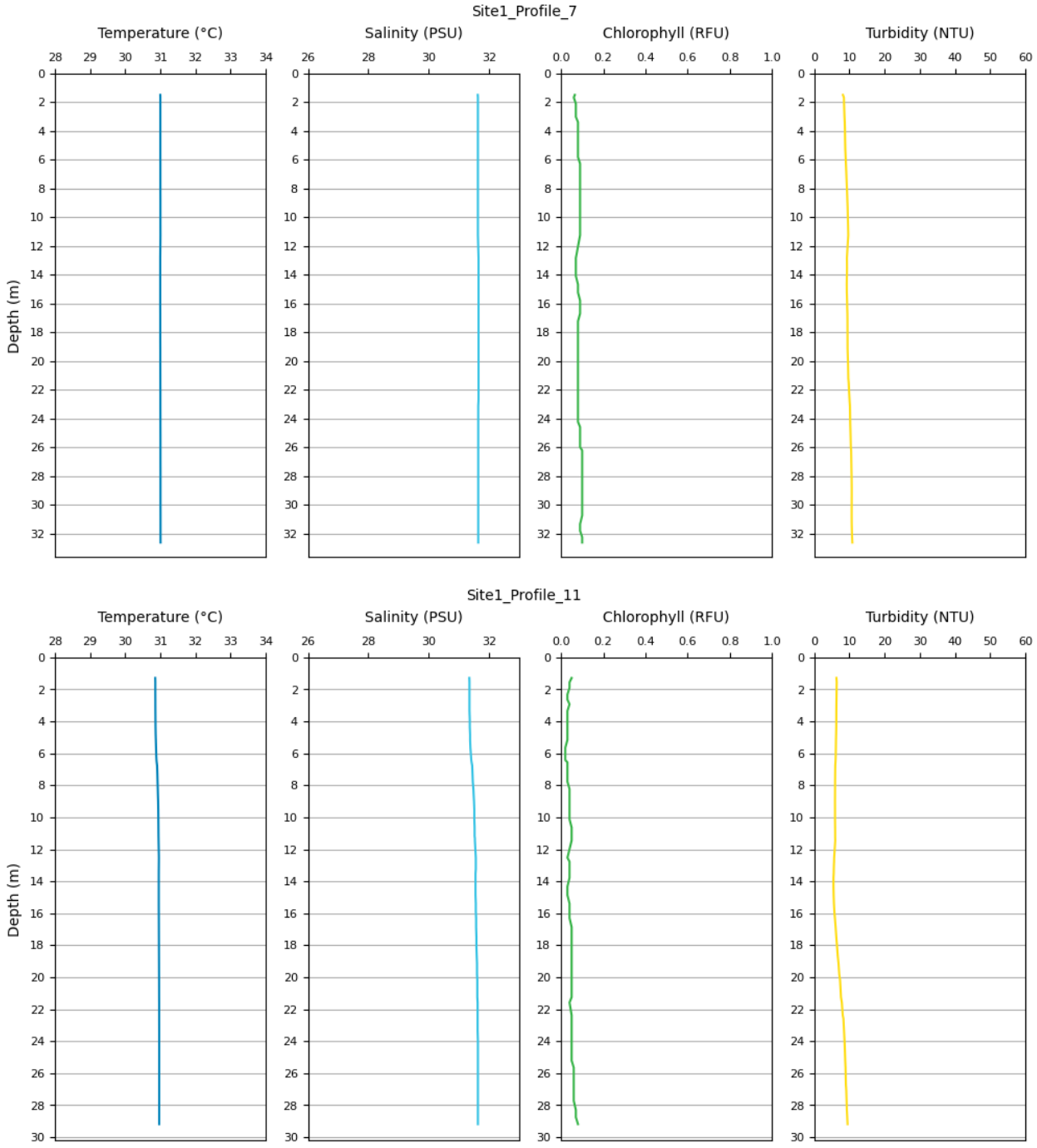

Figure 27. Measured temperature, salinity, chlorophyll and turbidity through the water column at Site 1 at high water (top) and during the ebb stage of the tide (bottom).

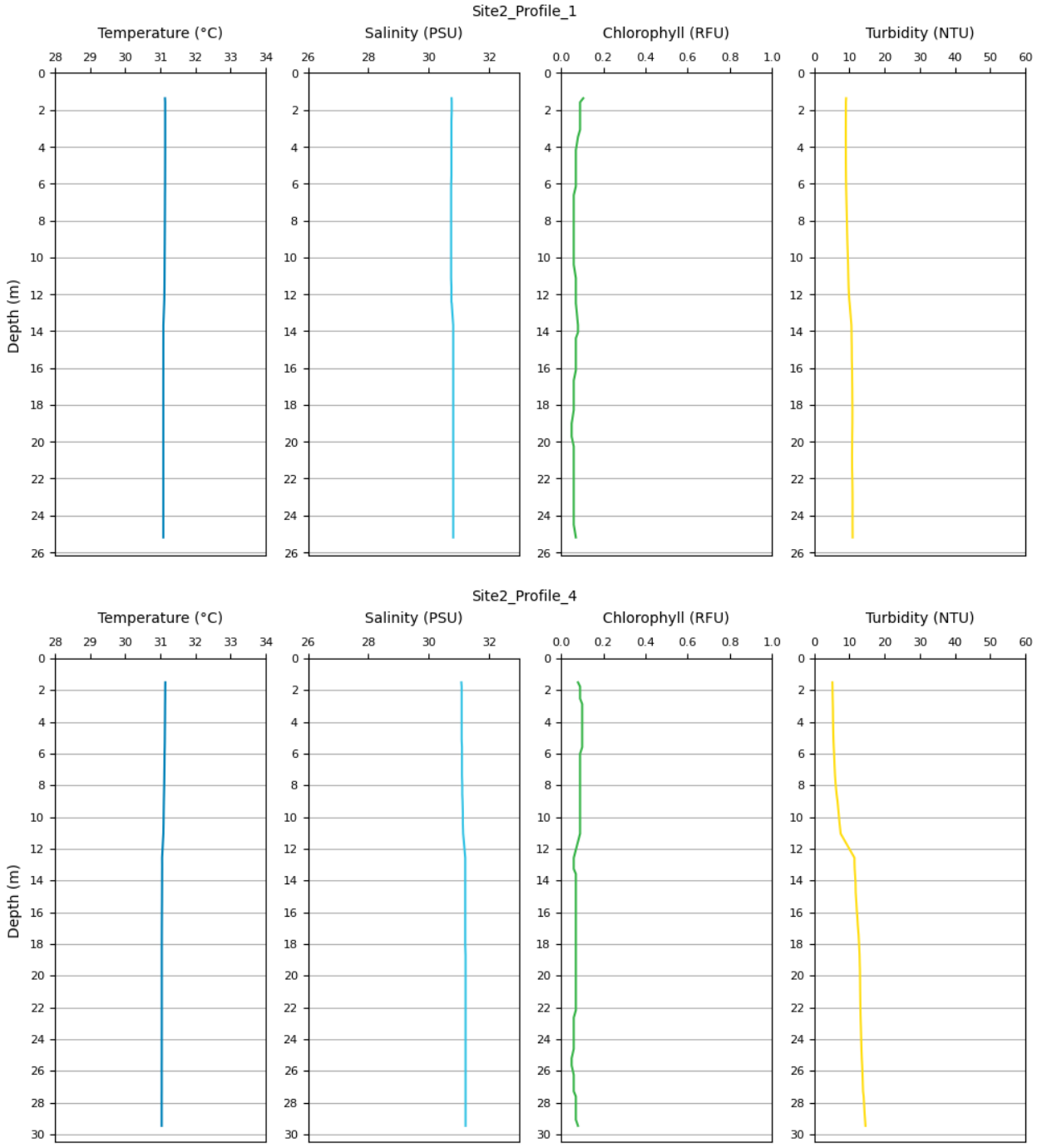

Figure 28. Measured temperature, salinity, chlorophyll and turbidity through the water column at Site 2 at low water (top) and during the flood stage of the tide (bottom).

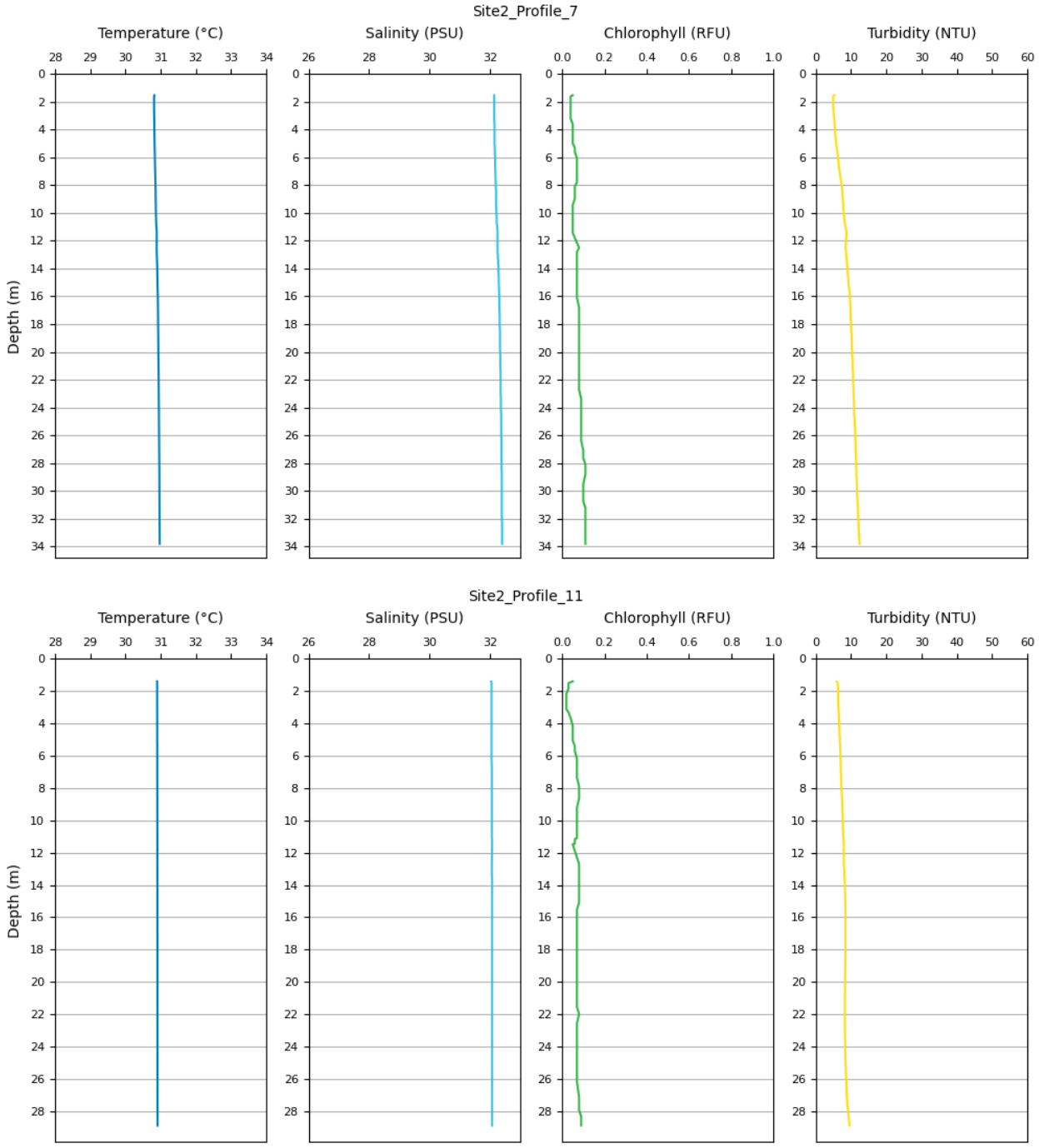

Figure 29. Measured temperature, salinity, chlorophyll and turbidity through the water column at Site 2 at high water (top) and during the ebb stage of the tide (bottom).

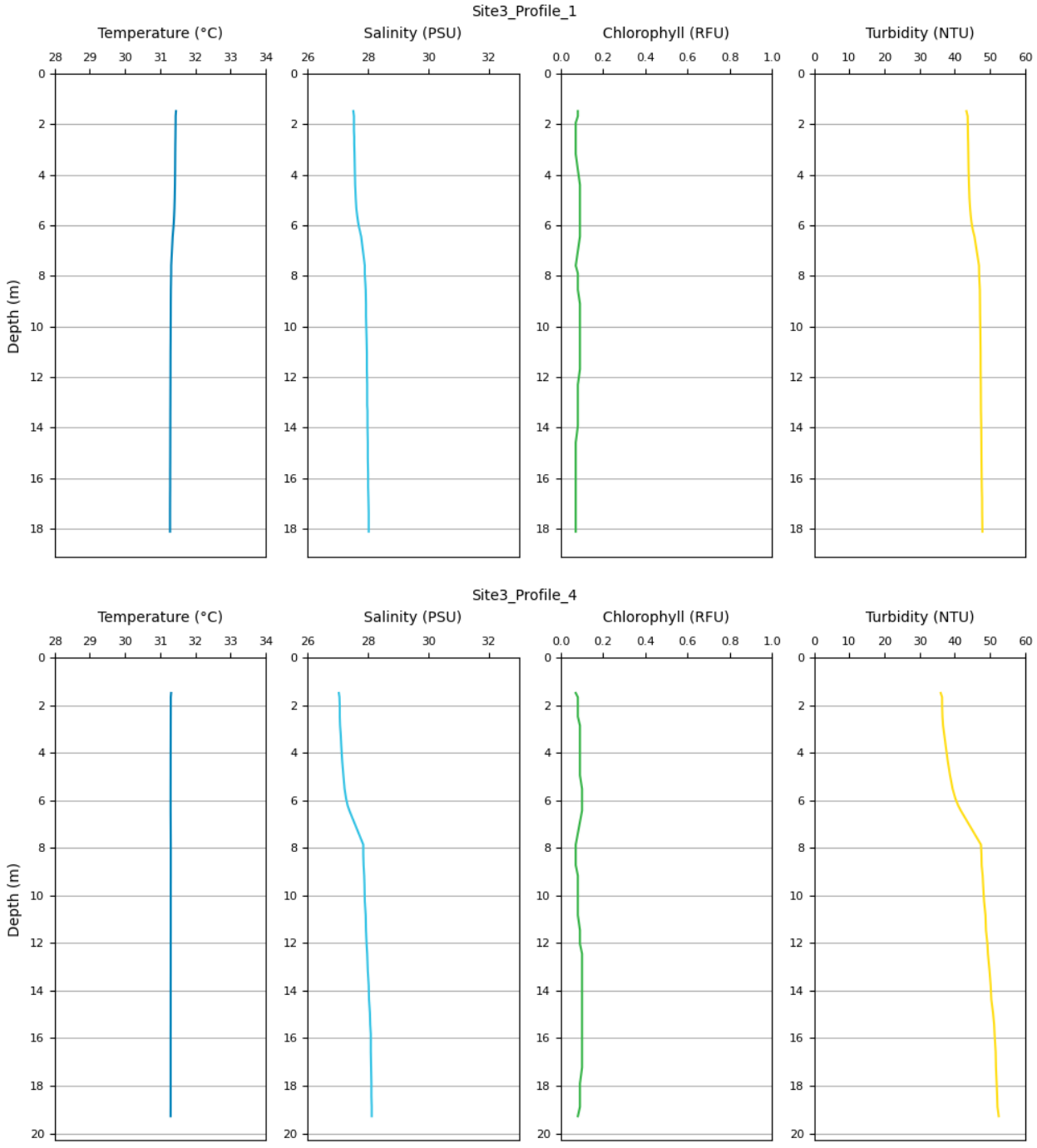

Figure 30. Measured temperature, salinity, chlorophyll and turbidity through the water column at Site 3 at low water (top) and during the flood stage of the tide (bottom).

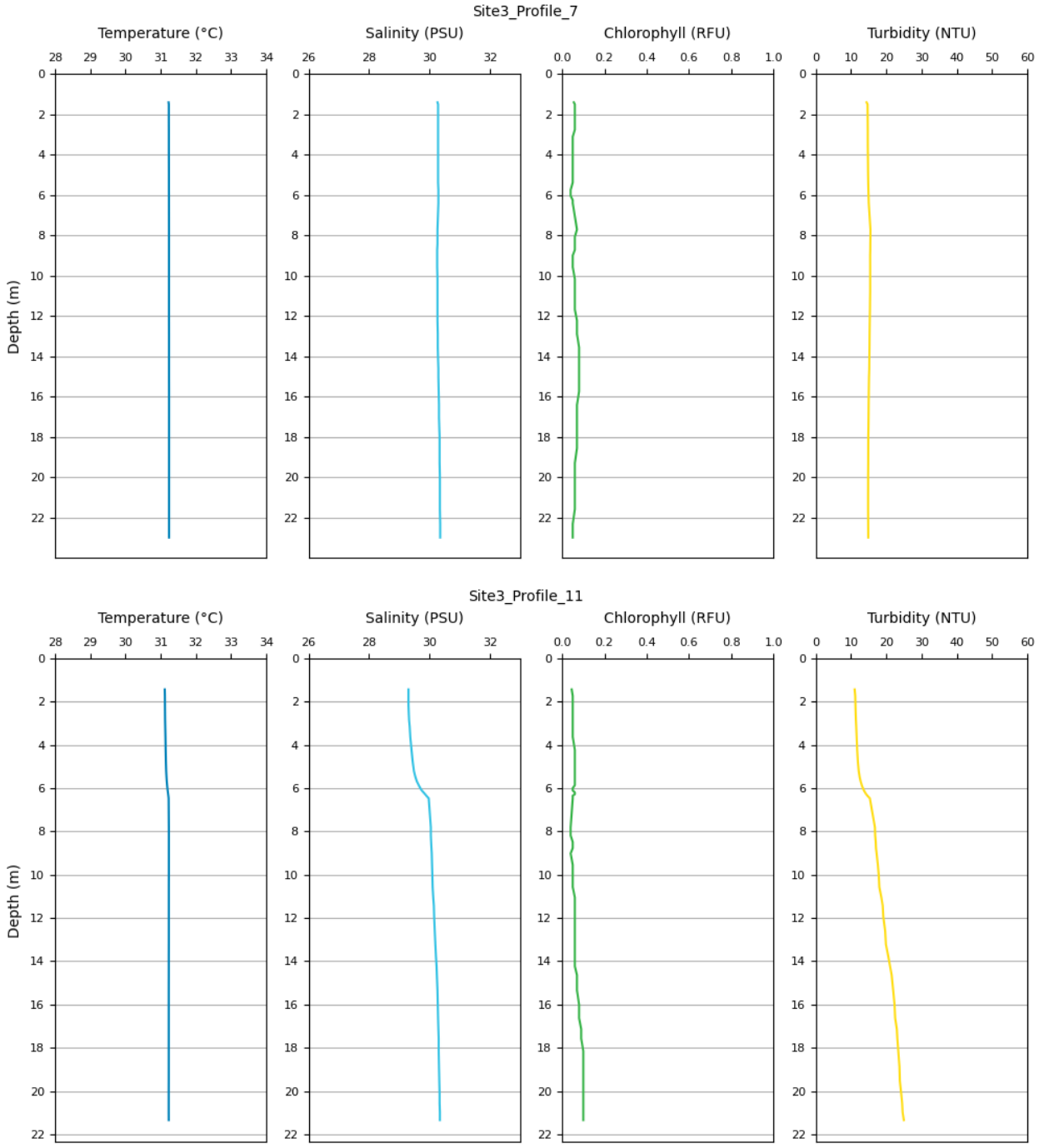

Figure 31. Measured temperature, salinity, chlorophyll and turbidity through the water column at Site 3 at high water (top) and during the ebb stage of the tide (bottom).

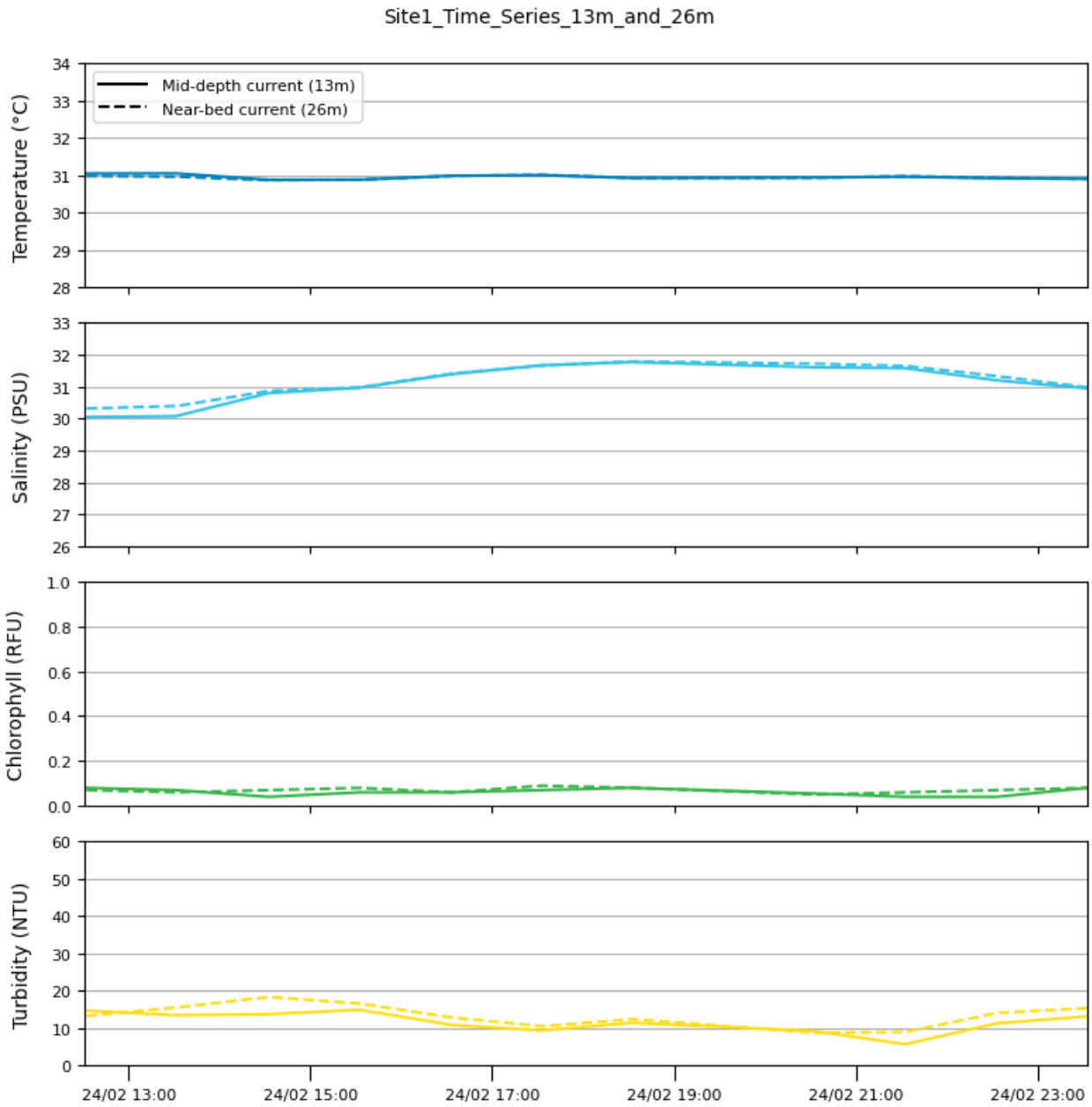

Figure 32. **Time series of mid depth and near-bed measured temperature, salinity, chlorophyll and turbidity over a spring tidal cycle at Site 1.**

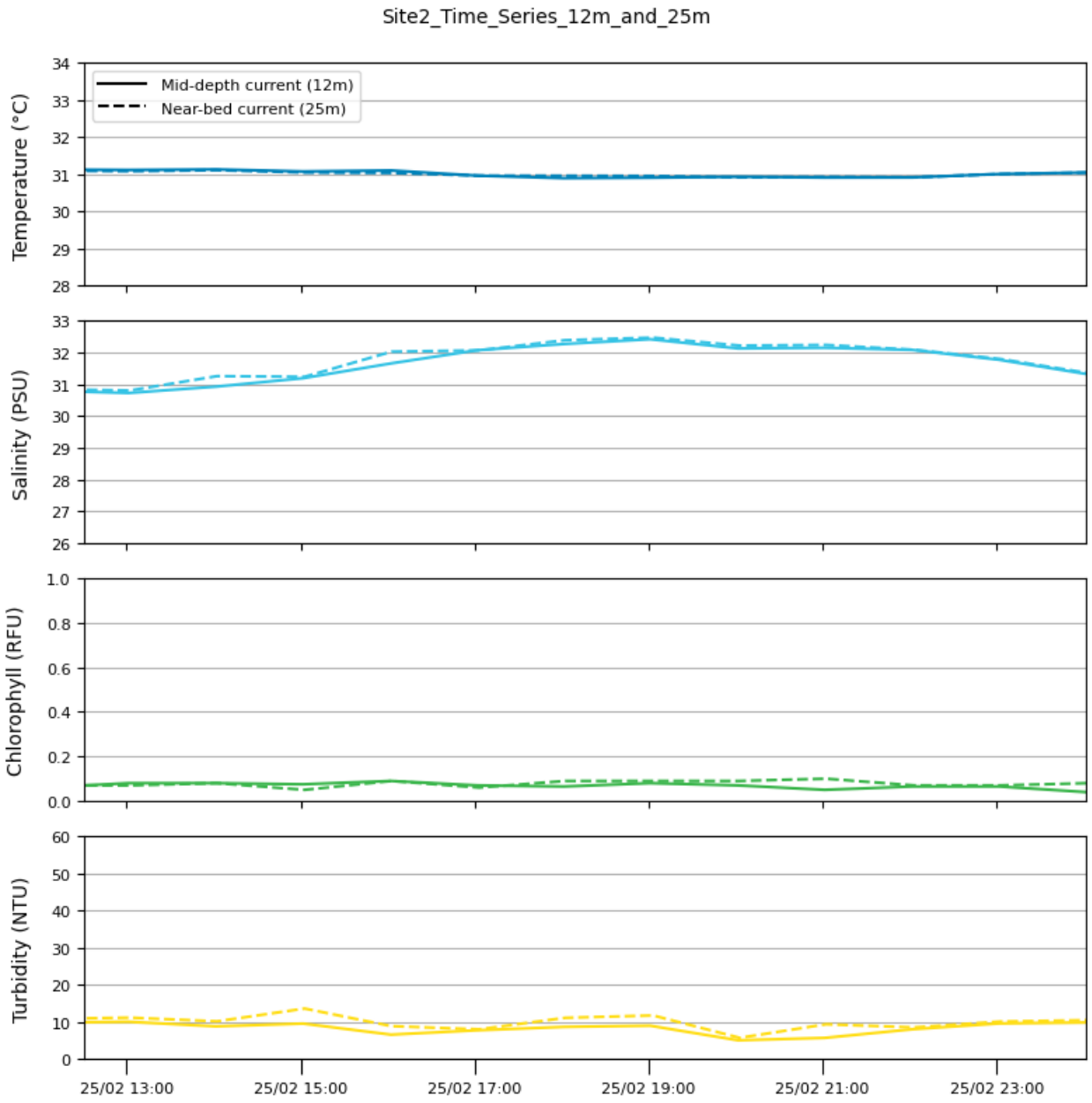

Figure 33. Time series of mid depth and near-bed measured temperature, salinity, chlorophyll and turbidity over a spring tidal cycle at Site 2.

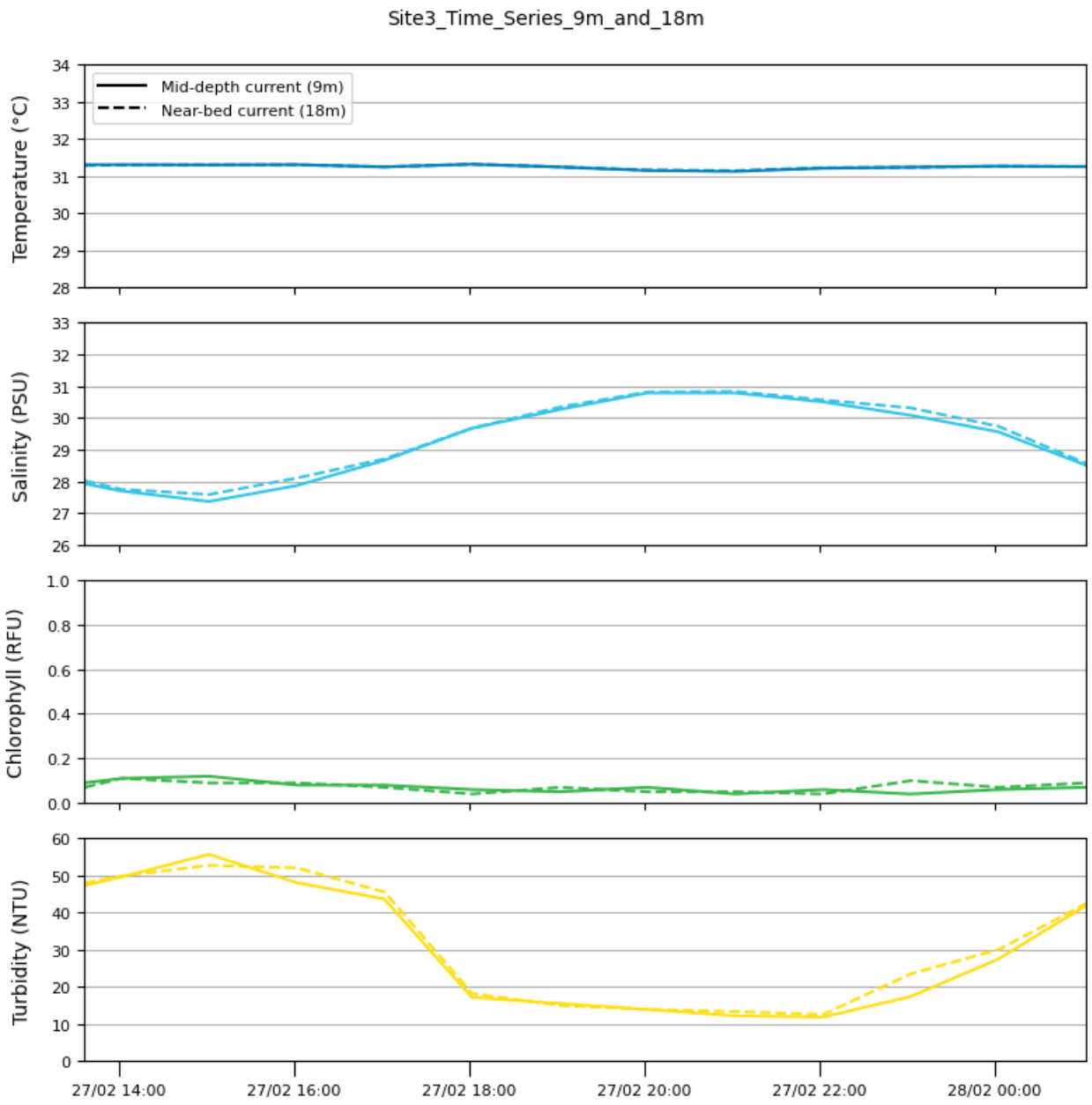

Figure 34. **Time series of mid depth and near-bed measured temperature, salinity, chlorophyll and turbidity over a spring tidal cycle at Site 3.**

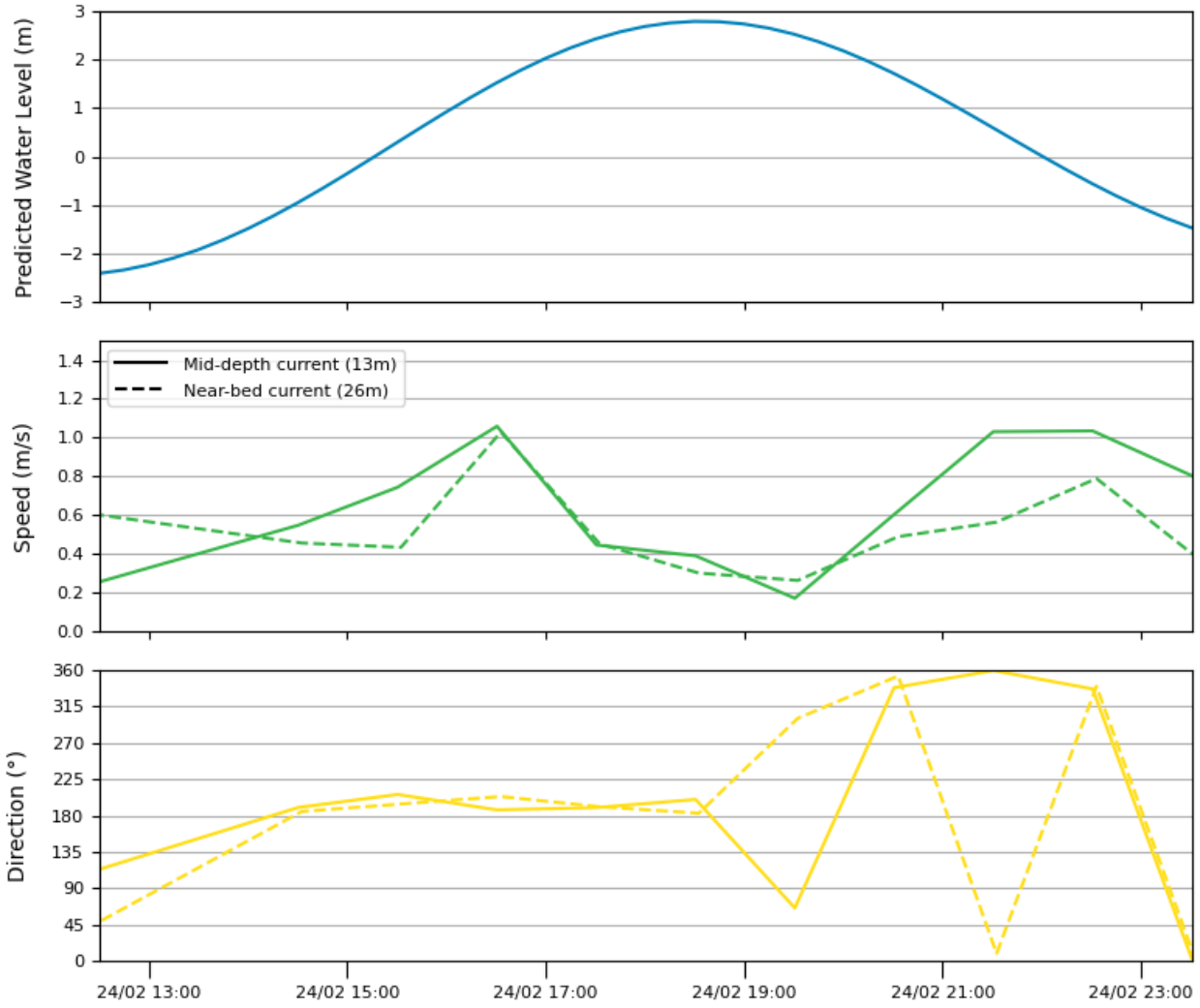

Figure 35. Time series of predicted water level and measured mid depth and near-bed current speed and direction over a spring tide at Site 1.

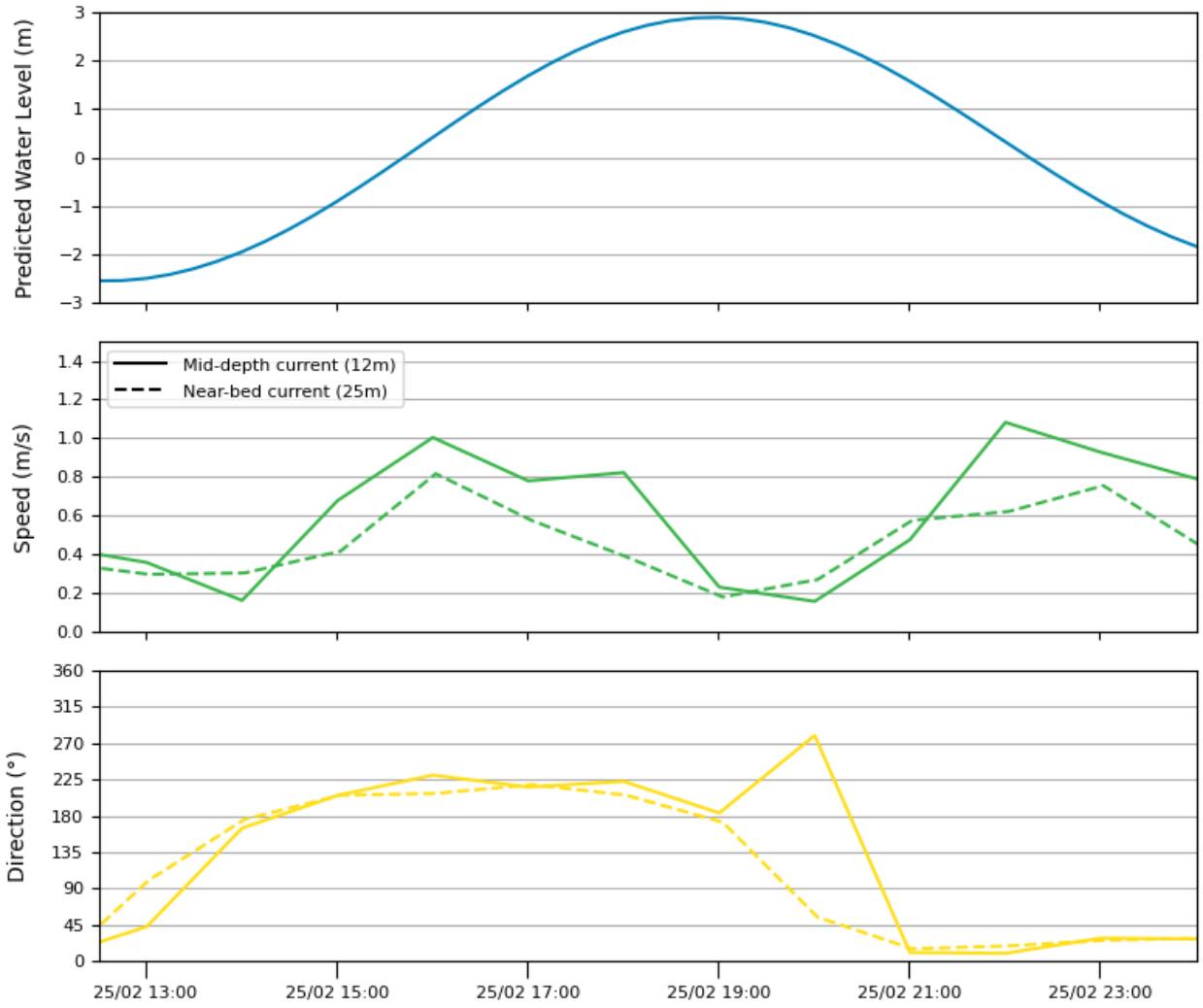

Figure 36. Time series of predicted water level and measured mid depth and near-bed current speed and direction over a spring tide at Site 2.

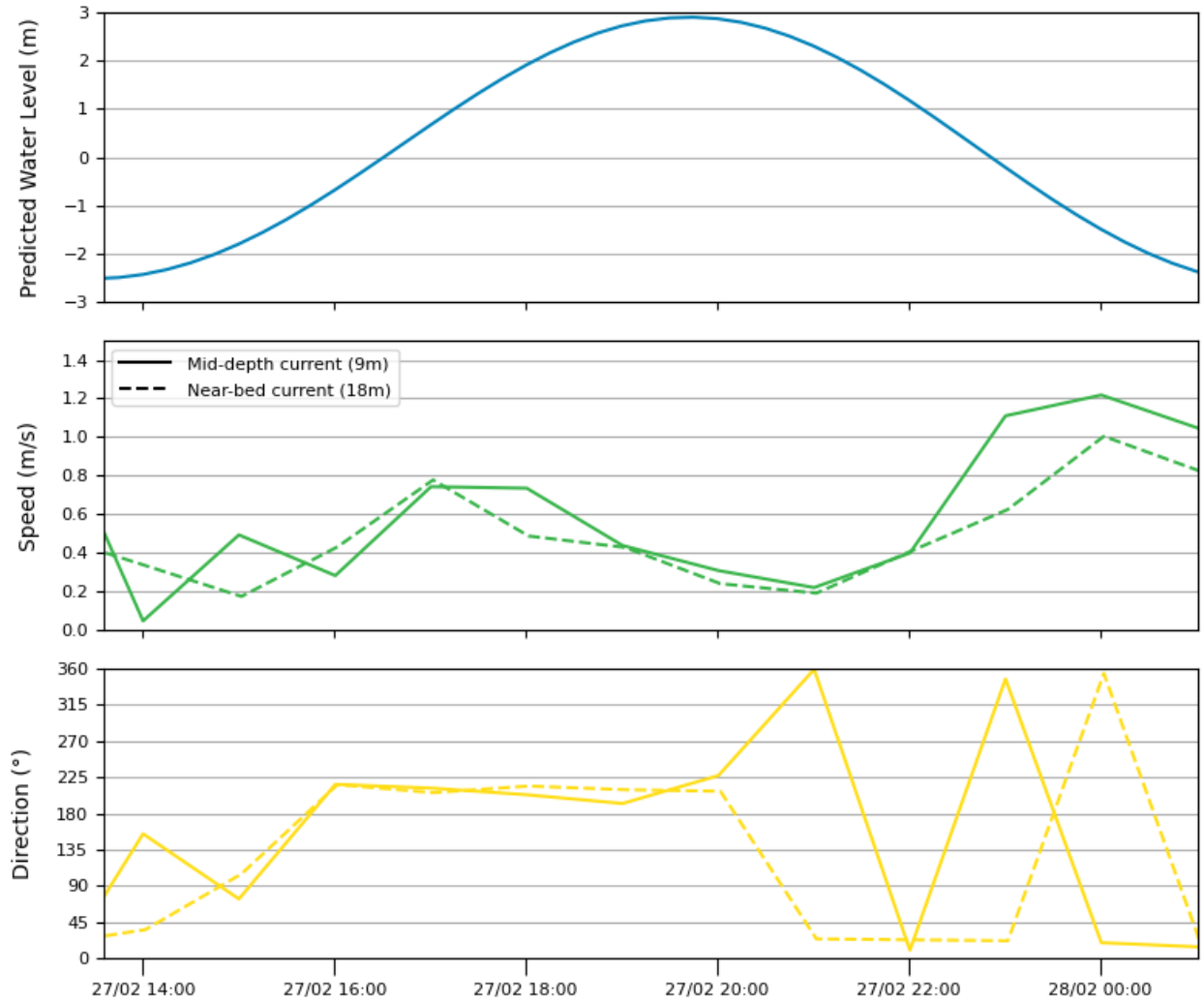

Figure 37. Time series of predicted water level and measured mid depth and near-bed current speed and direction over a spring tide at Site 3.

The correlation between the turbidity measured by the YSI Multi-Sonde Probe and TSS calculated in the laboratory based on concurrent water samples is shown in Figure 38. The plot shows an overall good correlation between the two datasets, although there is a high degree of variability in the correlation when the turbidity is relatively low (less than 20 NTU). The correlation is based on all of the data collected from all 13 water column profiles at each of the three sites, with turbidity sonde measurements and water samples collected at mid water column and near-bed over a 13-hour period at the three sites. To understand whether the correlation between turbidity and TSS varies significantly with depth through the water column (as would be expected if significantly more sand was present near the bed compared to the mid water column), separate plots for mid depth and near-bed are shown in Figure 39 and Figure 40. The plots show a good correlation at both depths, with a slightly stronger correlation mid depth than near-bed. The TSS-turbidity correlation factor varies from 2.59 mid-depth to 2.94 near-bed, while the correlation for all data lies mid-way between the two, with a value of 2.77 (i.e. 1 NTU = 2.77 mg/L). This compares to 1 NTU = 1.72 mg/L as calculated from dry season data collected in CG in July 2023, as reported in PCS (2024a).

As noted by PCS (2024a), measurements of turbidity by nephelometers are more sensitive to finer silt and clay particles than to sand. This means that if the sediment in suspension varies significantly spatially or temporally, the correlation between turbidity and TSS will also vary. Therefore, adopting a single correlation for varying conditions can result in an overprediction of the TSS when there is a higher proportion of silt and clay particles present or an underprediction of the TSS when there is a higher proportion of sand present. In this case, the similarity in the correlation at the two depths indicates that the suspended sediment present does not vary significantly between the two depths, but the difference between the wet season and dry season TSS-turbidity correlation factors indicates that there are differences in the suspended sediment between the two seasons. The suspended sediment present in the wet season has been assessed further by analysing the PSD and SEM feature data for the suspended sediments in the water samples. This is discussed below.

The suspended solids in the water samples were analysed using a Malvern Mastersizer to determine their PSD. To see how the percentage of sand-sized particles in suspension varied depending on the TSS, the correlation between the two has been plotted (Figure 41). The plot shows that for most of the samples less than 10% of the sediment in suspension was sand-sized. There was a negative correlation between TSS and the percentage of sand present in suspension, with more than 15% sand only being present at times when the TSS was lower (between 20 and 60 mg/L). When the TSS increased above 70 mg/L, the percentage of sand present in suspension typically remained below 5%, although one sample had 7% present. Further analysis of the samples following the PSD analysis showed that there were sand-sized organic matter particles present in some of the samples, which resulted in artificially high percentages of sand-sized particles measured as part of the PSD analysis. The samples with more than 10% sand-sized particles present were identified as having organic matter present, meaning that less than 10% sand particles were present in suspension in all samples.

The PSD data can also be used to further understand what the suspended sediment was composed of and how it varied spatially and temporally. Plots showing time series of the turbidity along with the percentage of clay (< 4 µm), silt (4 to 63 µm) and sand (> 63 µm) present in the suspended sediment at the mid depth and near-bed sampling depths over a spring tidal cycle at each of the three sites, are shown in Figure 42 to Figure 44. The plots show that at all three sites and for both the near-bed and mid water column samples, the suspended sediment was predominantly made up of silt, with a high percentage of clay and limited sand present. The median particle size (d_{50}) from all samples ranged between 4 µm and 14 µm (excluding the samples where organic matter was found to bias the percentage of sand-sized particles present), with an average of 8 µm, showing that the sediment in suspension was predominantly in the fine silt to clay size range (finer than 16 µm). At Sites 1 and 2, there was more than double the amount of silt present compared to clay (near-bed average of 26% clay compared to 67% silt at Site 1, and 28% clay compared to 64% silt at Site 2), while at Site 3 the amount of clay present was higher (near-bed average of 39% clay compared to 55% silt). At all three sites, the percent of sand present throughout all samples remained below 10% (excluding samples biased by organic matter), with near-bed values of 3.8% at Site 1, 6.5% at Site 2 and 4.3% at Site 3. Although the data indicate a higher percentage of sand present in suspension near-bed compared to mid water column, the average difference ranges from 0.4% at Site 1 to 1.2% at Site 3.

Given that the peak near-bed current speeds during the measurements were representative of spring tidal conditions and therefore high at the three sites (between 0.8 and 1.0 m/s), and that Sites 2 and 3 were located where several metres of sand was available on the seabed for transport, the results would be expected to show a high percentage of sand present in the samples if sand is regularly transported in suspension in this area of CG. Based on this, the results indicate that limited sand is transported in suspension in this area of CG. Furthermore, the data indicate that the majority of the suspended sediment in this region of CG is silt and clay-sized particles, indicating that sand transport in this region occurs predominantly as bedload transport as opposed to suspended load.

Overall, the data show that the sediment in suspension during a spring tidal cycle was predominantly made up of silt and clay-sized particles, with only a small amount of sand present both near-bed and mid water column. The consistency between the PSD through the water column, at the three sites and through a spring tidal cycle, provides confidence that adopting the correlation between turbidity and TSS based on all data at the three sites (i.e. 1 NTU = 2.77 mg/L) can be considered to be representative for the area of CG around the proposed operational area during the wet season. However, it is important to acknowledge that there is likely to be variability throughout the wet season.

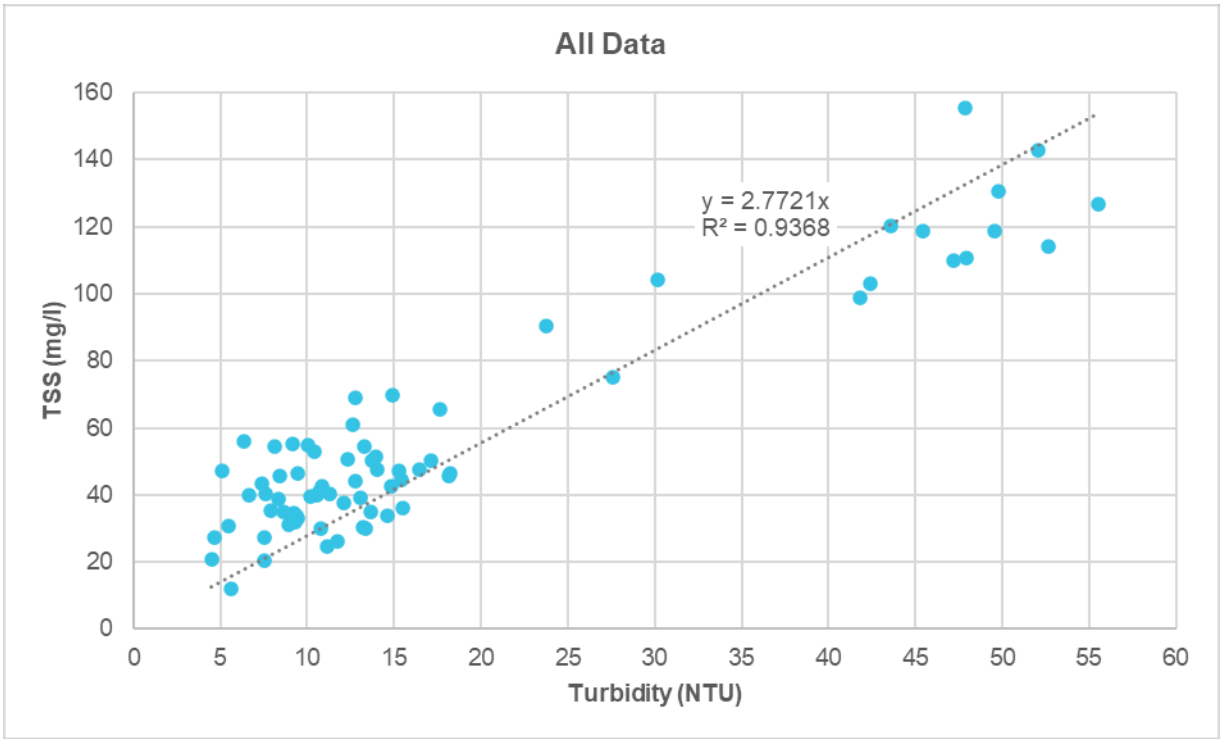

Figure 38. Correlation between measured in-situ turbidity and laboratory calculated TSS for all samples.

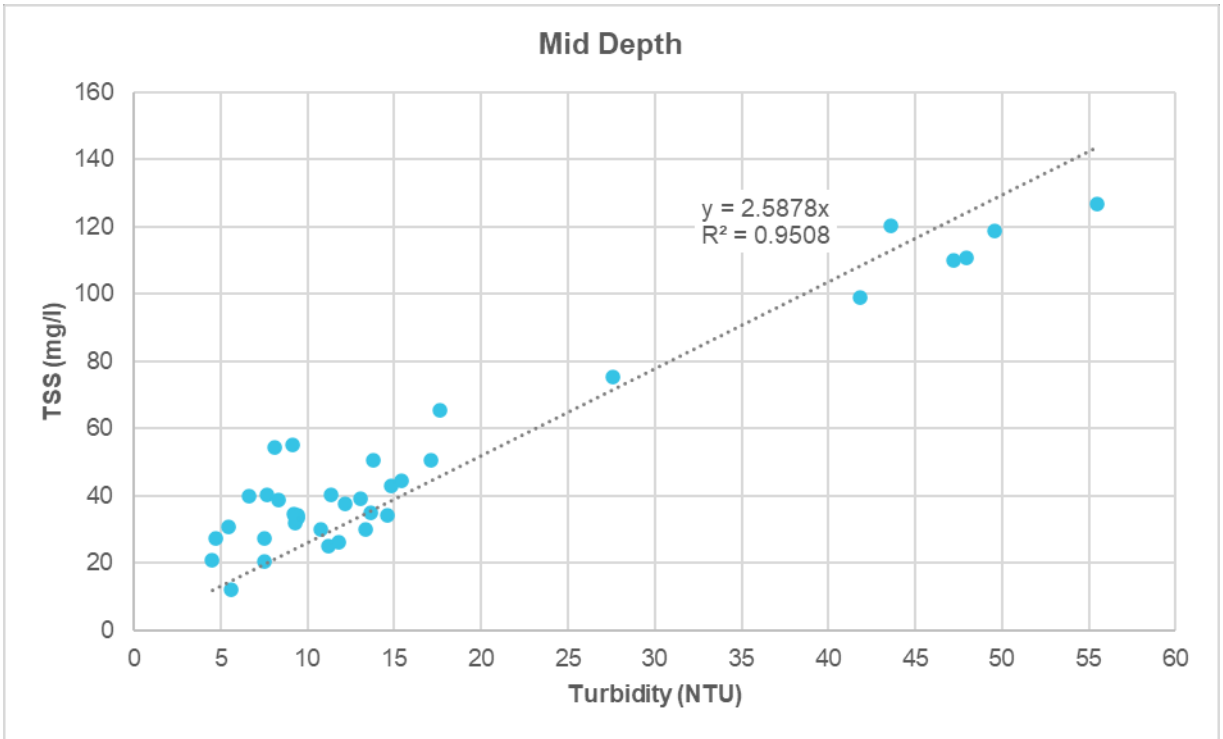

Figure 39. Correlation between measured in-situ turbidity and laboratory calculated TSS for the mid depth samples.

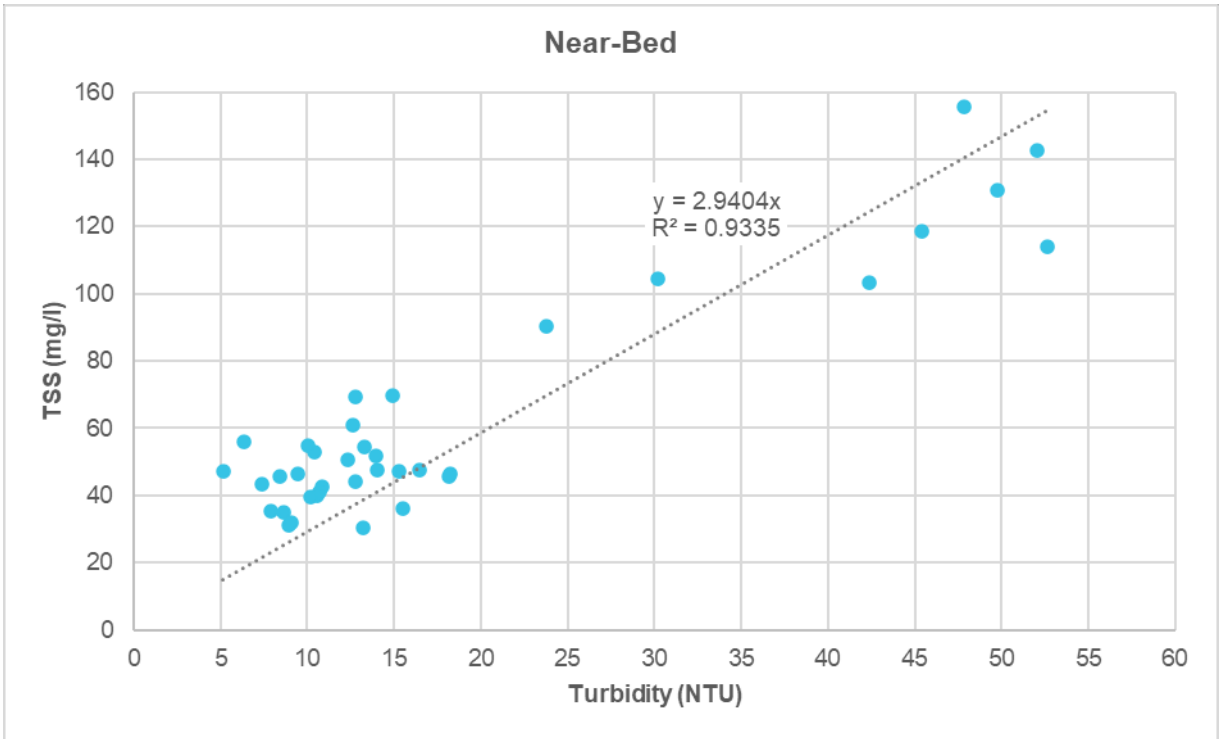

Figure 40. Correlation between measured in-situ turbidity and laboratory calculated TSS for the near bed samples.

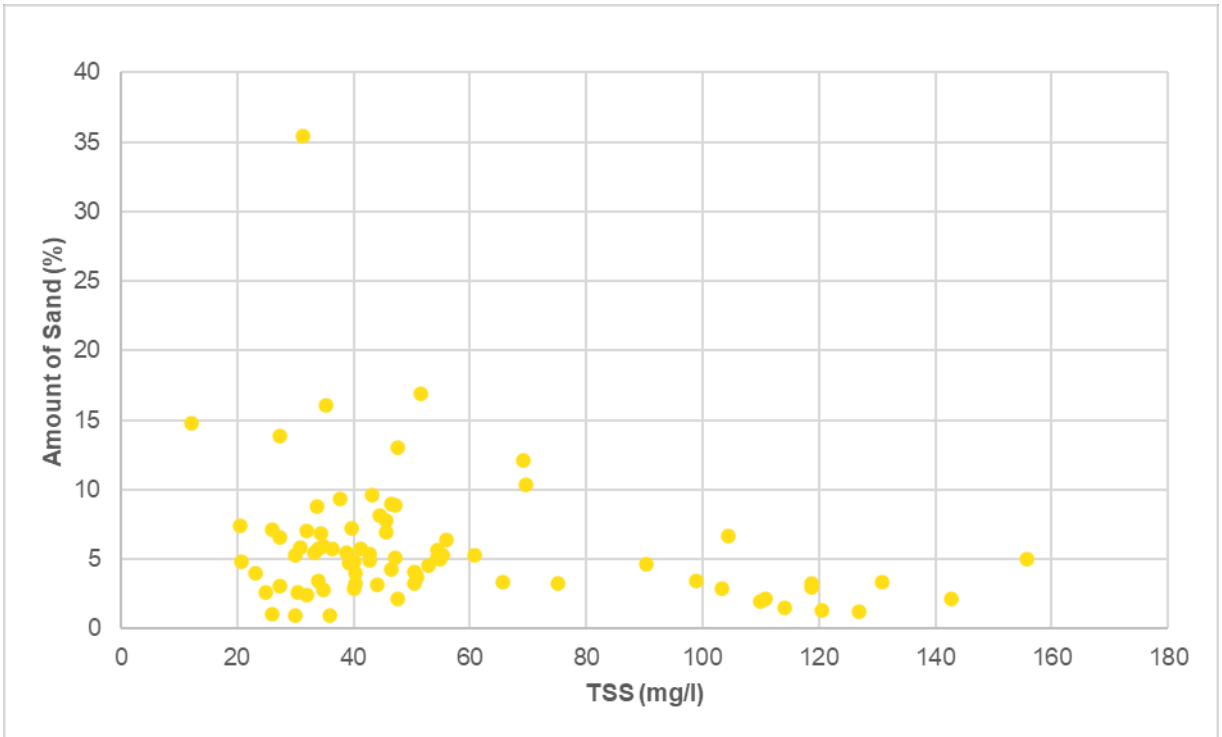

Figure 41. Correlation between laboratory calculated TSS and the percentage of sand present in suspension for all samples collected.

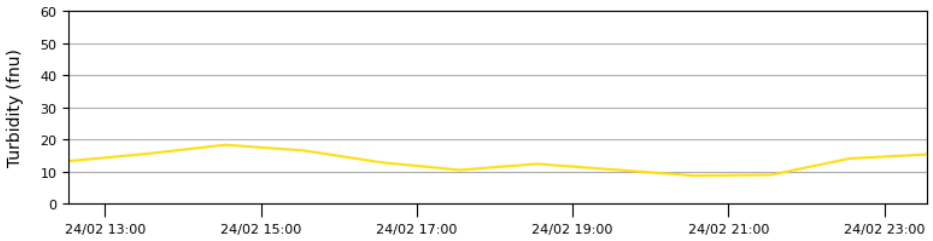

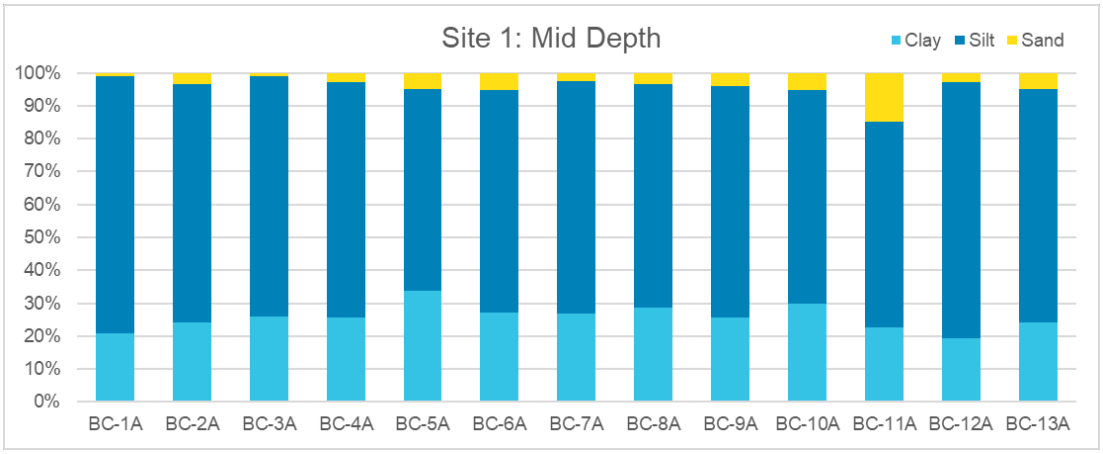

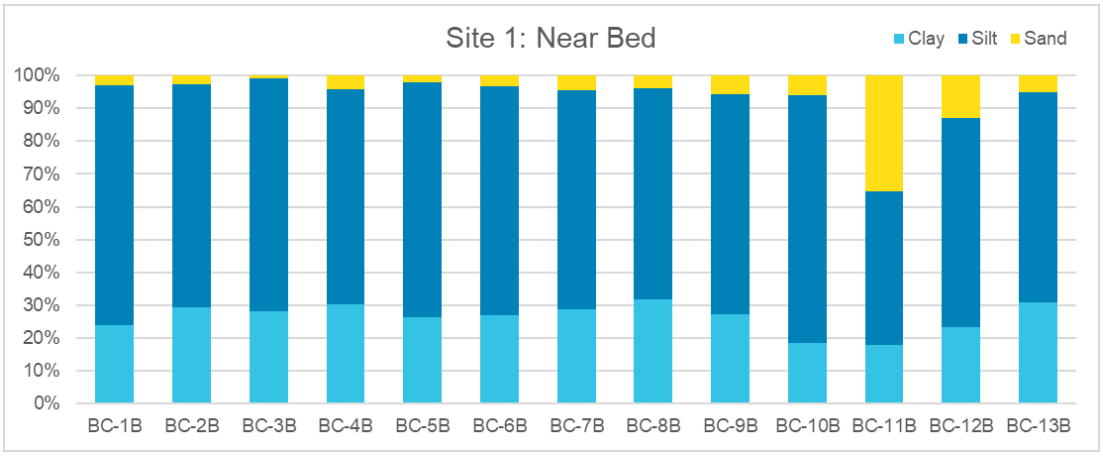

Figure 42. **Measured near-bed turbidity (top) and composition of the suspended sediment at mid depth (middle) and near-bed (bottom) over a spring tidal cycle at Site 1.** *Note: the high percentage of sand-sized particles in samples BC-11A, BC-11B and BC-12B are due to sand-sized organic matter being present, the actual percentage of sand will have been in line with the other samples (i.e. around 5%).*

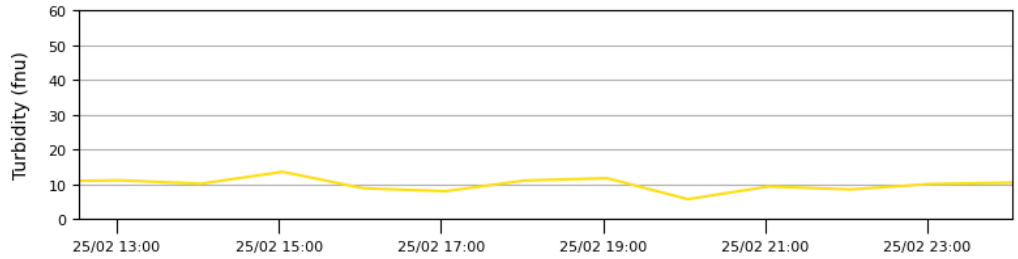

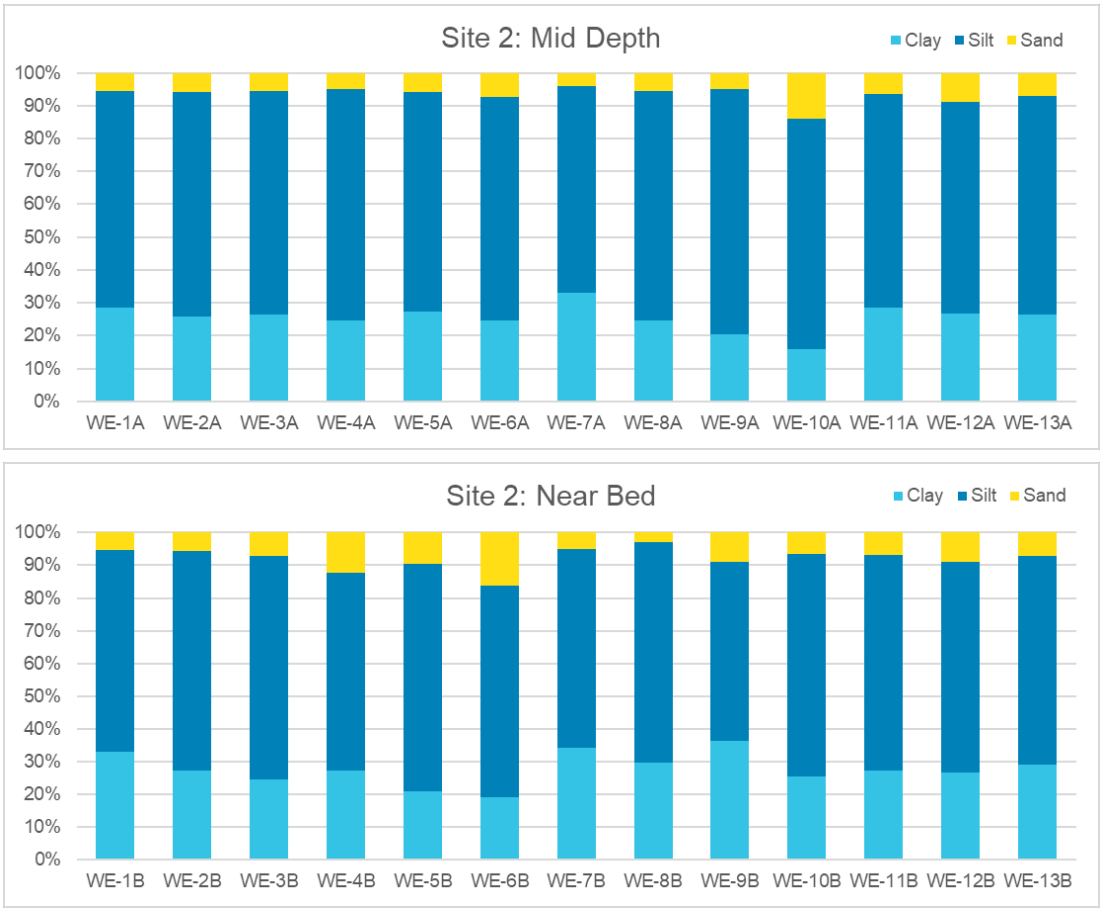

Figure 43. Measured near-bed turbidity (top) and composition of the suspended sediment at mid depth (middle) and near-bed (bottom) over a spring tidal cycle at Site 2. *Note: the higher percentage of sand-sized particles in samples WE-4B, WE-6B, WE-9B and WE-10A are due to sand-sized organic matter being present, the actual percentage of sand will have been in line with the other samples (i.e. 5 to 10%).*

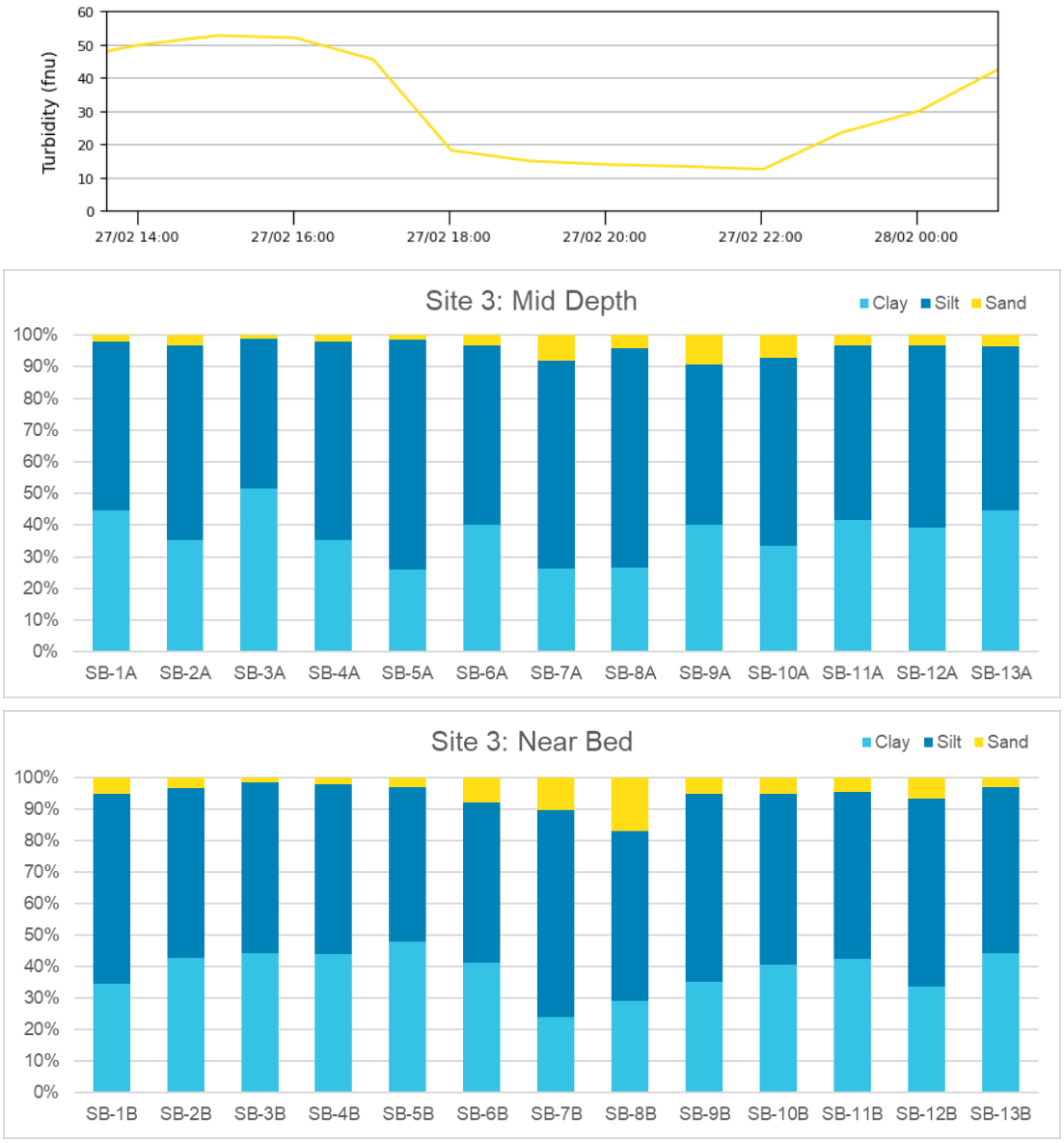

Figure 44. **Measured near-bed turbidity (top) and composition of the suspended sediment at mid depth (middle) and near-bed (bottom) over a spring tidal cycle at Site 3.** *Note: the higher percentage of sand-sized particles in samples SB-7A, SB-7B, SB-8B and SB-9A are due to sand-sized organic matter being present, the actual percentage of sand will have been in line with the other samples (i.e. around 5%).*

Results from the SEM elemental feature analysis showed that there were nine dominant elements throughout the samples which each had an average percent composition (based on particle areas) out of all samples of more than 1% and a maximum percent composition out of all samples of more than 5%. These elements were quartz, feldspar, magnesium aluminosilicate, magnesium silicate, iron silicate, calcite, clay/mica, halite and an agglomerate (silicate with halite). It is important to note that the agglomerate was predominantly made up of silicate and so could potentially be made up of predominantly quartz and/or feldspar particles with clay-sized particles encasing them. Out of the nine dominant minerals in the suspended sediment samples, five are the same as the eight dominant minerals determined from the bed sediment samples (quartz, feldspar, magnesium aluminosilicate, calcite and the silicate/halite agglomerate), while the other four (magnesium silicate, iron silicate, clay/mica and halite) were either not present or only present in trace amounts in the bed sediment samples. This difference is likely to be a result of some of these minerals only being present as particles in the clay to fine silt size range, meaning they will be deposited in areas with low current speeds and calm wave conditions (e.g. in the tidal creeks and mangrove areas fringing the main bay of CG).

Results from the SEM elemental feature analysis of the suspended sediment in the water samples, along with results from the closest available bed sediment sample (see Section 3 for further details), are shown for each of the three sites in Figure 45 to Figure 47. The results show the following.

- Site 1: At low water there is a significant difference in the minerals present in the mid-depth and near-bed samples, with 63% quartz present mid-depth but only 5% quartz present near-bed. This can be partially explained if the higher percentage of silicate with halite agglomerate present near-bed (59% compared to 22%) is assumed to be predominantly made up of quartz. The near-bed sample also contains feldspar (8%) and magnesium aluminosilicate (12%) which are only present in trace amounts in the mid-depth sample. Both samples also have a small amount of calcite present (2% to 4%) and halite (11%). At high water the composition of the suspended sediment in the mid-depth and near-bed samples was very similar, with the silicate with halite agglomerate being the dominant mineral following by magnesium aluminosilicate, feldspar and then quartz. Both samples also had calcite (up to 10%), clay/mica (2%) and halite (<1%) present. The samples therefore show an increase in the amount of feldspar, magnesium aluminosilicate, calcite and clay/mica present at high water compared to low water, with a reduction in the amount of halite (both depths), quartz (mid-depth) and silicate with halite agglomerate (near-bed). The bed sediment in the area is predominantly made up of quartz with some feldspar and magnesium aluminosilicate as well as agglomerates. Therefore, the quartz, feldspar, magnesium aluminosilicate and silicate with halite agglomerate could result from local resuspension of the bed sediment in the region, but the other minerals present must have already been in suspension and come from a source away from the site.

- Site 2: Similar to Site 1, there is a large difference in the minerals present in the mid-depth and near-bed samples, with the mid-depth sample being predominantly quartz (79%), while the near-bed sample was predominantly magnesium aluminosilicate (56%) with only a trace amount of quartz present (<1%). Both samples also contained feldspar (4% to 12%), silicate with halite agglomerate (3% to 8%), clay/mica (1%) and halite (4%) while the mid-depth sample also contained calcite (7%). At high water the composition of the suspended sediment in the mid-depth and near-bed samples was similar, with magnesium aluminosilicate and iron silicate being the dominant minerals followed by feldspar and the silicate with halite agglomerate. Both samples also contained small amounts of clay/mica (2% to 4%), calcite (1%) and halite (1%). The samples show a significant increase in the amount of iron silicate (both depths) and magnesium aluminosilicate (mid-depth) present at high water compared to low water, a small increase in the amount of clay/mica, a reduction in the amount of magnesium silicate (near-bed), halite (both depths), calcite (mid-depth) and quartz (mid-depth) and little change in the amount of feldspar, silicate with halite agglomerate and magnesium aluminosilicate (near-bed). The bed sediment in the area is predominantly made up of quartz with some feldspar, magnesium aluminosilicate, calcite and agglomerates. Therefore, the quartz, feldspar, magnesium aluminosilicate, calcite and silicate with halite agglomerate could result from local resuspension of the bed sediment in the region, but the other minerals present must have already been in suspension and come from a source away from the site.

- Site 3: Unlike the other two sites, the suspended sediment from mid-depth and near-bed at low water and high water all had similar mineral compositions. The SSC at this site was significantly higher than at the other two sites (50 to 150 mg/l at Site 3, compared to 25 to 50 mg/l at Sites 1 and 2) which may have resulted in less variability in the mineral composition. At Sites 1 and 2, the lowest SSC occurred at low water, mid-depth (25 and 33 mg/l) which was when the mineral composition was noticeably different to the other samples. For all the samples the dominant minerals were magnesium aluminosilicate and iron silicate, while calcite, clay/mica, magnesium silicate and silicate with halite agglomerate were also present in all samples. There isn't a consistent variation in mineral composition in both the mid-depth and near-bed samples from low water to high water except for an increase in magnesium silicate and silicate with halite agglomerate. The amount of iron silicate reduced by 9% in the mid-depth between low water and high water, while in the near-bed sample the iron silicate remained the same and the magnesium aluminosilicate reduced by 20%. In the near-bed samples, the amount of calcite and clay-mica increased by 5% and 6% respectively, but in the mid-depth samples, there was no change. The bed sediment in the area is predominantly made up of quartz with some feldspar, magnesium aluminosilicate and agglomerates also present. The only similar minerals from the suspended sediment samples are magnesium aluminosilicate and the silicate

with halite agglomerate, suggesting that the majority of the sediment in suspension was already in suspension, having been transported from a source away from the site.

The elemental feature results show that at Sites 2 and 3, the dominant minerals in the suspended sediment were magnesium aluminosilicate and iron silicate, which are clays resulting from the weathering and chemical breakdown of igneous and metamorphic rocks. Therefore, the majority of the sediment in suspension at these two sites is likely to have been clay particles which originated from the terrigenous sediment in the CG catchment. The composition of the suspended sediment at Site 1 was different to Sites 2 and 3, with quartz and feldspar consistently being present, the silicate with halite agglomerate typically being the dominant mineral, while magnesium aluminosilicate and iron silicate were not dominant minerals at the site. The reason for this difference is uncertain, but it is likely to be due to:

- Site 1 being located close enough to the entrance to CG to have not experienced the higher SSC from upstream which Site 3 experienced. Satellite imagery has shown that this occurs during the ebb stage of spring tides (PCS, 2024a); and
- Site 2 being located close to intertidal areas and creeks on the western shoreline of CG where some resuspension of previously deposited fine-grained silt and clay is likely to occur during spring tides. Site 1 is located away from any sources of fine-grained silt and clay and the elemental feature results indicate that the suspended sediment at this site is likely to have the highest contribution of locally suspended sediment.

All three of the sites have shown that calcite is present in the suspended sediment during both low water and high water. This indicates that there is an upstream source of the calcite, this is likely to be from the weathering of limestone from the CG catchment. The SEM analysis showed that the calcite particles in suspension were less than 10 µm in size, while the calcite particles present in the seabed samples near the entrance to CG and in King Shoals were up to 500 µm (and probably larger as this is the size that the sample was sieved prior to SEM analysis). The clay and fine silt size range calcite particles present in suspension, which are likely to be from an upstream source, are likely to be too small to be deposited on the seabed except in very sheltered locations, which explains why they were not present in the seabed samples from upstream in CG. The calcite in the bed sediment samples close to the entrance to CG and in King Shoals are predominantly larger particles than those in suspension, suggesting that they are from a different source which, given the spatial pattern of the calcite, is likely to be offshore.

At Sites 1 and 2, the amount of halite in the suspended sediment was much higher at low water compared to high water. This suggests that the halite is from an upstream source, and as halite was not present in the bed sediment (only as agglomerates) and was not present at Site 3, it is expected that the halite is not from a source upstream of CG (e.g. the West or East Arms) but has come from the draining of the upper intertidal areas (or supratidal areas through rainfall) along the shoreline of CG and then the ebb tide has transported these particles in suspension to Sites 1 and 2.

Overall, the results show that the majority of the sediment in suspension at the three sites was fine-grained silt and clay, with clay minerals being dominant at two of the three sites and an agglomerate of silicate and halite being dominant at the third site. Similarities in the mineral composition of the suspended sediment between Sites 2 and 3 and at low water and high water, indicates that the suspended sediment is likely to remain in suspension over a spring tidal cycle, with the suspended sediment predominantly from an upstream source.

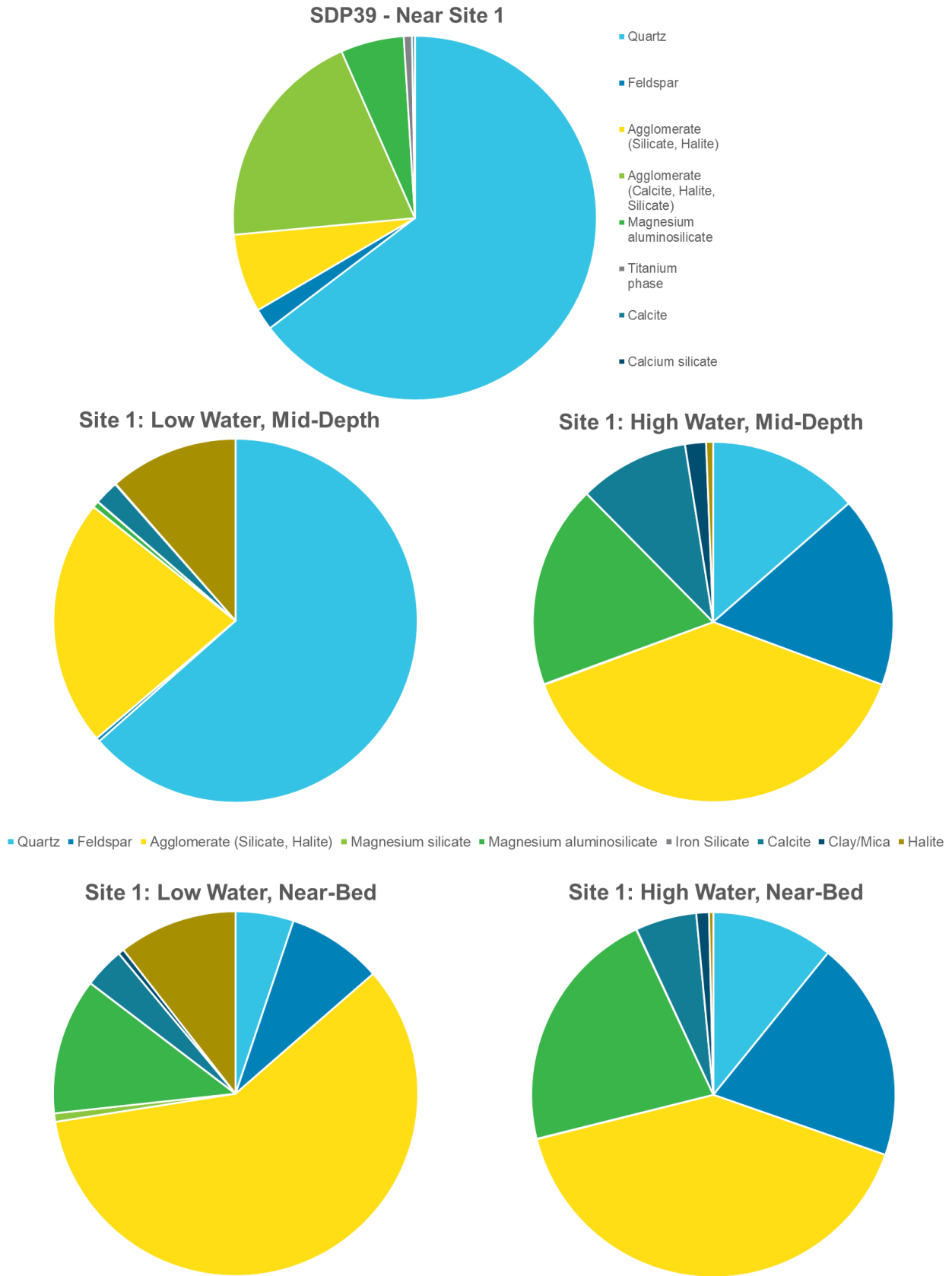

Figure 45. Elemental feature analysis results for the bed sediment close to Site 1 (top) and for the suspended sediment collected from Site 1 at low water and high water.

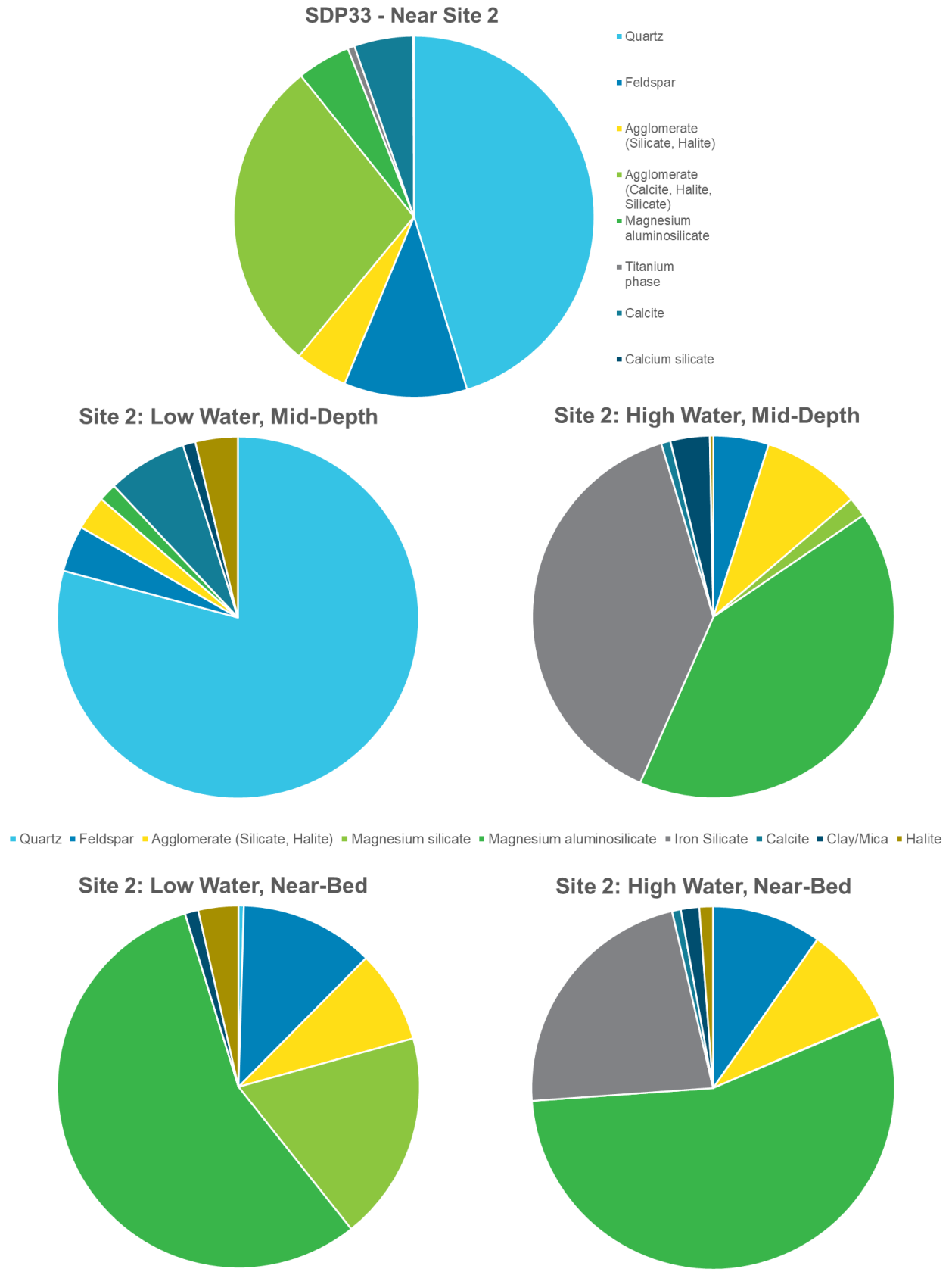

Figure 46. **Elemental feature analysis results for the bed sediment close to Site 2 (top) and for the suspended sediment collected from Site 1 at low water and high water.**

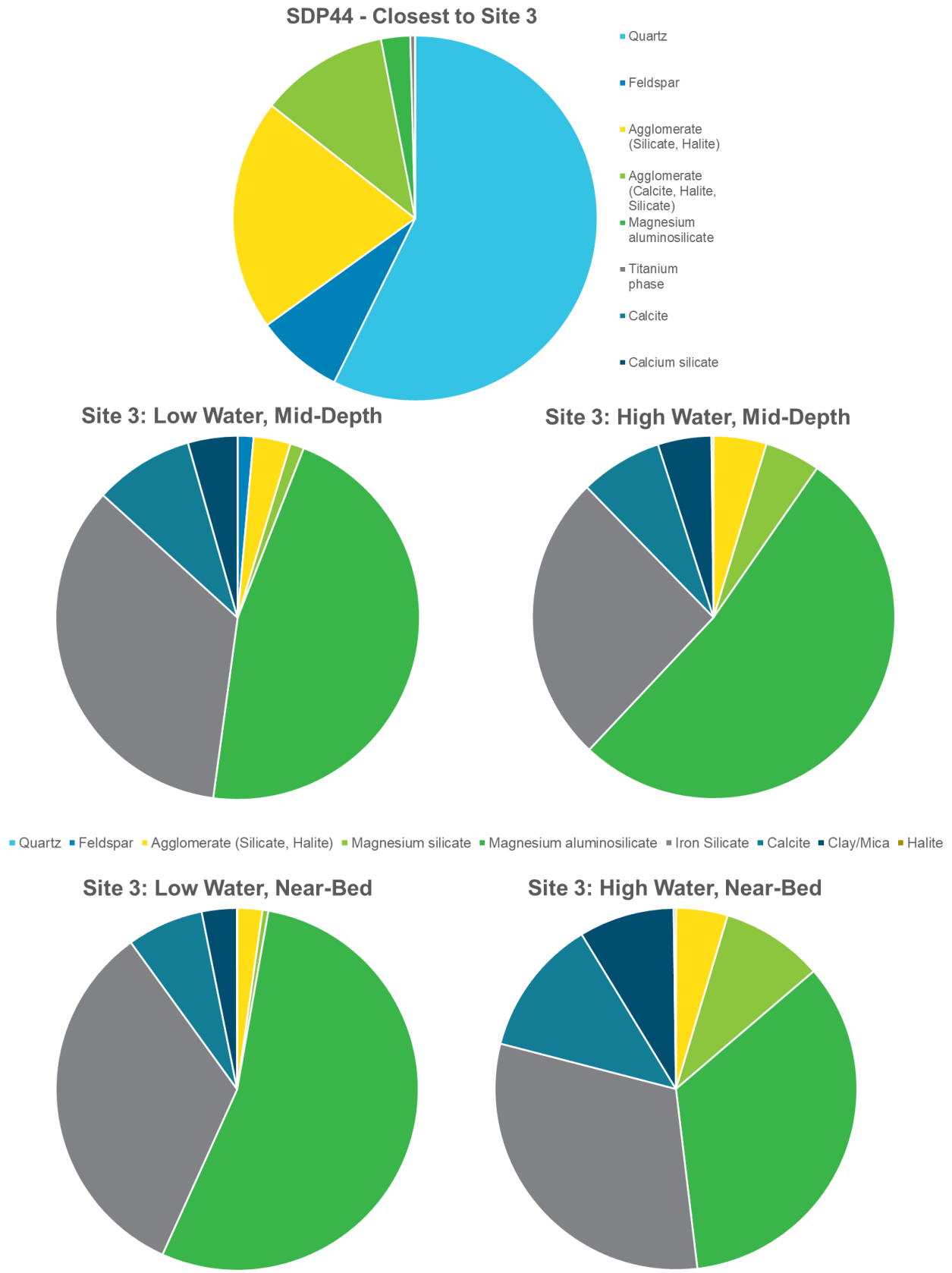

Figure 47. Elemental feature analysis results for the bed sediment close to Site 3 (top) and for the suspended sediment collected from Site 1 at low water and high water.

5. AWAC and ADCP Data

5.1. Data Overview

To provide measured timeseries data of water levels, waves and currents through the water column Nortek AWACs and Nortek Signature 500/1000 ADCPs have been deployed (herein both types of instrument are referred to as AWACs). The locations where the AWACs along with co-mounted sensors (discussed in Section 6) have been deployed, and are planned to be deployed, are shown in Figure 48. Details of the AWAC data which were available at this stage of the assessment are summarised below:

- AWAC-01: An AWAC was deployed on the seabed for 41 days from 9th June to 21st July 2023 and for 66 days from 3rd March to 8th May 2024 (water depth of 30.1 m MSL). Current data at 1 m bins through the water column along with water depth data were successfully recorded during both deployments. However, there was an issue with the instrument during the deployment in 2023 which meant that the wave data were not usable, but wave data were measured during the 2024 deployment.

- AWAC-02: An AWAC was deployed on the seabed in a water depth of 18.0 m MSL for 27 hours in 2023 (7th to 8th September 2023). Current data at 1 m bins through the water column along with water depth and wave data were successfully recorded during both deployments.

- AWAC-03: An AWAC was deployed on the seabed in a water depth of 19.2 m MSL for 46 hours (13th October to 15th October 2023). Current data at 1 m bins through the water column along with water depth and wave data were successfully recorded during the deployment.

- AWAC-04: An AWAC was deployed on the seabed in a water depth of 27.6 m MSL for 20 hours (7th to 8th September 2023). Current data at 1 m bins through the water column along with water depth data were successfully recorded during the deployment. However, there was an issue with the instrument which meant that the wave data were not usable.

- AWAC-06: An AWAC was deployed on the seabed in a water depth of 20.5 m MSL for 35 days (8th September to 13th October 2023), and for 65 days from 6th March to 10th May 2024. Current data at 1 m bins through the water column along with water depth and wave data were successfully recorded during the deployment.

- AWAC-07: An AWAC was deployed on the seabed in a water depth of 11.1 m MSL for 142 days (15th October 2023 to 5th March 2024). Current data at 1 m bins through the water column along with water depth and wave data were successfully recorded during the deployment.

- AWAC-11: An AWAC was deployed on the seabed in a water depth of 22.2 m MSL for 67 days (2nd March to 8th May 2024). Current data at 1 m bins through the water column along with water depth and wave data were successfully recorded during the deployment.

In addition, AWACs are currently deployed in CG and will provide additional hydrodynamic and wave data at the monitoring sites. Further details on the AWAC deployments and data processing are provided by PCS (2024c).

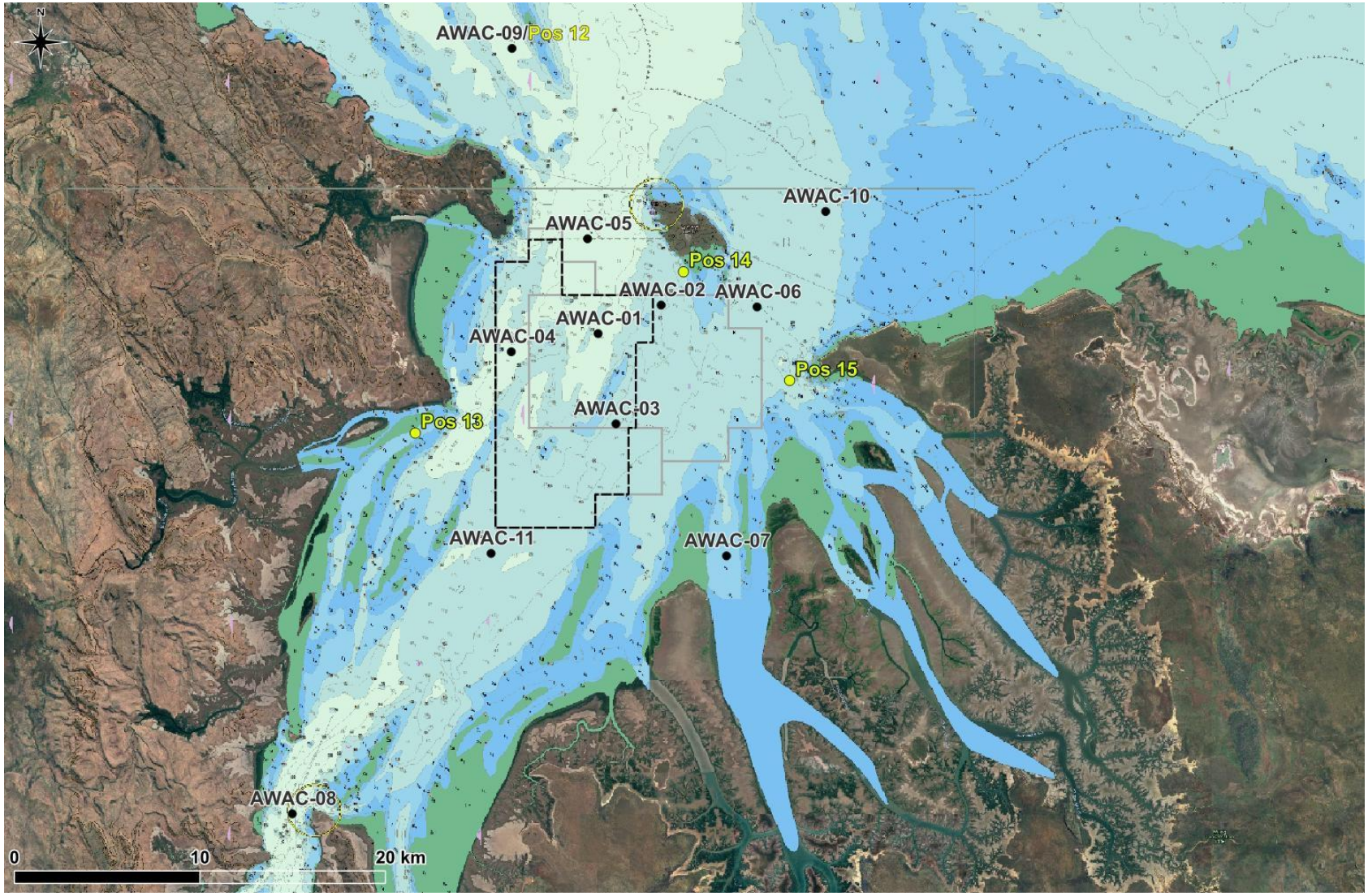

Figure 48. **Locations of the AWAC and Frame (sites called Pos) deployment sites in the CG.**

5.2. Results

5.2.1. Hydrodynamics

This section details the data from each of the AWAC deployments detailed in Section 5.1. Results from the first deployment at AWAC-01 in June to July 2023 are presented in PCS (2024a). The results are presented in chronological order.

5.2.1.1. AWAC-02, September 2023

Time series of water level, flow speed and direction for the short deployment at site AWAC-02 are shown in Figure 49. Flow speed is presented at three heights in the water column, the surface (layer 12), mid-depth (layer 6) and bed (layer 1). The flow speeds reduce through the water column, and speeds over the deployment period are less than 1 m/s. The flow direction is relatively consistent through the water column, with a south-southeast to south flood flow direction and a north-northwest to north ebb flow direction. The flow data suggests an ebb dominance at the site, although a longer time series is required to confirm this as it could also be a result of the tidal asymmetry over the measurement period.

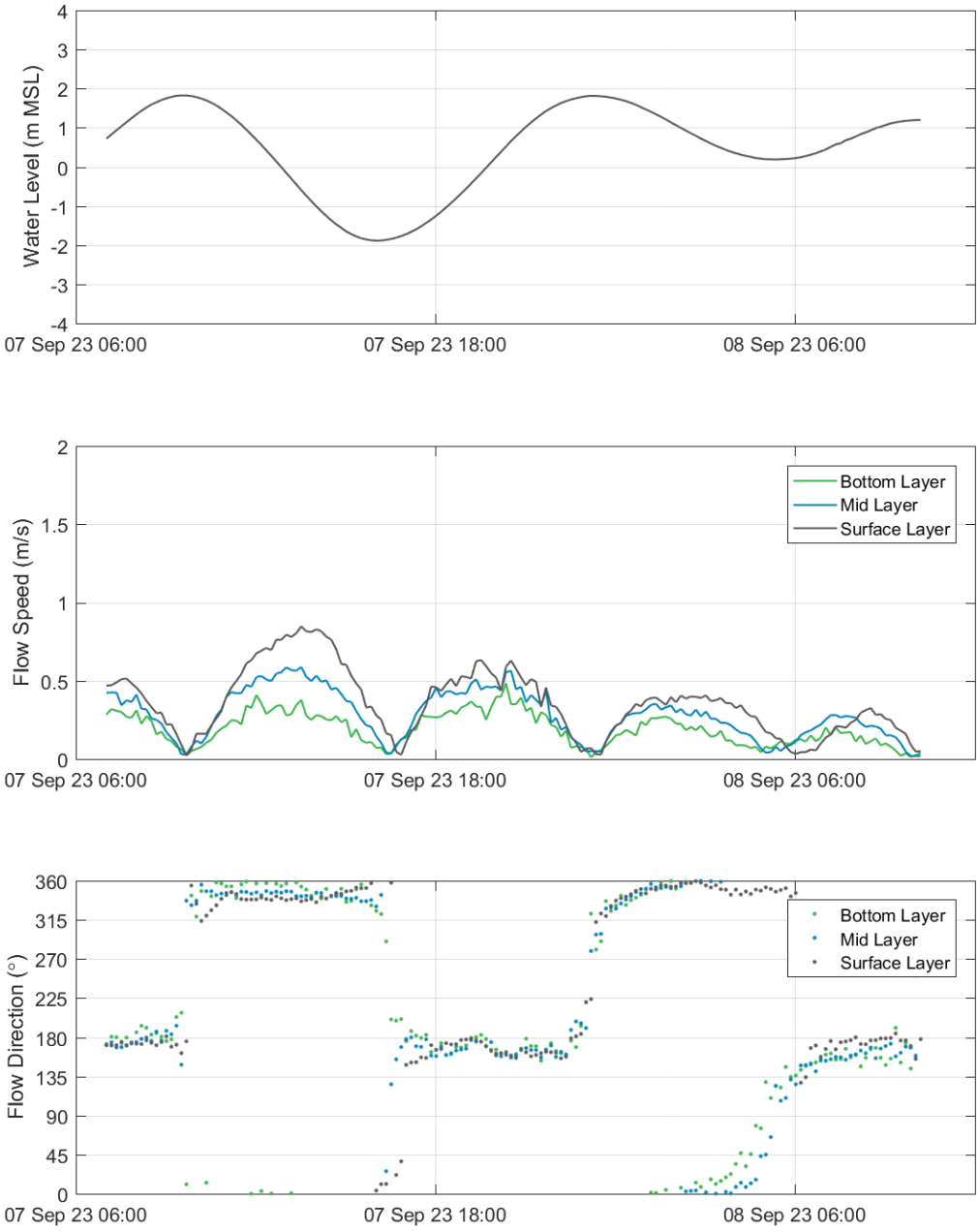

Figure 49. Time series plots of the water level, flow speed and flow direction at AWAC-02 in September 2023.

5.2.1.2. AWAC-04, September 2023

Figure 50 shows water level, flow speed and direction for the short deployment at AWAC-04. Water levels show a clear semi-diurnal tide, with a range of just under 4 m. The flow speed is shown at three heights in the water column, the surface (layer 24), mid-depth (layer 12) and bed (layer 1). Peak flow speeds over the period are 1 m/s, with surface flows showing some minor differences to mid and bed flows, this could be due to the presence of sandwaves in this area (as shown in Section 2) influencing how the flow speeds vary through the water column. The flow direction is relatively consistent through the water column and varies from south to south-southwest during the flood stage of the tide from north to north-northeast during the ebb stage of the tide.

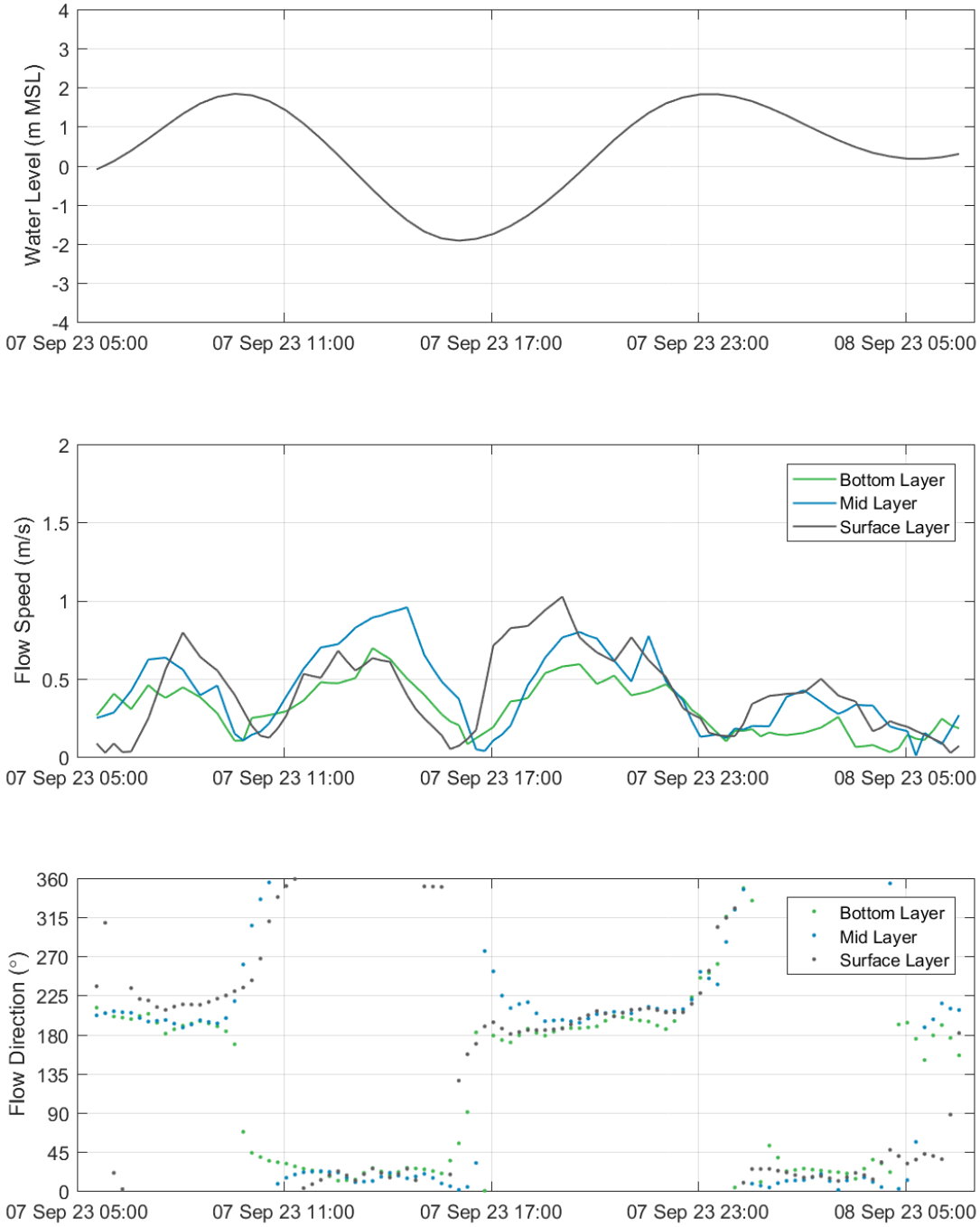

Figure 50. Time series plots of the water level, flow speed and flow direction at AWAC-04 in September 2023.

5.2.1.3. AWAC-06 September to October 2023

Figure 51 shows water level, flow speed and direction for the 35 day deployment AWAC-06 in September 2023. In addition, results over a 14 day spring-neap tidal cycle are presented in Figure 52. The largest spring and smallest neap tidal ranges over the period were approximately 6.5 m and 2 m respectively. The peaks in mid-depth flow speeds are typically less than 1 m/s, while the peaks in surface flow speed can reach 1.3 m/s. Figure 52 shows a 14 day spring-neap cycle, and presents flow speeds for three heights in the water column (surface (layer 14), mid-depth (layer 6) and bed (layer 1)). Flows are seen to reduce through the water column with differences in peak speeds of up to 0.5 m/s between the surface layer and the bed layer. There is no consistent dominance is the flood or ebb currents, with the dominance varying through the spring-neap tidal cycle for flood or ebb flows. The flow direction is relatively consistent through the water column and varies from south to south-southwest during the flood stage of the tide from north to north-northeast during the ebb stage of the tide.

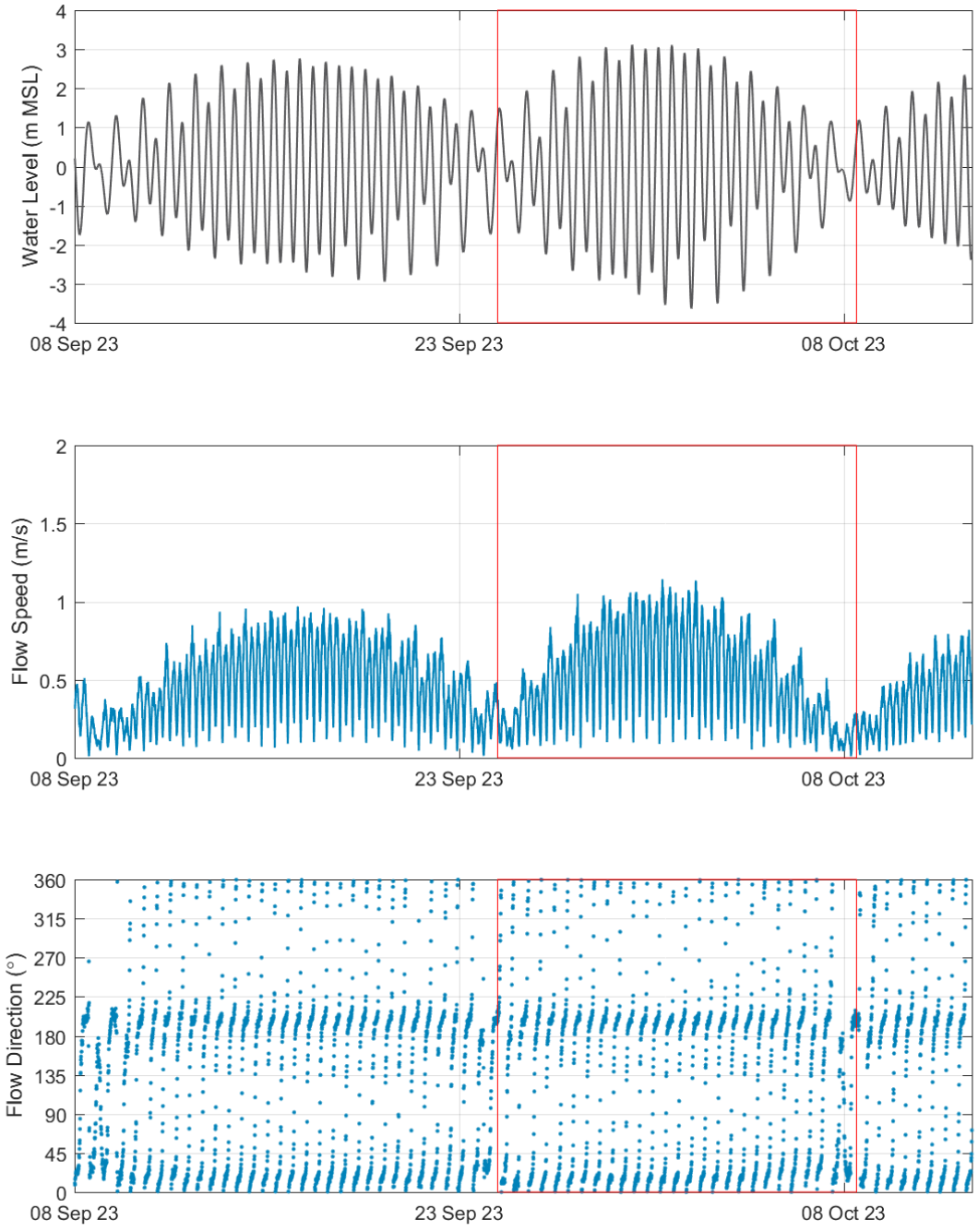

Figure 51. Time series plots of the water level, mid-depth flow speed and mid-depth flow direction at AWAC-06 from September to October 2023.

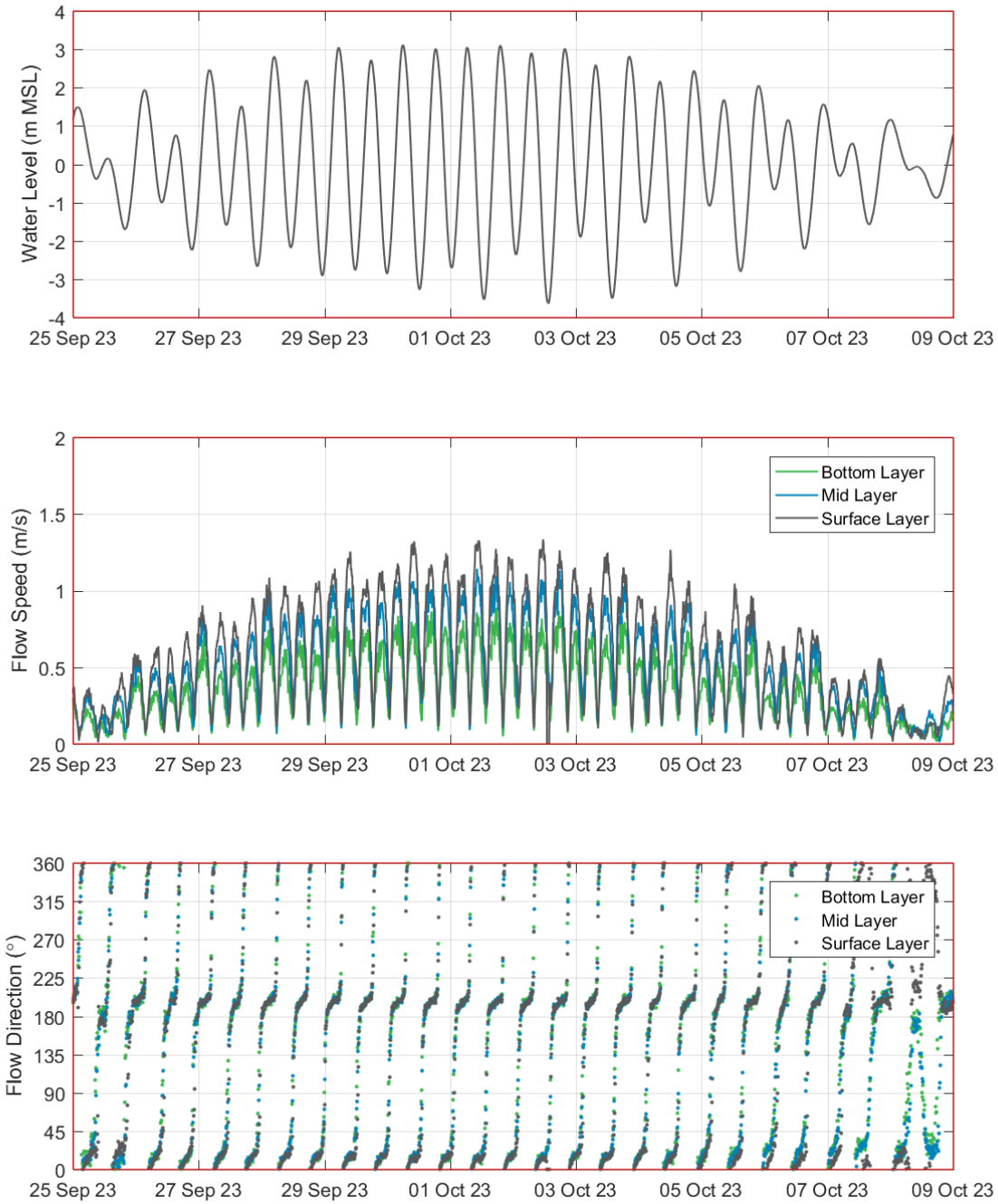

Figure 52. Time series plots of the water level, flow speed and flow direction at AWAC-06 over a 14 day spring neap tidal cycle.

5.2.1.4. AWAC-03 October 2023

Figure 53 presents water level, flow speed and direction for the short deployment at site AWAC-03. Flow speed is presented at three heights in the water column, the surface (layer 13), mid-depth (layer 7) and bed (layer 1). Flows reduce through the water column, with peak speeds of just over 1 m/s in the surface layer and 0.7 m/s in the bed layer. No consistent tidal dominance is evident for flood or ebb flows. The flow direction is relatively consistent through the water column and varies from south to south-southwest during the flood stage of the tide from north to north-northeast during the ebb stage of the tide.

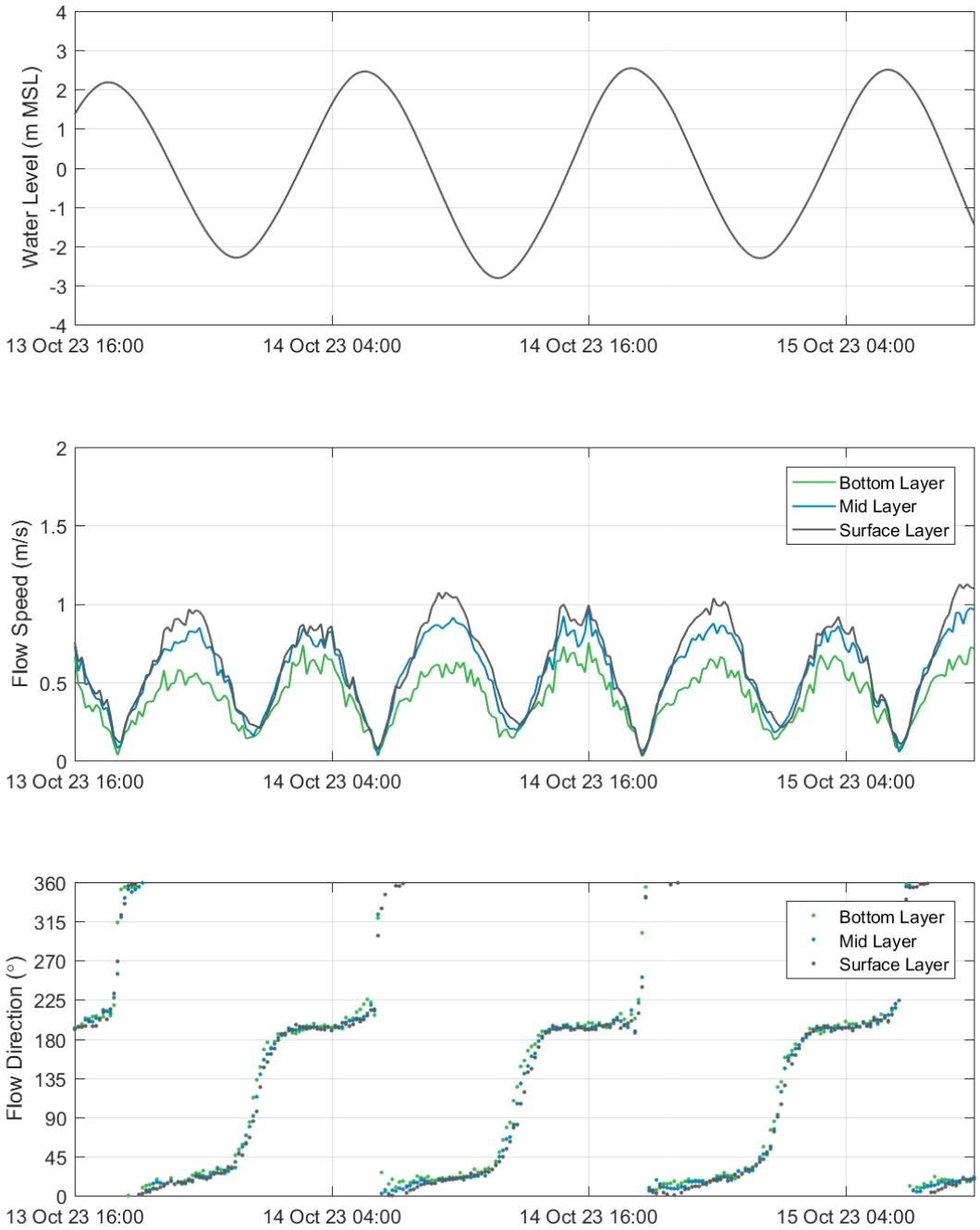

Figure 53. Time series plots of the water level, flow speed and flow direction at AWAC-06 in October 2023.

5.2.1.5. AWAC-07 October 2023 to March 2024

Figure 54 shows water level, flow speed and direction over the 142 day deployment AWAC-07. In addition, data over a 14 day spring-neap tidal cycle are shown in Figure 55. There are clear spring and neap periods, with corresponding maximum and minimum tidal ranges of approximately 7 m and 2 m respectively. The flow speeds vary between the different spring and neap cycles, with the largest mid-depth current speed of 1.5 m/s occurring in February 2024. Figure 55 shows a 14 day spring-neap cycle, and presents flow speeds for three heights in the water column (surface (layer 6), mid-depth (layer 3) and bed (layer 1)). The flow speed is highest in the surface layer and lowest in the bed layer, with a difference of approximately 0.2 to 0.3 m/s between the two layers. During spring tides the current speeds are highest during the ebb stage of the tide, but higher current speeds occur for a longer duration during the flood stage of the tide, as a result there is no consistent clear tidal dominance at the site. The flow direction is consistent through the water column and varies from south-southeast to south during the flood stage of the tide from north-northwest to north during the ebb stage of the tide.

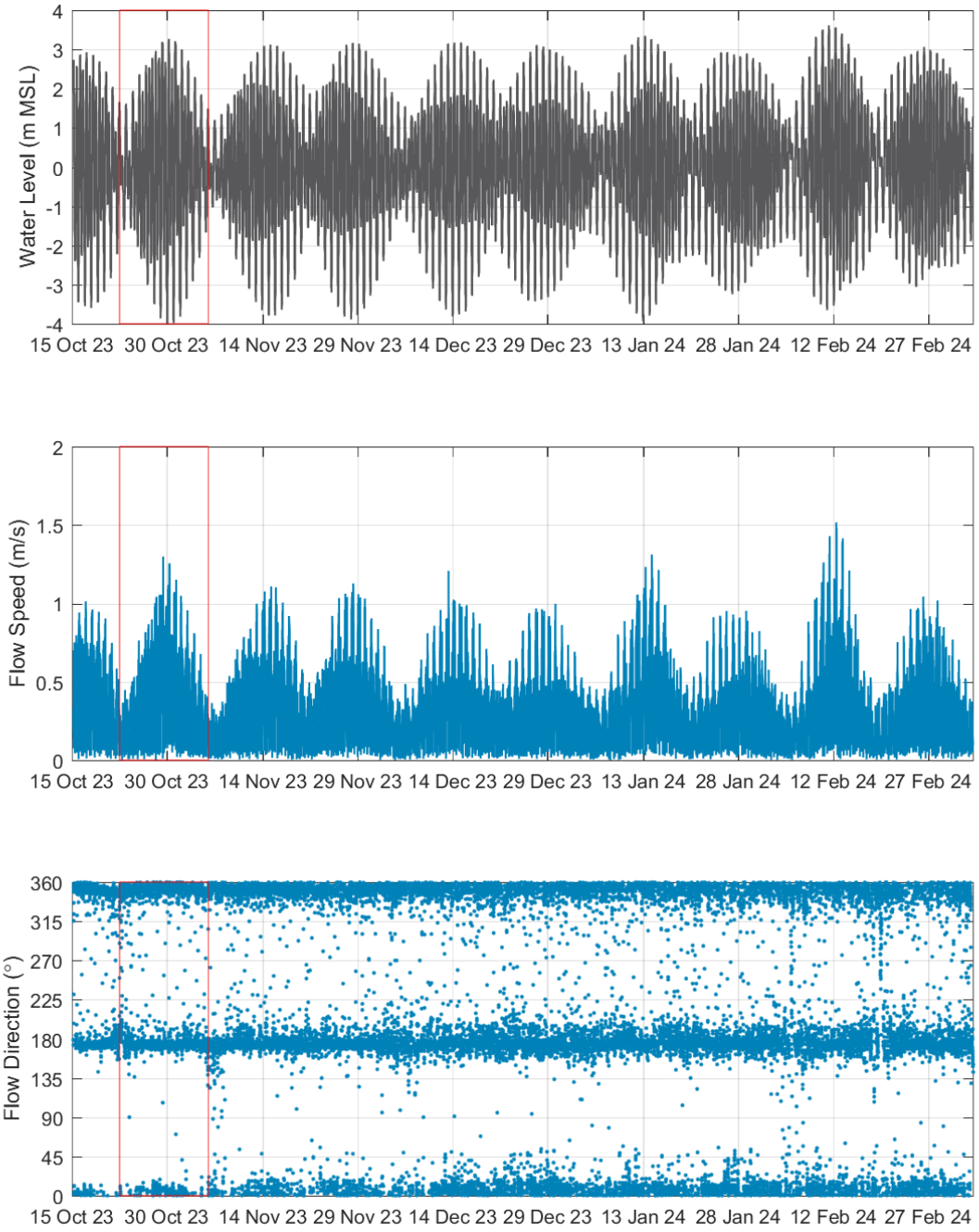

Figure 54. **Time series plots of the water level, mid-depth flow speed and mid-depth flow direction at AWAC-07 from October 2023 to March 2024.**

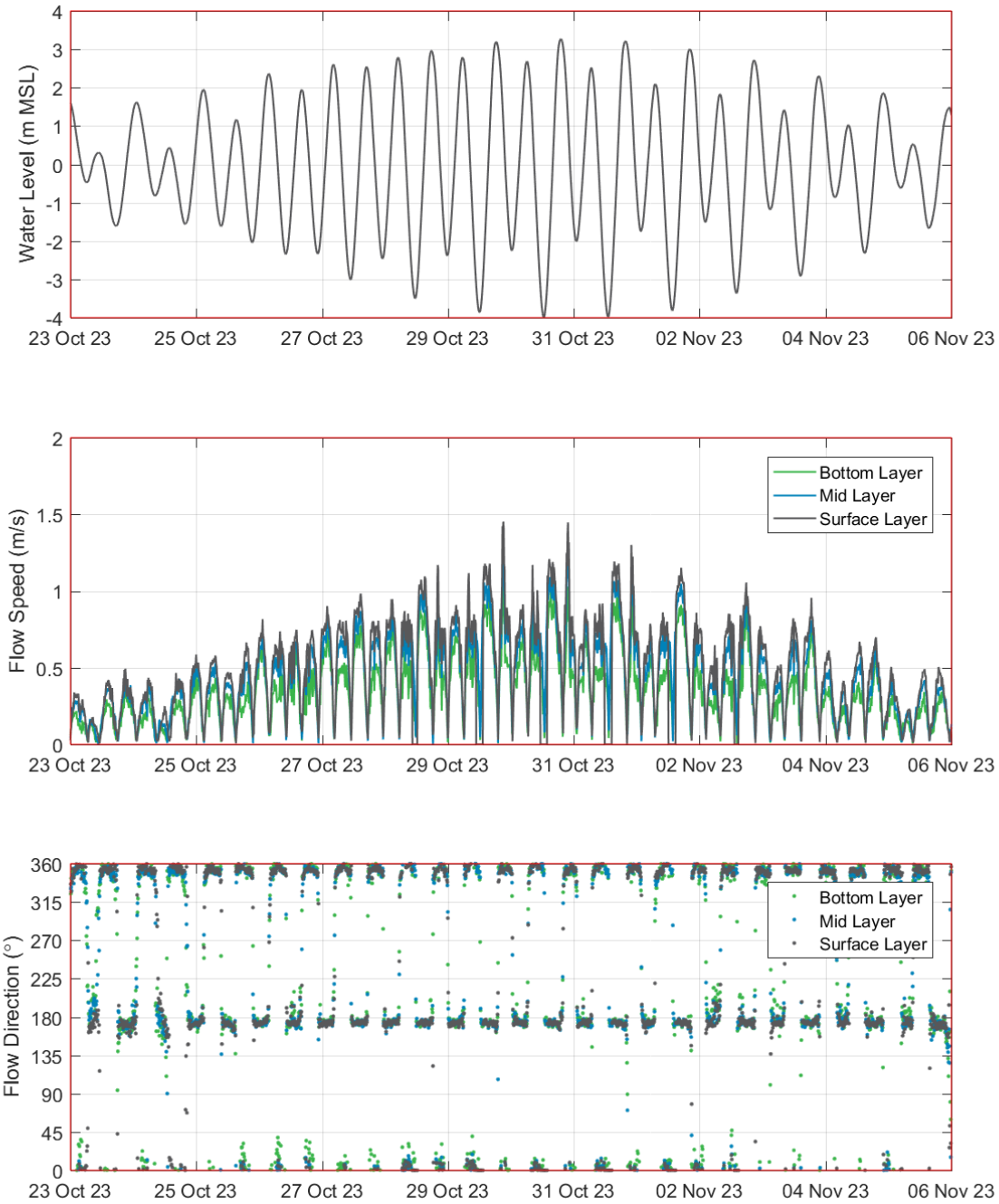

Figure 55. Time series plots of the water level, flow speed and flow direction at AWAC-07 over a 14 day spring neap tidal cycle.

5.2.1.6. AWAC-06 March to May 2024

Figure 56 shows water level, flow speed and direction for the 65 day deployment AWAC-06 (the second deployment at this site). In addition, data over a 14 day spring-neap tidal cycle are shown in Figure 57. Distinct spring and neap periods are evident, with corresponding maximum and minimum tidal ranges of approximately 6.5 m and 2 m respectively. The mid-depth peak flow speeds range from 0.5 m/s during neap tides to 1.5 m/s during spring tides. Figure 57 shows a 14 day spring-neap cycle, and presents flow speeds at three heights in the water column (surface (layer 11), mid-depth (layer 6) and bed (layer 1)). The flow speed is highest in the surface layer and lowest in the bed layer, with a difference of up to 0.5 m/s between the two layers. During spring tides the peak flow speeds are typically slightly higher during the ebb stage of the tide, with no clear dominance during smaller tides. The flow direction is relatively consistent through the water column and varies from south to south-southwest during the flood stage of the tide from north to north-northeast during the ebb stage of the tide.

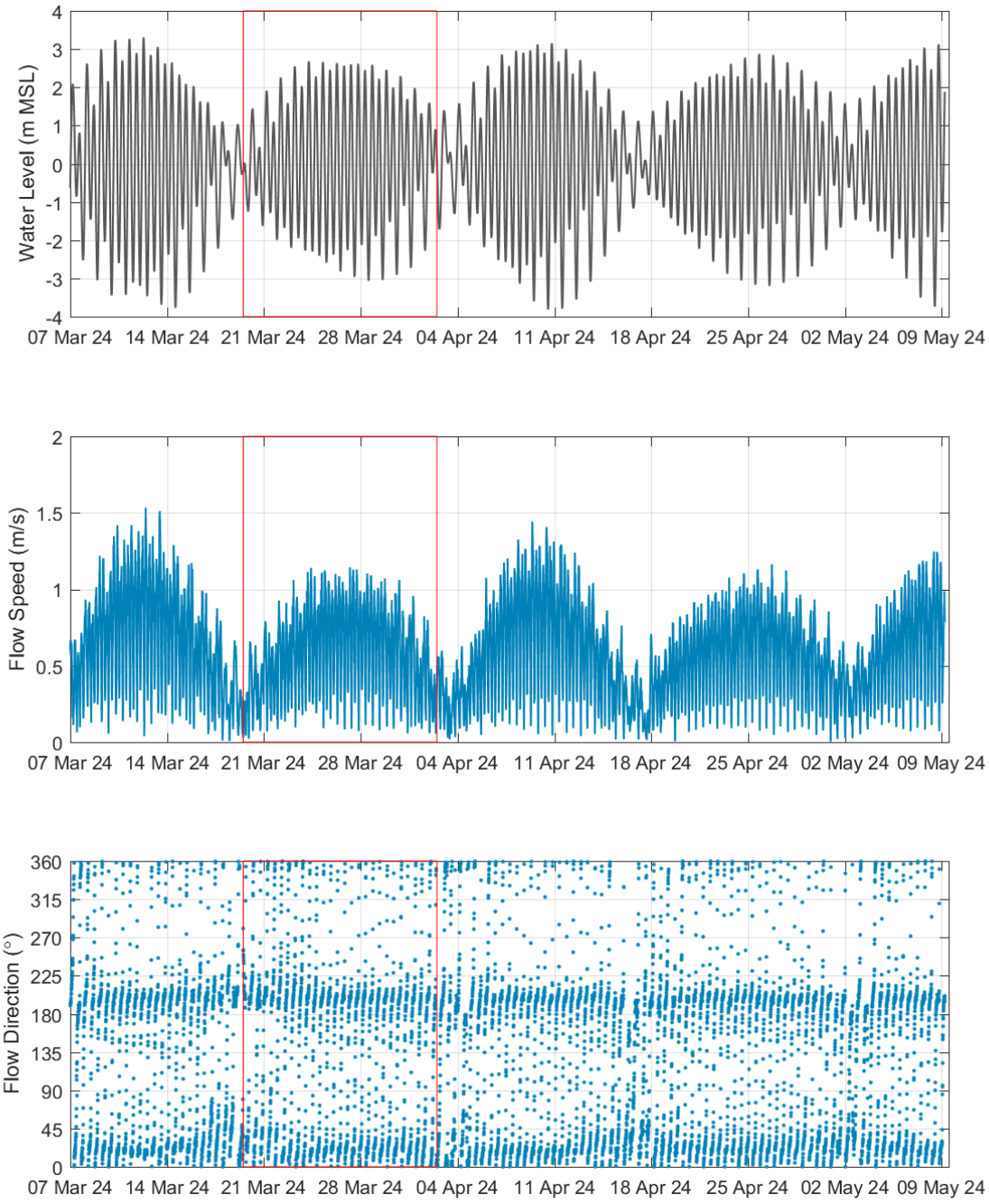

Figure 56. Time series plots of the water level, mid-depth flow speed and mid-depth flow direction at AWAC-06 from March to May 2024.

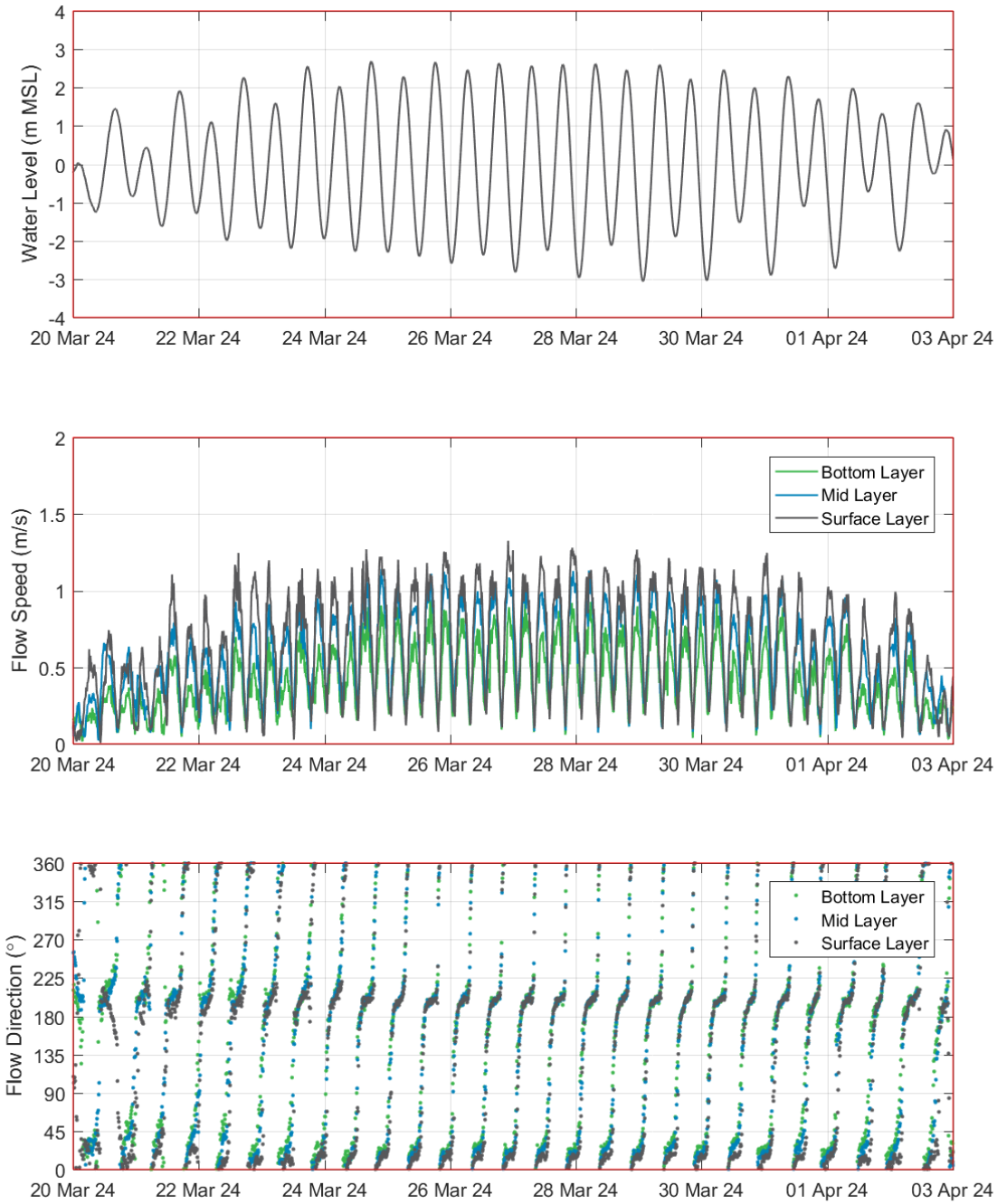

Figure 57. Time series plots of the water level, flow speed and flow direction at AWAC-06 over a 14 day spring neap tidal cycle.

5.2.1.7. AWAC-01 March to May 2024

Figure 58 shows water level, flow speed and direction for the 66 day deployment AWAC-01. In addition, data over a 14 day spring-neap tidal cycle are shown in Figure 59. There are clear spring and neap periods, with corresponding maximum and minimum tidal ranges of approximately 7 m and 2 m respectively. The flow speeds vary between the different spring and neap cycles, with the largest mid-depth current speed of 1.5 m/s occurring in March 2024. Figure 59 shows a 14 day spring-neap cycle, and presents flow speeds for three heights in the water column (surface (layer 22), mid-depth (layer 11) and bed (layer 1)). The flow speed is highest in the surface layer and lowest in the bed layer, with a difference of up to 0.8 m/s between the two layers. Current speeds during the ebb stage of the tide are typically higher than during the flood stage of the tide suggesting a slight ebb dominance at the site. The flow direction is consistent through the water column and varies from south-southeast to south during the flood stage of the tide from north-northwest to north during the ebb stage of the tide.

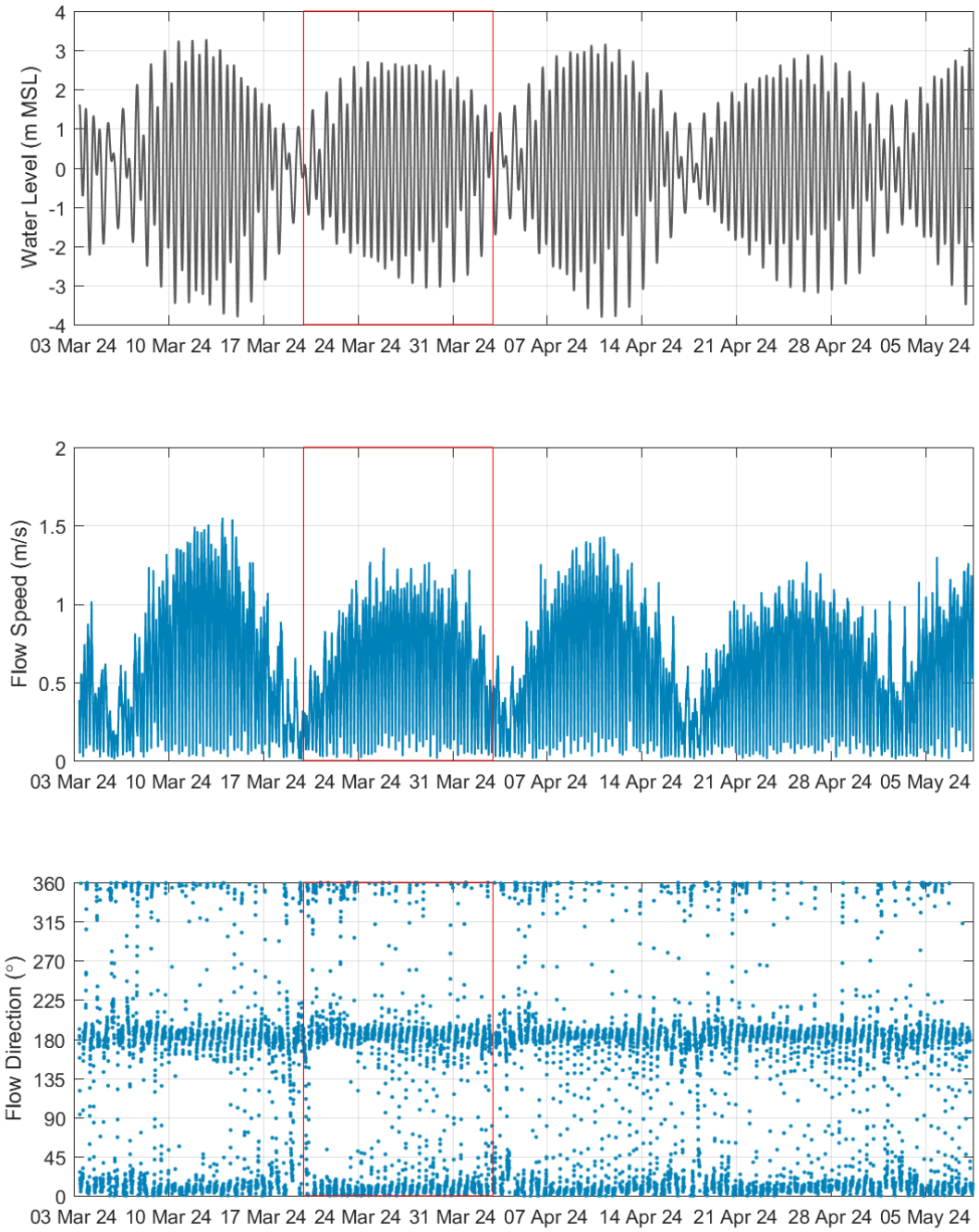

Figure 58. Time series plots of the water level, mid-depth flow speed and mid-depth flow direction at AWAC-01 from March to May 2024.

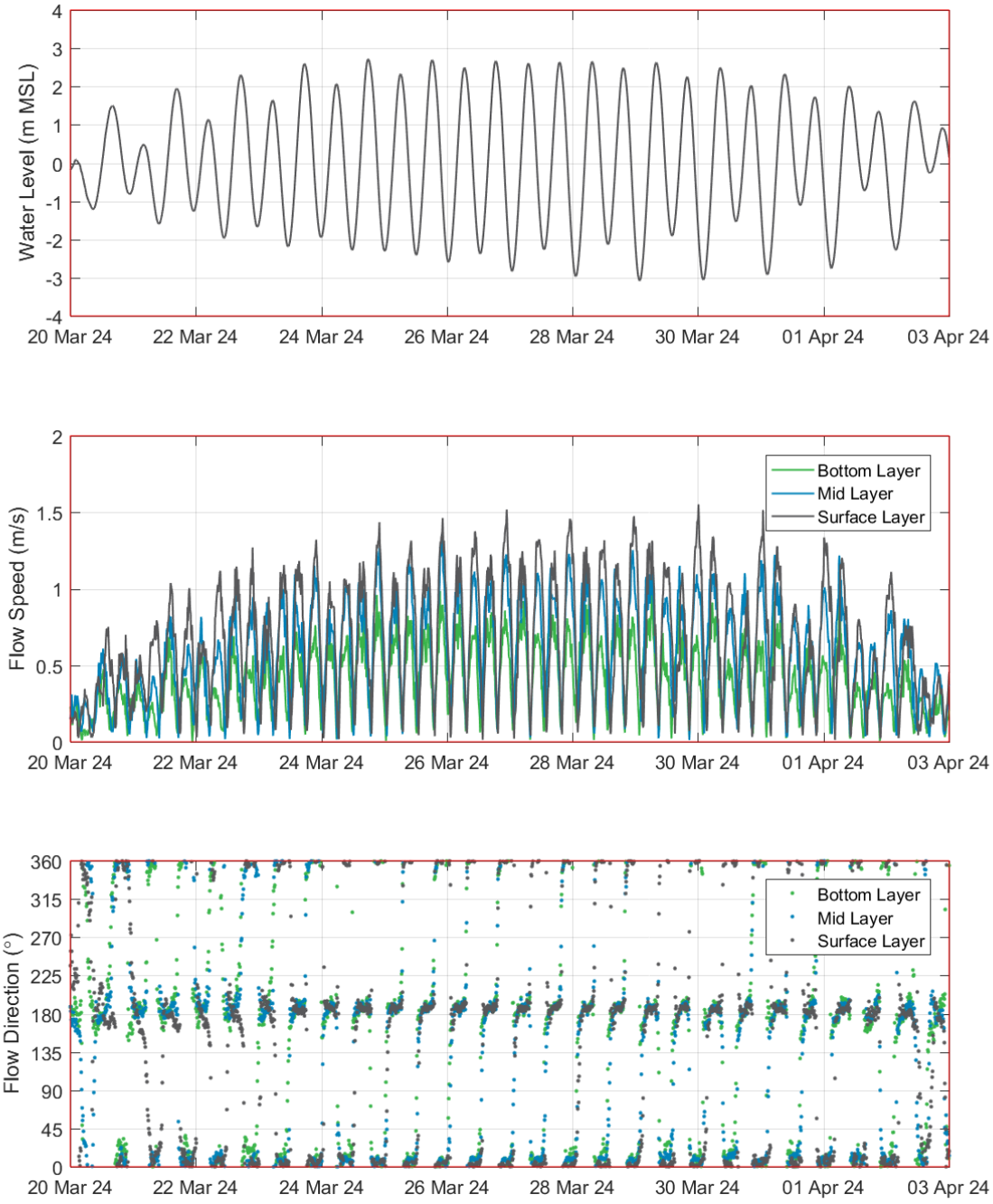

Figure 59. Time series plots of the water level, flow speed and flow direction at AWAC-01 over a 14 day spring neap tidal cycle.

5.2.1.8. AWAC-11 March to May 2024

Figure 60 shows water level, flow speed and direction for the 67 day deployment AWAC-11. In addition, data over a 14 day spring-neap tidal cycle are shown in Figure 61. There are clear spring and neap periods, with corresponding maximum and minimum tidal ranges of just over 7 m and 2.5 m respectively. The flow speeds vary between the different spring and neap cycles, with the largest mid-depth current speed of 1.5 m/s occurring in March 2024. Figure 61 shows a 14 day spring-neap cycle, and presents flow speeds for three heights in the water column (surface (layer 14), mid-depth (layer 7) and bed (layer 1)). The flow speed is highest in the surface layer and lowest in the bed layer, with a difference of up to 1.0 m/s between the two layers. There is a strong ebb dominance present in the surface layer, this dominance reduces with depth through the water column. The flow direction is consistent through the water column south-southeast flows during the flood stage of the tide from north-northwest flows during the ebb stage of the tide.

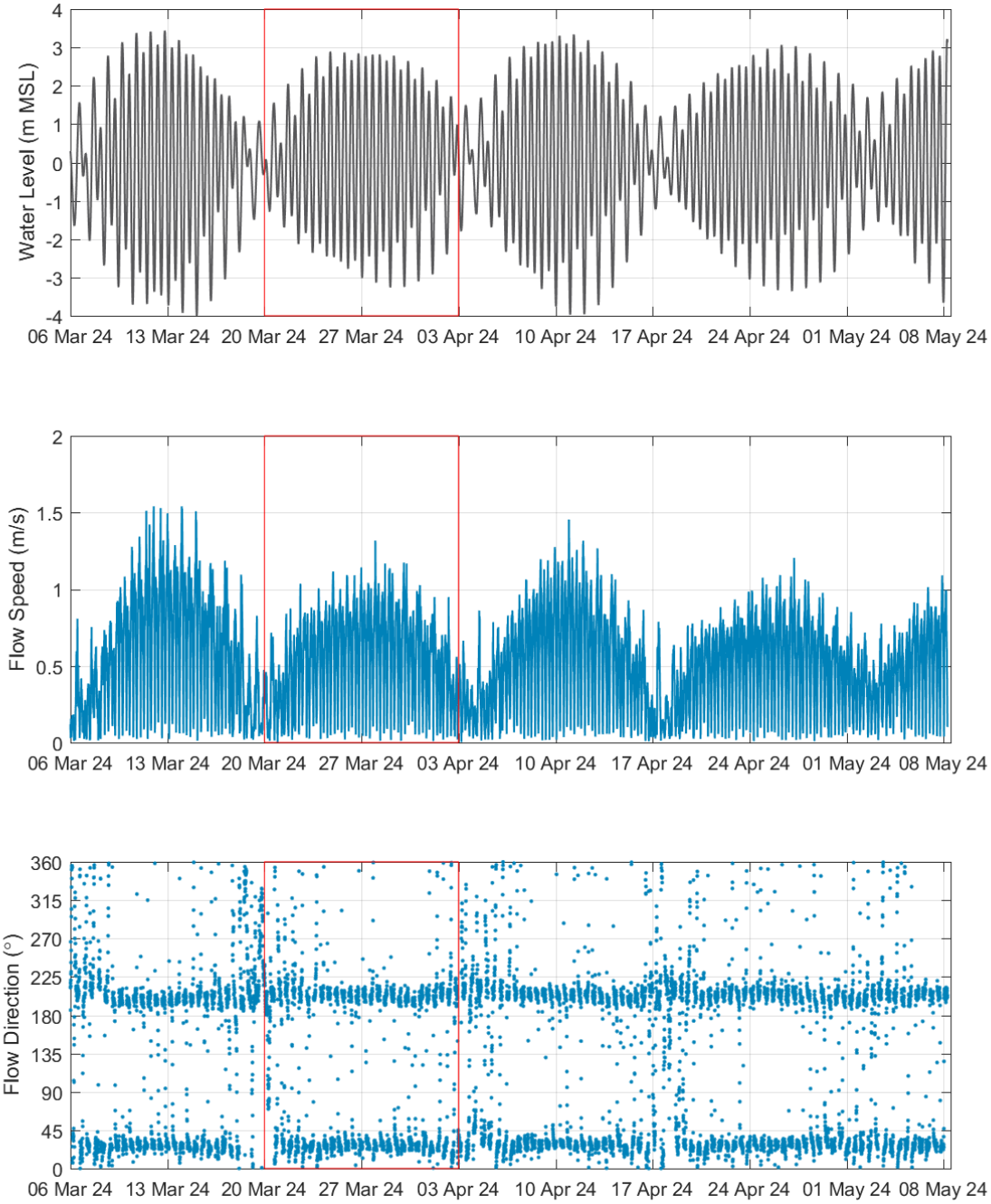

Figure 60. Time series plots of the water level, mid-depth flow speed and mid-depth flow direction at AWAC-11 from March to May 2024.

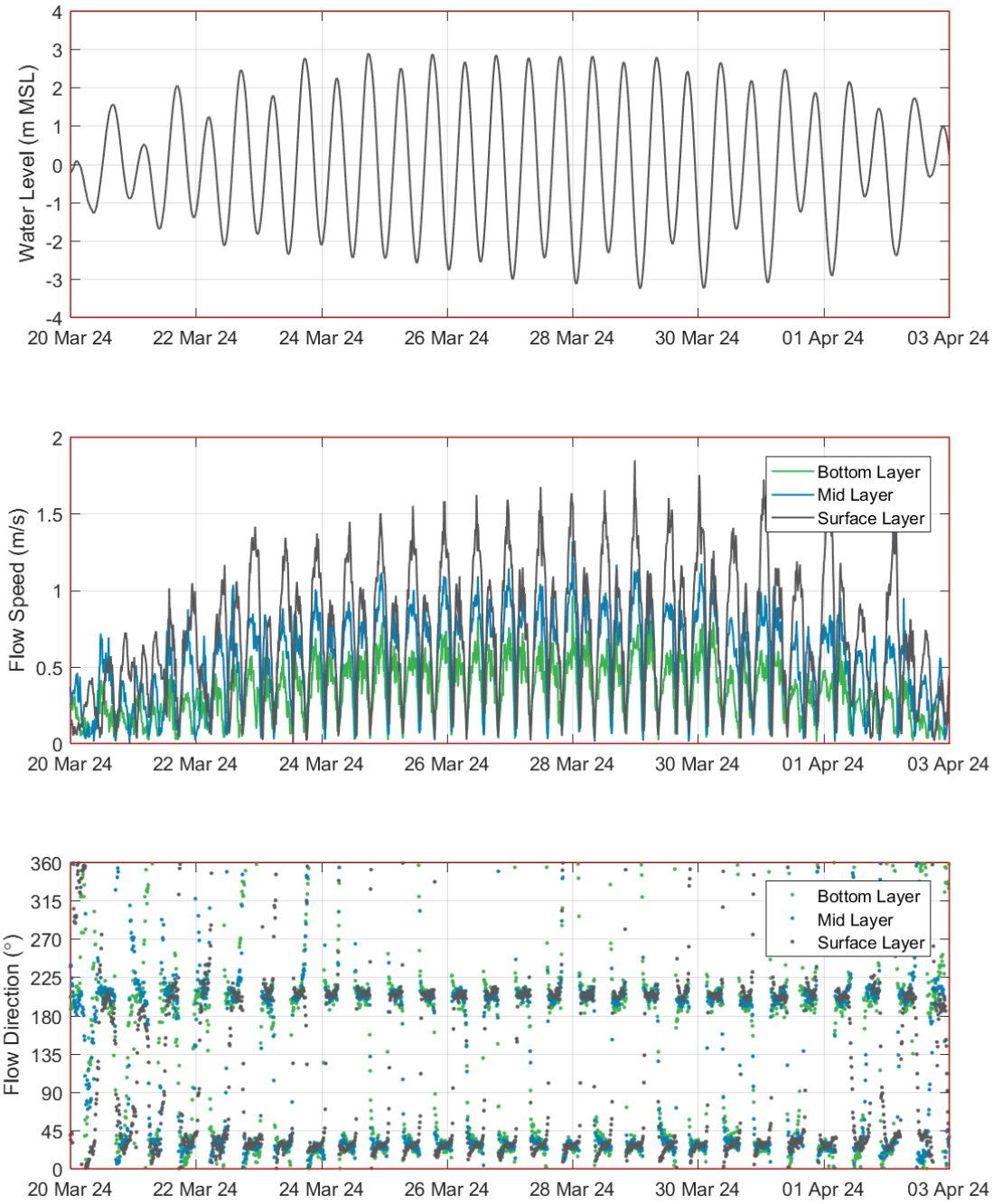

Figure 61. Time series plots of the water level, flow speed and flow direction at AWAC-11 over a 14 day spring neap tidal cycle.

5.2.2. Waves

This section presents the wave data from each of the AWAC deployments detailed in Section 5.1. Results are presented in chronological order.

5.2.2.1. AWAC-02 September 2023

Figure 62 displays wave height (H_{m0}), peak wave period (T_p) and mean wave direction (herein referred to as wave direction) over the deployment at AWAC-02. The H_{m0} over the period remains consistent at between 0.2 and 0.3 m, while the T_p increases from 1.5 to 4 seconds over the period and the wave direction is predominantly from the north northwest to north.

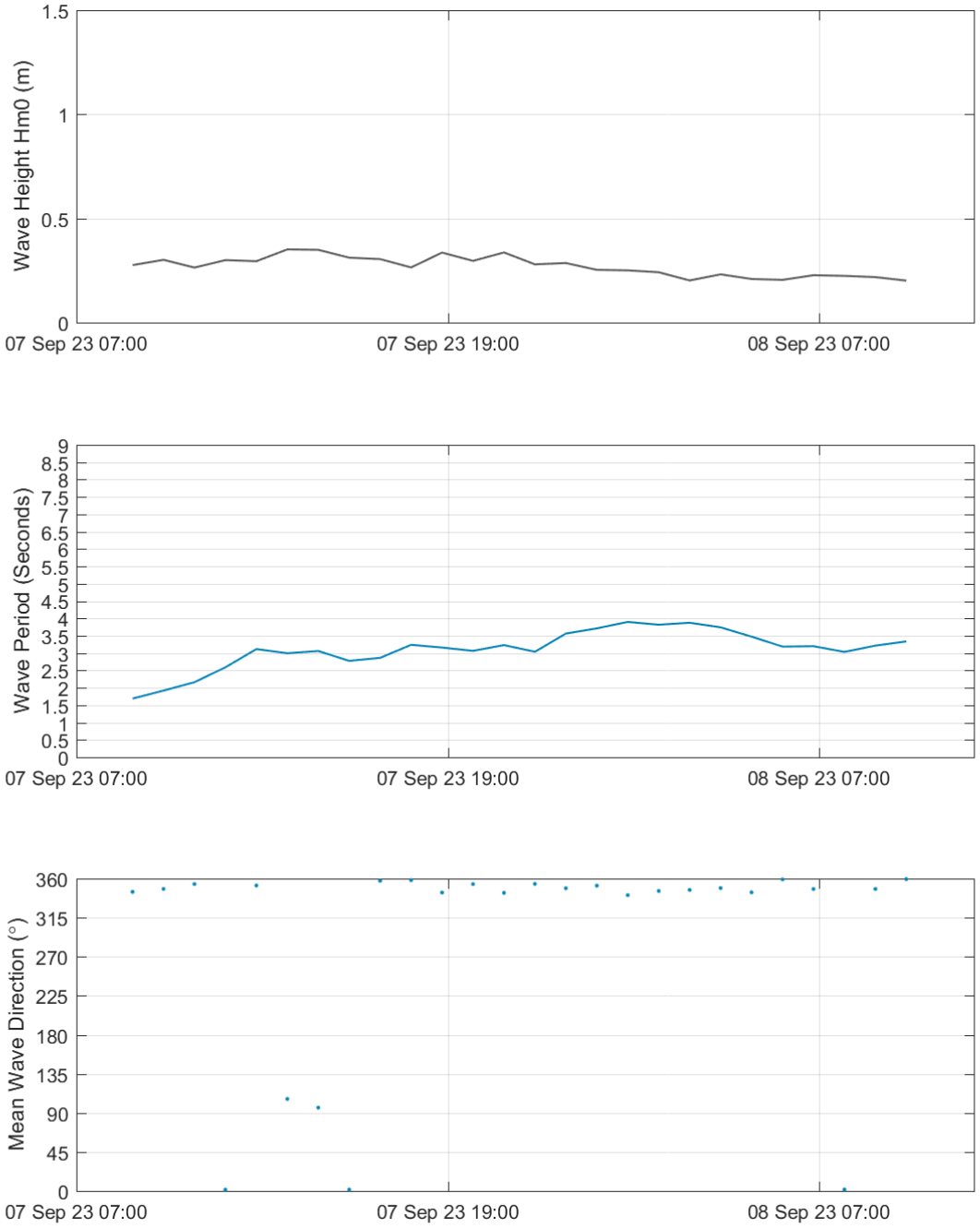

Figure 62. Time series plots of the H_{m0}, T_p and mean wave direction at AWAC-02 in September 2023.

5.2.2.2. AWAC-06 September to October 2023

Figure 63 shows the H_{m0}, T_p and mean wave direction over the 35 day deployment at AWAC-06. The H_{m0} over the period varies from 0.1 to 1.0 m, while the T_p varies between 1.5 and 8 seconds over the period and the wave direction is predominantly from the north to northeast. The data over the first and last 7 days show a clear diurnal variability, with an increase in H_{m0} and T_p occurring through the day, followed by a reduction overnight. This indicates that the local wind conditions are the main influence on the waves over these periods.

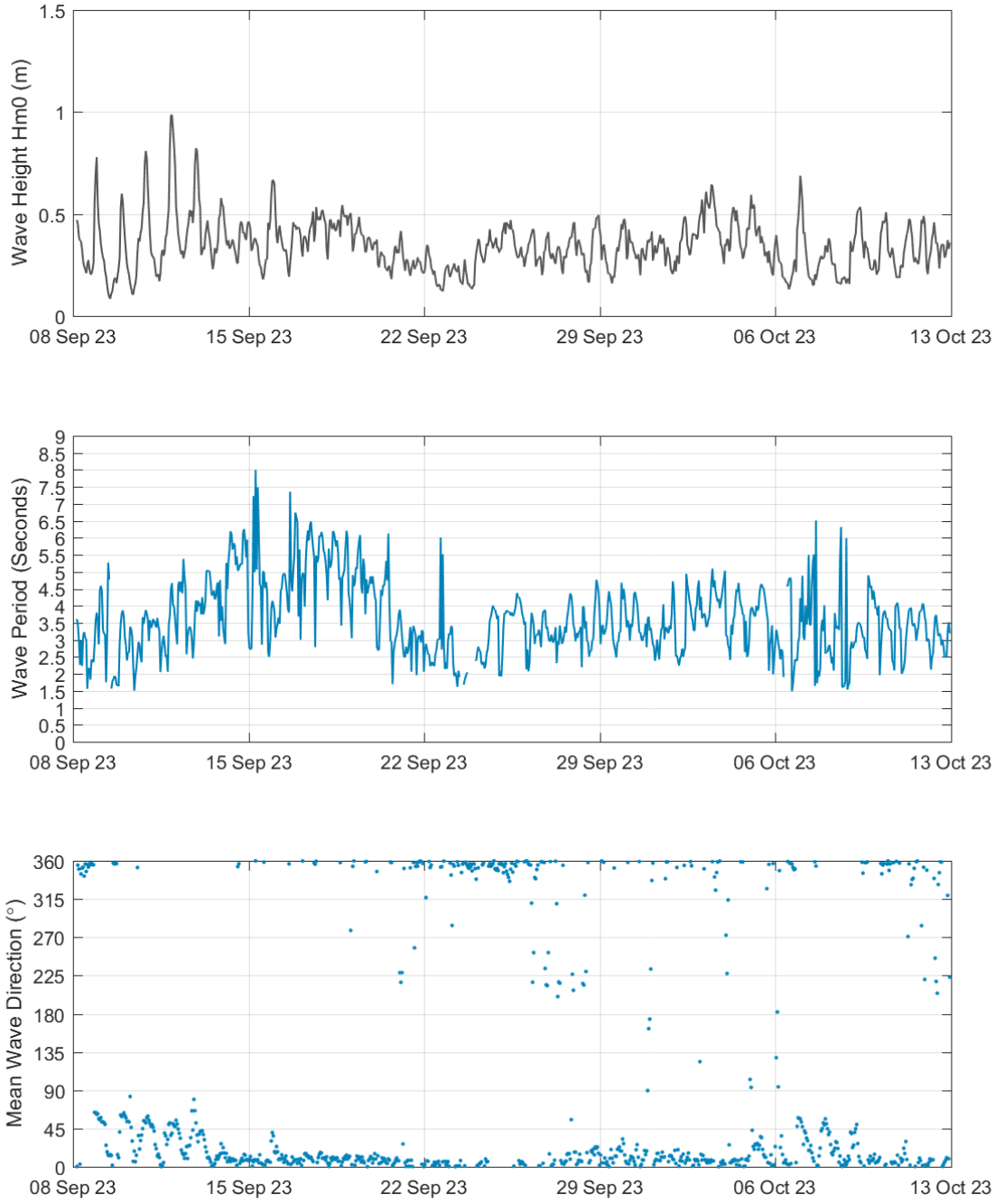

Figure 63. Time series plots of the H_{m0}, T_p and mean wave direction at AWAC-06 from September to October 2023.

5.2.2.3. AWAC-03 October 2023

Figure 64 shows the H_{m0}, T_p and mean wave direction over the 46 hour deployment at AWAC-03. The H_{m0} over the period varies from 0.15 to 0.4 m, while the T_p varies between 1.5 and 5.5 seconds over the period and the wave direction is predominantly from the north to northeast. The data show higher wave heights occurring through the day, followed by a reduction overnight.

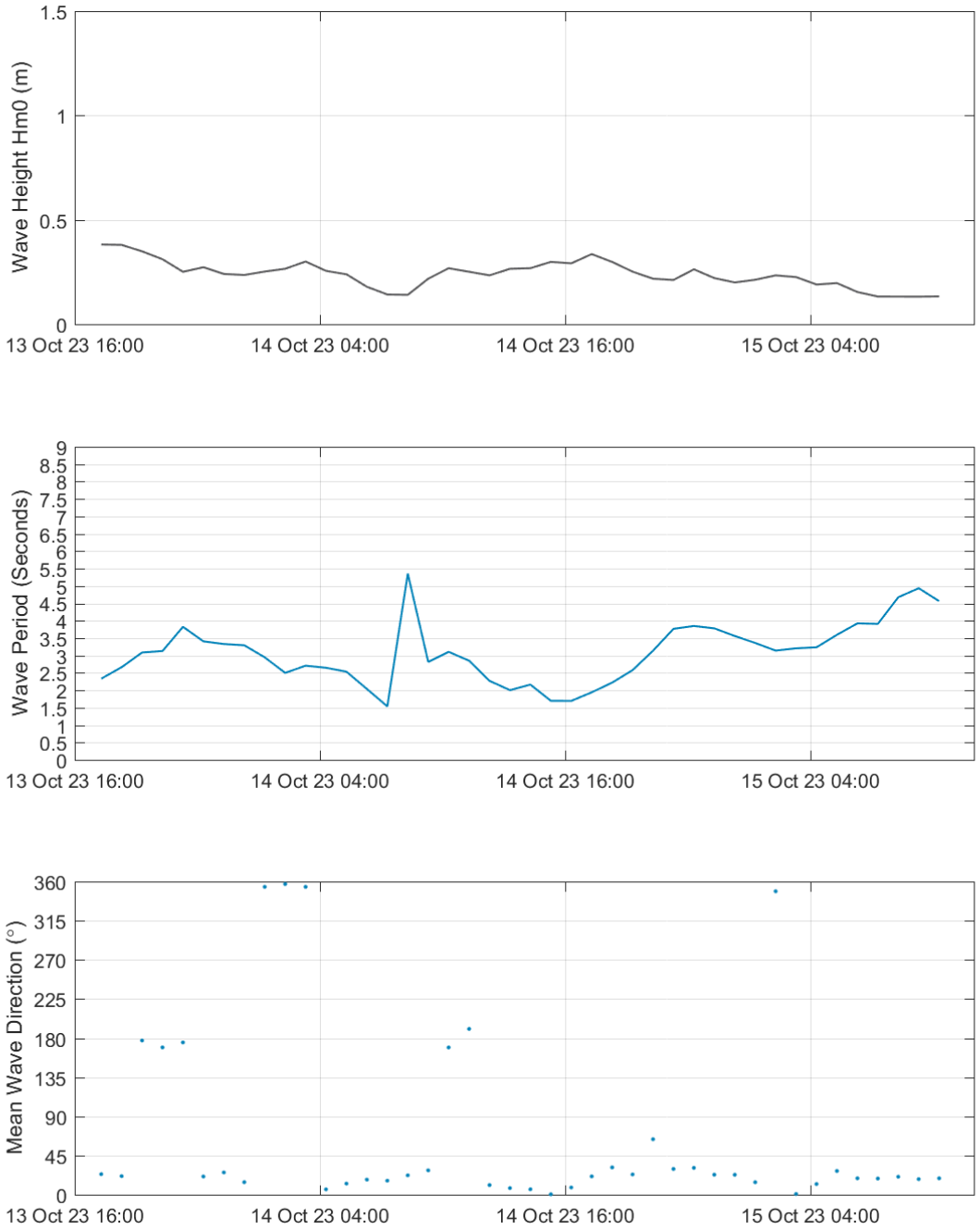

Figure 64. Time series plots of the H_{m0}, T_p and mean wave direction at AWAC-03 in October 2023.

5.2.2.4. AWAC-07 October 2023 to March 2024

Figure 65 shows the H_{m0}, T_p and mean wave direction over the 142 day deployment at AWAC-07. The H_{m0} over the period varies from 0.1 to 1.1 m, while the T_p varies between 1 and 8 seconds over the period and the wave direction is predominantly between the northwest and northeast. The data show a clear diurnal tidal signal in wave height during October to December, while in January and February the diurnal variability appears to be reduced indicating that a change in the wind conditions has changed the local wave conditions at the site. In addition, T_p is higher during January and February compared to October to December, indicating that waves generated offshore in Joseph Bonaparte Gulf (JBG) influence CG more often in the wet season compared to the dry season.

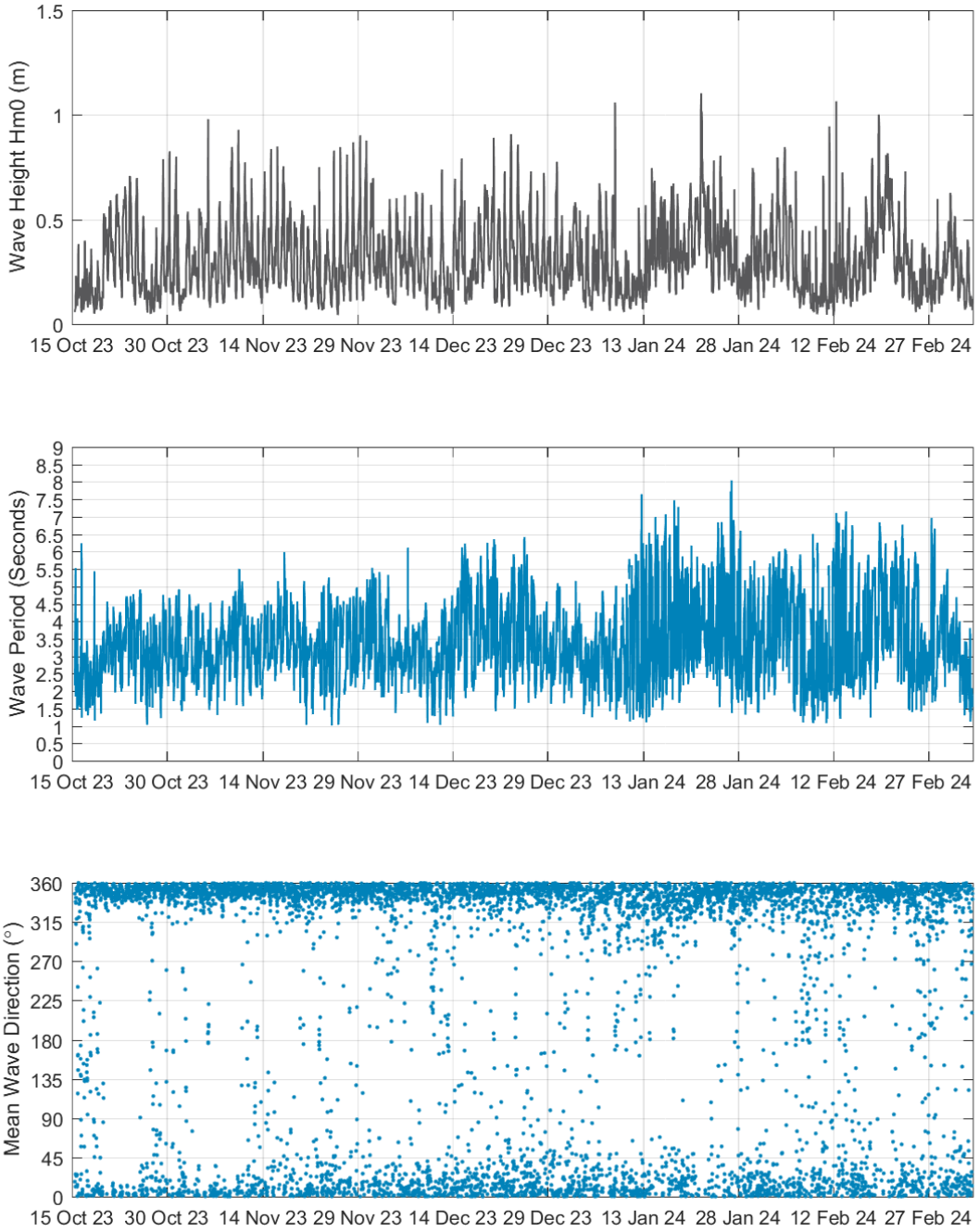

Figure 65. Time series plots of the H_{m0}, T_p and mean wave direction at AWAC-07 from October 2023 to March 2024.

5.2.2.5. AWAC-06 March to May 2024

Figure 73 shows the H_{m0}, T_p and mean wave direction over the 65 day deployment at AWAC-06. The H_{m0} over the period varies from 0.1 to 1.2 m, while the T_p varies between 1.5 and 8.5 seconds over the period and the wave direction is predominantly between the northwest and northeast. The wave conditions during March 2024 show more variability with limited diurnal variation while the wave conditions during April and May 2024 have less variability and experience a consistent diurnal variability. This suggests that the waves in March can be considered to be representative of wet season conditions (generated offshore in JBG), while the waves in April and May were more representative of dry season conditions (generated by local winds in CG).

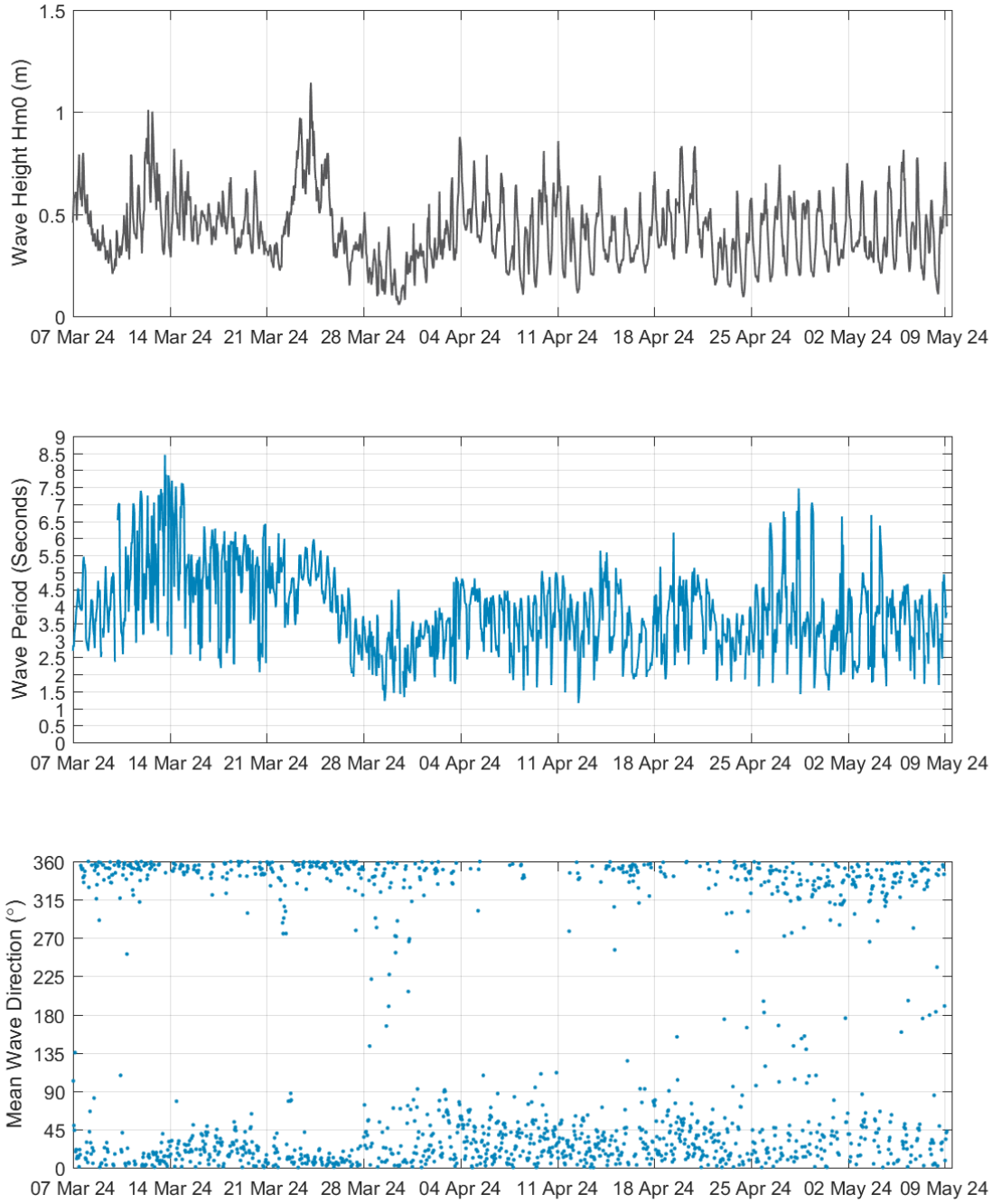

Figure 66. Time series plots of the H_{m0}, T_p and mean wave direction at AWAC-06 from March to May 2024.

5.2.2.6. AWAC-01 March to May 2024

Figure 67 shows the H_{m0}, T_p and mean wave direction over the 66 day deployment at AWAC-01. The H_{m0} over the period varies from 0.1 to 1.0 m, while the T_p varies between 1 and 9 seconds over the period and the wave direction is predominantly from the northwest to northeast. The T_p is noticeably higher during March with values of between 4 and 8 s for much of this period, while during April and May the T_p was typically between 2 and 5 s. As with the data at AWAC-06 this suggests that the waves in March can be considered to be representative of wet season conditions (generated offshore in JBG), while the wave in April and May were more representative of dry season conditions (predominantly generated by local winds in CG).

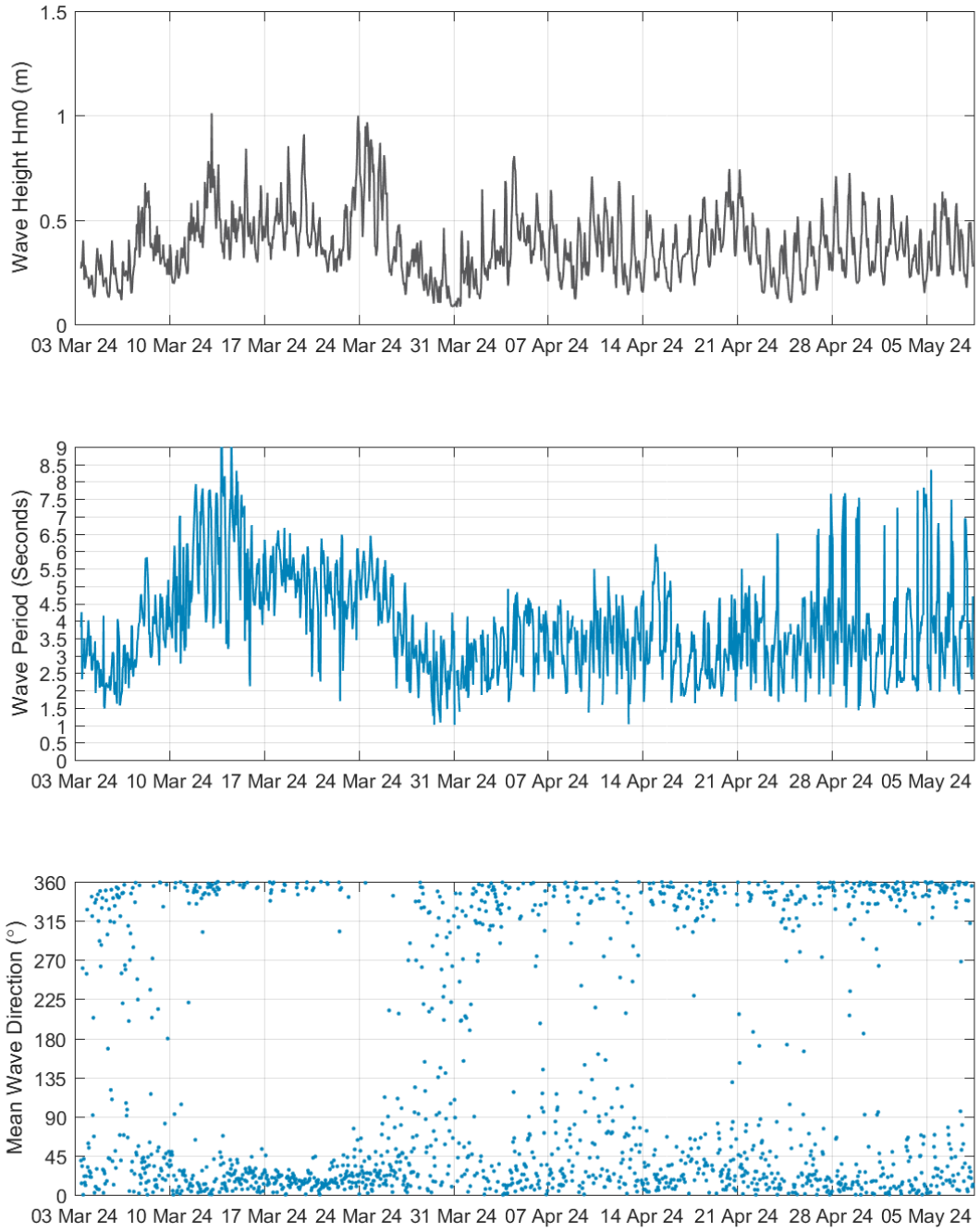

Figure 67. Time series plots of the H_{m0}, T_p and mean wave direction at AWAC-01 from March to May 2024.

5.2.2.7. AWAC-11 March to May 2024

Figure 68 shows the H_{m0}, T_p and mean wave direction over the 67 day deployment at AWAC-11. The H_{m0} over the period varies from 0.1 to 1.1 m, while the T_p varies between 1 and 8 seconds over the period and the wave direction is predominantly from the north to northeast. The T_p is slightly higher during March with values of between 3 and 6 s for much of this period, while during April and May the T_p was typically between 2 and 5 s. As with the data at AWAC-06 and AWAC-01, this is likely to be due to a change from wet season to dry season conditions, although the change is less at this site which could be a result of the site being located further into CG compared to the other two sites.

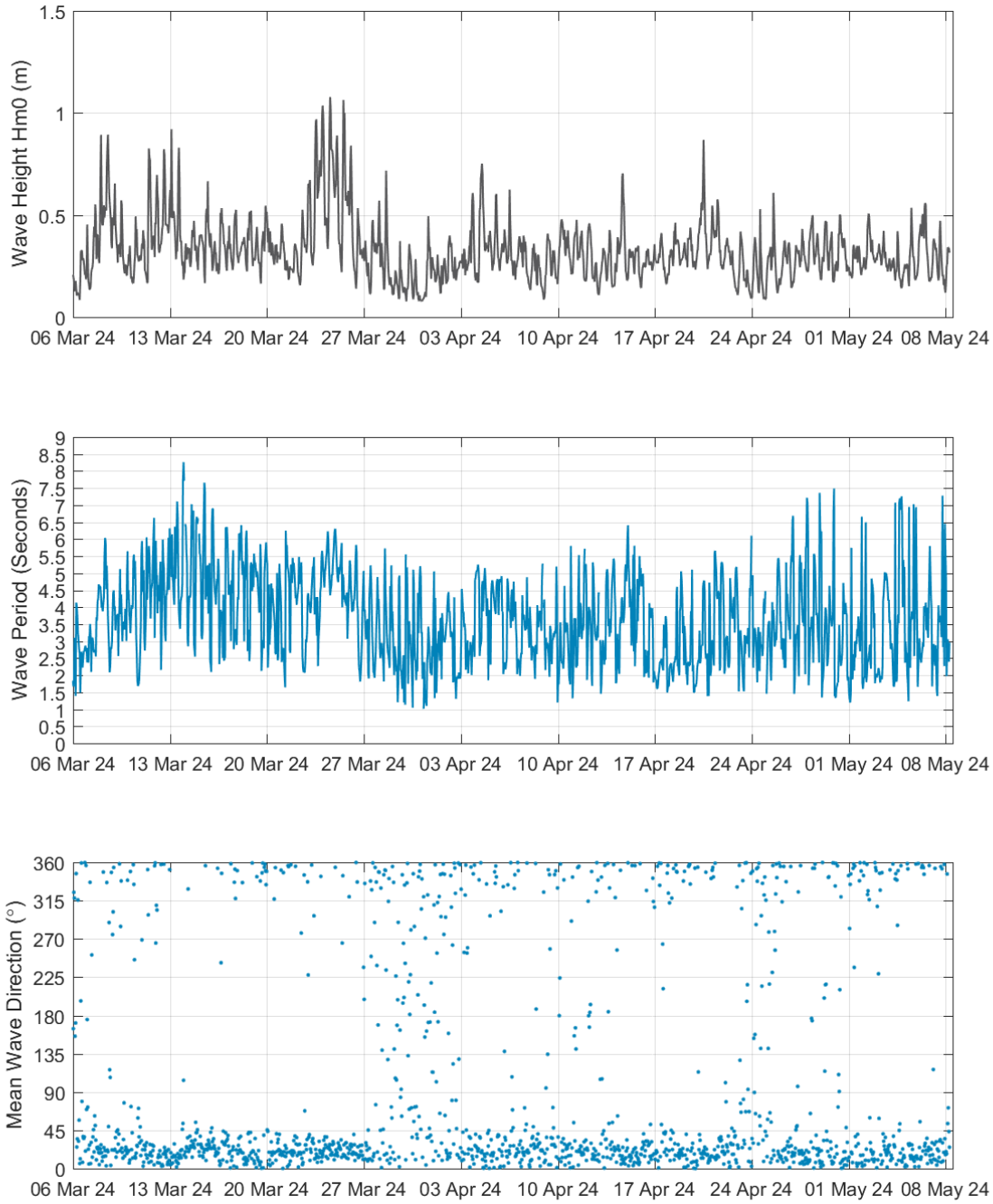

Figure 68. Time series plots of the H_{m0}, T_p and mean wave direction at AWAC-11 from March to May 2024.

5.2.2.8. March to May 2024 Comparison

A comparison between the measured wave conditions from March to May 2024 at AWAC-01 and AWAC-11 and at AWAC-06 and AWAC-11 are shown in Figure 69 and Figure 70. These three sites represent the eastern entrance to CG (AWAC-06, approximately 3 km to the east of Lacrosse Island), within the proposed operational area (AWAC-01,

approximately 7 km southwest of Lacrosse Island) and to the south of the proposed operational area (AWAC-11, approximately 20 km southwest of Lacrosse Island). Therefore, AWAC-06 will be the most exposed to offshore wave conditions, while AWAC-01 is likely to be more sheltered from offshore waves and AWAC-11 is likely to be the most sheltered location in terms of offshore waves.

The plots show that wave heights were smaller at AWAC-11 during the April to May period during dry season conditions compared to AWAC-06 and AWAC-01. However, during the wet season wave events in March, the wave height at AWAC-11 was larger than at the other two sites at certain times, indicating that ongoing wave growth occurred within CG due to local wind conditions for specific wind directions. Wave periods and wave directions were generally similar at the three sites, although the wave period at AWAC-11 was typically slightly lower compared to the other two sites during the wet season wave events.

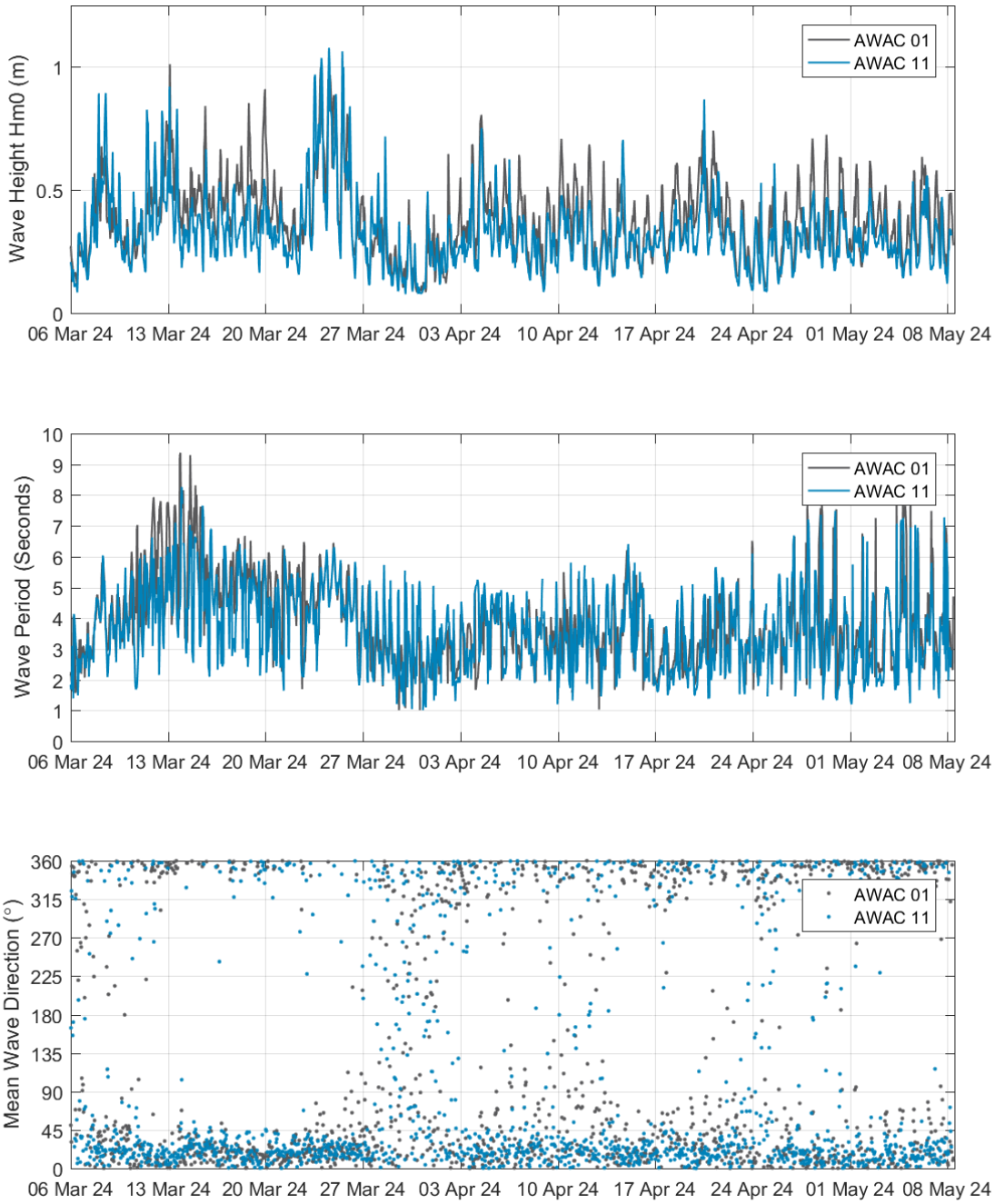

Figure 69. Comparison between wave conditions at sites AWAC-01 and AWAC-11 from March to May 2024.

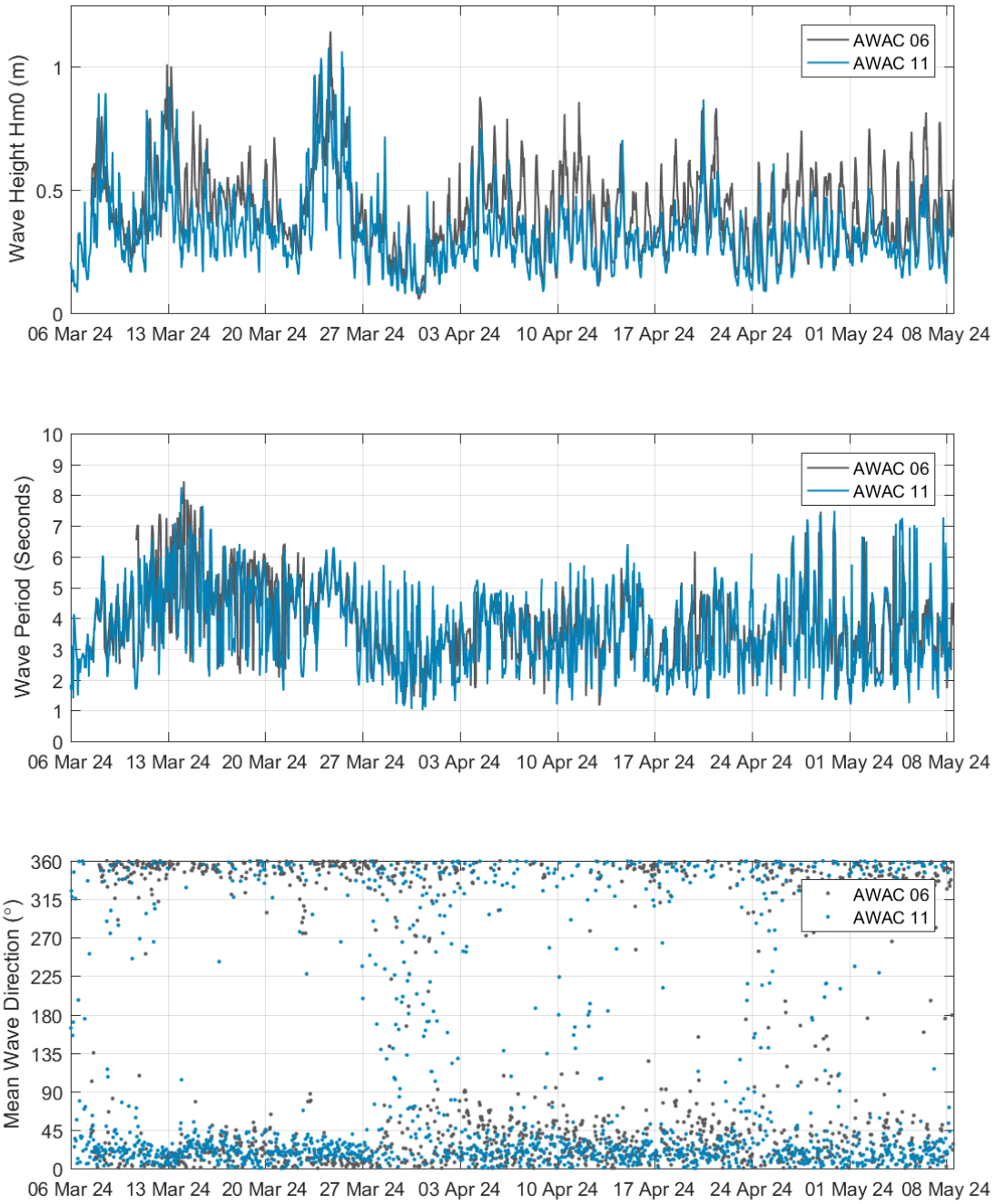

Figure 70. Comparison between wave conditions at sites AWAC-06 and AWAC-11 from March to May 2024.

6. In-situ Benthic Light and Water Quality Data

6.1. Data Overview

LI-COR LI-1500 light sensors and Manta Multiprobes have been attached to the same frame as the AWAC/ADCPs and to frames without an AWAC/ADCP (Pos 12 to Pos 15) to measure benthic photosynthetically active radiation (PAR), depth and water quality parameters (temperature, salinity, turbidity, depth, dissolved oxygen and pH). The available PAR, depth and water quality data which have been analysed as part of this assessment are summarised below and the monitoring sites are shown in Figure 48:

- AWAC-01: No benthic light or water quality instruments were attached to the AWAC frame for the deployment in June to July 2023. For the 66 day deployment from 3rd March to 8th May 2024 there was an issue with the LI-COR instrument meaning that no PAR data were recorded, but depth and water quality data were collected.
- AWAC-02: PAR, depth and water quality data were collected for 27 hours over 7th September to 8th September 2023.
- AWAC-03: There was an issue with the LI-COR instrument resulting in no PAR data being recorded. Water quality and depth data were collected for 46 hours over 13th October to 15th October 2023 but there was an issue with the turbidity sensor meaning that the turbidity data were unreliable (negative values).
- AWAC-04: PAR data were collected for 25 hours over 7th September to 8th September 2023, but no additional water quality or depth data were collected.
- AWAC-06: During the September to October 2023 deployment there was an issue with the LI-COR instrument meaning that the PAR data were unreliable, but PAR data were recorded at the site during the second deployment from 7th to 13th March 2024. Water quality and depth data were collected for 35 days from 8th September to 13th October 2023 and for 54 days from 7th March to 9th May 2024.
- AWAC-07: PAR data were collected for eight days from 15th October to 22nd October 2023. Water quality and depth data were collected for 142 days from 15th October 2023 to 5th March 2024, but there was an issue with the turbidity sensor meaning that the turbidity data were unreliable.
- AWAC-08: PAR data were collected for eight days from 2nd March to 9th March 2024. Water quality and depth data were collected for 108 days from 2nd March to 18th June 2024
- AWAC-11: PAR data were collected for eight days from 2nd March to 9th March 2024. Water quality and depth data were collected for 68 days from 2nd March to 12th May 2024.
- Pos-12: PAR data were collected for eight days from 4th March to 11th March 2024. Water quality and depth data were collected for 109 days from 4th March to 21st June 2024.
- Pos-13: PAR data were collected for eight days from 2nd March to 9th March 2024. Water quality and depth data were collected for 70 days from 2nd March to 8th May 2024.
- Pos-14: PAR data were collected for eight days from 3rd March to 10th March 2024. Water quality and depth data were collected for 109 days from 3rd March to 20th June 2024.

Additional PAR and water quality data are being collected in CG and will provide additional data at the monitoring sites.

6.2. Results

6.2.1. Benthic Light

The available benthic light data collected to date in CG has been analysed as part of this assessment to provide a better understanding of the conditions in CG. The data at all of the available sites showed very low benthic irradiance, with virtually no light at all and with most sites (except the shallowest two at Pos-13 and Pos-14) showing no temporal pattern in the benthic irradiance as would be expected due to variations in ambient light between day and night. In addition, at all sites except the shallowest two (Pos-13 and Pos-14), the upward and downward facing sensors did not show a consistent difference (i.e. the upward facing sensor always having higher values), suggesting that there was no light and the measurements by the two sensors were due to background noise caused by the accuracy and resolution of the sensors.

Example plots from the measurements at AWAC-02 (depth of 21.5 m MSL), AWAC-04 (depth of 28.5 m MSL), AWAC-11 (depth of 22.3 m MSL) as well as Pos-13 and Pos-14 (the shallowest two sites with a depth of 13.5 m MSL), are shown in Figure 71 to Figure 75. At sites AWAC-02, AWAC-04 and AWAC-11, the measurements are consistently less than 0.02 µmol/m^2/s and with no variability in the measurements between day and night. In contrast, the measurements at Pos-13 and Pos-14, which are 8 m shallower than any of the other sites, showed low levels of benthic light during daylight hours for up to five days (peaks ranging from 0.05 to 0.5 µmol/m^2/s at Pos-13 and 0.13 to 4.4 µmol/m^2/s at Pos-14), with the upward facing sensor recording higher values than the downward facing sensor (peaks of less than 0.1 µmol/m^2/s for downward facing sensor at Pos-13 and less than 0.5 µmol/m^2/s at Pos-14). Over this same period the measurements at the deeper AWAC-11 site within CG (22.3 m MSL compared to 13.5 m MSL) showed no benthic light, while the offshore site at King Shoals at Pos-12 (28 m MSL compared to 13.5 m MSL) experienced a single tide with a very low peak in benthic light of 0.025 µmol/m^2/s. Sentinel 3 satellite imagery was sourced to determine the cloud cover in the area over the measurement period for AWAC-02 and AWAC-04 and the imagery showed that there was no cloud cover over the CG at 10:00 am on both days, meaning that the very low benthic light measurements were not due to low ambient light over the period.

To better understand the conditions which resulted in elevated benthic light at Pos-13 and Pos-14, concurrent water level and turbidity data at the sites are shown along with the benthic light data in Figure 76 and Figure 77. The plots show that the benthic light coincided with neap tides when the turbidity was at its lowest (generally between 10 and 15 NTU at Pos-13 and less than 10 NTU at Pos-14). At Pos-13 the highest benthic light occurred during the morning (between 06:00 and 12:00) which coincided with high water during the measurement period. The reason for the elevated light to occur in the morning is likely to be related to the tidal state rather than the time of day, with lower turbidity water from offshore being present in CG around high water and the turbidity then increasing during the ebb stage of the tide as higher turbidity water from upstream flowed into CG, which significantly reduced the benthic light. At Pos-14 there was less variability in turbidity over the tidal cycle (due to the site being closer to the entrance to CG relative to Pos-13) and as a result the highest peaks in benthic light occurred around low water when the water depths were lowest. At both sites, when the average turbidity increased above approximately 20 NTU, there was no benthic light. The results therefore indicate that benthic light is available in the shallower regions of CG, but that in depths of 13.5 m MSL, the light is only available during neap tides when the turbidity is at its lowest, with no benthic light during other periods.

The benthic light data show that there is no benthic light available at the sites in CG in water depths of more than 20 m. This correlates with previous results from a drop camera that was deployed to the seabed at all 35 vibro-core sites in Block 4 in March 2023 and at all 132 benthic grab sites across CG and King Shoals in July and August 2023. All videos showed a completely blacked-out aphotic zone caused by a constantly suspended sediment layer for several metres above the seabed. Example plots from the drop camera through the water column are shown in Figure 78.

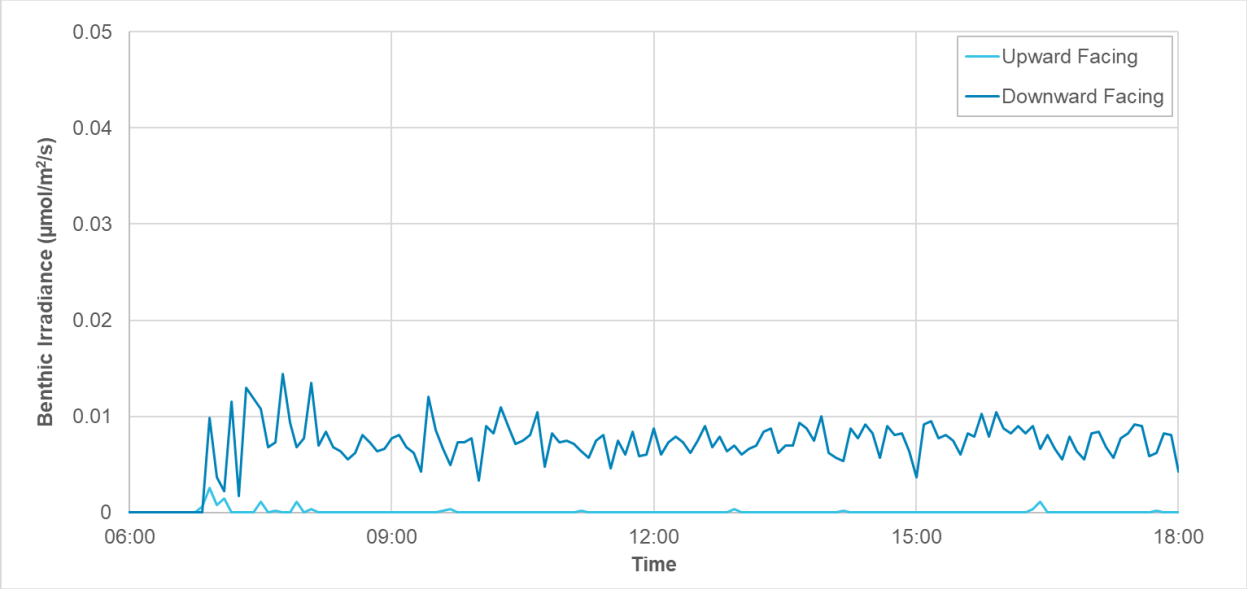

Figure 71. Time series of instantaneous benthic light at AWAC-02 on 07/09/2023.

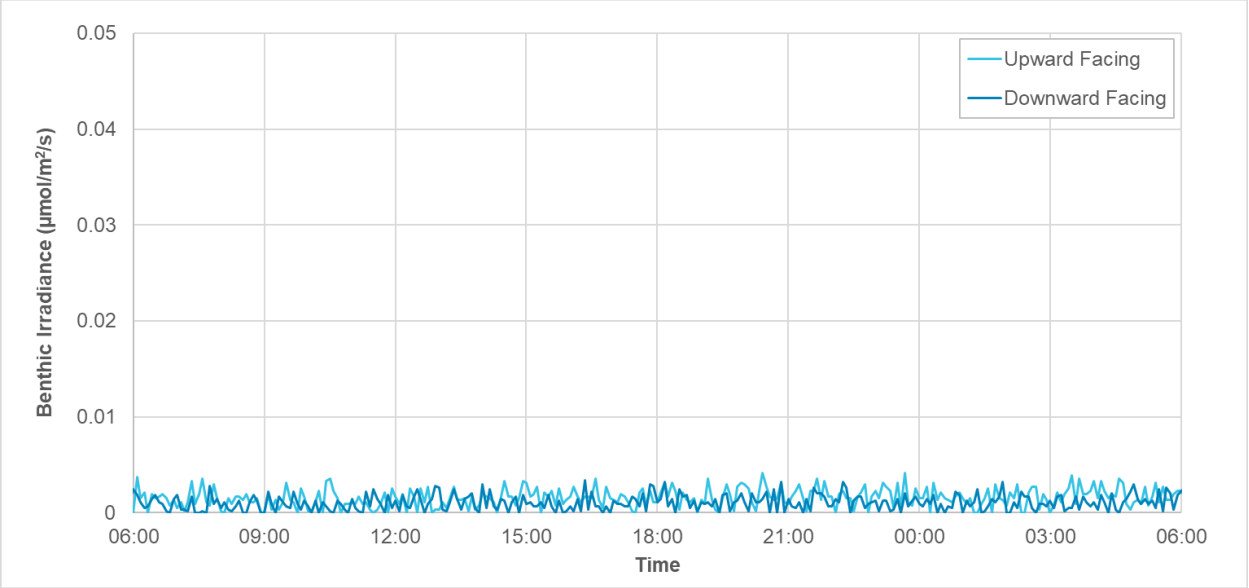

Figure 72. Time series of instantaneous benthic light at AWAC-04 from 07/09/2023 to 08/09/2023.

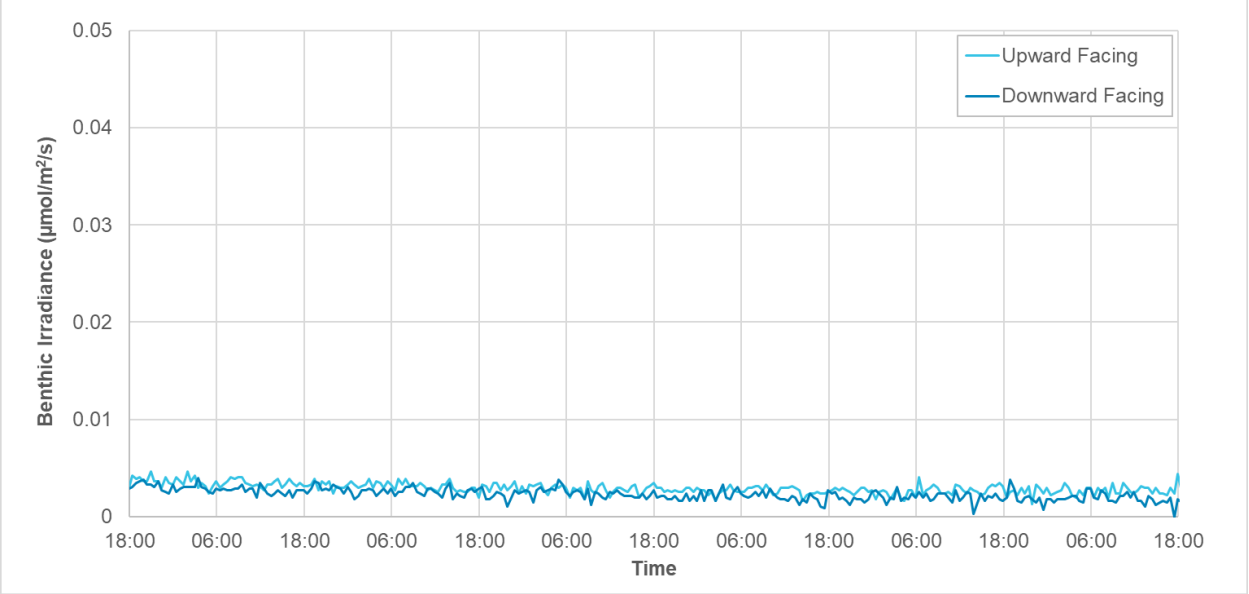

Figure 73. Time series of instantaneous benthic light at AWAC-11 from 02/03/2024 to 09/03/2024.

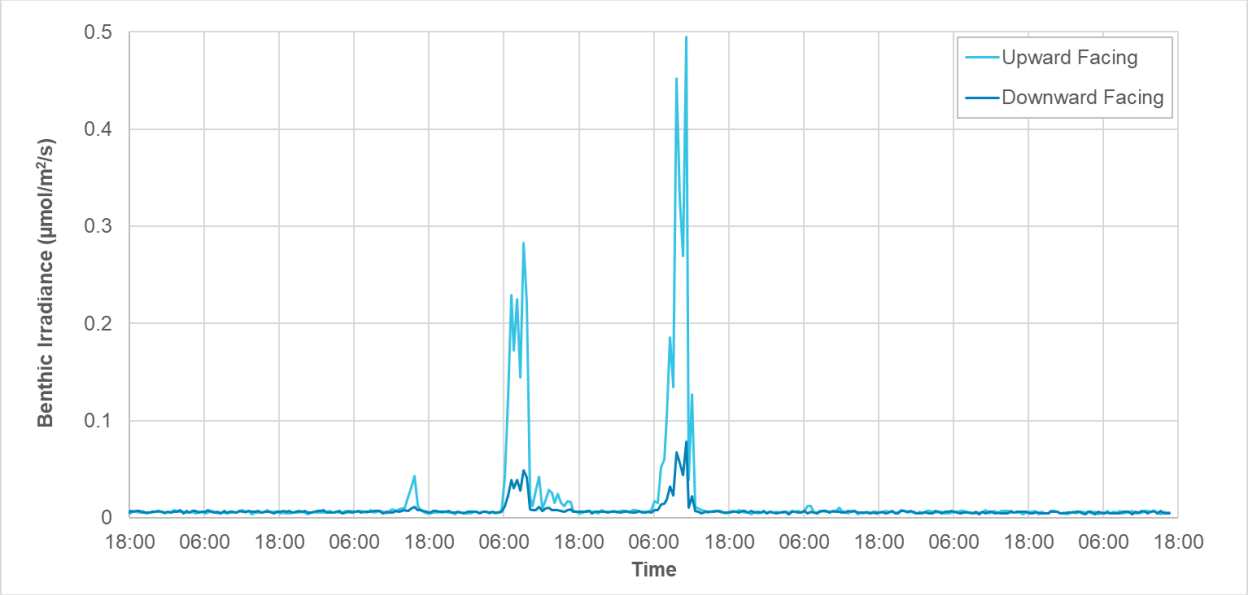

Figure 74. **Time series of instantaneous benthic light at Pos-13 from 03/03/2024 to 10/03/2024.**

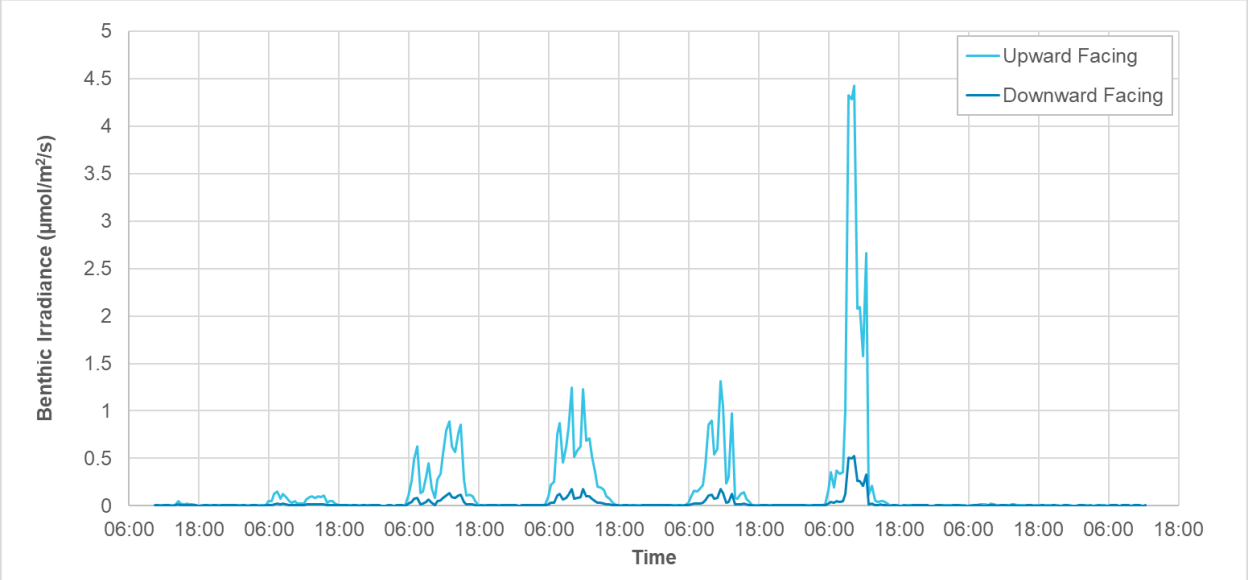

Figure 75. **Time series of instantaneous benthic light at Pos-14 from 03/03/2024 to 10/03/2024.**

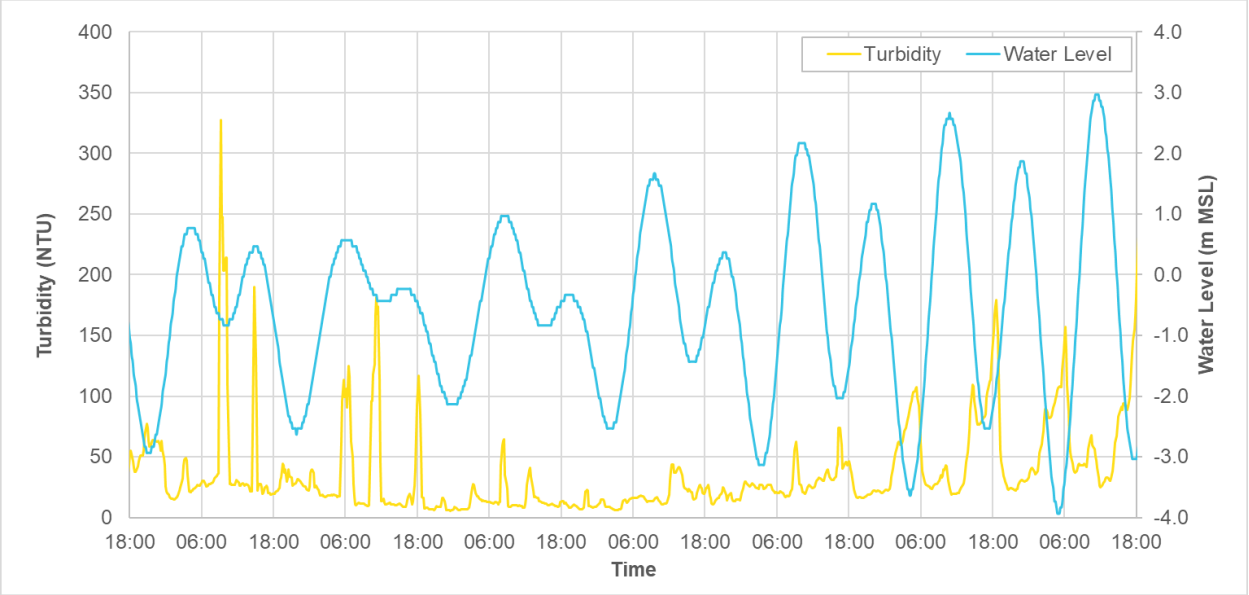

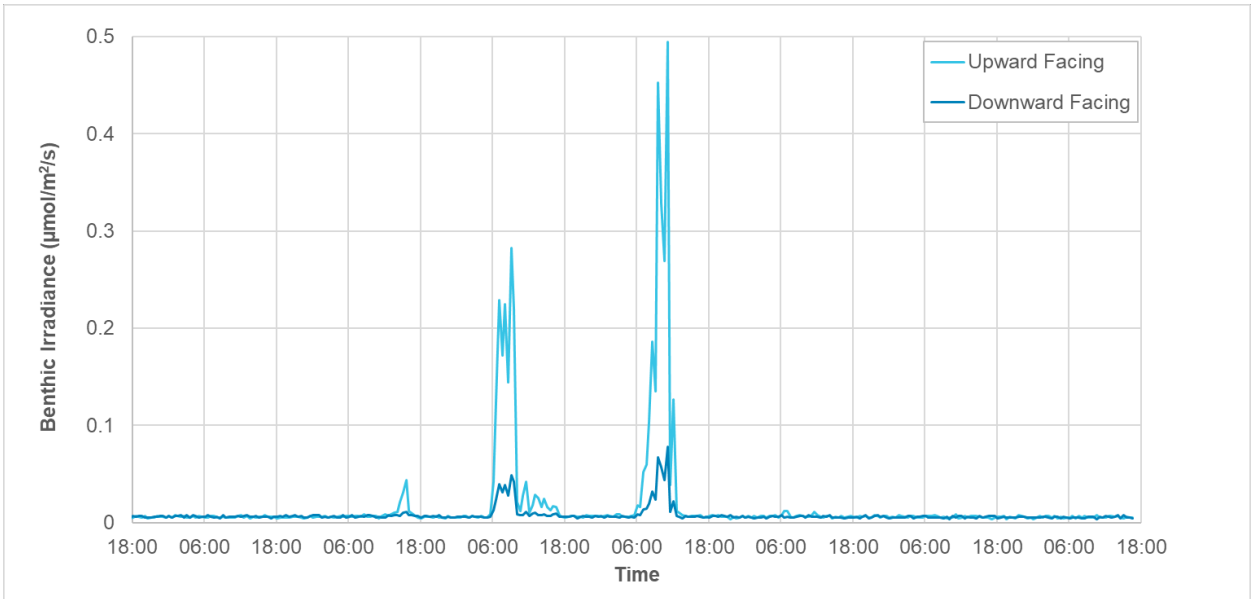

Figure 76. Time series of water level and turbidity (top) and instantaneous benthic light (bottom) at Pos-13 from 03/03/2024 to 10/03/2024.

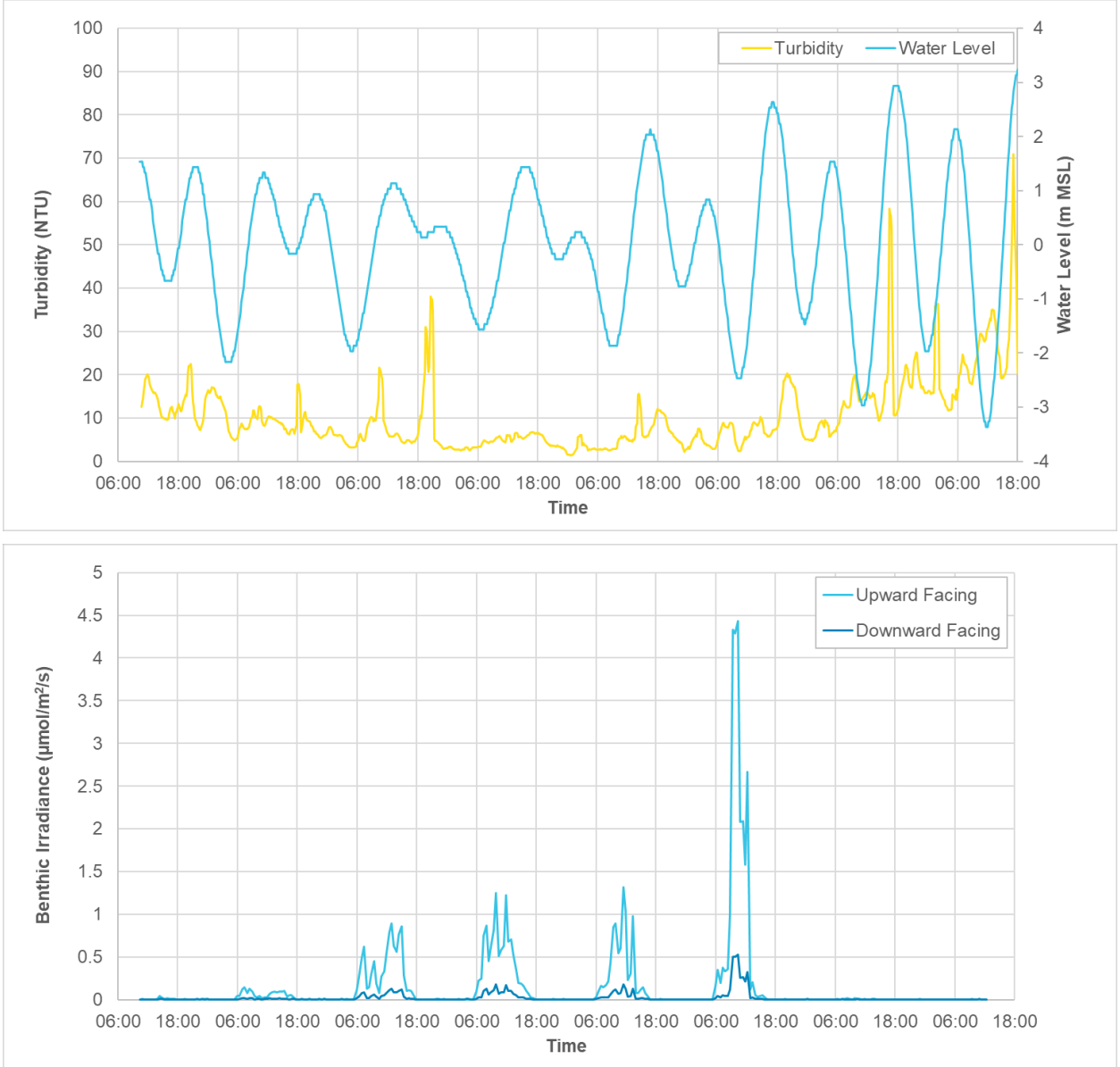

Figure 77. **Time series of water level and turbidity (top) and instantaneous benthic light (bottom) at Pos-14 from 03/03/2024 to 10/03/2024.**

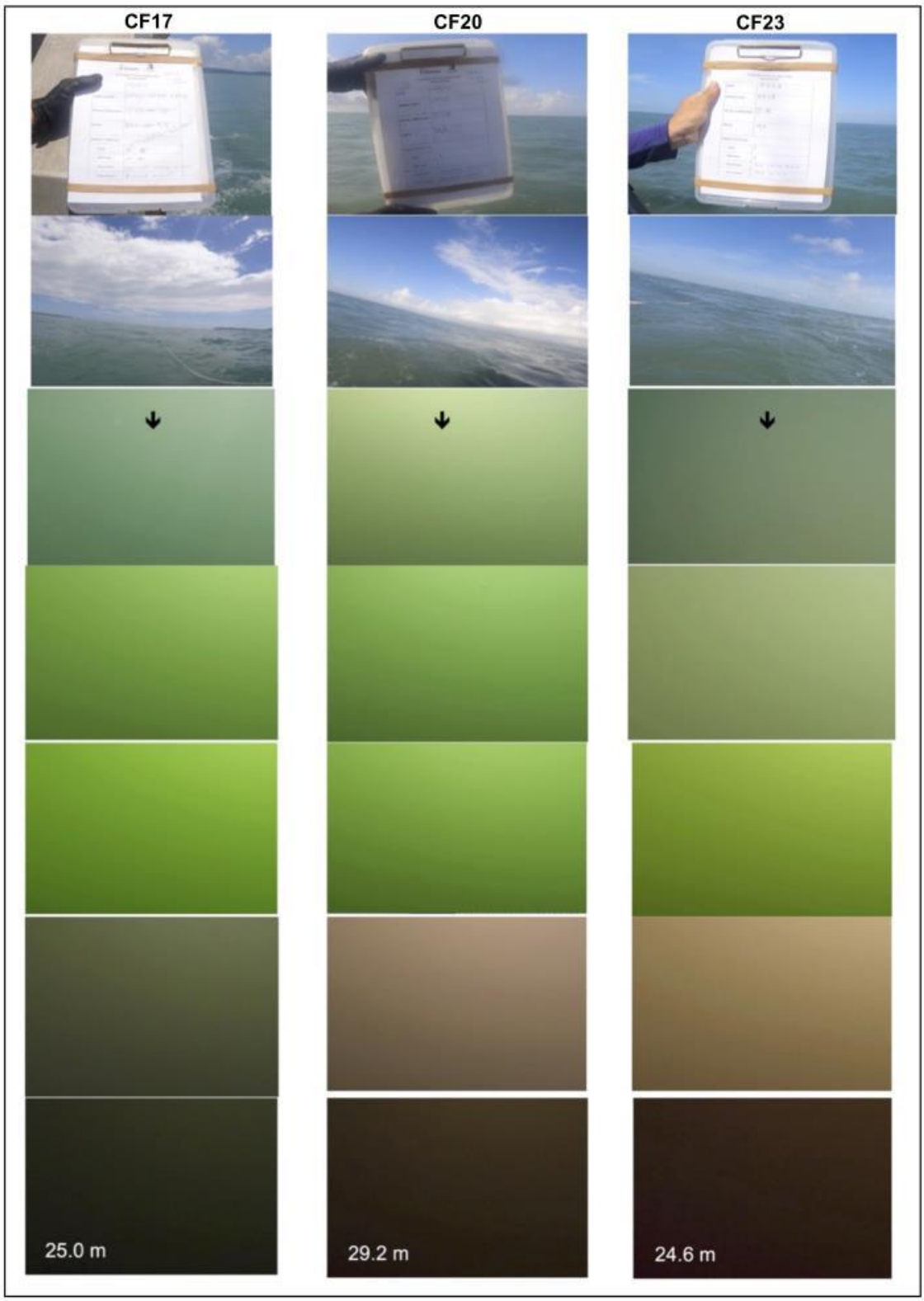

Figure 78. **Screen shots from three examples of the drop camera videos undertaken at 167 sites across CG and King Shoals in March 2023 and July-August 2023, showing a completely blacked-out aphotic zone. All of the videos show exactly the same (source: BKA, 2024d).**

6.2.2. Water Quality

Plots of the measured water quality data at all the sites are shown in Figure 79 to Figure 98. The measurements extend from September 2023 to June 2024 and cover 10 different measurement sites from the confluence between CG and the West Arm, out to King Shoals. The plots show the following.

- Temperature: the temperature varies gradually over time, with limited short-term variation over a tidal cycle (around 0.5 ºC). The water temperature varied from approximately 25 ºC in the dry season up to 32 ºC in the wet season (highest water temperatures recorded during December and January). The water temperature is relatively consistent between the sites, with concurrent data at the confluence with the West Arm and in King Shoals showing very similar water temperatures from March to June 2024. The data show a relatively consistent increase in water temperature between the dry season and the wet season, but with more variability occurring when the water temperature is reducing between the wet season and the dry season. The variability in the reduction in water temperature is likely to be related to the upstream freshwater discharge and the meteorological conditions during the wet season.

- Salinity: the salinity varies both spatially and temporally, with larger variations occurring during the wet season due to the increased freshwater discharge flowing into CG. The measured salinity varied between 10 and 34 PSU, with the lower value of 10 PSU only occurring at the furthest upstream site (at the confluence with the West Arm). The highest salinity measurements were in King Shoals, while the lowest measurements were at the furthest upstream site at the confluence with the West Arm, with the sites between varying depending on their relative distance between the two. The data also show that the salinity within CG also varies over a tidal cycle, with the highest salinity occurring at high water, due to the flood stage of the tide importing higher salinity offshore water into CG, and the lowest salinity occurring at low water after the ebb stage of the tide has brought low salinity water from upstream into CG. The measured data showed that the salinity could vary by up to 8 PSU over a tidal cycle, this occurred during the west season during a period of higher freshwater discharge.

- Turbidity: the data show that the turbidity in the region is highly variable both temporally and spatially. The turbidity was typically lower close to the entrance to CG and in King Shoals and higher further upstream. The turbidity was typically highest around low water, due to the ebb stage of the tide transporting higher turbidity water from upstream into CG, and lower around high water as a result of the flood stage of the tide transporting lower turbidity water from offshore into CG. At most sites there was a significant difference in turbidity between high and low water, with the largest difference of around 350 NTU. However, at the furthest upstream site (at the confluence with the West Arm) there was less variation through the tidal cycle due to the reduced influence of the lower turbidity water from offshore, meaning that the turbidity could remain high throughout the tidal cycle. At most sites there was a clear spring-neap tidal signal in the data, with high turbidity coinciding with the spring tides and lower turbidity coinciding with the neap tides. At the offshore site at King Shoals, this pattern was not as obvious, suggesting that the turbidity at this location is not as strongly influenced by the astronomical tide, but is likely controlled more by the wave conditions and other events which result in widespread increases in turbidity (e.g. a large freshwater discharge event).

- Dissolved Oxygen: data were only measured for dissolved oxygen from September 2023 to March 2024. Despite this there is still sufficient data to provide an understanding of dissolved oxygen in the region. The data show that the dissolved oxygen was consistently between 6 and 7 mg/L over the dry season conditions. During the wet season the dissolved oxygen was more variable, with values reducing down to 2 mg/L for short periods but typically varying between 4 and 6 mg/L. The measurements suggest that the values are relatively consistent throughout the region.

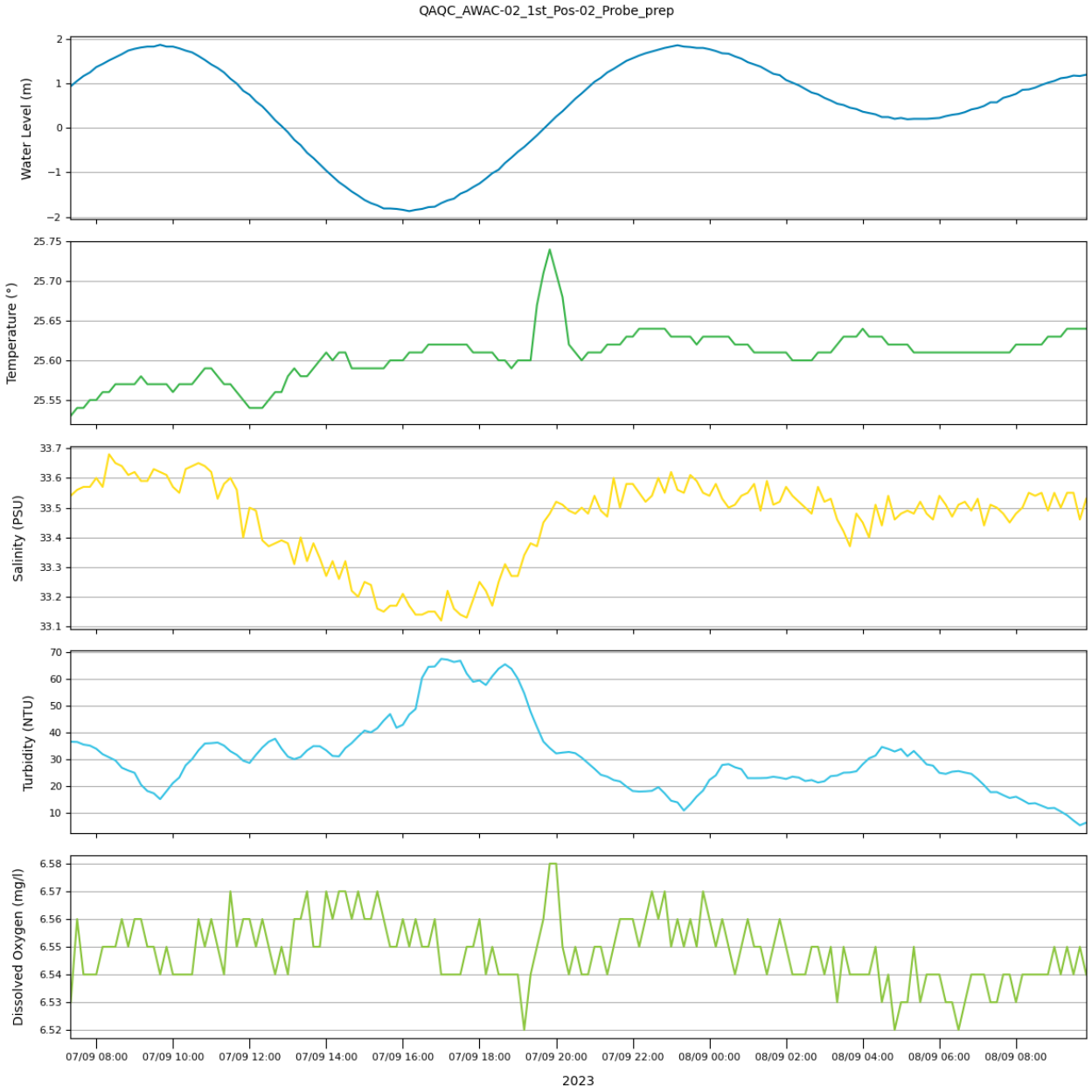

Figure 79. Time series of water level, temperature, salinity and turbidity measured at AWAC-02 in September 2023.

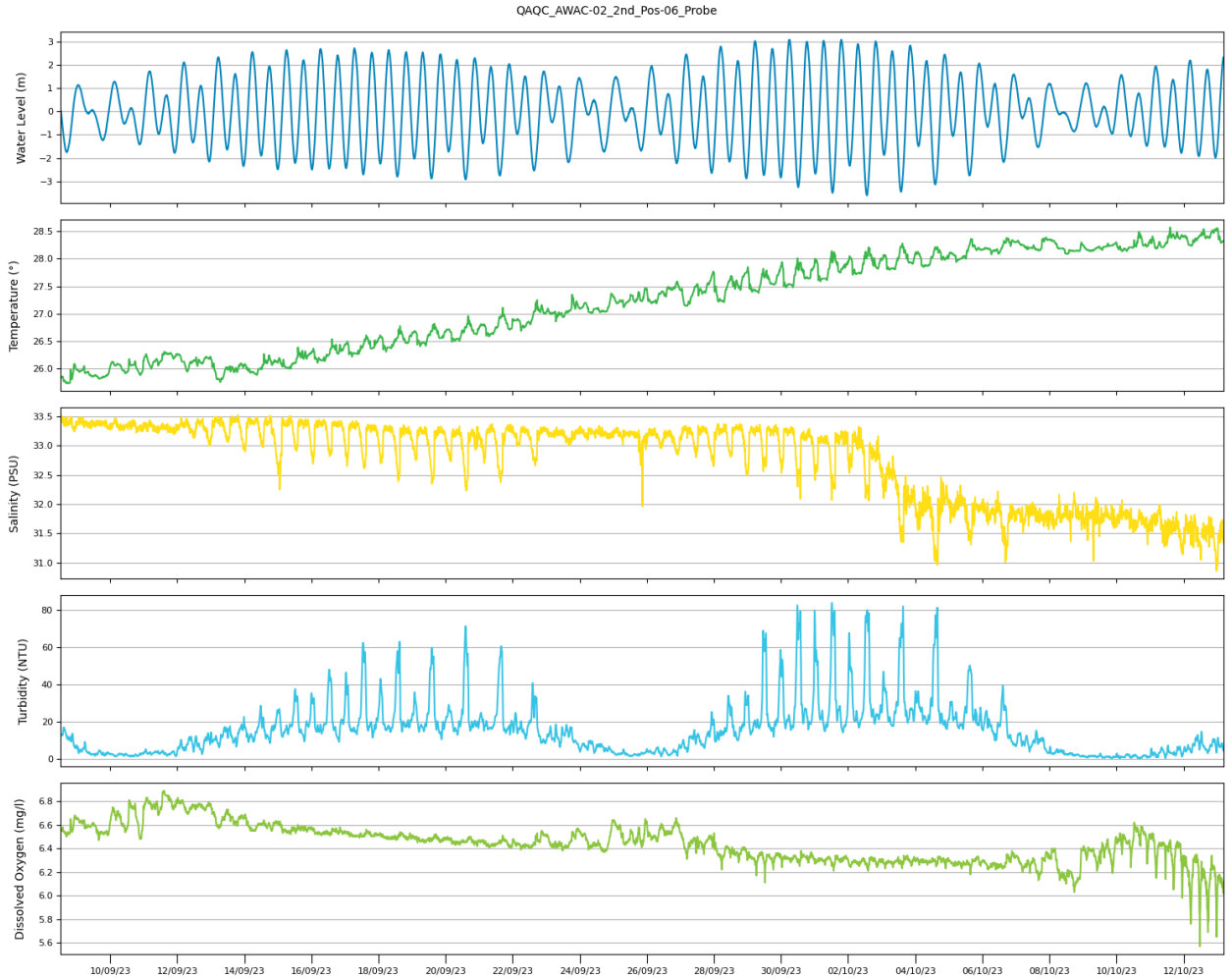

Figure 80. Time series of water level, temperature, salinity, turbidity and dissolved oxygen measured at AWAC-06 from September to October 2023.

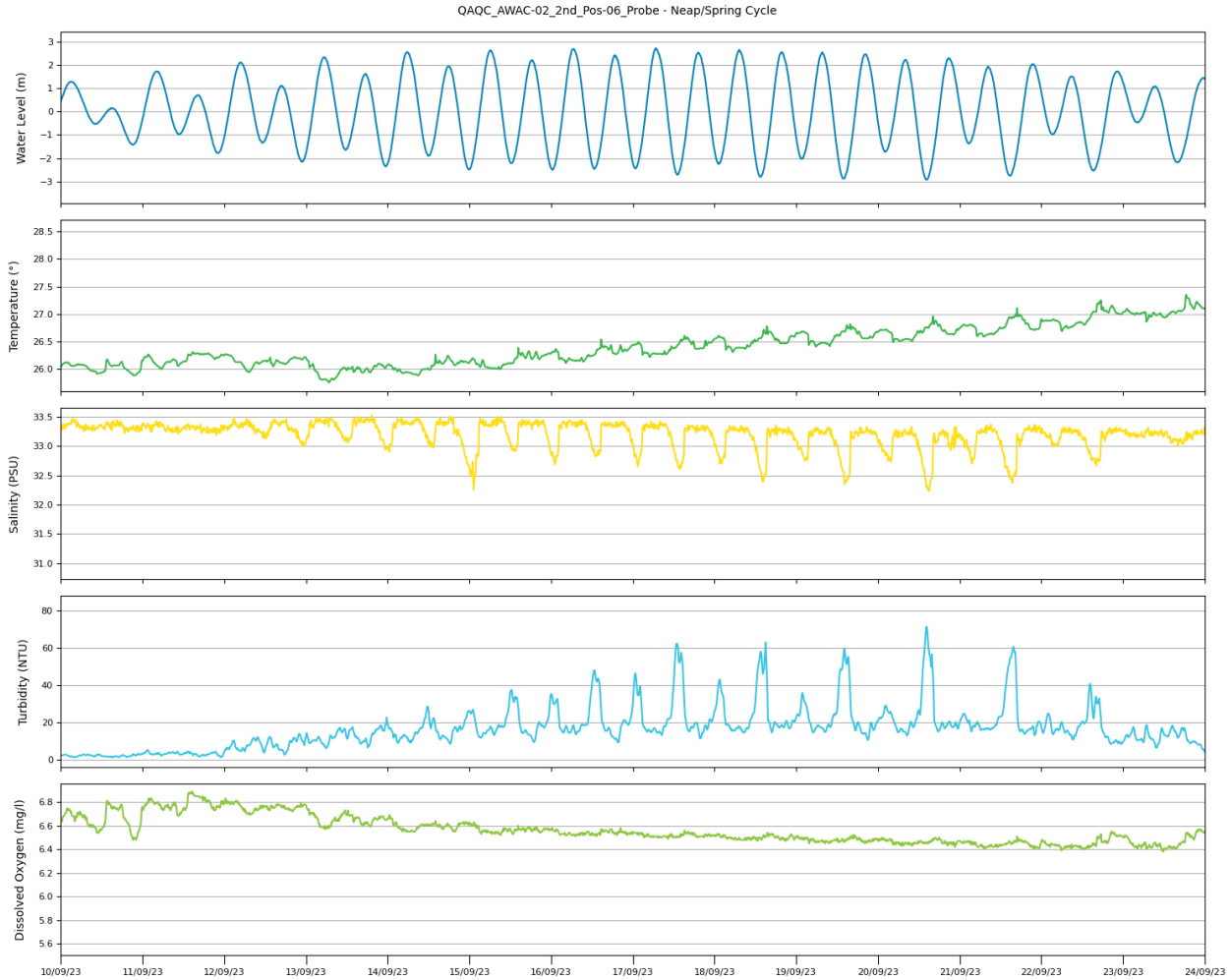

Figure 81. Time series of water level, temperature, salinity, turbidity and dissolved oxygen measured at AWAC-06 over a 14 day spring neap tidal cycle whole deployment period in September 2023.

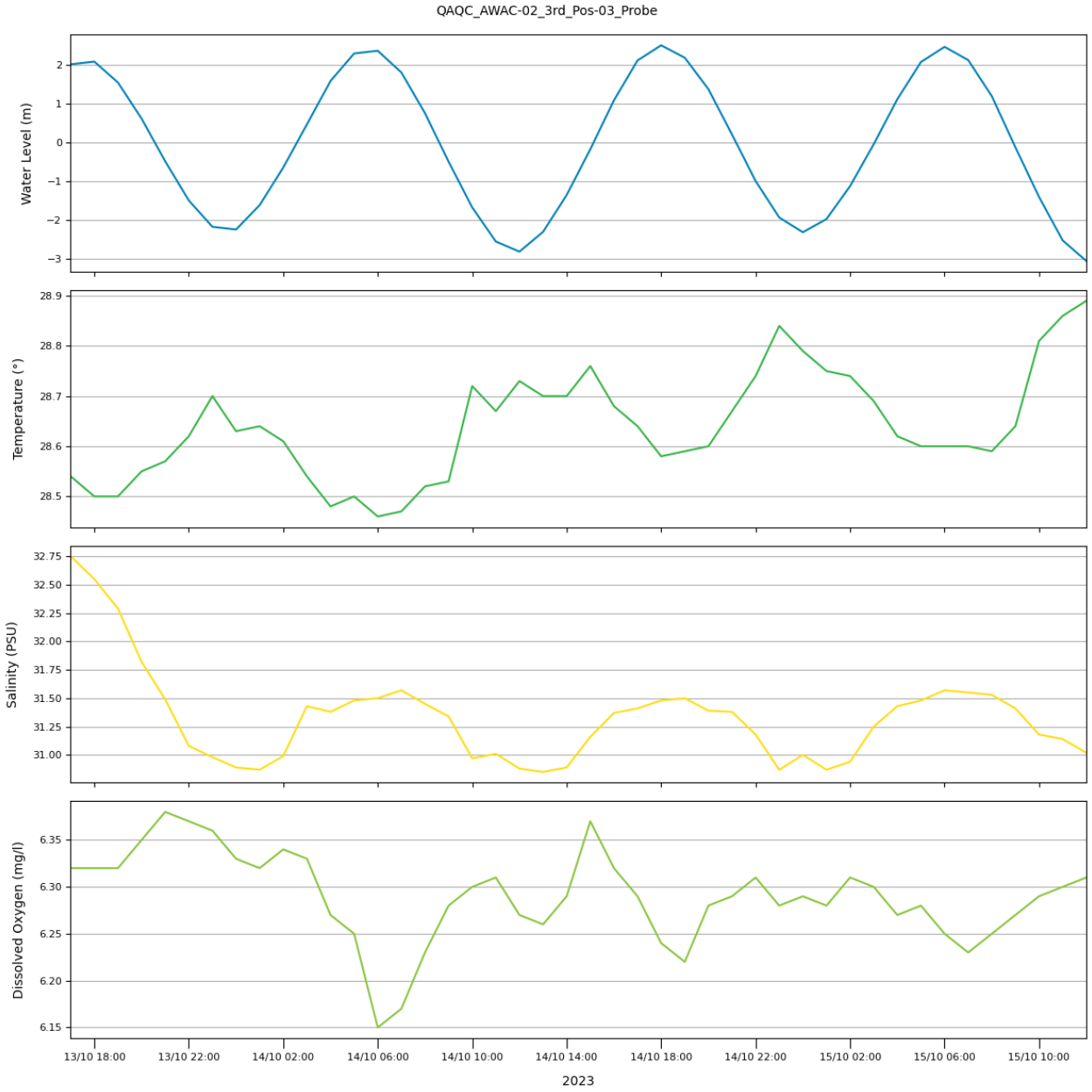

Figure 82. Time series of water level, temperature, salinity and dissolved oxygen measured at AWAC-03 in October 2023.

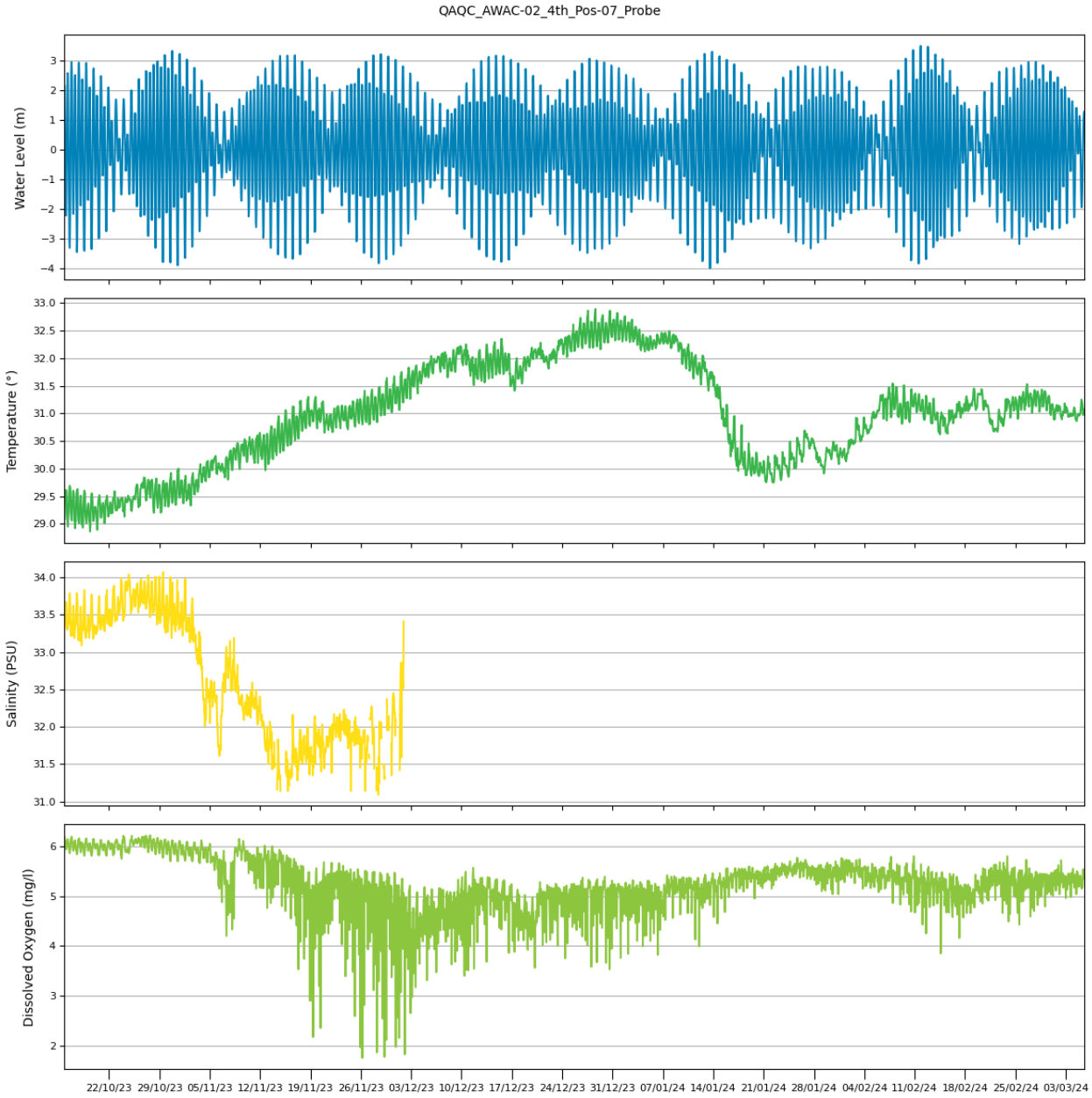

Figure 83. Time series of water level, temperature, salinity and dissolved oxygen measured at AWAC-07 over the whole deployment period from October 2023 to March 2024.

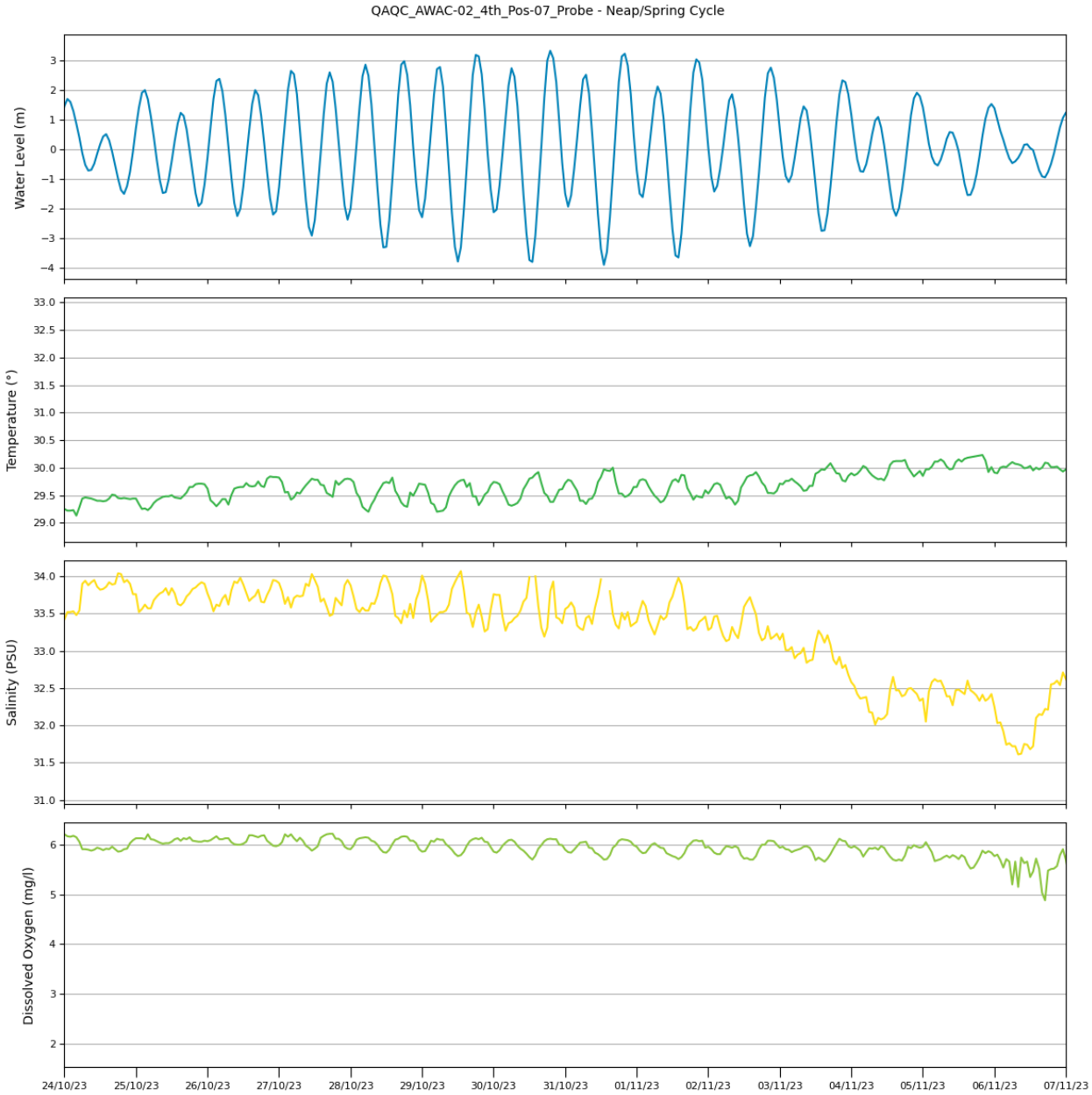

Figure 84. Time series of water level, temperature, salinity and dissolved oxygen measured at AWAC-07 over a 14 day spring neap tidal cycle in October 2023.

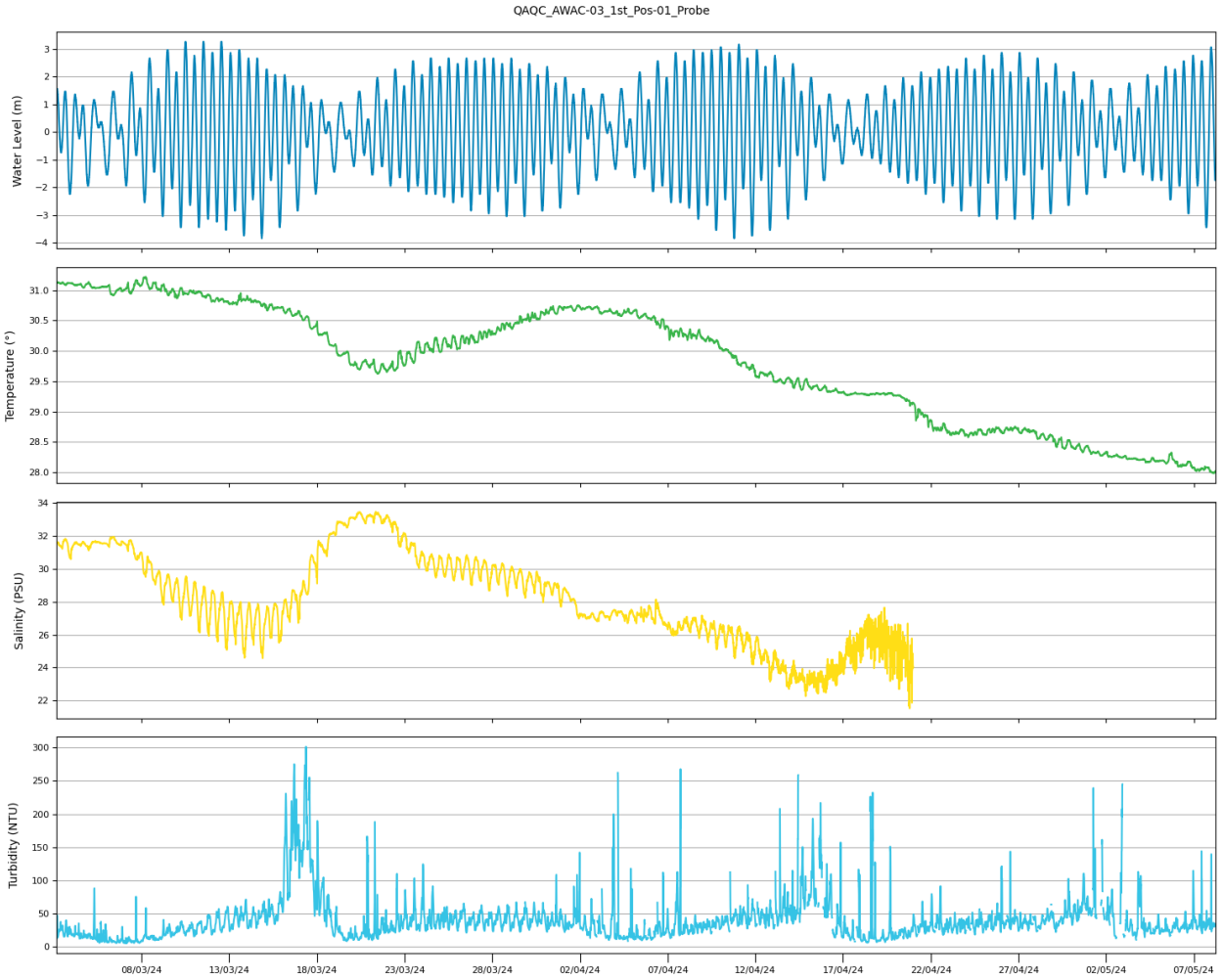

Figure 85. Time series of water level, temperature, salinity and turbidity measured at AWAC-01 over the whole deployment period from March to May 2024.

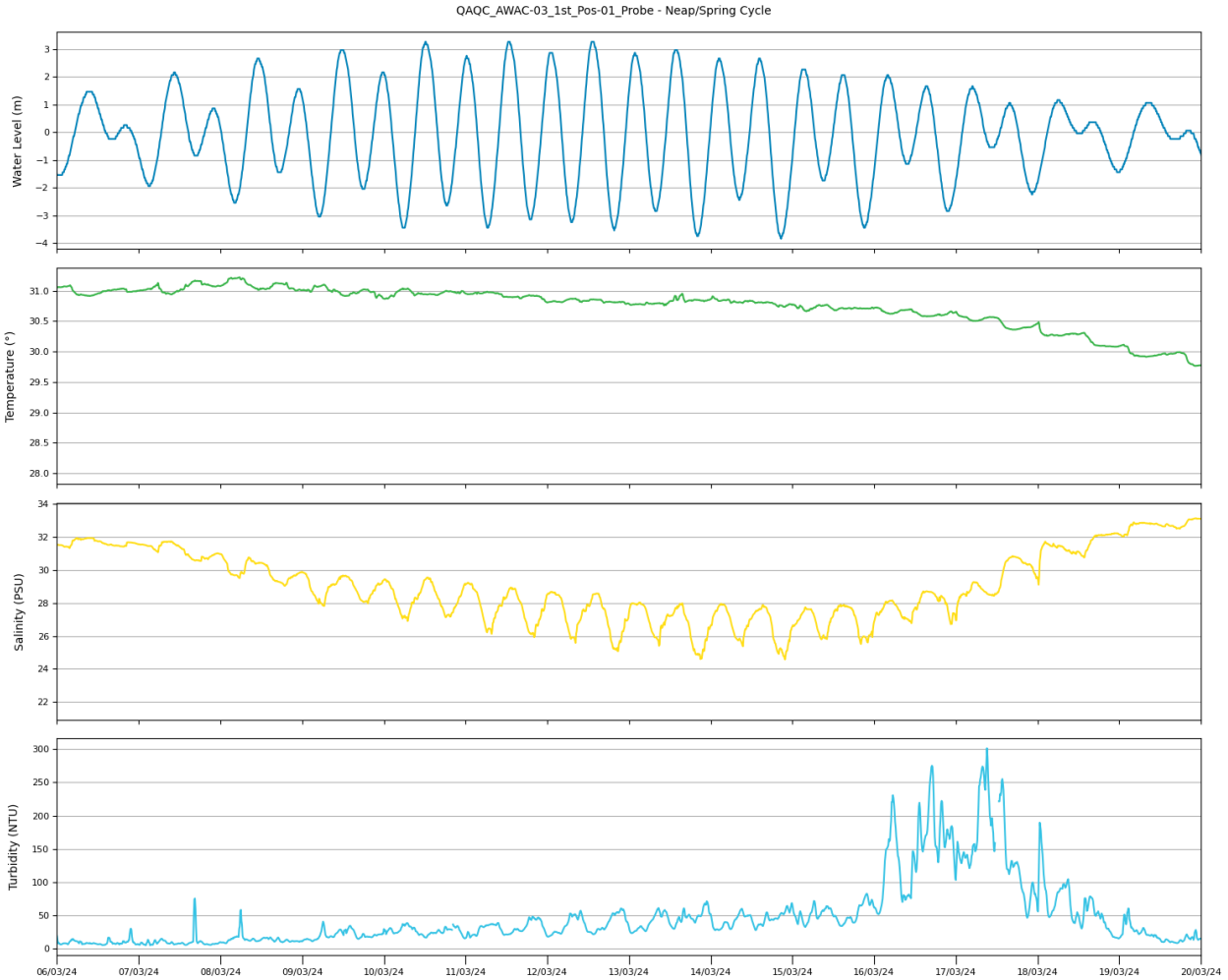

Figure 86. Time series of water level, temperature, salinity and turbidity measured at AWAC-01 over a 14 day spring neap tidal cycle in March 2024.

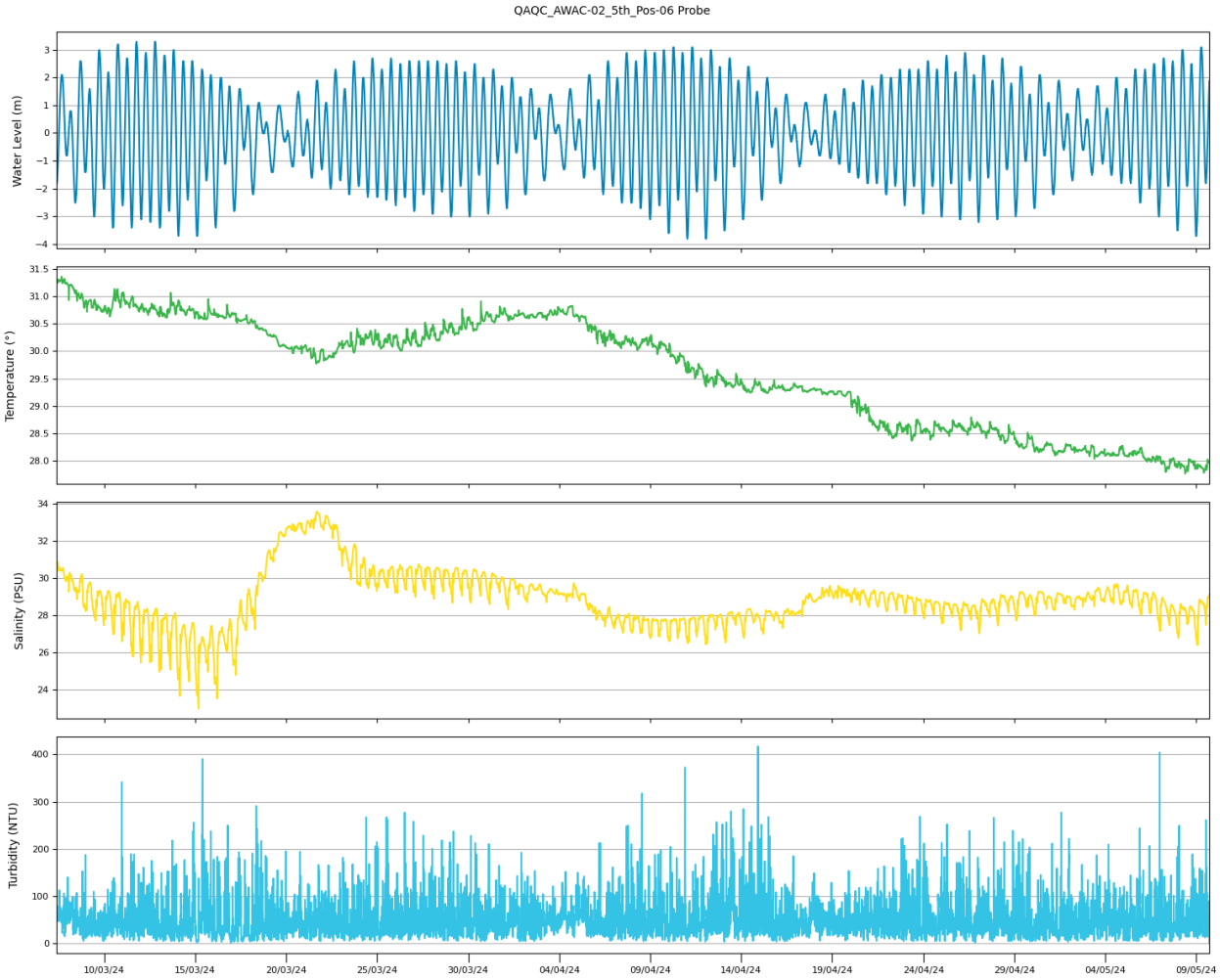

Figure 87. Time series of water level, temperature, salinity and turbidity measured at AWAC-06 over the whole deployment period from March to May 2024.

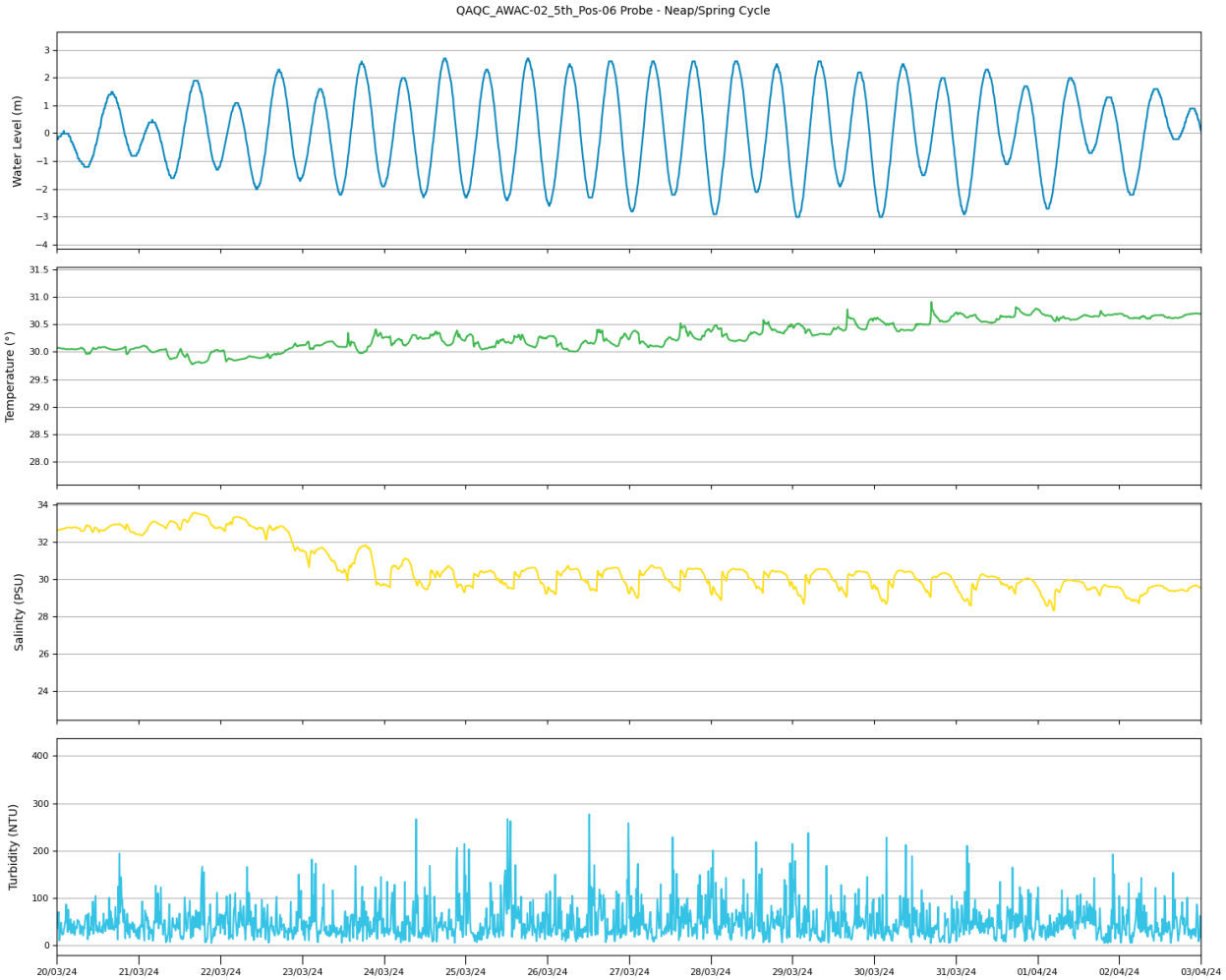

Figure 88. Time series of water level, temperature, salinity and turbidity measured at AWAC-06 over a 14 day spring neap tidal cycle in March 2024.

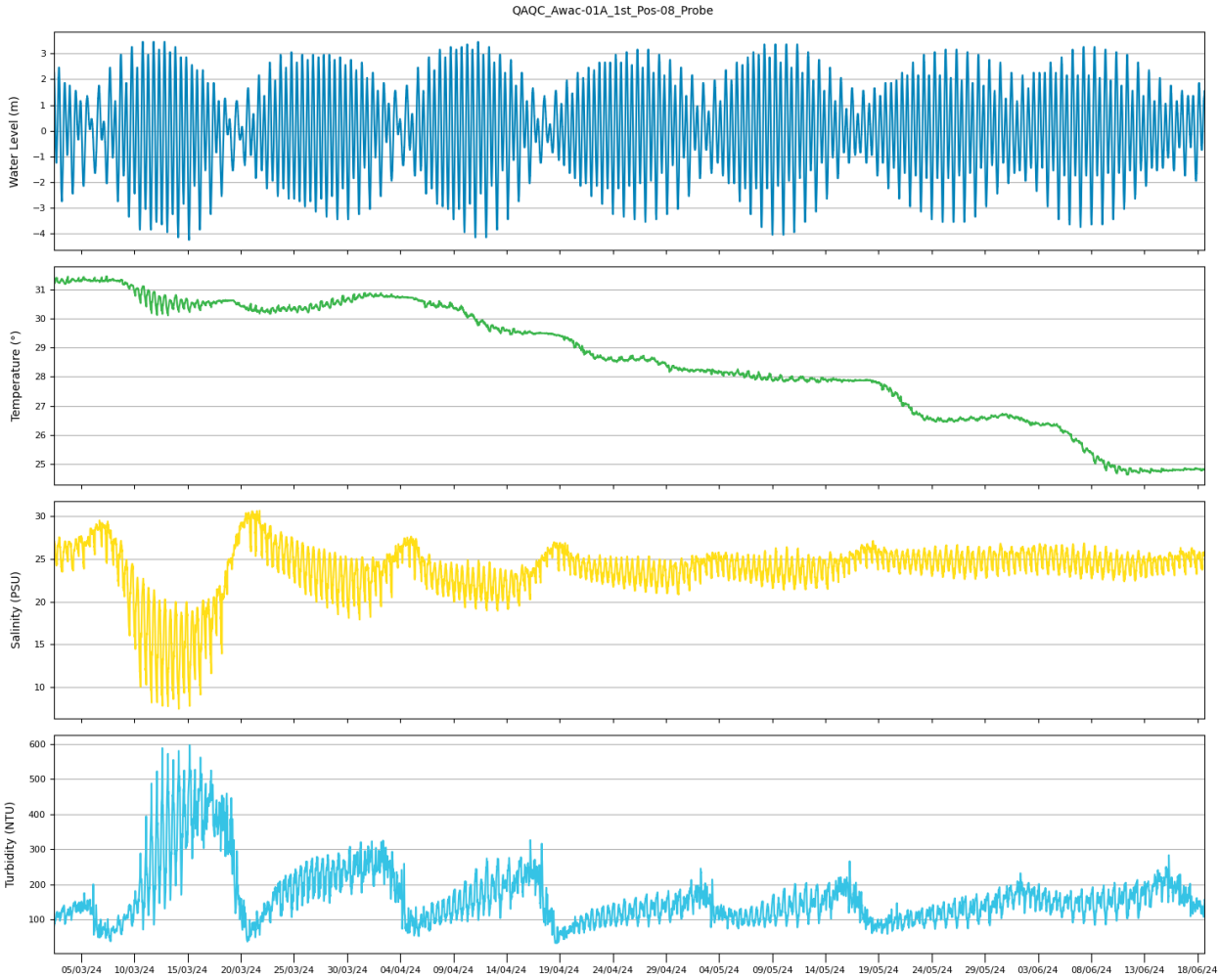

Figure 89. Time series of water level, temperature, salinity and turbidity measured at AWAC-08 over the whole deployment period from April to June 2024.

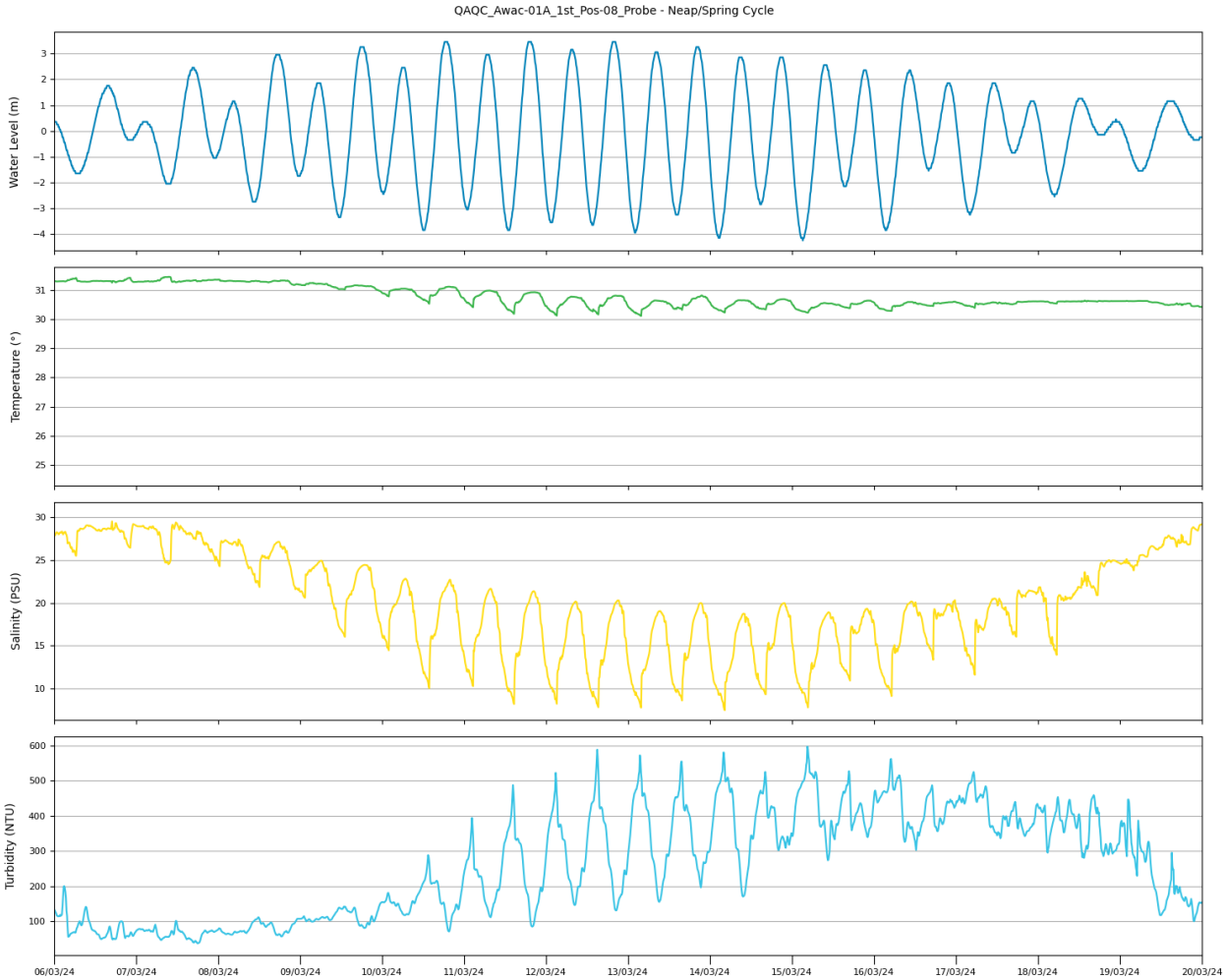

Figure 90. Time series of water level, temperature, salinity and turbidity measured at AWAC-08 over a 14 day spring neap tidal cycle whole deployment period in April 2024.

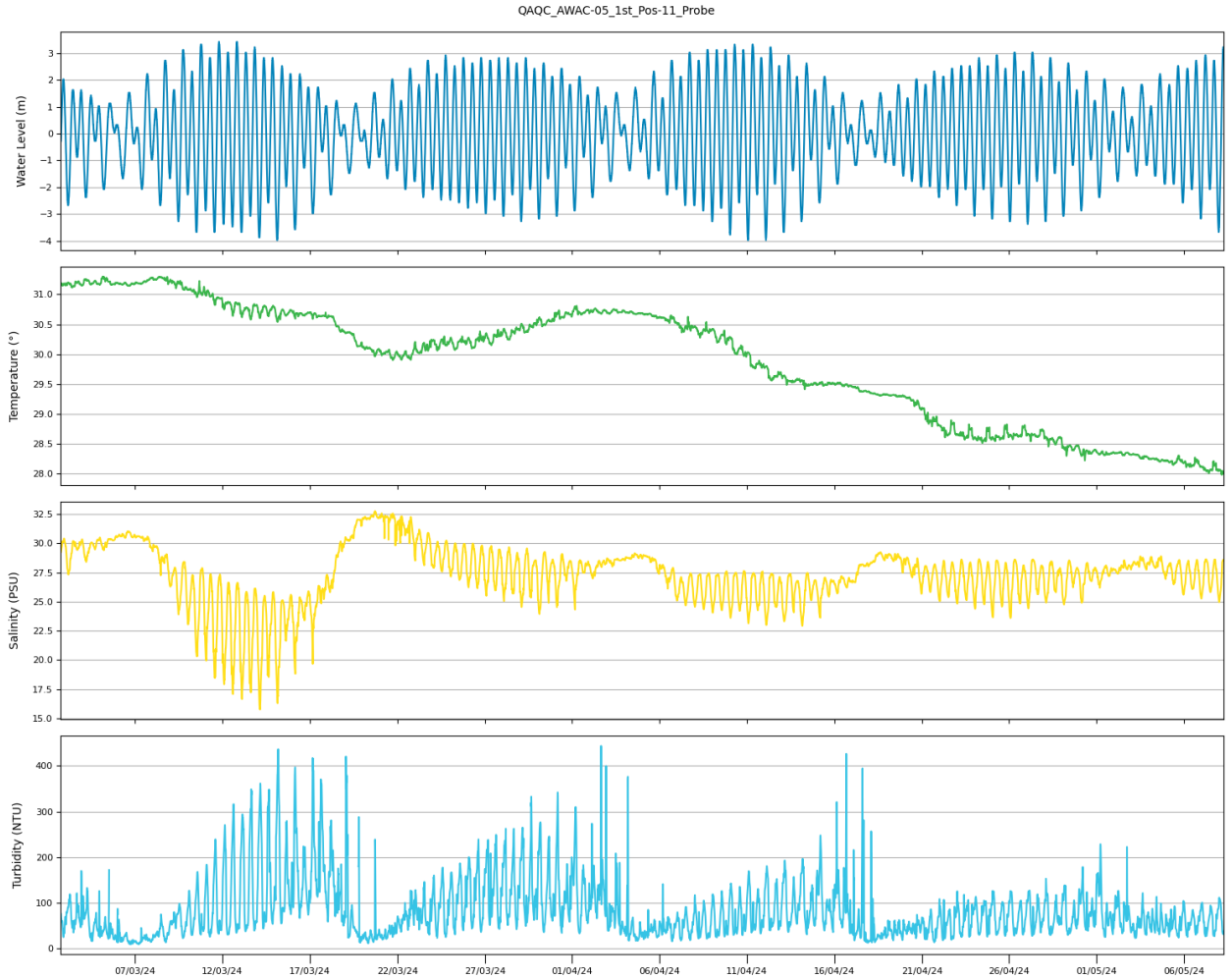

Figure 91. Time series of water level, temperature, salinity and turbidity measured at AWAC-11 over the whole deployment period from March to May 2024.

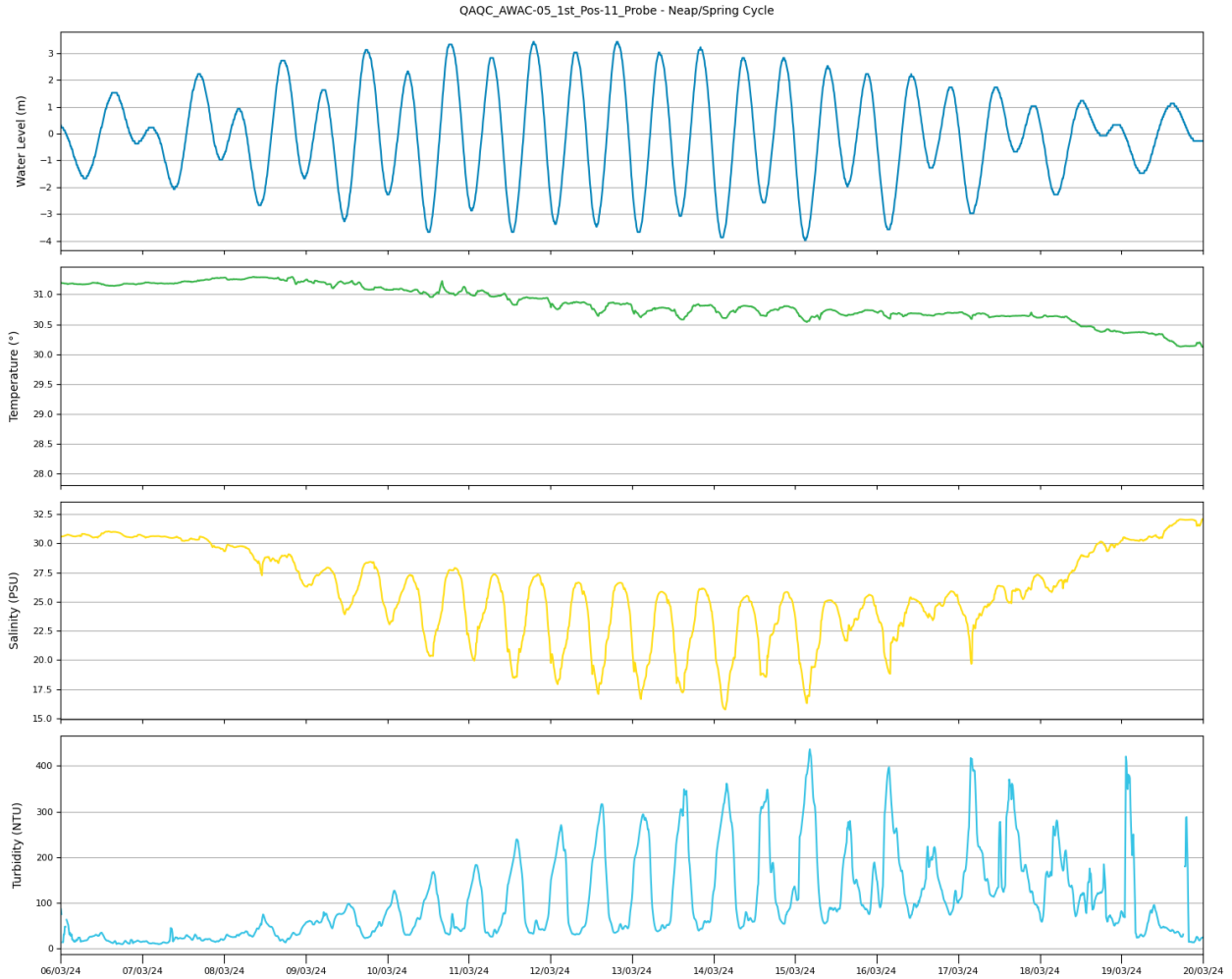

Figure 92. Time series of water level, temperature, salinity and turbidity measured at AWAC-11 over a 14 day spring neap cycle in March 2024.

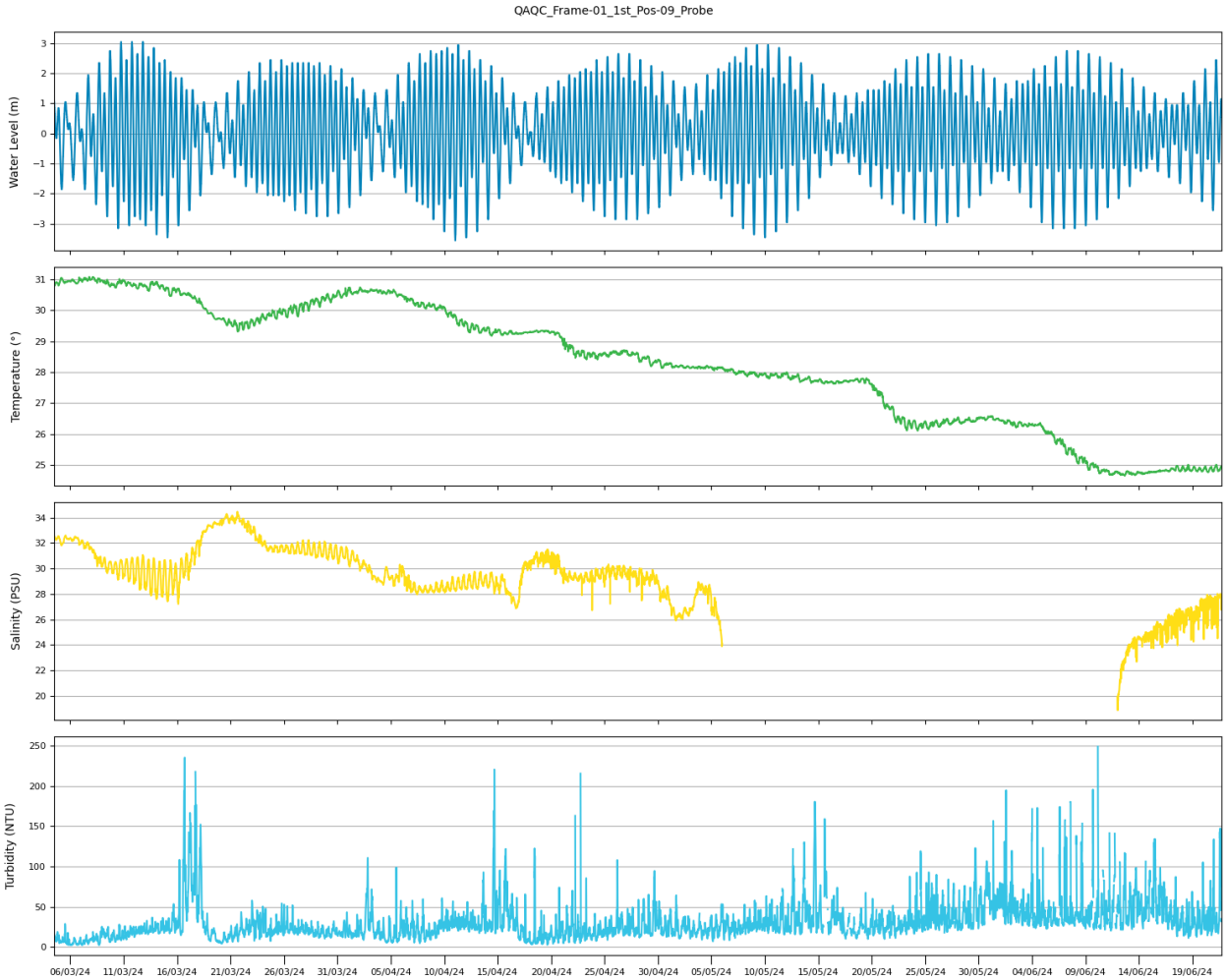

Figure 93. Time series of water level, temperature, salinity and turbidity measured at Pos-12 over the whole deployment period from March to June 2024.

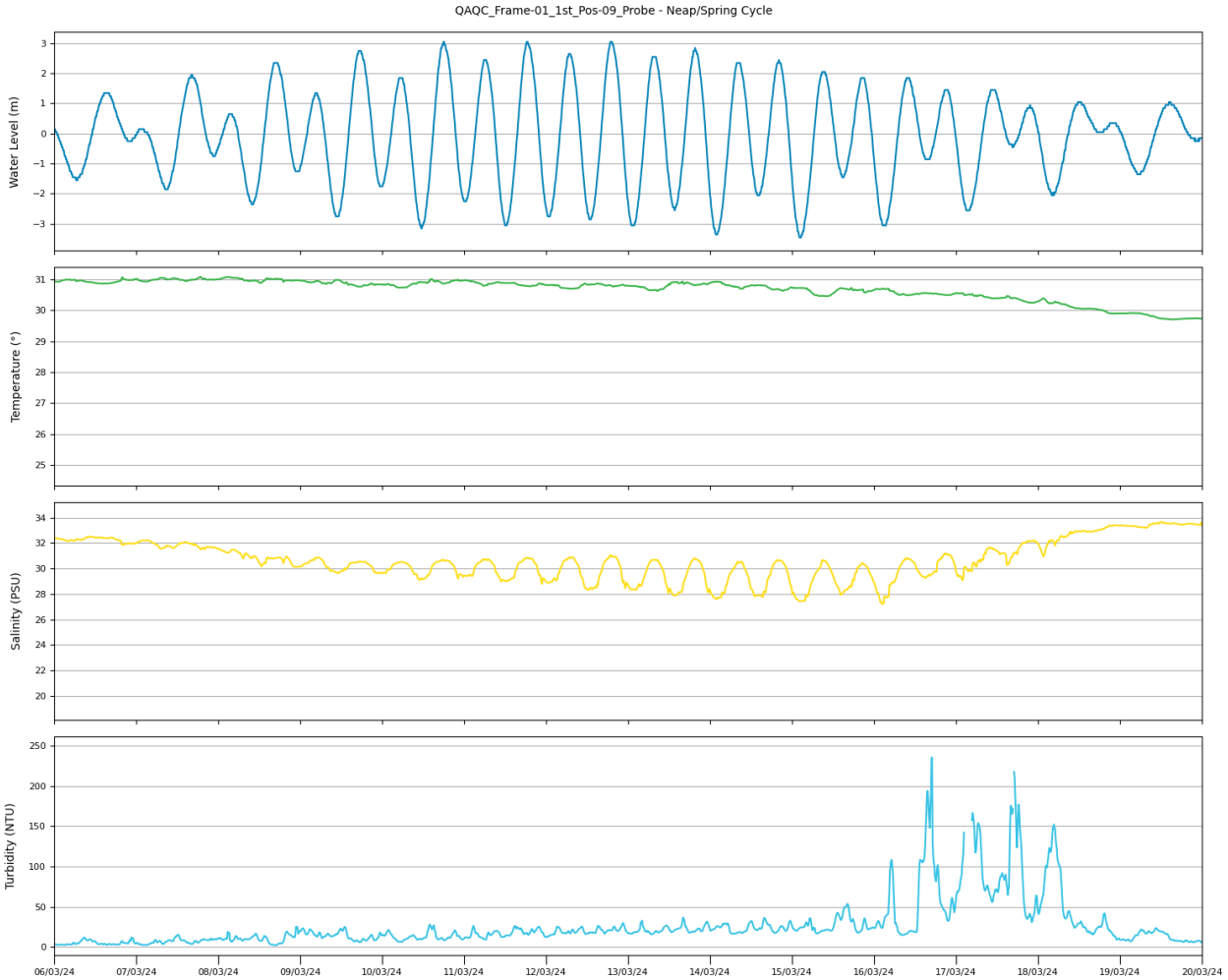

Figure 94. Time series of water level, temperature, salinity and turbidity measured at Pos-12 over a 14 day spring neap tidal cycle in March 2024.

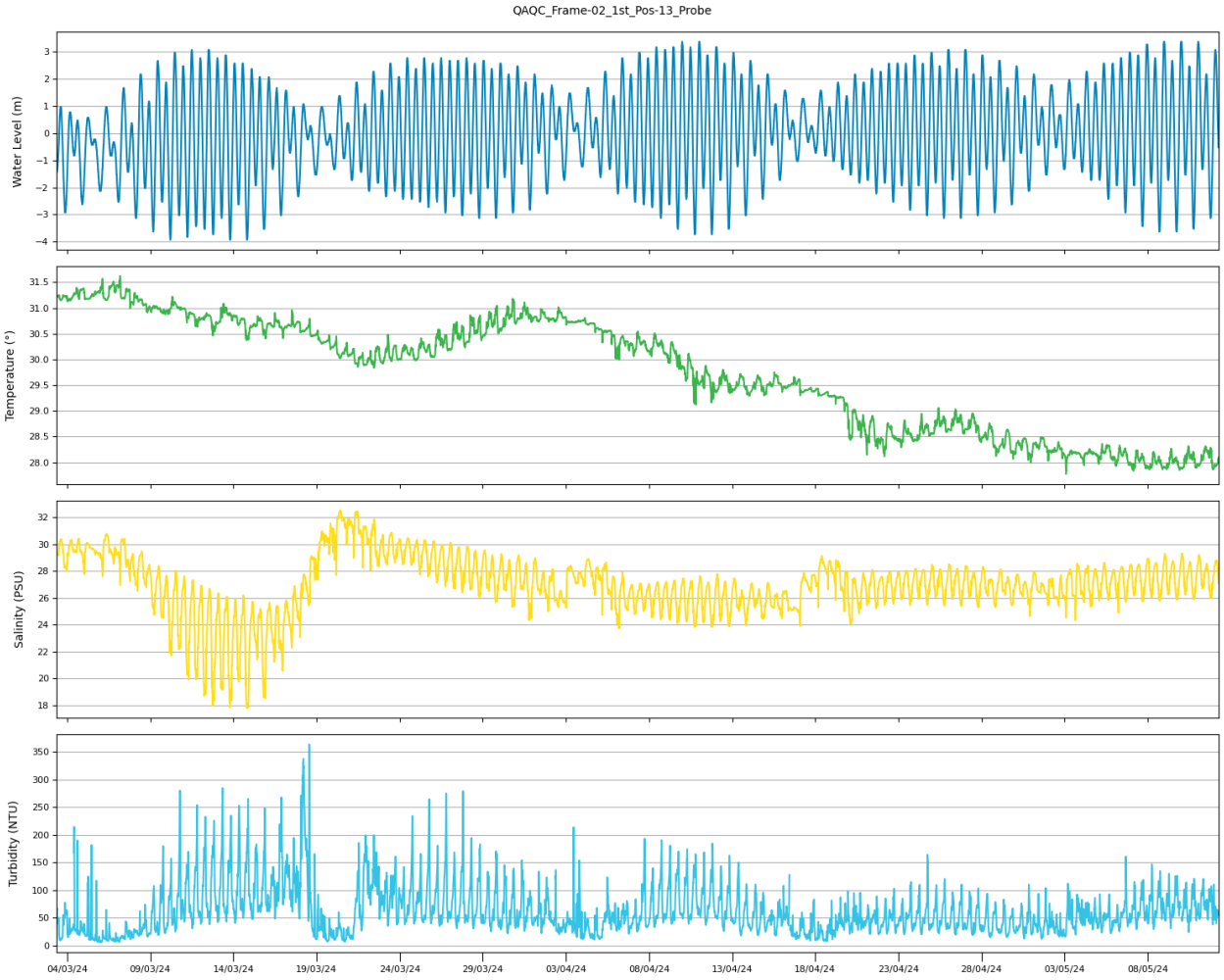

Figure 95. Time series of water level, temperature, salinity and turbidity measured at Pos-13 over the whole deployment period from March to May 2024.

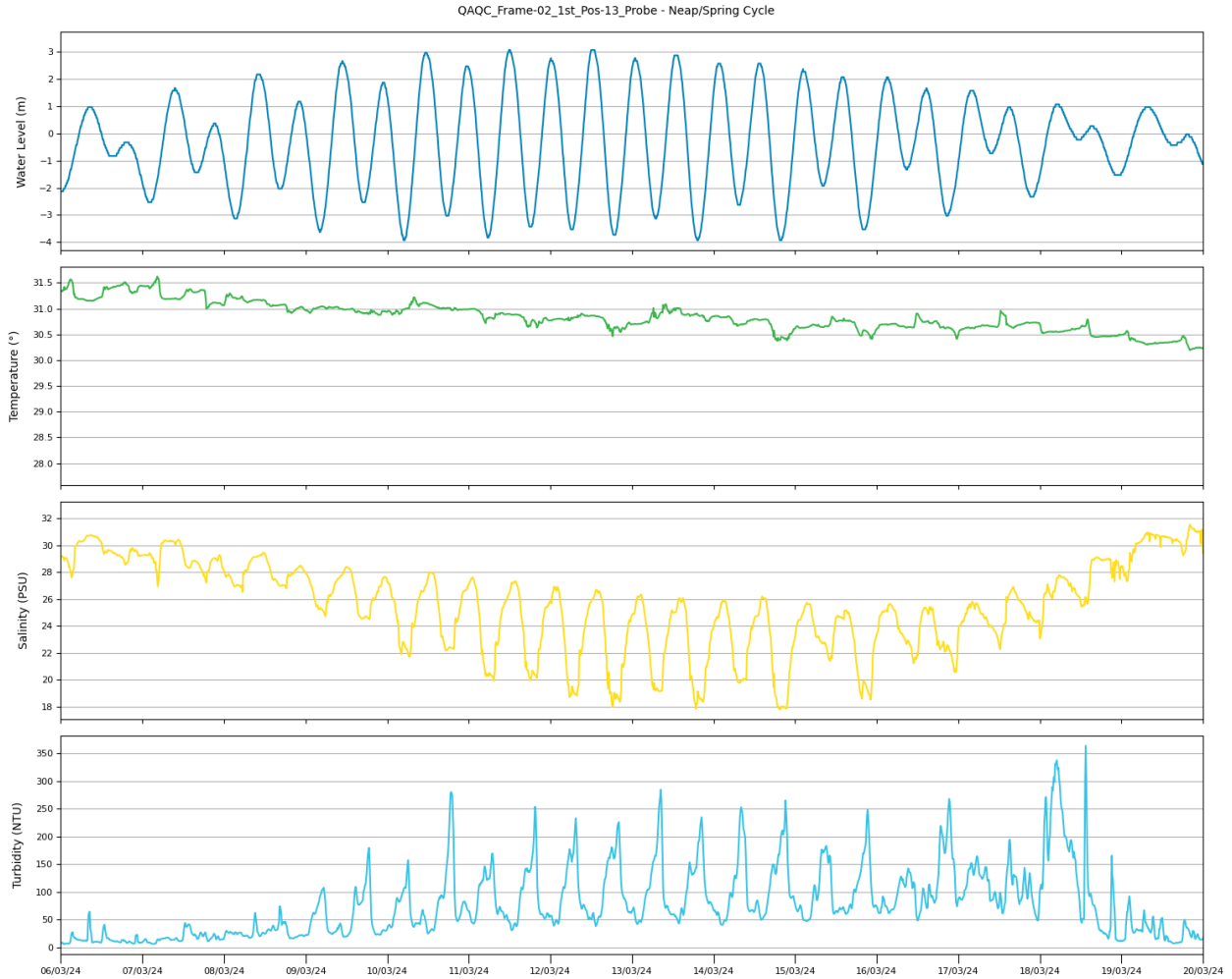

Figure 96. Time series of water level, temperature, salinity and turbidity measured at Pos-13 over a 14 day spring neap tidal cycle in March 2024.

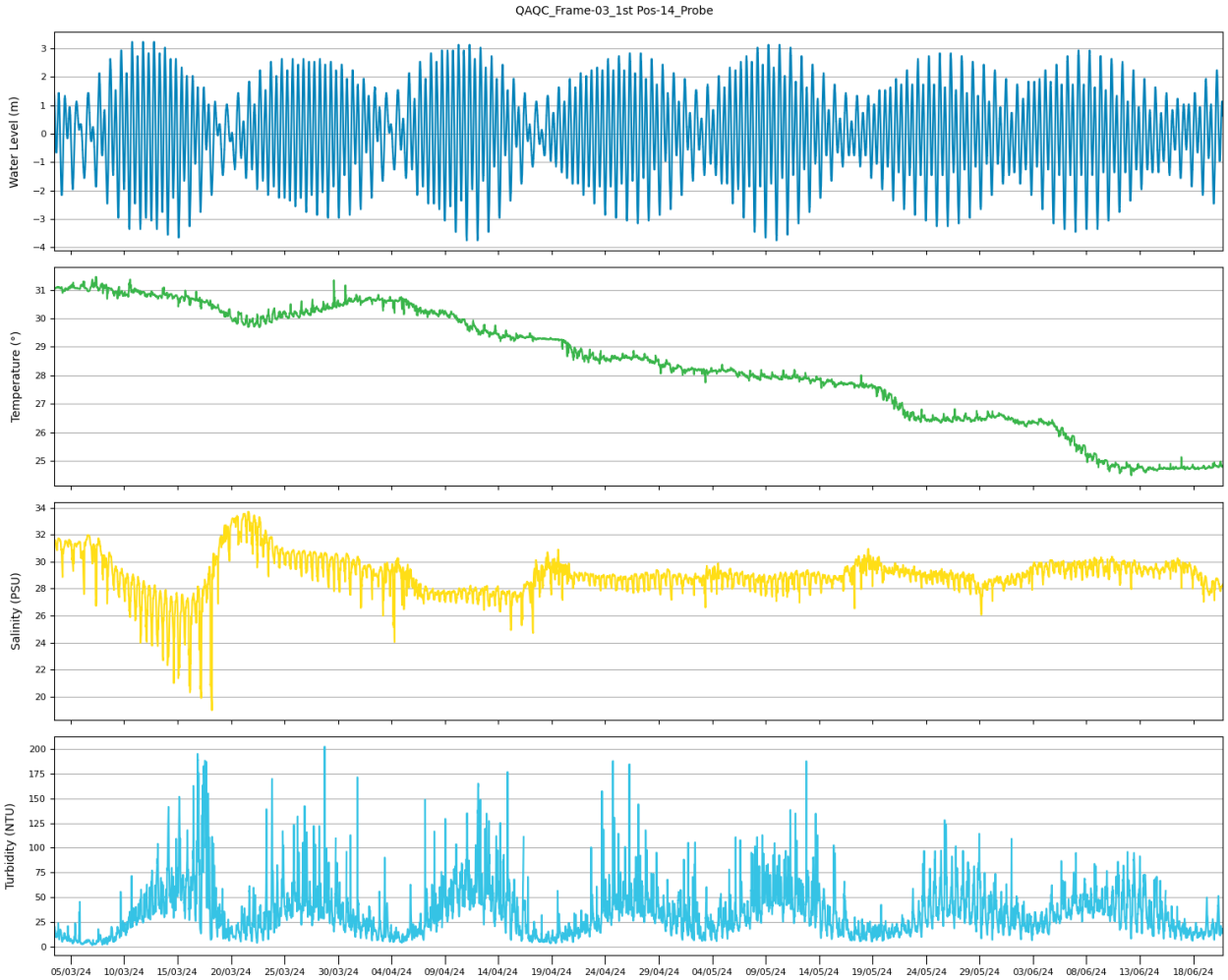

Figure 97. Time series of water level, temperature, salinity and turbidity measured at Pos-14 over the whole deployment period from March to June 2024.

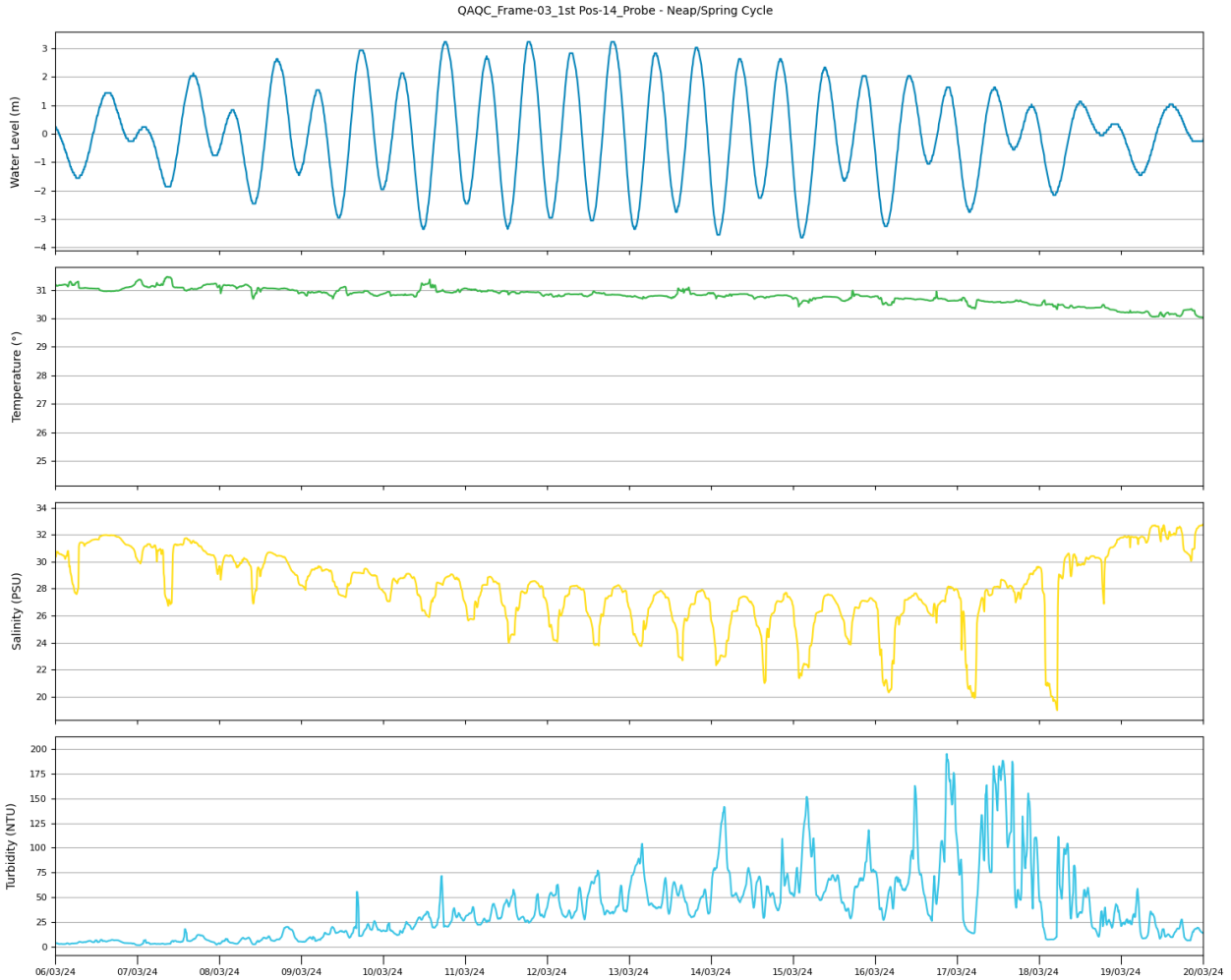

Figure 98. Time series of water level, temperature, salinity and turbidity measured at Pos-14 over a 14 day spring neap tidal cycle in March 2024.

7. LiDAR Data

7.1. Data Overview

BKA commissioned drone survey and remote sensing company Sensorem to undertake LiDAR and photogrammetry drone surveys of the four beaches where turtle nesting occurs in the seaward parts of CG (Figure 99). These are two beaches (one small and one large) at Cape Domett, Turtle Bay at Lacrosse Island and Turtle Beach West, west of Cape Dussejour. It was not possible to survey the beach at East Bank Point (Barnett Point) within CG where turtle nesting is also known to occur due to safety concerns regarding crocodiles in the area (video footage of this area was captured instead).

The drone surveys were undertaken between 22nd and 25th February 2024. The data were captured using a DJI Matrice 300 RTK with a Zenmuse L2 payload installed. At each beach two known points were surveyed using a Trimble R12 GNSS Receiver and one point was used to set up a D-RTK 2 base station to allow corrections to be sent to the DJI M300, which ensured that the data were captured to a high level of accuracy (root mean squared (RMS) horizontal and vertical errors of 0.02 and 0.05 m). The vertical datum from the surveys was relative to Australian Height Datum (AHD), the difference between AHD and MSL in CG is unknown but AHD is likely to be in the order of 0.2 m lower than MSL. The average ground sampling resolution was just under 0.02 m and the survey areas ranged from 0.16 km^2 at Turtle Bay to 1.14 km^2 at Turtle Beach West.

The captured drone data were processed by Sensorem to develop DEMs for each beach, and these were provided to PCS with a 0.05 m horizontal resolution. In addition, orthomosaic imagery for each beach was also provided at the resolution the imagery was captured.

7.2. Results

The LiDAR DEMs for each of the four beaches are shown in Figure 100 to Figure 103 along with cross-shore transect locations. The plots show that all four beaches have a gradually sloping bed in the lower intertidal area which becomes much steeper in the upper intertidal and supratidal areas.

Close up plots of the orthomosaic imagery of sections of the beaches are shown in Figure 104 to Figure 107. These images highlight the very high-resolution imagery that the drone provides, meaning that the combination of the DEM data and the orthomosaic imagery can be used to understand the elevation of the beach as well as features such as locations on the intertidal area of the beach where rock is present. The imagery shows that at Turtle Beach West, the main Cape Domett Beach and the small Cape Domett Beach, some of the lower intertidal areas are covered by rock and not sand, while at Turtle Bay, the imagery shows that large rocks are present at the northern and southern ends of the beach.

The LiDAR DEM elevation data at the four beaches have been compared with the other bathymetric/topographic data which are available at the cross-shore beach transects. The other available data are the Geoscience Australia (GA) high-resolution 30 m depth model (Geoscience Australia, 2023) and the Digital Earth Australia (DEA) 25 m intertidal elevation model (DEA, 2023). Plots comparing the cross-shore transect bathymetry between the 2024 LiDAR and the other two data sources are shown for the four beaches in Figure 108 to Figure 111. The plots show the following.

- The elevation from the DEA intertidal elevation model is generally similar to the 2024 LiDAR elevation, although there are differences of up to 1.5 m at Turtle Beach West. However, the DEA intertidal elevation data only extends up to 1 to 2.5 m AHD, meaning that prior to the 2024 LiDAR data, the only data available above this elevation was the GA 30 m depth model.

- The GA 30 m depth model elevation generally shows a reasonable level of agreement with the 2024 LiDAR elevation data up to the 0 m AHD contour, with differences typically less than 2 m. However, above the 0 m AHD contour, differences in elevation between the two are typically at least 2 m and can be more than 5 m.

The comparison highlights how the 2024 LiDAR drone data provides a significant improvement in the representation of the beach profile elevation, especially for the beach elevation above where the DEA 25 m intertidal elevation model extends (i.e. above 1 to 2.5 m AHD).

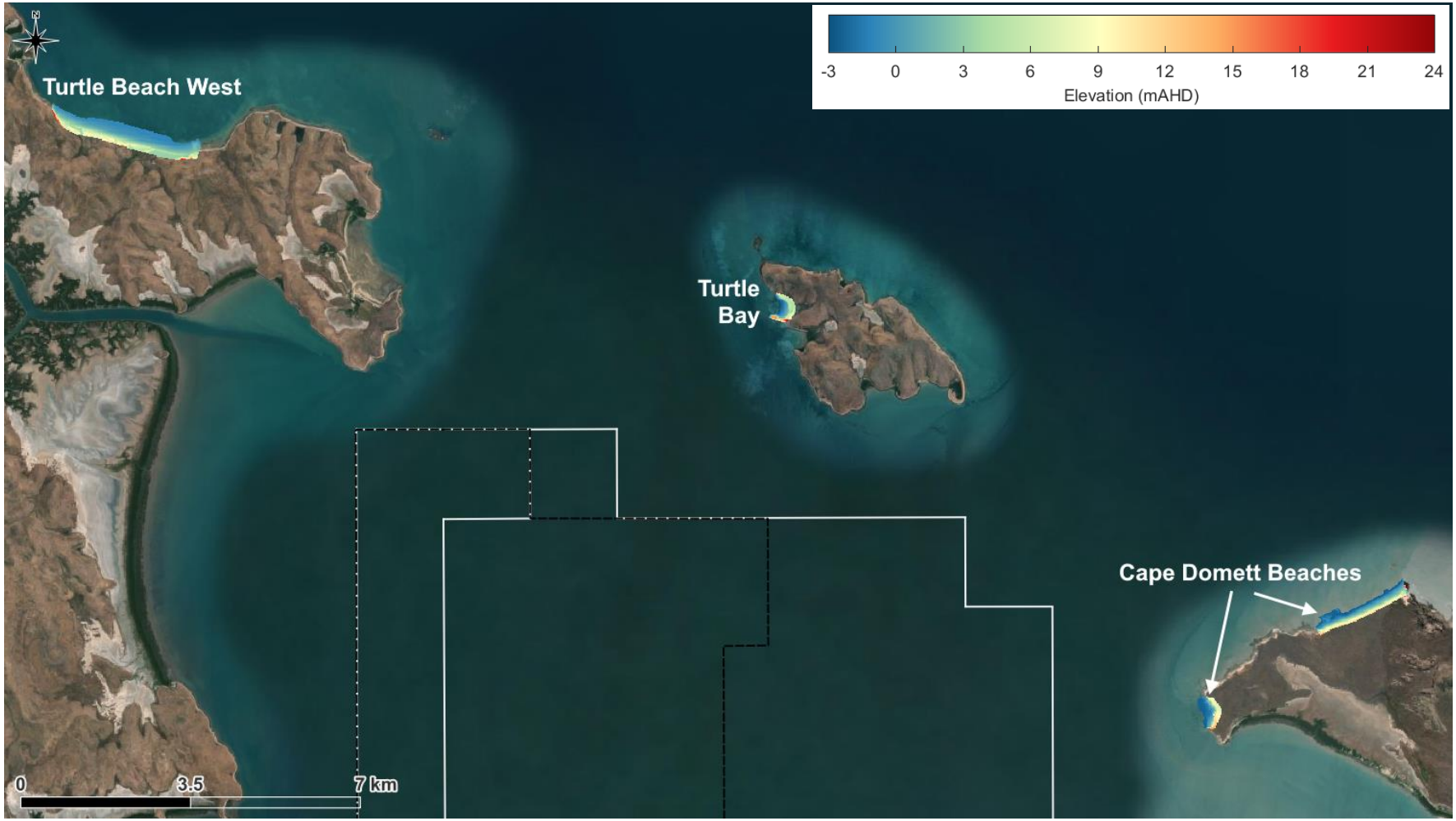

Figure 99. **Beaches where the LiDAR and Photogrammetry drone surveys were undertaken.**

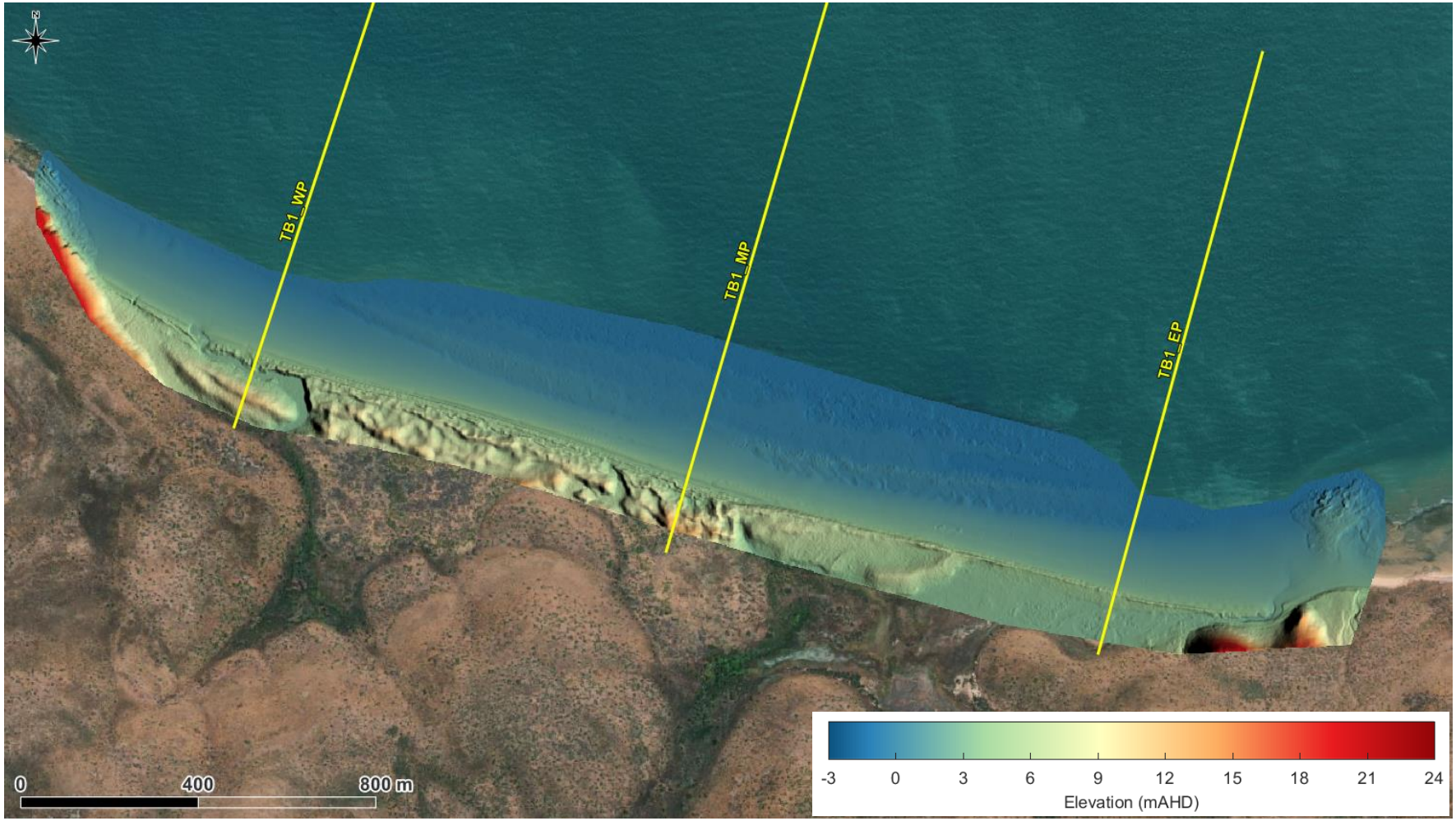

Figure 100. **The 2024 LiDAR DEM for Turtle Beach West along with cross-shore transects.**

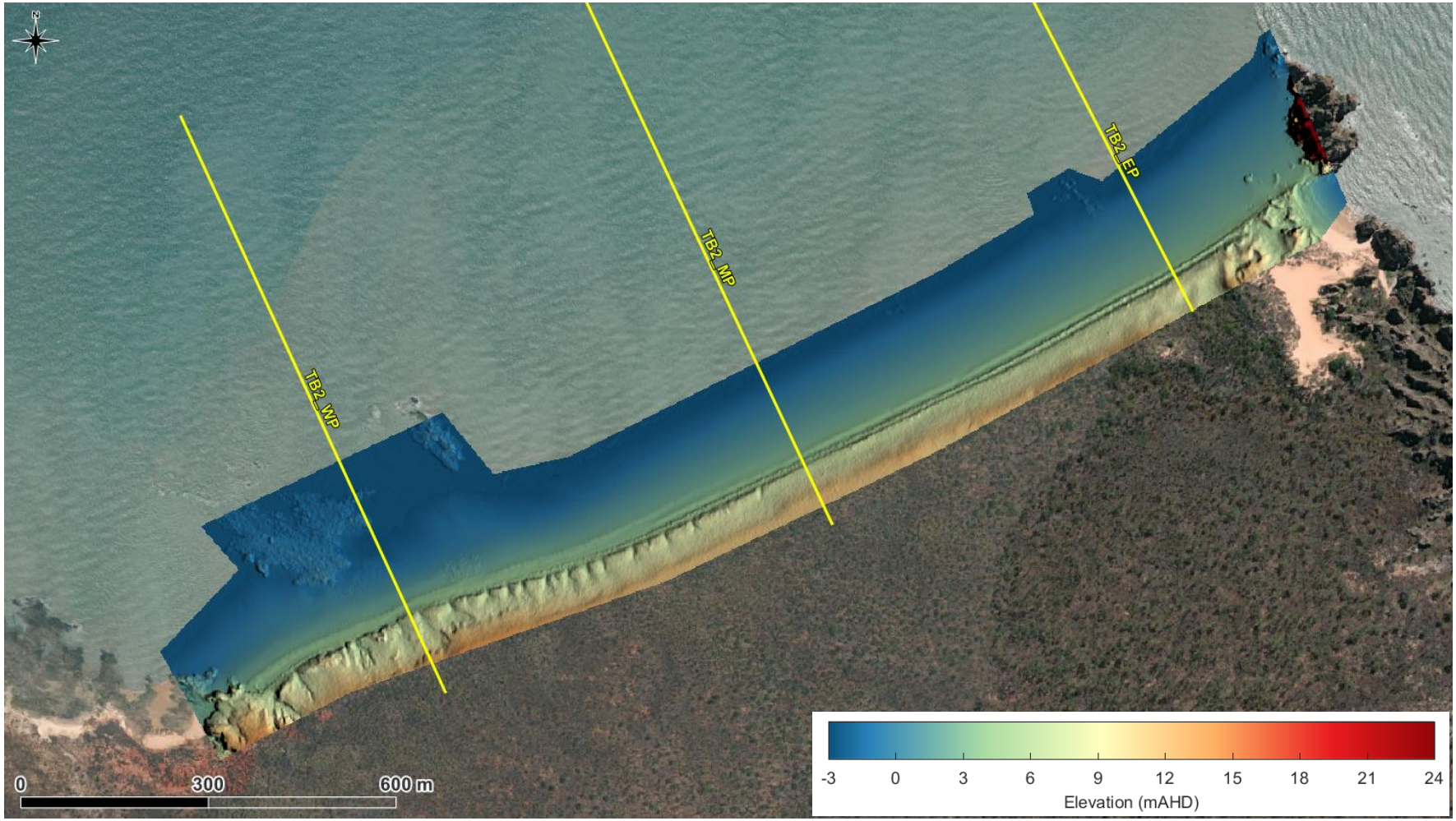

Figure 101. **The 2024 LiDAR DEM for the main Cape Domett Beach along with cross-shore transects.**

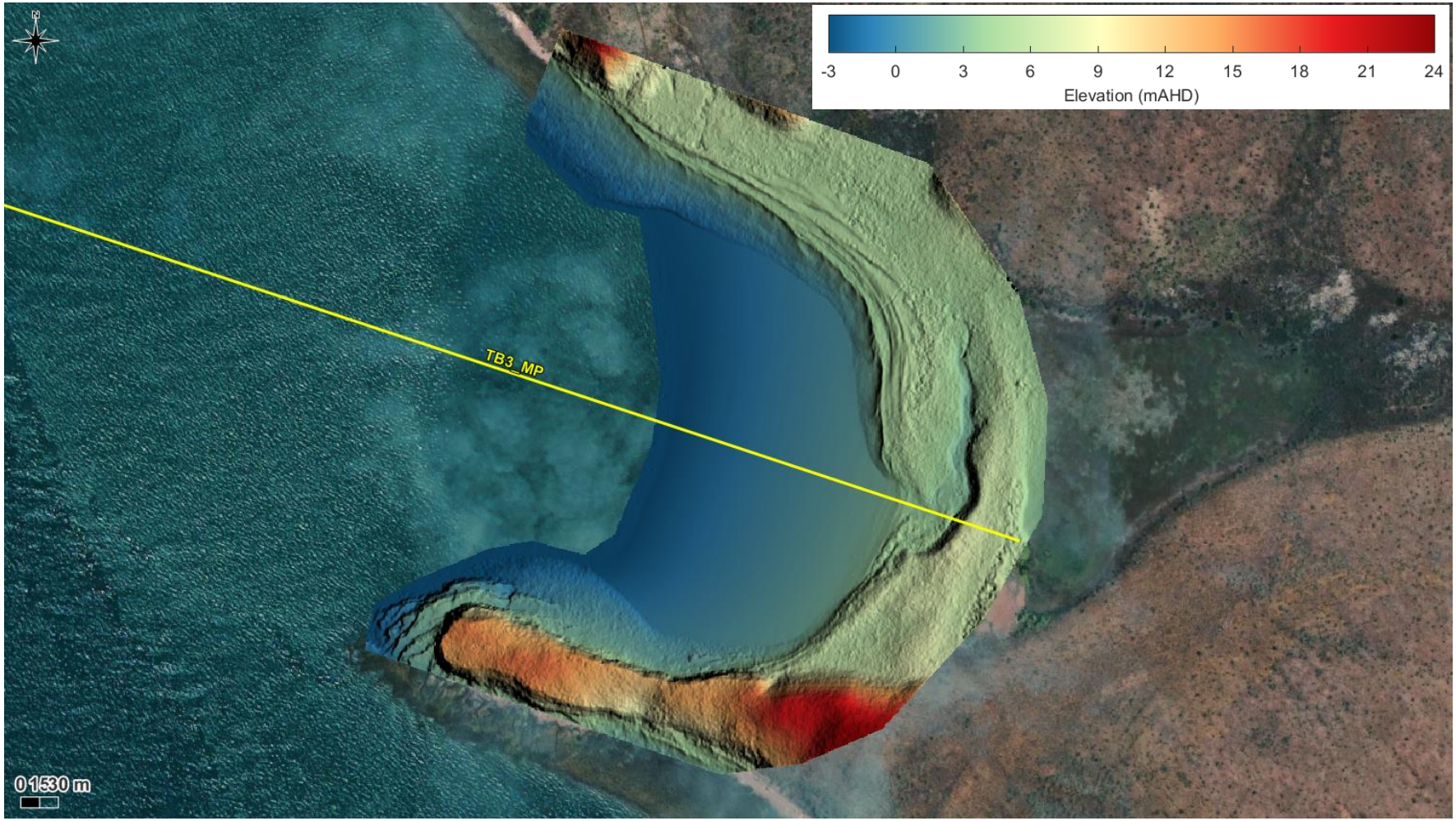

Figure 102. **The 2024 LiDAR DEM for Turtle Bay along with a cross-shore transect.**

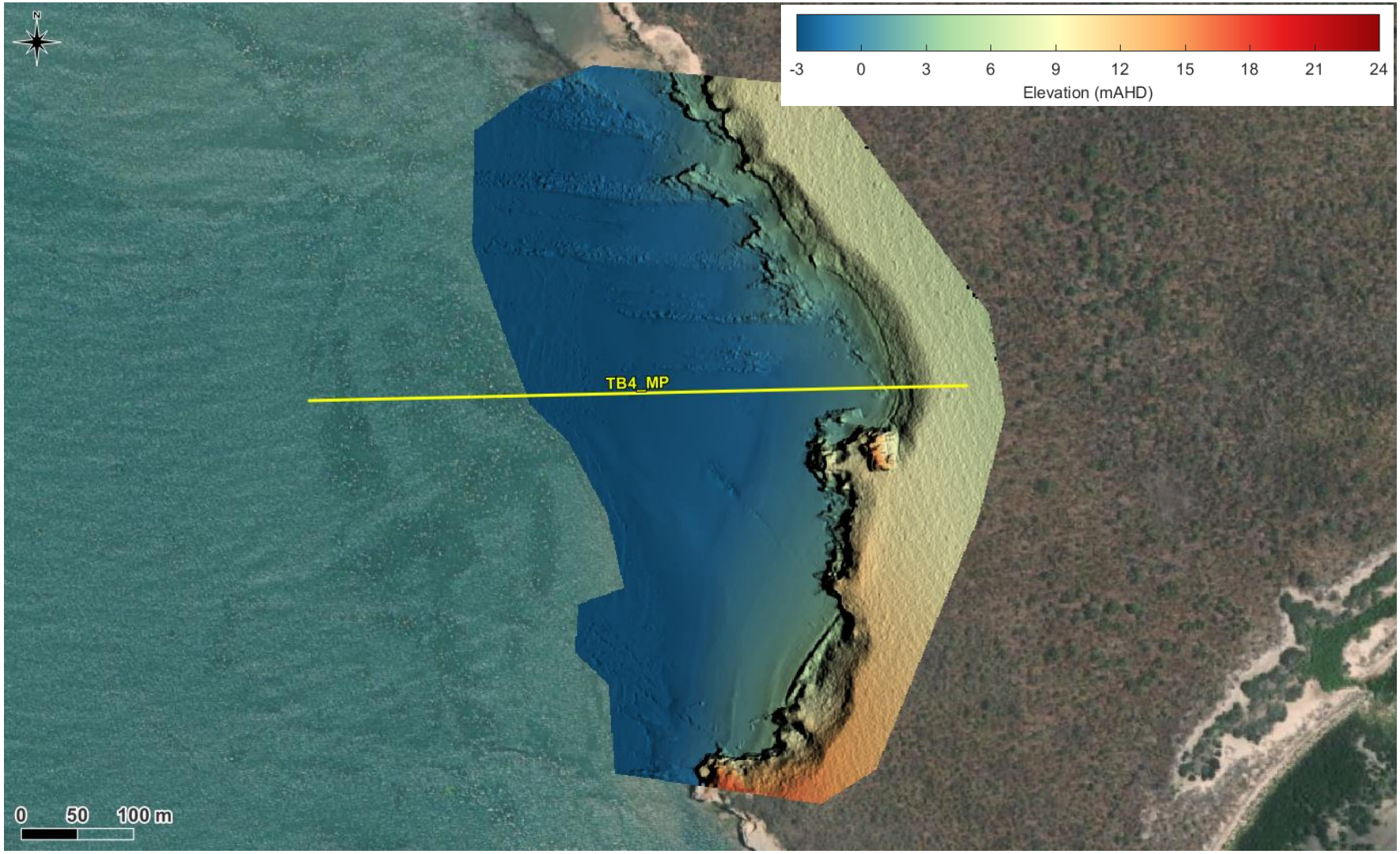

Figure 103. **The 2024 LiDAR DEM for the small Cape Domett Beach along with a cross-shore transect.**

Figure 104. **Close up of the 2024 orthomosaic imagery in the middle of Turtle Beach West.**

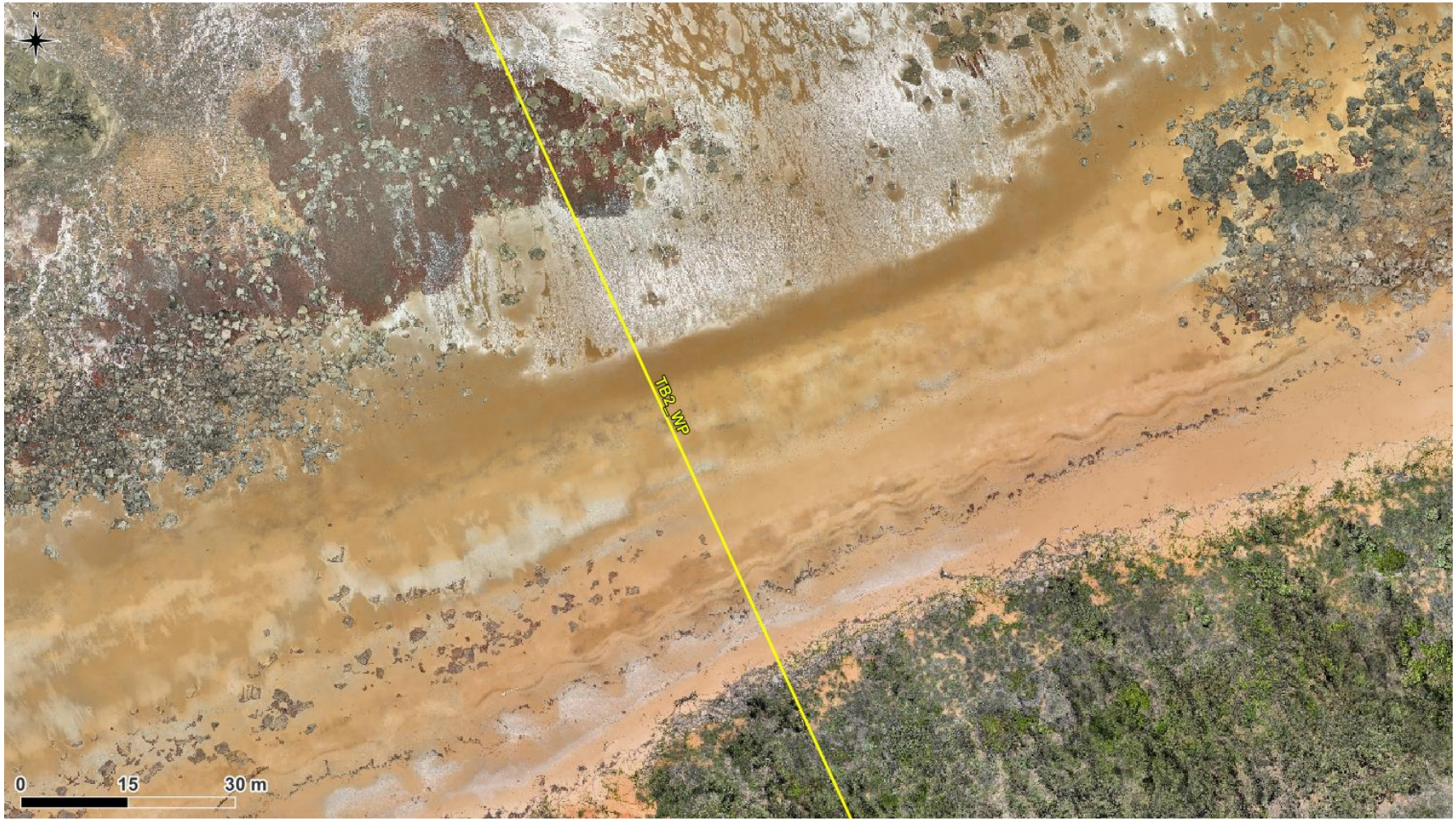

Figure 105. **Close up of the 2024 orthomosaic imagery at the western end of the main Cape Domett Beach.**

Figure 106. **Close up of the 2024 orthomosaic imagery at the southern end of Turtle Bay.**

Figure 107. **Close up of the 2024 orthomosaic imagery at the middle of the small Cape Domett Beach.**

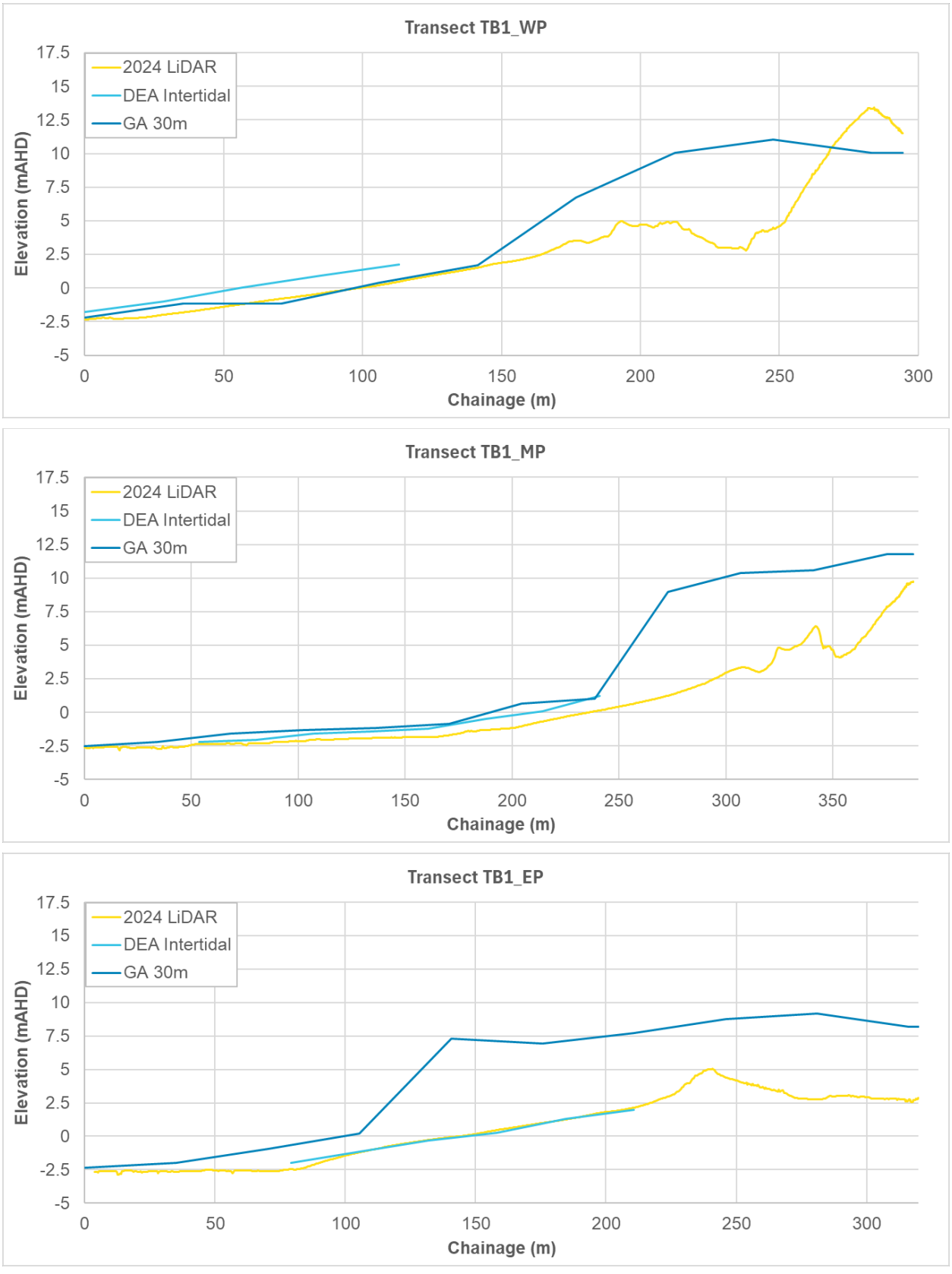

Figure 108. Bathymetry along the three cross-shore transects at Turtle Beach West (see Figure 100 for locations).

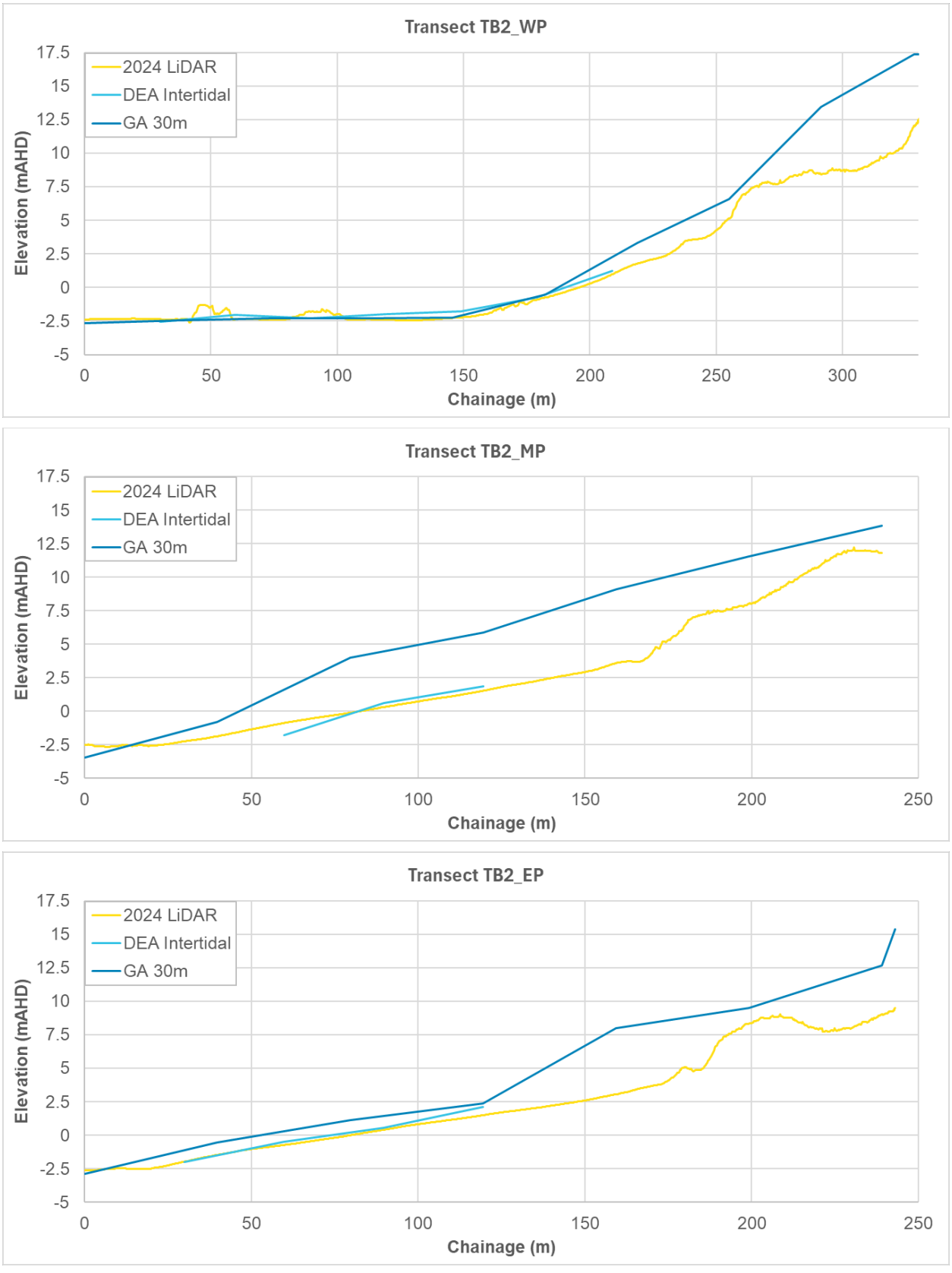

Figure 109. Bathymetry along the three cross-shore transects at the main Cape Domett Beach (see Figure 101 for locations).

Figure 110. Bathymetry along the cross-shore transect at Turtle Bay (see Figure 102 for location).

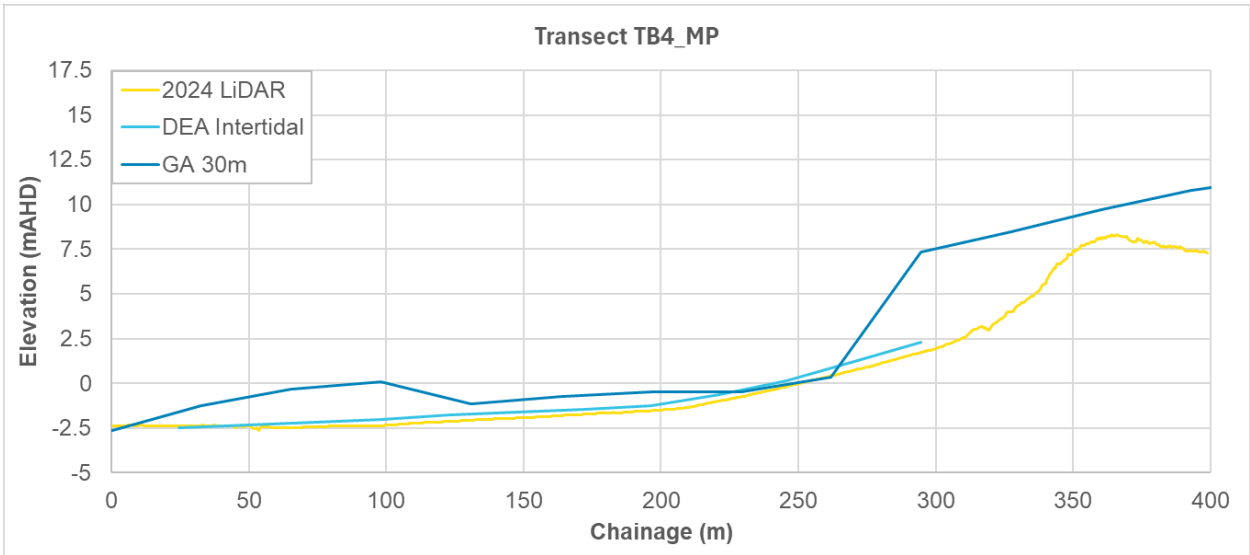

Figure 111. Bathymetry along the cross-shore transect at the small Cape Domett Beach (see Figure 103 for location).

8. Summary

This technical note has provided an analysis of some of the data collected by BKA during the 2024 wet season data collection campaign in CG in February and March 2024, plus data from in-situ self-logging instruments collected at other times, as indicated. The analysis has focused on bathymetric survey data, laboratory results from sediment sampling, vertical profiling data, AWAC and ADCP data, benthic light and water quality data and LiDAR elevation data and orthomosaic imagery of turtle nesting beaches. A summary of the key findings from the analysis are provided below.

- Bathymetry: The data from the multibeam survey have shown that there are extensive areas with sand waves and smaller megaripples present within the proposed operational area. Repeat bathymetric surveys of two Target Areas within the proposed operational area showed that the sand waves migrated at distances of 5 to 10 m over a 29-day lunar tidal cycle. The sand waves were predominantly migrating in a northerly direction, although some localised areas experienced a southerly migration. A high-level estimate of the regular ongoing sand supplied to the proposed operational area through sand wave migration due to typical conditions was calculated to be in the order of 375,000 m^3/yr. In addition, the asymmetry of the sand waves was used to predict the dominant bedload sand transport directions within the proposed operational area, with a net northerly transport dominating.

- Sediment Sampling: The samples have shown that sand is present throughout much of the region, with sand being the dominant sediment present in the West and East Arms and in the main body of CG. The sediment was more variable in the inlets, creeks and small rivers around CG, where silt and clay was present, as well as areas where gravel was dominant.

  Sediment upstream in the West and East Arms was made up of predominantly quartz and feldspar, with small quantities of other minerals also present. As both quartz and feldspar are known to be present in high percentages in the catchments which drain into CG, the sediment in the East and West Arms are considered to be supplied from the upstream catchments. Quartz and feldspar remain the most dominant minerals in the bed sediment throughout the majority of the main bay of CG where the sediment is predominantly sand. The similarity of the sediment in the central area of CG to where the West Arm joins CG, indicates that the sediment throughout the southern and central area of CG is predominantly from an upstream source.

  There is a reduction in the amount of quartz and feldspar present in the bed sediment close to the western entrance to CG and in King Shoals. There is also an increasing amount of calcite from the central CG in an offshore direction. As there is no calcite or calcium silicate present in the bed sediment in the West or East Arms, it can be concluded that these minerals are from an offshore source and the small amount present in CG are from the import of offshore sediment through the western and eastern entrances. Therefore, close to the entrances of CG, and within the proposed operational area, there is a combination of sediment from upstream of CG and sediment from offshore. In addition, the sediment present at King Shoals suggests that the majority of the sediment in this area is likely to be from an offshore source as opposed to being from within CG. This indicates that any dredging from within the proposed operational area would be unlikely to influence the supply of sediment to King Shoals.

- Vertical Profiling:

  - There was limited spatial or temporal variability in water temperature or chlorophyll, with a water temperature of around 31ºC throughout and chlorophyll typically remaining low below 0.2 RFU.

  - Mean salinity for all data from all profiles was 30.8 Practical Salinity Units (PSU) with a range of 26.9 PSU to 32.5 PSU. There was limited variation in salinity through the water column, but salinity was shown to vary over a tidal cycle, with a lower salinity at low water (following the ebb stage of the tide) and a higher salinity at high water (following the flood stage of the tide). The variation in salinity was highest at the furthest upstream site with variations of up to 4 PSU, while at the furthest downstream site the variation was smaller (up to 1.5 PSU).

  - Mean turbidity for all data from all profiles was 15.2 Nephelometric Turbidity Units (NTU) with a range of 4.0 NTU to 55.6 NTU (The turbidity at the two sites closest to the entrance to CG was similar, with values varying between 5 and 20 NTU. The turbidity at the furthest upstream site showed the largest variability and the highest turbidity values, with values ranging from 7 to 55 NTU. The highest turbidity was around low water and the lowest around higher high water, indicating that the suspended sediment resulting in the elevated turbidity was predominantly from an upstream supply.

  - A correlation factor of 2.77 between turbidity and TSS was developed based on wet season data (i.e. 1 NTU = 2.77 mg/L). This compares to 1 NTU = 1.72 mg/L as calculated based on dry season data collected in CG in July 2023, as reported in PCS (2024a). The difference between the two correlation factors suggests that there is a difference in the PSD of the suspended sediment between the two seasons, although there is likely to be temporal variability in the correlation factors during each season which could be higher than the difference between the two seasons.

  - The suspended sediment at all three monitoring sites was predominantly made up of silt and clay-sized particles, with limited sand present in suspension. The composition of the sediment in suspension was similar between the sites and over the spring tidal cycle, which gives confidence that the derived turbidity to TSS correlation is applicable for the area around the proposed operational area during the wet season.

  - The elemental feature analysis results showed that clay minerals were dominant at two of the three sites and an agglomerate of silicate and halite was dominant at the third site. Similarities in the mineral composition of the suspended sediment at low water and high water at two sites indicates that the suspended sediment is likely to remain in suspension over a spring tidal cycle and that the sediment was not locally suspended at the sites. At the site located in the middle of the proposed operational area, the mineral composition of the suspended sediment indicated that some of the suspended sediment could have been due to resuspension of sediment locally at the site.

  - Mean current velocity for all data from all profiles was 0.55 m/s with a range of 0.05 m/s to 1.22 m/s. The higher values are very high current velocities. Peaks in current speed occurred mid-way through the flood and ebb stages of the tide, with lower current speeds occurring around high water and low water (slack water), which is fully consistent with what would be expected. At Sites 1 and 2, the peak flood and ebb current speeds were approximately comparable (mid depth peaks of 1 m/s and near-bed peaks of 0.8 m/s), while at Site 3 the ebb current speeds were higher than the peak flood current speeds.

- AWAC and ADCP: Water level, current and wave data have been analysed at seven different sites within CG between September 2023 and May 2024. The data have shown how the current and wave conditions vary both spatially and temporally within CG. Peak current speeds at the sites typically ranged from just under 1 m/s to 1.5 m/s, with current speeds at highest at the surface and lowest at the bed, and differences between the two layers varying from 0.2 m/s to 1.0 m/s. The current data at all sites showed that the astronomical tide was the dominant force controlling the currents in the region. The measured wave data showed a change in the wave conditions between the dry season and the wet season, with diurnal variations in wave heights typically occurring during the dry season due to daily variation in local wind conditions, while during the wet season, larger wave events occurred which were generated offshore in CG. Comparison between wave conditions at the measurement sites showed slightly larger waves at the western entrance to CG during dry season conditions, but the potential for larger waves within CG compared to the western entrance during wet season wave events. This suggests that ongoing wave growth can occur within CG during larger wet season wave events but likely only for a narrow range of wind directions.

- Benthic Light and Water Quality:

  - At all the sites where benthic light measurements have successfully been collected in CG, the data show that limited benthic light was available on the seabed. The results have shown no benthic light was available on the seabed in depths of more than 20 m and at the shallowest site with a depth of 13.5 m MSL, low levels of benthic light were available just during neap tides when the turbidity was at its lowest, with no benthic light during other periods.

  - The water temperature varied from approximately 25 ºC in the dry season up to 32 ºC in the wet season (highest water temperatures recorded during December and January). The water temperature was relatively consistent between the monitoring sites. The data showed a relatively consistent increase in water temperature between the dry season and the wet season, but with more variability occurring when the water temperature reduced between the wet season and the dry season. The variability in the reduction in water temperature was likely to be related to the upstream freshwater discharge and the meteorological conditions during the wet season.

  - Larger variations in salinity occurred during the wet season due to the increased freshwater discharge flowing into CG. The measured salinity varied between 10 and 34 PSU, the highest salinity measurements were in King Shoals while the lowest measurements were at the furthest upstream site at the confluence with the West Arm, with the sites between varying depending on their relative distance between the two. The data also show that the salinity within CG varied over a tidal cycle, with the highest salinity occurring at high water, due to the flood stage of the tide importing higher salinity offshore water into CG, and the lowest salinity occurring at low water after the ebb stage of the tide has brought low salinity water from upstream into CG.

  - The turbidity was typically lower close to the entrance to CG and in King Shoals and higher further upstream. The turbidity was highest around low water, due to the ebb stage of the tide transporting higher turbidity water from upstream into CG, and lower around high water as a result of the flood stage of the tide transporting lower turbidity water from offshore into CG. At most sites there was a clear spring-neap tidal signal in the data, with high turbidity coinciding with the spring tides and lower turbidity coinciding with the neap tides.

  - The data showed that the dissolved oxygen was consistently between 6 and 7 mg/L over the dry season conditions. During the wet season the dissolved oxygen was more variable, with values reducing down to 2 mg/L for short periods but typically varying between 4 and 6 mg/L. The measurements suggested that the dissolved oxygen was relatively consistent throughout the region.

- LiDAR Data: A comparison between the 2024 LiDAR data and other available intertidal and supratidal beach elevation data was undertaken. This showed the following.

  - The new LiDAR data provides a significant increase in resolution compared to previous available data (0.02 m compared to 25 to 30 m).

  - The new LiDAR elevation data were generally similar to the Digital Earth Australia 25 m Intertidal elevation data, although at one of the beaches there were differences of up to 1.5 m.

  - Comparison with the Geoscience Australia 30 m depth model, which is the only available dataset for providing elevations for the upper beach profile (> 2.5 m AHD), showed typical differences of around 2 m, but with some differences of more than 5 m.

  - The LiDAR data are considered to provide a significant improvement in the representation of the beach profile elevation at the turtle nesting beaches compared to other available datasets.

Multiple sources of data from the 2024 wet season data collection campaign (February to March 2024) have shown that the sand which is present within the proposed operational area, is predominantly from a terrestrial source. Weathering of rock in the CG catchment has resulted in sand dominated by quartz and feldspar minerals, to be supplied to the West and East Arms. The sand is then transported downstream into the main body of CG and towards the entrances to CG. Close to the entrance to CG, the bed sediment is made up of a combination of terrestrial and offshore minerals, although the terrestrial minerals are strongly dominant. Limited suspension of sand occurs around the proposed operational area, with the majority of the sediment in suspension being clay to fine silt-sized particles, while the sand is predominantly transported by bedload transport.

9. References

BKA, 2024b. Cambridge Gulf Marine Sand Proposal – WA EP Act s38 Referral Report No. 2: *Proposal Setting & Existing Environment Descriptions*.

BKA, 2024d. Cambridge Gulf Marine Sand Proposal – WA EP Act s38 Referral Report No. 4: *Impact Assessments of Relevant Environmental Factors*.

Digital Earth Australia (DEA), 2023. Derived data product, DEA Intertidal Elevation. <https://www.dea.ga.gov.au/products/dea-intertidal-elevation>, viewed 11 October 2023.

Geoscience Australia, 2023. High-resolution depth model for Northern Australia – 30m. <https://ecat.ga.gov.au/geonetwork/srv/api/records/1010ac13-e033-489d-b9ce-ae11fd0e11ef>, viewed 10 October 2023.

PCS, 2024a. Cambridge Gulf Marine Sand Proposal – WA EP Act s38 Referral Report No. 5: *Metocean & Sediment Dynamics –System Understanding, Conceptual Model and Initial Modelling.*

PCS, 2024c. Cambridge Gulf Marine Sand Proposal – WA EP Act s38 Referral Report No. 5: *Metocean & Sediment Dynamics –System Understanding, Conceptual Model and Initial Modelling.* Annex 2: Factual Data Report.

Schlee, J., 1973. Atlantic Continental Shelf and Slope of the United States – Sediment Texture of the Northeastern Part. US Geological Survey, Professional Paper 529-L, 64 p.

Shepard, F.P., 1954. Nomenclature based on sand-silt-clay ratios. Journal of Sedimentary Research 24.

Sheppard, S.; Griffin, T.J.; Tyler, I.M.; Page, R.W., 2001. High- and low-K granites and adakites at a Palaeoproterozoic plate boundary in northwestern Australia. Journal of the Geological Society. 158 (3): 547–560.

Tyler, I.M., 1996. Geology and Landforms of the Kimberley. Department of Conservation and Land Management. 72 p.

Appendix A: Water Column Profile Plots

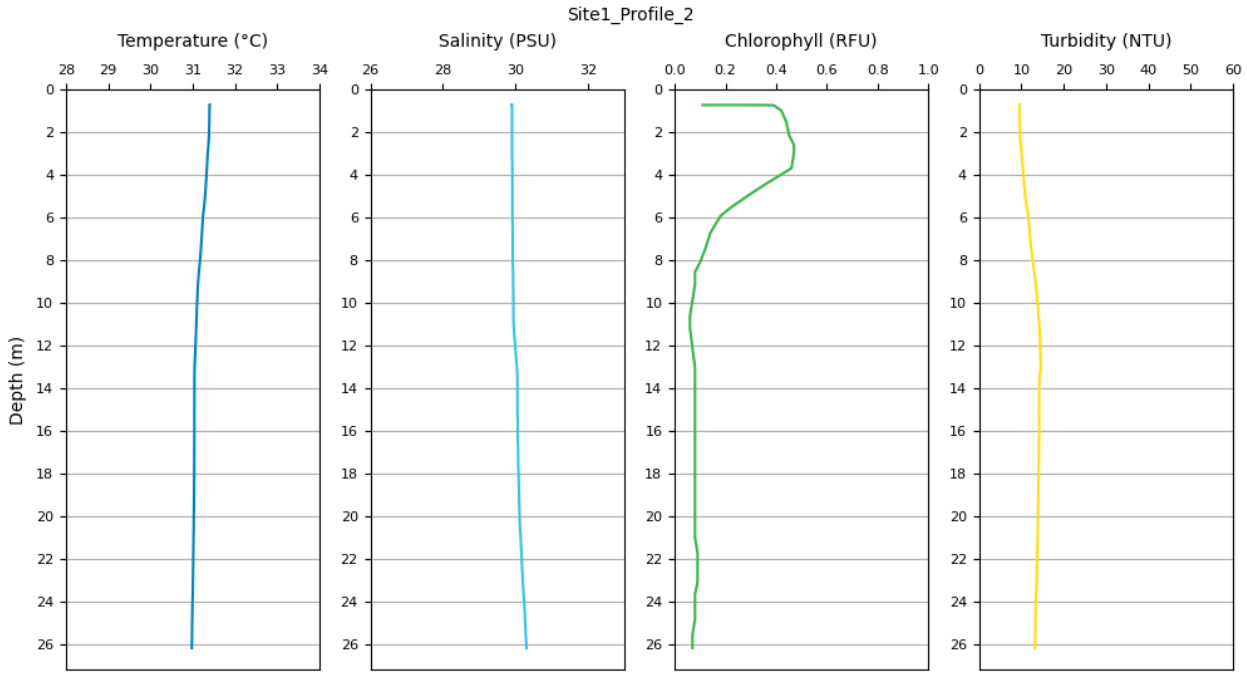

Figure A1. **Measured temperature, salinity, chlorophyll and turbidity through the water column at Site 1 at low water +1 hour.**

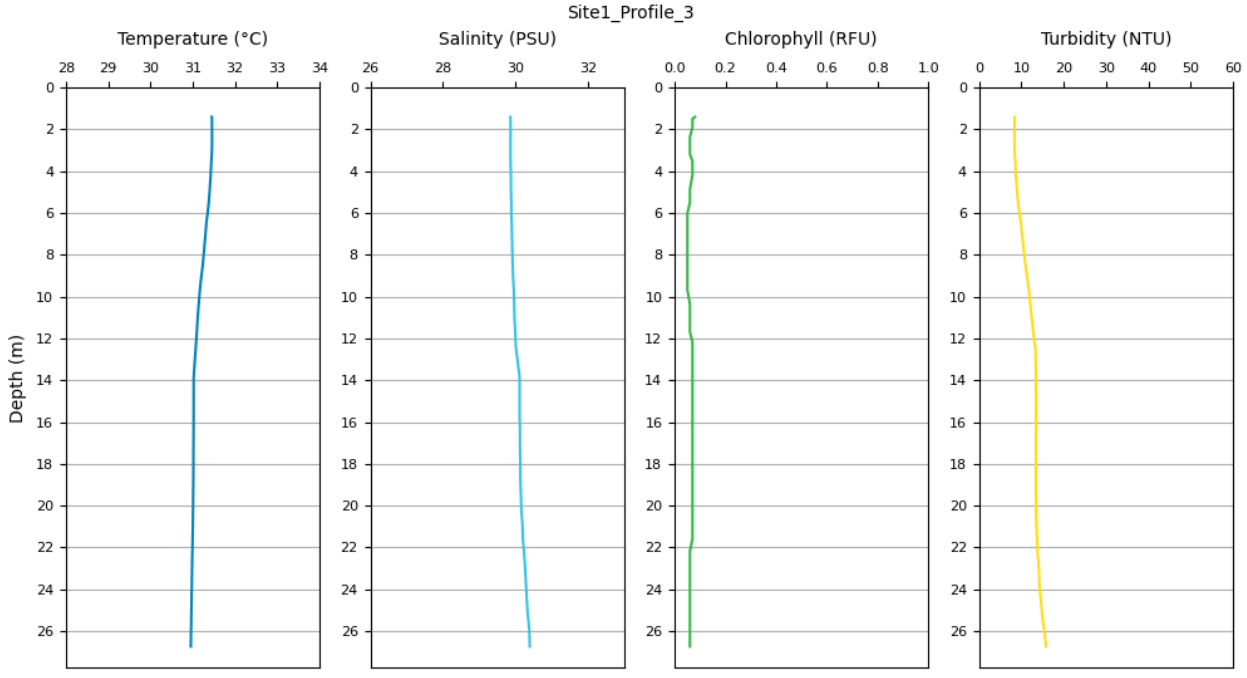

Figure A2. **Measured temperature, salinity, chlorophyll and turbidity through the water column at Site 1 at low water +2 hours.**

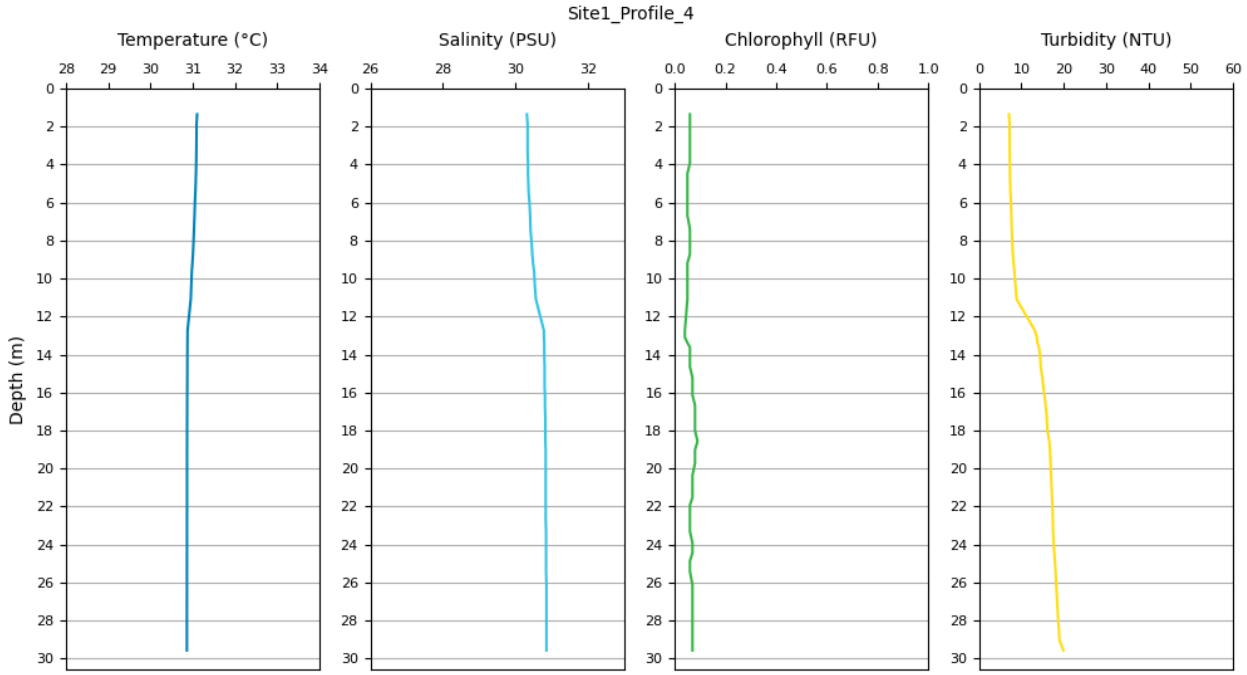

Figure A3. Measured temperature, salinity, chlorophyll and turbidity through the water column at Site 1 at low water +3 hours.

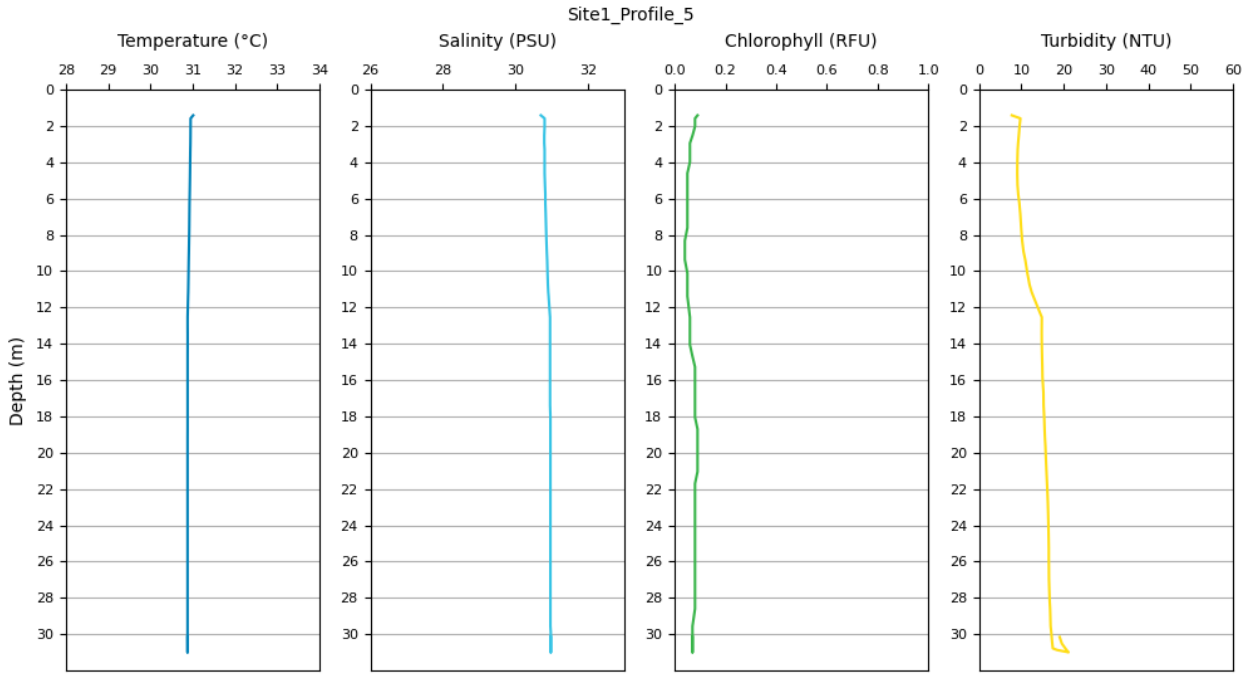

Figure A4. Measured temperature, salinity, chlorophyll and turbidity through the water column at Site 1 at low water +4 hours.

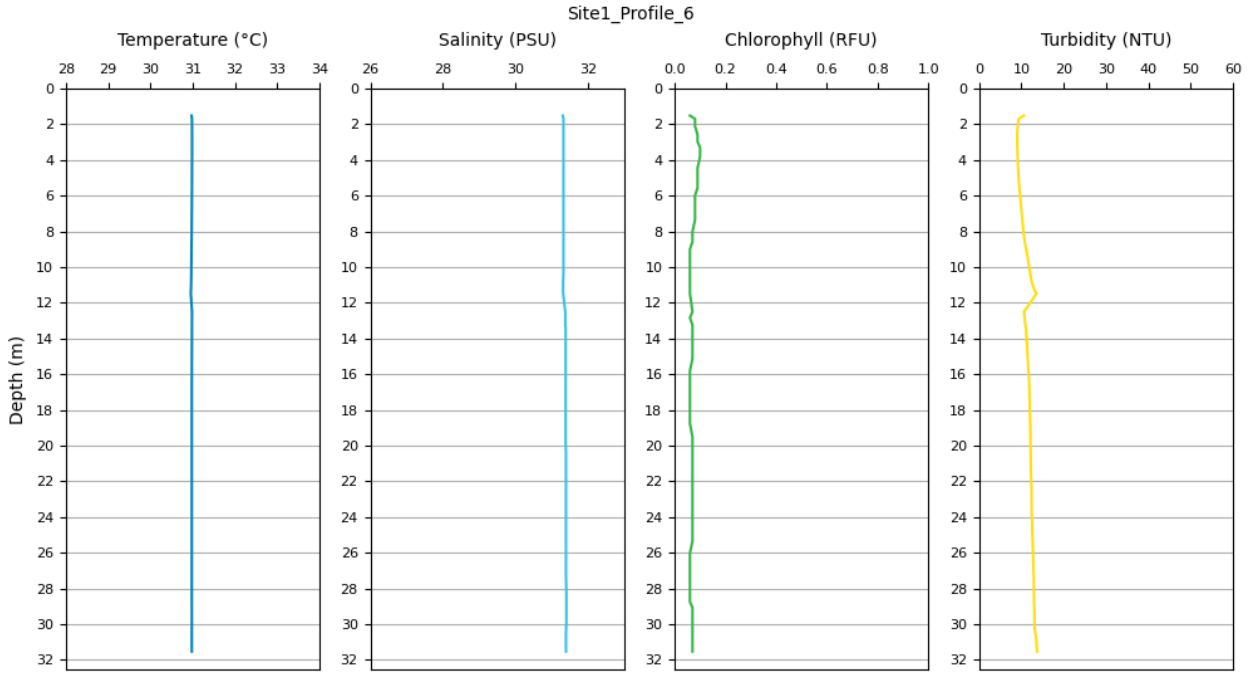

Figure A5. Measured temperature, salinity, chlorophyll and turbidity through the water column at Site 1 at low water +5 hours.

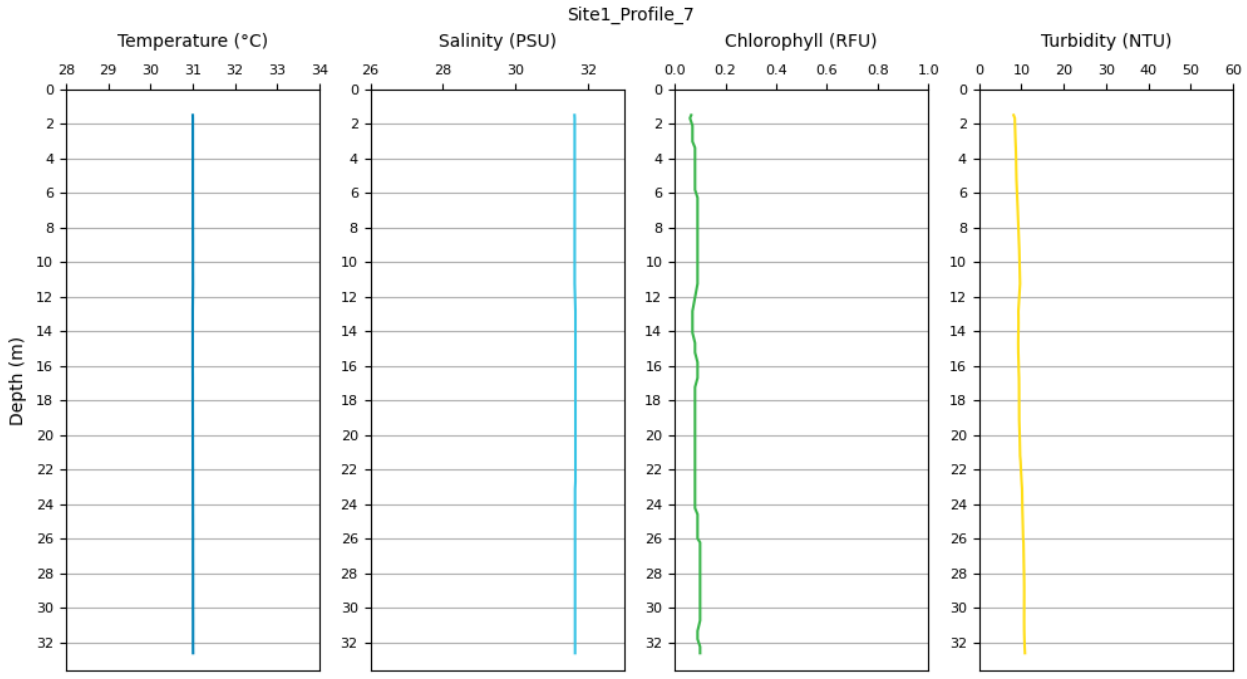

Figure A6. Measured temperature, salinity, chlorophyll and turbidity through the water column at Site 1 at low water +6 hours.

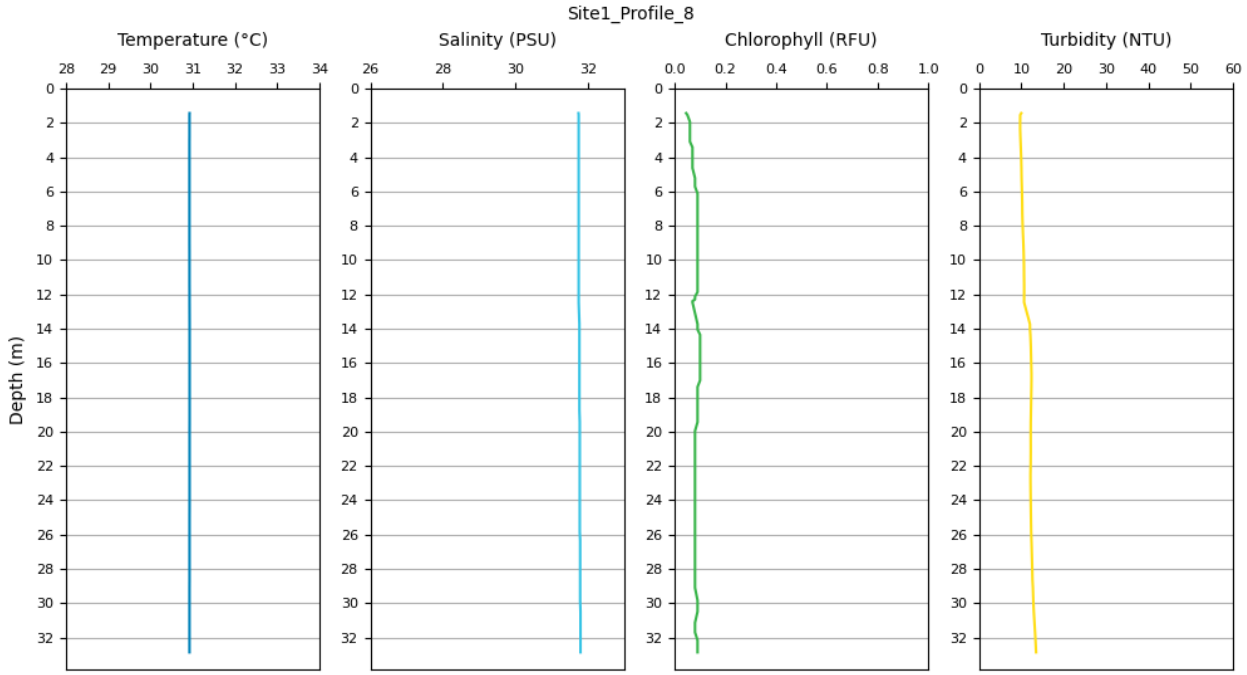

Figure A7. Measured temperature, salinity, chlorophyll and turbidity through the water column at Site 1 at low water +7 hours.

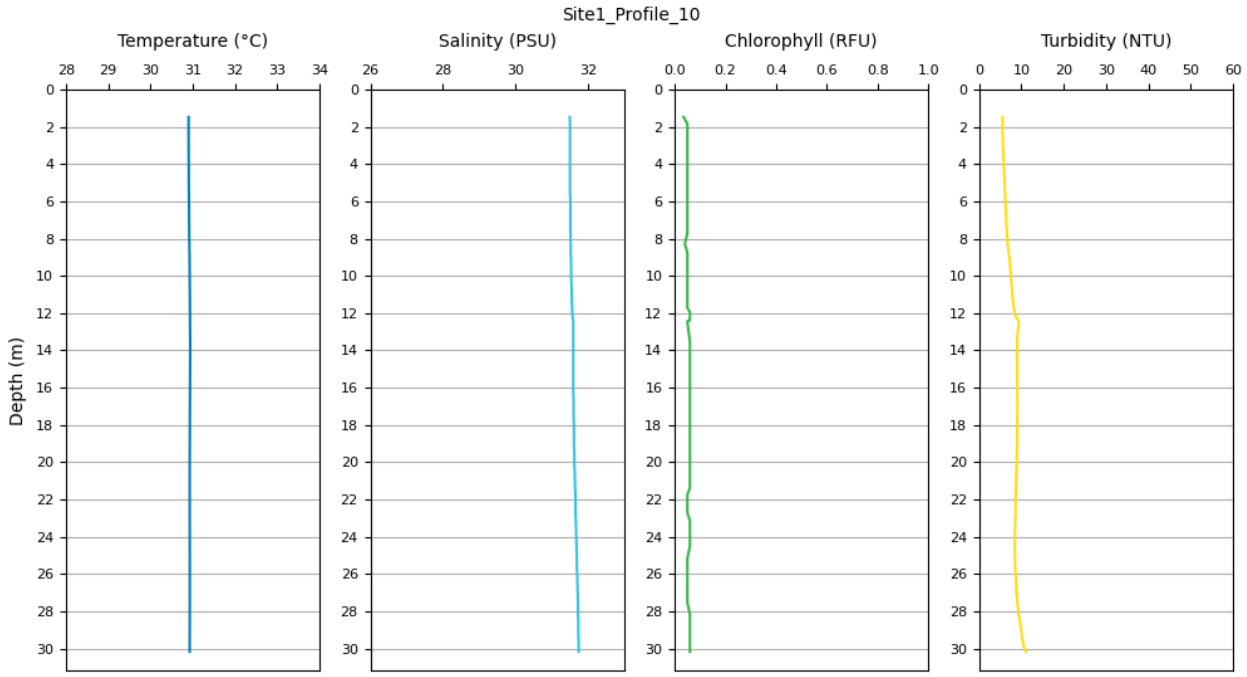

Figure A8. Measured temperature, salinity, chlorophyll and turbidity through the water column at Site 1 at low water +9 hours.

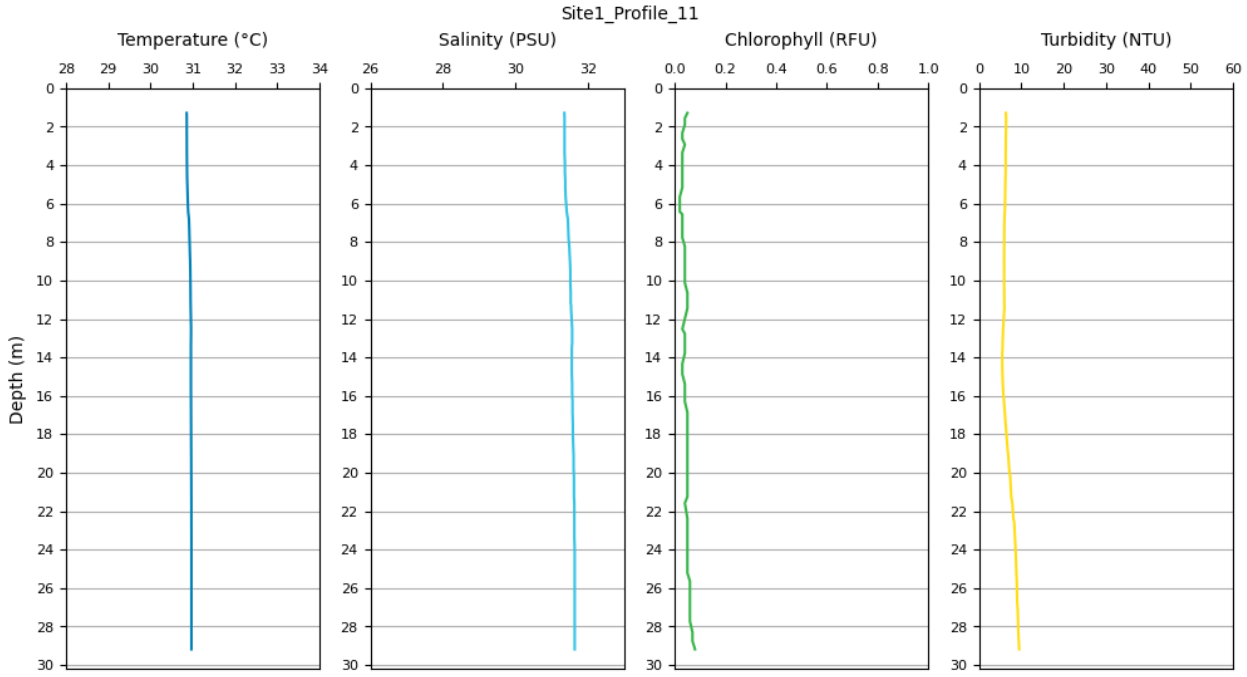

Figure A9. Measured temperature, salinity, chlorophyll and turbidity through the water column at Site 1 at low water +10 hours.

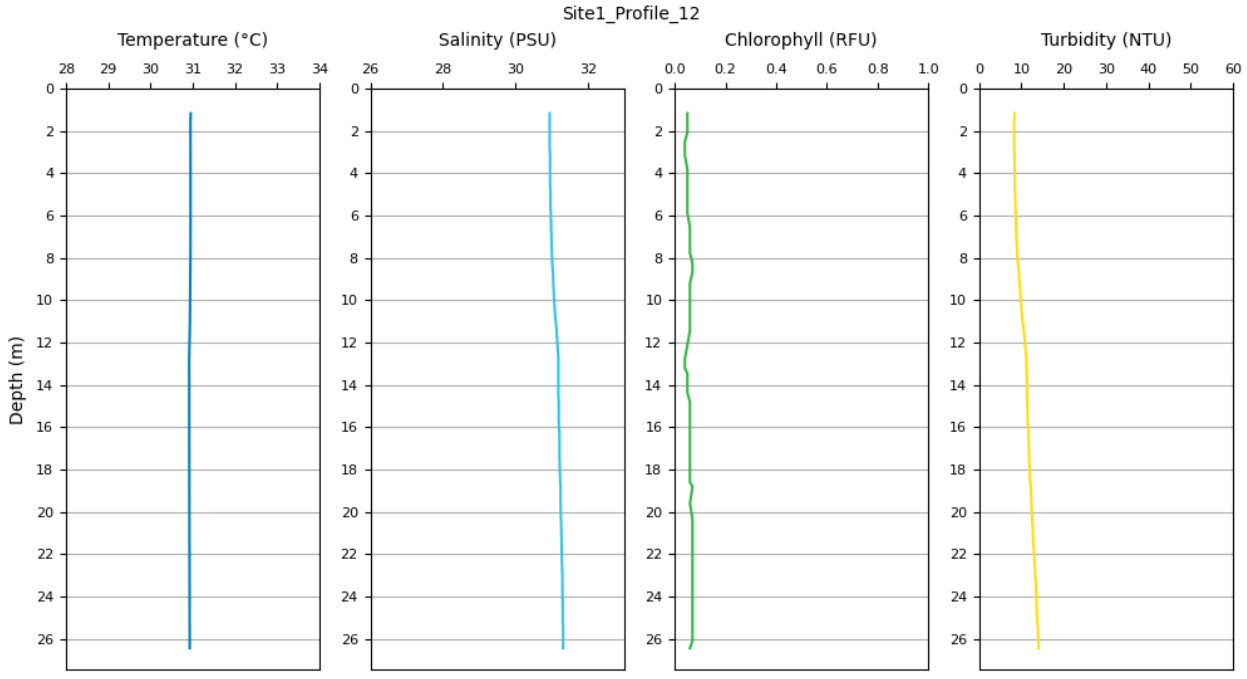

Figure A10. Measured temperature, salinity, chlorophyll and turbidity through the water column at Site 1 at low water +11 hours.

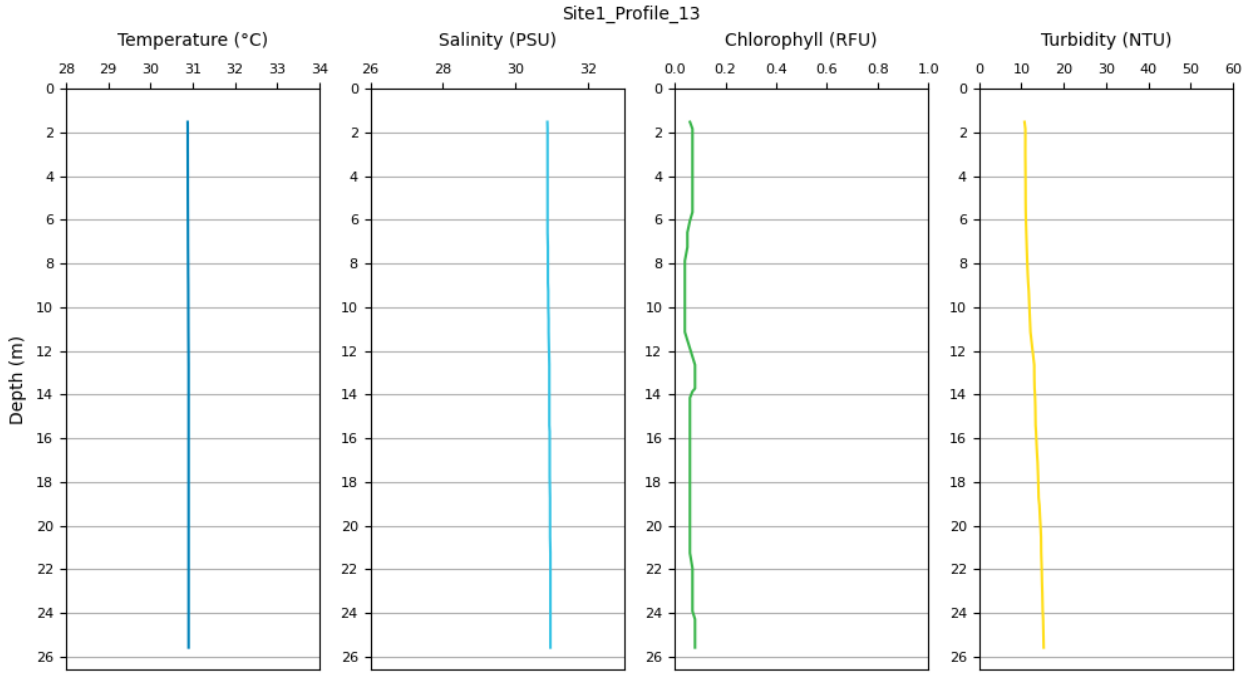

Figure A11. Measured temperature, salinity, chlorophyll and turbidity through the water column at Site 1 at low water +12 hours.

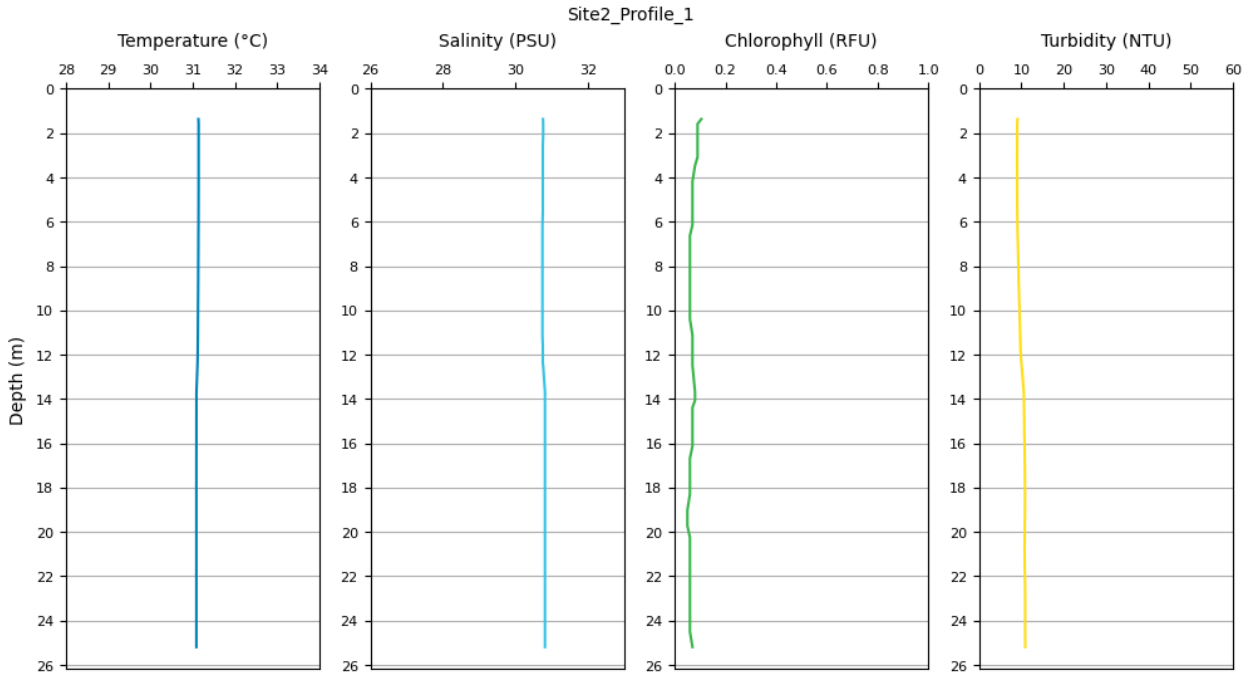

Figure A12. Measured temperature, salinity, chlorophyll and turbidity through the water column at Site 2 at low water.

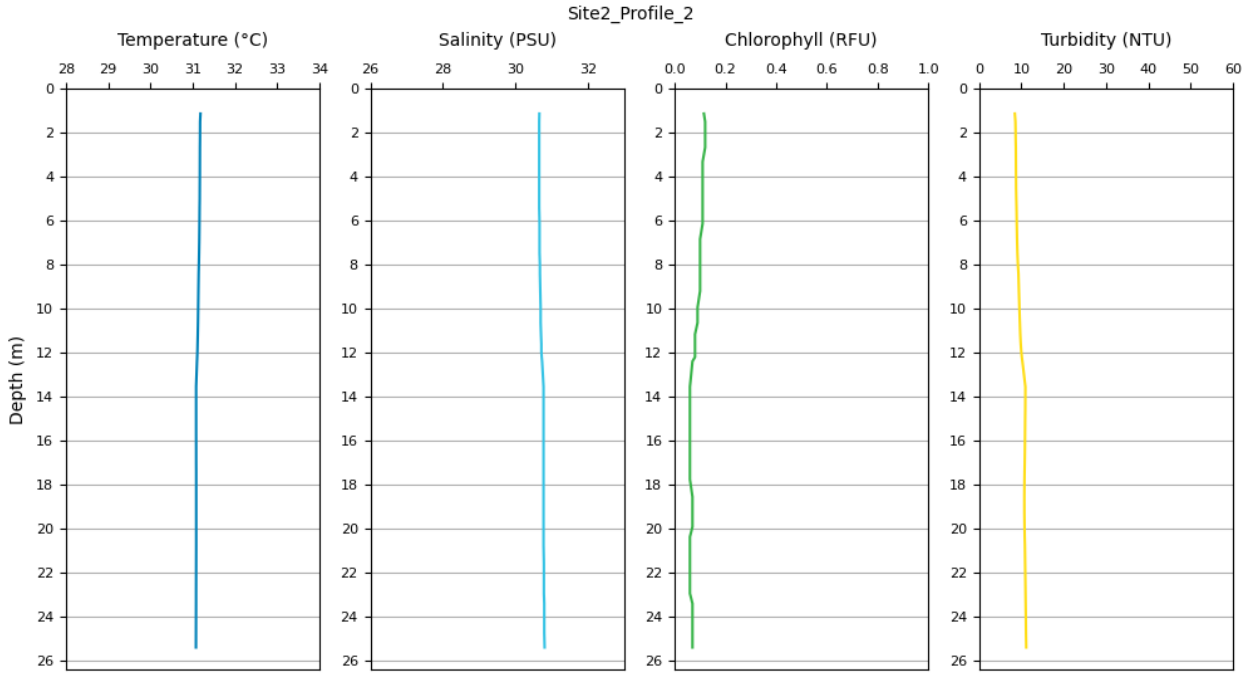

Figure A13. Measured temperature, salinity, chlorophyll and turbidity through the water column at Site 2 at low water +1 hour.

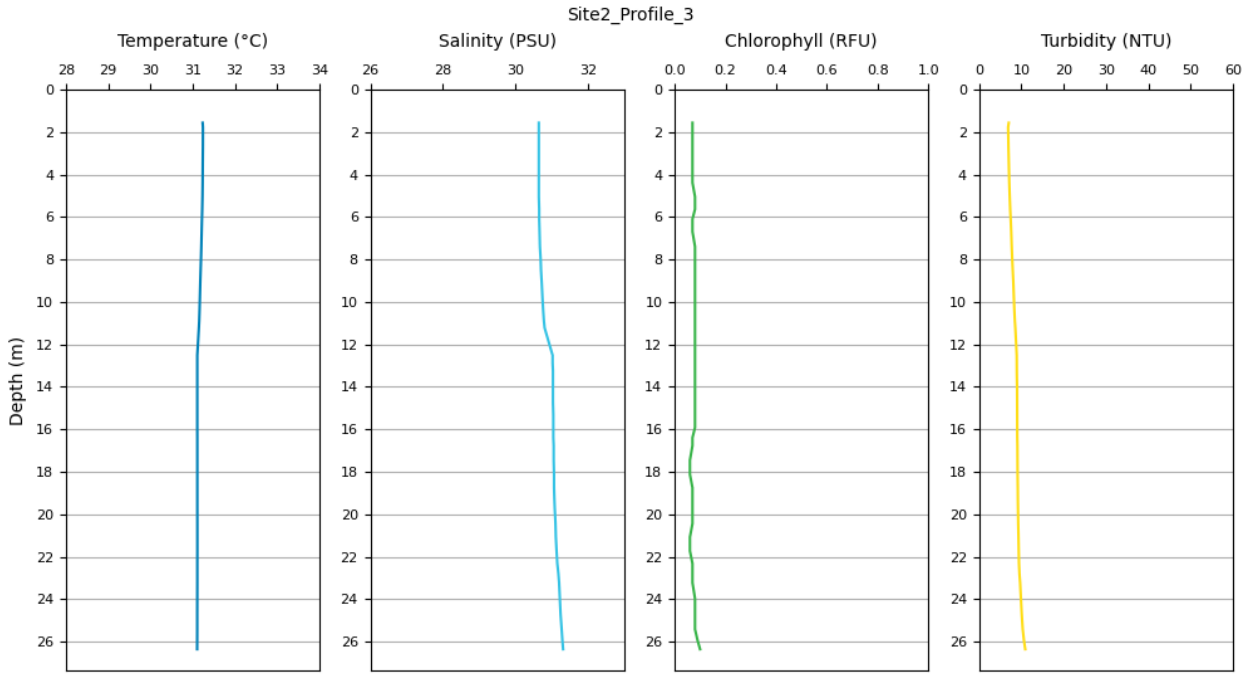

Figure A14. Measured temperature, salinity, chlorophyll and turbidity through the water column at Site 2 at low water +2 hours.

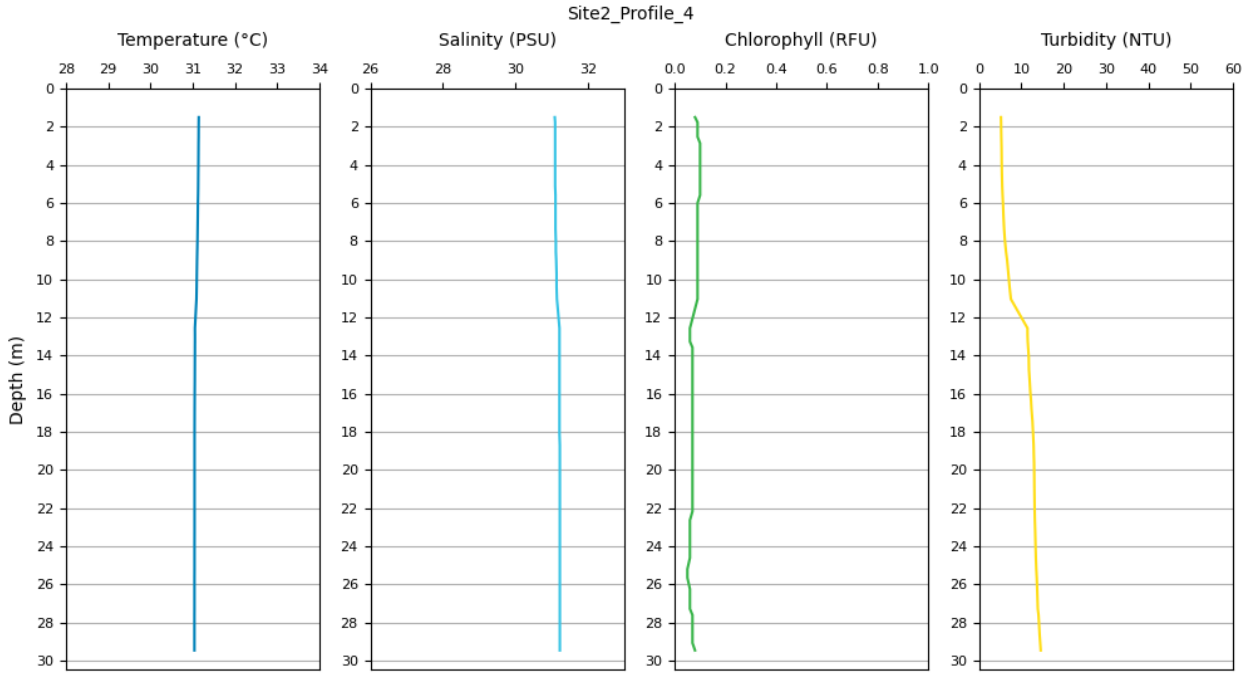

Figure A15. Measured temperature, salinity, chlorophyll and turbidity through the water column at Site 2 at low water +3 hours.

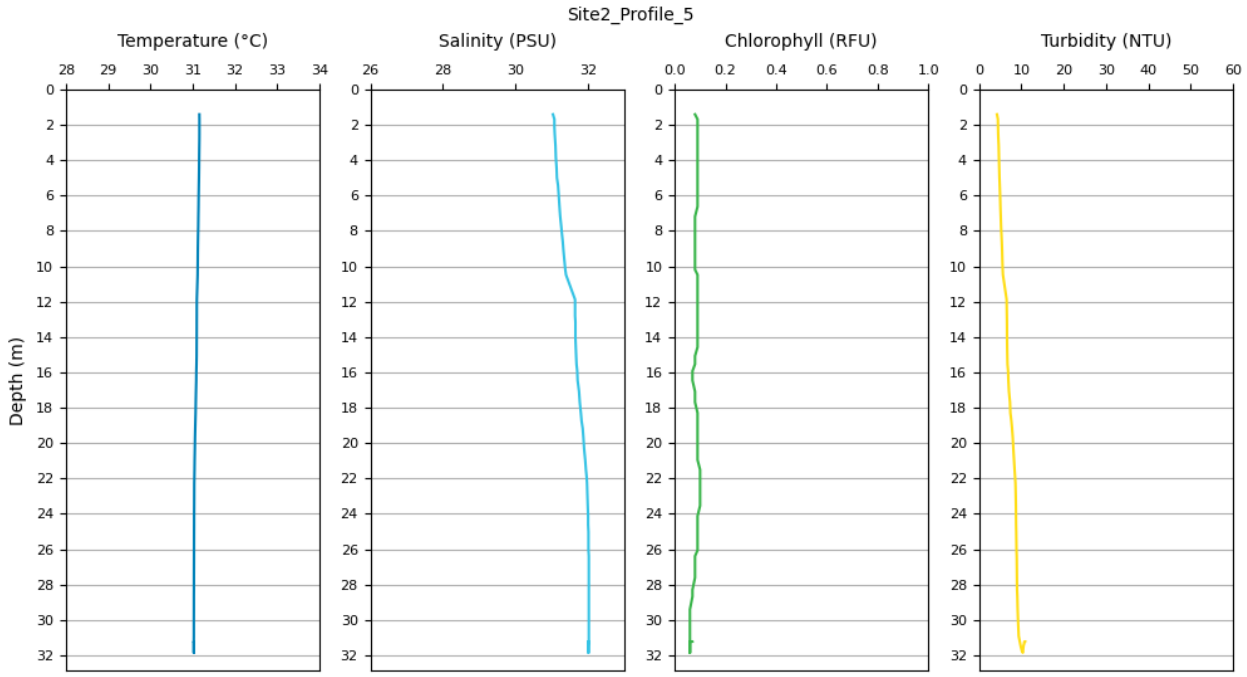

Figure A16. Measured temperature, salinity, chlorophyll and turbidity through the water column at Site 2 at low water +4 hours.

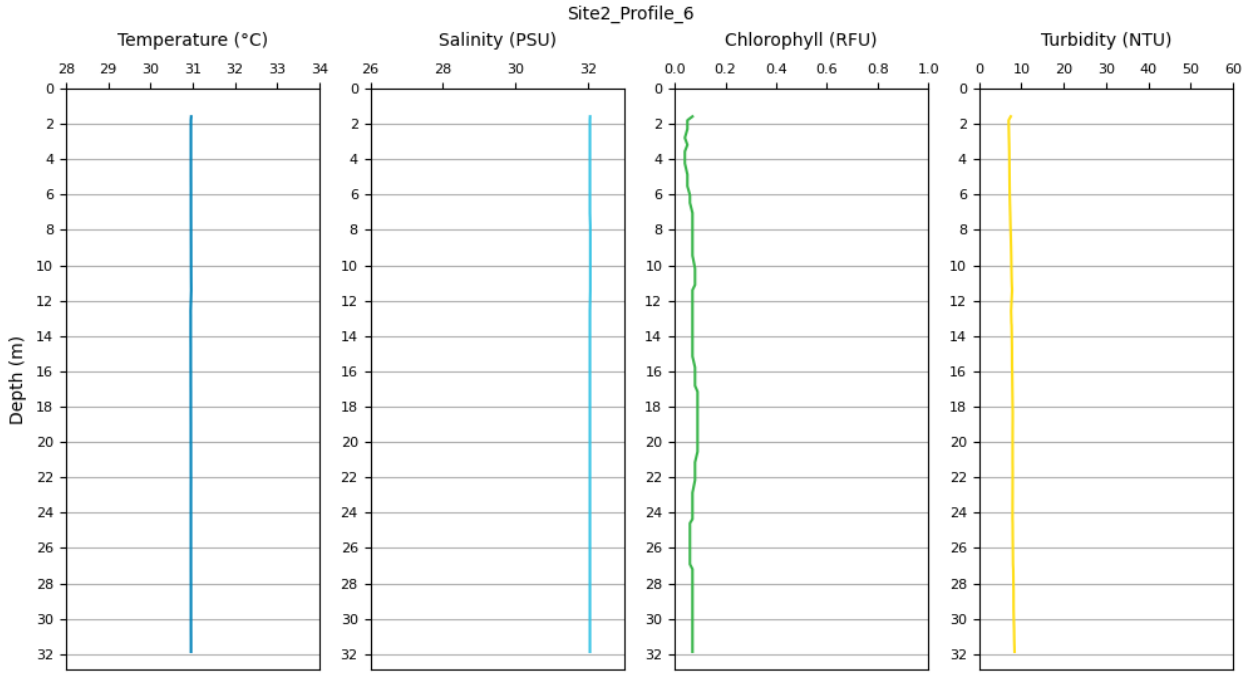

Figure A17. Measured temperature, salinity, chlorophyll and turbidity through the water column at Site 2 at low water +5 hours.

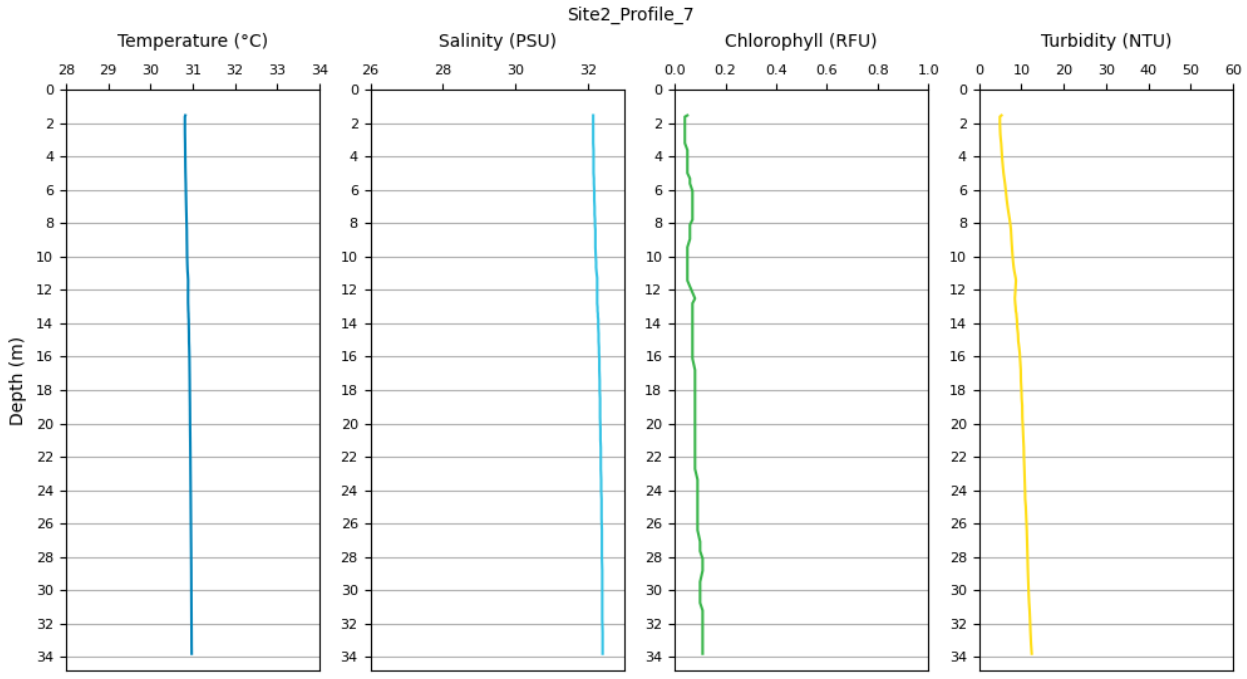

Figure A18. Measured temperature, salinity, chlorophyll and turbidity through the water column at Site 2 at low water +6 hours.

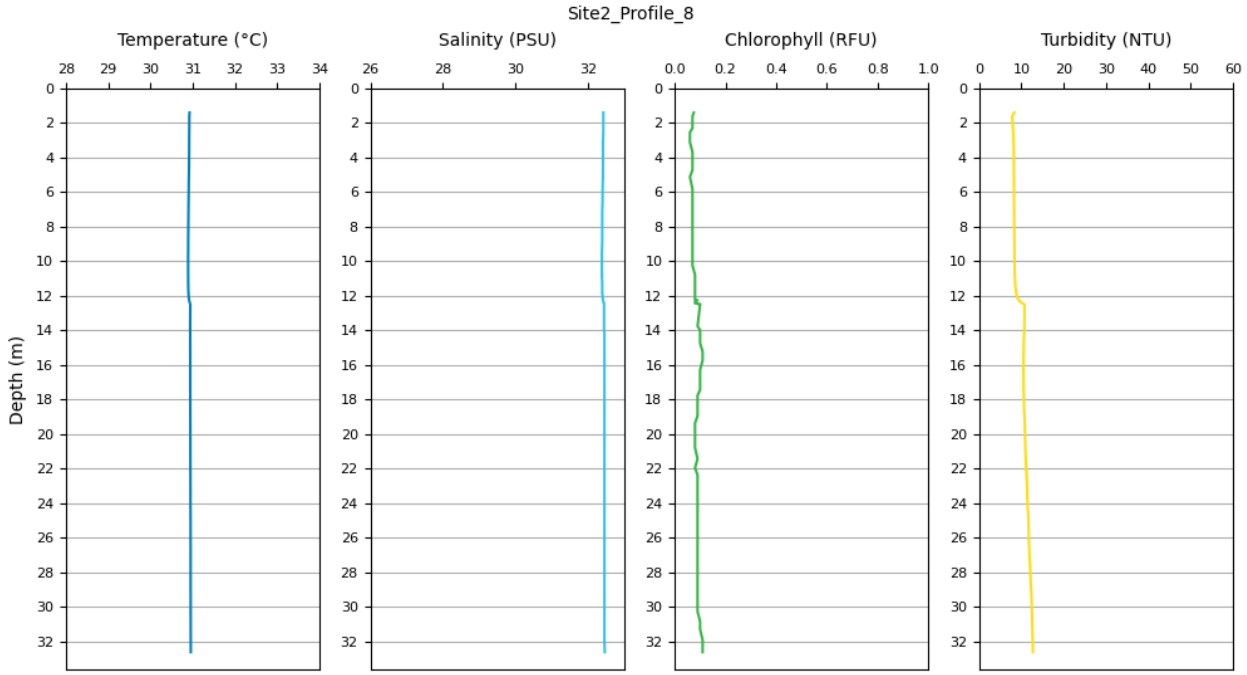

Figure A19. Measured temperature, salinity, chlorophyll and turbidity through the water column at Site 2 at low water +7 hours.

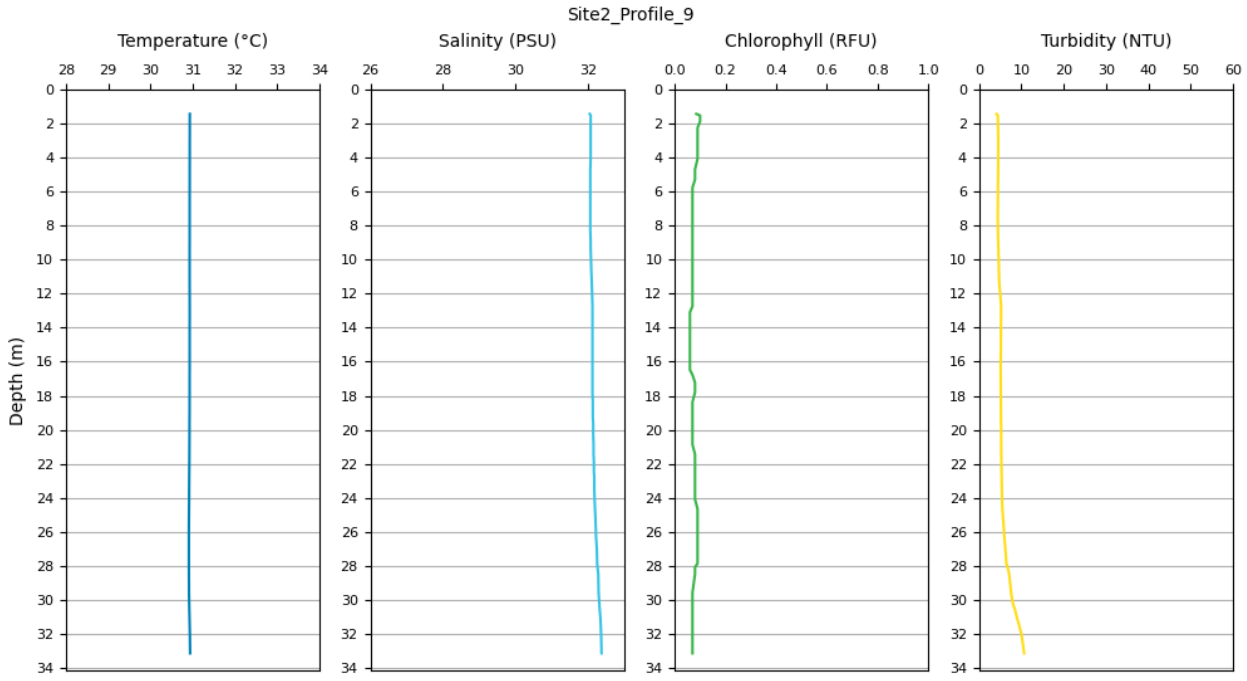

Figure A20. Measured temperature, salinity, chlorophyll and turbidity through the water column at Site 2 at low water +8 hours.

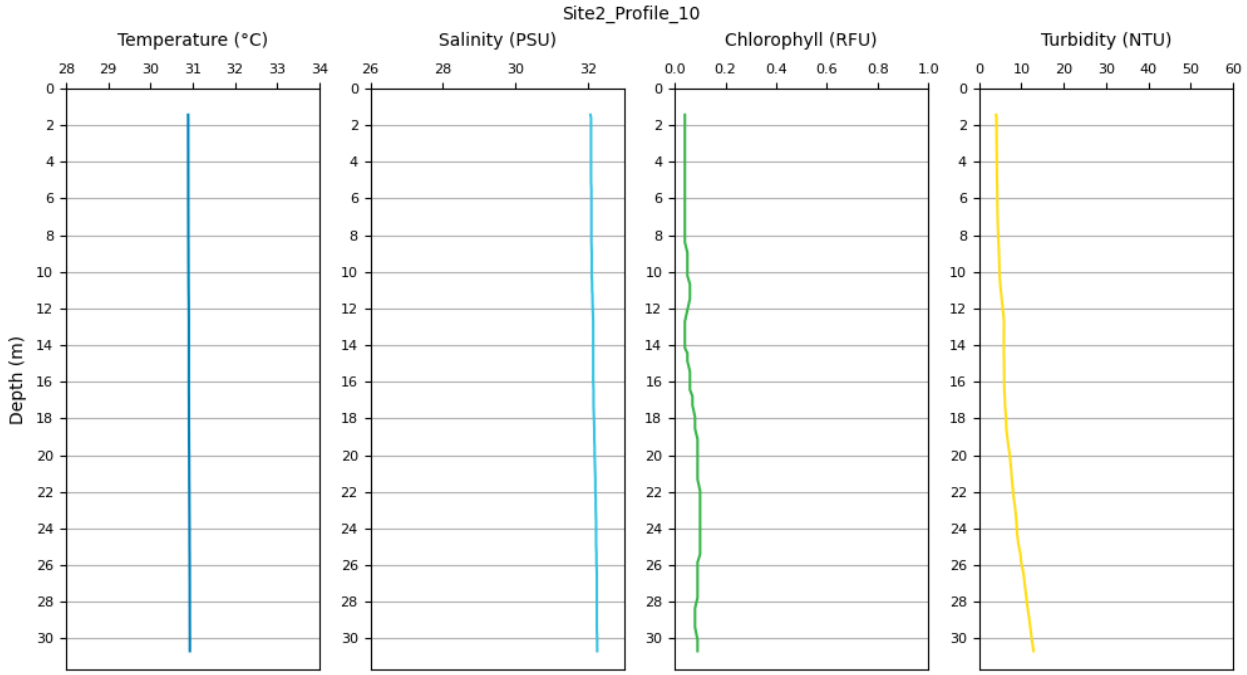

Figure A21. Measured temperature, salinity, chlorophyll and turbidity through the water column at Site 2 at low water +9 hours.

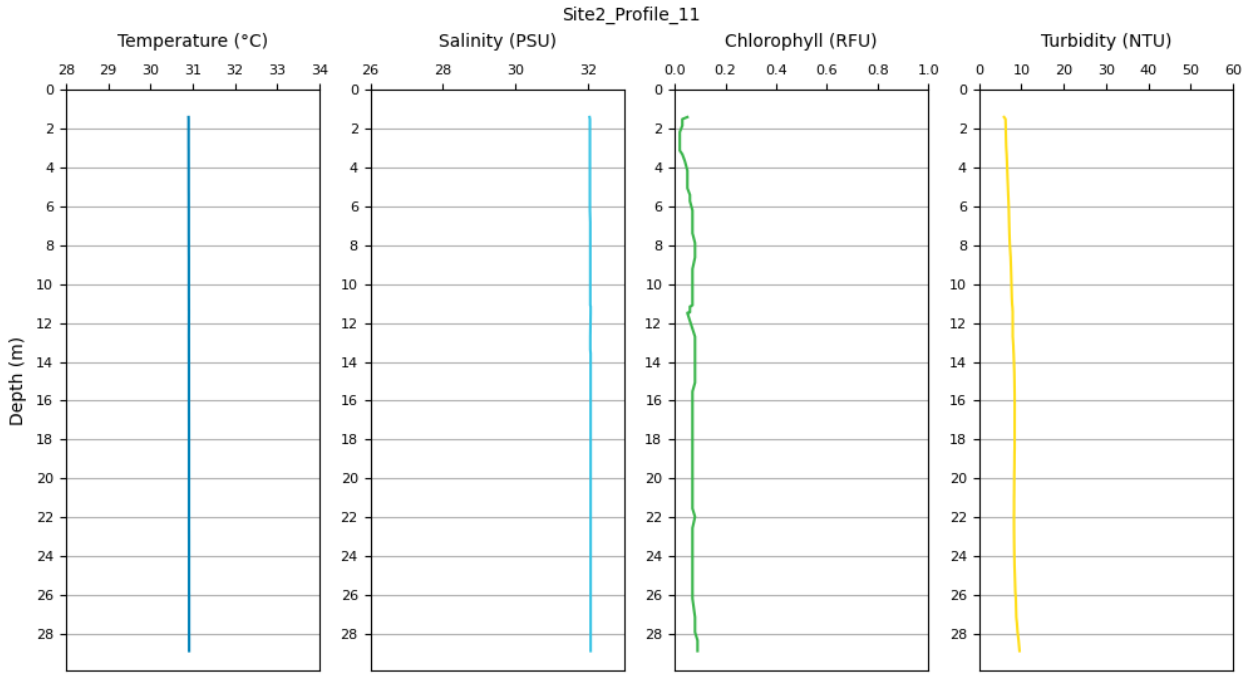

Figure A22. Measured temperature, salinity, chlorophyll and turbidity through the water column at Site 2 at low water +10 hours.

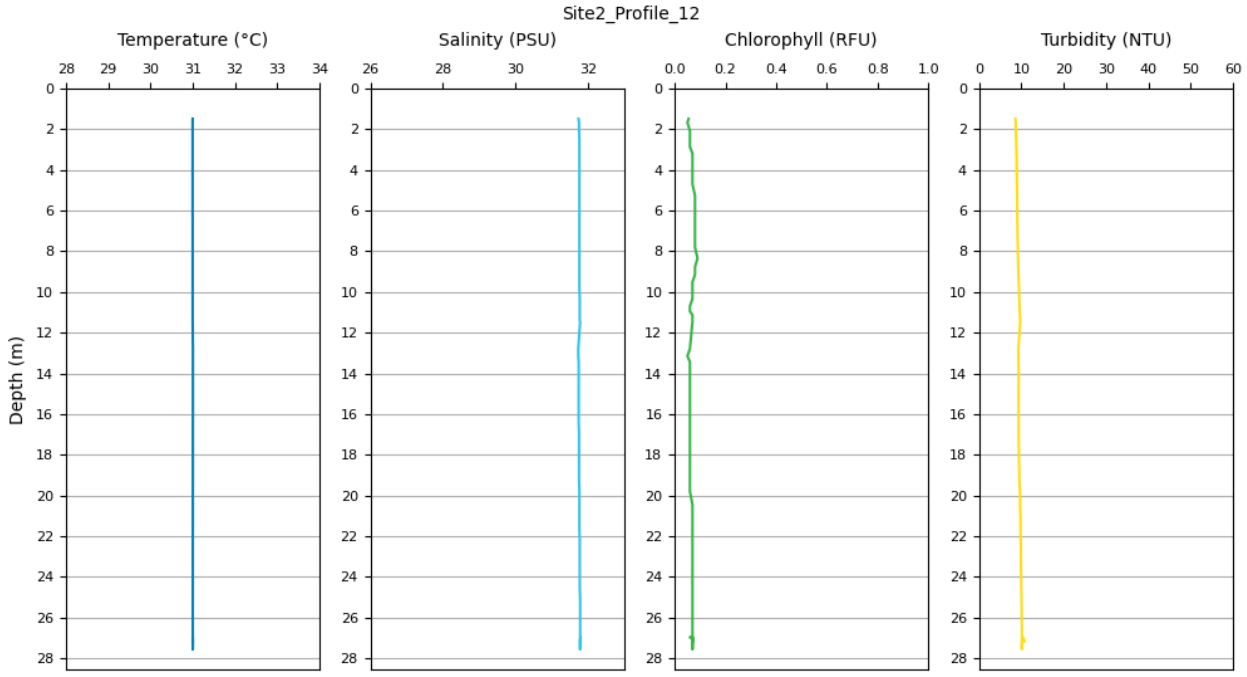

Figure A23. Measured temperature, salinity, chlorophyll and turbidity through the water column at Site 2 at low water +11 hours.

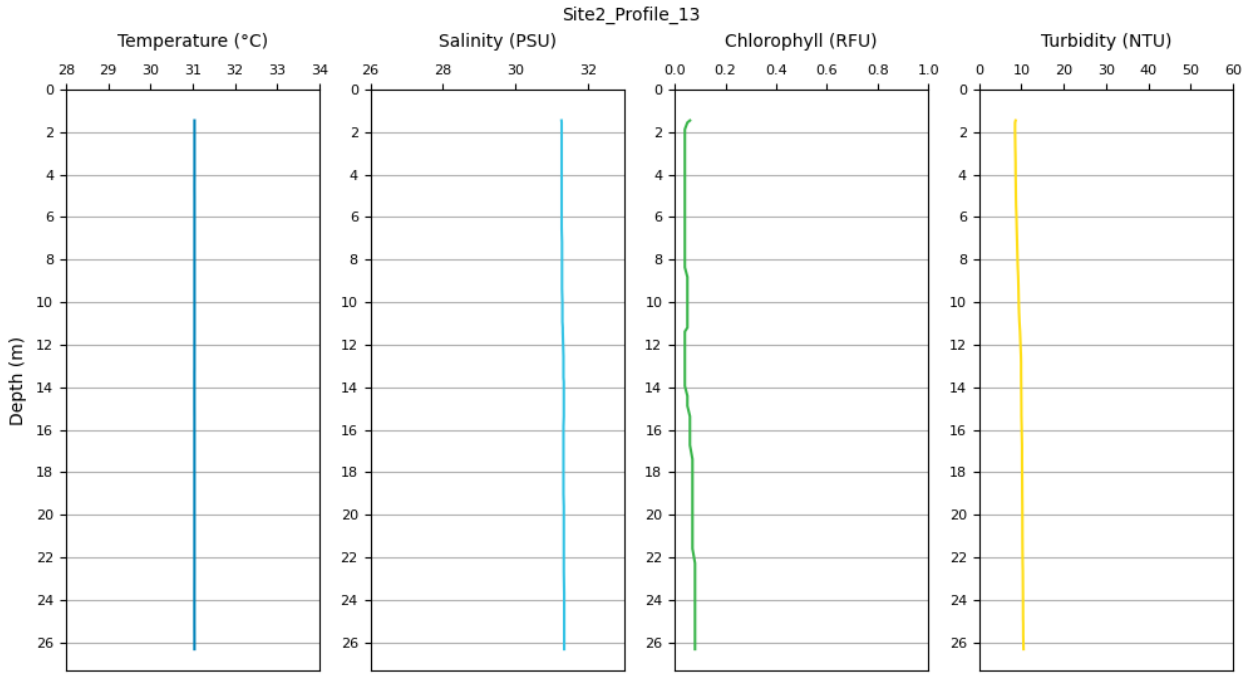

Figure A24. Measured temperature, salinity, chlorophyll and turbidity through the water column at Site 2 at low water +12 hours.

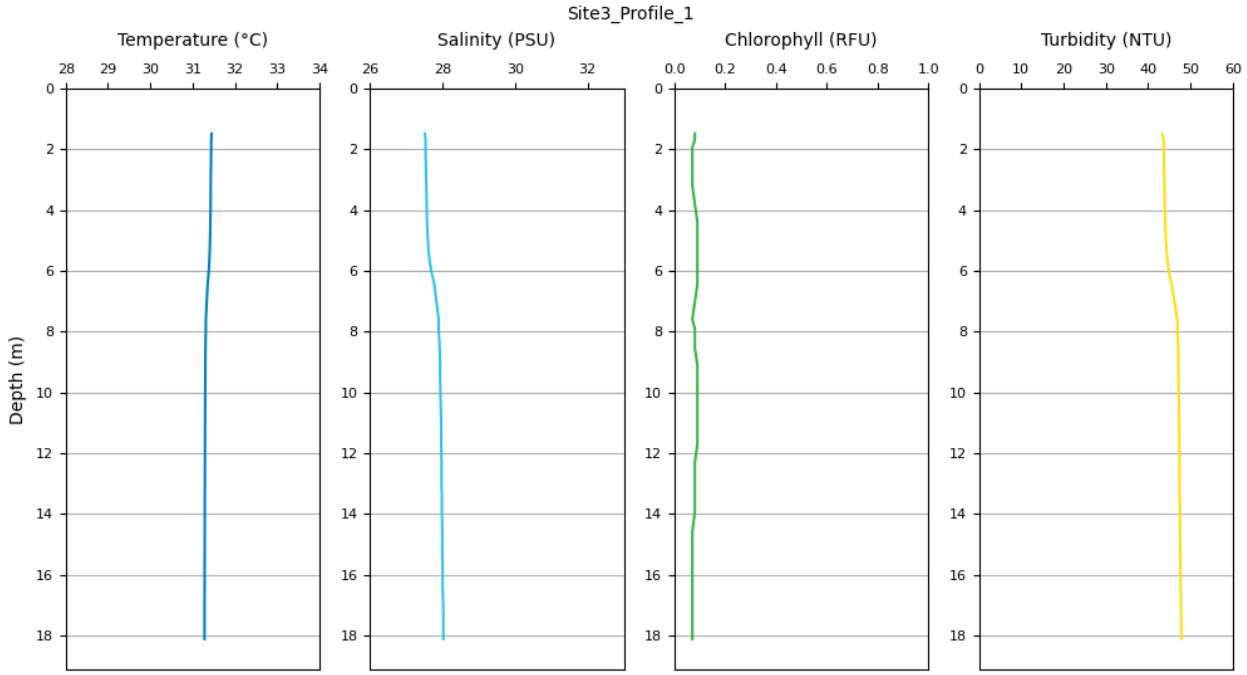

Figure A25. Measured temperature, salinity, chlorophyll and turbidity through the water column at Site 3 at low water.

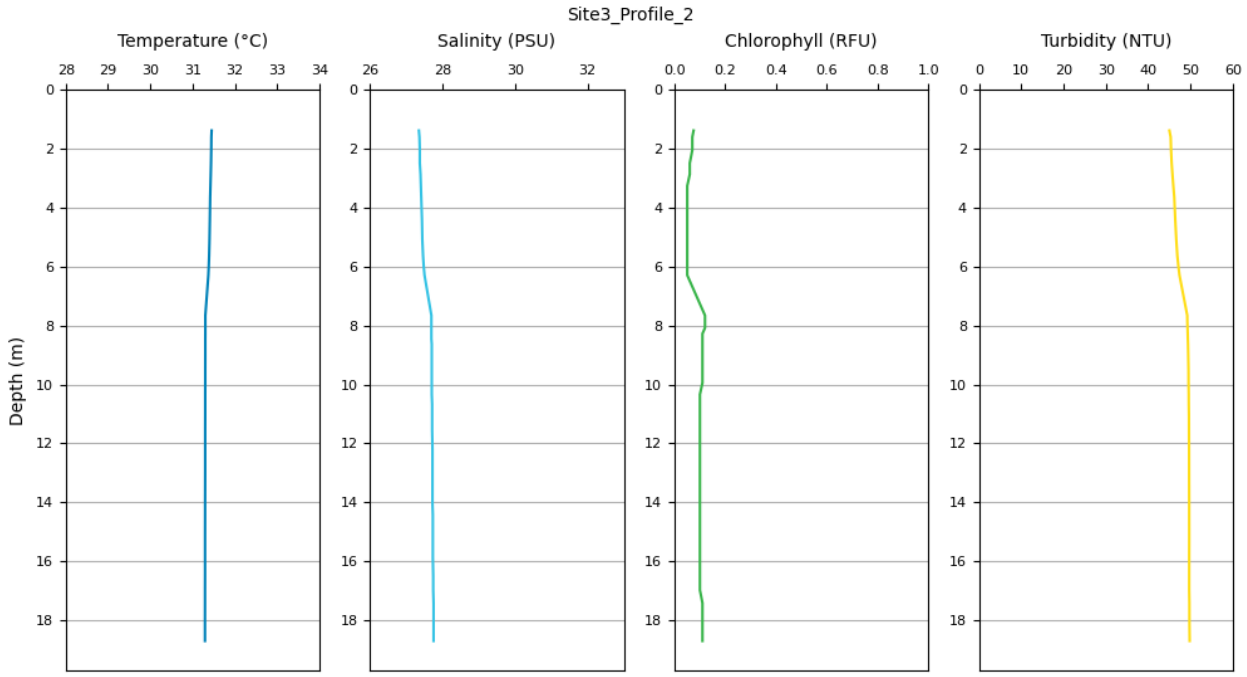

Figure A26. Measured temperature, salinity, chlorophyll and turbidity through the water column at Site 3 at low water +1 hour.

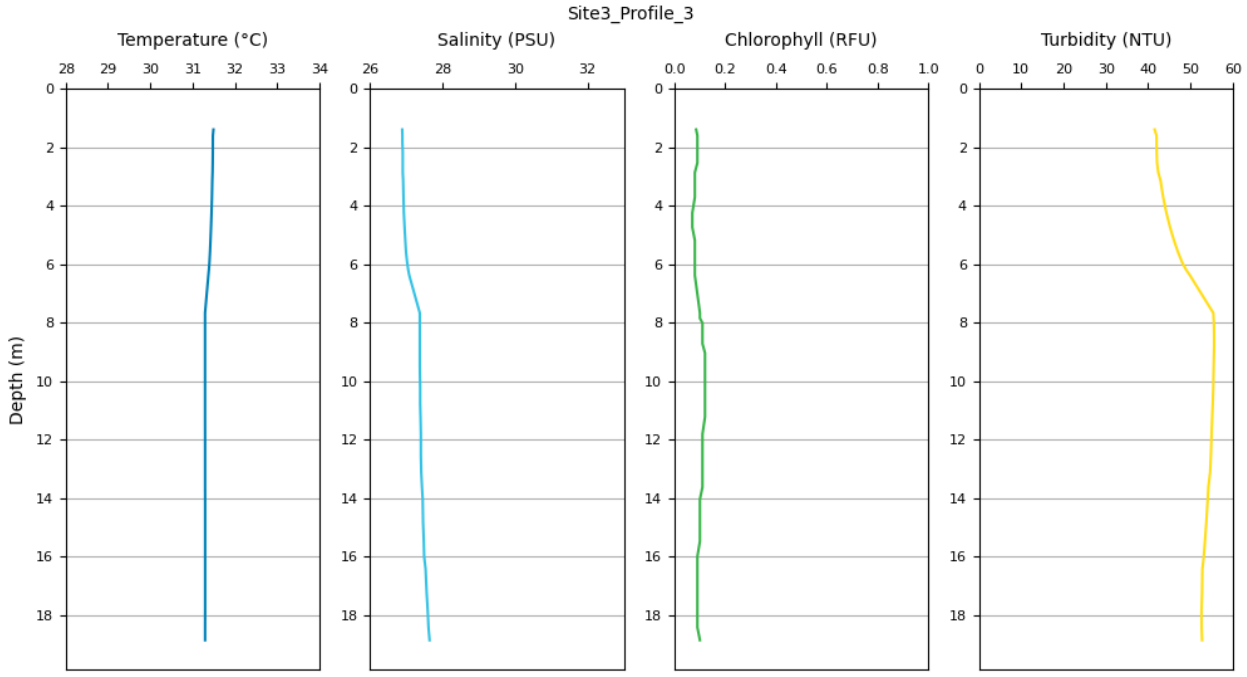

Figure A27. Measured temperature, salinity, chlorophyll and turbidity through the water column at Site 3 at low water +2 hours.

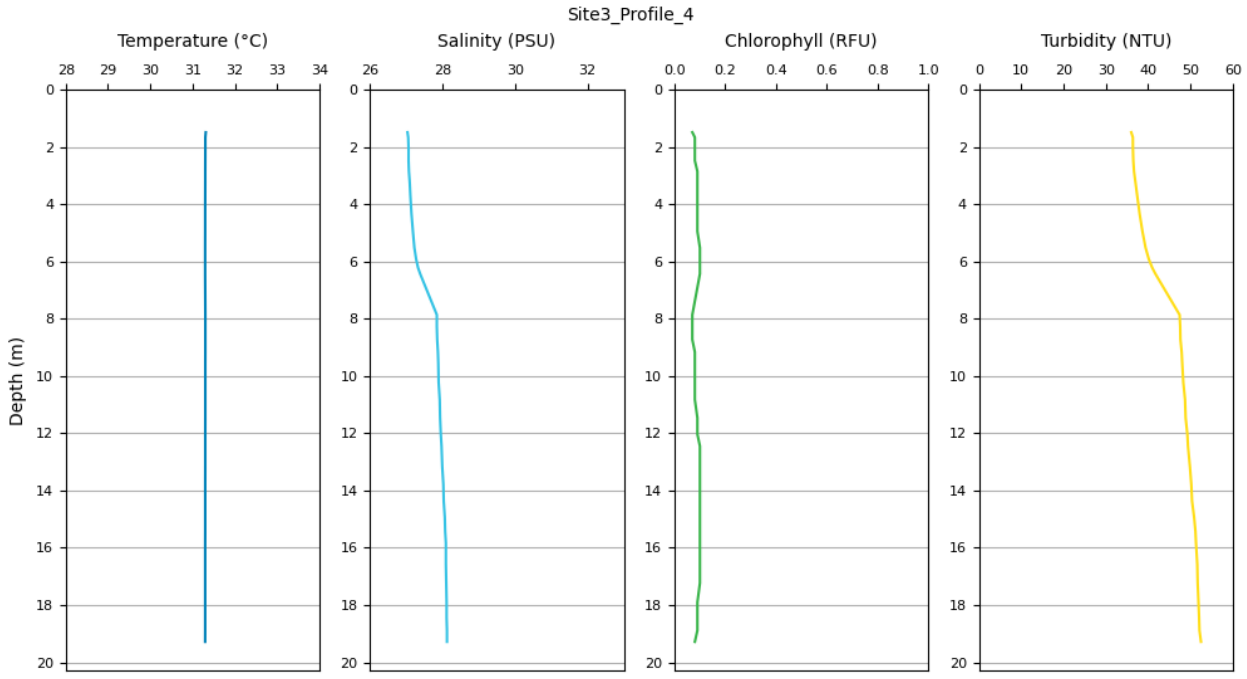

Figure A28. Measured temperature, salinity, chlorophyll and turbidity through the water column at Site 3 at low water +3 hours.

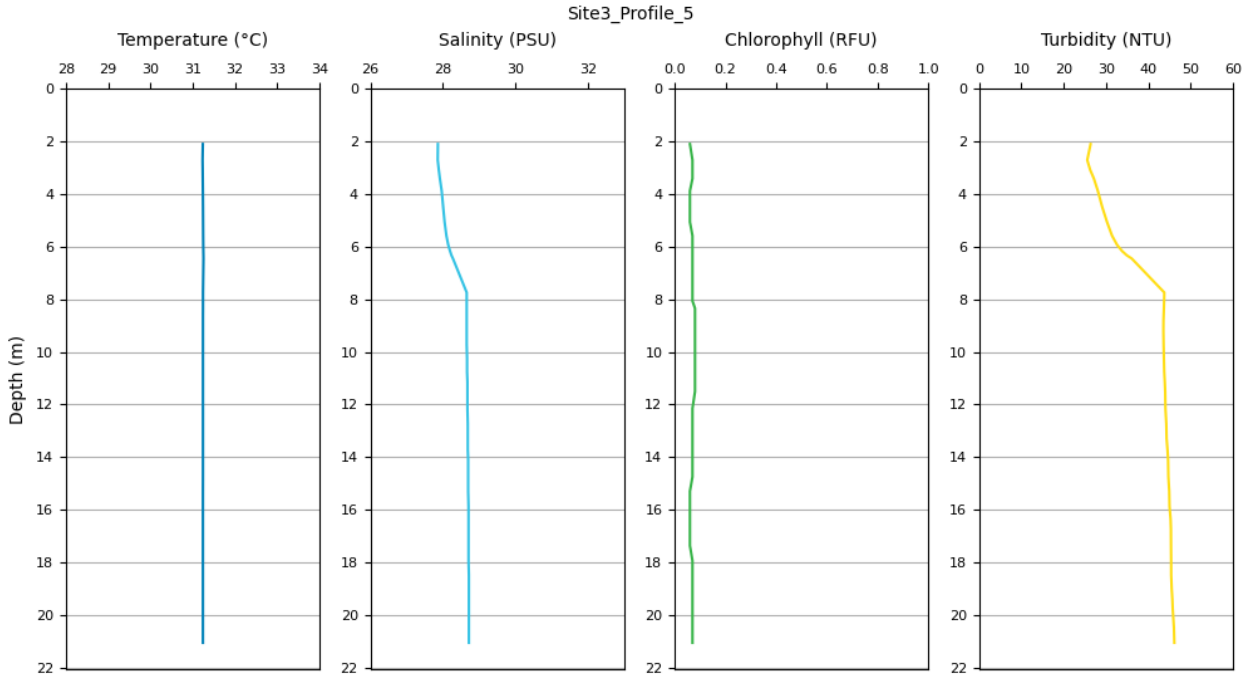

Figure A29. Measured temperature, salinity, chlorophyll and turbidity through the water column at Site 3 at low water +4 hours.

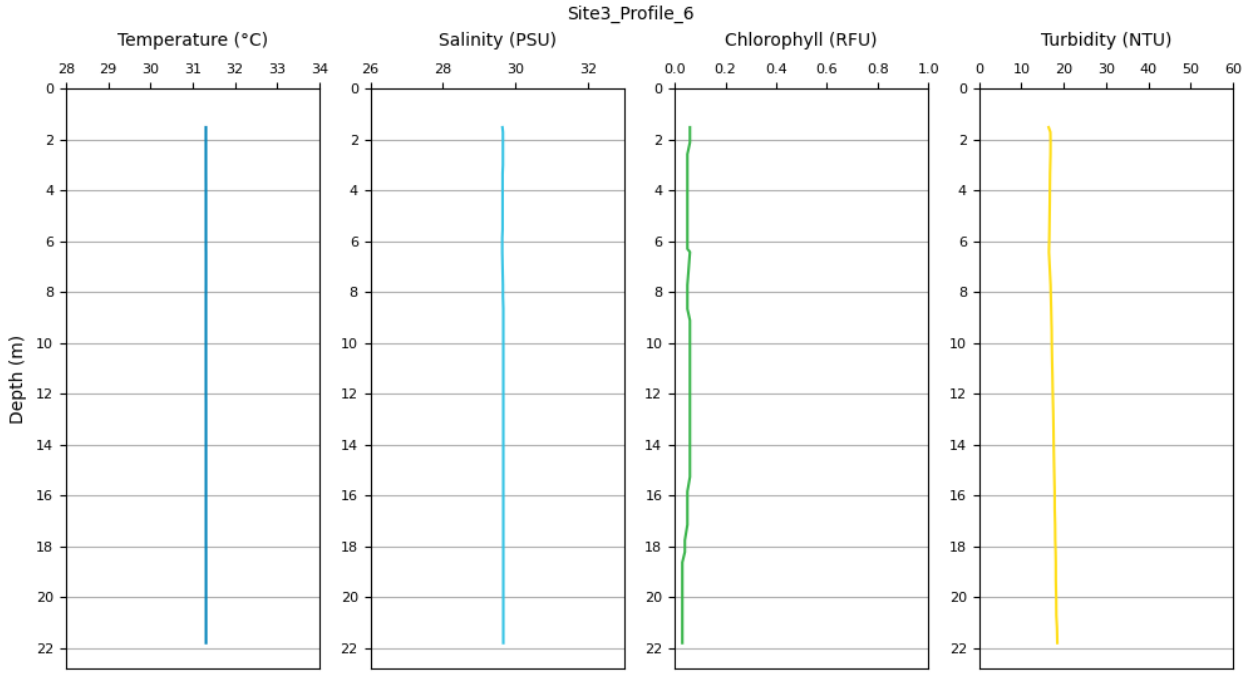

Figure A30. Measured temperature, salinity, chlorophyll and turbidity through the water column at Site 3 at low water +5 hours.

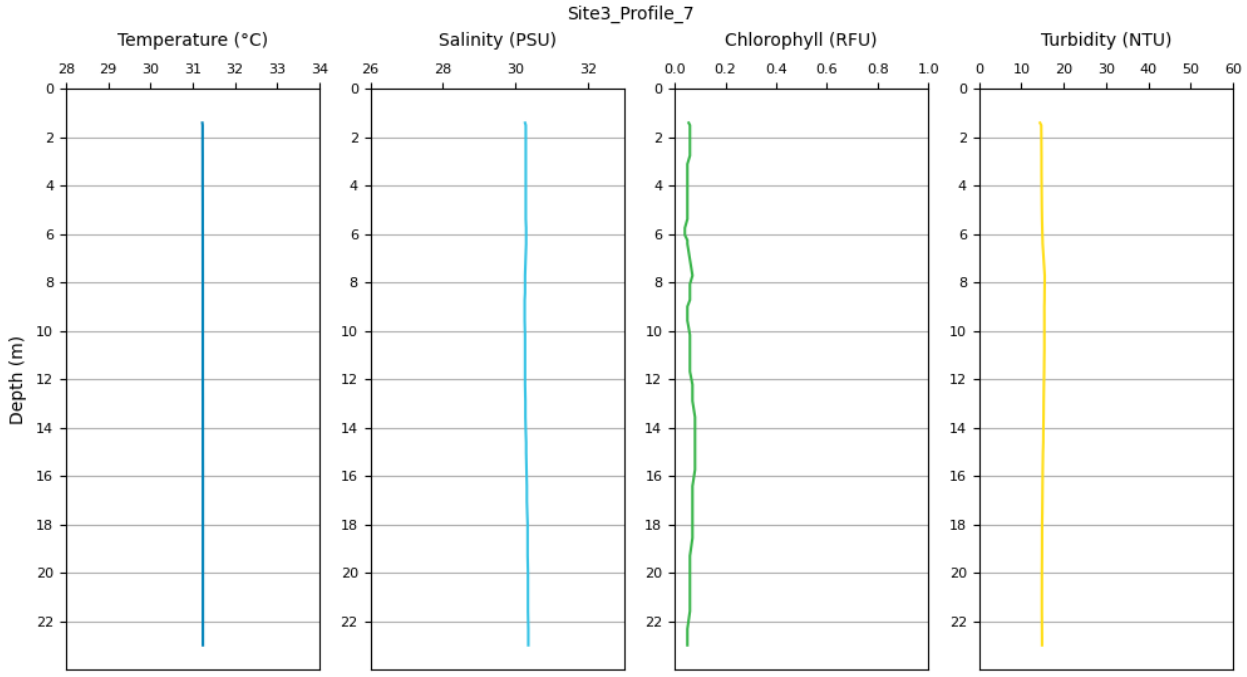

Figure A31. Measured temperature, salinity, chlorophyll and turbidity through the water column at Site 3 at low water +6 hours.

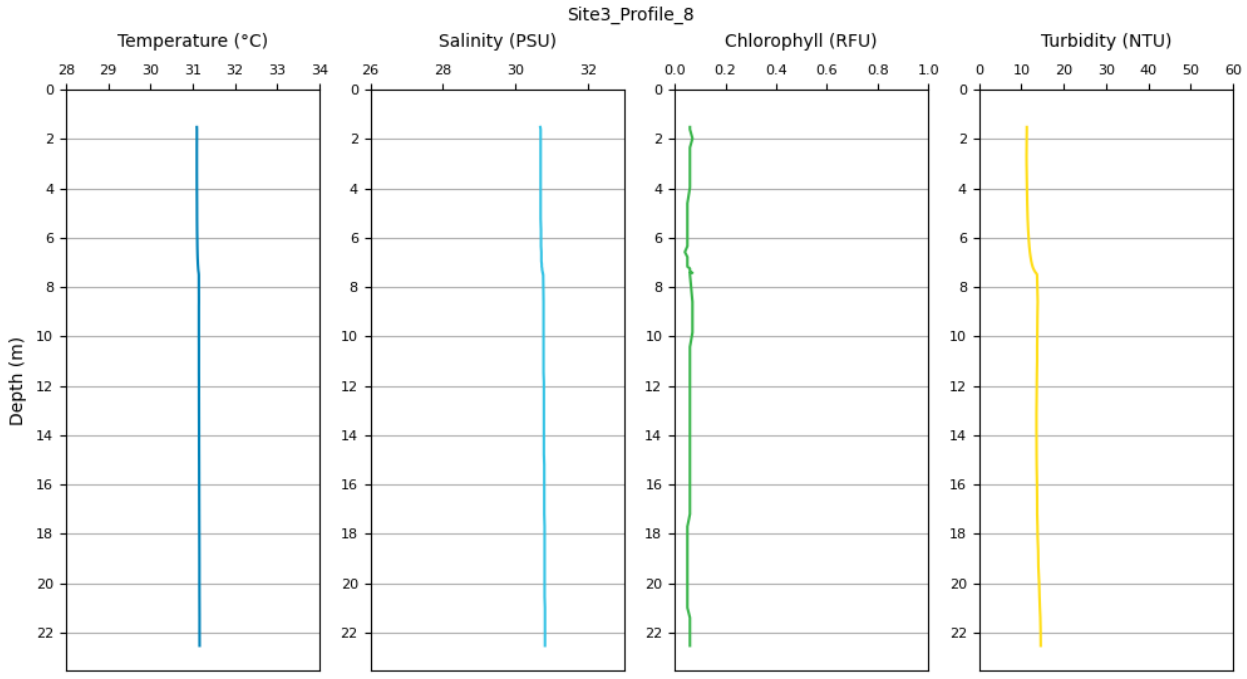

Figure A32. Measured temperature, salinity, chlorophyll and turbidity through the water column at Site 3 at low water +7 hours.

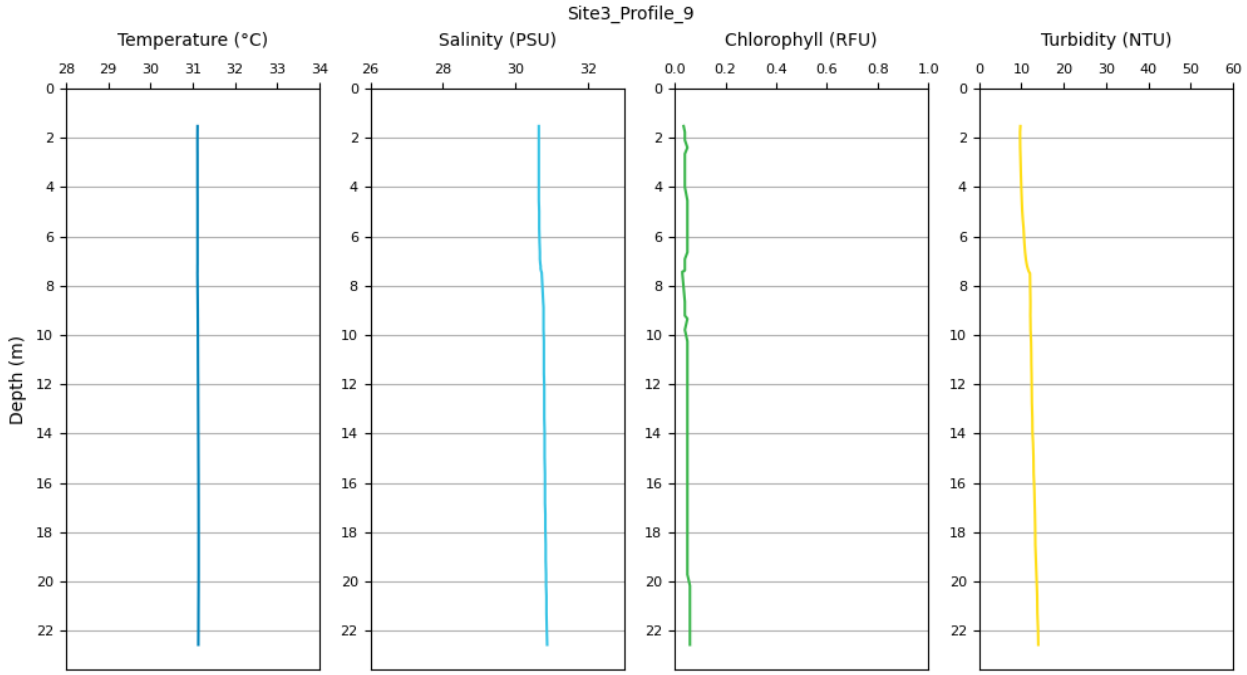

Figure A33. Measured temperature, salinity, chlorophyll and turbidity through the water column at Site 3 at low water +8 hours.

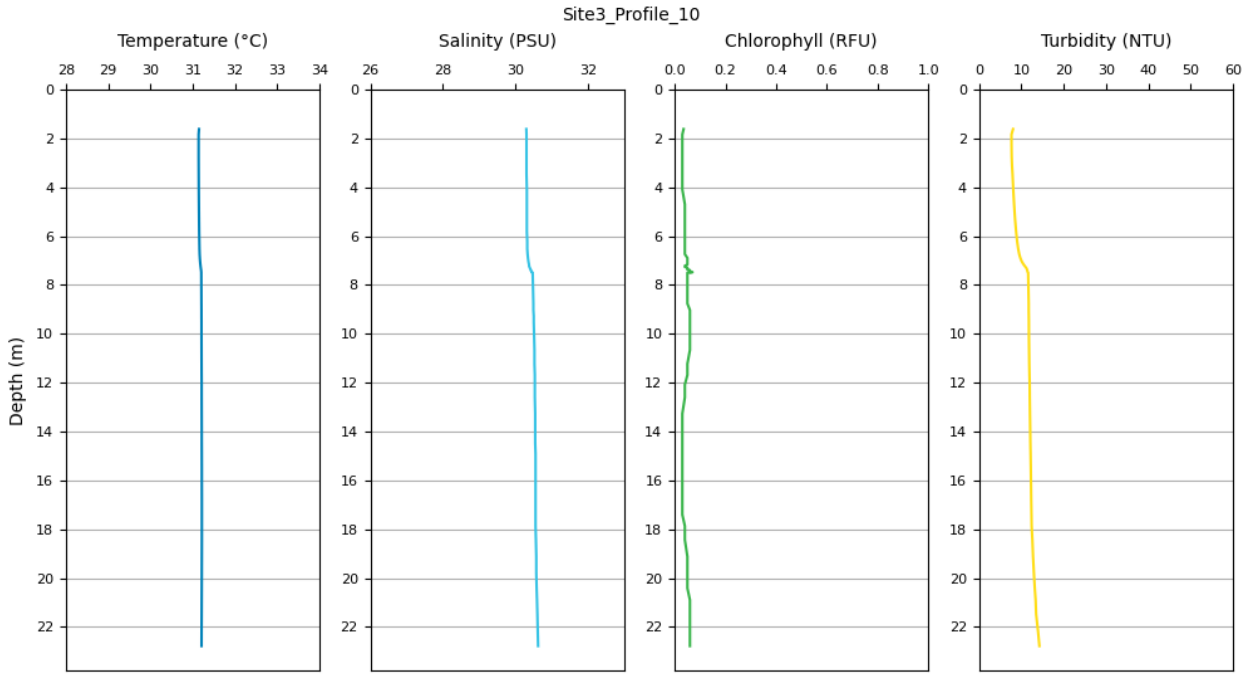

Figure A34. Measured temperature, salinity, chlorophyll and turbidity through the water column at Site 3 at low water +9 hours.

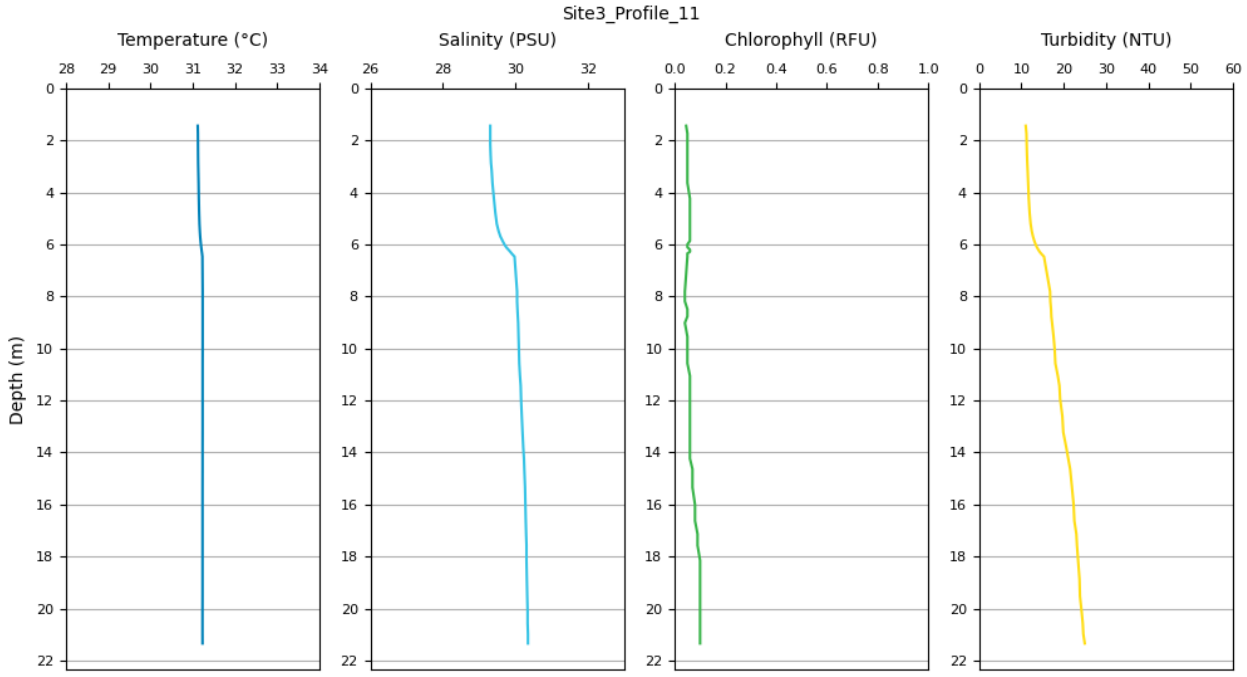

Figure A35. Measured temperature, salinity, chlorophyll and turbidity through the water column at Site 3 at low water +10 hours.

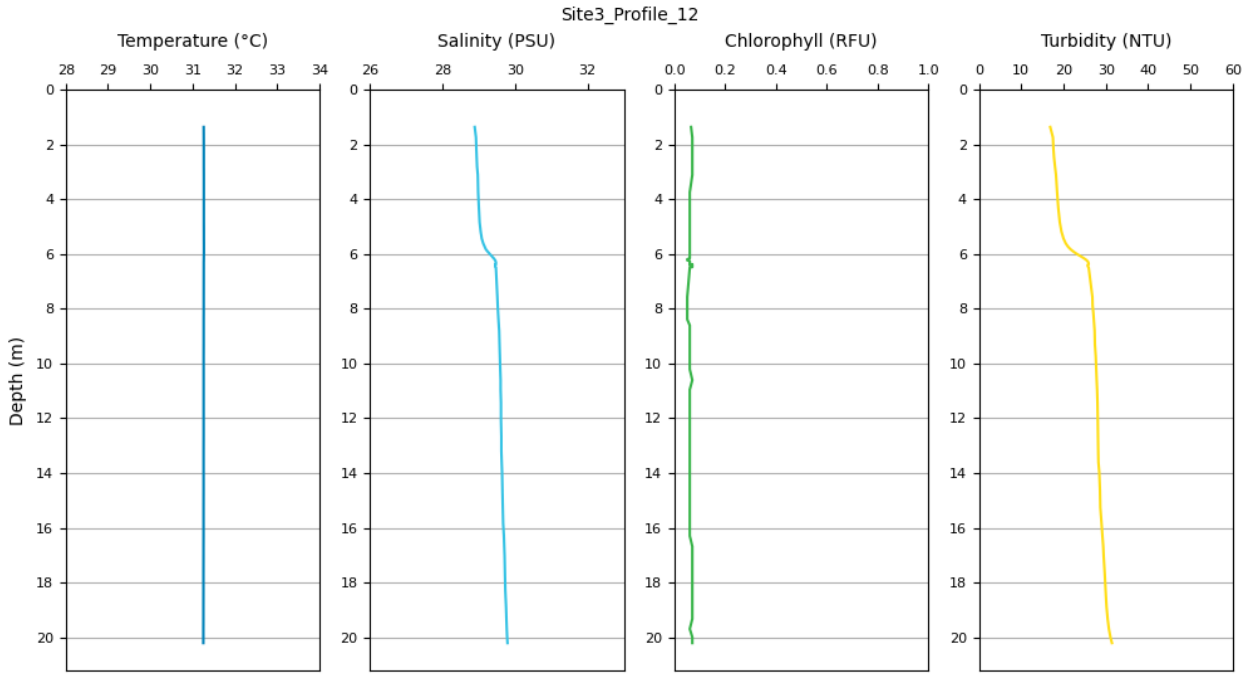

Figure A36. Measured temperature, salinity, chlorophyll and turbidity through the water column at Site 3 at low water +11 hours.

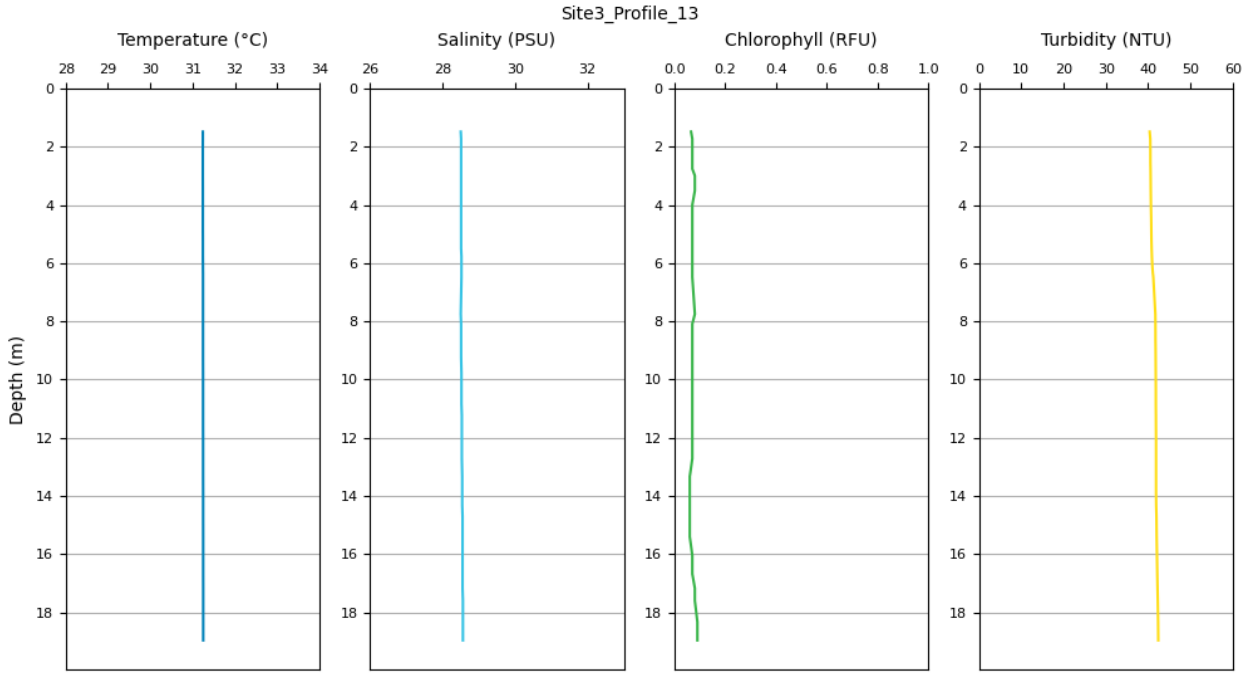

Figure A37. Measured temperature, salinity, chlorophyll and turbidity through the water column at Site 3 at low water +12 hours.